UNIVERSITY
OF HULL

Exploring the Role of Metals and Senescence in Cutaneous Wound Repair

A Thesis submitted for the Degree of Doctor of Philosophy at the University of Hull

by

Holly Nicola Wilkinson

BSc (Hons), The University of Manchester

MRes, The University of Manchester

September 2019

Abstract

Acute wound healing involves a tightly regulated cascade of cellular signalling and functional events. Deterioration at any stage of this sophisticated system can lead to healing impairment and chronic, non-healing wounds. Chronic wounds, which are prevalent in the elderly and diabetic, are a global socioeconomic burden and remain a major area of clinical unmet need. Improved understanding of the cellular and molecular aetiology of chronic wounds is essential to develop new therapies. The aim of this work was to explore the role of cellular senescence and the metallome in governing normal and pathological wound repair.

Novel data presented in this thesis show increased senescence in both aged and diabetic wounds, while biologically-important metals, such as calcium, were reduced. Transcriptional profiling of wounds strongly linked the transcriptome, metallome and senescence. A direct role for senescence in pathological healing was mechanistically demonstrated *in vitro*, *ex vivo* and *in vivo*. Crucially, pharmacological inhibition of the explicated senescence receptor, Cxcr2, accelerated diabetic wound healing *in vivo*. Collectively, these data reveal a hitherto unappreciated role for Cxcr2 in mediating cellular senescence during pathological skin repair.

Global profiling of the wound metallome highlighted significant changes in wound iron levels during late-stage healing. *In vitro* studies uncovered a new role for iron in mediating extracellular matrix deposition during wound remodelling, while reduced iron levels in diabetic wounds correlated with impaired ECM deposition. In summary, temporospatial metallome profiling identified multiple defects in metal-linked cellular processes in the pathological wound environment.

Taken together, the research platform delivered in this work will provide an unprecedented opportunity to further interrogate transcriptional and functional relationships between cellular senescence and the metallome in wound repair. Indeed, this research may underpin the development of novel, efficacious metal-targeted therapies for chronic healing wounds in the future.

Table of Contents

List of Figures

List of Tables

Abbreviations

AGEs = Advanced glycation end products

AgO = Silver oxide

AMP = Antimicrobial peptide

ANOVA = Analysis of variance

AX = Alloxan

BCA = Bicinchoninic acid assay

bFGF = Basic fibroblast growth factor

BM = Basement membrane

BMDM = Bone marrow-derived macrophage

BMP = Bone morphogenic protein

BSA = Bovine serum albumin

CAMK = Calcium/calmodulin-dependent protein kinase

CaSR = Calcium sensing receptor

CDK = Cyclin dependent kinase

CDKI = Cyclin dependent kinase inhibitor

CFU/mL = Colony forming units per milliliter

CM = Conditioned media

CO_2 = Carbon dioxide

CTCF = Corrected total cell fluorescence

Ctsg = Cathepsin g

DAG = Diacylglycerol

DAMP = Damage-associated molecular pattern

DAPI = 4′,6-diamidino-2-phenylindole

DAVID = Database for annotation, visualisation and integrated discovery

Dcytb = Duodenal cytochrome B

DE = Differentially expressed

DENB = Dey-Engley neutralising broth

DFU = Diabetic foot ulcer

DKO = Double knock-out

DM = Diabetes mellitus

DMEM = Dulbecco's minimal essential media

DMSO = Dimethyl sulphoxide

DMT1 = Divalent metal transporter 1

DNA = Deoxyribonucleic acid

DNA-SCARS = DNA segments with chromatin alterations reinforcing senescence

DPBS = Dulbecco's phosphate buffered saline

DWAT = Dermal white adipose tissue

E. coli = *Escheria coli*

ECM = Extracellular matrix

EGF = Epidermal growth factor

eNOS = Endothelial nitric oxide

EPS = Extracellular polymeric substances

ER = Endoplasmic reticulum

FAAS = Flame atomic absorption spectroscopy

FBS = Foetal bovine serum

FIH = Factor inhibiting hypoxia inducible factor

FITC = Fluorescein isothiocyanate

FPKM = Fragments per kilobase million

GAG = Glycosaminoglycan

GF = Growth factor

GM = Growth media

GPCR = G-protein coupled receptor

H_2O_2 = Hydrogen peroxide

HBSS = Hank's balanced salt solution

HCl = Hydrochloric acid

HDF = Human dermal fibroblast

HFE = Human hemochromatosis protein

HH = Hereditary hemochromatosis

HIF = Hypoxia inducible factor

HJV = Hemojuvelin

HNO_3 = Nitric acid

HO-1 = Heme oxygenase 1

H&E = Haematoxylin and eosin

ICC = Immunocytochemistry

ICP-MS = Inductively coupled plasma mass spectrometry

IFNγ = Interferon gamma

IHC = Immunohistochemistry

IL = Interleukin

IPA = Ingenuity pathway analysis

IP3 = Inositol 1,4,5-trisphosphate

IP3R = Inositol 1,4,5-trisphosphate receptor

IRE = Iron response element

IRP = Iron regulatory protein

KLF = Krüppel-like factor

KRT = Keratin

LA-ICP-MS = Laser ablation inductively coupled plasma mass spectrometry

LC = Langerhans cell

LC-MS = Liquid chromatography mass spectrometry

LIP = Labile iron pool

LOX = Lysyl oxidase

LPS = Lipopolysaccharide

MCP-1 = Monocyte chemoattractant protein 1

MCU = Mitochondrial uniporter

MDF = Murine dermal fibroblast

MDM2 = Mouse double minute 2 homolog

MEF = Murine embryonic fibroblast

MEK = Murine epidermal keratinocyte

MHA = Mueller Hinton agar

MHB = Mueller Hinton broth

MIF = Macrophage migratory inhibitory factor

MIP-1α = Macrophage inflammatory protein 1-alpha

MMP = Matrix metalloproteinase

MnSOD = Manganese superoxide dismutase

MOI = Multiplicity of infection

MSA = Mannitol salt agar

mTert = Mouse telomerase reverse transcriptase

Mφ = Macrophage

NAADP = Nicotinic acid adenine dinucleotide phosphate

NADPH = nicotinamide adenine dinucleotide phosphate

NaOH = Sodium hydroxide

$NaHCO_3$ = Sodium bicarbonate

NCX = Sodium-calcium exchanger

NDb = Non-diabetic

NFAT = Nuclear factor of activated T cells

NFκB = Nuclear factor kappa-light-chain-enhancer of activated B cells

NHEK = Normal human epidermal keratinocyte

NK = Natural killer (cell)

NTBI = Non-transferrin bound iron

O/N = Overnight

OCT = Optimum cutting temperature

OH- = Hydroxyl free radical

P. aer = *Pseudomonas aeruginosa*

P4H = Prolyl 4 hydroxylase

PAI-1 = Plasminogen activator inhibitor-1

PAMP = Pathogen-associated molecular patterns

PBS = Phosphate buffered saline

PCA = Principal component analysis

PCBP2 = Poly (rc) binding protein 2

PDGF = Platelet-derived growth factor

PHD = Prolyl hydroxylase

PI = Propidium iodide

PKA = Protein kinase A

Plat = Plasminogen activator, tissue

Plaur = Plasminogen activator, urokinase receptor

PMA = Phorbol 12-myristate 13-acetate

PMCA1b = Plasma membrane calcium ATPase 1b

PPB = Perl's Prussian blue

pRb = Retinoblastoma protein

P/S = Penicillin-streptomycin solution

PTH = Parathyroid hormone

qRT-PCR = Quantitative reverse transcription polymerase chain reaction

RNA = Ribonucleic acid

RNA-SEQ = Ribonucleic acid sequencing

ROS = Reactive oxygen species

RT = Room temperature

S. aur = *Staphyloccoccus aureus*

S1P = Sphingosine-1-phosphate

SASP = Senescence-associated secretory phenotype

SB = *Stratum basale*

SC = *Stratum corneum*

SDS-PAGE = Sodium dodecyl sulphate-polyacrylamide gel electrophoresis

SEM = Standard error of the mean

SERCA = Sarco(endo)plasmic reticulum Calcium-ATPase

SG = *Stratum granulosum*

SMA = Smooth muscle actin

SMAD = Mothers against decapentaplegic homolog

SODs = Superoxide dismutases

SPRR = Small proline-rich protein

SS = *Stratum spinosum*

STEAP3 = Six transmembrane epithelial antigen of the prostate 3

STZ = Streptozocin

T1DM = Type 1 diabetes mellitus

T2DM = Type 2 diabetes mellitus

TBI = Transferrin bound iron

TDM = THP-1-derived macrophage

TEWL = Transepidermal water loss

Tf = Transferrin

TfR1 = Transferrin receptor

TGFβ = Transforming growth factor beta

TIMP = Tissue inhibitor of metalloproteinase

TMF = Trace metal free

TNF = Tumour necrosis factor

TRP = Transient receptor potential

TRPV6 = Transient receptor potential vannaloid type 6

TUNEL = Terminal deoxynucleotidyl transferase dUTP nick end labeling

UTR = Untranslated region

UVR = Ultraviolet radiation

VDR = Vitamin D receptor

VEGF = Vascular endothelial growth factor

VLU = Venous leg ulcer

WT = Wild-type

YFP = Yellow fluorescent protein

Thesis Associated Publications

- Wilkinson HN, Roberts ER, Stafford AR, Banyard KL, Mace KA, Hardman MJ. Tissue iron promotes wound repair via M2 macrophage polarisation and the chemokines CCL17 and CCL22. Am J Pathol. 2019 Nov; 189(11): 2196-2208. [IF 4.1] [Editor's Choice]
- Wilkinson HN, Upson SE, Banyard KL, Knight R, Mace KA, Hardman MJ. Reduced iron in diabetic wounds: An oxidative stress-dependent role for STEAP3 in extracellular matrix deposition and remodelling. J Invest Dermatol. 2019 Nov; 139(11): 2368-2377 [IF 6.5]
- Wilkinson HN, Clowes C, Banyard KL, Matteuci P, Mace KA, Hardman MJ. Elevated local senescence in diabetic wound healing is linked to pathological repair via CXCR2. J Invest Dermatol. 2019 Apr; 139(5):1171-1181. [IF 6.5] [Highlighted article and commentary*]

  *Associated Commentary: Tomic-Canic M, DiPietro LA. Cellular Senescence in Diabetic Wounds: When Too Many Retirees Stress the System. J Invest Dermatol. 2019 Apr; 139(5): 997-999. [IF 6.5]

- Wilkinson HN, Iveson S, Catherall P, Hardman MJ. A Novel Silver Bioactive Glass Elicits Antimicrobial Efficacy against Pseudomonas aeruginosa and *Staphylococcus aureus* in an Ex Vivo Skin Wound Biofilm Model. Front Microbiol. 2018 Jul 3; 9: 1450. [IF 4]
- Wilkinson HN, Hardman MJ. The role of estrogen in cutaneous ageing and repair. Maturitas. 2017 Sep; 103: 60-64. [IF 3.3]

Thesis Associated Presentations

- Gordon Research Conference in Tissue Repair and Regeneration, New Hampshire, US (June 2019) – Defining A Role for CXCR2-Mediated Senescence in Diabetic Wound Repair (Poster)
- Gordon Research Conference in Tissue Repair and Regeneration, New Hampshire, US (June 2019) – Wound Metallomics: Identifying a New Role for Iron in Pathological Wound Repair (Poster)
- British Society of Cell Biology/British Society of Developmental Biology Spring Meeting, Warwick, UK (April 2019) – Diabetic CXCR2-Mediated Senescence Orchestrates Cellular Behaviour in the Wound Microenvironment (Poster)
- Allam Medical Lecture, Hull, UK (March 2019) – Wound Metallomics: Identifying a New Role for Iron in Pathological Wound Repair (Poster)
- 15th International Medical Postgraduate Conference, Prague (November 2018) – A Mechanistic Role for CXCR2-Mediated Cellular Senescence in Diabetic Wound Repair (Talk)

- Transatlantic Diabetic Lower Extremity and Chronic Wound Symposium, Santorini, Greece (October 2018) – Senescence and Diabetes in Wound Repair (Poster)
- PhD Life Sciences Symposium, Hull, UK (January 2018) – Ageing and Wound Healing (Talk and Poster)
- 3rd Basel-Manchester Forum on Skin repair, Switzerland (October 2017) – Calcium: A Global Regulator of Wound Healing (Poster)
- North England Cell Biology Forum Meeting, Hull, UK (September 2017) – Calcium: A Global Regulator of Wound Healing (Talk and Poster)
- PhD Life Sciences Symposium, Hull, UK (January 2017) – Exploring the Role of Metals in Wound Repair (Talk, Poster and Session Chair)
- 13th International Medical Postgraduate Conference, Prague (November 2016) - Exploring the Role of Metals in Wound Repair (Talk)
- Summer Showcase Symposium, Manchester, UK (July 2016) – Comparing Efficacy of Monofilament Debriding Devices in Wound Healing (Poster and Image)
- Centre for Doctoral Training in Regenerative Medicine Symposium, Manchester, UK (June 2016) – Exploring the Role of Metal Ions in Wound Healing (Poster)

Thesis Associated Prizes

- The Allam Lecture (Hull York Medical School, 2019) – Poster Prize (1st)
- 15th International Medical Postgraduate Conference (Prague, 2018) – Talk Prize
- Transatlantic Diabetic Lower Extremity and Chronic Wound Symposium (Santorini, 2018) – Poster Prize (1st)
- PhD Life Sciences Symposium Winner (University of Hull, 2018) – Poster Prize
- 3rd Basel-Manchester Forum on Skin Repair (Switzerland, 2017) – The Conference Prize
- North England Cell Biology Forum Meeting (Hull, 2017) – Talk Prize
- PhD Life Sciences Symposium (University of Hull, 2017) – Poster Prize (1st)
- MRC Max Perutz Award (Royal Society London, 2016) – Finalist
- Summer Showcase Symposium (University of Manchester, 2015) – Image Finalist

Acknowledgements

I would first and foremost like to thank my supervisors, Dr Barbara Guinn and Professor Matthew Hardman, for their continued support during the trials and tribulations of my research endeavours. Not only did they encourage me through my most tempestuous moments, but they also guided me down the path of experience, wisdom and clarity. For this, I am eternally grateful; it has been a minefield. I would also like to thank my industrial supervisor, Mr Paul Caterall, for his outrageous anecdotes about Theraglass and his contagious enthusiasm about the first PhD paper (it was a slippery slope from there). I would like to acknowledge the support and friendship of Dr Kimberly Mace, who took me under her wing and opened my mind to the world of macrophages, dude. I would further like to thank the plastics department at Castle Hill Hospital, particularly Mr Paolo Matteucci, for providing access to patient skin samples, which allowed most of the work in this thesis to be undertaken. I would also like to greatly acknowledge the Medical Research Council who supported this research as part of an MRC industrial CASE PhD Studentship (MR/M016307/1) with Theraglass Ltd. (London, UK).

Within Biomedical Sciences, I have to thank Mrs Ann Lowry for trusting me in her electron microscopy suite, Dr Cordula Kemp for her conversations about *Drosophila* and confocal microscopy, Mrs Ellie Beeby for always being happy and helpful, and Dr Cheryl Walter and Miss Jenna Jarvis for letting me isolate plasmid DNA in their laboratory. I would also like to acknowledge the help of Mr Robert Knight and Dr Anna Bird in the elemental analysis facility. Rocks are interesting – who knew?!

I am extremely grateful to everyone at Daisy for providing a collegial and nurturing environment. Although I cannot name everyone, I would like to specifically thank Dr Ruth Kennedy and Mr Chris Crow for their advice and help when I arrived in Hull with 70 crates to unpack and nowhere to put any of it, Dr Elizabeth Roberts, Dr Simon Fraser, Miss Francesca Longhorne, Mrs Rebecca Stinson and Mrs Hayley Foster for their friendship, and the ever-expanding Hardman group as of late. I would like to thank my family, my mum for walking my dogs, my dad for constantly asking if I have finished my PhD yet, and my Grandad for asking whether I plan to do a “super PhD” next, likely due to the fact that I have not left university in the past ten years. Finally, I would like to greatly acknowledge my sister, Kirsten, who is the only one who thinks I will “smash it”, although I have yet to figure out what “it” is.

Dedication

This thesis is dedicated to my two favourite ladies who began their lives when I started down this arduous path. This is for Luna and Tia, who have provided me with companionship, empathy and compassion during the last four years and have given me the perspective, inspiration and resilience to complete this journey. Thank you.

"You cannot teach a man anything; you can only help him discover it in himself". ~Galileo

Declaration

I confirm that this work is original and that if any passage(s) or diagram(s) have been copied from academic papers, books, the internet or any other sources these are clearly identified by the use of quotations marks and the reference(s) fully cited. I certify that, other than where indicated, this is my own work and does not breach the regulations of the University of Hull regarding plagiarism or academic misconduct in examinations. This piece of work is my own and does not contain any unacknowledged work from any other sources. I confirm that any patient information obtained to produce this piece of work has been appropriately anonymised.

Chapter 1: Introduction

1.1. The Skin

Skin is the largest organ of the human body, comprising around 15-17% of an individual's body weight and spanning up to $2m^2$ in adults (Zaidi & Lanigan, 2010). The skin performs a variety of important functions to maintain homeostasis, such as enabling thermostability and allowing the body to respond to extrinsic sensory stimuli, including heat and pressure (Kosikowska et al., 2015). Crucially, the skin acts as the primary barrier against the vagarious onslaughts of the external environment. It prevents desiccation through regulation of trans-epidermal water loss (TEWL; Hardman et al., 1998), and protects against mechanical, chemical, thermal and photic damage to vital internal structures (Takeo et al., 2015). The skin also defends against pathogenic infection by microorganisms through elegantly adapted host-microbiota interactions, and a sophisticated innate immune response (Naik et al., 2015). This thesis focuses on exploring the vital evolved mechanisms that the skin uses to quickly and efficiently close breaches to its barrier.

1.1.1. Skin Structure

The skin comprises of the epidermis, basement membrane (BM), dermis, and underlying subcutaneous adipose tissue, the hypodermis (**Figure 1.1**; Debeer et al., 2013). The hypodermis serves as an insulating layer and energy reserve, providing cushioning to underlying tissues (Frienkel & Woodley, 2001). The skin houses structures that convey its functionality, such as nerve endings and blood vessels; and appendages, including hair follicles, sweat glands, sebaceous glands and nails (Elias, 2007; Proksch et al., 2008). Although the structure of skin is largely conserved among mammals, subtle differences are still apparent. For example, skin from humans, non-human primates and pigs is attached to underlying muscle fascia, and maintains high elastic content relative to the skin of other mammals (Dorsett-Martin, 2004; Sullivan et al., 2001). Porcine skin retains similar epidermal thickness to human skin (as observed via infrared spectroscopy, Kong & Bhargava, 2011; Mahl et al., 2006) and is insulated by an abundant hypodermis (Debeer et al., 2013; Summerfield et al., 2015). Human and porcine skin also possess similar epidermal turnover and keratin protein expression, and comparable dendritic cell antigen

patterns (Sullivan et al., 2001; Summerfield et al., 2015). By contrast, murine skin is loose, much thinner than human skin, and lacks rete ridges (Treuting et al., 2012). Murine skin also holds considerably more hair follicles and a *panniculosus carnosus* muscle layer to allow rapid wound contraction following injury (Wong et al., 2010). Despite these marked differences, the overall composition of the skin, and the distribution of collagen and elastic fibres, remains comparable between humans and mice (Junqueira & Montes, 1983; Kielty & Grant, 2002). Indeed, species-specific similarities and differences must be considered when using non-human skin and wound models for translational research purposes (see **Table 1.1**).

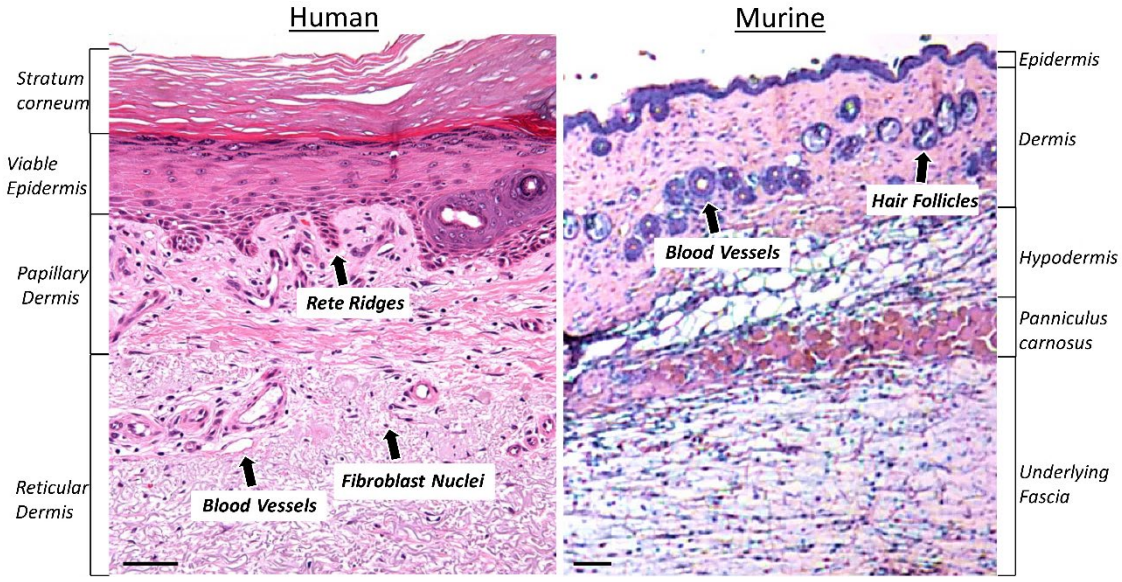

Figure 1.1. Comparative structural composition of human and murine skin. Haematoxylin and eosin staining shows the main features of human and mouse skin. Human epidermis and dermis are thicker, with a visible *stratum corneum*, while murine skin contains dense hair follicles and a *panniculus carnosus* muscle. Bar = 50 µm. *Histological images produced by the author (HNW)*.

Table 1.1. Key similarities between human, porcine and murine skin structure and wound healing. *

Feature	Species		
	Human	**Porcine**	**Murine**
Skin attachment	Firmly attached	Firmly attached	Loose
Hair	Sparse	Sparse	Dense
Panniculus carnosus	No	No	Yes
Primary healing mechanism	Re-epithelialisation	Re-epithelialisation	Contraction

**Adapted from Summerfield et al. (2015).*

1.1.2. The Epidermis

The epidermis is a superficial differentiated squamous epithelial layer, protecting the body against physical trauma, chemical damage and ultraviolet radiation (UVR) exposure (Braverman, 2000). Within the embryo, epidermal formation is dependent on expression of the transcription factor, p63. Upregulation of p63 is required to convert keratin 8 (Krt8)/18-expressing ectoderm into Krt5/14-positive epidermis (Byrne et al., 1994; Mills et al., 1999). Around 95% of the epidermis is composed of KRT-rich squamous keratinocytes, which migrate and differentiate through the four histologically distinct epidermal layers: the *stratum basale* (SB), the *stratum spinosum* (SS), the *stratum granulosum* (SG) and the *stratum corneum* (SC; Baroni et al., 2012; Hardman et al., 1999; **Figure 1.2**).

The skin is the only organ, other than the lungs, in direct contact with atmospheric oxygen (Stücker et al., 2002). As the epidermis is avascular, it relies heavily on apical diffusion of oxygen and nutrient transfer through contact with the dermis at the BM (Braverman, 2000). Epidermal thickness varies substantially based on body site. The thickest skin (up to 600 μm) is found on plantar and palmar regions (Debeer et al., 2013; Elias, 2007), where an extra supportive layer, the *stratum lucidum*, is sandwiched between the SC and SG (Zirra, 1976).

The epidermis primarily functions to continually replenish the SC; a layer of large, non-viable, impermeable corneocytes devoid of organelles, which act as the first barrier to intrusion and dehydration (Elias, 2004; Madison, 2003; Proksch et al., 2008). Over time, corneocytes of the SC are lost through desquamation, which allows the epidermis to circumvent extrinsic macromolecular damage accumulation (Tigges et al., 2014). Therefore, new keratinocytes must constantly replace the nonviable SC through the process of terminal differentiation (Allen & Potten, 1975). Differentiation is regulated by an epidermal calcium gradient, where keratinocytes become increasingly permeable to calcium as they migrate towards the apical (SC) surface (Eckert & Rorke, 1989). In human skin, the turnover rate of keratinocytes, migrating from the SB to the SC, is approximately 28 days (Harding, 2004; Lai-Cheong & McGrath, 2009).

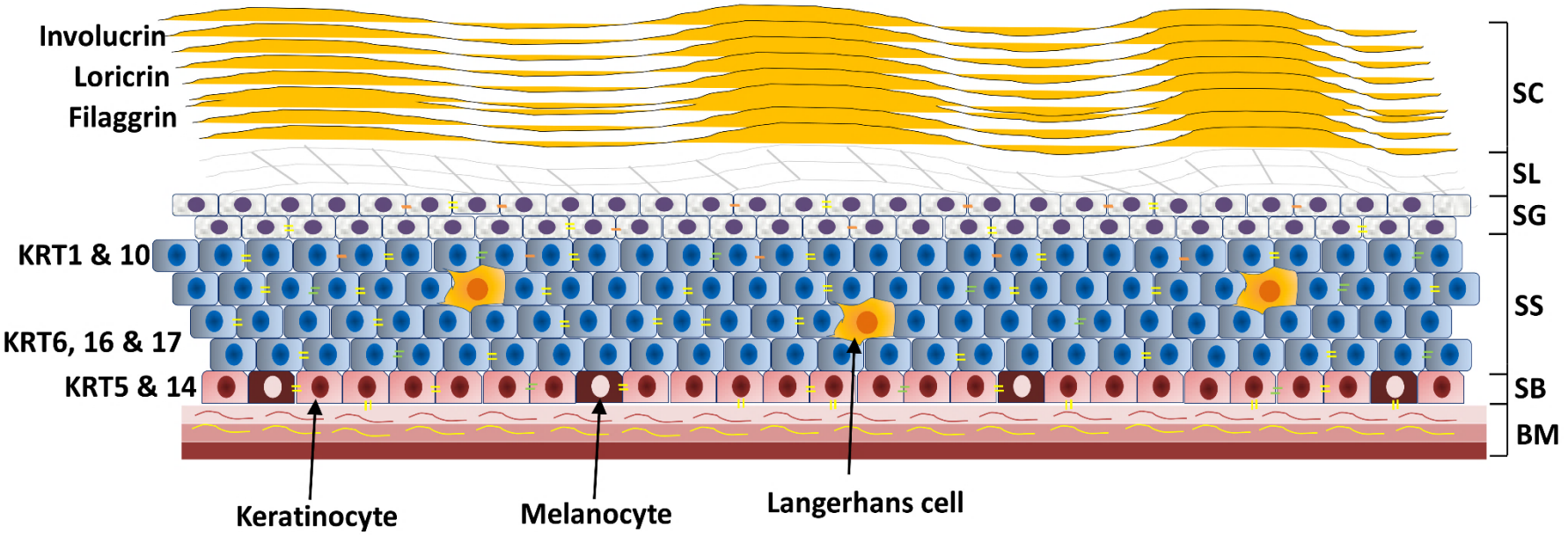

Figure 1.2. Epidermal structure and spatial localisation of keratin proteins. The epidermis is subcategorised into the following main layers: the *stratum corneum* (SC), the uppermost layer comprising of dead corneocytes; the *stratum granulosum* (SG), containing one or two layers of granular keratinocytes; the *stratum spinosum* (SS), spiny cells with limited mitosis and; the *stratum basale* (SB), a dynamic single layer of cells in contact with the basement membrane (BM). Langerhans cells are antigen-presenting cells found in the SS. The SB also contains pigment-producing melanocytes. Basal cells attach to the underlying BM via hemidesmosomes (vertical, yellow lines). Cell-cell attachment occurs via desmosomes (horizontal, yellow lines), tight junctions (horizontal, orange lines) and adherens junctions (horizontal, green lines; Otten et al., 2014). The *stratum lucidum* (SL) is only apparent in skin of the palmar, plantar and lip regions (Zirra, 1976). Spatial localisation of filament proteins is shown on the left, where keratins 5 and 14 (KRT5 & 14) are expressed in basal cells, and loricrin is found in the SC. *Illustration produced by the author (HNW).*

The columnar cells of the SB are connected to the BM through hemidesmosomes (Walko et al., 2015); while keratinocytes adhere to each other through major cell-cell adhesion molecules (e.g. desmosomes and adherens junctions, Smith & Fuchs, 1998). Desmosomal plaque proteins connect desmosomal cadherins to the keratinocyte cytoskeleton (Otten et al., 2014). Above the SB is the SS, a layer of spinous cells named because of their "spiny" appearance (Odland, 1960; Harding, 2004). Next is the SG, where keratinocytes appear angular and flattened, producing keratohyalin granules filled with cornified envelope components (Nemes & Steinert, 1999). Crucially, tight junctions, cell-cell junctions found only in the uppermost SS and the SG, provide a paracellular permeability barrier in the epidermis of mice (Furuse et al., 2002) and humans (reviewed in Niessen, 2007). The remaining 5% of non-keratinocyte epidermal cells includes melanocytes, merkel cells, and antigen-presenting Langerhans cells (LCs, Nestle et al., 2009).

1.1.2.1. Keratinocytes

As previously mentioned, the overall purpose of the keratinocyte is to transform from a highly proliferative cell to a non-proliferative, differentiated cell that becomes part of the non-viable, terminally differentiated SC (Eckert, 1989). Paracrine and endocrine signals from the dermis trigger a specific subset of stem cells within the SB to continually regenerate the epidermis (Lim et al., 2013; Walters & Roberts, 2002). Differentiating keratinocytes also produce, and respond to, chemical signals from neighbouring cells and the local microenvironmental niche (e.g. the native calcium gradient; Adams et al., 2015; Cumberbatch et al., 2003; Eckert, 1989). Indeed, recent findings demonstrate the importance of the phosphatases, DUSP6, PPTC7, PTPN1, PTPN13 and PPP3CA, in determining keratinocyte commitment to differentiation (Mishra et al., 2017), and the expression of these factors is regulated by topography (Zijl et al., 2019). Together, this sophisticated network of communication allows epidermal turnover to occur at a functional rate, thus maintaining skin barrier integrity.

During the process of terminal differentiation, keratinocytes produce a number of major structural proteins, such as KRT, loricrin, small proline-rich proteins (SPRRs) and filaggrin (Hardman et al., 1998). KRTs are the most comprehensive family of interfilament proteins, expressed solely in epithelia throughout the body (Bragulla & Homberger, 2009), and comprising around 30-40% of total keratinocyte protein

(Coulombe & Lee, 2012). KRTs are subcategorised into type I (acidic, e.g. KRT9-KRT19) or type II (basic, e.g. KRT1-KRT8; reviewed in Karantza, 2011) and their expression is entirely dependent on spatial localisation (Eckert, 1989; Lane & McLean, 2004; see **Figure 1.2**). KRTs form web-like structures within keratinocytes, attached via desmosomes (Proksch et al., 2008), therefore providing cell structural integrity (Homberg & Magin, 2014).

As well as forming the epidermis, keratinocytes perform important immunological barrier roles, acting as sentinels against bacterial invasion (Nestle et al., 2009). They express many pattern recognition receptors (e.g. toll-like receptors and nucleotide-binding oligomerization domain-like receptors) on their cell surface and within endosomes that respond to evolutionarily conserved microbial agents (pathogen-associated molecular patterns, PAMPs) and toxins (danger-associated molecular patterns, DAMPs; Nestle et al., 2009). Activation of PAMPS and DAMPS modulates inflammasome production and the secretion of pro-inflammatory cytokines, such as interleukin (IL)-1, IL-6 and tumour necrosis factor (TNF) alpha (Feldmeyer et al., 2007), and chemokines, such as CCL20 (Dieu-Nosjean et al., 2000). Initiation of the TH1-type immune response can then ensue, leading to LC and $CD8^{+ve}$ T cell recruitment (Roth et al., 2012). Keratinocytes also produce antimicrobial peptides (AMPs), such as β-defensins and cathelicidins, to combat pathogenic colonisation (Gilliet & Lande, 2008), and possess endogenous neurotransmitter receptors that modulate barrier permeability in response to fluctuating ion gradients (Baroni et al., 2012). Hence, due to their multimodal activities, it is not surprising that keratinocytes play a dominant role in the skin, and impairment in their functionality is implicated in a host of debilitating skin disorders (Harder et al., 1997).

1.1.3. The Basement Membrane

Keratinocytes of the SB sit atop the basal lamina, a layer of specialised fibrous proteins and connective tissue, collectively termed the BM (Martin, 1997). The BM attaches the epidermis to the dermis through anchoring filaments and hemidesmosomes that adhere to basal keratinocytes (Walko et al., 2015). Hemidesmosomes can be separated into two classes: type I in stratified and pseudostratified epithelia (Hieda et al., 1992), such as the skin, and; type II in simple epithelia, such as the intestine (Fontao et al., 1999). The BM also mediates cellular

cross talk (via molecular cross-talk selectivity) and allows LCs to migrate between the epidermis and the dermis (Clark, 1996; Noirey et al., 2002).

Throughout the body, BMs function to organise tissue infrastructure and modulate cell polarity (Wu et al., 2006). The skin BM can be divided into three layers, the *lamina lucida*, *lamina densa* and *sublamina densa*, and is composed of a network of extracellular matrix (ECM) proteins, including laminin 5, collagens IV and VII, and elastic fibres (Nishiyama et al., 2000; Varkey et al., 2014). Keratinocytes attach to the BM through integrins α6β4 and α3β1, which link to the actin cytoskeleton (Watt, 2002; Wu et al., 2006). Consequently, dominant mutations in BM complexes, such as KRT5 and KRT14, leads to loss of adhesion between the epidermis and dermis (acantholysis), and the development of blistering diseases (collectively termed epidermolysis bullosa, reviewed in Walko et al., 2015).

1.1.4. The Dermis

Underneath the BM is the dermis, a supportive, elastic layer of connective tissue derived from the embryonic mesoderm (Frienkel & Woodley, 2001). The dermis evolves throughout life, beginning in foetal development as a regenerative organ with no scarring (Leavitt et al., 2016). The dermis then becomes less cellular throughout childhood, and gradually thickens until the age of 50 (Haydont et al., 2019). Beyond this, skin structural changes occur because of intrinsic and extrinsic ageing (**Section 1.2; Figure 1.3**).

While the role of the epidermis is primarily as a skin barrier, the dermis acts as a supporting scaffold through its structural matrix of collagens and elastin fibres embedded in glucosamines, proteoglycans and glucosaminoglycans (GAGs; Quan & Fisher, 2015). Unlike the epidermis, which is constantly shed and replenished, the dermis is less proliferative and relies heavily on adaptation and damage repair mechanisms to maintain normal function (Tigges et al., 2014). The dermis houses an extensive web of blood vessels, contains far fewer cells than the epidermis, and comprises of a thin upper papillary layer, the *pars papillaris*, and a thick reticular layer, the *pars reticularis* (Smith et al., 1982; Eckert, 1989; Elias, 2007).

The superior surface of the dermis projects into the epidermis, forming dermal papillae with roles in sensation (through Meissner's Corpuscles, or touch receptors, García-Mesa et al., 2017). Epidermal rete ridges extend down into the papillary

dermis, which is characterised by an abundance of fibroblasts, immature matrix proteins (e.g. collagen type III), elastic proteins (e.g. fibrillin) and extensive vasculature (Sorrell & Caplan, 2004). On the other hand, the reticular dermis, which comprises around 80% of the total dermis, contains a much more extensive network of mature matrix proteins, mainly collagen type I and GAGs (Waller & Maibach, 2006). While dermal layer functional heterogeneity is a relatively new and fundamentally important discovery (reviewed in Rognoni & Watt, 2018), it is not surprising that fibroblasts of each dermal layer originate from two morphologically and physiologically distinct lineages, and contribute to skin homeostasis and regeneration in different ways (Driskell et al., 2013). In fact, many fibroblast niches exist. Fibroblasts isolated from the dermal papilla, for example, are spindle-shaped and proliferate rapidly, while fibroblasts of the reticular dermis are squarer, and play a major role in dermal contraction (Sorrell et al., 1996; Sorrell & Caplan 2004). Further differences between the two main fibroblast lineages include changes in matrix gene expression (Izumi et al., 1995), altered matrix metalloproteinases (MMPs) and tissue inhibitor of metalloproteinases (TIMPs), and differential growth factor (GF) expression (Janson et al., 2012; Mine et al., 2008).

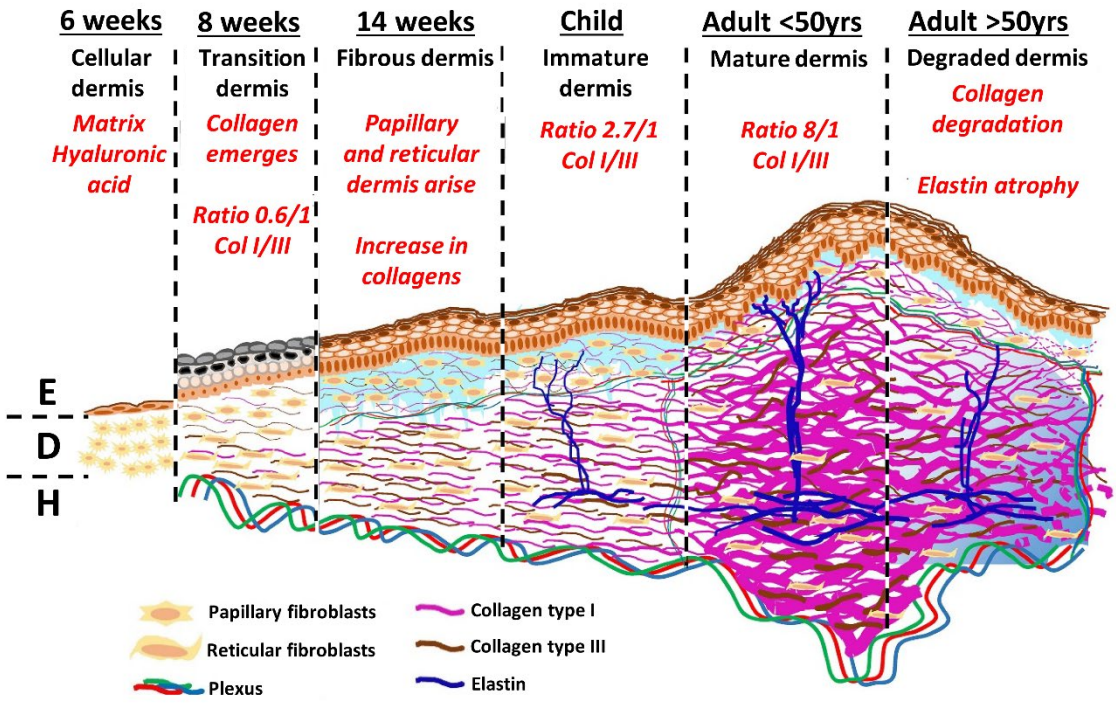

Figure 1.3. Structural components of dermal development. Throughout development the dermis thickens and becomes less cellular with reduced regenerative capacity. Beyond 50 years of age, the dermis degrades as a result of intrinsic and extrinsic skin ageing factors. E = epidermis. D= dermis. H = hypodermis. Col = collagen. *Figure adapted from Haydont et al. (2019).*

The blood supply to the dermis originates from the *cutaneous plexus*, which is found beneath the dermis but superior to the hypodermis. Capillaries extend out from the *cutaneous plexus* to supply oxygen to the reticular dermis, while the *subpapillary perplexus*, which demarcates the upper limit of the reticular dermis, feeds the capillaries of the dermal papillae (Sorrel & Caplan, 2004; Stücker et al., 2002). Although dominated by fibroblasts and matrix components, other cells within the dermis include mast cells, melanocytes, nevi (moles), and cells of haematopoietic origin, including resident dendritic cells and transient leukocytes (e.g. neutrophils and macrophages, Mφs; Gonzalez-Ramos et al., 1996; Lugović et al., 2001). The dermis also houses an array of skin appendages, such as sweat glands, sebaceous glands, hair follicles, nails and apocrine glands extending from the *lamina densa* to the subcutaneous adipose tissue (Baran et al., 2005). Like most tissues, the dermis is dynamic and is remodelled throughout life, yet many dermal ECM components are long lived, with half lives of 10 years or more (Humphrey et al., 2014).

1.1.4.1. Extracellular Matrix

As aforementioned, the major structural protein of the dermis is collagen I, accounting for up to 80% of dermal collagen, while the remainder is mostly collagen III. Elastin, the main elastic fibre type, comprises 2% of the dermis (Hwang et al., 2011), spans the entirety of the dermis, and is required to permit skin deformability and passive recoil (elasticity, Kielty & Grant, 2002). Indeed, the contrasting arrangement of collagens within the two dermal layers conveys their function. For example, the papillary dermis contains a thin meshwork of collagen fibrils to cope with mechanical stress, whereas the reticular dermis contains thicker, weaved collagen bundles to provide the skin with resilience (Frienkel & Woodley, 2001; Graham et al., 2010a; Smith et al., 1982).

Differential distribution of proteoglycans is also seen between the dermal layers, with a higher percentage of decorin found in the papillary dermis, and more versican located in the reticular dermis (Zimmermann et al., 1994). The principal dermal cell type, the mesenchymally-derived fibroblast, is primarily responsible for synthesis and degradation of fibrous (e.g. collagen) and non-fibrous (e.g. proteoglycans) matrix components (Frienkel & Woodley, 2001). Interestingly, during murine embryonic development, two key lineages of fibroblasts have emerged, the En1-lineage^{+ve} fibroblasts and the En1-lineage^{-ve} fibroblasts (Rinkevich et al., 2015).

Indeed, the fibrotic nature of fibroblasts has been shown to be limited by lineage, where only En1-lineage^{+ve} fibroblasts contribute to matrix deposition following dorsal murine skin injury (Rinkevich et al., 2015). Along with their major role in governing matrix remodelling, fibroblasts can also modulate the immune response through cytokine release (e.g. controlling Mφ polarisation, Donlin et al., 2014) and regulate hair cycle through growth factor production (Lin et al., 2015).

The ECM not only accommodates a rich scaffold of matrix proteins, but also contains a number of enzymes, cytokines and inhibitors. Here, the ECM provides a migratory scaffold and a network of communication (through cellular signalling, Frantz et al., 2010). Proteoglycans bind water to maintain skin hydration (Waller & Maibach, 2006), while the promiscuous adhesive proteins, fibronectins and laminins, control cell-to-matrix attachment through integrins (Mao & Schwarzbauer, 2005), modulate fibroblast differentiation (Torr et al., 2015), and influence fibroblast matrix gene expression (Hielscher & Gerecht, 2015).

Throughout life, the ECM of the dermis is remodelled, either through changes associated with ageing (e.g. UVR exposure), inflammatory disease, or during wound repair (Antonicelli et al., 2007). As part of the remodelling process, matrix proteins are degraded. This degradation is largely mediated by MMPs, a family of 25 zinc and calcium-dependent proteinases (Khasigov et al., 2001). Putative elastolytic MMPs include MMP-2, MMP-7, MMP-9, MMP-12, and MT1-MMP (Houghton et al., 2011), while MMP-1, MMP-2, MMP-8, MMP-9, MMP-13, MT1-MMP and MT3-MMP act as collagenases (Fields, 2013), described extensively in **Table 1.2**.

MMPs, expressed as pro-MMPs or zymogens, are activated through proteolytic cleavage of their N-terminal prodomains (Gao et al., 2015). MMP production can be endogenously inhibited via TIMPs (Gill & Parks, 2008), a family of proteins comprising four homologous members (TIMP1, TIMP2, TIMP3 and TIMP4; Brew et al., 2000). TIMP1 and TIMP3 are known to inhibit latent and pro-MMP-9, while TIMP2, TIMP3 and TIMP4 interact with pro-MMP-2 (Baker et al., 2002), thus preventing its activation. Knockout mouse studies further show the importance of TIMPs in ECM maintenance, where *Timp1*$^{-/-}$ mice have reduced myocardial fibrillary collagen (Lemaître et al., 2003) and exhibit increased fibrosis as a result of heightened inflammation (following liver injury, Wang et al., 2011).

Table 1.2. Classification of matrix metalloproteinases (MMPs). *

MMP	Substrate
MMP-1 (Collagenase-1)	Collagen I, II, III, VII, and X; aggrecan; serpins; alpha2-macroglobulin; kallikrein; chymase
MMP-8 (Collagenase-2)	Collagen I, II, and III; aggrecan; serpins; 2-MG
MMP-13 (Collagenase-3)	Collagen I, II, III, IV, IX, X, and XIV; gelatin; fibronectin; laminin; tenascin; aggrecan; fibrillin; serpins
MMP-2 (Gelatinase A)	Gelatin; collagen I, IV, V, VII, and X; laminin; aggrecan; fibronectin; tenascin
MMP-9 (Gelatinase B)	Gelatin; collagen I, III, IV, V and VII; aggrecan; elastin; fibrillin
MMP-3 (Stromelysin-1)	Collagen IV, V, IX, and X; fibronectin; elastin; gelatin; aggrecan; nidogen; fibrillin; E-cadherin
MMP-10 (Stromelysin-2)	Collagen IV, V, IX, and X; fibronectin; elastin; gelatin; laminin; aggrecan, nidogen; E-cadherin
MMP-11 (Stromelysin-3)	Serine protease inhibitors; 1-proteinase inhibitor
MMP-7 (Matrilysin)	Elastin; fibronectin; laminin; nidogen; collagen IV; tenascin; versican; 1-proteinase inhibitor; E-cadherin; tumor necrosis factor
MMP-12 (Metalloelastase)	Collagen IV; gelatin; fibronectin; laminin; vitronectin; elastin; fibrillin; 1-proteinase inhibitor; apolipoprotein A
MMP-14 (MT1-MMP)	Collagen I, II, and III; gelatin; fibronectin; laminin; vitronectin; aggrecan; tenascin; nidogen; perlecan; fibrillin; 1-proteinase inhibitor; alpha2-macroglobulin; fibrin
MMP-15 (MT2-MMP)	Fibronectin; laminin; aggrecan; tenascin; nidogen; perlecan
MMP-16 (MT3-MMP)	Collagen III; fibronectin; gelatin; casein; laminin; alpha2-macroglobulin
MMP-17 (MT4-MMP)	Fibrin; fibrinogen; tumor necrosis factor precursor
MMP-24 (MT5-MMP)	Progelatinase A
MMP-25 (MT6-MMP)	Gelatin
MMP-19 (RASI-1)	Gelatin; aggrecan; cartilage oligomeric matrix protein; collagen IV; laminin; nidogen; large tenascin
MMP-20 (Enamelysin)	Amelogenin; aggrecan; cartilage oligomeric matrix protein
MMP-28 (Epilysin)	Casein

**Adapted from Caley et al. (2015). The main classes are coloured as follows: Purple = Collagenases; Blue = Gelatinases; Green = Stromelysins; Orange = Membrane Type MMPs.*

Note: Other MMPs with unknown substrates include MMP-21, -22, -23, -26 and -27.

More recently, Gooyit et al. (2013) demonstrated (by mass spectrometry) that diabetic mouse wounds, which show delayed healing, have excessive Mmp-9. Further, inhibiting Mmp-9 in diabetic murine wounds led to accelerated wound repair, while inducing Mmp-8 in diabetic mice stimulated more rapid healing by increasing vascular endothelial GF (Vegf) and reducing Il-6 production (Gao et al., 2015). Therefore, it is clear that careful regulation of MMP and TIMP activity is vital in preventing excessive proteolysis and fibrosis (Arpino et al., 2015).

1.1.1.1.1. Collagen Synthesis

Collagens are a super family of ECM proteins, recognised by their right-handed triple helix formation and composed of homotrimer (e.g. collagen III) or heterotrimer (e.g. collagen I) α-chains. These α-chains contain Glycine-X-Y tripeptide repeats (reviewed in Fields, 2010), often Glycine-Proline-Y or Glycine-X-Hydroxylproline, where X and Y can be any amino acid other than glycine, proline or hydroxyproline (Shoulders & Raines, 2009). At this stage, the trimer (tropocollagen) molecules, must be post-translationally modified to form full collagen fibres (described below).

Unlike most protein modifications, which happen in the Golgi apparatus, initial assembly of collagen pre-pro-peptides (following translation from mRNA) occurs within the endoplasmic reticulum (ER; Malhotra & Erlmann, 2015). Within the ER, the tropocollagen signal peptide (an N-terminal) is dissolved, and the proline and lysine residues are hydrolysed by enzymes (prolyl hydroxylase and lysyl hydroxylase) assisted by multiple chaperones (e.g. HSP47; Nagata, 2003) to become hydroxyproline and hydroxylysine (Sricholpech et al., 2012). This stage cannot occur effectively without ascorbic acid, an essential cofactor of prolyl and lysyl hydroxylases (Peterkofsky & Udenfriend, 1965; Murad et al., 1981). Following the addition of sugar monomers to the hydroxyl groups (glycosylation), the propeptides twist into a triple helix of procollagen and are sent to the Golgi apparatus for export (Malhotra & Erlmann, 2015). Modification of this procollagen into tropocollagen occurs extracellularly, where collagen peptidases trim the loose ends of the procollagen, and lysyl oxidases (LOXs) mediate polymerisation of multiple tropocollagens (cross-linking) to form collagen fibrils (Herchenhan et al., 2015). The collagen fibrils, arranged in a head-to-tail fashion, can cross-link further to form a collagen fibre (Kadler et al., 1996; Kadler, 2017; **Figure 1.4**).

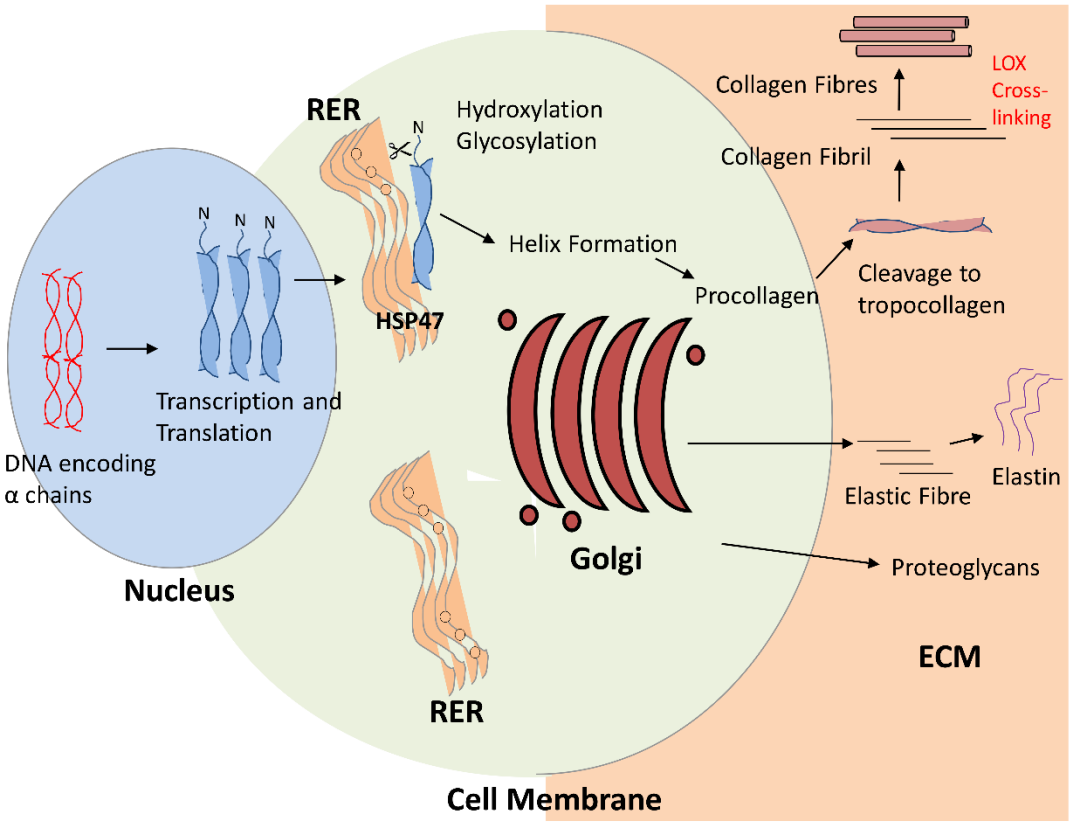

Figure 1.4. Matrix fibre synthesis. Within the nucleus, DNA (encoding collagen) is transcribed and translated to protein. The resultant tropocollagen is transported to the rough endoplasmic reticulum (RER) for post-translational modification. N-terminals of the peptides are cleaved and fibres are hydrolysed with the help of enzymes and chaperones (e.g. HSP47). The tripeptide is then transported to the Golgi apparatus (Golgi) for exocytosis as procollagen. In the extracellular matrix (ECM), collagen fibres are formed through cross-linking (by LOX enzymes). Other matrix fibres produced in a similar way are proteoglycans and elastin. *Figure produced by the author (HNW).*

Collagens are characterised by their suprastructure, where they fall into fibrillar, network, fibrillary-network, anchoring, transmembrane and multiplexin subtypes (reviewed in Birk & Bruckner, 2005). Along with the proper activity of chaperone proteins and enzymes, correct collagen formation is mediated through small leucine rich proteoglycans such as decorin and lumican (Hultgårdh-Nilsson et al., 2015). This is demonstrated *in vivo*, where decorin-null (Danielson et al., 1997) and lumican-null (Chakravarti et al., 1998) mouse skin has reduced tensile strength and abnormal collagen fibril assembly.

As already described, the ECM of the dermis comprises of mostly fibrillar collagens (80%), including collagen I, which dominates and is larger than collagen III (~20% of dermal ECM; Waller & Maibach, 2006). However, at least 12 other collagen types are apparent within the skin, including collagen type VI and collagen type VII. Collagen VI is a non-fibrillar collagen that performs a variety of crucial functions,

including aiding immune cell adherence and maintaining collagen I bundle assembly (Theocharadis et al., 2016). Collagen VII is necessary for epidermal-dermal adherence (Sakai et al., 1986), where defects in both *COL7A1* allelles can lead to recessive dystrophic epidermolysis bullosa (Fine et al., 2008). Indeed, injection of recombinant collagen VII into recessive dystrophic epidermolysis bullosa skin grafts on mice leads to restoration of normal skin function (e.g. dermal-epidermal adherence and collagen VII production; Woodley et al., 2013).

1.1.1.1.2. Elastin Production

As previously discussed, elastin is responsible for allowing reversible extension in lungs, blood vessels and the skin (Kielty & Grant, 2002). Elastic fibres typically maintain a half-life of approximately 70 years and undergo very little turnover, meaning that in humans, they are required to function throughout life. However, accumulation of damage occurs through mechanical stress, elastase activity, glucose-mediated cross-linking and accumulation of calcium and lipids. Thus, skin elastic recoil is reduced in a time-dependent fashion (Naylor et al., 2011; Scandolera et al., 2015). Elastin itself maintains no biological activity, but elastin-derived peptides have been associated with modulating free intracellular calcium levels (Faury et al., 1998), cell migration (Devy et al., 2010) and pro-inflammatory cytokine production (Baranek et al., 2007).

Although relatively stable, there are situations throughout life that require elastogenesis, such as development (Pierce et al., 1995) and wound repair (Zheng et al., 2006). Re-activation of elastin production is also observed in several diseases, including chronic obstructive pulmonary disease (Rangasamy et al., 2009). The soluble precursor responsible for elastin production is tropoelastin (60-70kDa in weight), which is post-translationally insolubilised and cross-linked (via LOXs) in the ECM to form amorphous elastin (Kagan & Li, 2003). Elastin production is guided upon a scaffold of elastic microfibrils (e.g. fibrillin; Kielty & Grant, 2002). A number of key dermal cytokines can also promote (e.g. transforming growth factor beta, TGF-β) or downregulate (e.g. basic fibroblast growth factor, bFGF) elastin production (reviewed in Sproul & Argraves, 2013).

1.1.5. The Hypodermis

The deepest skin layer is the ectodermally-derived hypodermis, sometimes referred to as the dermal white adipose tissue (DWAT) layer, which comprises of mesenchymally-derived adipose tissue (Sorrell & Caplan, 2004). The hypodermis protects underlying skeletal muscle, bone, tendons and joints by cushioning against physical trauma, while the adipose reserve also functions as thermal insulation and an energy store (Baroni et al., 2012). The depth of the hypodermis, like the other skin layers, depends entirely on its bodily location (Rittié & Fisher, 2015). In women, subcutaneous adipose tissue accounts for around 85-90% of total body fat regardless of body mass index, but in men, the ratio of white to visceral fat is much lower (Ross et al., 1993; reviewed in Fuente-Martín et al., 2013). DWAT adipocytes contain a large, semi-liquid, lipid-rich cytoplasm and are surrounded by a network of nerves and blood vessels (Matsumoto et al., 2007). Adipocytes produce a number of cytokines (adipokines) such as adiponectin and leptin. Therefore, the DWAT is not merely an energy reserve, but also acts as an important homeostatic endocrine organ (Hotamisligil, 2006). For example, imiquimod-induced dermatitis was exacerbated in mice with an adiponectin deficiency (Shibata et al., 2015), suggesting a unique role for adiponectin in modulating the skin immune response to irritation.

1.1.6. Other Integumentary Components

Skin appendages, such as nails, hairs, sebaceous glands and sweat glands, play important functions in maintaining skin homeostasis. Nails are highly keratinised structures found embedded into the epidermis, assisting in fine dexterity and providing physical protection from the environment (Saito et al., 2015). Hairs are anchored into the dermis or hypodermis, depending on the hair cycle stage, and provide an array of functions (Baran et al., 2005; reviewed in Paus & Cotsarelis, 1999). These include protecting the skin from mechanical insults, regulating body temperature, aiding courtship, allowing social communication and promoting wound repair (reviewed in Ito & Cotsarelis, 2008). External hair is a shaft of dead, keratinised cells, but inside the skin, it is part of the living follicle. Hair follicles consist of an outer root sheath containing multipotent stem cells that give rise to keratinocytes and melanocytes (Randall & Botchkareva, 2009), and an inner root sheath that provides support for the hair shaft (reviewed in Buffoli et al., 2014). Errector pilli muscles in the dermis also attach to the sheath of the hair follicle to

allow erection of the hair shaft, which insulates the skin from heat loss (Krause & Foitzik, 2006). Sebum-secreting sebaceous glands are connected to the hair follicle shaft to aid delivery of sebum to the SC, thus protecting the skin from friction, regulating TEWL, providing AMPs and antioxidants (e.g. vitamin E), and supplying pheromones for attraction (reviewed in Shi et al., 2015). The sweat glands, found deep in the dermis, are required for body cooling (Sato et al., 1989).

1.2. Ageing

Biological ageing is a rare occurrence in the animal kingdom, limited to only a handful of species. Human life expectancy has surpassed that of other animals (relative to body mass), due to both the advent of modern medicine and technological advances worldwide (Wilkinson & Hardman, 2017). Indeed, the ageing population has become a defining feature of the 21st century, where the number of people over the age of 65 is projected to grow from 524 million in 2010 to nearly 1.5 billion by 2050 (Al-Nuaimi et al., 2014). At the same time, the number of people living past the age of 80 is increasing, with progressively more becoming centenarians (Robine & Cubaynes, 2017). Unfortunately, increased longevity is associated with many chronologically-acquired physiological changes, resulting in a) heightened susceptibility to chronic, non-communicable disease and b) increased strain on healthcare providers' worldwide (Schieber & Chandel, 2014). Therefore, it is vital to understand the underlying mechanisms driving the ageing phenomenon to develop new biological strategies to tackle age-associated pathologies.

1.2.1. Mechanisms of Intrinsic Ageing

Ageing is a somatic process characterised by a gradual loss of function, reduced metabolism and increased susceptibility to stress (Tigges et al., 2014). Over many years, biological, demographic and epidemiological studies have attempted to address the underlying causes of ageing, with numerous proposed theories. Broadly speaking, these hypotheses can be split into two principal categories: a) damage theories (accumulation of cell and tissue damage) and; b) programmed longevity theories (intrinsic changes in genetic, endocrine and immunological function; reviewed in Libertini et al., 2015). Although discussed as separate entities, ageing is a multifactorial and complex process, involving a combination of mechanisms that often include senescence, oxidative stress and endocrine components.

1.2.1.1. Senescence

One of the most discussed cellular ageing mechanisms is senescence, described as the cessation of mitosis and critical shortening of telomeres (Campisi, 2011; Debacq-Chainiaux et al., 2016; Toutfaire et al., 2017). A number of factors, including stress and oncogene activation, can induce cellular senescence (Debacq-Chainiaux et al., 2016). Although unable to divide, senescent cells remain metabolically active and communicate to their cellular environments by secreting a range of cytokines, chemokines, proteases and GFs, collectively known as a senescence-associated secretory phenotype (SASP; Tchkonia et al., 2013). The SASP contributes to age-related diseases, such as cancer (Thangavel et al., 2011) and atherosclerosis (Zhou et al., 2006). Further, depletion of senescent cells can reduce age-associated pathology in murine progeroid models (Baker et al., 2011). A more detailed description of senescence, and an exploration into its role in normal and pathological wound repair, is provided in **Chapter 3**.

1.2.1.2. Oxidative Stress

The oxidative stress, or free radical theory, describes ageing as a consequence of sustained reactive oxygen species (ROS) damage. Combined environmental onslaught (e.g. UVR) and prolonged cellular metabolism (aerobic respiration) lead to increased ROS production (Bottai et al., 2013). ROS, including hydrogen peroxide (H_2O_2), superoxide and hydroxyl (OH-) free radicals, are highly unstable due to the presence of an unpaired electron. This excessive oxidation can cause DNA damage, proteolysis and lipid peroxidation through multiple strategies, such as cross-linking of nucleic acids and proteins, or the formation of advanced glycation end-products (AGEs; Balaban et al., 2005). ROS can also directly influence MMP activation (Haorah et al., 2007), or mediate MMP production through activator protein-1 transcription (Pimienta & Pascual, 2007), thus promoting proteolysis through multiple mechanisms. Collectively, these effects can be detrimental to normal cellular behaviour and ultimately lead to apoptosis and tissue degradation.

The body has a number of innate antioxidant defences to counteract oxidant damage. Antioxidants can include enzymes (catalase and peroxidase, Zhu et al., 2005), small electron donor molecules (ascorbic acid, tocopherols and nicotinamide adenine dinucleotide, reviewed in Zhang et al., 2015c) and superoxide dismutases (SODs). SODs are of particular interest, as they require redox active transition

metals to maintain their function. The three main mammalian SODs all contain a metal cofactor: SOD1, or CuZnSOD; SOD2, or MnSOD and; SOD3, or ecSOD (Fukai & Ushio-Fukai, 2011). Of note, estrogen retains potent antioxidant activity, reversing oxidative damage in ovariectomised rats (Abbas & Elsamanoudy, 2011), directly preventing ROS production and apoptosis in isolated rat mitochondria (Borrás et al., 2010), and preventing H_2O_2-mediated senescence in human umbilical vein endothelial cells (Ruan et al., 2014).

1.2.1.3. Endocrine Changes

Circulating levels of multiple hormones are altered throughout life in both genders, and these significant endocrine changes are implicated in both causing and exacerbating age-associated pathology (see Emmerson & Hardman, 2012 for a detailed review). Extended lifespan, combined with a stable age of menopausal onset, means that women are spending longer proportions of their lives in an estrogen-deficient post-menses state (Koebele & Bimonte-Nelson, 2016). Post-menopause, the primary source of estrogens originates from circulating adrenally derived 3β-hydroxy-5-androstene-17-one (Labrie et al., 2001). At the same time, levels of dihydrotestosterone remain constant in both sexes, while production of the cortisol precursor, 11β-hydroxysteroid dehydrogenase, increases with age (discussed in Emmerson & Hardman, 2012). The drop in circulating 17β-estradiol following the menopause leads to the rapid onset of infertility (Sowers et al., 2008), and in the long term, causes osteoporosis, cardiovascular disease (Clegg et al., 2017) and skin ageing (reviewed in Raine-Fenning et al., 2003). Intriguingly, menopausal decline in serum 17β-estradiol has also been linked to other mechanisms of ageing, including senescence and oxidative stress (Lopez-Otin et al., 2013), thus suggesting it to be a highly important age-regulating hormone.

1.2.2. Skin Ageing

Unlike other bodily organs, the skin is in direct contact with the external environment and is therefore subjected to extensive extrinsic ageing. As a result, skin ageing is characterised by a combination of intrinsic and environmental factors that exacerbate age-related structural and functional decline (Gosain & DiPietro, 2004; **Table 1.3** and **Figure 1.5**). Structurally, skin ageing leads to epidermal and dermal thinning, loss of dermal elasticity and collagen, increased pigmentation, and susceptibility to dermatoses, such as dryness (xerosis), wrinkling and infection

(Blume-Peytavi et al., 2016; Wilkinson & Hardman, 2017). Intrinsic ageing reduces cellular proliferation and blood flow, especially in the upper dermis (Chung et al., 2002; Gunin et al., 2014). Increased degradation of fibrous matrix (e.g. elastin; Robert et al., 1988), collagenous matrix (El-Domyati et al., 2002) and water-rich GAGs (Ghersetich et al., 1994) is also found, resulting in skin thinning and fine lines.

By contrast, extrinsic "photoageing" is accompanied by melanocyte accretion and redistribution, LC reduction and the accumulation of non-functional elastin (dermal elastosis) and elastic proteins (e.g. fibrillin-1; Toutefaire et al., 2017). Photoageing is responsible for the deep, leathery appearance of aged skin, a consequence of severe matrix changes and loss of anchorage (collagen VII) between the epidermis and dermis (Craven et al., 1997). Photo-exposed aged skin also appears thicker than photo-protected aged skin (El-Domyati et al., 2002). As UVB is absorbed by the epidermis (D'Orazio et al., 2013), UVA, which penetrates deeper into the skin, is primarily responsible for photoageing (Sheratt, 2009). Even in minimally UVR-exposed skin, early photo-damage effects are still observed, such as loss of fibrillin-1 (Langton et al., 2010). Toxic polycylic aromatic hydrocarbons from cigarette smoke and industrial processes can also contribute to exogenous skin ageing (Schroeder et al., 2006).

Table 1.3. Key structural similarities and differences between intrinsically aged and extrinsically aged skin. *

Feature	Intrinsically Aged	Extrinsically Aged
Epidermis	Thinned	Thickened
Dermis	Thinned	Thickened
Blood Flow	Reduced	Reduced
Elastin	Degraded	Accumulated
Epidermal-Dermal Junction	Normal	Loss of Anchorage
Inflammatory Cells	Increased	Increased

**As compared to young, healthy skin. Modified from Farage et al. (2008).*

Many conserved molecular changes govern the physiological effects of skin ageing. For example, UVR- and cellular metabolism-mediated ROS generation causes tyrosine phosphatase production, phosphorylation of tyrosine kinase receptors, and the activation of downstream signalling pathways (e.g. MAPK) and transcription factors (e.g. activator protein-1). Of interest, activator protein-1 is known to directly

suppress pro-collagen I expression and induce MMPs -1, -3 and -9 (Rittié & Fisher, 2015), therefore promoting matrix degradation. Senescent cells also accumulate throughout the dermis and epidermis in aged human skin, contributing to reduced skin function (Lupa et al., 2015; Toutefaire et al., 2017).

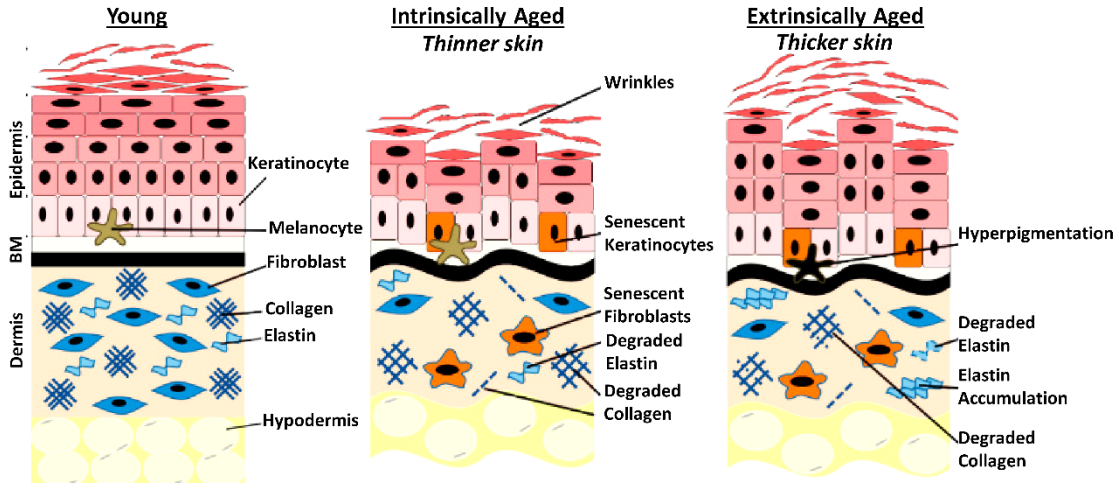

Figure 1.5. Key structural differences between young, intrinsically aged and extrinsically aged skin. Intrinsic ageing is characterised by thinner epidermis and dermis, and degradation of extracellular matrix (ECM) proteins. Extrinsically aged skin is thickened with increased pigmentation. Extrinsically aged skin also shows degradation of ECM, but accumulation of elastin. Both types of skin ageing lead to wrinkles, deformation of the basement membrane (BM) and senescent cell accumulation. *Adapted from Orioli & Dellambra (2018).*

As discussed above, the menopause is a key factor in age-related functional decline, and many common ageing skin features are associated with endocrine changes. Ageing and UVB exposure both cause excessive accumulation of 11β-hydroxysteroid dehydrogenase, which increases skin thinning and TEWL (Schoepe et al., 2006; Tiganescu et al., 2013; Tiganescu et al., 2015). By contrast, wrinkling, skin drying and loss of collagen is attenuated with estrogen treatment (e.g. topical 17β-estradiol; reviewed in Jackson et al., 2011; Thornton, 2013). Indeed, within five years of the menopause, up to 30% of collagens III and I are lost. In women, skin ageing correlates more definitively with estrogen deficiency than chronological advancement (Brincat et al., 1987).

Estrogen can be biosynthesised within the skin (Labrie, 2015), where resident skin cells are known to manufacture estrogens from 3β-hydroxy-5-androstene-17-one and cholesterol (Tiganescu et al., 2011). Regulation of cutaneous estrogen is therefore dependent on localised estrogen-metabolising enzymes, such as

aromatase, important for catalysing the conversion of androgens to estrogens, and 17β-hydroxysteroid dehydrogenases 1 (17βHSD1) and 2 (17βHSD2) for the conversion of estrone to 17β-estradiol (Labrie et al., 2001). It is therefore not surprising that estrogen receptor signalling occurs throughout the skin via two main nuclear hormone receptors, ERα and ERβ. Estrogen receptor expression and localisation is crucial for maintaining normal skin function, where ERβ signalling has emerged as a key opponent of skin ageing (Jackson et al., 2011). For example, Chang et al. (2010) demonstrated that treatment with ERβ-selective agonists (WAY-200070 and ERB-041) significantly dampened pro-inflammatory marker expression (e.g. MMP-1 and IL-6) in primary keratinocytes and fibroblasts, whereas ERα-selective agonist treatment had no effect. In the same study, topical application with the ERβ agonist, ERB-041, reduced wrinkling in UV exposed murine skin, thus protecting against photoageing.

1.3. Diabetes

Diabetes Mellitus (DM) is a chronic condition characterised by hyperglycaemia and a number of secondary complications, including ischemia and neuropathy (Jeffcoate & van Houtum, 2004). The two most common forms of DM are insulin-dependent type 1 DM (T1DM), caused by autoimmune destruction of β cells (Atkinson, 2014), and insulin non-dependent type II DM (T2DM). T2DM accounts for 90-95% of DM cases and is associated with insulin resistance and obesity, affecting around 350 million people worldwide (Lam & LeRoith, 2012). Despite technological and medical advances, it is expected that by 2030 DM, particularly T2DM, will affect almost half a billion people across the world (Graz et al., 2018; Lam & LeRoith, 2012). Indeed, T2DM has a large socio-economic impact. A patient over the age of 65 with T2DM on average costs healthcare providers twice as much as a patient in the same age group without T2DM (O'Shea et al., 2013). In 2012 alone, T2DM cost the National Health Service £11.7 billion, while T1DM cost £1.8 billion (Kanavos et al., 2012).

1.3.1. Detrimental Effects of Diabetes on Skin

Up to a third of patients with T2DM experience some form of skin complication, most severely chronic ulcers (Mendes et al., 2017; Quondamatteo, 2014). Unlike aged skin, DM skin structure and function has been greatly understudied, with diabetic mouse models widely used for this purpose. The pancreatic β cell-toxic glucose

analogs, streptozocin (STZ), or alloxan (AX), are used experimentally to induce T1DM (reviewed in Radenković et al., 2016). STZ and AX, although exerting their effects in a slightly different manner (Lenzen, 2008), ultimately cause pancreatic β cell destruction. Thus, animals treated with STZ or AX develop hyperglycaemia and insulopaenia (Radenković et al., 2016). Most researchers prefer using STZ over AX, as AX causes higher toxicity and a more complicated DM phenotype (Quondamatteo, 2014). A commonly used genetically modified T1DM model is the non-obese diabetic mouse. This mouse exhibits spontaneous immune destruction of pancreatic β cells, and therefore incorporates immune aspects of T1DM (Jayaraman et al., 2013). The most common T2DM model is the *db/db* mouse, which possesses a leptin receptor-based mutation (**Section 2.1**). Mice homozygous for this mutation develop insulin-resistance by two weeks of age, become obese by four weeks of age, and are hyperglycaemic by eight weeks of age (King, 2012; Quondamatteo, 2014).

Although limited, a number of skin changes have been reported with DM. For example, in DM patients, higher fasting blood glucose levels correlated with increased xerosis (Sakai et al., 2005). In a rodent model of T2DM, hyperglycaemic rats showed increased SC dryness and reduced SC integrity, which was not connected to any change in basal TEWL or filaggrin expression (Park et al., 2011). However, the authors did observe reduced epidermal lipid synthesis, reduced AMP production and impaired restoration of the SC following tape stripping in the T2DM rats, indicating compromised skin barrier. Indeed, DM patients display increased susceptibility to infections (Calvet et al., 2001; Joshi et al., 1999), and exhibit skin microbiota dysbiosis, with greater quantities of the opportunistic pathogen, *Staphylococcus aureus*, present in plantar regions (Redel et al., 2013).

Intriguingly, 1 in 200 diabetic patients experience a condition known as bullosis diabeticorum, or diabetic bullae, where spontaneous skin blistering occurs (Behm et al., 2012). This is mirrored in *db/db* murine skin, where reduced BM collagen IV expression (Rodgers et al., 2006) and reduced E-cadherin (cell-cell adhesion; Taylor et al., 2011) are observed, suggesting reduced epidermal structural stability. Thickened BMs are also apparent (diabetic patients, To et al., 2013; Zhang et al., 2009b), while the epidermis is thinner (in *db/db* mice and STZ-induced mice and rats, Sakai et al., 2003). Other epidermal features of DM include reduced

keratinocyte proliferation and abnormal basal Krt1 expression (in *db/db* mice, Taylor et al., 2011).

Diabetic skin is less mechanically stable, with lower elasticity and reduced mean breaking strength (in *db/db* mice and human diabetic skin; Argyropoulos et al., 2016; Bermudaz et al., 2011). Diabetic ECM is also characterised by high levels of collagen cross-linking, demonstrated by increased LOX at the mRNA and protein level (Argyropoulos et al., 2016), and increased production of AGEs (Bermudaz et al., 2011). These features may contribute to poor dermal integrity and delayed wound resolution, as blockage of the AGE receptor restores normal healing in *db/db* mice (Goova et al., 2001). Interestingly, investigations of skin proteolysis have shown contrasting findings, where reduced Mmp-9, Mmp-2, Timp-1, collagen I and collagen III expression were observed in *db/db* murine skin by Bermudaz et al. (2011), but increased MMP-1 and MMP-2 were shown in human (Argyropoulos et al., 2016) and murine (Ye et al., 2013) diabetic skin in other studies. Overall, it is clear that DM and ageing both greatly influence skin structure and function, which in turn, significantly impacts skin restoration ability following damage.

1.4. Wound Repair

The skin is the body's primary defence against the extrinsic environment, and thus it must repair any breaches to its barrier in a quick and efficient manner. Indeed, it is a dynamic and highly effective regenerative organ, progressing through a temporal series of complex cellular processes to return to a normal state – both architecturally and physiologically – following damage (Broughton et al., 2006; Stadelmann et al., 1998). The Latin terms *tumor*, *rubor*, *calor* and *dolor* (swelling, redness, heat and pain) were coined almost two thousand years ago to first describe the human wound healing response (Pratsinis et al., 2018). Nowadays, wound healing is classically simplified into four phases: haemostasis, inflammation, proliferation and matrix remodelling (**Figure 1.6** and **Figure 1.7**).

1.4.1. Phase 1 – Coagulation and Haemostasis

The first stage of wound repair is to trigger clot formation, thereby preventing exsanguination caused by vascular damage (Velnar et al., 2009). Platelets, first discovered in the 1880s (Coller, 2011), are now widely known to be key contributors to haemostasis and thrombosis (Golebiewska & Poole, 2015). Platelets

are activated through contact with blood vessel proteins, such as fibronectin and fibrinogen, and adhere to the vessel wall forming an insoluble clot of fibrin, fibronectin, vitronectin and thrombospondin (Velnar et al., 2009; Li et al., 2007). Endothelial cells from the damaged vasculature migrate into the wound bed, depositing a temporary scaffold of fibrin. The fibrin scaffold triggers platelets to release cytokines and GFs (e.g. platelet-derived GF, PDGF), which attract recruited inflammatory cells and resident skin cells to the site of injury (Witte & Barbul, 1997; Haertel et al., 2014). As the most abundant cell type during early repair, it is also not surprising that platelets play a role in preventing bacterial infection. For example, Tang et al. (2002) demonstrated that platelets produce a number of AMPs (e.g. PF-4 and CTAP-3) that exhibit direct bactericidal activity (reviewed in Golebiewska & Poole, 2015). Once the clot is formed, a number of factors are released to cause cessation of the coagulation process, thus preventing excessive thrombosis. Prostacyclin inhibits platelet aggregation, antithrombin III inhibits thrombin, and activated protein C degrades coagulation factors V and VII (Mann, 2003).

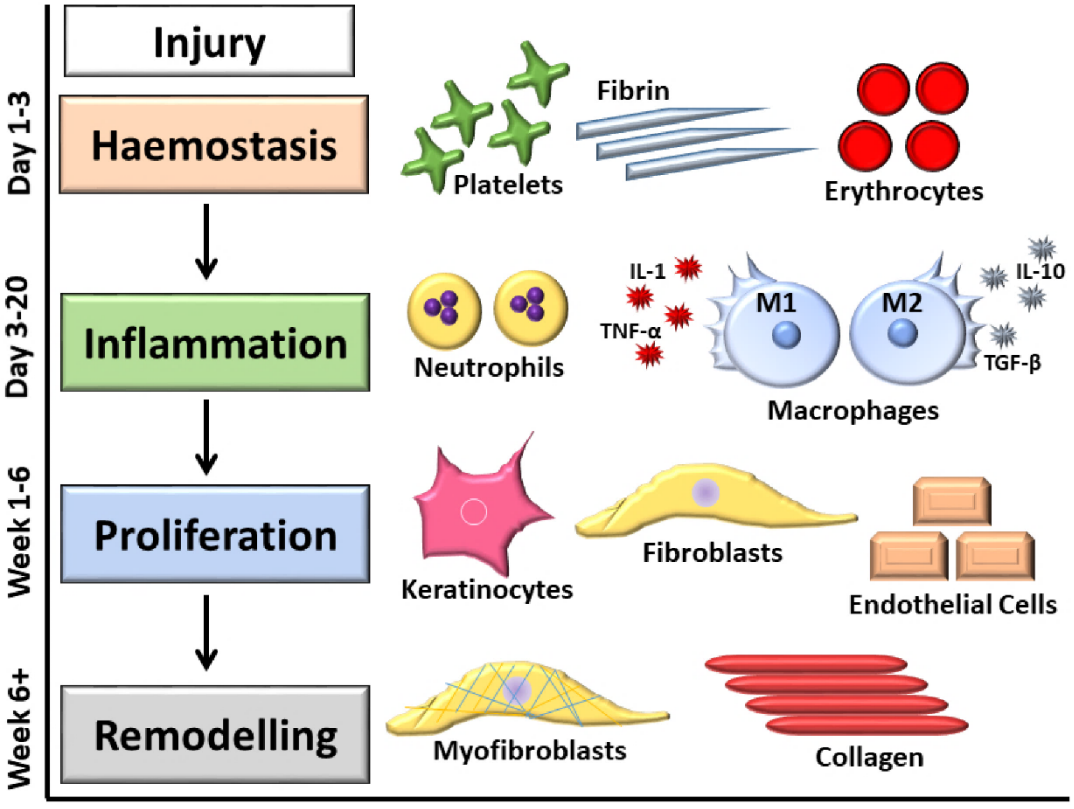

Figure 1.6. The four main stages of wound repair and when they occur in human healing. To the right are the main cellular and structural components of each stage, including polarised macrophages and their corresponding cytokines. *Figure from Wilkinson & Hardman (2017).*

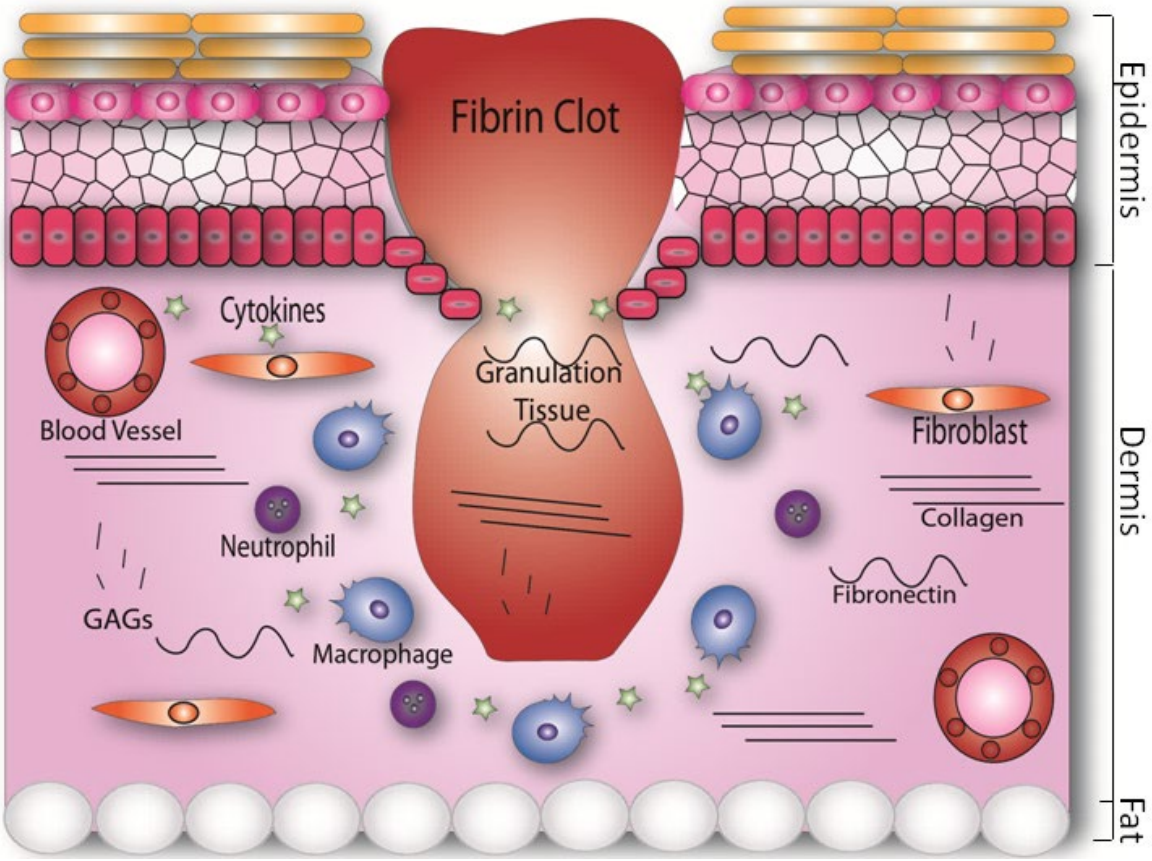

Figure 1.7. Structural schematic of an acute wound in early healing. Haemostasis is rapidly followed by immune cell infiltration (neutrophils and macrophages) and the formation of the granulation tissue (GT). Epidermal basal keratinocytes at the wound edges (dark pink) migrate to close the wound. Fibroblasts deposit structural proteins, such as glycosaminoglycans (GAGs), fibronectin and collagen to replace the GT. Later, keratinocytes undergo terminal differentiation to reform the epidermis, while fibroblasts differentiate into myofibroblasts for wound contraction. Inflammation abates and the wound remodels. *Illustration generated by the author (HNW).*

1.4.2. Phase 2 – Inflammation

The innate inflammatory response has crucially evolved to prevent pathogenic wound invasion. Upon damage, resident immune cells, such as mast cells, LCs, γδ T cells and Mφs, release a number of pro-inflammatory cytokines and chemokines that attract circulating leukocytes to the site of injury (reviewed in Martin & Leibovich, 2005). Pro-inflammatory molecules also stimulate increased endothelial expression of cell adhesion molecules, such as selectins, facilitating neutrophil and monocyte adhesion and diapedesis (reviewed in Muller, 2003). Neutrophils arrive at the wound site first, initially leaking into the wound from damaged vessels. They are also enticed by pro-inflammatory chemoattractants such as IL-1, TNF-α, TGF-β and bacterial endotoxins (e.g. lipopolysaccharides, LPS; Witte & Barbul, 1997). In response to pro-inflammatory signals, neutrophils, and other cells at the wound site,

release their own pro-inflammatory cytokines via signalling pathways such as the nuclear factor kappa-light-chain-enhancer of activated B cells (NF-κβ) cascade (Li et al., 2001). Neutrophils remove necrotic tissue and bacteria via phagocytosis and the release of ROS, AMPs, eicosanoids and proteolytic enzymes (Segel et al., 2011; Young & McNaught, 2011). Neutrophils also trap and kill pathogens in an extruded web of DNA coated with AMPs and cytotoxic histones (Brinkman et al., 2004).

Unless a wound is infected, neutrophils are cleared within 72 hours of injury onset. Most neutrophils are extruded from the wound site as they adhere to the fibrin scab, while any remaining neutrophils are removed by Mφ efferocytosis (Martin & Leibovich, 2005). Mφs are master effector cells in wound repair, due to their versatile functions and high plasticity. Indeed, Cd11b-specific Mφ deletion leads to delayed wound healing and increased inflammation (Mirza et al., 2009). In wounds, Mφs reach peak infiltration 72 hours after injury in mice and 7-days post-injury in humans (Baum & Arpey, 2005). Like neutrophils, Mφs engulf necrotic cellular debris and pathogenic material through evolutionarily conserved receptors, but also exhibit differential behaviours and morphological changes in response to cytokine stimulation (**Figure 1.8**; Mantovani et al., 2005).

Traditionally, two main subsets of Mφs are apparent in wounds: classically activated (M1-stimulated) Mφs and alternatively activated (M2-stimulated) Mφs. However, the M2 repertoire has now expanded and is seen as a spectrum of phenotypes governed by tissue status and environmental stimulus (Mosser & Edwards, 2008; Snyder et al., 2016). M1 Mφs, induced by pro-inflammatory stimuli such as LPS and interferon gamma (IFN-γ), promote inflammation by releasing ROS and inflammatory cytokines (e.g. IL-1, IL-6 and TNF-α). M1-stimulated Mφs phagocytose apoptotic neutrophils, replacing them as the main inflammatory mediator (Li et al., 2007). Later stages of inflammation are characterised by a switch to alternative activation, which can be stimulated by efferocytosis (Korns et al., 2011). Generally, M2-stimulated Mφs express anti-inflammatory cytokines (IL-4, IL-10, IL-13 and TGF-β1; Barrientos et al., 2008; Eming et al., 2007; Witte & Barbul, 1997) and produce arginase, a key player in effective wound repair (Witte & Barbul, 2003, Campbell et al 2013). M2-stimulated Mφs also release a myriad of GFs to mediate re-epithelialisation and fibroplasia (Li et al., 2007). More recently, Mφs have been shown to play a crucial role in angiogenic remodelling in mice and fish (Gurevich et

al., 2018). Together, these mechanisms promote scavenging of debris, bacteria and pro-inflammatory cells, and stimulate reparative processes to allow wound resolution (Mantovani et al., 2005).

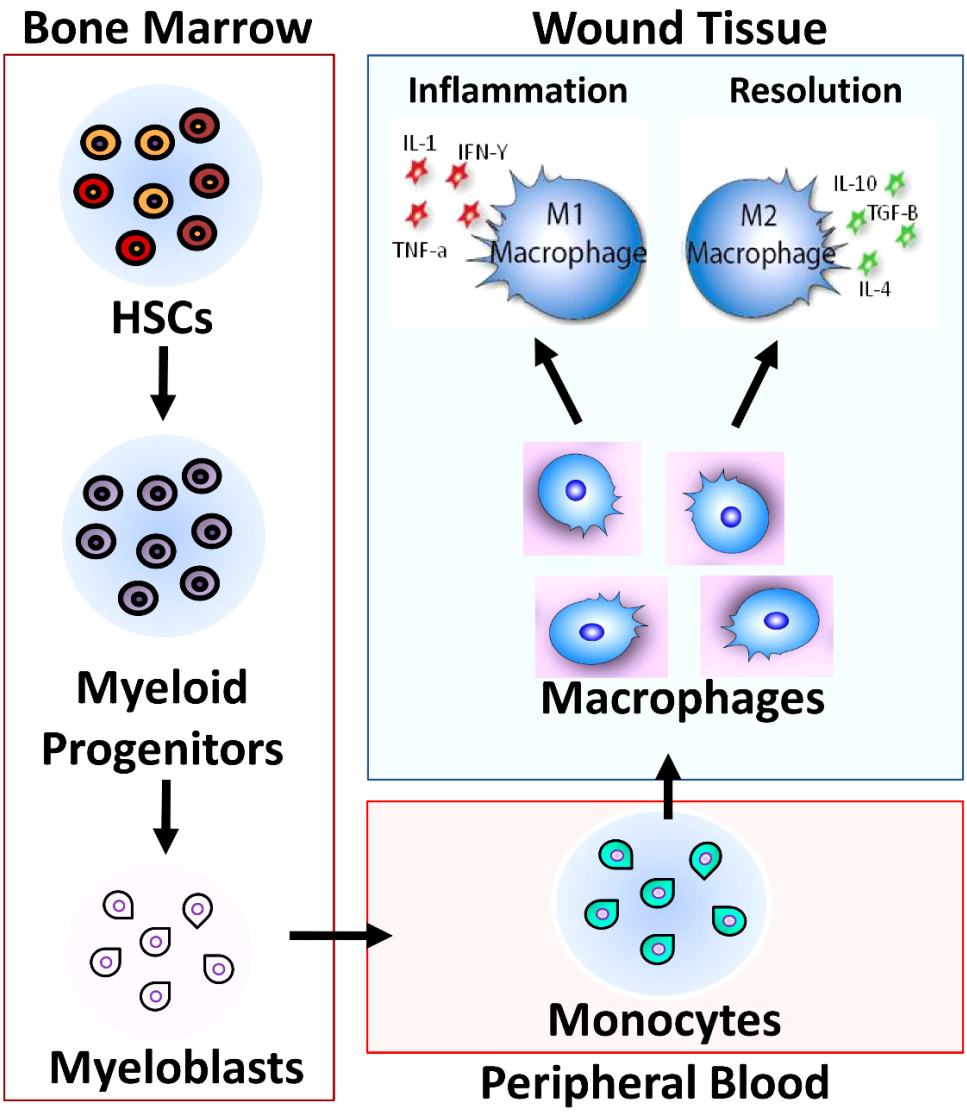

Figure 1.8. Macrophage differentiation and polarisation. Multipotential haematopoietic stem cells (HSCs) of the bone marrow give rise to myeloid precursors that differentiate into myeloblasts. Myeloblasts then become monocytes that enter the blood. Monocytes are recruited to sites of inflammation and differentiate into macrophages (Mφs). In wound tissue, both recruited and resident Mφs are polarised to M1 (pro-inflammatory) or M2 (anti-inflammatory) states via cytokine and chemokine signalling. *Illustration produced by the author (HNW).*

1.4.3. Phase 3 – Proliferation

As early as 12 hours post-injury, keratinocyte activation is triggered by H_2O_2 and calcium release, mechanical and electrical changes, exposure to pathogens, GFs and cytokines (Shaw & Martin, 2016). Keratinocytes at the wound edge thus become invasive to migrate across the wound and reform the epidermis, a process termed

re-epithelialisation (Bleaken et al., 2016; Young & McNaught, 2011). The wound edge keratinocytes lay down BM as they migrate (Shaw & Martin, 2016). Moreover, keratinocytes are recruited not only from the intact epidermis at the wound edges, but also from nearby hair follicles (Ito et al., 2005). Although the bulge region has long been deemed a niche for keratinocyte stem cells (Taylor et al., 2000), understanding of its role in wound healing has expanded considerably. Indeed, there is high plasticity between the hair follicle niches to allow hair regrowth (Rompolas et al., 2013), and only specific stem cells are recruited to wound repair. For example, $Krt15^{+ve}$ (Garcin et al., 2016) and $Krt19^{+ve}$ (Driskell et al., 2015) bulge stem cells are dispensible for re-epithelialisation, but Lgr5- and Lgr6-expressing cells from the bulge region and interfollicular epidermis show important adaptations for wound healing (Joost et al., 2018).

Activated keratinocytes undergo epithelial-mesenchymal transition, where they develop a migratory phenotype (e.g. flattening, elongation, development of lamellipodia projections, and modification of cell adhesion junctions; Li et al., 2007). Keratinocytes negotiate through debris and necrotic tissue of the wound bed through their interactions with structural proteins of the preliminary matrix via integrin receptors (Santoro & Gaudino, 2005). MMPs, particularly MMP-1 and MMP-9, are vital for keratinocyte migration as they aid in integrin receptor dissociation (Li et al., 2007). The production of other proteases, such as plasmin, further facilitates keratinocyte migration by degrading the initial wound bed (Martin, 1997). When keratinocytes from each wound edge meet, they have established a single epithelial layer termed the neoepidermis. At this point, migration terminates, keratinocytes adhere to the underlying matrix, and undergo terminal differentiation to regenerate the full epidermis (Baum & Arpey, 2005).

Fibroblast proliferation and migration into the granulation tissue is triggered by signals from endothelial cells and immune cells in early repair (Martin, 1997), and paracrine factors from migrating mesenchymal stem cells (Smith et al., 2010). Within the wound, resident and mesenchymal-derived fibroblasts respond to a milieu of signalling molecules (e.g. TGF-β1, PDGF, and other GFs) to either: (a) become pro-fibrotic, laying down ECM proteins or; (b) differentiate into myofibroblasts for wound contraction (Martin, 1997; Li et al., 2007). Myofibroblasts are characterised by an abundance of α-smooth muscle actin (α-SMA) and other

microfilament bundle components (e.g. γ-SMA, myosin and desmin) associated with generating strong contractile forces and focal adhesions (Li et al., 2007; Martin, 1997; Werner et al., 2007). Interestingly, knockout of the gene encoding α-SMA, *Acta2*, did not delay wound healing or alter fibroblast contraction in mice (Tomasek et al., 2013), thus suggesting compensation by other microfilaments. Myofibroblast contraction is facilitated by pseudopodial extensions, which allow cytoplasmic actin to bind to fibronectin in the matrix scaffold (Li et al., 2007). As myofibroblasts adhere to one another via desmosomes, binding to matrix fibrils causes overall wound contraction (Stadelmann et al., 1998).

Angiogenesis, the formation of new blood vessels, is triggered by a hypoxic environment where chemotactic factors such as VEGF, epidermal GF (EGF), TGF-α and angiogenin trigger: (1) degradation of the basal lamina of progenitor blood vessels to allow vascular sprouting; (2) chemotaxis; (3) proliferation and; (4) remodelling and differentiation (Velnar et al., 2009). The presence of the fibrin matrix also promotes angiogenesis by causing phenotypic changes in endothelial cells that influences their migration (Kalebic et al., 1983). The resulting endothelial cell capillary sprouts enter the wound bed and form a new network of capillaries. This capillary network provides essential nutrients to the granulation tissue - a new ECM that replaces the initial wound bed clot (Baum & Arpey, 2005).

1.4.4. Phase 4 - Matrix Remodelling

Matrix remodelling spans the entire tissue repair process, beginning with the initial deposition of a fibrin clot and ending several years later with the formation of a mature, type I collagen-rich scar (Li et al., 2007). Fibroblasts are responsible for: a) replacing the initial fibrin clot with hyaluronan, fibronectin and proteoglycans; b) the subsequent switch to procollagen production and; c) mature collagen fibril formation (Baum & Arpey, 2005). Proteoglycans aid formation of collagen fibrils and act as a conduit for the migration and activity of other wound cell types (e.g. endothelial cells and Mφs; Schultz & Wysocki, 2009).

As previously discussed, collagen composition in skin is approximately 80% collagen I: 20% collagen III. However, the collagen matrix of the granulation tissue predominantly comprises of the embryo-associated collagen III (~30%) and only 10% collagen I (Witte & Barbul, 1997). As healing progresses, collagen III is replaced by collagen I, which provides scar tissue with increased tensile strength

(Diegelmann & Evans, 2004; Young & McNaught, 2011). The integrity and architecture of the scar never returns to that of unwounded skin, achieving 80% of pre-wounding strength post-injury (Witte & Barbul, 1997; Young & McNaught, 2011). These sequential changes in ECM require a fine balance between collagen degradation and synthesis, achieved through temporal regulation of key MMPs. These collagenases, expressed by inflammatory cells, epidermal cells and fibroblasts, cleave native helical collagens throughout repair (Witte & Barbul, 1998).

Normally, tropoelastin expression ceases during late embryonic development and remains absent post-birth. However, during disease states and wound healing, elastin production resumes. In wound healing, degradation of the normal dermal matrix (by proteases and physical damage) causes release of elastin fragments, or elastikines, which become their own signalling molecules (Duca et al., 2004). Early in wound repair, tropoelastin expression is heightened, but elastin fibre arrangement is aberrant. In fact, elastin fibres are often not apparent in scar tissue until many months following injury (Almine et al., 2012; Amadeu et al., 2004).

1.5. Aberrant Wound Healing

Acute wound repair follows an orderly cascade of cellular signalling and behavioural events to ensure rapid closure of the skin barrier. Complications at any stage of this reparative process can result in healing impairment (see **Figure 1.9**). The most significant aberrations result in wounds that fail to heal entirely. These "chronic" wounds, which predominately affect the elderly and diabetic, are a major area of unmet clinical need, reducing quality of life and causing a huge socio-economic burden (Bjarnsholt et al., 2008; Harding et al., 2002; Watson et al., 2011). For example, in 2012-2013, 2.2 million wounds were treated by the National Health Service, costing an estimated £4.5-£5.1 billion (Guest et al., 2015). Thus, it is clear why chronic wounds are considered a "silent epidemic" (Lindholm & Searle, 2016).

The three main types of chronic wounds are diabetic foot ulcers (DFUs), venous leg ulcers (VLUs) and pressure ulcers, deemed chronic if they fail to heal within 12 weeks (Sheehan et al., 2003; e.g. Wagner scale; **Table 1.4**). Pressure ulcers most frequently occur in patients who are immobilised for extended periods, where sustained pressure and shear forces result in ulceration, predominately of the skin covering bony prominences (Defloor, 1999; Liu et al., 2016). VLUs, by far the most

prevalent chronic wound type (Hall et al., 2014), are the result of oedema and hypoxia caused by venous insufficiency (Kranke et al., 2015). DFUs are particularly debilitating and can lead to lower limb amputation, thus increasing subsequent risk of death (Moulik et al., 2003; Walsh et al., 2016). DFUs are common in diabetic patients and usually begin as acute wounds. However, complications, such as chronic low-level inflammation and hyperglycaemia, influence the wound healing response, leading to poor clinical outcome (Baltzis et al., 2014). Hyperglycaemia impairs leukocyte function, and causes non-enzymatic glycation of collagen and the formation of AGEs, thus perpetuating inflammation (Pradhan et al., 2009). Diabetes also triggers long-term damage to the microvasculature (Young & McNaught, 2011), resulting in local tissue hypoxia, arterial vasculopathy and/or lower limb neuropathy– all extreme risk factors for chronic wound development (Walsh et al., 2015). In fact, it is estimated that 25% of diabetics will develop a chronic wound during their lifetime (Boulton, 2013).

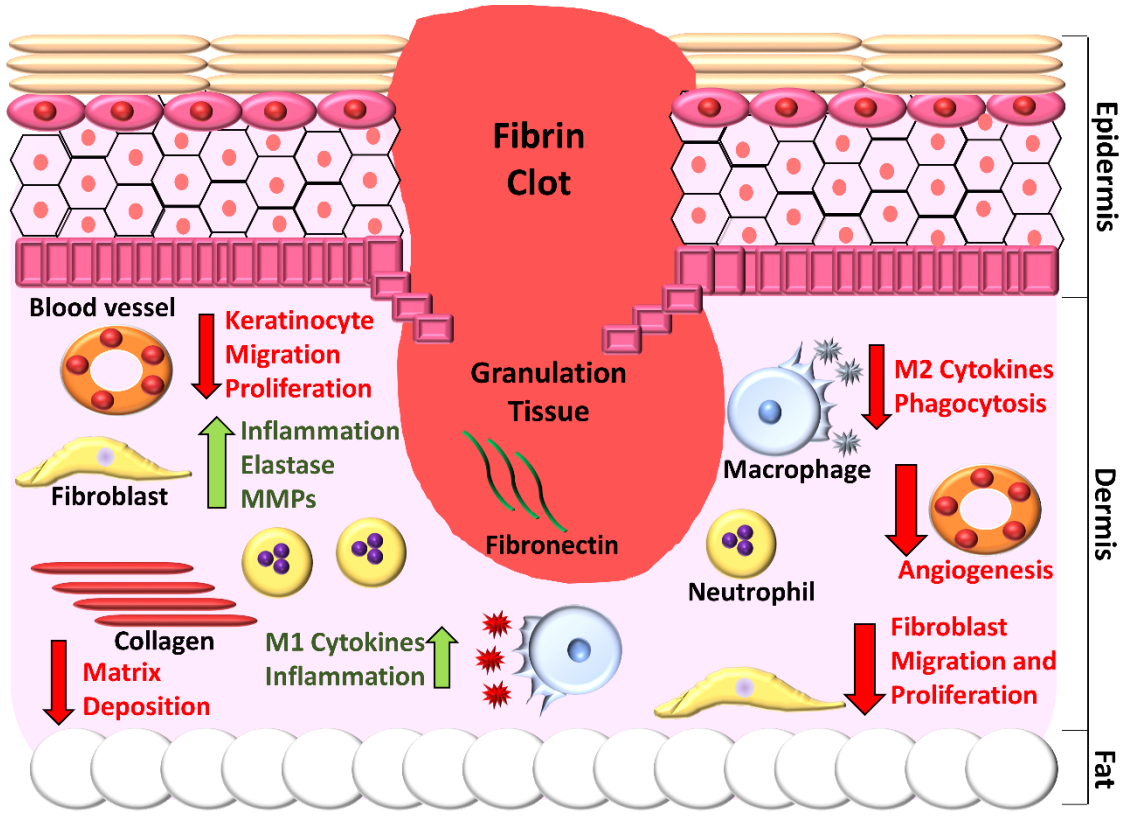

Figure 1.9. Cellular defects associated with pathological healing. Delayed healing in aged and diabetic wounds is associated with increased (green arrows) inflammation and reduced (red arrows) cellular proliferation and migration. *Image adapted from Wilkinson & Hardman (2017).*

It is important to note that the causes of wound chronicity, although simplified above, are often multifactorial and complex. Wound chronicity is influenced by local (e.g. ischemia) and systemic factors (e.g. age, malnutrition and disease), along with imbalances in cytokine and GF levels (Harding et al., 2002). However, in recent years, the most discussed contributor to chronicity is the persistence of wound infection (Dow et al., 1999; James et al., 2008; Wolcott et al., 2015; discussed in **Chapter 6**). Therefore, current treatments are largely aimed at reducing and preventing microbial wound contamination.

Table 1.4. Wagner wound categorisation system for diabetic foot ulcers. *

Category	Description
0	Intact skin
1	Superficial ulcer
2	As 1 but extending to tendon or bone
3	As 2 but with osteomyelitis or absess
4	Gangrene in toes and/or forefoot
5	Midfoot or hindfoot gangrene

**Modified from Margolis et al. (2002).*

1.5.1. Current Chronic Wound Therapies

Wound management often begins with assessment of the patient and wound aetiology (Kranke et al., 2015; Velnar et al., 2009). The most common intervention is debridement, or the removal of necrotic, infected, or hyperkeratotic tissue (Velnar et al., 2009) via sharp, surgical, enzymatic, autolytic, chemical, biological and mechanical processes (O'Brien, 2002; Stephen-Haynes & Thompson, 2007). Surgical debridement is painful, invasive, and requires implementation by a skilled professional (Gwynne & Newton, 2006). By contrast, the development of simple debriding devices has opened the possibility of self (home) care (Dogra & Rai, 2014; Wilkinson et al., 2016). Debridement is designed to remove infected and necrotic tissue, and expose the underlying vasculature to trigger a wound healing response (Stephen-Haynes & Thompson, 2007). Following debridement, wounds are irrigated with saline or an antibacterial solution at a pressure defined for the wound type (Velnar et al., 2009). Finally, a tailored dressing is applied to protect the wound from infection and provide an optimum environment for healing (Fonder et al., 2008). Autologous skin grafts can also be applied following irrigation, particularly

for the treatment of VLUs, although there remains a risk of dehiscence and further healing failure (Harding et al., 2002; Webster et al., 2012).

Recently, there has been a shift towards advanced therapies, largely based on new-found knowledge of the physiological disturbances associated with wound chronicity. For example, previous research has demonstrated a remarkable reduction in GFs in the milieu of chronic wounds compared to acute wounds (Higley et al., 1995; Yager et al., 1997). Studies involving the use of GFs *in vitro* (chronic wound-derived fibroblasts, Stanley et al., 1997), *in vivo* (VEGF on mouse wounds, Nauta et al., 2013; b-FGF on rat wounds, McGee et al., 1988; topical FGF on rat wounds, Ma et al., 2007) and in clinical studies (topical EGF, Brown et al., 1989), have revealed promising wound healing effects. Despite this, only PDGF (brand name REGRANEX, Smith and Nephew Ltd, Hull, UK) is approved for use in the clinic (Rees et al., 1999). Since its implementation, REGRANEX has shown varied effectiveness (Demidova-Rice et al., 2012). Other GFs, such as FGF (Japan) and EGF (Cuba) have been used clinically, with variable efficacy, high cost and controversial risks (e.g. cancer; Frykberg & Banks, 2015). Despite this, new GF therapies have the potential for improved clinical outcome, such as GF-incorporated matrices to improve diabetic wound healing *in vivo* (Ishihara et al., 2019).

Other less-risky treatments include the use of hyperbaric oxygen to increase tissue oxygenation (Kranke et al., 2015), and vacuum assisted closure (VAC), whereby negative pressure is applied to the wound to remove infected and inflamed milieu and promote wound closure (Vuerstaek et al., 2006). Traditional dressings have also evolved and now contain a myriad of material properties that aid regeneration, while incorporating substances with known pro-healing or antimicrobial effects (reviewed in Skórkowska-Telichowska et al., 2013). An adequate dressing is designed to maintain a moist environment while removing excess wound exudate (Baltzis et al., 2014). However, current treatments and best practice are only aimed at addressing secondary causes of chronicity, meaning chronic wounds often persist or recur (Velnar et al., 2009). Therefore, there remains a clinical unmet need to develop novel therapies that are financially, physiologically and practically suitable for chronic wound care.

1.6. Modelling Wound Repair

In vitro assays are widely used to model specific cellular aspects of healing (e.g. Liang et al., 2007), yet these assays fail to encompass the complexity of the *in vivo* environment. The development of more dynamic *in vitro* approaches, such as 3D skin equivalents, has partially reduced the need for animal and human studies (Itoh et al., 2013). However, artificially cultured 3D skin equivalents lack glands, immune cells and blood vessels, with studies only just beginning to address these problems (Kuo et al., 2018; Mazio et al., 2019). Human whole skin can also be induced to heal *ex vivo*, but availability can be limited. *Ex vivo* cultured skin also only remains viable of a few days and lacks immune cell infiltration. Thus, late stage wound responses (e.g. matrix remodelling) and granulation tissue formation cannot be studied effectively (Ansell et al., 2012; Zhou et al., 2018a). Porcine skin is yet another option, as wound closure occurs primarily through re-epithelialisation, mimicking human healing (Ueck et al., 2017). Despite the availability of non-animal models, mice are still extensively used in skin research (Godin & Touitou, 2007).

So why are mice favoured? Rodents are loose-skinned, have considerably more hair follicles than humans and a *panniculosus carnosus* muscle layer which allows rapid wound contraction following injury (Wong et al., 2010). Further, the mouse epidermis is much thinner than human (50 μm), making it difficult to produce partial-thickness wounds (Davidson et al., 1998). However, rodents are a less sentient *in vivo* species than pigs, are easier to manipulate, and heal with the same conserved mammalian stages of healing (Godin & Touitou, 2007). Moreover, the multitude of transgenic mouse lines available (reviewed in Maio, 2013) allows temporal and spatial investigation of the molecular basis of wound healing *in vivo*. Mouse models are often chosen due to their tractability, but strain-specific and species-specific differences must be considered when using non-human models for translational research purposes.

Wounding in mice involves full-thickness excisional biopsies or full-thickness incisional wounds to the dorsum, as these are highly reproducible (Ansell et al., 2014). However, the method of applying these wounds varies between laboratories, and healing rates can be affected by the analgesics and anaesthetics used (Hanci et al., 2012), the way the wound is initially created (punches, scissors, laser), and how it is treated (Ansell et al., 2012). In most studies, wounds are left to heal via

secondary intention (Galiano et al., 2004), which means they will largely close through contraction in mice. As a result, a number of researchers splint the wound to prevent contraction, or occlude the wound with dressings to increase the contribution of re-epithelialisation to skin repair (Scherer et al., 2009). These methods change the wound environment and rate of healing entirely (Dyson et al., 1997). Standardising methodology for *in vivo* murine studies is therefore essential for comparing and progressing current and future wound research.

1.6.1. Chronic Wound Models

Researchers have developed a number of pre-clinical delayed healing models, from pressure ulcers in mice using magnets (Strong et al., 2015) to burn wounds in pigs (Sheu et al., 2014; see **Table 1.5**). As those suffering with non-healing wounds tend to be diabetic or elderly, it follows that the most widely used chronic wound models involve diabetic and aged rodents (Roper et al., 2015). As previously discussed, both T1DM and T2DM can be modelled in mice. T1DM is most commonly induced through STZ injection, and STZ-induced mice show significantly delayed wound repair (Blecher et al., 2012; Hozzien et al., 2015; Long et al., 2016). More applicable to humans are the T2DM murine models of leptin deficiency (*ob/ob* mice) or leptin receptor deficiency (*db/db* mice). These mice are morbidly obese by 6-8 weeks of age, go on to develop T2DM (reviewed in O'Brien, 2014), and their wounds fail to heal at the same rate as their non-diabetic, heterozygous littermates (Seitz et al., 2010). However, there remains controversy as to whether delayed healing in diabetic mouse models is a result of hyperglycaemia, leptin deficiency or obesity (reviewed in Ansell et al., 2012).

Mice are aged for 1-2 years to imitate age-associated deterioration in wound repair (reviewed in Kim et al., 2015). Another viable ageing model is the ovariectomised mouse, where removal of the ovaries mimics the human menopause (Han et al., 2015). Loss of circulating sex hormones, particularly 17β-estradiol, leads to accelerated ageing and a delayed wound healing phenotype comparable to that of aged mice (Campbell et al., 2010). Unlike diabetic models, which are limited to comparison against diabetic wounds, aged models have the advantage that they emulate a more generalised chronic healing response, as age is a primary risk factor for the development of all types of chronic wound (Ansell et al., 2012).

Table 1.5. Examples of animal chronic wound models. *

Model		Primary Characteristics	Model Limitations	Reference
Animal	**Method**			
Porcine	Bipedicle flap. Full-thickness excisions.	Less skin perfusion, pressure and less oxygen.	Advanced surgical skills required.	Roy et al., 2009.
Murine	Magnetic ischemia devices.	Long-term inflammation.	Invasive. Included reperfusion phases.	Saito et al., 2008.
Porcine	UVR exposure. Full-thickness excisions.	Delayed granulation, delayed angiogenesis and delayed re-epithelialisation	UVR causes non-generalised effects. Healing returned to normal after 2 weeks.	Bernatchez et al., 1998.
Porcine	Streptozotocin injection. Full-thickness excisions.	Persistent hyperglycemia. Delayed re-epithelialisation.	Wounds healed after 18 days.	Velander et al., 2008.
Murine	Genetic. Full-thickness excisions.	Hyperglycaemia and delayed re-epithelialisation.	Difficult to distinguish between obesity and diabetes effects.	Wetzler et al., 2000.
Porcine	Streptozotocin injection. Full-thickness excisions. Inoculation with *S. aureus*.	Sustained tissue infection and delayed re-epithelialisation.	Substantial re-epithelialisation after 12 days. Long-term diabetes not assessed.	Hirsch et al., 2008.
Murine	Genetic. Full-thickness excisions. *P. aeruginosa* biofilms.	Sustained tissue infection and delayed re-epithelialisation.	Issues with dressing attachment and wound occlusion.	Zhao et al., 2012.
Murine	20 months old. Full-thickness excisions.	Delayed healing.	Fully closed after 9 days. Ageing in house takes time.	Nishio et al., 2008.

**Table adapted from Seaton et al. (2015) to include mouse data and aged wounds. Wound types, separated by colour, as follows: Reperfusion, burns, diabetic ulcers, infected diabetic ulcers, aged ulcers.*

1.7. The Metallome

Metal ions and metal complexes are ubiquitous throughout the body, orchestrating the action and inaction of cellular signalling pathways, regulating gene transcription and playing vital roles in catalysis (Szpunar, 2004). The metallome, the global distribution of metals and metalloids within the body, is therefore fundamental in

coordinating cellular behaviour and tissue architecture (Dlouhy & Outten, 2013). As the skin is a highly cellular, dynamic organ encompassing an array of diverse signalling responses, cellular processes and tissue structures, it follows that the metallome should play a crucial part in maintaining normal skin homeostasis.

1.7.1. Endogenous Metals in Chronic Disease

As metals provide critical functions throughout the body, it is understandable that abnormal alterations in metal homeostasis can result in, or be associated with, disease. For example, altered serum and tissue magnesium concentrations are found in diabetes (Resnick et al., 1993), cardiovascular disease (reviewed in Chakraborti et al., 2002) and neurodegenerative disorders (Andrasi et al., 2000; Çilliler et al., 2007). In fact, an inverse relationship is observed between magnesium and insulin levels in diabetes (Ma et al., 1995), while low dietary magnesium is associated with increased risk of cardiovascular events (Qu et al., 2013), stroke (Larsson et al., 2012), and hypertension (Paolisso & Barbagallo, 1997). Prospective studies have even demonstrated that individuals who have higher dietary intake of magnesium are less likely to develop T2DM (Hruby et al., 2014; Kim et al., 2010), and in a number of trials, supplementation with magnesium is correlated with lower post-fasting blood glucose (Castellanos-Gutiérrez et al., 2018; Hruby et al., 2014) and reduced insulin (ELDerawi et al., 2018). It is thus unsurprising that magnesium regulates enzymes involved in glucose transport and metabolism (Gales et al., 2014). Despite ample meta-analysis data, understanding of the underlying molecular basis of magnesium in disease is lacking (Guasch-Ferré et al., 2013).

Zinc is also intimately involved with insulin synthesis, as zinc deficiency and supplementation have drastic effects on diabetic animals (reviewed in Taylor, 2005). Here, mice that overexpress CuZnSODs and metallothioneins within their islet β cells are resistant to STZ and AX-induced T1DM (Kubisch et al., 1994), while dietary zinc supplementation also imparts the same protective influence against pancreatic β cell destruction (Ho et al., 2001). The defensive effects of zinc even extend to T2DM mouse models. For example, in *ob/ob* (Begin-Heick et al., 1985) and *db/db* (Simon & Taylor, 2001) mice, dietary zinc supplementation attenuated fasting hyperglycaemia and hyperinsulinemia, and prevented obesity in the *db/db* model. By contrast, a zinc deficient diet in *db/db* animals led to hyperglycaemia and insulopaenia (Simon & Taylor, 2001).

Further literature describes how iron, copper and calcium accumulate and interplay with pathology. Indeed, damage to metal regulatory mechanisms (e.g. via oxidative stress) leads to accumulation of iron and copper in many hepatic disorders, such as non-alcohol fatty liver disease (Dongiovanni et al., 2015; reviewed in Feldman et al., 2015). Impairment in calcium homeostasis causes a multitude of abnormalities throughout the body (Elsholz et al., 2014; Jiang et al., 2016), therefore crucial mechanisms have evolved to tightly and efficiently regulate intracellular free Ca^{2+} (Brini & Carafoli, 2009). Many calcium-associated proteins (e.g. calmodulin) and receptors (e.g. CaSR, discussed in **Chapter 4**) are also used as biomarkers in a range of pathologies, from alzheimer's disease (O'Day et al., 2015) to cancers (Tennakoon et al., 2016) and endocrine disorders (reviewed in Ward & Riccardi, 2012).

Although a large body of research pertains to investigating and observing metal changes in pathological conditions, the metal-specific basis of these biological and chemical defects remains to be elucidated. Similarly, the actions by which metals are transported and incorporated into intracellular systems is not fully understood. Advancing understanding of the human genome, combined with the development of sophisticated analytical techniques (Szpunar, 2004), offers an unprecedented opportunity to identify the unique relationships between metals and metalloproteins in health, and determine their subsequent roles in disease.

1.7.2. Endogenous Metals in Skin

Within the skin, the most important endogenous metal ions are zinc, calcium, magnesium, iron and copper (Dlouhy & Outten, 2013; Lansdown et al., 1999). Iron is the most abundant transition metal of the skin, although its absolute concentration varies between individuals (Wright et al., 2014). Importantly, the clinical manifestations of iron deficiency (e.g. anaemia) result in drastic skin changes, such as pallor and hyperpigmentation (Marks & Shuster, 1970). Iron may also play a significant role in fibroblast senescence, due to its pro-inflammatory influences in human and murine tissues (Sindrilaru et al., 2011). Furthermore, increased iron, which promotes oxidative and nitrative damage, correlates convincingly with elevated expression of the known senescence markers, γH2AX and p16INK4α (Sindrilaru et al., 2011; Sindrilaru & Scharffetter-Kochanek, 2013). The effects of iron in skin are explored more extensively in **Chapter 5**.

The second most abundant transition metal, zinc, is more copious within the epidermis than the dermis (Inoue et al., 2014) and forms complexes (mostly metallothioneins) within basal keratinocytes that are essential for regulating cellular mitosis, migration and differentiation (Lansdown et al., 2007). Interestingly, the epidermal zinc gradient contrasts with the calcium gradient, as zinc and calcium exert opposing effects on keratinocytes (Emri et al., 2015). In the presence of excess zinc, levels of calcium-binding proteins, such as calmodulin, rapidly decline (Heng et al., 1993; Lengyel et al., 2000). As the skin harbours 20% of the body's zinc, it is not surprising that zinc deficiency leads to a number of skin complications, such as psoriasis (Prasad, 1976; Vallee & Falchuk,1993) and impaired wound healing (in rats, Oberleas et al., 1971; in the clinic, Rahmat et al., 1974).

Magnesium is another important cutaneous metal, and a major cofactor for adenosine triphosphate, nucleic acids and many metabolic enzymes (Li & Zhou, 2011). Thus, magnesium maintains normal functioning of tissues throughout the body. Magnesium is also crucial in regulating ion channel permeability, as it influences the transmembrane transport of Ca^{2+}, K^{+}, and Na^{2+} (Permyakov & Uversky, 2013). Finally, the most deliberated, versatile, and probably the most important metal ion is calcium, found within intracellular and extracellular reservoirs throughout the body (Menon et al., 1985). Calcium tightly regulates epidermal permeability and cell function by maintaining its own gradient, which is also essential for epidermal stratification (Elsholz et al., 2014). Calcium effects in skin and wound healing are described in **Chapter 4**.

1.7.3. Endogenous Metals in Cutaneous Repair

Metal ions and metal complexes maintain the overall integrity of the skin, but also prevent skin infection (Wright et al., 2014), protect against skin disease (reviewed in Prasad, 1976; Vallee & Falchuk, 1993), and interact with diverse signalling pathways important in wound repair (Lansdown et al., 1999; Dlouhy & Outten, 2013). It is therefore unsurprising that metals play a number of potential roles in wound repair (summarised in **Figure 1.10**).

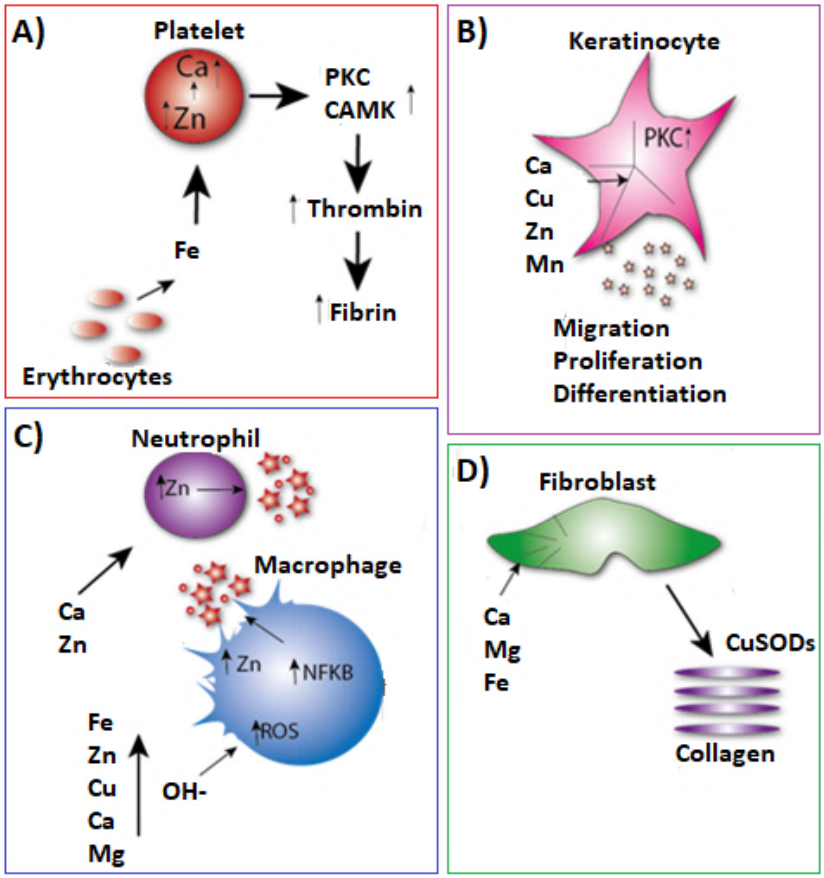

Figure 1.10. Wound-relevant processes that may be influenced by endogenous metal ions. A) Metals alter fibrin clot formation during haemostasis. **B**) Metals stimulate release of pro-inflammatory cytokines (stars) during inflammation. **C**) Metals influence keratinocyte activation, and actinomyosin filament formation/contraction during re-epithelialisation. **D**) Collagen deposition and fibroblast contraction are modulated by metals during the remodelling phase. Calcium (Ca), zinc (Zn), copper (Cu), manganese (Mn), iron (Fe) and magnesium (Mg). *Image produced by the author (HNW)*.

1.7.3.1. Haemostasis

Following injury, waves of Ca^{2+} are exhibited seconds after wounding in invertebrates (*Caenorhabditis elegans*, Xu & Chisholm, 2011; *Drosophila melangaster*, Ghannad-Rezaie et al., 2012; Razzell et al., 2013) and vertebrates (Klepeis et al., 2001; Tran et al., 1999; Yoo et al., 2012). During haemostasis, Ca^{2+} influx into platelets (Parekh & Putney, 2005) leads to transcriptional modification of protein kinase A (PKA), PKC and Ca^{2+}/Calmodulin-dependent protein kinase (CaMK; Tran et al., 1999; Pászty et al., 1998; Harper & Poole, 2010). Subsequently, Ca^{2+} modulates clotting factor expression, conversion of prothrombin and fibrinogen to thrombin and fibrin, respectively (Detwiler et al., 1978; reviewed in Lundblad et al., 2000), and platelet adhesion and GF production (Fréchette et al., 2005; reviewed in Lansdown, 2002). Interestingly, zinc exerts its effects through

modulating intracellular calcium to promote coagulation (Csermely & Somogyi, 1989; O'Dell, 2000), while the substantial influence of iron and iron-related proteins in regulating thrombosis has been extensively studied (Pretorius et al., 2013). The role of magnesium in clotting is less well known, yet magnesium has been investigated as a potential treatment for coagulatory disorders (Canton et al., 1987, Harnett et al., 2001; Sekiya et al., 1996). Unlike calcium, magnesium appears to reduce coagulation via antiplatelet and antithrombotic mechanisms (Ravn et al., 1996a, Ravn et al., 1996b, Sheu et al., 2002). Therefore, in early wound repair, endogenous Mg^{2+} levels are probably controlled to prevent exsanguination (Lansdown, 2002).

1.7.3.2. Inflammation

During inflammation, calcium modulates motility, membrane function and ROS production (Fujimaki et al., 2003; Lansdown et al., 2007; Razzell et al., 2013). A surge in Ca^{2+} is observed in activated neutrophils, allowing effector functions, such as phagocytosis, ROS production, and chemotaxis (Fujimaki et al., 2003; Razzell et al., 2013; Zhang et al., 2014a). External stimuli, such as LPS, also activates the influx of Ca^{2+} in Mφs to trigger inflammatory processes (Zhou, et al., 2014), while blockade of store operated calcium channels dampens inflammatory cytokine release in co-cultures of peripheral blood mononuclear cells and myoblasts (Beringer et al., 2018). Further, zinc is crucial for humoral and cell-mediated immunity (reviewed in Keen & Gershwin, 1990), and the functioning of a number of pro-inflammatory cytokines (e.g. IL-1, IL-2, IL-6, IFN-y and TNF-α; reviewed in Wessels et al., 2017) and immune cell activating transcription factors (e.g. MTF-1 and NF-κB; Martin & Leibovich, 2005; Wellinghausen et al., 1997). By contrast, iron and magnesium play more passive roles in inflammation, where iron leakage from damaged erythrocytes increases ROS (Pretorius et al., 2013; Sindrilaru et al., 2011) and magnesium acts as a second messenger for calcium (Mazur et al., 2007).

1.7.3.3. Proliferation and Matrix Remodelling

Calcium aids the proliferative phase of wound healing by orchestrating stratification of keratinocytes (reviewed in Elsholz et al., 2014), upregulating PDGFR and VEGFR (reviewed in Cordeiro & Jacinto, 2013), modulating angiogenesis, and increasing fibroblast proliferation, differentiation and maturation (reviewed in Varga-Szabo et al., 2009). In normal wound repair, zinc complexes govern multiple cellular

processes, from functional migration to ECM assembly (reviewed in Lansdown et al., 2007), and during angiogenesis, zinc finger proteins stimulate VEGF transcription in various ways (reviewed in Dai et al., 2004).

Although unresolved, magnesium is known to promote VEGF-2-induced endothelial cell migration (Hong et al., 2006; Maier et al., 2004) and GF release (e.g. EGF), thus stimulating keratinocytes (reviewed in Cordeiro & Jacinto, 2013; Li & Zhou, 2011). Interestingly, EGF has been identified as a magnesiotropic hormone, promoting cellular Mg^{2+} accumulation via the transient receptor potential (TRP) channel, TRPM6 (Groenestege et al., 2007). Magnesium also affects keratinocyte contractility (Wolf & Cittadini, 2003), which may extend to fibroblasts (Ferré et al., 2010; reviewed in Gill & Parks, 2011). Of note, long-term magnesium deficiency arrests proliferation and triggers senescence in primary human fibroblasts, possibly via oxidative stress mechanisms (Killilea & Ames, 2008).

1.8. Summary

The skin has evolved crucial mechanisms to quickly and efficiently close breaches to its barrier. In the elderly and diabetic, wound healing is fundamentally impaired, leading to excessive inflammation, reduced re-epithelialisation and delayed matrix deposition. These obstructions to normal repair underlie the development and persistence of non-healing wounds. As the ageing population increases, the incidence of chronicity is on the rise, putting strain on healthcare providers worldwide. Modern treatments are inadequate, focussing on alleviating secondary symptoms rather than addressing underlying chronic wound aetiology. As a result, there is an urgent need to develop therapies based on the cellular and molecular causes of poor healing.

Currently, the literature ascribes central functions for endogenous metals in regulating skin homeostasis, inflammatory processes and wound repair. However, there is a paucity of empirical evidence for these effects during *in vivo* wound healing, and present knowledge is based mainly on *in vitro* assessment of functional responses. For example, studies addressing the wound reparative effects of calcium are limited to *in vitro* assays (e.g. Zhou, Li et al., 2014) or *in vivo* experiments in less sentient organisms (e.g. zebrafish, Yoo et al., 2012). While important and interesting, these models are a long way from encompassing the complexities of the *in vivo*

mammalian wound healing environment. There is clear scope to explore the metallome in skin and wound physiology, and in pathological contexts such as ageing and diabetes. Investigating the central role of metals in wound healing may therefore contribute to future understanding of chronic wound aetiology and progress the development of effective new treatments.

1.9. Hypothesis and Aims

1.9.1. Hypothesis

The central research hypothesis for this thesis is that endogenous metals play critically important, hitherto unappreciated, roles in normal healing and that metal perturbation is a contributing factor to pathological healing. It follows that: a) injury and healing will lead to temporal and spatial changes in the global skin metallome and; b) manipulation of tissue metals holds the potential to promote healing.

1.9.2. Aims

The central aims of the thesis were as follows:

Aim 1: To explore novel aspects of diabetic wound healing pathology; a focus on cellular senescence. A pre-requisite to metal profiling studies is detailed characterisation of the pathological healing (*db/db*) mouse model. Pilot data from the Hardman group suggest a potential correlation between cellular ageing (senescence) and diabetic healing pathology. This will be explored in detail, using a combination of *in vitro*, *in vivo* and *ex vivo* wound healing models.

Aim 2: To characterise the temporospatial changes in endogenous metals during normal and pathological repair. Here the focus will be to conduct a systematic temporo-spatial evaluation of endogenous metal levels across a wound healing time course in normal and pathological (aged and *db/db*) murine wound models. Laser ablation inductively coupled plasma mass spectrometry (LA-ICP-MS) will be combined with histological analysis (e.g. immunohistochemistry) and correlative gene expression profiling (RNA-seq). This will permit, for the first time, correlation of wound metallomic, genomic and structural changes. Methodologies will be adapted throughout to ensure minimal trace metal contamination.

Aim 3: To elucidate the cellular and molecular role of specific metals in wound healing. *In vitro* assays will dissect the wound-relevant effects of specific metals (administration and sequestration) on a range of cell types (keratinocytes, fibroblasts, bone marrow-derived Mφs, and THP-1 cells). Detailed mechanistic studies will depend on the specific roles identified. Translational relevance will be tested using a model of human *ex vivo* wound repair.

Aim 4: To evaluate 3D bioactive glass as a metal delivery vehicle to promote healing and deliver antimicrobial efficacy. Although successfully used in bone regeneration, the effects of bioactive glass on wound repair are less well characterised. Here, a combination of *in vitro* and *in vivo* studies will be used to test cellular healing promotion. In addition, silver functionalised bioactive glass will be evaluated for stability and antimicrobial efficacy with/without metal functionalisation. More complex biofilm experiments will assess effects on host-biofilm interaction and virulence.

Chapter 2: Materials and Methods

2.1. Animal Experimentation

Female wild-type (WT, C57BL/6J), non-diabetic (NDb, $LEPR^{-/+}$) and diabetic (Db, $LEPR^{-/-}$) mice were obtained from Envigo Ltd (UK) and housed in the Biological Services Facility (The University of Manchester, UK) with *ad libitum* access to food and water. The Db mice used were homozygous for a point mutation in the leptin receptor, which results in leptin receptor deficiency and impaired signalling through the adipocyte-derived hormone, leptin (Sharma et al., 2003). As a result, these mice are morbidly obese and display many of the hallmark features of diabetes, such as increased serum insulin, hyperglycaemia and polyuria (Hummel et al., 1972). As a control group for the Db mice, their heterozygous littermates were used (NDb).

Young WT, NDb and Db mice were wounded at 8-10 weeks old, while aged WT mice were wounded at 87 weeks of age. Cages were kept under constant temperature, humidity and a 12-hour light-dark cycle. All animal procedures were carried out according to Home Office regulations under project licence 70/8136 and the personal licence of the author (HNW). Every effort was made to abide to practices of the 3Rs (Replacement, Reduction, Refinement; Burden et al., 2015), developed to reduce the number of, and suffering of, animals in experimental research. Therefore, where achievable, the number of mice used in experiments was determined as the least number of animals required to gain statistical significance, as concluded from previous power calculations within the group (Ansell et al., 2014).

2.1.1. Wounding

2.1.1.1. Incisional Wounds

Mice were anaesthetised with 2% isoflurane in 2L min^{-1} oxygen and nitrous oxide. Incisional wounds were created following an established protocol (Ashcroft et al., 2003). Briefly, the dorsal area was shaved and disinfected with 70% isopropyl alcohol swabs containing 2.5% chlorhexidine (Shermond, Leicester, UK) and two full-thickness 1 cm dorsal incisions were created using sterile no.11 scalpel blades (Swann-Morton, Sheffield, UK). The wounds were made 2 cm below the base of the animal's skull, 0.5 cm either side of the midline (as shown in **Figure 2.1**), deep

enough to cut through the *panniculus carnosus* muscle. Buprenorphine was administered as an analgesic post-wounding (0.1 mg/Kg). Mice recovered from surgery in a scantainer at 37°C, and were returned to normal housing separately for the duration of the experiment. Mouse weights were recorded and were maintained during experiments. Wounds were left uncovered and allowed to heal via secondary intention unless otherwise stated.

2.1.1.2. Excisional Wounds

Full-thickness excisional dorsal wounds were created with sterile 6 mm biopsy punches (Stiefel, Middlesex, UK), or trace metal free (TMF) sterile titanium instruments (World Precision Instruments, Hertfordshire, UK) for ICP-MS analysis. Excisional wounds were made down to the *panniculus carnosus*, 2 cm from the base of the skull and 0.5 cm from the midline of the animal (**Figure 2.1**). Excision skin was fully removed with sterile forceps and scissors. Animals were administered analgesic and allowed to recover. Individual experimental groups are outlined in each relevant chapter.

2.2. Tissue Collection

Mice were sacrificed via a rising concentration of carbon dioxide (CO_2) and a second approved Schedule One method was used to confirm death (cervical dislocation).

2.2.1. Skin and Wound Collection

Wounds were photographed for macroscopic wound area analysis using a FujiFilm FinePix S5700 camera (Fujifilm, Bedford, UK). Dorsal skin (above the wound area) was shaved and wounds were excised down to the underlying muscle using sterile scissors and forceps (titanium instruments for TMF work). Wounds were bisected at their midpoint, giving four wound halves from each mouse. One half was placed in formalin fixative (**see Appendix 2A.1**); one half was flash frozen in liquid nitrogen and stored at -80°C for biochemical analysis; one half was flash frozen in optimum cutting temperature medium (OCT, CellPath, Powys, UK) and; one half was collected in a TMF vacutainer (BD Biosciences, Berkshire, UK) at -80°C for ICP-MS (**Section 2.5**; see **Figure 2.1**). Normal dorsal skin was also excised for analysis.

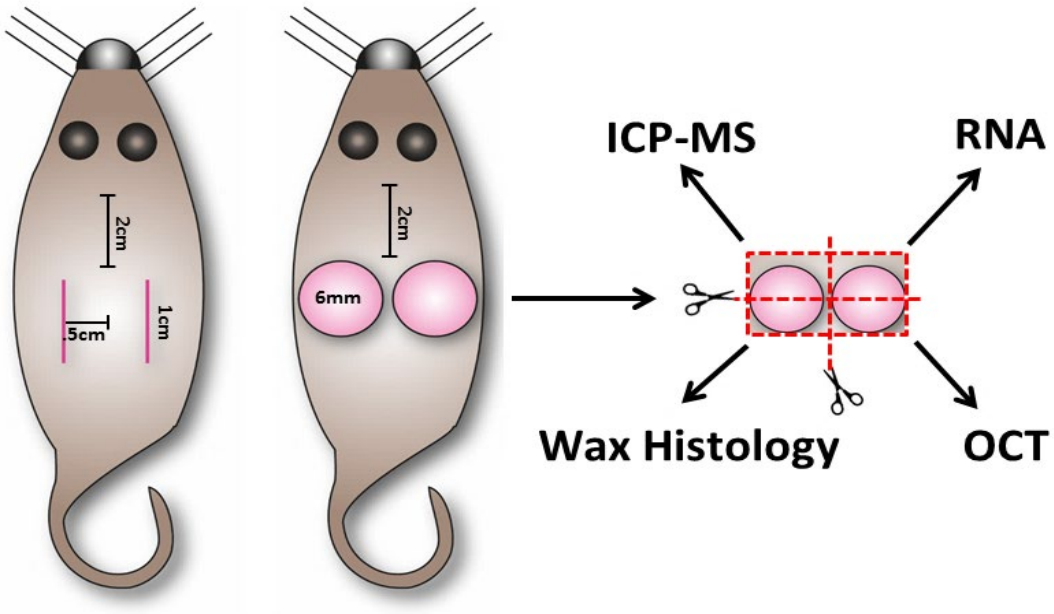

Figure 2.1. Example of incisional and excisional wounding in mice. Wounds are created 2 cm below the base of the skull and 0.5 cm either side of the midline of the animal. Scalpel blades are used for 1 cm incisions (left), while biopsy punches (or titanium instruments) are used to create 6 mm excisions (right). Wounds are made down to the *panniculus carnosus* and left to heal via secondary intention. Upon collection, wounds are excised and bisected at their midpoint for various analyses (shown to the right). ICP-MS = inductively coupled plasma mass spectrometry. OCT = optimum cutting temperature medium. *Illustration created by the author (HNW).*

2.2.2. Isolation of Murine Epidermal Keratinocytes and Dermal Fibroblasts

Murine hair was removed from the ventral side of the body using Veet® wax strips (Reckitt Benckiser, Berkshire, UK). Skin was cut away from the underlying fascia and placed in tubes containing Hank's Balanced Salt Solution (HBSS, Sigma-Aldrich, Dorset, UK) and 2% (v/v) Antibiotic-Antimycotic solution (Gibco, Thermo Fisher Scientific, Leicestershire, UK) on ice for cell isolation.

Skin collected in HBSS was washed in Dulbecco's phosphate buffered solution (DPBS; Gibco). Skin was cut into strips and floated on 0.2% (w/v) Dispase II (Sigma-Aldrich) in petri dishes, epidermis side up to ensure the epidermis was not submerged in the enzyme mixture. Petri dishes were incubated at 4°C overnight (O/N). The next day, the epidermis was peeled away from the dermis and incubated in 0.25% (v/v) trypsin (Gibco) for five minutes. Trypsin was neutralised with 10% heat-inactivated foetal bovine serum (FBS; Gibco), and the cells were passed through a 70 µm cell strainer (Thermo Fisher Scientific) and pelleted via

centrifugation (300 x g for five minutes). Murine epidermal keratinocytes (MEKs) were re-suspended in CNT07 media (CellnTec, Caltag Medsystems, Buckingham, UK) with 100 U/mL penicillin and 100 μg/mL streptomycin (P/S; Gibco) in collagen IV-coated plates (**Appendix 2A.2**) at a density of 5 x 10^4 cells per cm^2.

The dermis was cut into small pieces and incubated in enzymes within the Whole Skin Dissociation Kit (Miltenyi Biotec Ltd., Surrey, UK) for three hours at 37°C. The mixture was then dissociated further using the gentleMACS dissociator skin protocol (Miltenyi Biotech Ltd.) as per manufacturer's instructions. The fibroblast cell mixture was passed through a 70 μm cell strainer, centrifuged to pellet (300 x g for five minutes), and re-suspended in 1 mL culture media (dermal fibroblast media, **Appendix 2A.3**). Murine dermal fibroblasts (MDFs) were seeded at 1x10^5 cells/mL culture media in 25cm^3 vented capped flasks, and incubated at 37°C and 5% CO_2.

2.2.3. Isolation of Bone Marrow-Derived Macrophages

Bone marrow for subsequent Mφ experiments was isolated from the femoral and tibial bones of sacrificed animals. Bones were cut transversally at the joints and bone marrow was flushed from the medullary canal using a 27-gauge needle and 10 mL syringe filled with bone marrow medium (see **Appendix 2A.4**; modified from Pajarinen et al., 2015). A 19-gauge needle attached to a 10 mL syringe was used to gently disaggregate the bone marrow clumps. The bone marrow cell mixture was then passed through a 70 μm cell strainer, and cells counted and re-suspended into culture plates at a concentration of 2 million cells per mL. To freeze, cells were pelleted, re-suspended at five million cells per mL in 90% FBS and 10% dimethyl sulphoxide (DMSO, Thermo Fisher Scientific), and frozen at a rate of 1°C per minute prior to liquid nitrogen storage.

2.3. Human Skin Experimentation

All skin was collected from theatres at Castle Hill hospital (Cottingham, UK) under full UREC (FEC_47_2017) and LREC (17/SC/0220) approval. Samples were collected with full informed, written, patient consent. Skin was collected in holding media (Dulbecco's Modified Eagle Medium [DMEM] plus 2X antibiotic-antimycotic solution, both Gibco) and kept on ice during transport.

2.3.1. *Ex Vivo* Wounding

Skin was removed from holding media and adipose tissue was cut away with sterile scissors. Skin was then placed in sterile HBSS with 4% antibiotic-antimycotic and shaken vigorously to remove blood and loose adipose tissue. HBSS washing was repeated and any remaining adipose tissue was cut away with scissors. The skin was then washed twice in DPBS and the epidermis was dried completely with sterile gauze pads. A 2 mm biopsy punch (Stiefel) was used to excise the epidermis and papillary dermis, creating a partial-thickness wound. The skin was then completely excised as a 6 mm skin explant. Explants were placed on a nylon filter membrane (Merck-Millipore, Hertfordshire, UK) on a stack of three absorbent pads (Merck-Millipore) in 6 mm^2 dishes containing 5 mL of media (**Figure 2.2**). General explant culture media was DMEM containing 10% FBS, 100 U/mL penicillin, 100 µg/mL streptomycin and 2.5 µg/mL amphotericin B (all Gibco). Plates were incubated at 37°C with 5% CO_2. Media was changed every 2 days until collection in fixative (as above). Wound treatments are outlined where applicable.

2.3.2. Isolation of Human Dermal Keratinocytes and Fibroblasts

Skin was cut into strips and incubated O/N at 4°C in 0.2% (w/v) Dispase II in DPBS (Sigma-Aldrich). Normal human epidermal keratinocytes (NHEKs) were isolated as described for MEKs. The cell suspension was pelleted via centrifugation (300 x g for five minutes) and re-suspended in EpiLife™ medium (Gibco) on coating matrix (Gibco) at a density of 5 x 10^4 cells per cm^2. The plates were incubated at 37°C and 5% CO_2. Human dermal fibroblasts (HDFs) were isolated as per MDFs.

2.4. Histology

2.4.1. Tissue Processing

Wounds harvested in formalin fixative (**Appendix 2A.1**) were left at room temperature (RT) for 24 hours, then transferred to 70% ethanol: 30% dH_2O for at least 18 hours. After this time, tissue processing was carried out using the steps provided in **Table 2.1**. Wounds were then embedded in paraffin wax (Raymond Lamb, Thermo Fisher Scientific) in metal molds on a Histocore Arcadia C cold plate (Leica Biosystems, Milton Keynes, UK) with the cut edge oriented towards the base of the mold (for murine skin and wounds). This allowed sections of the wounds to be oriented in a transverse plane. For 2 mm human biopsies, whole explants were

embedded horizontally and trimmed uniformly to reach the centre of each wound. Serial sections were then taken from the centre of the wounds at 5 µm on a Leica RM225 microtome and placed on slides coated in VECTABOND® Reagent (Vector laboratories, Peterborough, UK; see **Appendix 2A.6**). Slides were dried at 37°C overnight and stored at RT until histological analysis.

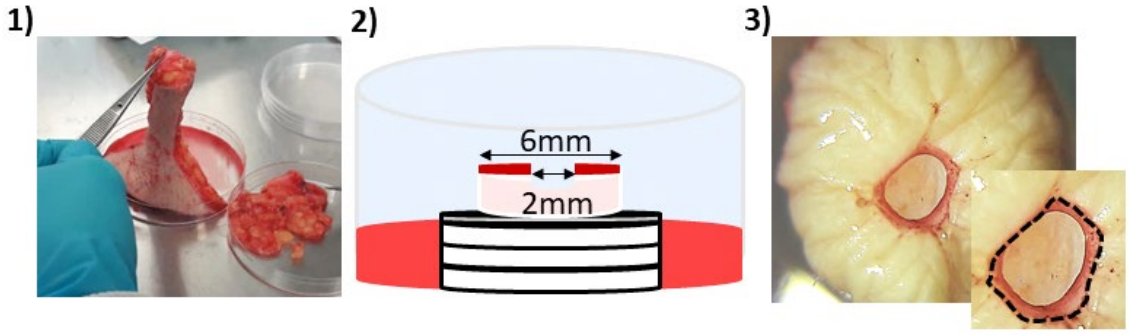

Figure 2.2. Schematic depicting the human *ex vivo* explant culture set up. Partial thickness wounds (2mm) are created within 6mm skin explants, cultured on absorbent pads at the air-liquid interface. Nutrient transfer from the media occurs through a filter membrane. **1** = skin, **2** = culture setup, **3** = wounded explant following 3 days of culture (wound = dotted line, red staining = % re-epithelialisation). *Illustration created by the author (HNW).*

Table 2.1. Processing stages for wax embedding murine and human tissues. *

Stage	Time	Temperature
90% Ethanol	30 minutes	RT
95% Ethanol	30 minutes	RT
100% Ethanol	30 minutes	RT
100% Ethanol	50 minutes	RT
Xylene	30 minutes	RT
Xylene	45 minutes	RT
Wax	1 hour	60°C
Wax	1 hour	60°C

**RT = room temperature.*

2.4.2. Haematoxylin and Eosin Staining

Wax sections were de-waxed in xylene (Thermo Fisher Scientific) for 20 minutes at RT and rehydrated through an ethanol gradient (100%, 100%, 90%, 70%, 50%, two minutes each) to dH_2O. Slides were rinsed again in dH_2O to remove residual ethanol. Slides were stained with filtered Shandon's Haematoxylin (Thermo Fisher Scientific) for one minute, rinsed in tap water, and counterstained in 5% (w/v) Eosin B in dH_2O (Sigma-Aldrich) for three seconds. Slides were rinsed in dH_2O until clear,

dehydrated through an ethanol gradient (50%, 70%, 90%, 100%, 100%, one minute each) and cleared in xylene for 10 minutes. Slides were mounted with Pertex® mounting medium (CellPath) and allowed to dry fully before imaging.

2.4.3. Masson's Trichrome Staining

Masson's Trichrome staining was used as an alternative structural stain to Haematoxylin and Eosin (H&E). Sections were brought to dH_2O and mordented in saturated picric acid for one hour at RT. Slides were then stained with Weigart's Haematoxylin for 10 minutes and rinsed in dH_2O. Slides were immersed in Biebrich Scarlet-Acid Fuschin solution for two minutes, rinsed in dH_2O, and differentiated in phosphomolybdic-phosphotungstic acid solution for 10 minutes. Slides were counterstained in Alanine Blue for five minutes followed by 1% (v/v) acetic acid (three minutes), dehydrated rapidly in 95% and 100% ethanol (one minute each), and mounted in Pertex®. Reagent recipes are provided in **Appendix 2A.7**.

2.4.4. Immunohistochemistry

Slides brought to dH_2O were boiled in antigen retrieval buffer (citrate buffer, pH 6; see **Appendix 2A.8**) for 2-3 minutes. Once cool, slides were rinsed in dH_2O and endogenous peroxidase activity was blocked with 0.3% (v/v) H_2O_2 (Sigma-Aldrich) in dH_2O for 30 minutes at RT. H_2O_2 was rinsed from the slides with phosphate buffered saline solution (PBS; see **Appendix 2A.9**) for 15 minutes. For subsequent staining, VECTASTAIN® ELITE ABC kits (Vector Laboratories; see **Appendix 2A.10**) were used. Sections were blocked in 10% animal serum for 20 minutes to block non-specific antibody binding. Excess serum block was tapped from the sections, which were subsequently incubated in primary antibodies at the dilutions specified in **Table 2.2**. Known positive and negative controls were included for each antibody, and a PBS control (instead of primary antibody) was included on each slide to rule out non-specific binding (e.g. avidin-biotin background or secondary-binding). Following primary incubation, sections were rinsed in PBS and incubated in appropriate peroxidase-linked anti-igG secondary antibody for 30 minutes at RT. Slides were washed in PBS again and incubated in ABC reagent for 30 minutes at RT. ABC reagent contains horse radish peroxidase (HRP) and avidin to amplify the signal from the HRP-linked secondary antibody. Following a final PBS wash, colorimetric detection was achieved by incubating sections in NovaRED™ Peroxidase (HRP) Substrate (Vector Laboratories; see **Appendix 2A.11**). All sections were incubated

in NovaRED™ for the same amount of time and rinsed in dH_2O. Slides were counterstained with Shandon's Haematoxylin for 15 seconds, rinsed in tap water and dehydrated, cleared and mounted as described previously.

Table 2.2. Primary antibodies used for immunohistochemistry. *

Antibody	Working Conc.	Incubation Time	Temperature	Manufacturer	Host Species
α-SMA	0.5 µg/mL	O/N	4°C	Abcam	Mouse
Arginase I	0.5 µg/mL	1hr	RT	Santa Cruz	Goat
Caspase 3	0.5 µg/mL	O/N	4°C	R&D systems	Goat
Collagen I	0.5 µg/mL	O/N	4°C	Abcam	Rabbit
Collagen III	0.5 µg/mL	O/N	4°C	Abcam	Rabbit
Ferritin	0.5 µg/mL	O/N	4°C	Abcam	Rabbit
Fibronectin	0.5 µg/mL	O/N	4°C	Santa Cruz	Mouse
Keratin 6	1 µg/mL	O/N	4°C	Covance	Rabbit
Keratin 14	1 µg/mL	O/N	4°C	Covance	Rabbit
Ki67	100 µg/mL	O/N	4°C	Novacastra	Mouse
Mac3	5 µg/mL	O/N	4°C	BD Biosciences	Rat
MIF	10 µg/mL	O/N	4°C	R&D systems	Goat
Ly-6G	1 µg/mL	O/N	4°C	ThermoFisher	Rat
Nos2	1 µg/mL	O/N	4°C	Santa Cruz	Rabbit
p16	1 µg/mL	O/N	4°C	Santa Cruz	Rabbit
p21	1 µg/mL	O/N	4°C	Abcam	Rat
PDGFA	1 µg/mL	O/N	4°C	Santa Cruz	Mouse

**Concentration and incubation times for antibodies was determined by antibody titration and optimisation studies. Heat induced epitope retrieval was achieved with citrate buffer (pH 6). O/N = overnight for 16 hours.*

2.4.5. Perl's Prussian Blue Staining

Perl's Prussian Blue (PPB) staining was performed on wax embedded tissue sections to visualise iron deposits in skin and wound tissue. All solutions were stored in brown glassware cleaned in 1% (v/v) TMF nitric acid (HNO_3) and rinsed in Farmer solution (equal parts of potassium ferricyanide and sodium thiosulphate) to remove metal ion contamination. Rehydrated sections were incubated in a 50:50 solution of 5% (w/v) potassium ferricyanide (in dH_2O; Sigma-Aldrich) and 5% (v/v) hydrochloric acid (HCl) for 10 minutes at RT, then rinsed in dH_2O (as in Sindrilaru et al., 2011). Slides were counterstained in 5% (w/v) Neutral Red (Sigma-Aldrich), dehydrated in ethanol, cleared in xylene and mounted in Pertex®.

2.4.6. Picrosirius Red Staining

Picrosirius red staining was used to quantify collagen content in wound tissue. Rehydrated sections were immersed in Picrosirius Red solution (0.5 g Sirius Red in 500 mL saturated picric acid, Sigma-Aldrich) for one hour at RT, differentiated in

two changes of 0.5% (v/v) acetic acid (10-15 minutes each), rehydrated, cleared and mounted in PERTEX®. Under polarising light, collagen fibres are birefringent, with immature collagens (e.g. collagen type III) appearing yellow-green and mature collagens (e.g. collagen type I) appearing orange-red (Junqueira et al., 1979). Images were therefore imaged under polarising light using a Nikon Eclipse E400 microscope (Nikon UK Ltd., Surrey), SPOT camera (SPOT imaging, Image Solutions UK Ltd., Preston) and polarising filter set (Thermo Fisher Scientific). Analysis of collagen fibre composition was performed in ImageJ v.1.8 (National Institutes of Health [NIH], US) using a macro designed to measure the threshold intensity of green and red channels within each image.

2.4.7. Senescence-Associated Beta Galactosidase Staining

Senescence-associated beta galactosidase staining (SA-βGAL) was used to assess levels of senescent cells between pathological (aged and Db) and normal (young and NDb) skin and wounds (**Chapter 3**). SA-βGAL is a well-known marker for indicating senescence, where senescent cells and aged tissue express high levels of SA-βGAL activity (discussed in Itahana et al., 2013). Cryo-sectioned tissue was fixed in 0.5% (v/v) glutaraldehyde (Sigma-Aldrich) in PBS (pH 7.4) for 15 minutes at RT. Sections were rinsed with PBS (pH 7.4) for 5 minutes at RT, then rinsed twice in PBS containing 1 mM $MgCl_2$ (adjusted to pH 5.5 for mouse and pH 6.0 for human). Sections were incubated in X-Gal solution (**Section 2.A.12**) in the dark for 16 hours at 37°C, rinsed 3 x 5 minutes in PBS (pH 7.4) and post-fixed in 4% (v/v) paraformaldehyde in PBS for 30 minutes at RT. Sections were rinsed in PBS (3 x 5 minutes), counterstained in nuclear fast red (Sigma-Aldrich), dehydrated, cleared and mounted in Pertex®. Brightfield images were captured as in **Section 2.4.9**.

2.4.8. Terminal Deoxynucleotidyl Transferase dUTP Nick End Labelling

Terminal deoxynucleotidyl transferase dUTP nick end labelling (TUNEL) is a staining technique used to detect late stage apoptosis via labelling of double strand DNA breakage (Labat-Moleur et al., 1998). TUNEL was performed using an *in situ* Cell Death Detection Kit (Roche, Sigma-Aldrich). Briefly, OCT sections were fixed in methanol at -20°C for 10 minutes and rinsed in dH_2O. Antigen retrieval was performed with proteinase K solution (**Appendix 2A.13**) for 20 minutes at 37°C. Slides were rinsed in PBS and incubated in TUNEL reaction mixture at 37°C for 30 minutes, rinsed three times in PBS, and mounted in MOWIOL mounting reagent with

4',6-diamidino-2-phenylindole (DAPI; **Appendix 2A.14**). Images were captured at 10X and 40X magnification on a Zeiss Axio Vert. A1 microscope with AxioCam|cm1 camera (Carl Zeiss Microscopy Ltd, Cambridge, UK) using DAPI and fluorescein isothiocyanate (FITC) filters. Images were merged and numbers of $FITC^{+ve}$ cells versus total $DAPI^{+ve}$ cells counted using ImageJ v.1.8.

2.4.9. Histological Image Analysis

A Nikon Eclipse E400 microscope with SPOT camera and software (Image solutions UK Ltd.) was used to visualise all non-fluorescent, non-polarised stained slides. For wound area and width measurements, H&E and KRT14 stained images were captured at 4X magnification. For other epidermal measurements and cell counts, images were captured at 20X magnification. Wound measurements and cell counts were analysed in ImagePro-Plus v.6.3.0 (Media Cybernetics, Finchampstead, UK). Scale bars and calibrations were created from graticules taken on the Nikon Eclipse E400 microscope and SPOT camera (above).

Wound area was determined as the area from the normal skin margins on either side of the wound, down to the *panniculus carnosus* muscle, and underneath the wound clot or epidermis (depending on healing stage). Wound width was determined as the width between the normal skin margins on either side of the wound (see **Figure 2.3**). Percentage wound re-epithelialisation (closure) was determined by dividing the sum of the lengths of the newly formed epidermis (neo-epidermis) by the full wound distance (see **Figure 2.4**).

KRT6 immunohistochemistry (IHC) was used to measure epidermal hyperproliferation and differentiation (Mommers et al., 2000). An average of the distance contribution and neo-epidermal area was taken from the left and right wound sides. Neo-epidermal area and distance was quantified in ImagePro-Plus v6.3.0. $Ki67^{+ve}$ epidermal basal cells were counted within 500 μm of the leading wound edge. Cells two frames from the leading edge were included in epidermal TUNEL analysis. Dermal cell counts were determined from five representative pictures of each wound (**Figure 2.5**). Stained cells were counted using ImagePro-Plus v.6.3.0 and a colour threshold tool. Areas were determined to give positively stained cells per mm^2 of tissue.

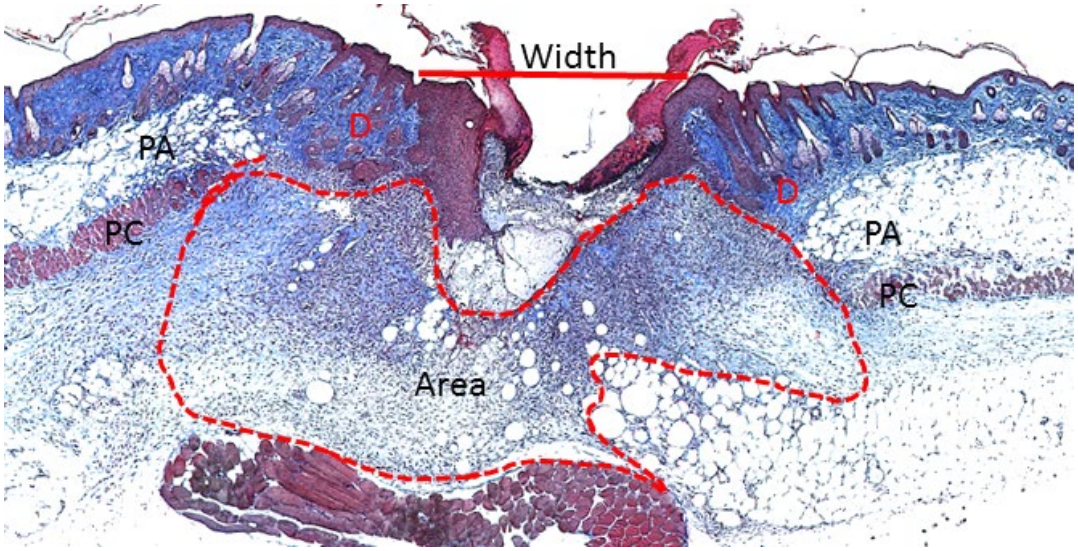

Figure 2.3. Masson's Trichrome staining showing wound width and area measurements. Width (red line) is measured to the normal skin (**D** to **D**). Wound area (dotted red line) is measured as the granulation tissue under the wound clot to the *panniculous adiposus* (**PA**) and *panniculus carnosus* (**PC**) on either side of the wound, down to the underlying body wall. Adipose tissue (white, bubbles) below the PC is excluded. Aged incisional wound at day 7 post-injury. *Histology by HNW*.

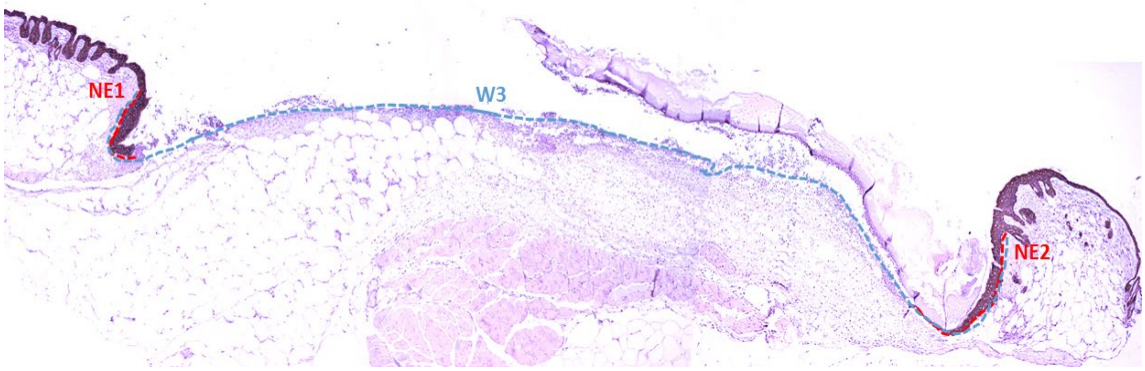

Figure 2.4. Keratin 14 immunohistochemistry demonstrating measurement of re-epithelialisation. Re-epithelialisation (percentage wound closure) is determined by measuring the distance of the newly formed epidermis (neo-epidermis, **NE**) on either side of the wound (**NE1** and **NE2**) as a percentage of total wound width (**W3**). Diabetic excisional wound at day 3 post-injury. Red staining = keratin 14. *Histology by the author (HNW)*.

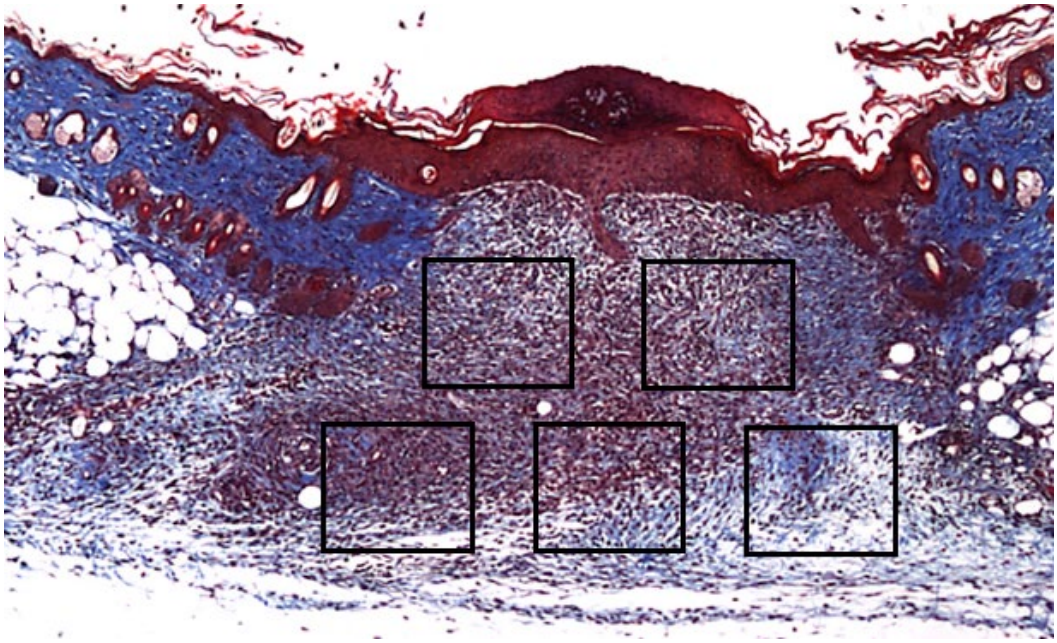

Figure 2.5. Example of dermal cell count measurements. From each wound, five representative images (five boxes, above) are taken within the granulation tissue at 20X magnification. Average number of positively-stained cells per mm^2 for each wound is determined in ImagePro v.6.3.0. Masson's Trichrome stain of a young, day 7 incisional wound. *Histology by the author (HNW)*.

2.5. Inductively Coupled Plasma Mass Spectrometry

Inductively coupled plasma mass spectrometry (ICP-MS) is a method most commonly used for detecting metal concentrations in non-biological samples, but was repurposed to measure total metal abundance in skin and wounds (see **Figure 2.6** and **Figure 2.7**). Tissue from mice and humans was frozen at -80°C and freeze dried in TMF vacutainers at -50°C and 0.03-0.04 mBAR for 3 days. Freeze-dried tissue samples, along with a certified reference material (DOLT-5 dogfish liver, National Research Council, Canada) were weighed in trace metal free 50 mL falcons and dissolved overnight in a 50:50 solution of concentrated TMF HNO_3 and 30% H_2O_2 (as in Ouypornkochagorn & Feldmann, 2010). Blanks containing only HNO_3 and H_2O_2 were included and showed no trace metal contamination. The next day the samples, blanks and reference material were further digested in a MARS 6 microwave with a MARSXPRESS™ vessel (CEM Microwave Technology Ltd., Dublin, UK) at 400W power using the following cycling parameters: Ramp to 75^0C for 5 minutes; hold at 75^0C for 30 minutes; ramp to 95^0C for 5 minutes and; hold at 95^0C for 60 minutes. Once cool, NORMATOM® TMF water (VWR, Leicestershire, UK) was added to each digested sample to make a final concentration of 25% HNO_3. Higher concentrations of HNO_3 are not recommended as they alter the efficiency of sample ionisation (Evans et al., 2003). Samples were analysed on an Agilent 7500cx

inductively coupled plasma mass spectrometer (Agilent Technologies, UK). Internal standards ranged from 1-100 ppb (parts per billion), were prepared in 25% HNO_3, and used as calibration. A water reference standard (CRM 1643E) was also included for verification of the internal standards.

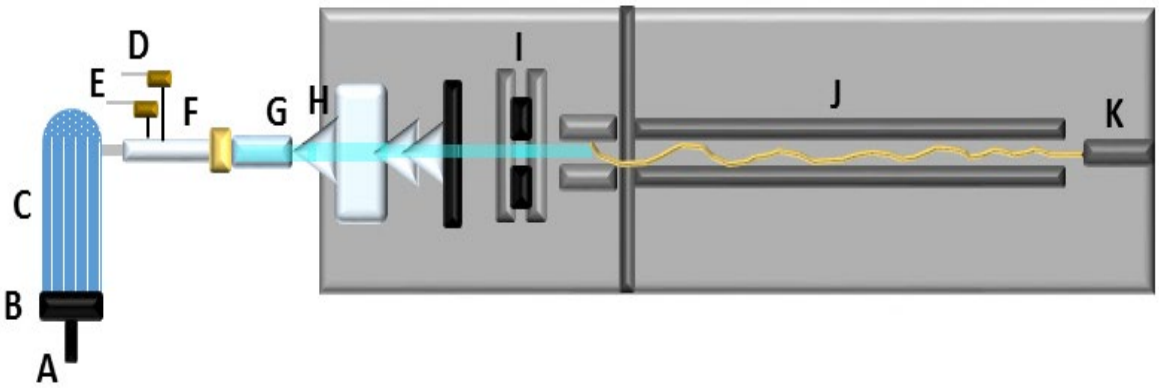

Figure 2.6. Schematic of the ICP-MS set up. A digested sample is vapourised by a pneumatic nebuliser (**A**) and transported through a carrier gas (**B**) into the spray chamber (**C**). The sample aerosol is passed into the plasma (enters the system through **D**, created through auxillary gas, **E**) contained in the torch (**F**). The torch contains a high power, high frequency electrical current which creates a magnetic field. The high current causes free electrons from the sample to collide with argon atoms, producing ions and electrons. Once a stable high plasma temperature is reached, the aerosol droplets are rapidly dried, decomposed, vaporised, atomised, and finally ionised by the removal of an electron. The positively charged ions (**G**) hit the interface cones (**H**) which extract the ions into the mass spectrometer vacuum system. Electrostatic lenses (**I**) keep the ions in a compact ion beam as they pass through to the mass spectrometry chamber. The most common mass analyser in ICP-MS is the quadrupole (**J**). The quadrupole is a combination of direct and alternating current that separate the ions based on their mass to charge ratio (m/z). As the system contains only positively charged ions, the m/z is equal to the mass of the ion, making spectrum interpretation easier than other mass spectrometry methods. Finally, the electron multiplier (**K**) detects each ion as it exits the quadrupole, storing information on the m/z for each ion to create a mass spectrum (**Figure 2.9**; as discussed in Bradshaw et al., 1989 & Baker & Miller-Ihli, 1999). *Illustration created by the author (HNW).*

2.6. *In Vitro* Analysis

2.6.1. Passage of Cells

Confluent, adherent cells were split using 0.25% trypsin. Trypsin was neutralised with media containing 10% FBS, or with trypsin neutralising solution (Cascade Biologics, Thermo Fisher Scientific) in serum-free culture. For suspension cells (THP-1 cells), cell suspension was removed from flasks without the need to trypsinise. Cell suspensions were pelleted via centrifugation at 300 x g for five minutes and split into plates or flasks for subsequent assays or passaging.

In culture, primary cells can divide a finite number of times (~50) before dying, and show signs of ageing when they approach this limit, originally described in primary

HDFs (Hayflick & Moorhead, 1961). This phenomenon has been attributed to telomeres, which critically shorten with increased replication (Allsopp et al., 1995), eventually eliciting a DNA damage response that triggers senescence (IJpma & Greider, 2003; **Chapter 3**). For most assays, primary murine or primary human cells were used. Therefore, for functional, transcriptional and translational studies, cells were used between their fourth and seventh passages. As cells were used in early passages, monitoring for senescence was not required. Primary keratinocytes were used immediately after isolation due to their inherent nature to differentiate

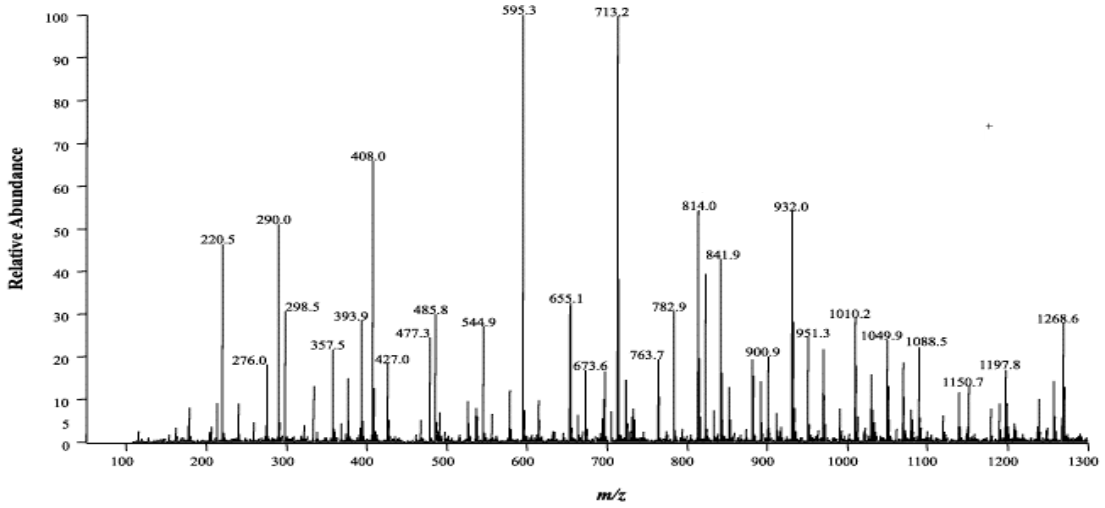

(reviewed by Watt, 2002). Similarly, primary Mφs were either used immediately for assays or frozen in liquid nitrogen prior to their differentiation from bone marrow.

Figure 2.7. Example of a mass spectrum output for ICP-MS analysis. The mass spectrum provides a qualitative representation of the sample, where the magnitude of each peak is proportional to the concentration of an element in a sample. Calibration standards of known abundance are included, allowing direct comparison of the signal intensities between standards and samples to generate numerical data. *Figure from Augusti et al. (2004)*.

2.6.2. Scratch Migration Assay

Scratch migration assays were performed to assess the migratory ability of keratinocytes and fibroblasts following treatment. Confluent flasks of cells were seeded into 24 well plates and left for 2 days to settle and reach an exponential growth phase (determined by in house growth kinetic measurements). By this point, scratches were performed on confluent wells by scratching a line through the centre of the well with a sterile 1 mL filter tip. For all scratch assays, cells were starved to 2% FBS (unless grown in serum-free culture) with treatments added. A 0hr scratch was included on each plate by staining the well with 1% (w/v) Crystal Violet (Sigma-

Aldrich). Plates were incubated at 37°C and 5% CO_2 until collection. Upon collection, media was aspirated from the wells, which were rinsed in DPBS, incubated in Crystal Violet and topped with dH_2O (as above). For imaging, dH_2O was aspirated and plates were photographed on a Nikon E400 microscope. Percentage closure was deduced from the zero-hour scratch measured in ImageJ v.1.8.

2.6.3. Adhesion Assay

Plates were coated in collagen I (Sigma-Aldrich) for HDF adhesion (see **Appendix 2A.15**). Cells were seeded into wells at a density of 1 x 10^5 per well (12 well plate) and incubated for 30 minutes at 37°C and 5% CO_2 to allow attachment. After this time, media was aspirated, wells were washed in DPBS to remove non-adherent cells and adherent cells were stained with 1% Crystal Violet solution. Images were taken on an E400 Nikon microscope as previously described and attached cells per mm^2 enumerated in ImagePro-Plus v. 6.3.0.

2.6.4. MTS Tetrazolium Assay

An MTS Tetrazolium Assay was performed using CellTiter96® AQ_{ueous} One (Promega, Southampton, UK), a colorimetric assay for detection of viable cells. Here, phenazine ethosulfate is reduced within viable cells, exits the cell and converts tetrazolium salt into soluble formazan. The amount of soluble formazan is then quantified (Riss et al., 2016). This assay was repurposed to measure THP-1 cell adherence (**Section 5.3.12.2**). CellTiter96® (20 µL) was added to each well, incubated as per manufacturer's instructions and read at 492 nm on a plate reader (ThermoScan, Thermo Fisher Scientific).

2.6.5. Fibroblast Contraction Assay

A contraction assay was modified from Vernon & Gooden (2002) to assess the contractile ability of HDFs *in vitro*. A 10X DMEM/MEM and sodium bicarbonate ($NaHCO_3$) solution was prepared from powder (Thermo Fisher Scientific), with 1% penicillin-streptomycin and 2.5 µg/mL amphotericin B solution. On ice, 4 mL collagen type I from rat tail (Corning, New York, US) was added to 500 µL 10X DMEM/MEM (and 10X $NAHCO_3$), 200 µL 0.1M sodium hydroxide (NaOH) and 300 µL FBS. Cells were seeded at 1.5 x 10^5 cells per mL collagen solution and left to gel at 37°C and 5% CO_2 for 20-30 minutes. Wells were then topped up with media containing treatments. Gel discs were dislodged from the sides of the culture wells

and plates were incubated at 37°C and 5% CO_2 until collection. Contracted gels were imaged and gel weights were obtained using a microbalance.

2.6.6. Flow Cytometry

Flow cytometry was used to assess cell viability via propidium iodide (PI, Thermo Fisher Scientific) and calcein AM (BD Biosciences) staining. PI is a cell impermeable dye that intercalates with DNA. When bound to DNA, the fluorescent intensity of the dye increases 20-fold (Arndt-Jovin & Jovin, 1989), therefore causing intensive staining of the nuclei of cells with disrupted cell membranes (e.g. late apoptotic and necrotic cells; Rieger et al., 2011). The forward-angle light scatter (or cell diameter) and side-angle light scatter (or cell granularity) of the cells can also be used as an assessment of viability. Here, necrotic cells initially swell due to loss of membrane integrity, and apoptotic cells gain increased granularity due to the formation of apoptotic bodies (Vermes et al., 2000).

On the contrary, live cells can be stained with calcein AM, a lipophilic dye that enters cells through the cell membrane. Cleavage of calcein from acetoxymethyl esters requires hydrolysis by esterases (only apparent in live cells), resulting in release of an intense green fluorescence (Bratosin et al., 2005). Viability of HDFs was assessed following calcium and iron treatment via calcein AM staining, although iron is known to quench calcein (Tenopoulou et al., 2007). HDFs were seeded into 6 well plates and treated at 80% confluence for up to 11 days. Upon collection, media and cells were pelleted and counted via trypan blue exclusion. Cell pellets were washed with sterile PBS/sodium azide (0.15% v/v NaN_3 in PBS), re-suspended in PI (10 µg/mL working concentration) or calcein AM (5 µM working concentration) and incubated at RT for 10 minutes (PI) or 30 minutes (calcein AM). PI was read on the FL-2 (585/42) and FL-3 (670/LP) channels (emission filters), while calcein AM was read on the FL-1 (530/30) channel, of a BD FACSCalibur™ (BD Biosciences). Applied gains and voltages across all channels were kept equivalent between treatment groups. Cell viability was assessed from the peak shift of ethanol-treated (PI) or control live (calcein AM) cells (**Figure 2.8**).

2.6.7. Matrix Work

2.6.7.1. Preparation of Cell-Derived Matrix Proteins

HDFs were seeded into 24 well plates with coverslips (for scanning electron microscopy and immunofluorescence), or 6 mm^2 dishes (for ECM) and incubated at

37°C and 5% CO_2 until confluent. Media was aspirated, cells were washed in DPBS and treatment media was added. Media was replaced every 3 days and cells were left to deposit matrix for 11 days at 37°C and 5% CO_2. Five days prior to collection, media was changed for the final time. HDFs were collected at 3 days for RNA.

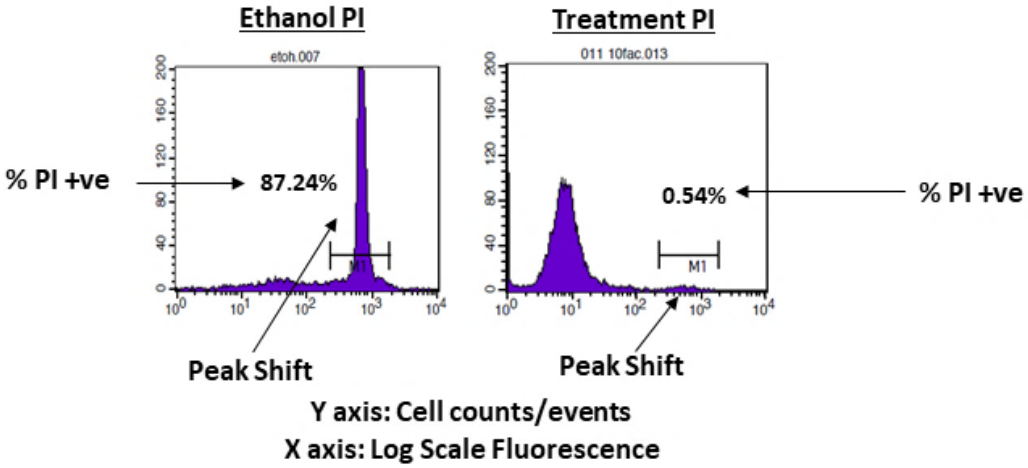

Figure 2.8. Example of propidium iodide flow cytometry analysis. Voltages applied within each channel are adjusted to visualise cell populations as peaks on histograms (cell counts versus fluorescence). Cells with the highest fluorescent intensity shift towards the right (e.g. ethanol treated, propidium iodide [PI] stained cells). Markers are placed on control peaks (ethanol peak for PI, control live peak for calcein AM) and the marker placed in the control position for each treatment. Thus, for stained cells, a higher shift to the right results in a higher percentage of cells falling within the marker range and being classed as positive for dye uptake. *Image by the author (HNW).*

2.6.7.2. Preparation of Cell Lysates

Media was collected in tubes on ice and supplemented with (western blot analysis) or without (zymography) 1 mM Halt protease and phosphatase inhibitor cocktail (Pierce, Thermo Fisher Scientific) before storing at -80°C. Cells were pelleted, placed on ice and lysed with ice-cold RIPA buffer (150 mM sodium chloride, 1% Triton X-100, 0.5% sodium deoxycholate, 0.1% SDS, 50 mM Tris-HCl [pH 8.0] and 1X Halt protease and phosphatase inhibitor cocktail) for two minutes. Lysates were collected in cold Lobind Eppendorf tubes, sonicated for 3 x 10 second pulses and centrifuged at 12, 000 rpm and 4°C for 20 minutes. Supernatant was collected into fresh, cold Lobind Eppendorf tubes and stored at -20°C until use.

2.6.7.3. Extraction of Extracellular Matrix

Media was aspirated from dishes and HDFs were removed from the deposited matrix with denuding buffer (see **Appendix 2A.15**). The remaining ECM was rinsed

gently with DPBS and treated with 10 µg/mL DNAse I (Roche, Sigma-Aldrich) in DPBS for 30 minutes at 37°C and 5% CO_2. ECM protein was extracted with 500 µL UPX buffer (Expedeon, Cambridgeshire, UK). The samples were vortexed briefly and left on a MACSmix™ Tube Rotator (Miltenyi Biotec) at 4°C O/N. The samples were then heated to 100°C on a heat block for 5 minutes, cooled for one hour at 4°C, and centrifuged at 13, 000 rpm at 4°C for 15 minutes. The supernatant was collected in fresh Lobind Eppendorf tubes and stored at -80°C.

2.6.7.4. Western Blotting

2.6.7.4.1. Sample Preparation and Gel Separation

Western blotting was performed to measure the expression of proteins in cells. Here, protein samples were separated by molecular weight on sodium dodecyl sulfate-polyacrylamide gel electrophoresis (SDS-PAGE) gels, transferred to nitrocellulose membranes and incubated in primary antibodies for detection of proteins of interest. HRP-linked secondary antibodies were bound to the primary antibodies, and HRP substrate was detected via chemiluminescence.

To determine protein concentrations within samples, a Pierce Bicinchoninic Acid (BCA; Thermo Fisher Scientific) assay was used as per manufacturer's instructions. Bovine serum albumin was included to produce a standard curve. Cell and ECM protein was collected as previously described, protein concentration was adjusted, and protein samples were added to electrophoresis sample loading buffer prior to loading in SDS-PAGE separating gels with 4% stacking gels (recipes in **Appendix 2A.17-2A.19**). Acrylamide percentage in the separating gel was dependent on the protein of interest. High molecular weight proteins (e.g. COL1A1 and FN1) were run on 7% gels, while low molecular weight proteins (e.g. ferritin and PDGFA) were run on 12% gels. A Precision Plus Protein™ Kaleidoscope™ pre-stained standard (Biorad Laboratories Ltd.) was included in the first lane (5 µL) as a molecular weight marker. Gels were run for 1.5-2 hours at 90V in a mini protean III gel tank (Biorad Laboratories Ltd.) using 1X tris-glycine-SDS (TGS) running buffer (**Appendix 2A.20-2A.21**).

2.6.7.4.2. Protein Transfer

Following SDS-PAGE, gels were transferred onto nitrocellulose membranes (0.2 µm; Amersham, GE Healthcare Life Sciences, Buckinghamshire, UK). Nitrocellulose, thick

filter papers (Thermo Fisher Scientific) and blotting sponges (Biorad Laboratories Ltd.) were soaked in transfer buffer (**Appendix 2A.22**) prior to assembly of the Mini Trans-Blot Electrophoretic Transfer Cell apparatus (Biorad Laboratories Ltd.; **Figure 2.9**). Gels were stacked closest to the cathode and transferred at 4°C and 70V for 1-2 hours, depending on the size of the proteins of interest. Longer transfer times were required for larger proteins. The transfer was checked by assessing the protein ladder transfer, and proteins were visualised on the nitrocellulose membranes via Ponceau S (0.1% solution in 5% acetic acid, Sigma-Aldrich) staining.

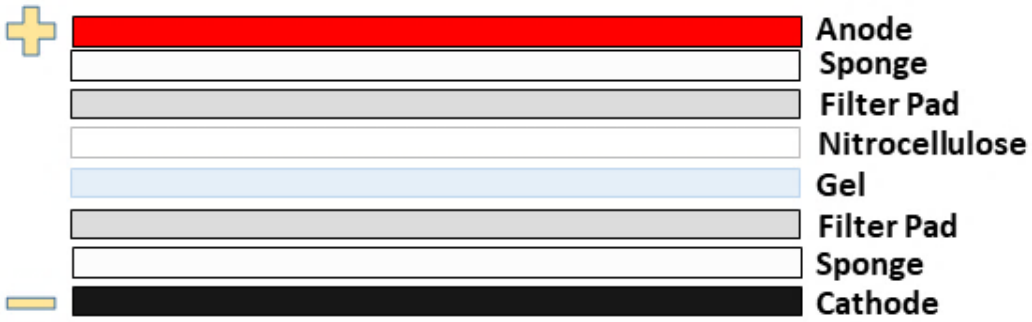

Figure 2.9. Assembly of apparatus used for wet transfer of proteins onto nitrocellulose membrane. Sponges, filter pads and nitrocellulose are pre-wetted in transfer buffer and assembled in an open transfer cassette. The gel is removed from the glass plate, rinsed in running buffer and placed on top of the filter pad closest to the cathode ("-"). The nitrocellulose membrane is placed on top of the gel and air bubbles are removed from the system using a roller. The cassette is closed tightly, added to a tank of transfer buffer and current is applied. *Figure drawn by the author (HNW).*

2.6.7.4.3. Immunoblotting

Membranes containing transferred proteins were blocked overnight at 4°C in 5% (w/v) non-fat milk (in TBST, see **Appendix 2A.23-2A.24**). Membranes were washed in 1X TBST, primary antibodies were diluted in 0.5% non-fat milk block, and membranes sealed with primary antibody (**Table 2.3**) for one hour at RT. Membranes were washed in 1X TBST and incubated in HRP-conjugated secondary antibody (GE Healthcare Life Sciences), diluted in 1X TBST, for one hour at RT. Following final TBST washes to remove unbound secondary antibody, chemiluminescent detection was achieved using SuperSignal™ West Pico PLUS chemiluminescent substrate (Thermo Fisher Scientific). X-ray film (CL-exposure film, Thermo Fisher Scientific) exposure was carried out in a dark room. Films were: a) developed (developer and replenisher, Kodak, Hertfordshire, UK); b) rinsed in 5% acetic acid in dH_2O; c) fixed (Kodak fixer and replenisher) and; d) rinsed in tap water and left to dry. Bands were quantified as relative expression of the control via densitometric analysis in ImageJ v.1.8. Beta actin was used as a loading control.

Membranes were stripped in mild stripping buffer (**Appendix 2A.25**) and re-probed with separate antibodies.

Table 2.3. Antibodies used for immunoblotting. *

Primary Antibody	Raised in	Conc.	Manufacturer	Secondary	Dilution	Transfer Conditions
Beta Actin	Mouse monoclonal	1 µg/mL	Sigma-Aldrich	Anti-Mouse HRP	1:5000	70V 1.5hr
Collagen I	Mouse monoclonal	0.4 µg/mL	Sigma-Aldrich	Anti-Mouse HRP	1:1000	70V 2hr
Fibronectin	Mouse monoclonal	0.3 µg/mL	Santa Cruz	Anti-Mouse HRP	1:500	70V 2hr
Vimentin	Mouse monoclonal	0.4 µg/mL	Santa Cruz	Anti-Mouse HRP	1:500	70V 2hr
PDGFA	Mouse monoclonal	0.4 µg/mL	Santa Cruz	Anti-Mouse HRP	1:500	70V 1.5hr
Collagen 6A1	Mouse monoclonal	0.4 µg/mL	Santa Cruz	Anti-Mouse HRP	1:500	70V 2hr
Ferritin	Mouse monoclonal	0.4 µg/mL	Santa Cruz	Anti-Mouse HRP	1:500	70V 1.5hr

**Primary antibody dilutions were determined by optimisation experiments. All antibodies were incubated at room temperature for one hour with constant agitation. Conc. = concentration.*

2.6.7.5. Liquid Chromatography Mass Spectrometry

Liquid chromatography mass spectrometry (LC-MS) was used to determine the protein expression profiles of cell-derived ECM following metal treatment. This technique allows for the separation of proteins via liquid chromatography prior to mass spectrometry analysis, thus is useful for the identification of thousands of peptides in an efficient and reproducible manner (Ocak et al., 2009).

Protein was extracted from denuded ECM using UPX buffer (as described above). For label free LC-MS analysis, isolated protein requires reduction, denaturing, alkylation and trypsin digestion (Gundry et al., 2009). Isolation of protein with UPX buffer negates the need to reduce the proteins. Therefore, the FASP Protein Digestion Kit (Expedeon) was used for denaturing, alkylation and trypsin digestion of proteins. Kit reagents were prepared and all steps followed as per manufacturer's instructions. For trypsin digestion, Thermo Scientific™ Pierce™ MS Grade Trypsin Protease (Thermo Fisher Scientific) was used. The collected filtrate was transferred to a clean Lo-bind Eppendorf tube and acidified with 0.5% (v/v) trifluoracetic acid. Insoluble proteins were pelleted (13, 000 rpm for 10 minutes) and clear filtrate was collected in fresh tubes and stored at -80°C until desalting.

Desalting is a fundamental requirement to ensure all salts and buffers that can interfere with mass spectrometry applications are removed (Gundry et al., 2009). Here, reverse phase resins capture the proteins within the column, allowing elution following washes. Pierce™ C18 Spin Columns (Thermo Fisher Scientific) were used for the capture of hydrophobic proteins. The subsequent eluted proteins were dried in a centrifugal vacuum evaporator (45°C for 30 minutes) and stored at -80°C until mass spectrometry analysis. For analysis, dried protein was re-suspended in 30 µL of LC-MS loading buffer (0.1% formic acid with 2% acetonitrile in LC-MS grade water). Samples were then loaded into a refrigerated tray in the UltiMate™ 3000 RSLCnano System using an Acclaim™ PepMap™ 100 C18 LC Column (75 µm x 250 mm; both Thermo Fisher Scientific) for liquid chromatography. Each sample was injected into the column in duplicate with blanks (0.1% formic acid with 2% acetonitrile in LC-MS grade water) run between each sample. Mass spectrometry was performed using a Bruker Impact qQTOF and ProteinScape 3.1 software (Bruker, Coventry, UK). Proteins were identified using the MASCOT 2.1 database.

2.6.7.6. Matrix Immunocytochemistry

Fibroblast-derived ECM was visualised via fibronectin, collagen III and collagen I immunocytochemistry (ICC; **Table 2.4**). HDFs were denuded or stained with their ECM. Wells were blocked in 1% bovine serum albumin (BSA, in DPBS) for 1 hour at RT. Primary antibodies were added to the wells in 1% BSA (in DPBS) and stored at 4°C O/N. Primary antibodies were aspirated from the wells, the wells were rinsed in DPBS, and cells were incubated in Alexa Fluor™-conjugated secondary antibodies (Thermo Fisher Scientific) at a 1:200 concentration (in DPBS) for 1 hour at RT. Wells were rinsed well in DPBS, and coverslips were mounted onto slides containing MOWIOL mounting medium (see **Appendix 2A.14**). Stained ECM was visualised via confocal microscopy and quantified via corrected total cell fluorescence (CTCF; McCloy et al., 2014) or threshold analysis in ImageJ v.1.8.

2.6.7.7. Confocal Microscopy

A confocal laser scanning microscope (LSM 710, Zeiss) equipped with 2.5x, 10x and 20x objective lenses and ZEN 10 software (Carl Zeiss Ltd., Cambridge, UK) was used to image ICC stained cells and double immunofluorescence on paraffin embedded tissue sections. DAPI, Alexa Fluor® 488, Alexa Fluor® 594 and Alexa Fluor® 647 were excited using the 405 nm diode, 488 nm argon, 561 nm and 633 nm lasers,

respectively. Pinhole size was equalled between all lasers for optimum confocality. Settings for each laser (laser power, master gain, digital gain and digital offset) were kept consistent within experiments to avoid bias and allow accurate intensity determination and quantification. All images were exported as LSM files and imported into ImageJ v.1.8 for subsequent analysis.

Table 2.4. Primary antibodies used for immunocytochemistry. *

Primary Antibody	Dilution	Raised in	Manufacturer
Arginase1	0.5 µg/mL	Goat Polyclonal	Santa Cruz
Calmodulin 1	1 µg/mL	Mouse Monoclonal	Abcam
CASR	2 µg/mL	Mouse Monoclonal	Abcam
Collagen I	0.5 µg/mL	Mouse Monoclonal	Santa Cruz
Collagen III	0.5 µg/mL	Mouse Monoclonal	Santa Cruz
CXCL2	0.5 µg/mL	Goat Polyclonal	Abcam
Ferritin	0.5 µg/mL	Rabbit Monoclonal	Abcam
Fibronectin	0.5 µg/mL	Mouse Monoclonal	Santa Cruz
Keratin 1	1 µg/mL	Rabbit Polyclonal	Covance
Keratin 14	1 µg/mL	Rabbit Polyclonal	Covance
Loricrin	1 µg/mL	Rabbit Polyclonal	Covance
Nos2	2 µg/mL	Rabbit Polyclonal	Santa Cruz
p16	1 µg/mL	Rabbit Polyclonal	Santa Cruz
p21	1 µg/mL	Mouse Monoclonal	Abcam
PDGFA	1 µg/mL	Mouse Monoclonal	Santa Cruz

**All primary antibodies incubated overnight.*

2.6.7.8. Scanning Electron Microscopy

Cells seeded on coverslips were left to deposit matrix for 11-14 days as previously described. Media was aspirated, cells were rinsed in DPBS, and coverslips were fixed in 2.5% glutaraldehyde (in dH_2O) for 2 hours. Coverslips were rinsed in DPBS (3 x 10 minutes) to remove glutaraldehyde, and stored overnight at 4°C in fresh DPBS.

The following day, coverslips were dehydrated up and ethanol series (30%, 50%, 70%, 90%, 100% and 100%, 15 minutes each) prior to critical point drying (CPD) with CO_2. CPD is vital for SEM imaging to prevent water molecules interfering with the vacuum within the SEM, and to prevent subsequent collapse of tissue specimens (Bray, 2000). Within the CPD apparatus, absolute ethanol (stored in molecular sieve) was exchanged with liquid CO_2 over an hour, with ethanol flushed twice during this time. The temperature of the apparatus was then increased to 41°C on a thermocirculator (HU1000-E3500, Betta-Tech Controls Ltd., Milton Keynes, UK), making the temperature inside the chamber 37°C and the pressure 1400psi. As the critical point of CO_2 is around 35°C and 1,200psi (Bray, 2000), the CO_2 vapourises without changing density or surface tension, thus tissue structure is maintained. Following CPD, coverslips were mounted onto pegs and sputter coated in carbon prior to imaging on a Zeiss EVO60 scanning electron microscope.

2.6.8. Transfection

2.6.8.1. Bacterial Transformation

Bacterial transformation was performed using Subcloning Efficiency™ DH5α™ Competent Cells (Thermo Fisher Scientific). Briefly, 1-10 ng plasmid DNA was mixed with 50 µL of competent cells and incubated on ice for 30 minutes. Cells were heat shocked by transferring to 42°C for 20 seconds, then returning to ice for two minutes. Pre-warmed Super Optimal broth with Catabolite repression medium (Thermo Fisher Scientific) was added to the competent cells, which were then incubated at 37°C for an hour with 225 rpm shaking. The resultant culture was plated onto antibiotic-containing selective agar plates. For the pUC19 plasmid control, used to determine transformant efficiency, selective plates contained 100 µg/mL ampicillin. For the pUNO1 control vector and pUNO1-hCXCL2 plasmid, the selective plates contained 100 µg/mL blasticidin. Plates were incubated at 37°C O/N and colonies present (e.g. transformed colonies) selected for plasmid amplification in Luria-Bertani broth containing blasticidin at 100 µg/mL.

2.6.8.2. Plasmid Purification

Plasmid DNA was purified from cultures of transformants using a QIAGEN plasmid midi kit (Qiagen, Manchester, UK) following manufacturer's instructions. DNA was eluted in Tris-EDTA buffer (Sigma-Aldrich) and plasmid purity was determined using a SimpliNano nanodrop spectrophotometer (Thermo Fisher Scientific).

2.6.8.3. Transfecting Mammalian Cells

Lipid-mediated transfection of HDFs was performed using Lipofectamine 3000 (Thermo Fisher Scientific) following manufacturer's instructions. An empty pUNO1 vector was included as a plasmid control and a yellow fluorescent protein (YFP) plasmid (a kind gift from Dr Cheryl Walter, Biomedical Sciences, The University of Hull) added as a control for transfection efficiency. After 48 hours, control cells were visualised for YFP expression using the Livecyte™ imaging platform. Transfected HDFs were collected for ICC and SA-βGAL staining. Experiments performed with the transfected cells are described in detail in **Chapter 3**.

2.6.9. Murine Macrophage Assays

2.6.9.1. Macrophage Growth and Differentiation

Mononuclear phagocyte progenitor cells from bone marrow were cultured in bone marrow medium (**Appendix 2A.5-2A.6**). WT and NDb cells were cultured in low glucose media, while aged and Db cells were cultured in high glucose media, to more closely mimic a pathological environment (Kanter et al., 2012). In the presence of proper cytokine stimulation (e.g. with Mφ colony-stimulating factor, M-CSF), mononuclear phagocytes proliferate and differentiate through monoblast, promonocyte and monocyte stages before becoming Mφs (reviewed in Ushach & Zlotnik, 2016; **Chapter 1**). L929 cells (CCL-1, ATCC, Middlesex, UK), which secrete M-csf (Rios et al., 2017), were cultured to provide conditioned media (CM) for Mφ differentiation (see **Figure 2.10**). Media was collected from L929 cells every 2 days, sterile-filtered (0.22 μm) and stored at -20°C until use. Mφs were differentiated for 7 days, serum starved and polarised.

2.6.9.2. Macrophage Polarisation

On day 7 post-seeding, Mφs were serum-starved for six hours prior to activation. To classically activate (M1-polarise) Mφs, cells were treated with 100 ng/mL Ifn-γ (Gibco, Thermo Fisher Scientific) and 1 μg/mL LPS (Sigma-Aldrich). To alternatively activate (M2-polarise) Mφs, 50 μg/mL InVivoMab anti-Ifn-γ (BioXCell, New Hampshire, US) and 20 ng/mL Il-4 (Sigma-Aldrich) was added to fresh culture media. Non-polarised Mφs were treated with media only. Treatments were added at the time of polarisation for RNA, or the following day for phagocytosis. Cells were incubated O/N at 37°C and 5% CO_2 and collected for analysis via ICC, quantitative

real-time polymerase chain reaction (qRT-PCR; see **Appendix 2A.32** for primer sequences), or used in phagocytosis experiments.

2.6.9.3. Macrophage Phagocytosis

Phagocytosis assays were performed to functionally assess the effects of metal treatments on Mφs. Following polarisation, media was aspirated and replaced with metal-containing media for six hours. For phagocytosis, *Escheria coli* (*E. coli*) Bioparticles™ were incubated at a multiplicity of infection (MOI) of 10 (10 particles per Mφ) for two hours at 37°C and 5% CO_2. Mφs were collected, fixed in 4% (v/v) formaldehyde solution in PBS, permeabilised in 0.1% Triton X-100 (in PBS) and counterstained with Rhodamine Phalloidin (Invitrogen, Thermo Fisher Scientific) in sterile 1% BSA (w/v, in PBS). Imaging was performed via confocal microscopy, and quantification (CTCF) performed in ImageJ v.1.8. For flow cytometry, THP-1 cells were treated and incubated as above, lifted from their wells with 0.25% trypsin/EDTA (Thermo Fisher Scientific) and resuspended in 0.25% (w/v) BSA. THP-1 cells were then analysed on a BD FACSCalibur™ and CellQuest Pro™ software.

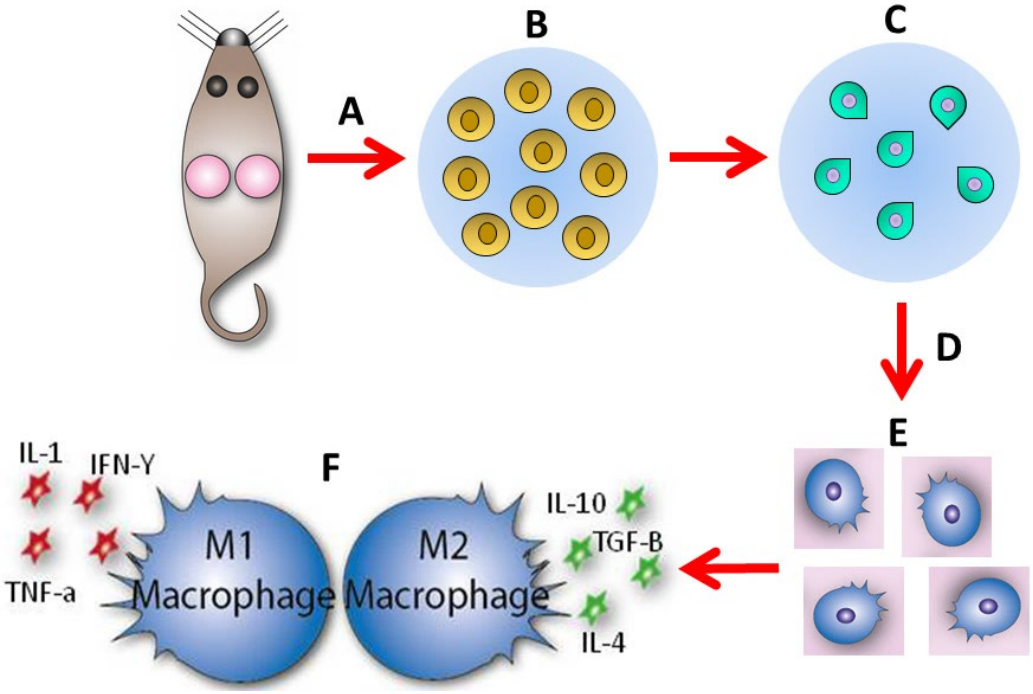

Figure 2.10. Illustration of bone marrow isolation and macrophage culture. Bone marrow is collected from mice (**A**) to isolate myeloid progenitor cells (**B**). Monocytes (**C**) are stimulated with macrophage colony-stimulating factor from L929 cells (**D**) to cause differentiation into macrophages (**E**). Macrophages are polarised to pro-inflammatory (M1) or anti-inflammatory (M2) states with various cytokines (**F**). *Illustration created by the author (HNW).*

2.6.10. LiveCyte™ Live Cell Imaging

To visualise changes in cell behaviour (e.g. migration) in real-time following treatment, the Livecyte™ (PhaseFocus, Sheffield, UK) was used. The Livecyte™ uses a quantitative phase imaging technique known as ptychography to allow label-free, high contrast, phase imaging of cells overtime, thus circumventing the need for fluorescent labels that may damage cells (Suman et al., 2016). Further, as the method records diffraction patterns of individual cells over time, the images can be re-focused post-imaging, preventing the loss of images through focal drift (Kasprowicz et al., 2017). The diffraction patterns are processed by an algorithm to provide information on cell characteristics, such as cell thickness, weight and migration (Kasprowicz et al., 2017). The Livecyte™ was specifically used in **Section 4.4.8** to quantify changes in cell migration following treatment. Scratch assays were prepared and plates inserted into the Livecyte™ imaging platform. Central areas within each well were focused and the acquisition software started. Data was analysed using scratch analysis and single cell segmentation within the CAT software (PhaseFocus). Tiff stacks, videos and CSV files were exported. Single cell segmentation was analysed in R v.3.6.1. (R Core Team, 2019) using 'ggplot2' (Wickham, 2016), 'reshape' (Wickham, 2007), 'dplyr' (Wickham et al., 2019), 'plyr' (Wickham, 2011) and 'matrixStats' (Bengtsson, 2018) packages.

2.7. Quantitative Real-Time Polymerase Chain Reaction

2.7.1. RNA Extraction from Cells and Tissue

Each snap frozen half wound (stored at -80°C) was cut into <1mm pieces and incubated in 1 mL cold TRIzol™ Reagent (Invitrogen, Thermo Fisher Scientific) in Eppendorf tubes. Tissue was homogenised (IKA T10 basic homogeniser, Oxford, UK) for 30 seconds and incubated at RT for five minutes in TRIzol™ Reagent. To every 1 mL TRIzol™ Reagent, 200 µL chloroform was added to each Eppendorf tube and vigorously shaken for 15 seconds. Tubes were centrifuged for 15 minutes at 4°C and 13, 000 rpm. The aqueous phase, containing RNA, was removed and purified using the spin column method in the Invitrogen™ Ambion™ PureLink™ RNA Mini Kit (Thermo Fisher Scientific) following manufacturer's instructions. RNA was stored at -80°C until use. For cells, media was aspirated, wells were rinsed in DPBS and TRIzol™ Reagent was added (750 µL TRIzol™ Reagent per 1 x 10^6 cells). Cells were scraped and added to Eppendorf tubes, and RNA isolated as above.

2.7.2. cDNA Synthesis

Prior to synthesis into complimentary DNA, RNA concentration was determined via a SimpliNano nanodrop spectrophotometer (Biochrom Ltd., Cambridge, UK) and samples adjusted to a final concentration of 1 µg RNA per µL, made up to 10 µL with RNAse free water (Thermo Fisher Scientific). Each sample was incubated in 1 µL Random Primers (Promega) and 1 µL dNTP mix (Promega), denatured at 70°C for five minutes and cooled on ice for two minutes. cDNA mastermix was prepared by adding 100U Bioscript reverse transcriptase (Bioline, London, UK), 4 µL transcription buffer (Bioline), 1 µL RNAse OUT (Invitrogen) and 2.5 µL RNAse free water to each sample. Samples were then placed on a thermocycler (TC-412, Techne, Staffordshire, UK) for set cycling parameters (**Appendix 2A.26**).

2.7.3. Quantitative Real-Time PCR

Primers were designed so that nucleotide sequences were between 18-30 nucleotides long and amplicon product size less than 300. GC content was kept between 40-60% and annealing temperature was between 65-70°C. Sequences of more than four repeated bases were discarded to prevent secondary structure formation (e.g. hairpin loops and primer dimers; Bustin et al., 2009). Nucleotide sequences were obtained from the NCBI gene database and primers designed using Primer3Plus software (Untergasser et al., 2007). Forward and reverse sequences were designed on alternating exons to prevent amplification of contaminating gDNA and sequences were uploaded into BLAST to ensure specificity (Ye et al., 2012). Products were checked by assessing amplification curves (below).

Samples were diluted by three orders of magnitude and plated into 96 well PCR plates. 2X Takyon for SYBR assay (Eurogentec, Hampshire, UK) was added to each well with forward and reverse primers (**Appendix 2A.32-2A.34**). Plates were analysed on a CFX Connect™ platform using CFX Manager™ software (Biorad Laboratories Ltd.). The optimised qRT-PCR cycling protocol is provided (**Appendix 2A.27**), where annealing temperature was optimised for each set of primers used.

Primer amplification was deemed acceptable when amplification curves crossed the relative fluorescent unit (RFU) threshold before 35 cycles (**Figure 2.11**). Primer specificity was shown via melt curve analysis, where a single peak confirmed amplification of a single product (**Figure 2.12**). For analysis, relative expression (based on quantitation cycle values) was determined from a sample standard

(**Figure 2.13**) and a standard curve produced (**Figure 2.14**). Again, primers were deemed optimal if the efficiency of the amplification was between 90-110% and the R^2 of the standard curve equal to one (as per the minimum information for publication of qRT-PCR experiments guidelines, Bustin et al., 2009). Any data sets that fell beyond the optimal range were excluded from analysis.

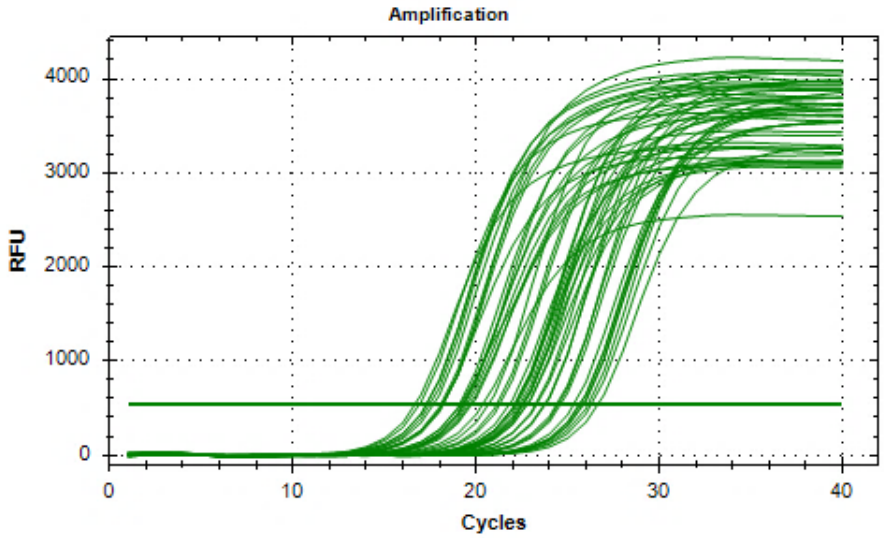

Figure 2.11. Example of good primer amplification. Good primers pass the relative fluorescent unit (RFU) threshold between 15 and 35 cycles, as shown.

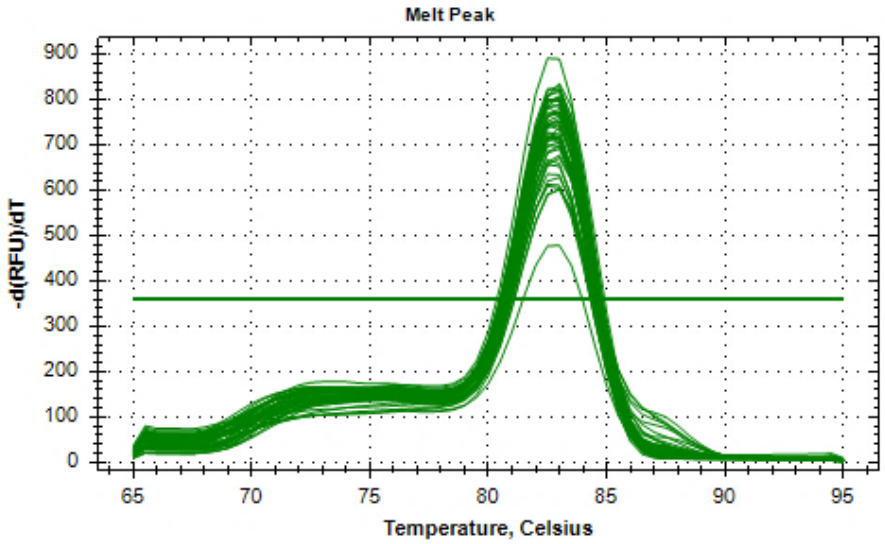

Figure 2.12. Single melt curve peak demonstrating primer specificity. The melt peak plots the rate of change in fluorescence (y axis) against the cycling temperature (x axis). The highest fluorescence is shown when primer annealing (double stranded [ds] DNA) is observed. As the temperature increases, dsDNA denatures and fluorescence is reduced. A single peak indicates primer annealing at a specific temperature and thus, amplification of a single product. Primers with multiple peaks and samples with sub-optimal amplification were excluded from analysis.

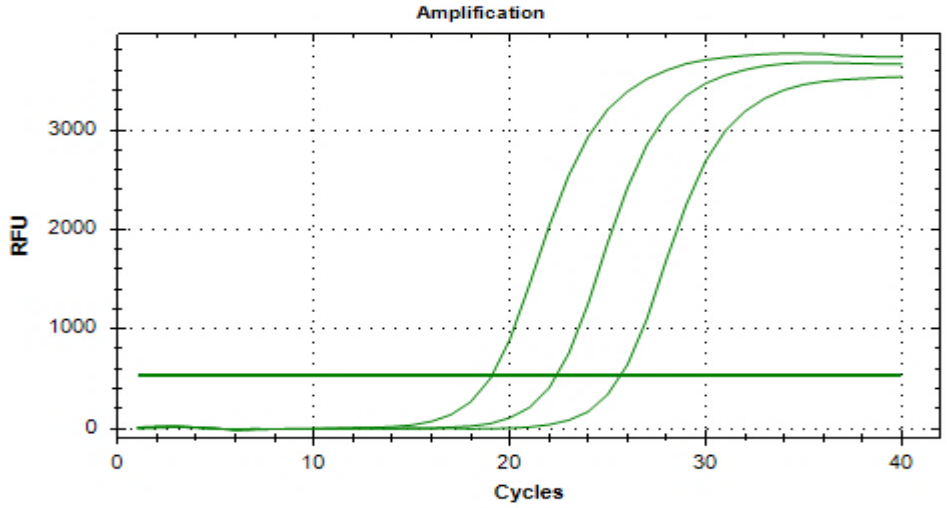

Figure 2.13. Selection of standards to produce a standard curve. A sample, diluted by three orders of magnitude, is chosen to produce a standard curve of the dataset. The dilutions must show equal spacing and adequate amplification (<35 cycles).

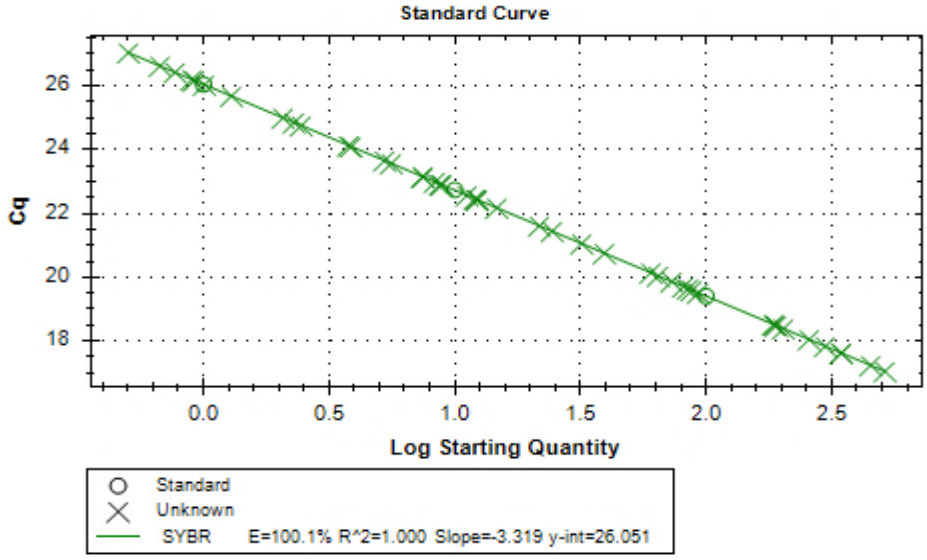

Figure 2.14. Example of a standard curve for data amplified from one primer set. Standards from **Figure 2.13** are shown (circles). All other samples are plotted on the regression line (crosses). Amplification efficiency should fall between 90-100% and the R^2 must equal one. Cq = cycle quantity.

2.8. Microbiological Assays

2.8.1. Bacterial Culture

Reference strains of *P. aeruginosa* (NCTC 10781) and *S. aureus* (NCTC 13297) were chosen as they are directly relevant to chronic wound infection (Price et al., 2009). Glycerol stocks of bacteria stored at -80°C were streaked onto Mueller Hinton agar (MHA; Oxoid, Hampshire, UK) plates and incubated at 37°C for 24-48 hours to produce viable colonies. A single viable colony was added to 10 mL Mueller Hinton

broth (MHB; Oxoid) and shaken (140 rpm, Labnet 211DS shaking incubator, Labnet International, US) for 16 hours (O/N) at 37°C. For all assays, O/N cultures were adjusted to 0.5 on the McFarland turbidity scale (as described in Balouiri et al., 2016), unless otherwise stated (see **Figure 2.15**).

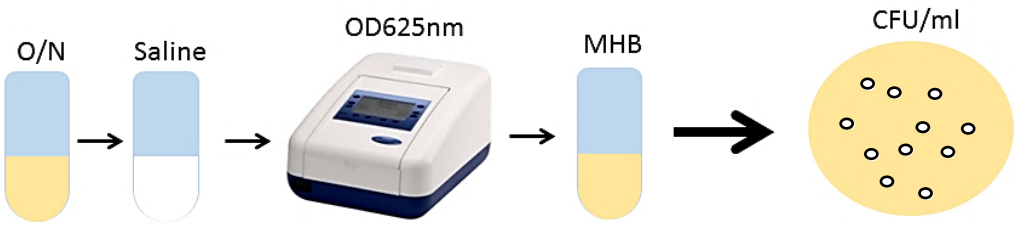

Figure 2.15. Determination of bacterial starting concentrations from overnight cultures. Bacterial overnight (O/N) cultures are adjusted to an optical density (OD) of 0.08-0.12 at 625 nm on a Jenway spectrophotometer (Jenway 7310, Cole-Parmer, UK) using 0.85% sterile saline as the diluent. OD-adjusted suspensions are diluted 1 in 150 in Mueller Hinton (MH) broth to give starting concentrations between 5 x 10^5 and 1 x 10^6 colony-forming units per ml (CFU/mL), confirmed by plating on MH agar (to enumerate viable colonies, white circles). *Illustration by the author (HNW).*

2.8.2. Agar Diffusion

Sterile 1 cm^2 pieces of Tegaderm™ pad (3M, Bracknell, US) were coated in emollient treatments (described in **Section 6.3.1**) and added to MHA plates containing 5 x 10^5-1 x 10^6 colony forming units per mL (CFU/mL) bacteria. Plates were incubated statically at 37°C in air for 24 to 48 hours. Growth inhibition zones were imaged with a Nikon camera (Finepix S5700) and measured in ImageJ v.1.8. Agar diffusion tests were repeated in three independent experiments for each bacterial species.

2.8.3. Time-Kill Assays

Adjusted cultures (above) were added to sterile universal tubes with treatments described in **Section 6.3.1**. Tubes were incubated at 37°C with 140 rpm shaking for 24 hours, and collected at intervals (0.5, 1, 2, 4 and 24 hours). Upon collection, tubes were vortexed, and 100 µL of bacterial broth was removed from each tube and added to 900 µL Dey-Engley Neutralising broth (DENB; Fluka, Sigma-Aldrich). A neutralising broth test was performed prior to experiments to ensure the DENB neutralised the antimicrobial treatments under study (**Appendix 2A.28**). Samples were serial diluted, plated on MHA, and incubated for 24 hours at 37°C to determine CFU/mL. The time-kill assay was repeated in three independent experiments.

2.8.4. Stability and Kinetics

To test the stability of cream preparations, Theraglass™ treatments were incubated at 4°C, RT and 37°C for 24-120 hours. At each 24-hour interval, treatments were collected for agar diffusion assays. To test the kinetics of antimicrobial soluble factor release, Theraglass™ powders (1 g per tube) were incubated in 5 mL sterile DPBS at RT on a rocker over a period of 24-144 hours, and collected at 24-hour intervals. At each time point, supernatant was removed and replaced with fresh DPBS. Tegaderm™ pad was soaked in the collected supernatant and added to bacterial plates for agar diffusion testing as above.

2.8.5. Minimum Inhibitory Concentration and Minimum Bactericidal Concentration Assays

Treatments were prepared to 20% in sterile DPBS. The minimum inhibitory concentration (MIC) and minimum bactericidal concentration (MBC) for each treatment was determined by a broth microdilution method using MHB (as in Balouri et al., 2016). Here, 50 µL MHB was added to each well of a 96 well plate, with treatments serial diluted down each row. O/N cultures were adjusted to a starting concentration of 5×10^5 CFU/mL and added to the wells (above), except MHB control wells that contained no bacteria or treatments. For co-cultures, adjusted bacterial suspensions were mixed in a 1:1 ratio and added to 96 well plates. The experimental plate was set up four times for each bacterial group. Plates were incubated statically at 37°C for 20 hours. For MIC assays, 10 µL of PrestoBlue® Cell Viability reagent (Thermo Fisher Scientific) was added to each well. Plates were incubated at 37°C for 15 minutes, read at 570 nm, and values were subtracted from background values gathered at 600 nm. The MIC was determined as the minimum concentration of treatment that caused <90% reduction in bacteria (ascertained from the OD of untreated bacteria wells). For the MBC assay, 100 µL was removed from each treatment well, serial diluted in DENB, and plated on MHA to determine the lowest concentration of antimicrobial treatment that prevented viable colony growth.

2.8.6. Biofilm Formation Assay

To test whether Theraglass™ could inhibit biofilm formation in the bacterial species, a standard 96-well microtiter biofilm formation plate assay was performed (as described in O'Toole, 2011), and set up as for the MIC/MBC experiments. Plates were incubated under aerated conditions at 37°C for 48 hours. Plates were then

submerged in dH_2O to remove planktonic bacteria, and biofilm wells were stained with 125 µL 0.1% Crystal Violet (Sigma-Aldrich) for 20 minutes at RT. Plates were washed in dH_2O and dried O/N at RT. To solubilise the Crystal Violet, 200 µL of 30% (w/v) glacial acetic acid (Thermo Fisher Scientific) was added to the wells. Plate absorbance was measured at 570 nm and biofilm formation categorised as in Christensen et al. (1989) based on the ODs obtained (**Figure 2.16**).

$OD \leq ODc$	*= non-adherent*
$ODc < OD \leq 2 \times ODc$	*= weak biofilm*
$2 \times ODc < OD \leq 4 \times ODc$	*= moderate biofilm*
$4 \times ODc < OD$	*= strong biofilm*

Figure 2.16. Classification system used for biofilm formation. Optical densities (ODs) obtained at 570nm are used to determine the OD cut-off (ODc), deduced as three standard deviations above the mean OD of the negative control. If the OD of a biofilm falls below or equal to the ODc, it is classed as non-adherent. If the OD of a biofilm is over four times the ODc, it is categorised as a strong biofilm.

2.8.7. Biofilm Culture

Planktonic bacteria (adjusted to 0.5 on the MacFarland turbidity scale) were added in 20 µL droplets to sterile nylon filter membranes (Merck-Millipore, UK) on MHA and biofilms were left to form at the air-filter interface for 72 hours at 37°C. Every 24 hours, membrane biofilms were transferred to fresh MHA plates using sterile forceps. For co-culture experiments, planktonic cultures of *P. aer* and *S. aur* were mixed in a 1:1 ratio and added to filter membranes, as ratiometric analysis proved this to lead to the most equal ratio of the two species (**Appendix 2A.29**).

2.8.7.1. *Ex Vivo* Porcine Wound Biofilm Preparation

Fresh porcine skin, collected under University ethical approval (FEC_21_2017) from a local abattoir, was held in growth medium (GM) consisting of HG DMEM with 10% FBS, 1% penicllin-streptomycin solution, 10 µg/mL Gentamicin and 2.5 µg/mL amphotericin B. The subcutaneous adipose tissue was removed, the skin was washed in HBSS containing 2X Antibiotic-Antimycotic, and washed in DPBS prior to wounding. The porcine skin was cut into $1cm^2$ squares and the epidermis was completely removed to create a wound bed which was inoculated with 72 hour established biofilms. A 0.2 µm filter membrane was placed on top of absorbent pads (Merck-Millipore) soaked in GM. Each porcine biofilm explant was placed on filter membranes to provide an air: liquid interface, thus allowing nutrient transfer to the

skin without submersion (modified from Olivera & Tomic-Canic, 2013). The skin was cultured at 37°C and 5% CO_2 for 24 hours to aid biofilm attachment. Treatments were then added to each biofilm. Non-treated biofilm controls and uninoculated porcine wound controls were also included.

2.8.7.2. Porcine Wound Biofilm Collection

Post-treatment (24 hours), porcine wound biofilms were bisected at their midpoint and: flash frozen for RNA and protease analysis; embedded in OCT for histological staining and; collected for viable colony enumeration. For viable colony counts, tissue was cut into pieces <1 mm and added to 1 mL MHB with 5 mL sterile 3 mm borosilicate glass beads (Sigma-Aldrich). Samples were vortexed and 100 µL of suspension was removed from each universal tube, serial diluted in DENB and spread on MHA (for single species). For co-culture biofilms, bacteria were plated on MHA (to count total colonies), mannitol salt agar (MSA, *S. aureus* selective) and cetrimide agar (*P. aeruginosa* selective). Plates were incubated at 37°C for 20-24 hours and counted (CFU/mL).

2.8.7.2.1. Microbiological Staining

Samples embedded in optimal cutting temperature media (OCT, Cell Path, UK) were cryo-sectioned at 10 µm on a Leica CM1950 cryostat. Gram-Twort, Acridine Orange (Sigma-Aldrich), and Concanavalin A (ThermoFisher) staining was used to visualise porcine wound biofilm load.

2.8.7.2.1.1. Gram-Twort Staining

A modified Gram-Twort stain was carried out as previously reported (Olett, 1947). Here, sections were fixed in ice cold methanol (-20°C) for 10 minutes at RT, stained for three minutes with 0.5% Crystal Violet in 25% ethanol (Sigma-Aldrich) and counterstained for 3 minutes in Gram's Iodine solution (Thermo Fisher Scientific). Slides were then differentiated in 2% acetic-alcohol (acetic acid in ethanol) and counterstained with a 9:1 solution of 0.2% Neutral Red and 0.2% Fast Green (both Sigma-Aldrich) in 100% ethanol. Sections were differentiated again, rapidly dehydrated in 100% ethanol and mounted with Pertex® mounting medium (Cell Path). Images were captured at 100x magnification on a Nikon E400 microscope with SPOT camera. Biofilm thickness analysis was performed in ImageJ v.1.8.

2.8.7.2.1.2. Acridine Orange

Acridine Orange is a useful stain to enumerate bacteria in host tissue. At low pH (~3.5), eukaryotic cells emit a green fluorescence and prokaryotic cells emit an orange fluorescence when excited by blue light (Neeraja et al., 2017). Here, methanol-fixed sections were incubated in Acridine Orange solution (2 mg/mL in dH_2O; Sigma-Aldrich) for five minutes at RT in a dark chamber, rinsed in dH_2O, and mounted in Fluoroshield™ mounting medium (Sigma-Aldrich).

2.8.7.2.1.3. Concanavalin A

Concanavalin A is a lectin that specifically binds to carbohydrates in host tissue and extracellular polymeric substances (EPS) from biofilms (Strathmann et al., 2002). Therefore, Concanavalin A was used to visualise host tissue and biofilm matrix. Counterstaining with DAPI allowed direct visualisation of bacterial cells. Methanol fixed OCT sections were incubated in Concanavalin A Alexa Fluor™ 488 Conjugate (50 µg/mL; Thermo Fisher Scientific) at 4°C O/N, rinsed in PBS and mounted in MOWIOL 4-88 containing DAPI (**Appendix 2A.14**). Fluorescent images were taken on a Zeiss Axio Vert. A1 microscope with AxioCam|cm1 camera (Carl Zeiss Microscopy Ltd, Cambridge, UK) at x40 magnification using FITC and DAPI channels.

2.8.7.2.2. Bacterial qRT-PCR

Snap frozen samples were cut into <1 mm pieces and biofilm aggregates were dissociated from porcine skin via bead-beating in 1 mL Invitrogen™ RNAlater™ Stabilization Solution (Thermo Fisher Scientific) and 5 mL sterile borosilicate glass beads. The supernatant fraction was centrifuged at 4°C and 10, 000 rpm to pellet the bacterial cells. RNA was isolated in two ways depending on bacterial species. For the Gram-negative *P. aeruginosa*, cell pellets were re-suspended in Max™ Bacterial Enhancement Reagent (Thermo Fisher Scientific) following the manufacturer's protocol. To break down the cell walls of *S. aureus* in single and co-culture biofilms, cell lysis was achieved by incubating pellets in 100 µL Tris-EDTA buffer with 10 mg/mL lysozyme and 25 µg/mL lysostaphin (all Sigma-Aldrich) for 20 minutes at 37°C (as in Resch et al., 2005). RNA was then isolated from all bacterial species with TRIzol® reagent and the aqueous phase purified with the Invitrogen™ Ambion™ PureLink™ RNA Mini Kit following manufacturer's instructions. RNA quantity was assessed using a SimpliNano Nanodrop spectrophotometer and reverse transcribed with Bioscript (Bioline) as outlined in previously. cDNA samples were diluted by

three orders of magnitude and qRT-PCR performed as described above. Primer sequences are available in the **Appendix 2A.34**.

2.8.7.2.3. Bacterial Zymography

Porcine biofilms dissociated via the glass bead method were centrifuged at 10,000 x g and 4°C for 10 minutes. The supernatant fraction (containing extracellular proteases) was removed, sterile-filtered (0.22 µm, Merck-Millipore) and stored at -80°C until use. Gelatin zymography was performed to assess extracellular protease activity (Caballero et al., 2001). Supernatant was run on 7.5% acrylamide gels containing 0.2% porcine skin gelatin (Oxoid) under non-reducing conditions at 70V and 4°C. The Precision Plus Protein™ Kaleidoscope™ Prestained Protein Standards (Bio-Rad Laboratories Ltd.) were used to determine molecular weights of the separated proteins in the gel. MMP2 and MMP9 standards (Biotechne, Abingdon, UK) were used as an internal control. Gels were washed in 2.5% Triton X-100 (Sigma-Aldrich) to remove SDS and incubated in gelatinase resolving buffer (**Appendix 2A.30**) for 24 hours at 37°C. In areas of high activity, proteases digest the gels. The gels were stained blue using 0.2% amido black (Thermo Fisher Scientific), thus revealing digested areas that appeared white (Leber & Balkwill, 1997). Gels were imaged on a lightbox and densitometric analysis was performed in ImageJ v.1.8. Relative density was determined from the control (untreated biofilm).

2.8.7.2.4. Colorimetric Protease Analysis

The Azocasein method (Andrejko et al., 2013) determined total extracellular protease activity. Here, 100 µL supernatant was added to 100 µL Azocasein (Sigma-Aldrich) solution (5 mg/mL in 0.1 M Tris-HCl, pH 8.8) and incubated at 37°C for 3 hours. The reaction was stopped with 10% trichloroacetic acid (25 µL per tube) and samples were centrifuged at 14, 000 rpm for 15 minutes at RT. To each well of a 96 well plate, 50 µL 0.5 M NaOH was added to 50 µL Azocasein supernatant in triplicate. NaOH was used as a blank, bacterial protease (Sigma-Aldrich) was included as an internal control for protease activity, and absorbance was measured at 405 nm. For the Azocasein assay, one protease activity unit was defined as an absorbance increase (OD_{405nm}) of 0.02 per hour (Andrejko et al., 2013).

2.8.7.3. Human *Ex Vivo* Biofilms

Following assessment of Theraglass™ in a porcine biofilm model, the host response was further elucidated in a more translationally relevant *ex vivo* human wound

biofilm model. Established 72-hour single and co-culture biofilms were transferred to 2 mm partial-thickness wounds in the centre of 6 mm biopsies (described above). Treatments were administered following biofilm establishment (24 hours) and human biofilm biopsies were cultured for a further 24 hours at 37°C and 5% CO_2. Samples were collected for biofilm colony enumeration and histology.

2.9. Statistical Analysis

Experiments were performed with three or more biological and/or technical replicates in three independent experiments where applicable. All data are illustrated as mean +/- standard error of the mean. Data analysis was performed in Microsoft® Excel 2016 (Microsoft Corporation, London, UK), R v.3.6.1. (Core Team, 2019; **Chapter 4**) including the 'car' (Fox & Weisberg, 2011; **Chapter 6**) package, and GraphPad Prism 7 (GraphPad Software, California, US). Normal distribution of data was determined via Shapiro-Wilks tests and parametric statistical analysis performed to deduce significance at the $P < 0.05$ level. Independent two-tailed Student's *t* tests were performed when comparing two independent groups. One-way analysis of variance (ANOVA) was performed when comparing one variable across three or more independent groups. Two-way ANOVA was performed when comparing two or more variables across two or more independent groups. For ANOVA, relevant *post-hoc* (Tukey's honest significant differences, Dunnett's and Sidak's) analysis was performed where appropriate.

Chapter 3: A Novel Role for Cellular Senescence in Acute and Pathological Wound Repair

Data presented in this chapter also appears in the following publication:

Elevated local senescence in diabetic wound healing is linked to pathological repair via CXCR2.

Authors: Holly N. Wilkinson[1], Christopher Clowes[2], Kayleigh L. Banyard[1], Paolo Matteuci[3], Kimberly A. Mace[4] and Matthew J. Hardman[1]

2019 J Invest Dermatol

139, Issue 5, Pages 1171–1181. DOI: 10.1016/j.jid.2019.01.005

Affiliations:

[1]Centre for Atherothrombosis and Metabolic Disease, Hull York Medical School, The University of Hull, HU6 7RX, United Kingdom. [2]Research and Development Department, Royal Stoke University Hospital, University Hospitals of North Midlands NHS Trust, ST4 6QG, United Kingdom. [3]Hull University Teaching Hospitals NHS Trust, United Kingdom. [4]Faculty of Biology, Medicine and Health, The University of Manchester, M13 9PT, United Kingdom.

See also commentary:

Cellular Senescence in Diabetic Wounds: When Too Many Retirees Stress the System. Marjana Tomic-Canic & Luisa A. DiPietro. 2019 J Invest Dermatol 139, Issue 5, Pages 997–999. DOI: 10.1016/j.jid.2019.02.019

Author contributions: All *in vitro* and *ex vivo* work was carried out by HNW. *In vivo* wound healing experiments were carried out by HNW and CC. Analysis of cells and tissue was carried out by HNW. Scratch analysis was performed by KLB. HNW performed *in vivo* experiments within the laboratory of KAM. PM provided access to human tissue. HNW, PM, KAM and MJH were involved in final drafting of the manuscript. HNW and MJH were involved in study concept, design and manuscript preparation.

3.1. Introduction

Senescence, first described by Hayflick & Moorhead (1961), is a defined process that globally regulates cell fate. On a cellular level, senescence is an intrinsic mechanism, triggered by both external and internal stressors. This stress then leads to a stable, essentially irreversible, loss of cellular proliferation (Demaria et al., 2014; Jun & Lau, 2010). From an evolutionary perspective, senescence developed as an autonomous anti-tumorigenic mechanism, there to halt incipient neoplastic transformation (Campisi & Robert, 2014). Senescent cells also exist in noncancerous tissues, accumulating exponentially with increasing chronological age (Campisi & d'Adda di Fagagna, 2007; Jun & Lau, 2010). The role of senescence in these non-cancerous states remains to be fully elucidated. This chapter will explore the role of senescence in the context of pathological wound healing.

3.1.1. Senescence as an Anti-Tumour Mechanism

A number of age-related and stress-related mechanisms induce senescence. These include repeated cell division (replicative senescence; Hayflick & Moorhead, 1961), mitogenic signals (reviewed in Tchkonia et al., 2013), increased ROS (Passos et al., 2010), DNA breaks (Di Micco et al., 2006) and epigenomic damage (Pazolli et al., 2012). Given that senescence evolved as an anti-cancer mechanism, it is unsurprising that activated oncogenes (e.g. BRAFE600 or RASV12; Dikovskaya et al., 2015) trigger cell cycle arrest. In higher eukaryotes, stressors and oncogenes subsequently cause the activation of anti-tumorigenic networks, controlled by transcriptional regulators such as p53 and retinoblastoma protein (pRb; Campisi & Robert, 2014). Sitting at the nexus of the complex anti-tumorigenic networks is p53, which maintains broad range stress detection (Shi & Gu, 2012). p53 directly transactivates the proliferation inhibitor, p21 (He et al., 2007), preventing cyclin dependent kinase (CDK) 2-mediated pRb inactivation (Beauséjour et al., 2003). Similarly, p16 transcription prevents CDK4- and CDK6-mediated phosphorylation of pRb (Takahashi et al., 2006).

As pRb naturally binds to E2F/DP transcription factor complexes (Dimova & Dyson, 2005), consequent failure to phosphorylate pRB (by CDKs) inhibits transcription of E2F target genes, thus preventing cell cycle progression from the G1 to S phase (Narita et al., 2003; Malumbres & Barbacid, 2005). Interestingly, it appears that p21 is often upregulated before p16, even though both mechanisms can act alone or in

combination (van Deursen, 2014). The complex senescence signalling pathways are reviewed in Campisi, (2013; simplified and summarised in **Figure 3.1**).

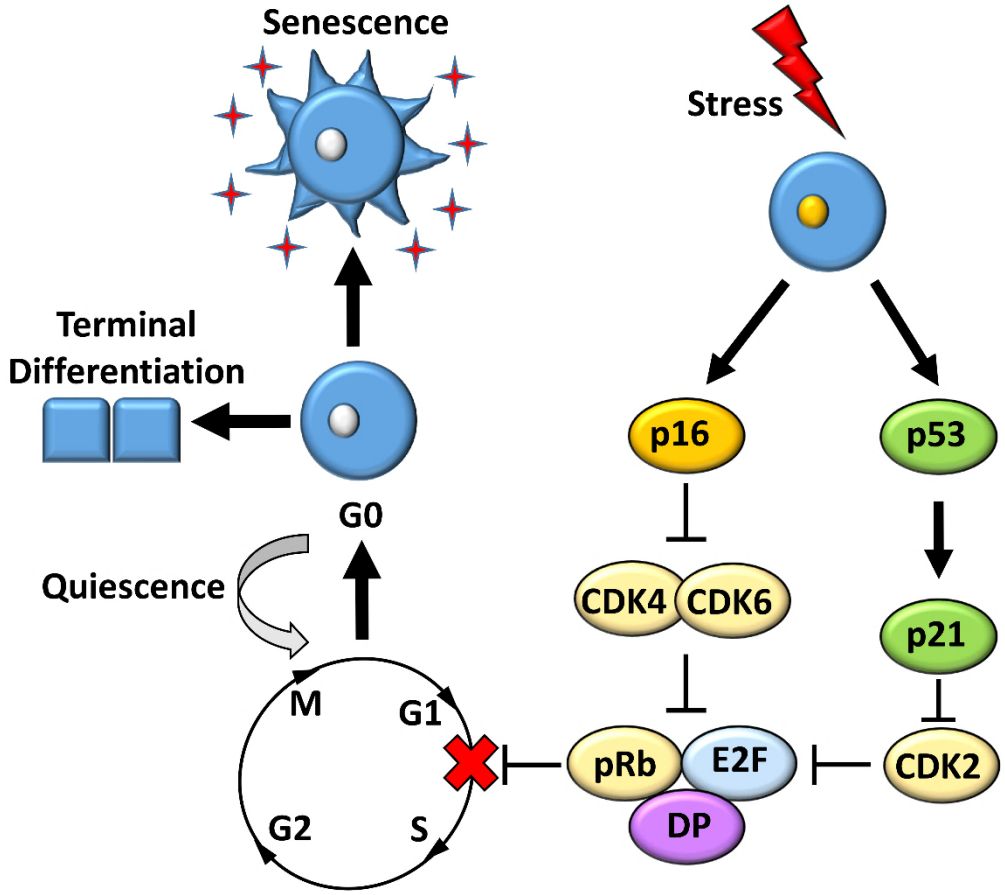

Figure 3.1. Principle pathways of senescence induction. Intrinsic and external stressors (e.g. ultraviolet radiation, oxidation and mutagens) trigger p16 and p53 tumour suppressor activities. Cyclin dependent kinase (CDK) 4 and CDK6 activity is inhibited by p16, while CDK2 is silenced by p21, transactivated by p53. CDK inhibition prevents retinoblastoma protein (pRb) phosphorylation and dissociation of the E2F/DP transcription factor complex, thus preventing cell cycle progression (from the G1 to S phase). Cell cycle arrest (G0) can be reversible (e.g. quiescence), lead to terminal differentiation, or cause senescence. Fully senescent cells produce a senescence-associated secretory phenotype (stars) which contributes to age-related disease. *Figure produced by the author (HNW).*

The CDK inhibitors (CDKIs) fall into two distinct classes with similar, yet defined functions. The INK4 class comprises the well-conserved $p15^{Ink4b}$ (encoded by the gene *CDKN2B*), $p16^{Ink4a}$ (*CDKN2A*), $p18^{Ink4c}$ (*CDKN2C*) and $p19^{Ink4d}$ (*CDKN2D*), which bind CDK4 and CDK6 (Sharpless, 2004). By contrast, the Cip/Kip family of CDKIs include $p21^{Cip1/Waf1/Sdi1}$ (encoded by the gene *CDKN1A*), $p27^{kip1}$ (*CDKN1B*) and $p57^{kip2}$ (*CDKN1C*; Besson et al., 2008), capable of binding to a broad range of CDKs and cyclins (Sherr & Roberts, 1999). The CDKIs are not only valuable in preventing

uncontrolled cellular division, but also aid other arrested cellular states, such as reversible quiescence (e.g. p21, Barr et al., 2017) and terminal differentiation (e.g. p21 for myotube formation, Pajalunga et al., 2007; p18 for differentiation of B cells into plasma cells, Tourigny et al., 2002). Furthermore, it has even been shown that members of the Cip/Kip family are necessary for embryonic development (p27 and p57 in mice, Tateishi et al., 2012), where attenuation of p21 leads to patterning defects (Muñoz-Espín et al., 2013; Storer et al., 2013).

Intriguingly, *CDKN2A,* the INK4a/ARF locus, is lost in many human cancers (Karsai et al., 2007; Mohseny et al., 2010). While INK4a directly controls pRB, ARF itself is required to stabilise p53 by sequestering the main p53 repressor, mouse double minute 2 homolog (MDM2; Pomerantz et al., 1998; Stott et al., 1998). Hence, MDM2 prevents transactivation of p53 to elicit potent tumorigenic activities (Shi & Gu, 2012). Although the p53/p21 and p16 pathways globally determine cell fate, the relative contribution of these pathways to senescence is thought to be cell-type specific (Campisi & d'Adda di Fagagna, 2007; Krizhanovsky et al., 2008).

Unlike quiescent cells, which undergo revocable cell cycle arrest, cellular senescence is irreversible under normal biological conditions. Morphologically, senescent cells show a distinct flattened and elongated appearance compared to dividing cells (Campisi & d'Adda di Fagagna, 2007). Senescent cells may also exhibit regions of highly condensed chromatin, known as senescence-associated heterochromatic foci (SAHF; van Deursen, 2014) and DNA segments with chromatin alterations reinforcing senescence (DNA-SCARS), resulting from DNA damage (Rodier et al., 2011). SAHFs contain chromatin alterations, such as γH2AX and H3K9Me3 (Chandra & Zang, 2013; van Deursen, 2014), and stain notably with DAPI (Kosar et al., 2011; Narita et al., 2003). These modifications in chromatin sequester E2F target genes, thus potentiating senescence (Shah et al., 2013). Alternative markers of senescence include other p53 regulated tumour-suppressor genes, such as decoy receptor 2 (Pare et al., 2019), loss of the nuclear lamina protein, lamin b1 (Wang et al., 2017a) and centrosome aberrations (Ohshima, 2012; reviewed in Tigges et al., 2014).

Often, β-D-galactosidase, a lysosomal hydrolase encoded by the *GLB1* gene, is used as an archetypal senescence biomarker (Debacq-Chainiaux et al., 2009; Dimri et al., 1995). Ordinarily, β-D-galactosidase is detected in non-senescent cells at pH 4, but cellular senescence causes expansion of the lysosomal compartment and results in

β-D-galactosidase activity that can be detected at pH 6, which is thus termed SA-βGAL (Kuilman et al., 2010). Multiple authors have demonstrated that SA-βGAL accumulates in ageing tissues (Dimri et al., 1995; Sigal et al., 1999), while others question specificity, arguing that SA-βGAL activity is visible in non-senescent cells (Krishna et al., 1999; Lee et al., 2006). Despite this, SA-βGAL remains the gold standard technique for detecting cellular senescence and is often used in conjunction with other key biomarkers, such as p16 and p21, to confirm senescence (Biran et al., 2017; Baker et al., 2016; Matjusaitis et al., 2016). Senescence cell characterisation is summarised in **Figure 3.2**.

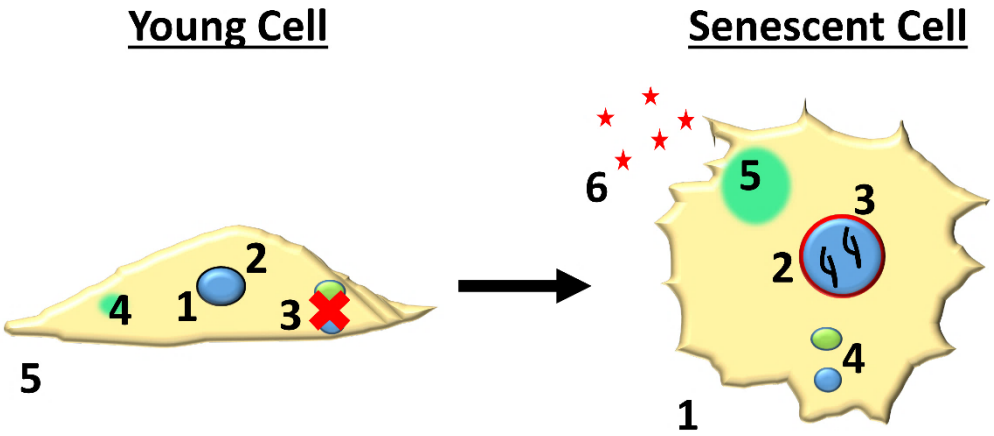

Figure 3.2. Characteristics of senescent cells. Senescent cells are characterised by morphological changes (**1**), chromatin modifications (e.g. senescence-associated heterochromatin foci, SAHF, **2**), loss of nuclear envelope protein, lamin b1 (**3**), increased p16 and p21 (**4**), senescence–associated β-D-galactosidase (β-GAL) activity (**5**), and production of a senescence-associated secretory phenotype (SASP, **6**). By contrast, young cells are proliferative (**1**), have normal nuclear envelope function (**2**), low p16 and p21 activity (**3**), normal β-GAL activity (**4**) and no hyper-secretory SASP (**5**). *Figure produced by the author (HNW).*

Although unable to divide, senescent cells are metabolically active and often possess a SASP, demonstrated by increased secretion of pro-inflammatory cytokines (e.g. IL-1α, IL-6, IL-8), GFs (TGF-β, insulin GFs, Elzi et al., 2012) and proteases (MMPs) that alter the tissue microenvironment (Freund et al., 2010). More recently, the characterised SASP has been extended to include lipids such as eicosanoids (Lopes-Paciencia et al., 2019). The SASP feature of senescent cells is a DNA damage response, and is not apparent in cells that naturally senesce due to overexpression of p16 and p21 (Coppe et al., 2011). The SASP heavily contributes to age-related functional decline (Rodier et al., 2009) and many chronic diseases (e.g. atherosclerosis, Erusalimsky & Kurz, 2005).

Paradoxically, the SASP can influence pre-cancerous development in proximal tissues (Collado et al., 2007) and thus promote tumorigenic activities, such as epithelial-to-mesenchymal transition (Krtolica et al., 2001; Campisi et al., 2011). Indeed, many SASP proteins, including the growth-regulated oncogenes and VEGF, are potent mitogenic drivers (Coppe et al., 2006; Coppe et al., 2010). The plasticity of the SASP across different cell types (reviewed in Campisi, 2013; Lupa et al., 2015) complicates understanding of its role within tissues, summarised in **Figure 3.3**.

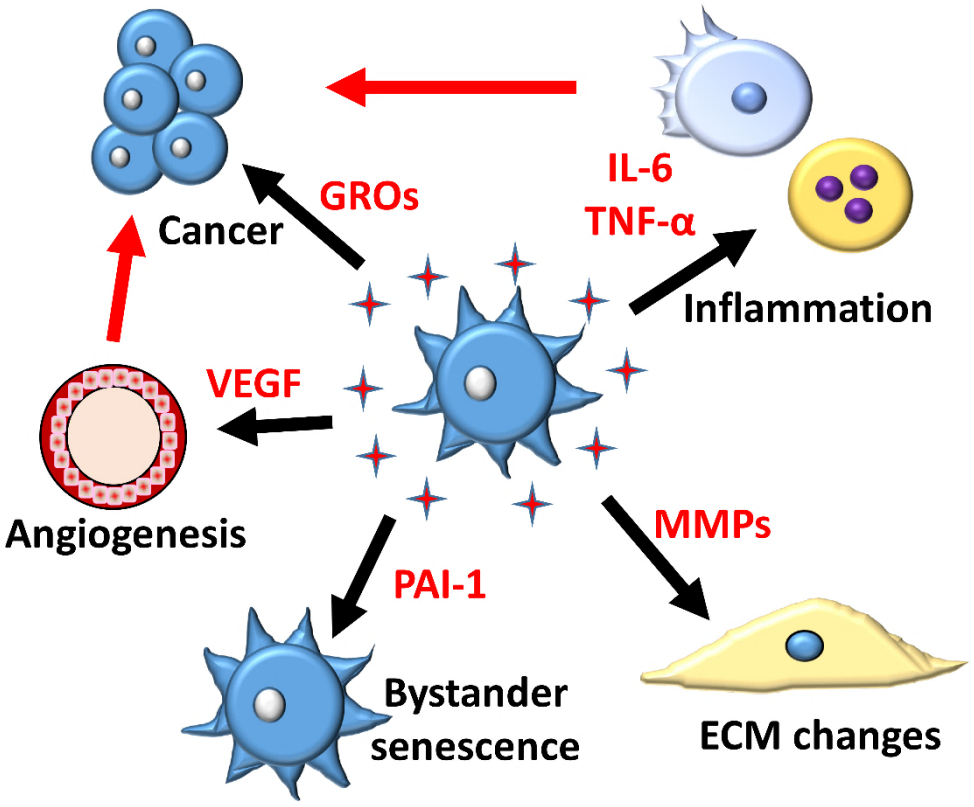

Figure 3.3. Biological roles for the senescence-associated secretory phenotype. Senescent cells produce a senescence-associated secretory phenotype (SASP) comprising pro-inflammatory mediators that influence extracellular matrix (ECM), inflammation and angiogenesis (wound healing processes; main components in red). The SASP also promotes senescence development in nearby cells ("bystander" senescence). The production of growth regulating oncogenes (GROs) in the SASP drives tumour formation and epithelial-mesenchymal transition, while inflammation and angiogenesis induce tumorigenic activity (red arrows). The SASP has been functionally linked to ageing, diabetes, fibrosis, wound healing and cancer. *Figure produced by the author (HNW).*

3.1.2. Senescence and Ageing

There is an intimate link between senescence and ageing, as it has been suggested that both exist to limit lifespan (Sharpless, 2004). For example, natural cellular ageing results in telomere shortening, which serves as a "mitotic clock" (Randle et

al., 2001). The importance of telomeres in preventing ageing onset becomes apparent in individuals with ataxia telangiectasia, a progeroid disease characterised by deficiency in ataxia telangiectasia mutated kinase and development of premature telomere shortening (Metcalfe et al., 1996). Intriguingly, mice with telomere attrition also show hallmark features of ageing, particularly in their skin, including alopecia and loss of subcutaneous adipose tissue (Rudolph et al., 1999).

Once telomeres are diminished, further cellular division results in proliferative arrest and/or apoptosis (Allsopp et al., 1995; Fumagalli et al., 2012), with cells only able to evade this outcome via sophisticated telomere repair mechanisms. One of these is telomerase, highly produced in human stem cells and cancer cells (Martinez & Blasco, 2011). Telomerase extends the length of telomeres by adding DNA repeats, thus allowing unrestrained cellular division (Childs et al., 2014). Intriguingly, some cell types, particularly epithelial cells, undergo p16-induced senescence despite ectopic telomerase expression (e.g. Kiyono et al., 1998; Rheinwald et al., 2002). Hence, telomere length alone may not determine a cell's senescent fate.

Telomerase can restrain senescence and promote mitogenic activity via mechanisms independent of regulating telomere length. For example, mice expressing the catalytic subunit of telomerase (mouse telomerase reverse transcriptase, mTert) spontaneously produced mammary gland tumours despite having same length telomeres as their controls (Artandi et al., 2002). Further, mice expressing Krt5-mTert showed heightened proliferation in SB keratinocytes, and were more likely to develop skin papillomas following chemical carcinogenesis (González-Suárez et al., 2001). Interestingly, murine cells possess much longer telomeres than human cells (Kipling & Cooke, 1990), and most murine cells are telomerase positive (Prowse & Grieder, 1995). Yet, senescence is a feature often observed in short passages of primary murine cells (mouse embryonic fibroblasts, MEFs) due to the stress-induced shock of *in vitro* culture (Sherr & Depinho, 2000).

Telomere erosion is not the sole cause of senescence during ageing. Normal cellular metabolism results in accumulation of oxidative damage, underpinning the free radical theory of ageing, discussed in **Section 1.2.1**. Intriguingly, MEF culture can be extended by lowering tissue culture oxygen tension, therefore circumventing oxidation-induced senescence (Parrinello et al., 2003). Concurrently, human diploid fibroblasts (Duan et al., 2005) and endothelial cells (Ruan et al., 2014) undergo

senescence following oxidant (H_2O_2) damage. Notably, exposure to UV as part of photoageing increases ROS production in skin (Herrling et al., 2006), with melanocytes being more highly susceptible to ROS damage than fibroblasts and keratinocytes (Jenkins et al., 2011). Jenkins et al. (2010) elucidated a crucial feedback loop between p16 and ROS, where ROS upregulates p16 in skin cells, and knockdown of p16 causes increased oxidative DNA damage. Hence, it is clear that a strong correlation exists between oxidant damage, senescence and ageing.

Despite species-specific differences, both p21 and p16 have strong causal links with ageing in human (Berry et al., 2017; Dungan et al., 2017; Kim et al., 2015) and murine (Choudhury et al., 2007; Baker et al., 2008; Baker et al., 2013) experimental models. For example, gene expression analysis indicated that p16 accumulates throughout the body in aged rodents, confirmed at the protein level in the islets, uterus and spleen (IHC, Krishnamurthy et al., 2004). Of further relevance is the fervent association between increased skin ageing and $p16^{+ve}$ (Waaijer et al., 2012) and SA-βGAL^{+ve} (Dimri et al., 1996; Ressler et al., 2006) cell accumulation.

The mechanisms underpinning cellular senescence in the context of cancer are well understood, yet causal roles for senescence in driving age-related pathology have only recently been discovered. In one example, Baker et al. (2011) directly demonstrated the effects of $p16^{+ve}$ cell eradication on age-related disease. Here, following constitutive expression of the checkpoint protein BubR1, hallmark features of premature ageing (e.g. cataracts and sarcopenia) were alleviated by $p16^{+ve}$ cell eradication. The CDKIs may also promote assisted cell cycling by extending cell lifespan following accumulated age-related damage (van Deursen, 2014). Overall, it is unsurprisingly that a large body of literature pertains to the involvement of senescence in ageing onset and age-related disease progression (e.g. atherosclerosis, Erusalimsky & Kurz, 2005).

3.1.3. Senescence in Diabetes

Systematic approaches have validated that healthy ageing and T2DM are both characterised by a decrease in organismal complexity and increased inflammation (Spazzafumo et al., 2013). These data importantly highlighted that complexity reduces at an accelerated rate in diabetic patients, hence diabetes can be seen as a state of accelerated ageing (Prattichizzo et al., 2016). Further, serious diabetic comorbidities (renal and cardiovascular defects) are not only associated with

ageing, but are also observed in young diabetic patients (Harjutsalo et al., 2008; Vlassara & Striker, 2011). It is thus unsurprising that mechanisms involved in ageing (e.g. senescence and inflammaging) are now being explored in diabetes research.

As aforementioned, senescent cells cause widespread disruption of normal tissue architecture, by virtue of their lack of function and their SASP (Coppe et al., 2010). Major SASP components, such as MMPs, cause matrix proteolysis (Khasigov et al., 2001), while secretion of potent inflammatory mediators (e.g. TNF-α) triggers immune cell influx into tissues (Witte & Barbul, 1997). Indeed, there is growing epidemiological evidence suggesting that this heightened immune response, known as 'sterile' inflammation, contributes to many age-related pathological states (neurological, Bitto et al., 2010; cardiovascular, Erusalimsky & Kurz, 2005; Prattichizzo et al., 2016).

Although complex, the onset of diabetes is typified by many autoimmune and inflammatory features. Likewise, obesity drives immune cell build-up (Schafer et al., 2016), and may mediate insulin resistance and diabetic pathogenesis (Minamino et al., 2009; Spranger et al., 2003). For example, obese mice express many hallmark SASP factors, including monocyte chemoattractant protein 1 (Mcp-1, Sartipy & Loskutoff, 2003), macrophage (Mφ) inflammatory protein 1α (Mip-1α; Xu et al., 2003) and Il-6 (Yoshimoto et al., 2013). Increased SASP components (MCP-1, IL-8; Coppe et al., 2008) are also observed in obese human subjects (Kim et al., 2006a; Utsal et al., 2012). Of note, removal of SASP factors, such as *Tnf*, protects obese mice from hyperglycaemia and insulinopenia (Uysal et al., 1997).

Obesity itself is related to senescence, as obese mice have higher levels of SA-βGAL in their adipose tissue, and elevated p53 and p21 mRNA (Minamino et al., 2009). By contrast, caloric restriction (Masoro, 2006) and exercise (Schafer et al., 2016) reduce adipose tissue senescence in experimental models. Other areas found to be highly senescent in diabetes include the pancreatic β cells (greater p27, Uchida et al., 2005) and the aorta (greater SA-βGAL, Brodsky et al., 2003). Further, plasminogen activator inhibitor 1 (PAI-1), a marker of senescence, is upregulated in the plasma of non-insulin dependent diabetic patients (Juhan-Vague et al., 1989).

A characteristic symptom of diabetes is hyperglycaemia, caused by insulin resistance or insulinopenia (Stumvoll et al., 2005). High glucose in *in vitro* systems directs premature senescence in multiple cell types, causing accelerated growth that

leads to advanced replicative exhaustion (Maeda et al., 2015; Yokoi et al., 2006). Hyperglycaemia also promotes AGE production (Coughlan et al., 2011). In the food industry, AGEs are produced to improve food bioavailability and taste by rapid high temperature protocols (O'Brien & Morrissey, 1989). Yet, within the body, AGE formation is a drawn-out process due to lower temperatures and lower glucose availability. AGEs are thus a distinctive feature of advanced lifespan (Ott et al., 2014).

AGEs contribute to many age-related comorbidities, such as reduced tissue elasticity (Badenhorst et al., 2003) and inflammation (Uribarri et al., 2007). They cause widespread cellular damage (through protein cross-linking and ROS, Van Puyvelde et al., 2014), further contributing to the patho-biochemistry of many diabetic complications, including neuropathy (Sheetz & King, 2002). AGEs are a feature of replicative senescence, where accelerated replication leads to build-up of oxidised proteins (in human fibroblasts, Sitte et al., 2000). Similarly, AGEs can directly potentiate senescence as AGE treatment induces cellular senescence in cardiac fibroblasts (SA-βGAL staining, Fang et al., 2016). As a result, senescence can be seen as an outcome and driver of the diabetic condition.

3.1.4. Macrophages and Senescence

Many SASP factors found in diabetes attract Mφs (e.g. MCP-1; Coppe et al., 2008), thus Mφs are major components of metainflammation, and contribute to diabetic pathogenesis and senescence induction. Indeed, fundamental roles for Mφs in mediating metabolically driven metainflammation have been elucidated, with many Mφ-specific cytokines forming part of the SASP (Kamei et al., 2006; Prattichizzo et al., 2018; Xu et al., 2003). Mφs, which differentiate from peripheral blood monocytes, are important tissue resident phagocytes that perform crucial regulatory functions in innate and adaptive immunity (Mosser & Edwards, 2008). As the SASP consists of many pro-inflammatory mediators (e.g. IL-6, TNF-α, IL-8; Coppe et al., 2008; Freund et al. 2010) known to act on classical Mφ receptors (e.g. CXCR1, CXCR2, CX3CR1, reviewed in Sagiv & Krizhanovsky, 2013), the SASP not only promotes Mφ influx, but selects for the anti-tumour, pro-inflammatory M1 phenotype (Mosser & Edwards, 2008). This has been demonstrated previously, where senescent (p53-expressing) hepatic stellate cells produced M1-stimulants in their SASP (e.g. IFN-y and IL-6), and non-senescent (non-p53 expressing) hepatic stellate cells produced M2-stimuli (e.g. IL-4; Lujambio et al., 2013). The SASP may

also contain granulocyte-Mφ colony-stimulating factor and granulocyte colony-stimulating factor (Freund et al., 2010), therefore initiating monocyte recruitment to target tissues (Mosser & Edwards, 2008).

Mφ migratory inhibitory factor (MIF, first coined independently by Bloom & Bennett, 1966 and David, 1966), is an evolutionarily conserved cytokine that amplifies inflammation (Lue et al., 2002), and is heavily linked to wound repair (Hardman et al., 2005). MIF is secreted as part of the SASP, and can induce CXCR2-dependent monocyte chemotaxis in senescent environments (Bernhagen et al., 2007). Intriguingly, MIF promotes insulin secretion by pancreatic β cells, and potentiates T2DM by reducing glucose uptake and increasing insulin resistance in target tissues (reviewed in Toso et al., 2008). Further, *Mif* $^{-/-}$ *Ldlr* (low density lipoprotein receptor) $^{-/-}$ mice show lower fasting glucose, reduced insulin levels and dampened inflammation compared to controls (Verschuren et al., 2009).

The SASP is facilitated by a number of important immune response-regulating transcription factors, such as NF-κB. For example, the early SASP includes production of IL-1α, which acts on its receptor, IL-1R, therefore initiating a signalling cascade that activates NF-κB (Orjalo et al., 2009). Stimulation of NF-κB and partner cascades (e.g. ccaat-enhancer-binding proteins) subsequently promotes inflammatory cytokine transcription and drives sustained senescence (Salminen & Kaarniranta, 2011). Additionally, multiple authors have shown that induction of senescence leads to activation of NF-κB gene sets (as determined by gene ontology analysis, Kuilman et al., 2010; Lujambio et al., 2013), while p53 and NF-κB are also linked in coregulatory (in Mφs, Lowe et al., 2014) and antagonistic (in HeLa cells, Huang et al., 2007) manners.

The inflammatory phenotype driven by the SASP can promote many chronic inflammatory disorders, but also contributes to senescent cell clearance. For instance, the pro-inflammatory environment attracts natural killer (NK) cells, neutrophils, T cells, and of course, Mφs (reviewed in Oishi & Manabe, 2016). Previously, Xue et al. (2007) demonstrated a key role for NK cells in removing senescent hepatoblasts. In fact, NK cells recognised and eliminated senescent hepatic stellate cells in a model of CCL4-induced liver fibrosis (Krizhanovsky et al., 2008), and relieved senescence in chronic pancreatis (in rats, Fitzner et al., 2012) and multiple myeloma cells (Soriani et al., 2009). Therefore, despite its detrimental

effects in driving inflammation, it is likely that the SASP fundamentally evolved to govern cancer and senescence by virtue of immune cell clearance. Indeed, the SASP will be discussed in the context of its role in wound repair in this chapter.

3.1.4.1. Chemokines and Their Receptors

Chemokines, which form part of the SASP, are cellular signalling molecules most widely recognised for their potent chemoattractant abilities (reviewed in Sokol & Luster, 2015). Consequently, chemokine receptors exist to modulate cell communication and cellular influx into tissues. In wound healing, chemokines from wound Mφs, fibroblasts and keratinocytes send out signals to attract other cells to the site of injury, triggering the wound repair response (reviewed in Ridiandries et al., 2018). Thus, chemokine signalling is vital to allow optimal innate and adaptive immune function and tissue repair.

Chemokines are relatively small proteins with highly conserved sequences, hence similarity is found between mouse and human cytokine analogues. There are four main classes of chemokines: XC (1 member), CXC (17 members), CXC3 (1 member) and CC (28 members), based on the pattern of their cysteine (C) residues (Kelner et al., 1994; Miller & Mayo, 2017). Chemokines signal through g-protein coupled receptors (GPCRs) and atypical chemokine receptors (reviewed in Vacchini et al., 2016). Intriguingly, chemokine receptors display complex networks of interactions, with differential affinity and promiscuity for the 50 endogenous chemokines (summarised in **Figure 3.4**). For example, CCR2 is stimulated by CCL2, CCL7, CCL8, CCL11, CCL13 and CCL16, while CCR9 is only activated by CCL25 (Zweemer et al., 2014). When chemokines bind to their associated cell surface receptor, this causes a conformational change in the GPCR and the Gα subunit dissociates and interacts with an effector (e.g. phospholipase C). Effector interaction then initiates secondary messenger cascades (e.g. Ca^{2+} and cyclic AMP) that actuate downstream signalling pathways (e.g. PKB and PKC). GPCR signalling subsides when g-protein receptor kinase phosphorylates the GPCR and stimulates β-arrestin binding, ultimately leading to receptor internalisation and degradation (Hanlon & Andrew, 2015).

Within the bone marrow, CXCL12 is required to maintain the haematopoietic stem cell population, and primes stem cell development into different immune cell lineages (Arthur et al., 2016; Sugiyama et al., 2006). Maturation of the progenitor cells then ensues when CXCL12/CXCR4 signalling is downregulated. Expression of

chemokine receptors determines the function and fate of immune cells in the peripheral blood. Indeed, pro-inflammatory ($Ccr2^{+ve}$) and anti-inflammatory ($Cx3cr1^{+ve}$) murine monocytes are characterised by their receptors (Ingersoll et al., 2011). Subsequent differentiation of monocytes into Mφs is dependent on chemokine signals from the local tissue microenvironment (Martinez et al., 2006), while polarised Mφs retain distinct chemokine expression profiles. M1 Mφs express CXCL9 and CXCL10 and M2 Mφs express CCL17, CCL18, CCL22 and CCL24, among others (Shapouri-Moghaddam et al., 2018).

Interestingly, chemokines can be solubilised in the extracellular space, or bind to matrix proteins (e.g. GAGs) to form a gradient of chemical signalling (Monneau et al., 2016; Sarris et al., 2012). For example, CXCL12α has been shown to bind to heparin sulphate to promote myoblast adhesion and migration (Thakar et al., 2017). Of note, proteins such as TNF-inducible gene 6 can inhibit chemokine-GAG interactions (Dyer et al., 2016), and chemokines can be cleaved by proteases (Denney et al., 2009). Therefore, it is clear that the chemokinome is a complex, extensive network of ligands that remains vital for cellular communication. As chemokines are heavily influenced by the local milieu and stroma, their roles in tissue repair, infection and pathology are of wide interest. The therapeutic development of chemokine receptor-targeted pharmaceuticals further highlights their clinical importance (Roy et al., 2017). Intriguingly, the role of chemokine receptor signalling in wound healing pathology and senescence remains understudied. Current knowledge of chemokine receptor expression in wound cells is provided in **Figure 3.5**.

3.1.5. Senescence in Wound Repair

Historically, senescence has been described as a stochastic chronic mechanism related to pathology and ageing. However, a small number of studies have shown that transient senescence, and an associated short-lived SASP, is useful in the tissue repair environment. Krizhanovsky et al. (2008) demonstrated a role for senescence knockdown (e.g. $p53^{-/-}$) in attenuating CCL4-induced liver fibrosis. More recently, Jun & Lau (2010) revealed senescence induction in fibroblasts following skin injury. Here, the matricellular adhesion protein CCN1 was crucial for fibroblast senescence, acting through nicotinamide adenine dinucleotide phosphate (NADPH) oxidase 2 to increase intracellular ROS. Intriguingly, as senescent cells produce ECM degrading

proteases, the presence of Ccn1 (Jun & Lau, 2010) and Ccn2 (Jun & Lau, 2017) protects against fibrosis following murine skin injury.

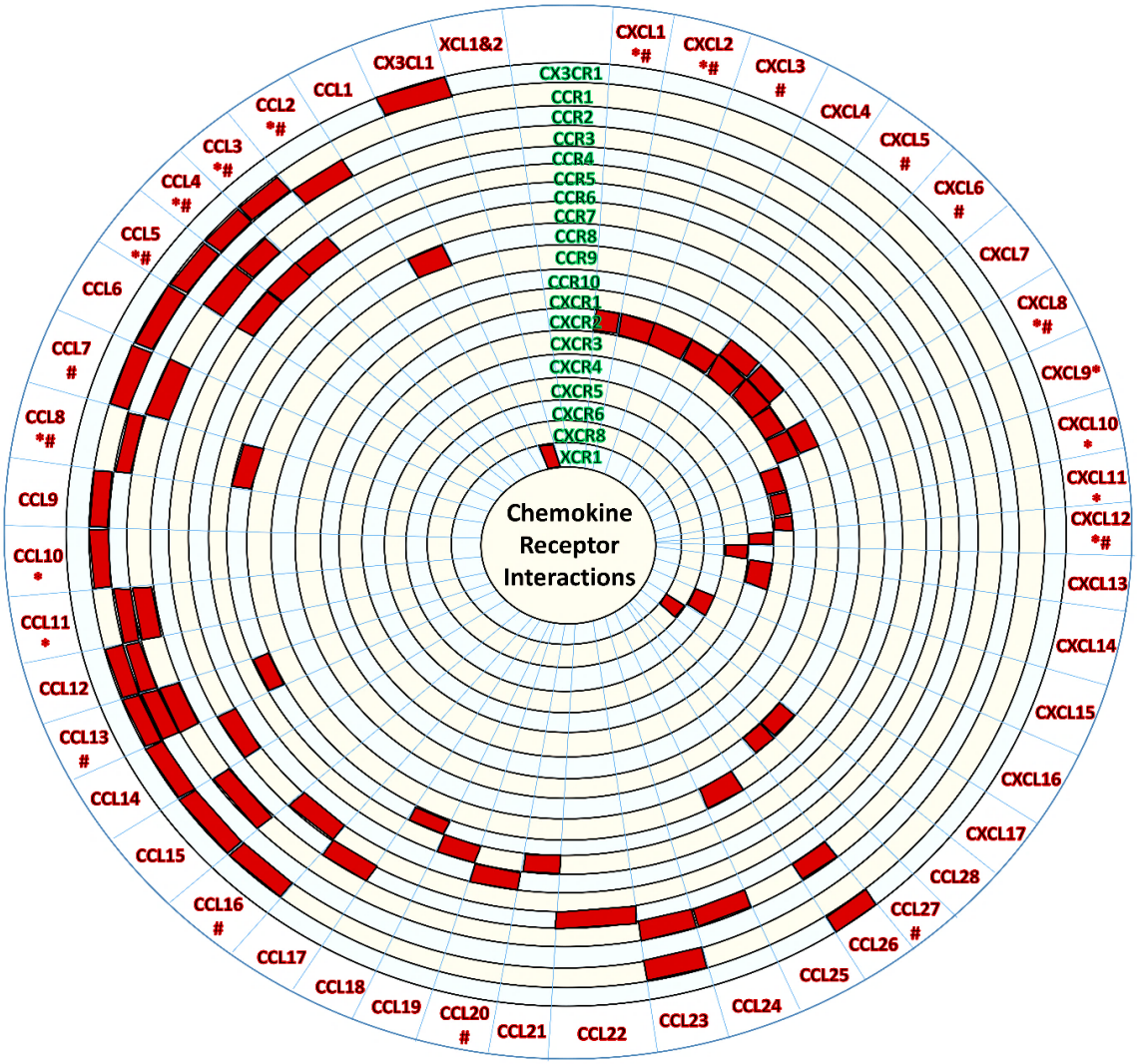

Figure 3.4. Classical chemokine receptor interactions. The major typical chemokine receptors matched to their ligands in a network (red tiles). Data obtained from Hughes & Nibbs (2018) and Zweemer et al. (2014). Atypical receptors are not shown. * = linked to wound healing (Bünemann et al., 2018; Ridiandries et al., 2018). # = linked to senescence (Acosta et al., 2008; Dulkys et al., 2004; Sagiv & Krizhanovsky, 2013). *Image produced by the author (HNW).*

Generation of the p16-3MR mouse, in which $p16^{+ve}$ cells can be detected and eliminated by the drug ganciclovir (GCV), allowed Demaria and colleagues (Demaria et al., 2014) to elucidate the temporal dynamics of senescent cells during wound healing, and determine how senescent cell attenuation contributes to wound repair. Here, eliminating $p16^{+ve}$ and $p21^{+ve}$ cells (using a murine p16/p21 double knockout, DKO) led to delayed wound healing. However, removing $p16^{+ve}$ or $p21^{+ve}$ cells

individually did not significantly reduce senescence or alter wound healing. Further, the authors deduced that the wound senescent cells were of mesenchymal origin (e.g. likely fibroblasts), producing Pdgfa as part of their SASP, an important growth factor for myofibroblast differentiation and wound resolution.

Although already discussed for their role in pathogenesis and the SASP, Mφs are important facilitators of multiple aspects of wound repair, including granulation, angiogenesis and tissue remodelling (reviewed in Koh & Dipietro, 2011). Mφs switch from a pro-inflammatory (M1-like) state to a pro-healing (M2-like) state to aid wound resolution (Lucas et al., 2010). In delayed healing, such as diabetes, a heightened pro-inflammatory Mφ response is observed (Bannon et al., 2013; Khanna et al., 2010). It follows that Mφs are strong candidates for involvement in the senescence aspect of cutaneous repair.

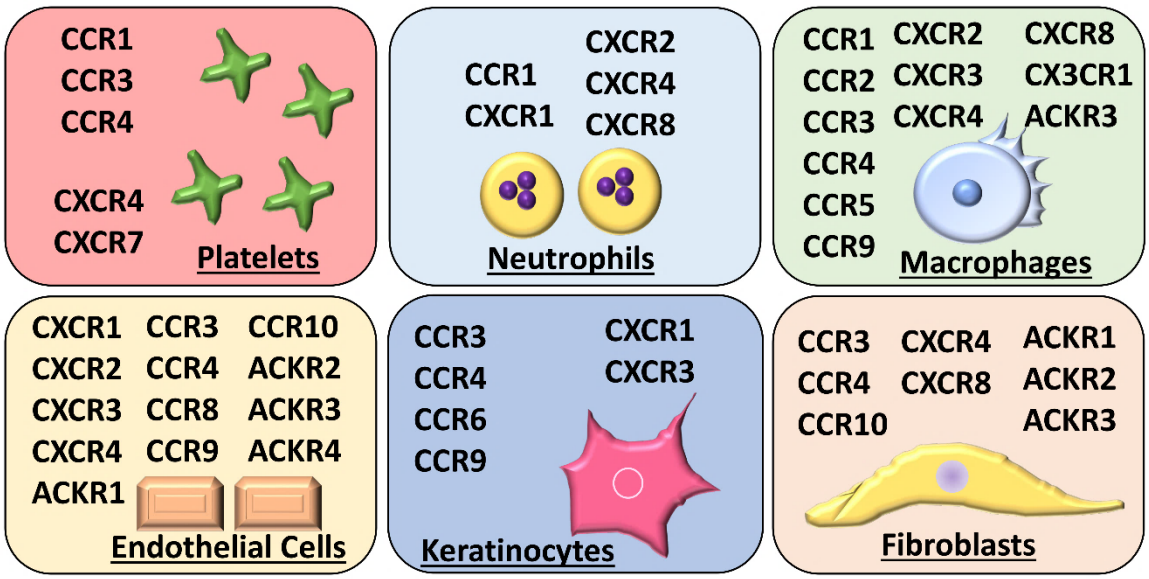

Figure 3.5. Chemokine receptor expression in wound-relevant cell types. Expression of chemokine receptors in major wound-relevant cells. Platelets (Chatterjee et al., 2015; Mancuso & Santagostino, 2017), neutrophils (Hughes & Nibbs, 2018), macrophages (Hughes & Nibbs, 2018; Sokol & Luster, 2015), endothelial cells (Bünemann et al., 2018), keratinocytes (Bünemann et al., 2018) and fibroblasts (Bünemann et al., 2018; Hughes & Nibbs, 2018). *Produced by the author (HNW).*

3.2. Chapter Aims

It was hypothesised that senescence plays an important role in the delayed healing phenotype observed in diabetes. The specific aims of this chapter were to:

1) **Characterise the expression of hallmark senescence biomarkers** in skin and wounds from murine models of normal (young and non-diabetic) and delayed (aged and diabetic) healing. Mφs play a crucial role in mediating senescence in multiple tissue types, thus diabetic Mφs were also screened for specific SASP components (e.g. Cxcl2).
2) **Explore the phenotypic cellular effects of senescence.** As Demaria et al. (2014) established that wound senescent cells were mesenchymal; the subsequent role of the diabetic Mφ SASP in mediating fibroblast senescence was established using HDFs.
3) **Evaluate the translational relevance of this research**. Here, an explicated diabetic SASP receptor (CXCR2) was blocked *in vitro*, during *ex vivo* human wound repair, and in Db murine wounds *in vivo*.
4) **Determine how p21 attrition influences wound healing.** Attenuation of the senescence markers p16 and p21 leads to delayed murine wound repair *in vivo* (Demaria et al., 2014). Hence, a $p21^{-/-}$ mouse model was used to determine the role of p21 in the inflammatory and proliferative aspects of wound healing.

3.3. Materials and Methods

3.3.1. Animal Experiments

Senescence was first assessed in skin and wound tissue from normal (young) and pathological (aged and diabetic) murine models (n = 6 per group, **Section 2.1**). Female p21$^{-/-}$ mice (Cdkn1a<tm1Led>/J) were obtained from the Jackson Laboratory (#016565) and maintained on a C57BL/6J background (as in Yosef et al., 2017). Experiments with p21$^{-/-}$ mice and WT controls (C57BL/6J) were performed at The Weizmann Institute of Science (Israel; n = 5 per group). For CXCR2 receptor antagonist experiments, Db mice were split into vehicle and treatment groups (n = 6) and excisional wounds created to the dorsum of each mouse. Treatments were administered via subcutaneous injection at the wound site every 2 days, with wounds collected at day 7 post-injury (illustrated in **Figure 3.4**). Wounding procedures and tissue collection are described in **Section 2.1**.

3.3.2. Histological Analysis

Masson's Trichrome staining was used to measure wound width, wound area and percentage re-epithelialisation of wounds, while IHC assessed the cellular aspects of wound healing. Immune cell influx was measured via Mac3 (Mφ) and Ly6-G (neutrophil) staining of granulation tissue. Mφ polarisation was determining via nitric oxide synthase 2 (Nos-2; M1-polarisation) and Arginase 1 (M2-polarisation) staining of p21$^{-/-}$ wound tissue. Matrix remodelling was evaluated via picrosirius red staining. Cellular proliferation was measured via counting Ki67^{+ve} cells in the granulation tissue and neo-epidermis of p21$^{-/-}$ wounds. Levels of Mif, α-Sma (fibroblast differentiation) and Pdgfa (SASP factor) were also determined in p21$^{-/-}$ mice. Tissue senescence was established via measuring SA-βGAL positive cells from OCT (optimum cutting temperature medium) sections (as in Krizhanovsky et al., 2008). As p16 and p21 are widely used markers of senescence, immunohistochemistry elucidated p16 and p21 changes in skin and wounds.

3.3.2.1. Image Analysis

Images were taken at x4 (Masson's Trichrome staining) and x20 magnification (all other histological staining) and analysed using Image Pro-Plus v.6.2.0 (Media

Cybernetics, Finchampstead, UK) as in **Section 2.4.9**. Statistical analysis was performed as in **Section 2.9**.

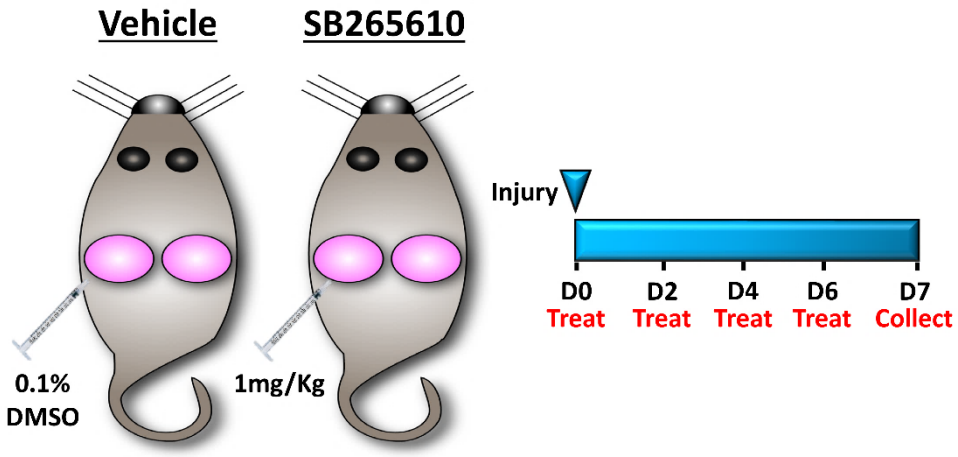

Figure 3.6. Design of Cxcr2 antagonist experiments for diabetic wounds. Excisional wounds were created on the dorsum of female, diabetic mice (8 weeks old). Mice were wounded and treated with vehicle (0.1% DMSO in DPBS) or antagonist (1mg/Kg SB265610 in vehicle) via wound bed injection. Treatments were administered every 2 days and wounds were collected at day 7 (D7) post-injury. *Figure produced by the author (HNW).*

3.3.3. SASP Conditioning Experiments

NDb and Db Mφs were isolated from bone marrow (n = 5 mice), differentiated and cultured as described in **Section 2.6.9**. Stimulation media was aspirated and replaced with fresh serum-free DMEM. Mφs were cultured for a further 48 hours and conditioned media (CM) was collected and sterile-filtered (through a 0.2 µm filter, Merck-Millipore) for conditioning experiments. RNA was extracted from the Mφs to determine senescence profiles (*Cdkn1a* and *Cdkn2a* mRNA), polarisation state (*Nos2* and *Ym1* mRNA) and ligand/receptor expression (*Cxcl1*, *Cxcl2* and *Cxcr2* mRNA). Mφs were also stained for senescence (p16 and p21) and polarisation (Nos-2 and Arginase-1) markers via immunocytochemistry (ICC).

Young (>50) and aged (<80) primary human dermal fibroblasts (HDFs) were isolated (n = 3 per group; **Section 2.3.2**). HDFs were treated with Mφ CM for 24 hours at 37°C and 5% CO_2 and collected for RNA. Data is presented as heatmaps, produced in GraphPad Prism v.7.0 (GraphPad Software Inc, California, US).

3.3.3.1 Characterising the Diabetic Macrophage Secretome

A Proteome Profiler Mouse Cytokine Array Kit (R&D systems, Abingdon, UK) was used to assess cytokine profiles of NDb and Db Mφ CM. Films were developed and

integrated density analysis performed in ImageJ v.1.8 (as for western blot, **Section 2.6.7.6**). As antibody array profiling does not elucidate changes in protease activity, gelatin zymogram analysis was used for this purpose (**Section 2.8.7.2.3**). Zymography gels were repeated in four independent experiments. MMP-2 activity was determined using densitometric analysis (ImageJ v.1.8) and ratios taken relative to the control group (NDb, non-polarised CM).

3.3.4. Transfection

HDFs were transfected with a control plasmid (pUNO1-mcs), or CXCL2-containing plasmid (pUNO1-CXCL2; both InvivoGen, Toulouse, France), which was amplified via bacterial transformation and purification (described in **Section 2.6.8**). Optimum concentrations of plasmid DNA and Lipofectamine® 3000 reagent (Thermo Fisher Scientific) were determined via counting YFP^{+ve} cells (on the Livecyte™, **Section 2.6.10**). Optimisation is shown in **Table 3.1**.

To ascertain whether CXCL2 transfection led to potentiation of a CXCL2-driven SASP and induction of p21, transfected cells were collected 2 days and 6 days post-transfection. ICC, qRT-PCR and gelatin zymography was performed as described above. HDF CM was profiled with a Proteome Profiler Human Cytokine Array Kit (Biotechne) following manufacturer's instructions.

3.3.5. Scratch Analysis

To determine how CXCR2 blockade affects *in vitro* keratinocyte migration, the CXCR2 antagonist, SB265610 (Biotechne), was used at 100 nM concentration, along with the CXCR2 ligands, CXCL1 and CXCL2 (30 ng/mL). Confluent monolayers of HaCaTs (obtained from AddexBio, San Diego, UK) were scratched, treated, and incubated at 5% CO_2 and 37°C for eight hours.

Scratch assays were also performed at 24 hours, with SB265610 used in conjunction with the CXCR2 ligands, CXCL1 and CXCL2 (described in **Table 3.2**). This allowed determination of the effects of combinatorial ligand treatment, while elucidating the specificity of the CXCR2 antagonist.

3.3.6. Human Wounding Experiments

The effects of CXCR2 antagonist were next determined in *ex vivo* human wound biopsies (**Section 2.3.1**). Treatments (100 nM SB265610 and a DMSO vehicle control) were applied topically to each wound. Wounds were cultured for 24 hours

at 37°C and 5% CO_2. Epidermal wound closure (KRT14 IHC) and epidermal basal cell proliferation (Ki67 IHC) were measured. Later stage wound healing was also assessed (3 days post-injury), including the treatments described in **Table 3.2**. Epidermal repair was measured via KRT14 and KRT6 IHC.

Table 3.1. Optimisation of transfection efficiencies using Lipofectamine® 3000 reagent and yellow fluorescent protein plasmid DNA.

Time	Lipofectamine® 3000	DNA	Positive cells	Negative cells	Transfection Efficiency (%)
6hr	0.75 µL	0.25 ng	0	419	0
6hr	0.75 µL	0.5 µg	18	504	3.448275862
6hr	0.75 µL	1 µg	34	386	8.095238095
6hr	1.5 µL	0.25 ng	34	244	12.23021583
6hr	1.5 µL	0.5 µg	44	552	7.382550336
6hr	1.5 µL	1 µg	65	341	16.00985222
6hr	1.5 µL	2 µg	39	345	10.15625

3.3.7. RT² Profiler PCR Arrays

PCR arrays were performed on vehicle-treated and SB265610-treated Db wounds. RNA was isolated and reverse transcribed into cDNA as described in **Section 2.7**. cDNA was diluted 100-fold and added to RT² Profiler PCR Array (Qiagen) plates with 2X Takyon SYBR mastermix (Eurogentec). qRT-PCR was performed and data was analysed using CFX Manager™ software (Bio-Rad Laboratories).

Table 3.2. Treatments used for *in vitro* and *ex vivo* human wound experiments.

Treatment Group	Concentration
DMSO	0.1% (v/v)
CXCL1	30 ng/mL
CXCL2	30 ng/mL
CXCL1 & CXCL2	15 ng/mL & 15 ng/mL
SB265610	100 nM
CXCL1 & SB265610	30 ng/mL & 100 nM
CXCL2 & SB265610	30 ng/mL & 100 nM
CXCL1 & CXCL2 & SB265610	15 ng/mL & 15 ng/mL & 100 nM

3.4. Results

3.4.1. Senescent cell accumulation in skin pathology.

To quantify differences in senescent cell numbers between normal (young) and pathological (Db and aged) skin, SA-βGAL staining was performed (**Figure 3.7A-D**). The greatest number of SA-βGAL^{+ve} cells was found in aged epidermis ($P < 0.001$), aged dermis ($P < 0.001$) and aged hair follicles ($P < 0.01$), compared to young. Interestingly, a trend towards increased dermal SA-βGAL was observed in Db tissue, approaching significance in dermis ($P = 0.06$).

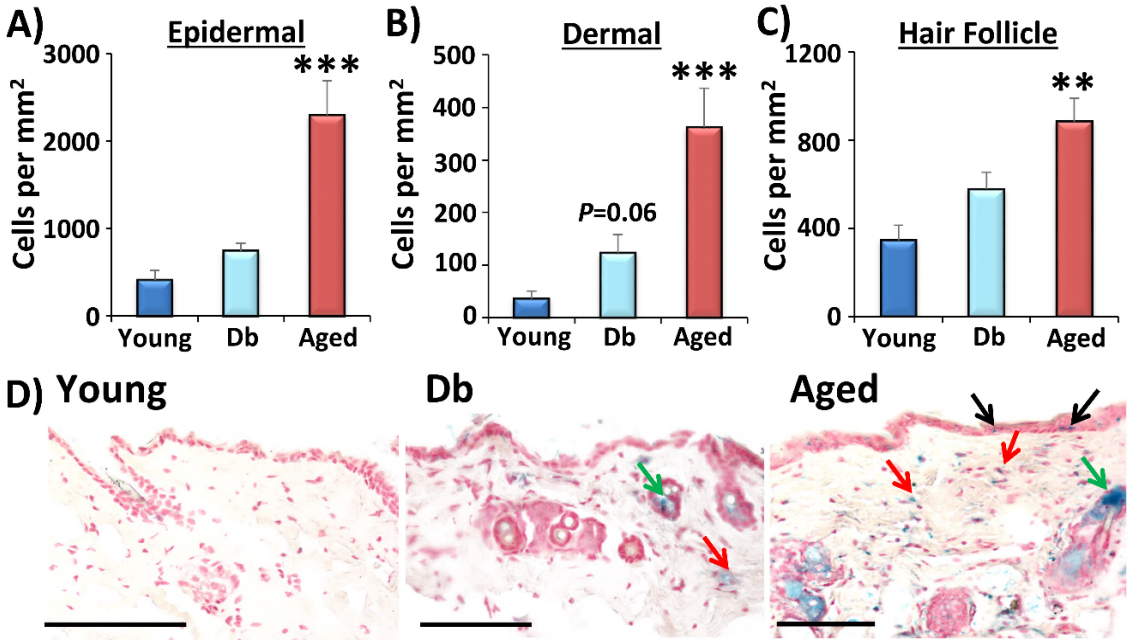

Figure 3.7. Profiling SA-βGAL in uninjured skin from normal and pathological murine wound models. Senescence-associated beta galactosidase (SA-βGAL) staining demonstrates increased senescent cells (blue) in epidermis (**A**), dermis (**B**) and hair follicles (**C**) of aged skin. Representative images of SA-βGAL^{+ve} epidermal cells (black arrows), dermal cells (red arrows) and hair follicle cells (green arrows) are shown in **D** with a neutral red counterstain. n = 5-6 animals per group. Data represent mean + SEM. Bar = 100 μm. Db = diabetic. ** = $P < 0.01$, *** = $P < 0.001$ One-way ANOVA with Dunnett's correction for multiple hypotheses (versus young).

To further characterise the senescence in Db and aged skin, IHC was performed using the well-documented CDKIs, p16 and p21. In agreement with SA-βGAL staining, significantly more p16^{+ve} cells were observed in aged dermis ($P < 0.001$; **Figure 3.8A, D**), with a trend towards induction of p16^{+ve} cells in aged hair follicles (**Figure 3.8B, D**). Ageing also led to heightened accumulation of p21^{+ve} dermal cells (**Figure 3.8C-D**; $P < 0.05$). Interestingly, little increase in p16^{+ve} or p21^{+ve} cells was observed in unwounded Db skin.

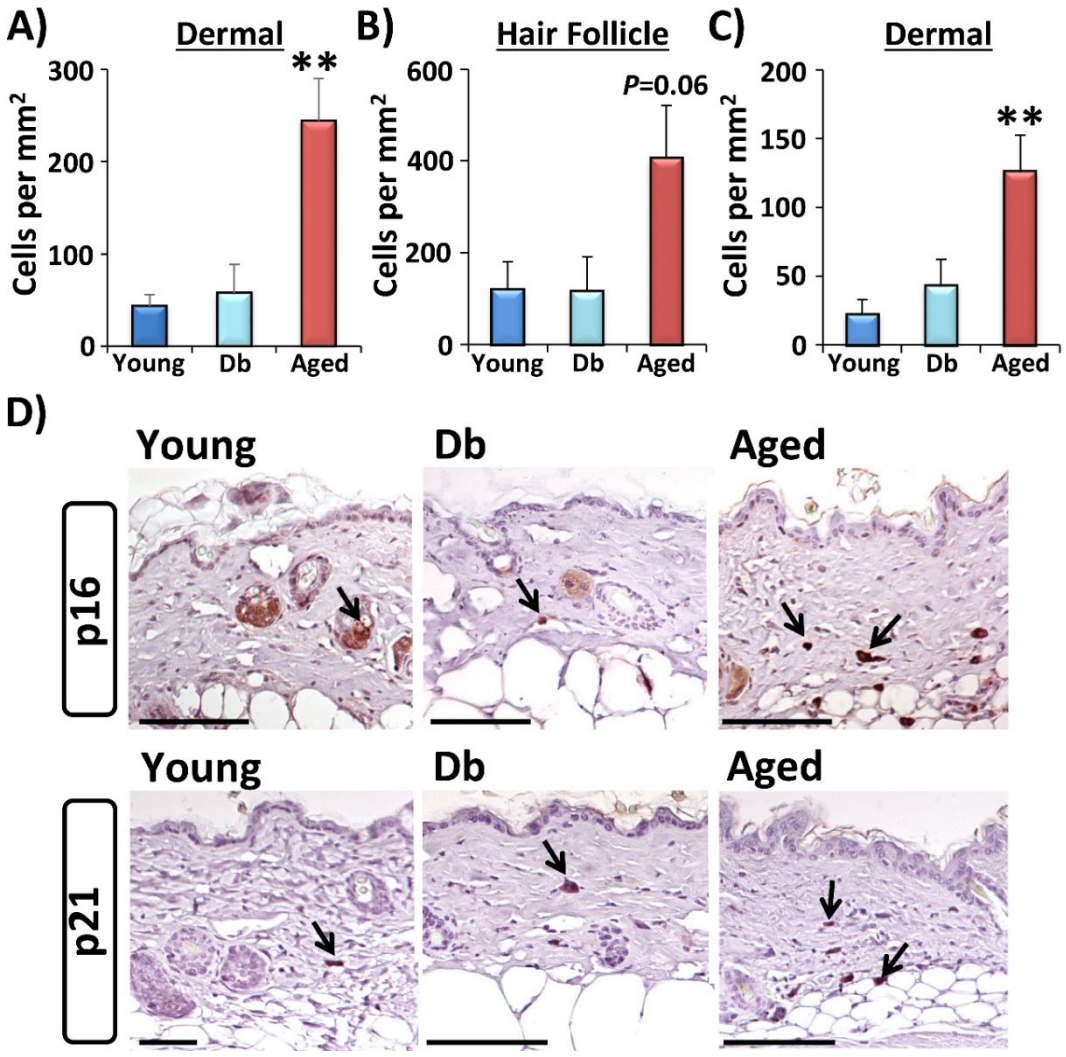

Figure 3.8. Profiling p16 and p21 in uninjured skin from normal and pathological murine wound models. Immunohistochemistry (IHC) illustrates increased p16^{+ve} (dermal, **A**; hair follicle, **B**), and p21^{+ve} (dermal, **C**) cells in aged skin (compared to young). IHC images depict p16^{+ve} and p21^{+ve} cells (brown red) by black arrows (**D;** n = 5-6 mice per group). Db = diabetic. Mean + SEM. Bar = 100 µm. ** = $P < 0.01$. One-way ANOVA with Dunnett's correction for multiple hypotheses (versus young).

3.4.2. Planimetric and cellular analysis confirms delayed wound healing in pathological models.

Aged and Db mice are widely used models of pathological repair (Ashcroft et al., 1997; reviewed in Ansell et al., 2012). To confirm that the mice used in this study demonstrated pathological healing, wound closure at day 7 (D7) post-injury was assessed via histology and compared to normal healing controls. Masson's Trichrome staining confirmed delayed healing in the aged (**Figure 3.9**) and Db (**Figure 3.10**) mouse models. Wound area (aged, $P < 0.05$; Db, $P < 0.01$) and wound width (aged, $P < 0.001$; Db, $P < 0.001$) were significantly larger in the aged (**Figure**

3.9A-C) and Db (**Figure 3.10A-C**) wounds compared to young and NDb controls, respectively. Percentage epidermal closure was also significantly delayed (aged, $P < 0.001$; Db, $P < 0.05$), with ageing (**Figure 3.9D**) and diabetes (**Figure 3.10D**).

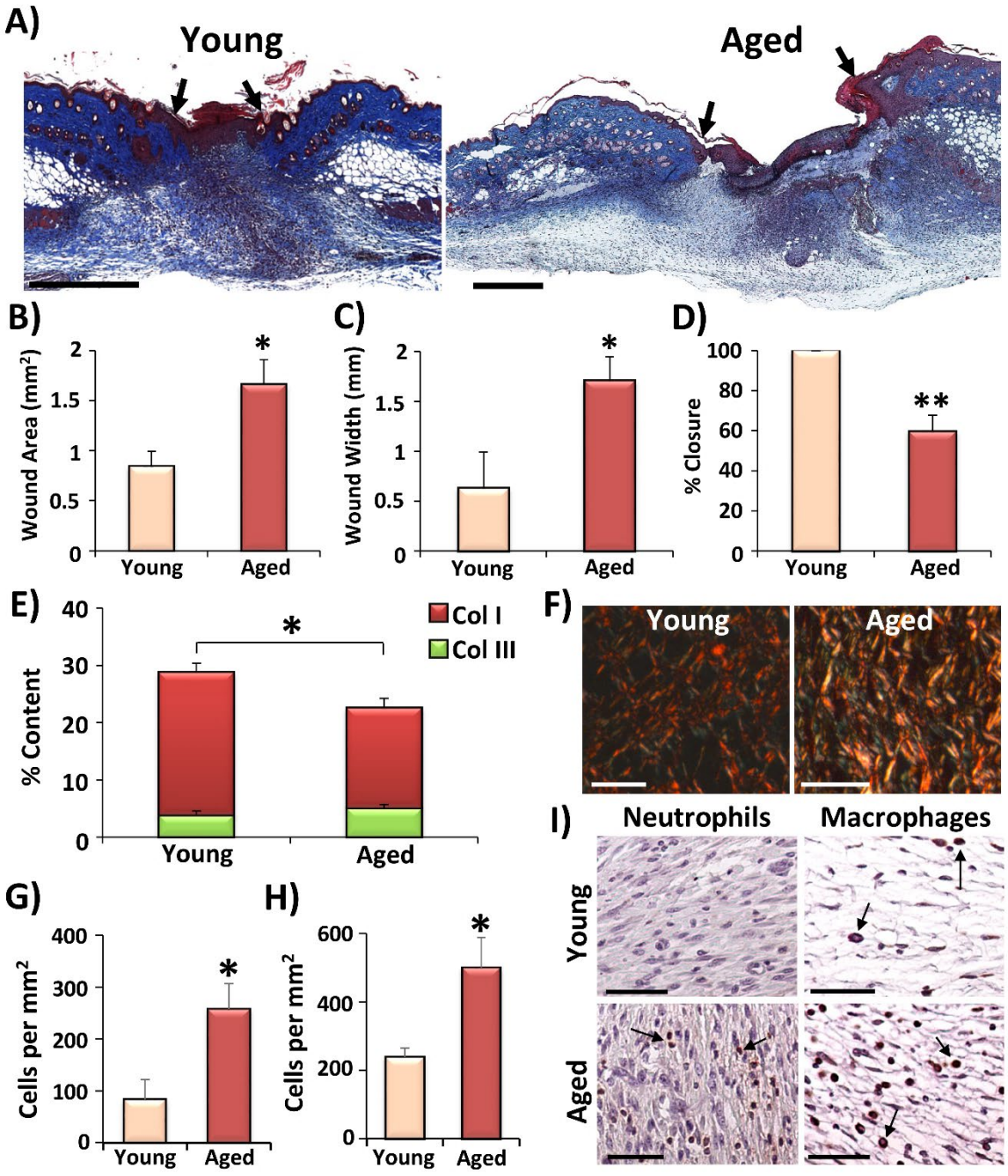

Figure 3.9. Confirmation of a delayed wound healing phenotype in aged mice. Masson's Trichrome staining of young and aged (**A**) wounds (day 7 post-injury) demonstrates a delay in wound repair in the aged model. Black arrows depict wound edges. Wound area (**B**), wound width (**C**) and percentage epidermal closure (**D**) were measured. Bar = 500 µm. Collagen type I (COL I, red birefringence) content (**E**), assessed by picrosirius red staining (**F**), was significantly reduced in aged wounds. White bar = 100 µm. Immunohistochemistry shows increased neutrophils (**G**, **I**) and macrophages (**H**, **I**) in aged wounds. Black arrows = brown-red positive staining. Black bar = 50 µm. n = 6 mice per group. Mean + SEM. * = $P < 0.05$, ** = $P < 0.01$, two-tailed independent Student's *t* tests.

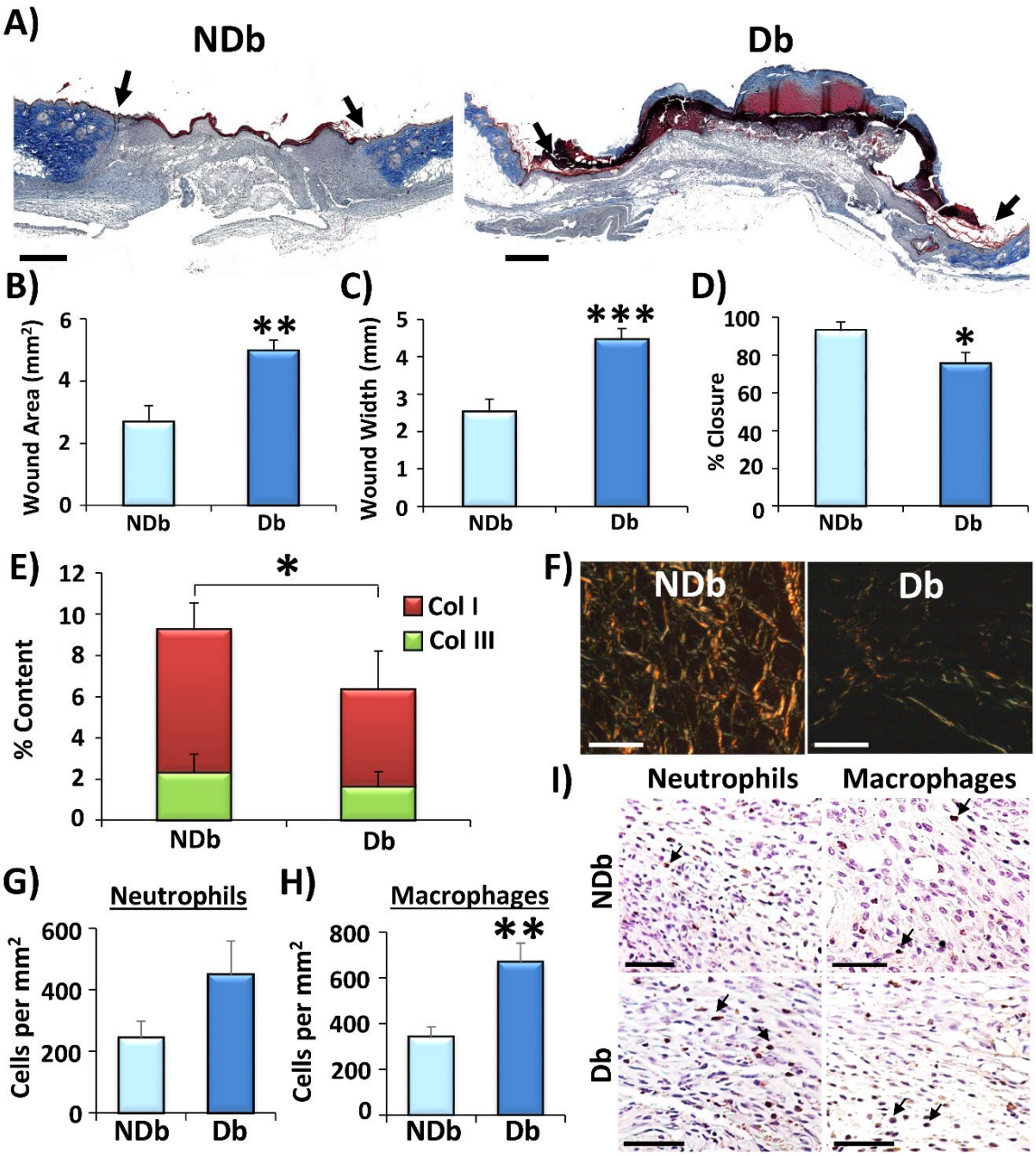

Figure 3.10. Confirmation of the diabetic pathological wound healing phenotype. Diabetic (Db) and non-diabetic (NDb) wounds at day 7 post-injury were Masson's Trichrome stained (**A**, bar = 500 µm). Black arrows depict wound edges. Wound area (**B**) and wound width (**C**) were significantly larger in Db wounds, while percentage epidermal closure (**D**) was delayed. Db wounds displayed reduced collagen type I (COL I, red birefringence) content (**E**), as illustrated by picrosirius red staining (**F**, white bar = 100 µm). Neutrophil (**G**) and macrophage (**H**) wound cell counts and representative immunohistochemistry (**I**) are provided. Black arrows = brown-red positive staining. Bar = 50 µm. Mean + SEM. * = $P < 0.05$, ** = $P < 0.01$, *** = $P < 0.001$. n = 4-6 mice per group. Two-tailed independent Student's *t* tests were performed on all data sets.

As wound healing progresses, ECM deposited early in repair (e.g. collagen type III) is gradually replaced by more permanent, late-stage matrix proteins (e.g. collagen type I; Martin & Nunan, 2015). Picrosirius red staining was used to measure matrix maturation. Here, aged ($P < 0.05$; **Figures 3.9E-F**) and Db ($P < 0.05$; **3.10E-F**,) wounds displayed reduced orange-red birefringence (i.e. less collagen type I) than normal healing control wounds.

Finally, the inflammatory status of the pathological wounds was confirmed via immunohistochemistry, giving an indication of wound resolution (Martin, 1997). Substantially greater wound site neutrophils ($P < 0.05$) and Mφs ($P < 0.05$) were observed in aged wounds compared to young (**Figure 3.9G-I**). Mφ infiltration was significantly elevated in Db wounds compared to NDb ($P < 0.01$; **Figure 3.10H-I**), while neutrophils displayed a trend towards increased levels in Db wounds.

3.4.3. Injury-induced senescence is increased in pathological wounds.

Significantly greater numbers of SA-βGAL^{+ve} cells were visualised in aged ($P < 0.05$) and Db ($P < 0.01$) wounds (D7) compared to normal healing controls (**Figure 3.11A-C**). Aged wounds presented similar levels of p16 (**Figure 3.11D**), but significantly more p21^{+ve} cells (**Figure 3.11F**), to young wounds. Db wounds displayed a non-significant trend towards increased p16 (**Figure 3.11E**) and p21 (**Figure 3.11G**) compared to NDb. Further, qRT-PCR profiling of skin (D0) and D7 wounds from young, Db and aged mice confirmed heightened senescence in aged skin (**Figure 3.12A-D**) where *Cdkn1a* ($P = 0.05$), *Cdkn1b* ($P < 0.05$), *Cdkn2a* ($P < 0.01$) and *Trp53* (p53; $P < 0.01$) were all upregulated. Intriguingly, aged wounds displayed significant downregulation of the senescence markers, and no change in senescence was observed between young skin and wounds at the mRNA level. Of note, Db wounds exhibited significant induction of *Cdkn1a* ($P < 0.05$; **Figure 3.12A**), thus suggesting a potential link between diabetic wound senescence and p21. Together, these data demonstrate that: (a) senescent cells accumulate in delayed healing wounds and; (b) senescence is differentially affected by pathology.

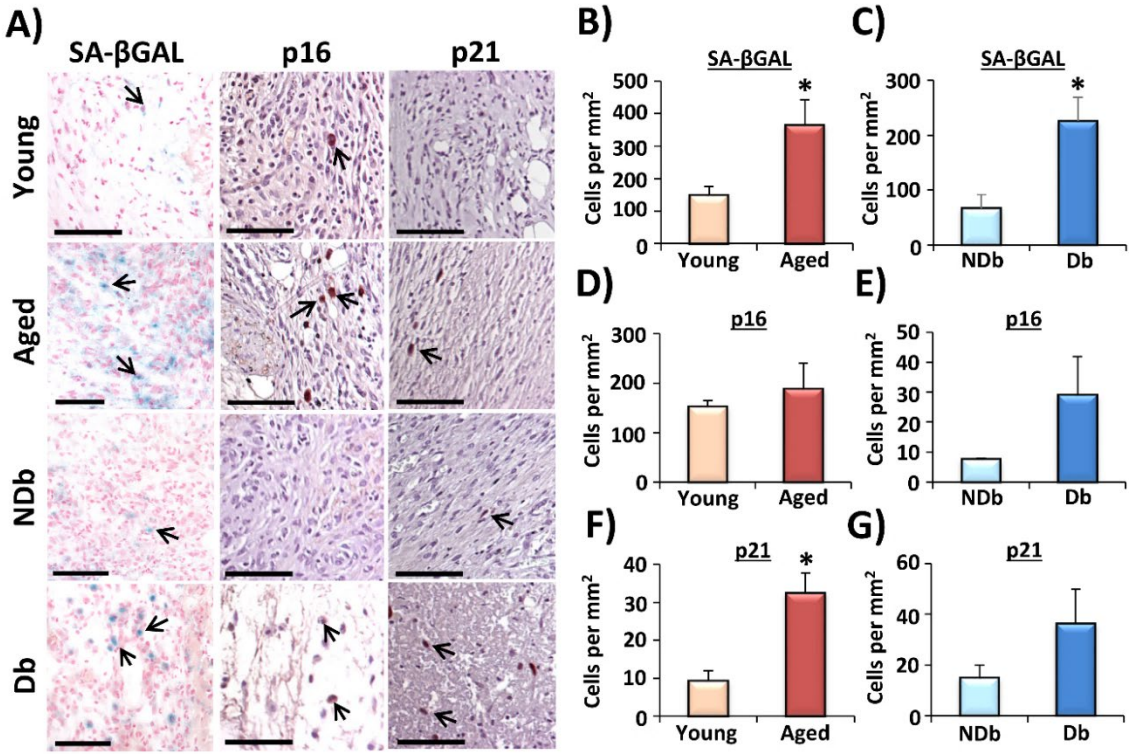

Figure 3.11. Accumulation of senescent cells correlates with pathological wound healing. Senescence-associated beta galactosidase (SA-βGAL, blue, black arrows) staining comparing young and aged, and non-diabetic (NDb) and diabetic (Db), wounds at day 7 post-injury (**A-C**, n = 6 per group). Immunohistochemistry showing p16^{+ve} cells (**A, D-E**) and p21^{+ve} cells (**A, F-G**, n = 4-6 per group. Brown-red p16^{+ve} and p21^{+ve} cells = black arrows. Mean + SEM. Bar = 100 μm. * = $P < 0.05$, two-tailed, unpaired Student's *t* tests.

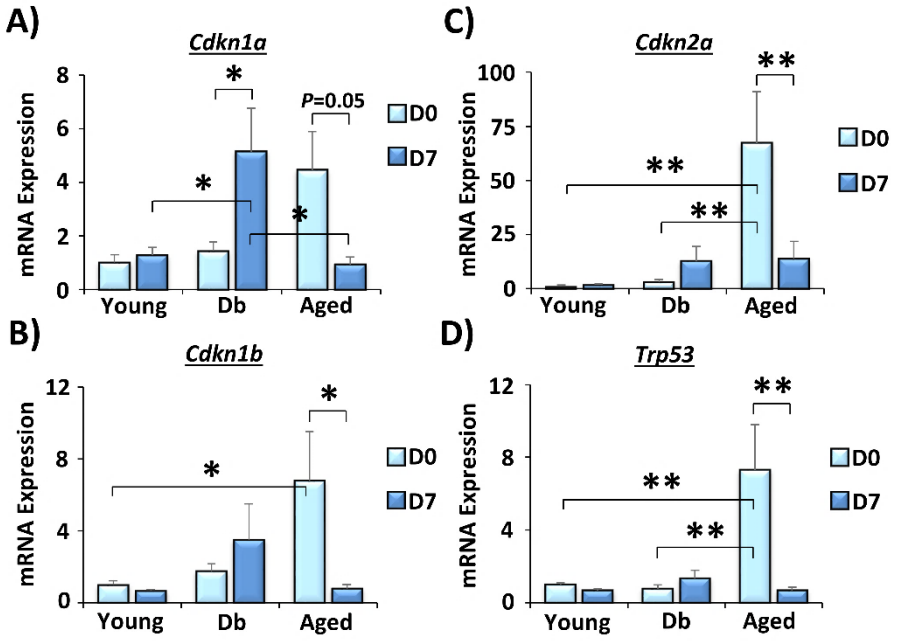

Figure 3.12. Aged skin displays a senescent gene profile, while diabetic wounds show p21 mRNA induction. qRT-PCR for senescent genes *Cdkn1a* (p21, **A**), *Cdkn1b* (p27, **B**), *Cdkn2a* (p16, **C**) and *Trp53* (p53, **D**). All genes are upregulated in aged normal skin (D0). *Cdkn1a* is significantly induced in diabetic (Db) wounds at day 7 post-injury (D7). n = 3 mice per group. Data = mean + SEM. * = $P < 0.05$, ** = $P < 0.01$. Significance was determined via two-way ANOVA with Sidak's correction.

3.4.4. Diabetic wound macrophages exhibit elevated senescence.

Senescence is a known intrinsic ageing mechanism, but its role in diabetes has only recently been described (Palmer et al., 2015). Therefore, immunofluorescence of wound Mφs in combination with p16 was performed, revealing high levels of senescence in Db Mφs (60%) compared to NDb ($P < 0.001$; **Figure 3.13**). This novel finding led to further exploration of the Db Mφ senescent phenotype.

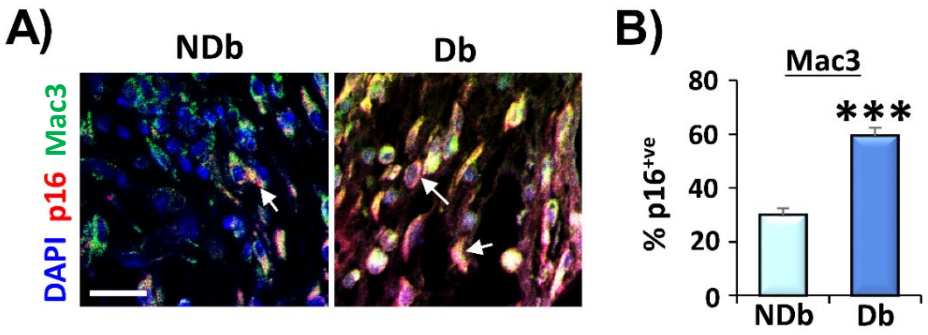

Figure 3.13. Diabetic wound macrophages are highly senescent. Immunofluorescent staining (**A**) for p16 (senescence) and Mac3 (macrophages) demonstrates increased $p16^{+ve}$ macrophages in diabetic (Db) wounds (compared to non-Db, NDb; **B**). n = 5 mice per group. Bar = 20 μm. Data = mean + SEM. *** = $P < 0.001$. Independent two-tailed Student's *t* test.

3.4.5. Diabetic macrophages possess a secretome which influences macrophage-fibroblast cross-talk.

Since injury-induced senescence is dependent on pathology, and delayed wound healing is characterised by deleterious Mφ function (Bannon et al., 2013), Db Mφ senescence was next profiled to establish its SASP-related influence on the wound environment (summarised in **Figure 3.14A**). Here, CM was collected from polarised Mφs for SASP array profiling, while the Mφs were collected for SA-βGAL, ICC and qRT-PCR. Finally, CM was administered to primary HDFs to determine how Db Mφ SASP influenced fibroblast senescence induction (qRT-PCR). SA-βGAL staining revealed heightened senescence in Db Mφs, regardless of polarisation state ($P < 0.001$; visualised in **Figure 3.14B**, quantified in **Figure 3.14C**). As expected, Db M1- ($P < 0.05$) and M2-stimulated ($P < 0.001$) Mφs presented increased *Cdkn1a* expression (**Figure 3.14D**), while M1-stimulated Db Mφs displayed elevated levels of *Cdkn2a* ($P < 0.01$, **Figure 3.14E**). Mφ polarisation was assessed using validated markers of polarisation (*Nos2* and *Ym1*), where NDb Mφs more readily shifted to M1 ($P < 0.001$) and M2 ($P < 0.01$) states than Db Mφs (**Figure 3.14F-G**). These data clearly demonstrate that Db Mφs are less responsive to polarisation and more senescent than NDb Mφs.

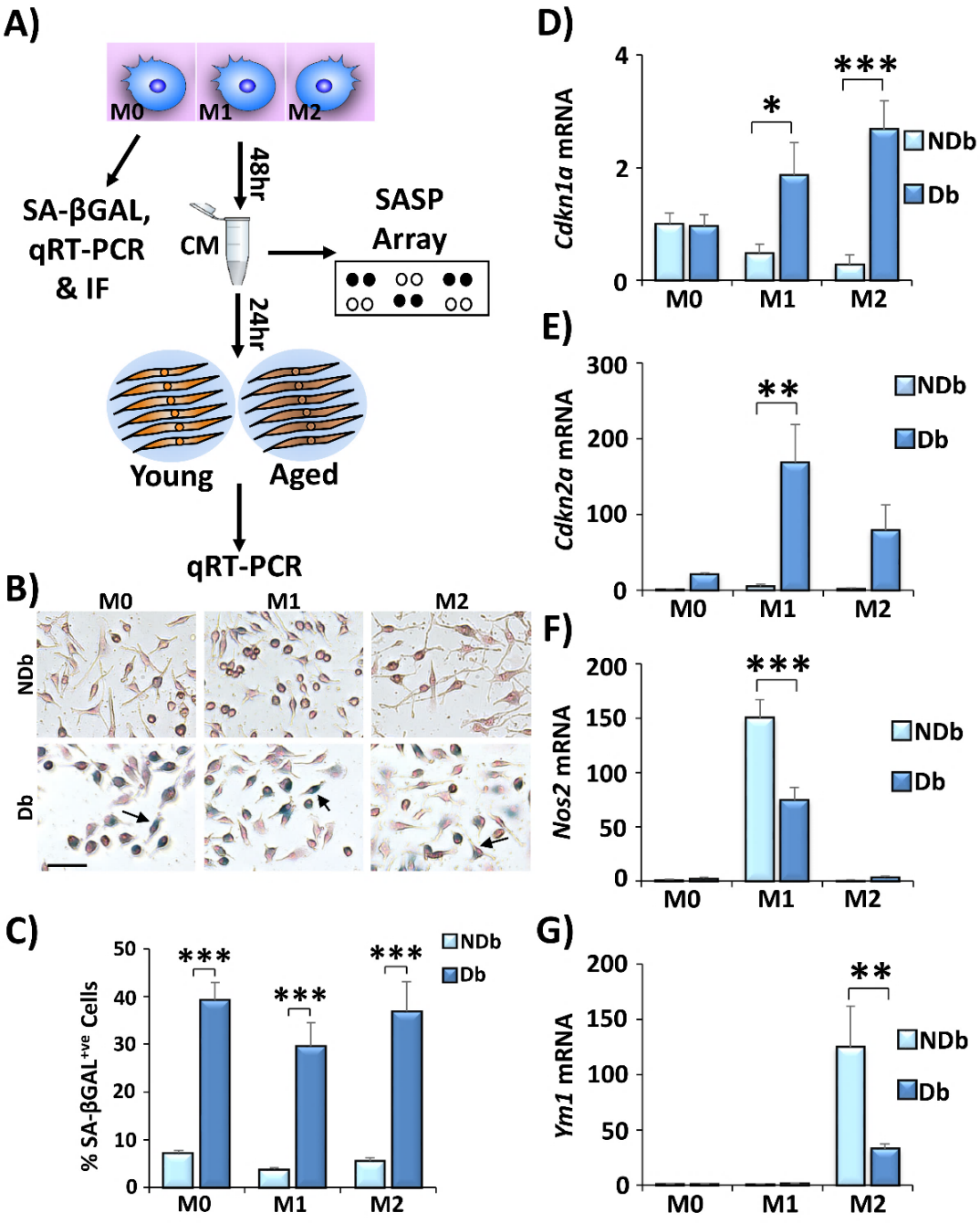

Figure 3.14. Diabetic bone marrow-derived macrophages are intrinsically susceptible to senescence. A schematic of the experimental set-up for testing macrophage (Mφ) senescence and Mφ effects on the local environment (**A**). Non-stimulated (M0), or stimulated (M1 and M2) Mφs from non-diabetic (NDb) and diabetic (Db) mice were profiled via SA-βGAL staining, qRT-PCR and immunofluorescence (IF). Conditioned media (CM) was collected from Mφs 48 hours post-stimulation and: a) profiled for cytokines (SASP array); or b) directly placed on human fibroblasts (young and aged, n = 3 donors per group). SA-βGAL demonstrates that Db Mφs are highly senescent (**B**, quantified in **C**). Bar = 50 µm. qRT-PCR further confirms the Db senescent phenotype with significantly higher levels of *Cdkn1a* (gene encoding p21, **D**) and *Cdkn2a* (p16) expression (**E**). Db Mφs are also less readily polarised to M1 (*Nos2*, **F**) and M2 (*Ym1*, **G**) states. n = 5 animals per group. Data = mean + SEM. * = $P < 0.05$, ** = $P < 0.01$, *** = $P < 0.001$. Significance determined via two-way ANOVA with Sidak's correction (NDb versus Db).

ICC staining for M1 and M2 markers demonstrated similar effects, where lower Nos-2 and Arginase-1 expression was apparent in Db Mφs (**Figure 3.15A**). Due to the observed differences in both polarisation state and p16 and p21 transcription, the cytokine profile of Mφ CM was characterised using antibody arrays. Here, a number of SASP-relevant soluble factors were elevated in the Db Mφ secretomes, in both M1- and M2-stimulated Mφs (**Figure 3.15B-C**). For visualisation purposes, the data are shown as fold changes (NDb versus Db). A number of cytokines and chemokines were upregulated in Db Mφ CM, including Cxcl1, Rantes, Cxcl2, Mip-1α, Tnf-α, Il-1ra and Timp-1, all now subsumed as SASP components (Chien et al., 2011). Fold changes below two-fold difference are displayed in a separate chart (**Figure 3.16A**). Individual fold changes (in descending order) are also provided for individual M1 (**Figure 3.16B**) and M2 (**Figure 3.16C**) comparisons.

Returning to the Db Mφs, qRT-PCR verified upregulation of *Cxcl1* and *Cxcl2* and *Cxcr2* at the mRNA level (**Figure 3.17A**). Gelatin zymography was used to explore relative changes in protease activity. Here, increased activity of the key wound gelatinase, MMP-2, a key component of the SASP, was revealed in Db M0 and M2-stimulated CM (compared to NDb, $P < 0.05$, **Figure 3.17B**). To confirm that Cxcl2 (and Cxcl1 and Cxcr2) were Db-specific SASP factors linked to wound repair, transcriptional profiling of these chemokines was performed in normal skin (D0) and wounds (D7) from young and pathological (Db and aged) murine models. In concurrence with the Mφ data, *Cxcl1* ($P < 0.001$), *Cxcl2* ($P < 0.05$) and their common receptor, *Cxcr2* ($P < 0.05$; Baggiolini, 2001), were all significantly elevated in Db wounds, but not in aged or young wounds (**Figure 3.17C-E**, respectively).

Previously, Demaria et al. (2014) demonstrated that a mesenchymal SASP influenced fibroblast differentiation during wound repair. Given the reported similarities between mouse and human fibroblast SASP components (Coppe et al., 2010), the influence of the Db murine Mφ SASP was investigated on human fibroblasts. Both young and aged HDFs were directly treated with Db (and NDb) CM and profiled with a panel of ECM (*COL1A1*, *COL3A1*, *FN1*), senescence (*CDKN2A*, *CDKN1A*, *NFE2L2*, *SERPINE1*) and SASP (*PDGFA*, *CXCL1* and *CXCL2*) markers (**Figure 3.17F**). Interestingly, both *CXCL1* and *CXCL2* were themselves induced in human fibroblasts treated with Db CM. Db Mφ SASP also indiscriminately upregulated levels of *SERPINE1* (encoding PAI-1), a well-known marker of fibroblast senescence

(Kortlever et al., 2006), in young HDFs ($P < 0.05$). Significant elevations in *SERPINE1* in aged HDFs were only apparent following Db M1 CM treatment ($P < 0.01$).

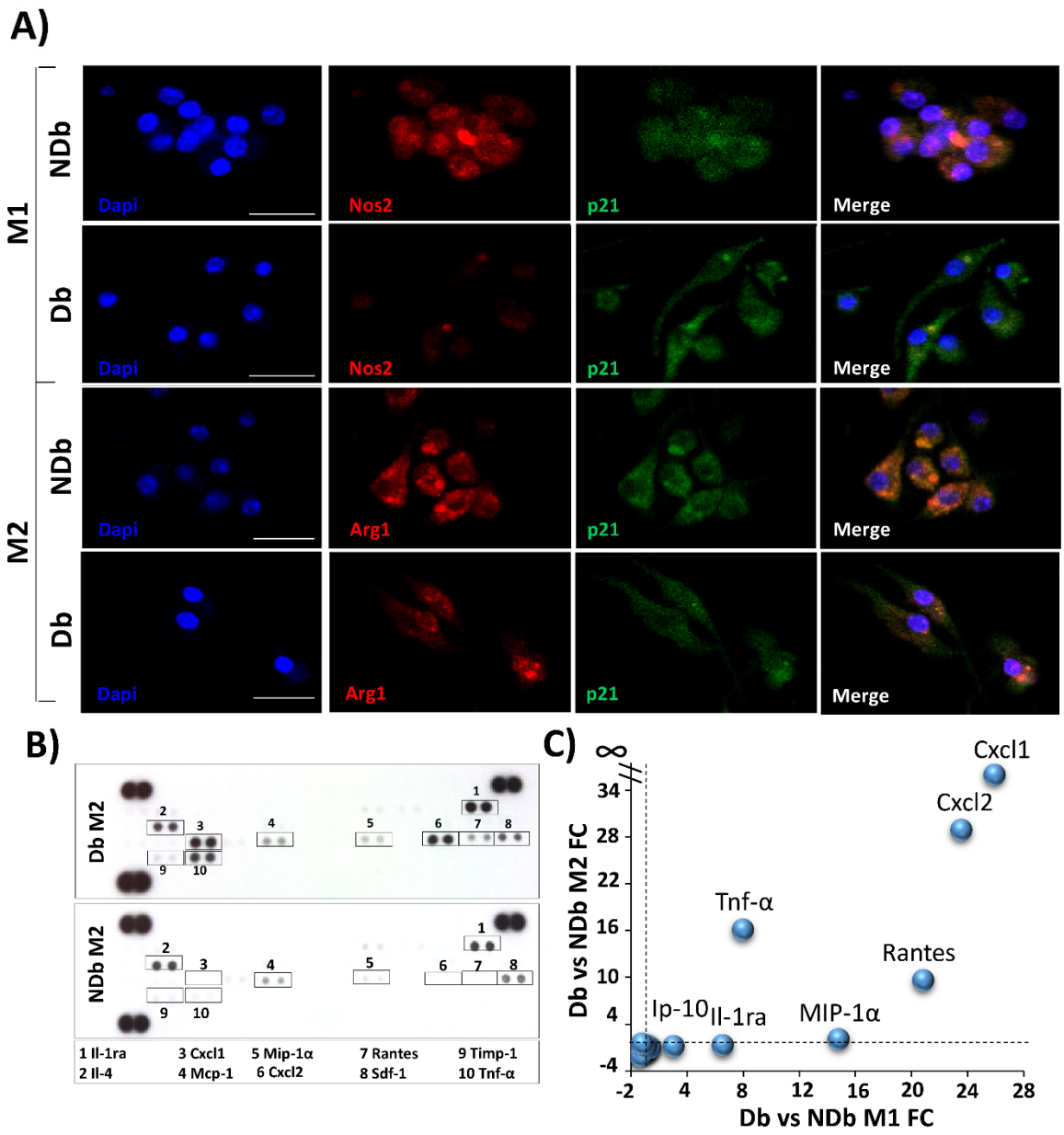

Figure 3.15. Diabetic macrophages produce a senescent secretome governed by Cxcr2. Immunofluorescence demonstrates reduced polarisation capacity of diabetic (Db) (**A**) compared to non-diabetic (NDb) macrophages (Mφs). Nos2 = Nos-2. Arg1 = Arginase-1. Bar = 20 μm. M1 = pro-inflammatory. M2 = anti-inflammatory. Conditioned media (CM) was collected from NDb and Db M1 and M2 Mφs and investigated via cytokine array (representative M2 blots, **B**). Quantification (**C**) depicting substantial differences in the listed cytokines (FC = fold change), of which the Cxcr2 ligands, Cxcl1 and Cxcl2, showed the most differential changes between NDb and Db Mφs. n = 5 animals per group. Cytokine arrays were repeated in two independent experiments.

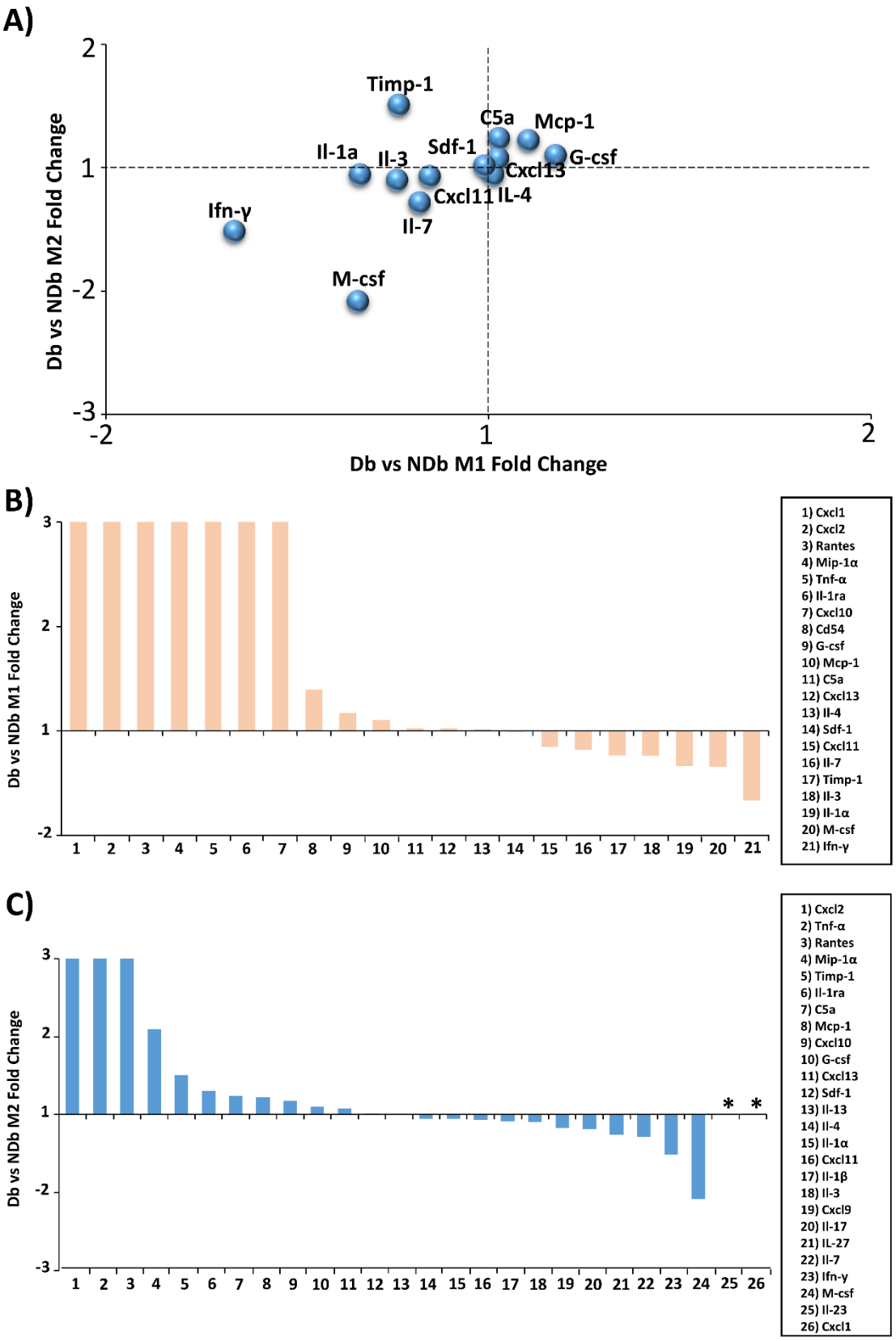

Figure 3.16. Further profiling of the diabetic macrophage secretory phenotype. Cytokines demonstrating little to no fold change difference between non-diabetic (NDb) and diabetic (Db) macrophage (Mφ) conditioned media are shown in **A**. Individual fold change graphs for M1-stimulated (**B**) and M2-stimulated (**C**) Mφs is also provided, in order of magnitude (descending, left to right). Key provided in legends. * = not expressed in the NDb condition.

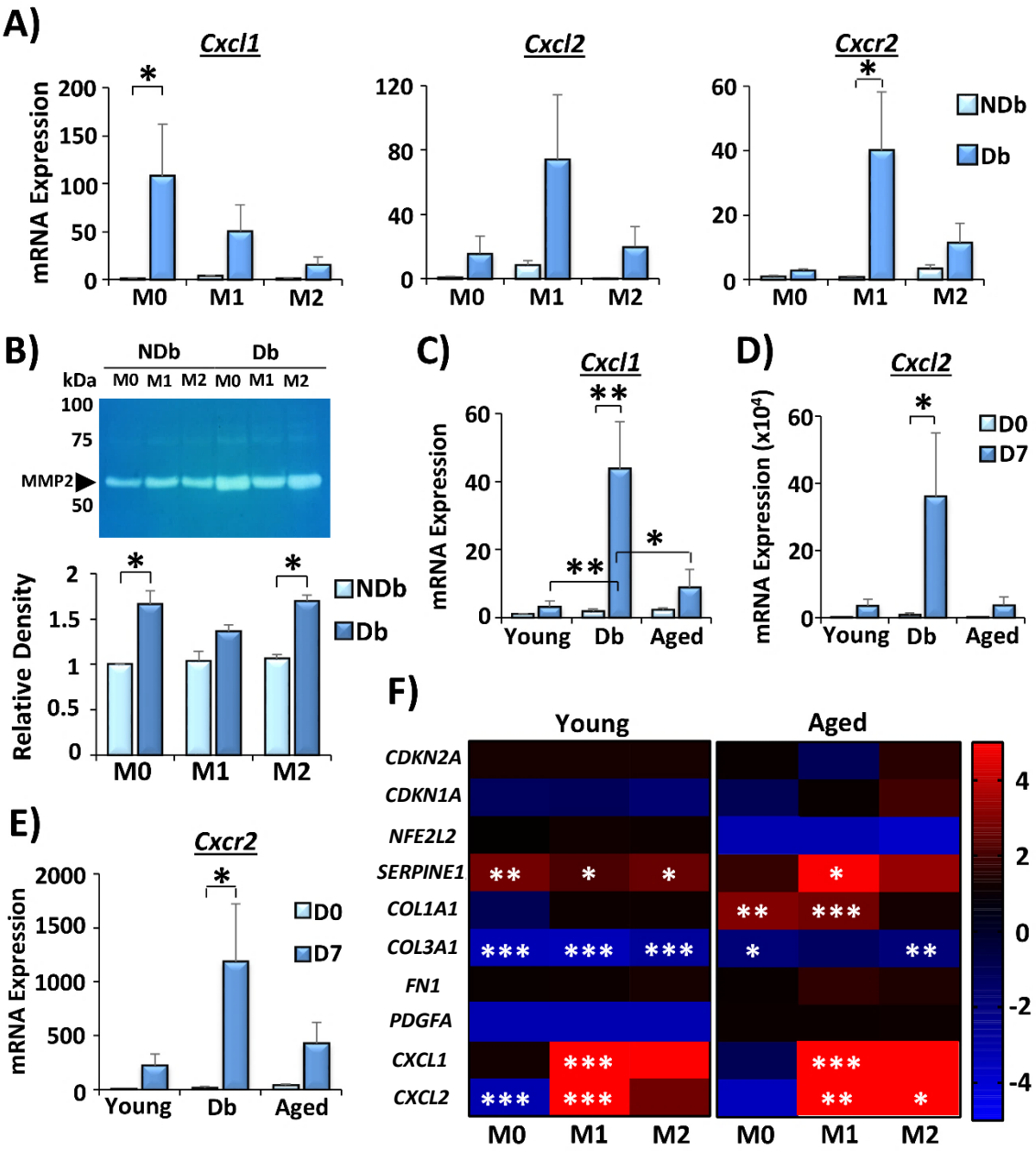

Figure 3.17. Diabetic macrophages and wounds are enriched for a Cxcr2 secretome that alters fibroblast chemokine expression. qRT-PCR illustrates changes in *Cxcl1*, *Cxcl2* and *Cxcr2* (**A**) in diabetic (Db) macrophages (Mφs). A gelatin zymogram (**B**) demonstrates increased MMP-2 activity in diabetic (Db) M0 and M2-polarised cells (graphed below zymogram, compared to non-diabetic, NDb). n = 5 animals per group. qRT-PCR shows significant induction of *Cxcl1* (**C**), *Cxcl2* (**D**) and *Cxcr2* (**E**) in diabetic (Db) wounds at day 7 (D7) post-injury (compared to normal skin, D0). n = 3 mice per group. Conditioned media (CM) from non-diabetic (NDb) and diabetic (Db) Mφs was added to cultured young and aged human dermal fibroblasts (HDFs). Heatmaps display Db versus NDb fold change in genes (**F**). Values above 4-fold difference are coloured bright red, and below -4, bright blue. Db Mφ CM upregulates *SERPINE1* (encoding PAI-1) and the chemokines, *CXCL1* and *CXCL2* in young and aged HDFs, respectively. n = 3 human donors per group. Mean + SEM. * = $P < 0.05$, ** = $P < 0.01$, *** = $P < 0.001$. Two-way ANOVA with Sidak's correction (versus NDb or D0).

3.4.6. Ectopic expression of CXCL2 propagates a CXCL2-driven secretome that influences senescence in non-transfected fibroblasts.

Signalling through Cxcr2 promoted senescence in MEFs (Acosta et al., 2008), while Db murine wounds (D7) and Mφs were characterised by heightened Cxcr2 and its ligands (Cxcl1 and Cxcl2). As Cxcl1/2-rich Db Mφ CM promotes CXCR2 ligand production and induction of *SERPINE1* in HDFs, ectopic CXCL2 was next induced in HDFs. Briefly, HDFs were transfected with a CXCL2 expression plasmid and collected: a) 2 days post-transfection to determine the influence of transfected CXCL2 on cellular senescence and; b) 6 days post-transfection to establish whether transfected HDFs produce a CXCL2-rich SASP capable of potentiating CXCL2 signalling and senescence to non-transfected HDFs.

ICC was performed to measure CXCL2, confirming that HDFs treated with CXCL2 plasmid exhibited significantly higher CXCL2 levels at day 2 (D2, $P < 0.05$) and day 6 (D6, $P < 0.001$) post-transfection (**Figure 3.18A-B**). CXCL2-transfected cells at D6 showed high levels of p21 nuclear localisation ($P < 0.001$; **Figure 3.18DC-D**). Further, the percentage of YFP^{+ve} cells (positive control) did not rise between D2 and D6 post-transfection (**Figure 3.18E**), confirming that ectopic expression of CXCL2, and not transfection itself, potentiates CXCL2 signalling in HDFs. Senescence induction was further confirmed via p16 ICC (**Figure 3.18F-G**) and staining for SA-βGAL (**Figure 3.18H-I**). Here, p16 expression was significantly elevated in the CXCL2 transfection group at D6 ($P < 0.001$), while SA-βGAL^{+ve} cells were increased following CXCL2 transfection ($P < 0.001$). Together, these data confirm that CXCL2 induction drives senescence in HDFs.

CM was collected and evaluated via antibody arrays to profile HDF SASP. Intriguingly, CXCL2-exposed cells upregulated multiple SASP cytokines (Coppe et al., 2011), including MIF, IL-6, IL-8, CXCL1, CXCL12 and PAI-1 (**Figure 3.19A-B**). MMP2 activity was higher in CXCL2-exposed HDFs at both D2 and D6, compared to non-exposed HDFs ($P < 0.05$; **Figure 3.19C**), with higher MMP2 activity in CXCL2-exposed cells at D6 than at D2 ($P < 0.05$). Finally, qRT-PCR revealed upregulation of *MMP2* ($P < 0.05$) and *COL3A1* ($P < 0.01$) in CXCL2-exposed HDFs (**Figure 3.19D**).

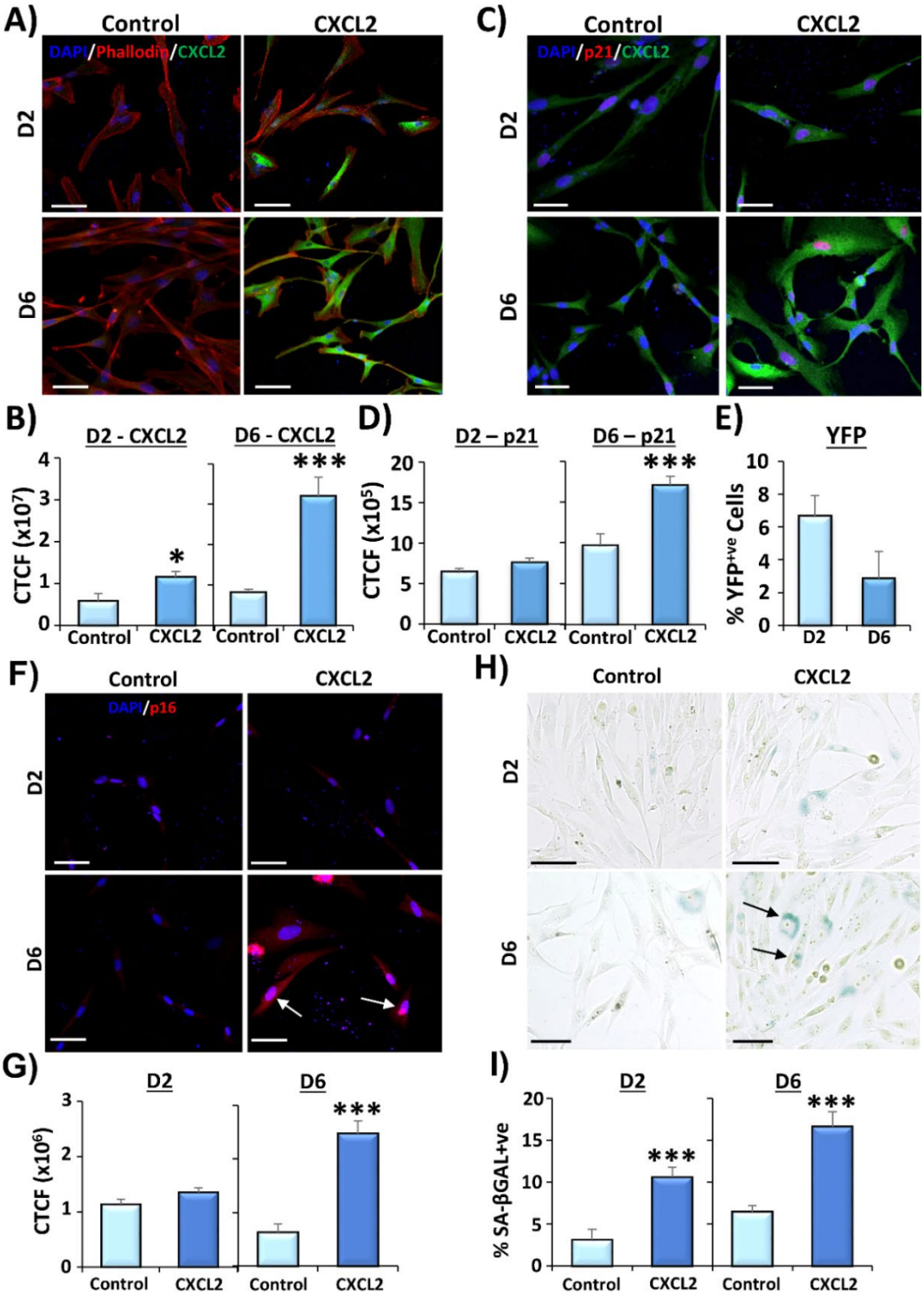

Figure 3.18. Ectopic CXCL2 induction promotes senescence in primary human dermal fibroblasts. Primary human dermal fibroblasts (HDFs) transfected with a control plasmid and CXCL2-containing plasmid were collected at day 2 (D2) and day 6 (D6) post-transfection. Immunocytochemistry reveals increased CXCL2 expression in CXCL2-transfected HDFs at D2 and D6 (**A-B**). Nuclear p21 staining is elevated at D6 post-transfection in the CXCL2 treatment group (**C-D**). YFP^{+ve} cells were counted for transfection efficiency (**E**). CXCL2-transfected HDFs also have higher p16 staining (**F-G**) and senescence-associated beta galactosidase (SA-βGAL; **H-I**). CTCF = corrected total cell fluorescence. Bar = 50 µm. n = 3 donors. Mean + SEM. * = $P < 0.05$, ** = $P < 0.01$, *** = $P < 0.001$. Significance determined via independent two-tailed Student's *t* tests.

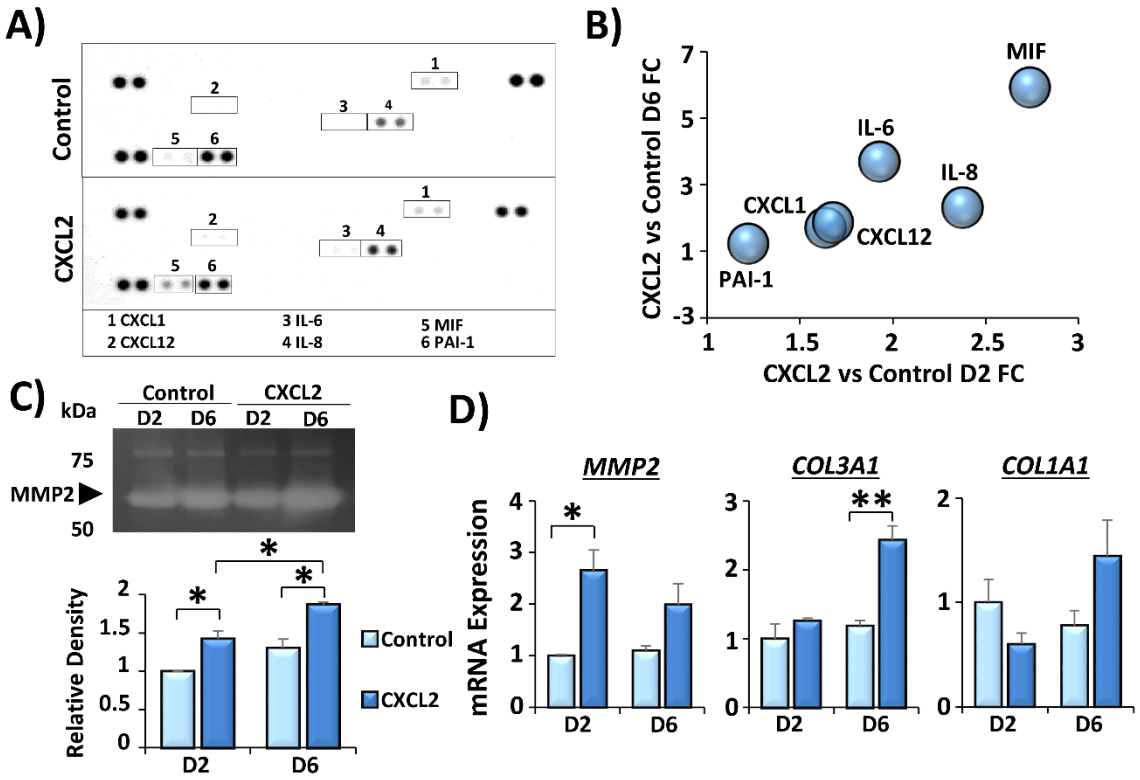

Figure 3.19. CXCL2-expressing human dermal fibroblasts exhibit upregulation of established senescence-linked cytokines and proteases. Antibody cytokine arrays were performed on conditioned media from control and CXCL2 transfected human dermal fibroblasts (HDFs) at 2 days (D2) and 6 days post-transfection (representative blot, **A**; quantified, **B**). FC= fold change. Gelatin zymography elucidates changes in MMP-2 expression (**C**; representative gel, top panel; quantification, bottom panel). HDFs were also collected to assess mRNA changes in *MMP2*, *COL3A1* and *COL1A1* via qRT-PCR (**D**). n = 3 donors. Data show mean + SEM. * = $P < 0.05$; ** = $P < 0.01$. Significance determined via two-way ANOVA with Tukey *post-hoc* analysis.

3.4.7. Human *ex vivo* wound healing is accelerated by blockade of the CXCR2 receptor.

Increased secretion of CXCL2 is apparent in Db Mφs (**Figure 3.15-3.17**), induces senescence in HDFs (**Figure 3.18**), and exerts its effects through the CXCR2 receptor (Acosta et al., 2008). Thus, the next aim was to determine the translational wound healing relevance of blocking CXCR2 (using the antagonist, SB265610, Bradley et al., 2009) in wound healing models *in vitro* (8 hours) and *ex vivo* (24 hours). HaCaT monolayers were scratched *in vitro* and percentage closure of scratch wounds was measured from a zero-hour control. Blockade of CXCR2 with SB265610 led to a significant ($P < 0.05$) improvement (>10%) in HaCaT scratch wound closure at 8 hours (**Figure 3.20A-B**).

Treatment with the CXCR2 ligands, CXCL1 and CXCL2, led to a substantial delay in scratch wound closure during the same period (~15%, $P < 0.01$, **Figure 3.20C-D**). Early *ex vivo* wounding experiments corroborated these effects, where SB265610 improved epidermal closure (**Figure 3.20E-F**; $P < 0.05$) and elevated epidermal basal cell proliferation in the epidermis adjacent to the wound (**Figure 3.20G-H**; $P < 0.05$) at 24 hours post-injury. Together, these data suggest that obstruction of signalling through the canonical senescence receptor, CXCR2, promotes early epidermal stages of healing.

As CXCR2 blockade showed promising effects in early epidermal wound healing models, its efficacy, along with the activity of its ligands, CXCL1 and CXCL2, was next evaluated during a longer treatment period. *In vitro*, CXCL1 and CXCL2 significantly delayed HaCaT scratch wound closure at 24 hours ($P < 0.05$ and $P < 0.01$, respectively), while CXCR2 blockade (SB265610) significantly improved ($P < 0.05$) scratch wound repair (**Figure 3.21A-B**). The specificity of SB265610 was confirmed via co-treatment with CXCL1, CXCL2, or the two ligands in combination. Intriguingly, when the two ligands were used in combination, they retained their ability to significantly delay wound closure, even with the CXCR2 antagonist ($P < 0.001$).

In human *ex vivo* wounds, SB265610 accelerated epidermal wound repair (~30%) at 3 days post-injury ($P < 0.01$). In the presence of SB265610, combinatorial ligand treatment (CXCL1 and CXCL2) still delayed epidermal wound closure ($P < 0.05$), while treatment with SB265610 and CXCL1 alone led to the same delayed effect ($P < 0.05$). Interestingly, when CXCL2 was used in combination with SB265610, the delayed healing phenotype was rescued (from ~40% with CXCL2 alone to ~80% with SB265610 co-treatment; **Figure 3.22A-B**). Thus, these data suggest SB265610 to be more selective for CXCL2 than CXCL1 *ex vivo*. Finally, neo-epidermal proliferation (KRT6 staining, **Figure 3.22A**, **C**) was significantly impaired only in wounds co-treated with SB265610 and CXCL1 ($P < 0.05$), further suggesting that SB265610 retains reduced potency against CXCL1 than CXCL2. Together, these data clearly demonstrate that blocking the canonical senescence receptor, CXCR2, promotes human epidermal wound healing *in vitro* and *ex vivo*.

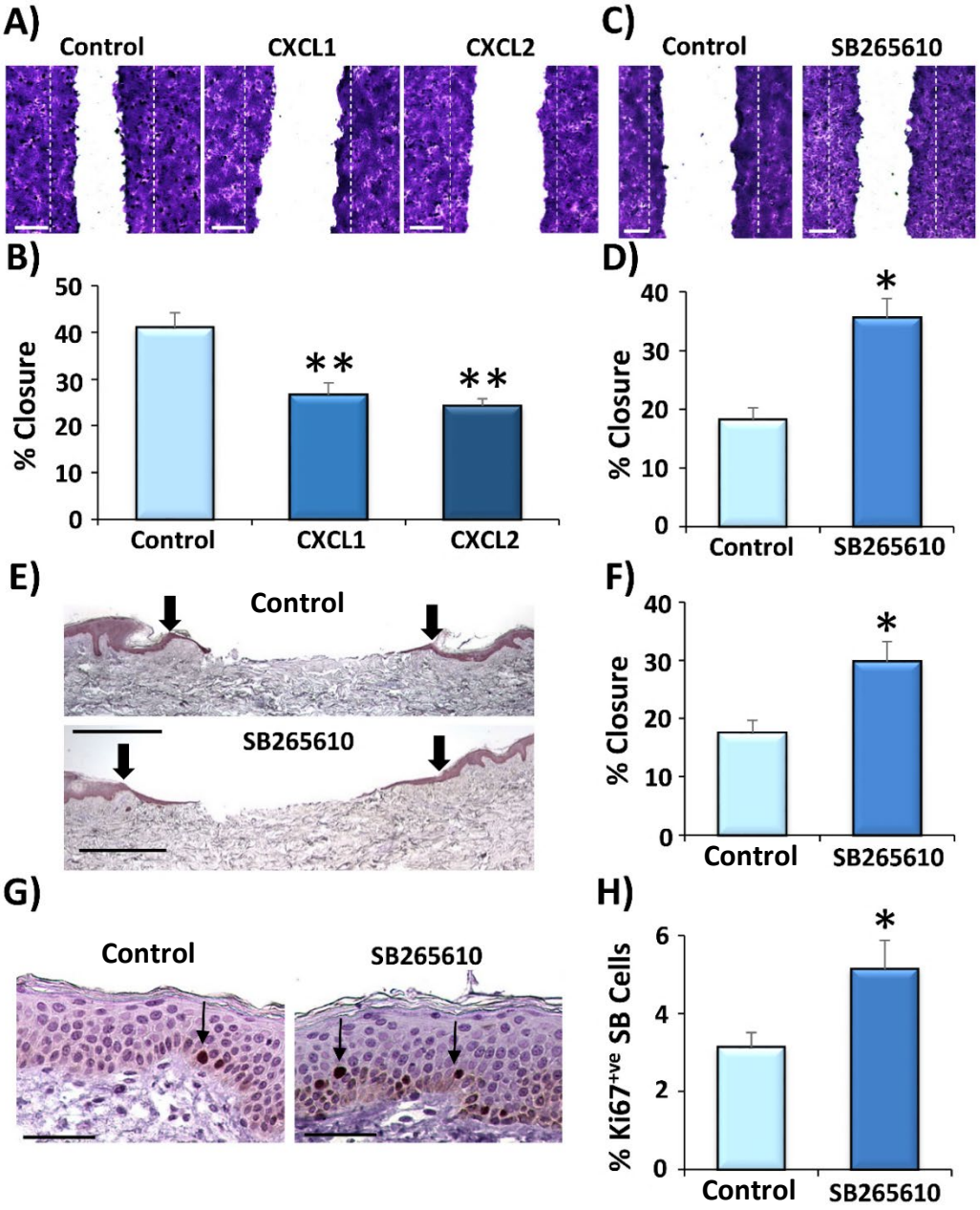

Figure 3.20. Classical signalling through CXCR2 delays early wound closure, while blocking of CXCR2 promotes *in vitro* and *ex vivo* keratinocyte migration. HaCaT keratinocytes were scratched in a confluent monolayer and treated with the CXCR2 ligands, CXCL1 and CXCL2. Representative Crystal Violet stained scratches (**A**, **C**). Original scratch = white dotted lines. At 8 hours post-scratching, CXCL1 and CXCL2 significantly reduces migration (**B**). However, blocking the CXCR2 receptor with an antagonist (SB265610) accelerates keratinocyte migration (**D**). Bar = 250 µm. Wounds were created in *ex vivo* human skin biopsies and treated with the CXCR2 antagonist, SB265610, for 24 hours. Representative keratin 14 immunohistochemistry (IHC; **E**) demonstrates an increase in epidermal migration following antagonist treatment (**F**; black arrows depict wound edges, migrating epidermis = red). Bar = 500 µm. Representative Ki67 IHC shows proliferating basal keratinocytes (black arrows, red-brown cells; **G**), increased following SB265610 treatment (**H**). Bar = 50 µm. n = 6 donors, n = 3 biopsies per donor, per treatment. Data = mean + SEM. * = $P < 0.05$, ** = $P < 0.01$. Significance was determined via one-way ANOVA and Dunnett's *post hoc* (**B**, versus control) or independent two-tailed Student's *t* tests (**D, F, H**).

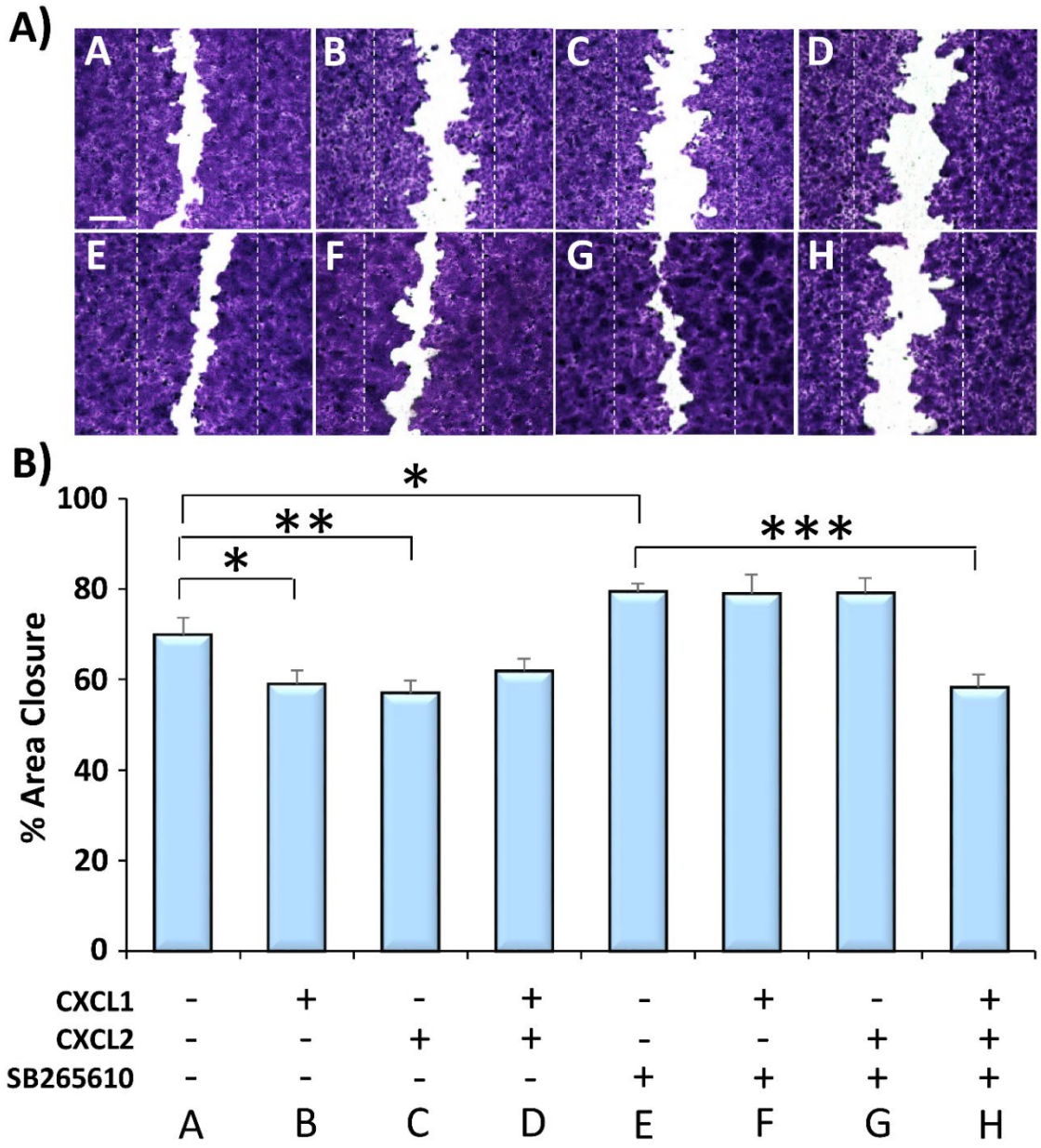

Figure 3.21. Inhibition of CXCR2 signalling promotes HaCaT scratch migration. The CXCR2 ligands, CXCL1 and CXCL2, impairs *in vitro* scratch wound closure (**B**, at 24 hours), while treatment with the CXCR2 antagonist, SB265610, accelerates scratch wound closure (representative of three independent experiments). Further, treatment with CXCL1 and CXCL2 independently with the CXCR2 antagonist rescues the ligand-induced delay in HaCaT migration, yet SB265610 fails to improve HaCaT migration when both ligands are used in combination. Crystal Violet-stained scratches presented in **A**. Letters in **A** relate to treatments in **B**. White, dotted lines = original scratch. Bar = 250 µm. Mean + SEM. * = $P < 0.05$, ** = $P < 0.01$, *** = $P < 0.001$. Independent two-tailed Student's *t* tests compared the shown groups.

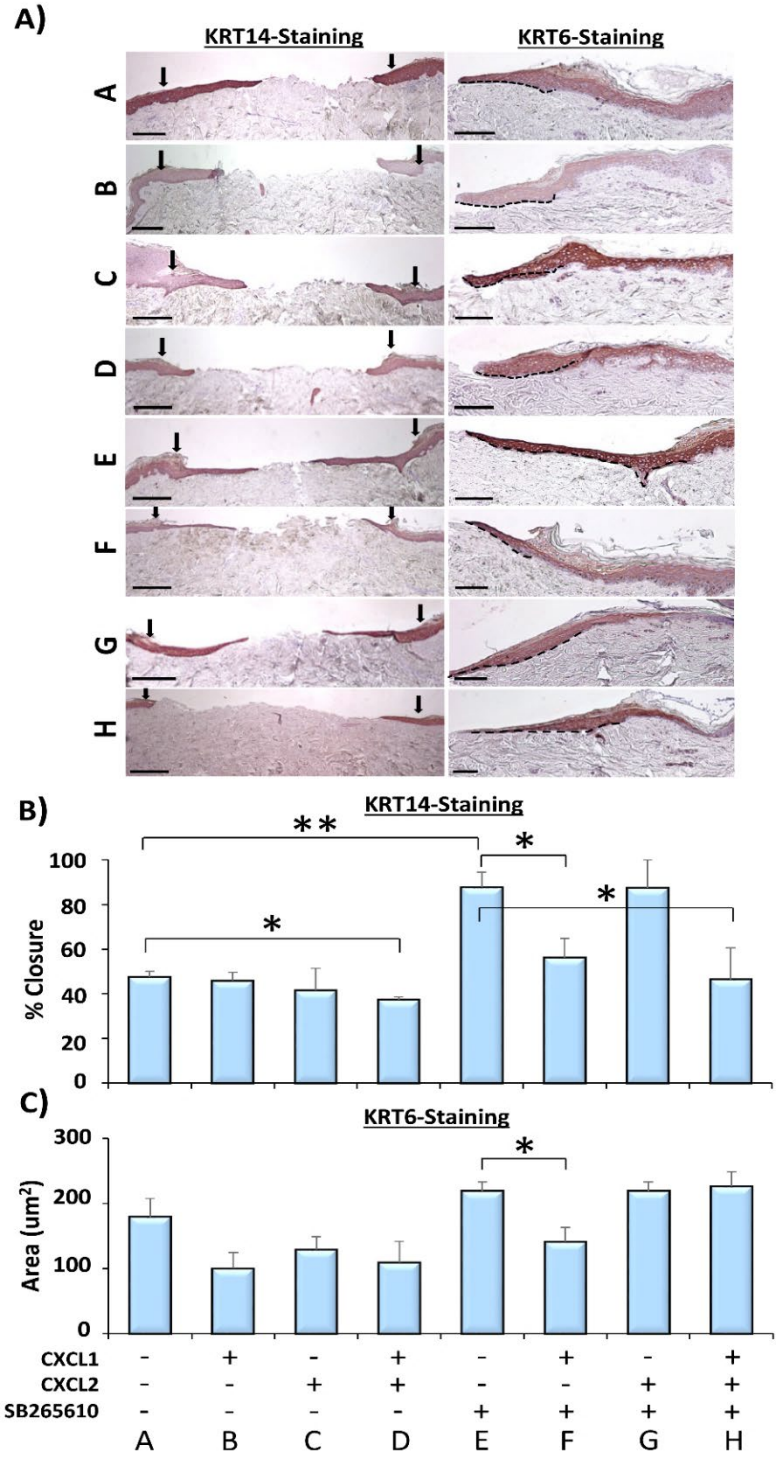

Figure 3.22. Human *ex vivo* wound repair is accelerated by blockade of CXCR2. Keratin 14 (KRT14) staining (**A** and **B**) demonstrates increased epidermal wound closure after 3 days following CXCR2 antagonist (SB265610) treatment (arrows show wound edges, bar = 200 μm), whereas combined treatment with CXCL1 and CXCL2 delays healing. Combining SB265610 with CXCL2, but not CXCL1, rescues the delay in wound healing, but SB265610 does not rescue healing with combinatory ligand treatment. Letters in **A** relate to treatments in **B**. Keratin 6 staining (KRT6, **A**, right panels; bar = 50 μm), depicts increased neo-epidermal proliferation following SB265610 treatment, inhibited by CXCL1 (**B**). Dotted lines = neo-epidermis. n = 3 donors per treatment. Data = mean + SEM. * = $P < 0.05$, ** = $P < 0.01$. Two-tailed, unpaired two-tailed Student's *t* tests.

3.4.8. Blocking Cxcr2 promotes *in vivo* diabetic wound repair by reducing inflammation and senescence.

As Db mice exhibit heightened Cxcr2, which is known to drive senescence, the effects of blocking Cxcr2 were next assessed during *in vivo* Db murine healing. Here, vehicle or SB265610 were administered subcutaneously to excisional wounds, which were collected at D7 post-injury (**Figure 3.23**). Interestingly, treatment with SB265610 led to a significant reduction in histological wound width ($P < 0.01$; **Figure 3.23A-B**) and wound area ($P < 0.05$; **Figure 3.23A, C**), but had no effect on re-epithelialisation (**Figure 3.23A, D**). Characterisation of wound inflammation revealed significantly fewer neutrophils in antagonist-treated wounds ($P < 0.05$; **Figure 3.23E, H**). To determine whether the observed improvement in healing was due to reduced senescence, Db wound Mφs were stained with p16. Here, SB265610-treated wounds exhibited significantly less $p16^{+ve}$ Mφs ($P < 0.001$; **Figure 3.23G, I**).

Bone marrow derived Mφs from control-treated and SB265610-treated Db mice displayed no significant changes in polarisation (*Nos2* and *Ym1*; **Figure 3.24A, B**) or levels of the senescence markers *Cdkn1a*, *Cdkn1b* or *Trp53* (**Figure 3.24C-E**). Only *Cdkn2a* was differentially expressed in M0 and M2-polarised Mφs (**Figure 3.24F**). Thus, the effects of subcutaneous SB265610 administration appear localised to wound tissue Mφs. Overall, SB265610 improved Db murine healing by dampening inflammation and reducing Mφ senescence.

3.4.9. Transcriptional analysis reveals an altered gene expression profile in SB265610-treated diabetic skin and wounds.

To understand the effects of SB265610 treatment at the molecular level, transcriptional profiling (PCR array) was performed on skin and wounds from vehicle-treated and SB265610-treated Db mice. Treatments were injected into the wound site only, with normal skin collected from the dorsal region above the wound. Scatterplots depict changes in 84 genes analysed, with comparisons made between skin and wounds within and between treatment groups. Interestingly, SB265610-treated skin showed upregulation of more genes than control skin (>1.5-fold change difference; **Figure 3.25**).

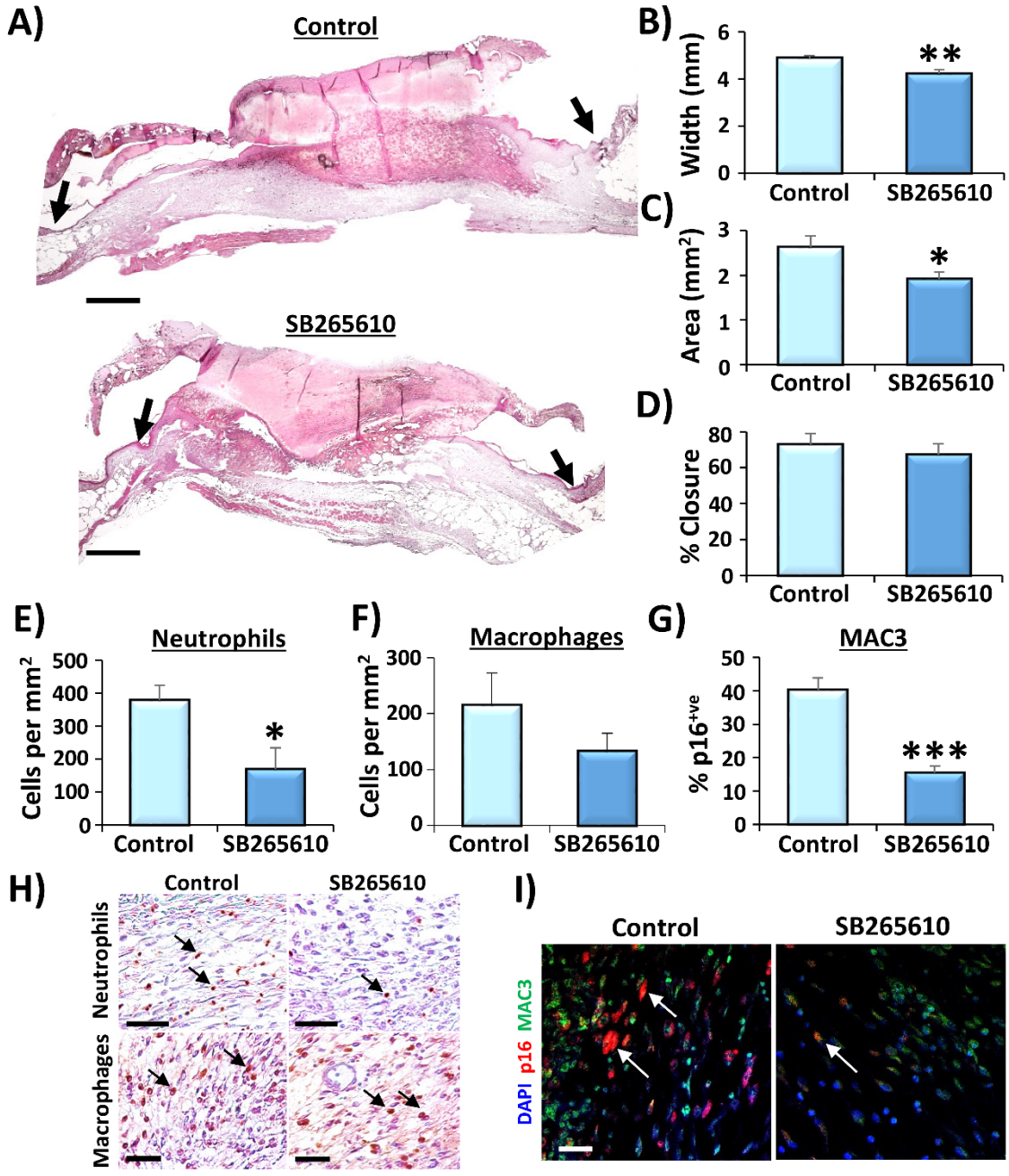

Figure 3.23. Blocking CXCR2 significantly improves diabetic wound healing *in vivo*. Diabetic wounds were treated with the CXCR2 antagonist, SB265610, or a vehicle control and collected at day 7 post-injury (n = 6 per group). Haematoxylin and Eosin (**A**, bar = 500 µm) staining was used to quantify wound width (**B**) and area (**C**), which are significantly reduced following SB265610 treatment. Arrows depict wound edges. Keratin 14 staining (**D**) reveals no changes in epidermal closure. SB265610-treated wounds have significantly reduced neutrophil infiltration (**E**). Although macrophage (Mφ) numbers are only modestly reduced (**F**), SB265610 treatment significantly reduces Mφ senescence (**G**). Representative immunohistochemistry (**H**) and immunofluorescence (**I**). Bars = 50 µm. Arrows depict positively stained cells. Mac3 = Mφs. p16 = senescence. Mean + SEM. * = $P < 0.05$, ** = $P < 0.01$, *** = $P < 0.001$. Unpaired two-tailed Student's *t* tests.

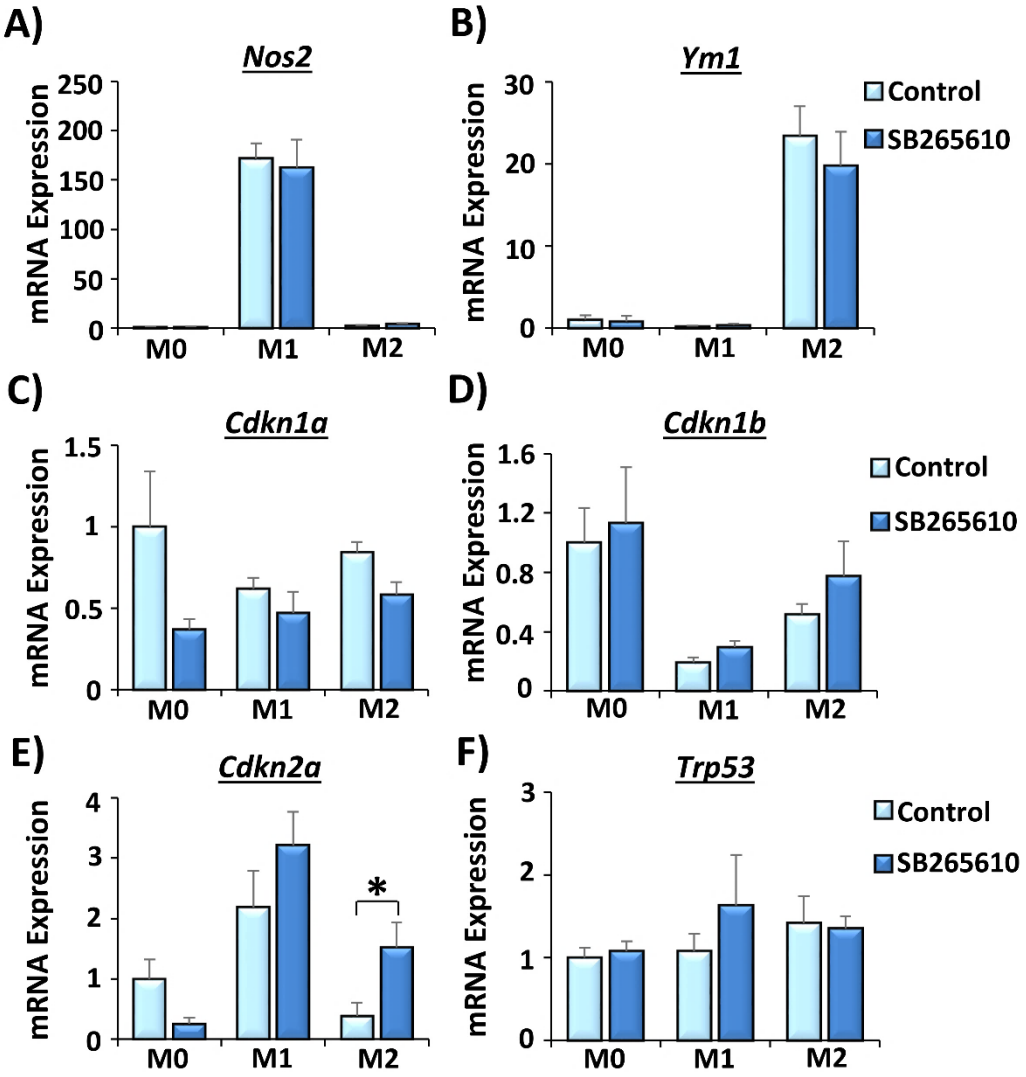

Figure 3.24. Bone marrow-derived macrophages from SB265610-treated mice do not display aberrant polarisation or altered senescence marker expression. Diabetic bone marrow was collected from mice subcutaneously treated with a CXCR2 antagonist, SB265610, or a vehicle control (n = 6 per group). Macrophages (Mφs) were differentiated and polarised (M0, M1 and M2 states), and profiled via qRT-PCR. M1 (*Nos2*, **A**) and M2 (*Ym1*, **B**) polarisation is unaffected by SB265610 treatment. *Cdkn1a* (**C**), *Cdkn1b* (**D**) and *Tp53* (**F**) are unchanged with SB265610 treatment. Only M2 polarised Mφs display altered *Cdkn2a* expression following SB265610 treatment (**E**). Data show mean + SEM. * = $P < 0.05$, ** = $P < 0.01$, *** = $P < 0.001$. Two-way ANOVA and Tukey *post-hoc* analysis.

Alterations in transcriptional signatures were less apparent in SB265610-treated wounds than in skin (**Figure 3.26**). However, *Ifn-γ*, *Mif* and Wnt Family Member 5A (*Wnt5a*) were significantly increased following SB265610 treatment ($P < 0.05$), while cathepsin g (*Ctsg*) was higher in vehicle-treated wounds ($P < 0.05$). As expected, substantial differences in gene upregulation were shown between skin and wounds from SB265610-treated (**Figure 3.27**) and control-treated (**Figure 3.28**) Db mice. For example, wounding induced upregulation of the matrix-related

genes, *Col1a1* ($P < 0.01$; $P < 0.001$), *Col1a2* ($P < 0.01$; $P < 0.001$), *Col3a1* ($P < 0.01$), *Col5a1* ($P < 0.01$; $P < 0.001$), *Col5a2* ($P < 0.01$), *Mmp9* ($P < 0.01$) and *Timp1* ($P < 0.01$) in the SB265610 group and control group, respectively. Higher transcription of the chemokines, *Cxcl1* ($P < 0.01$) and *Cxcl3* ($P < 0.01$), plasminogen activator, tissue (*Plat*; $P < 0.01$), plasminogen activator, urokinase receptor (*Plaur*; $P < 0.001$; $P < 0.05$), and WNT1 inducible signalling pathway protein 1 (*Wisp1*; $P < 0.01$; $P < 0.001$), were also found in wounds. These data suggest there are high levels of specific inflammatory markers in skin from SB265610-treated mice, which could illustrate a compensatory mechanism for dampened wound-site inflammation. Similarly, it is difficult to discern the influence of transcriptional upregulation of a small number of inflammatory markers on wound repair.

3.4.10. Elimination of p21-dependent senescence attenuates late-stage wound repair by inhibiting fibrogenesis.

Previous authors have shown that wound-induced senescence is important for normal healing (Jun & Lau, 2010; Demaria et al., 2014). To assess the contribution of p21-driven senescence to wound healing, $p21^{-/-}$ mice (and controls) were wounded, and tissue collected on days that correlated with the inflammatory (D3) and proliferative (D7) stages of wound repair. Interestingly, lack of $p21^{+ve}$ cells did not impact on early stages of wound healing (D3; **Figure 3.29**). However, by D7, $p21^{-/-}$ wounds were significantly larger than control wounds (wound area, $P < 0.05$, **Figure 3.29A**, **D**; wound width, $P = 0.07$, **Figure 3.29B**, **D**) and failed to reach full epidermal closure ($P < 0.05$; **Figure 3.29C**, **D**). D7 $p21^{-/-}$ wounds displayed a substantially less mature wound matrix (red birefringence on picrosirius red staining) compared to WT controls ($P < 0.001$; **Figure 3.29E-F**).

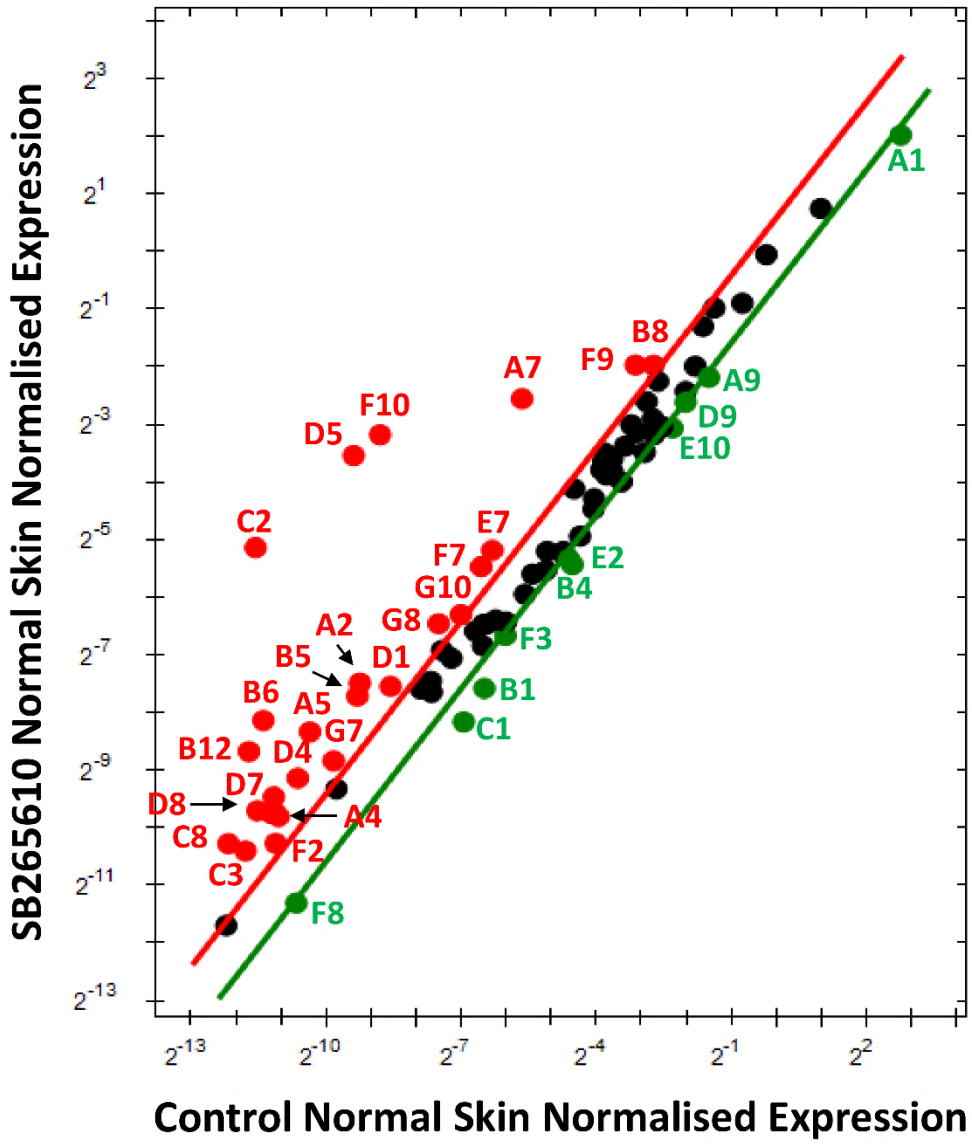

	1	2	3	4	5	6	7	8	9	10	11	12
A	*Acta2*	*Actc1*	*Angpt1*	*Ccl12*	*Cd7*	*Cd40lg*	*Cdh1*	*Col14a1*	*Col1a1*	*Col1a2*	*Col3a1*	*Col4a1*
B	*Col4a3*	*Col5a1*	*Col5a2*	*Col5a3*	*Csf2*	*Csf3* *	*Ctgf*	*Ctnnb1*	*Ctsg*	*Ctsk*	*Ctsl*	*Cxcl1*
C	*Cxcl11*	*Cxcl3*	*Cxcl5*	*Egf*	*Egfr*	*F13a1*	*F3*	*Fga*	*Fgf10*	*Fgf2*	*Fgf7*	*Hbegf*
D	*Hgf*	*Ifng*	*Igf1*	*Il10*	*Il1b* *	*Il2*	*Il4*	*Il6*	*Il6st*	*Itga1*	*Itga2*	*Itga3*
E	*Itga4*	*Itga5*	*Itga6*	*Itgav*	*Itgb1*	*Itgb3*	*Itgb5*	*Itgb6*	*Mapk1*	*Mapk3*	*Mif*	*Mmp1a*
F	*Mmp2*	*Mmp7*	*Mmp9*	*Pdgfa*	*Plat*	*Plau*	*Plaur*	*Plg*	*Pten*	*Ptgs2* *	*Rac1*	*Rhoa*
G	*Serpine1*	*Stat3*	*Tagln*	*Tgfa*	*Tgfb1*	*Tgfbr3*	*Timp1*	*Tnf*	*Vegfa*	*Vtn*	*Wisp1*	*Wnt5a*

Figure 3.25. Skin from SB265610-treated mice displays an altered gene expression profile to control skin. Diabetic skin was collected from the dorsum of treated mice at day 7 post-injury. Wounds were collected for RNA and profiled via qRT-PCR. Altered genes are shown in red (higher in SB265610 group) and green (higher in vehicle group). Threshold set to 1.5-fold change difference in expression. Black points = no change between vehicle and SB265610 groups. Table key below displaying genes, colour coded as graphed. Significance displayed as asterisks. * = $P < 0.05$, deduced via *t* tests. Data normalised to *Actb*, *B2m*, *Gapdh*, *Gusb* and *Hsp90ab1*. n = 3 mice per group.

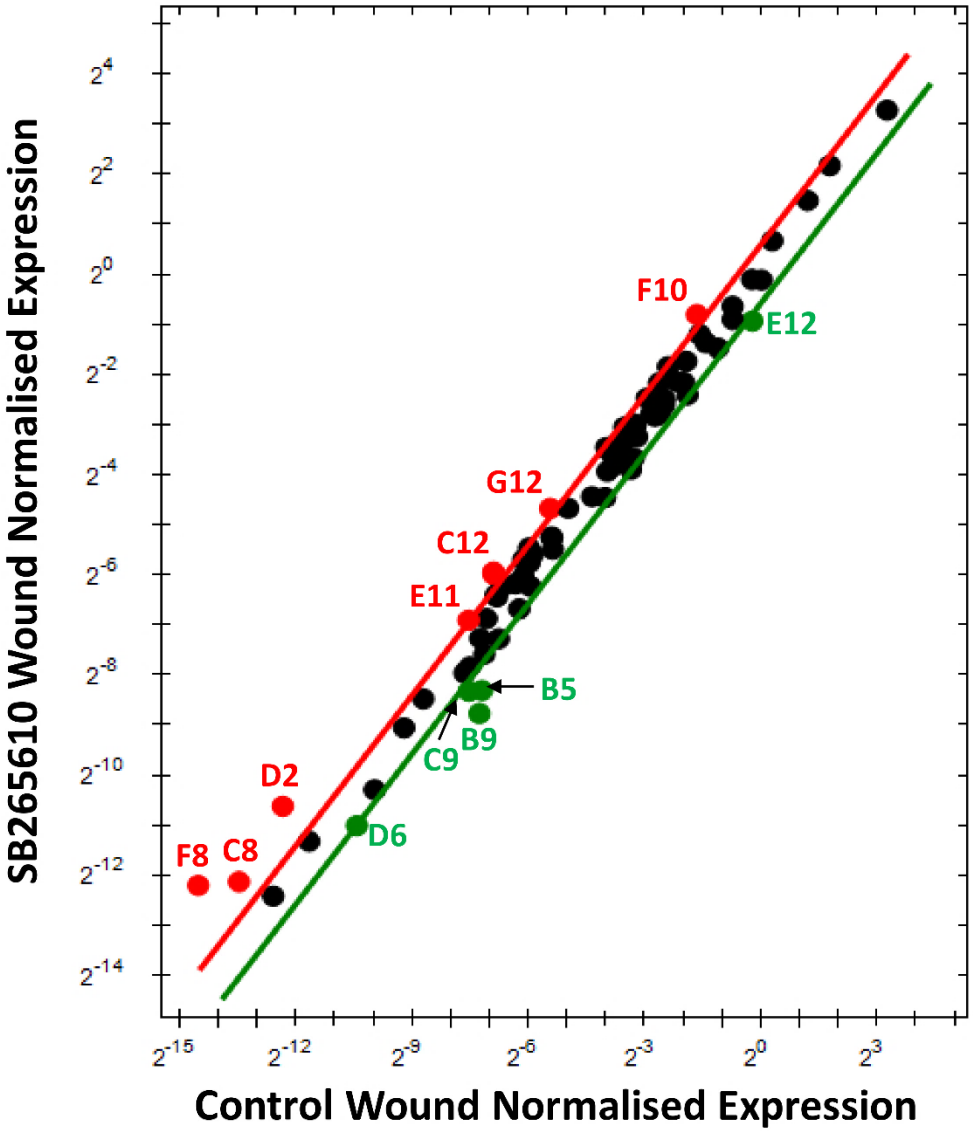

	1	2	3	4	5	6	7	8	9	10	11	12
A	*Acta2*	*Actc1*	*Angpt1*	*Ccl12*	*Cd7*	*Cd40lg*	*Cdh1*	*Col14a1*	*Col1a1*	*Col1a2*	*Col3a1*	*Col4a1*
B	*Col4a3*	*Col5a1*	*Col5a2*	*Col5a3*	*Csf2*	*Csf3*	*Ctgf*	*Ctnnb1*	*Ctsg* *	*Ctsk*	*Ctsl*	*Cxcl1*
C	*Cxcl11*	*Cxcl3*	*Cxcl5*	*Egf*	*Egfr*	*F13a1*	*F3*	*Fga*	*Fgf10*	*Fgf2*	*Fgf7*	*Hbegf*
D	*Hgf*	*Ifng* *	*Igf1*	*Il10*	*Il1b*	*Il2*	*Il4*	*Il6*	*Il6st*	*Itga1*	*Itga2*	*Itga3*
E	*Itga4*	*Itga5*	*Itga6*	*Itgav*	*Itgb1*	*Itgb3*	*Itgb5*	*Itgb6*	*Mapk1*	*Mapk3*	*Mif* *	*Mmp1a*
F	*Mmp2*	*Mmp7*	*Mmp9*	*Pdgfa*	*Plat*	*Plau*	*Plaur*	*Plg*	*Pten*	*Ptgs2*	*Rac1*	*Rhoa*
G	*Serpine1*	*Stat3*	*Tagln*	*Tgfa*	*Tgfb1*	*Tgfbr3*	*Timp1*	*Tnf*	*Vegfa*	*Vtn*	*Wisp1*	*Wnt5a* *

Figure 3.26. Wound gene expression profiles are altered in diabetic mice following SB265610 treatment. Diabetic wounds, treated with a vehicle control or SB265610, were collected at day 7 post-injury for transcriptional profiling. Red = higher expression in the SB265610 group. Green = higher expression in the vehicle group. Threshold fold change in expression = 1.5. Black points = no change between groups. Table shows genes tested. Significance displayed as asterisks. * = $P < 0.05$, deduced via *t* tests. Data normalised to *Actb*, *B2m*, *Gapdh*, *Gusb* and *Hsp90ab1*. n = 3 mice per group.

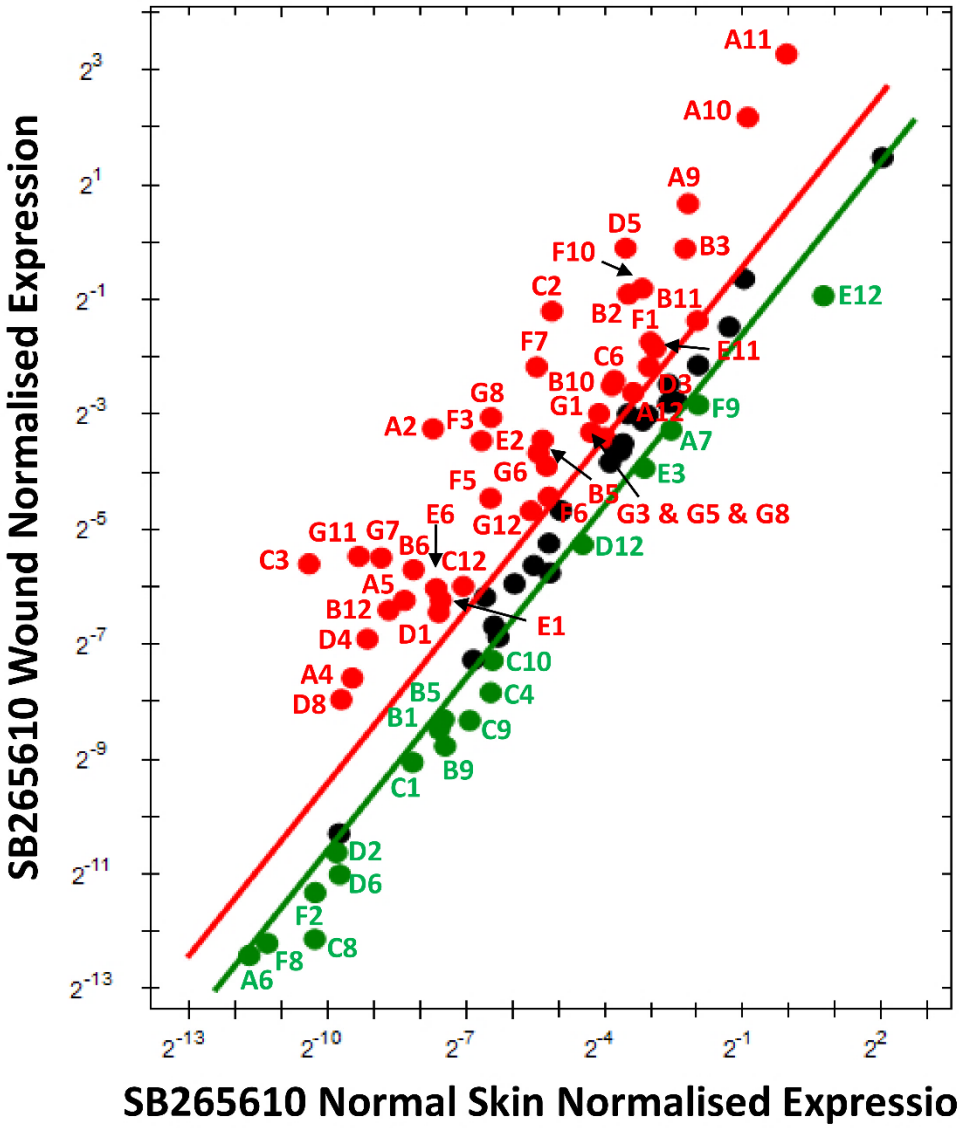

	1	2	3	4	5	6	7	8	9	10	11	12
A	*Acta2*	*Actc1*	*Angpt1*	*Ccl12*	*Cd7*	*Cd40lg*	*Cdh1*	*Col14a1*	*Col1a1* **	*Col1a2* **	*Col3a1* **	*Col4a1*
B	*Col4a3*	*Col5a1* *	*Col5a2* **	*Col5a3*	*Csf2*	*Csf3* *	*Ctgf*	*Ctnnb1*	*Ctsg*	*Ctsk*	*Ctsl*	*Cxcl1* **
C	*Cxcl11*	*Cxcl3* **	*Cxcl5*	*Egf*	*Egfr*	*F13a1*	*F3*	*Fga* *	*Fgf10* *	*Fgf2*	*Fgf7*	*Hbegf*
D	*Hgf*	*Ifng* *	*Igf1*	*Il10* *	*Il1b* **	*Il2* *	*Il4*	*Il6*	*Il6st*	*Itga1*	*Itga2*	*Itga3*
E	*Itga4*	*Itga5*	*Itga6*	*Itgav*	*Itgb1*	*Itgb3*	*Itgb5*	*Itgb6*	*Mapk1*	*Mapk3*	*Mif*	*Mmp1a*
F	*Mmp2*	*Mmp7*	*Mmp9* *	*Pdgfa*	*Plat* **	*Plau*	*Plaur* ***	*Plg*	*Pten*	*Ptgs2*	*Rac1*	*Rhoa*
G	*Serpine1*	*Stat3*	*Tagln*	*Tgfa*	*Tgfb1*	*Tgfbr3*	*Timp1* **	*Tnf* *	*Vegfa*	*Vtn*	*Wisp1* **	*Wnt5a*

Figure 3.27. Gene expression profiles comparing skin and wounds from SB265610-treated diabetic mice. Diabetic skin and wounds treated with SB265610 were collected at day 7 post-injury for qRT-PCR. n = 3 mice per group. Red = higher expression in SB265610 wounds. Green = higher expression in SB265610 skin. Threshold = 1.5-fold change in expression. Black points = no change between groups. Table shows genes tested, colour-coded as displayed in graph. Significance = asterisks. * = $P < 0.05$, ** = $P < 0.01$, *** = $P < 0.001$, deduced via *t* tests, Data normalised to *Actb*, *B2m*, *Gapdh*, *Gusb* and *Hsp90ab1*.

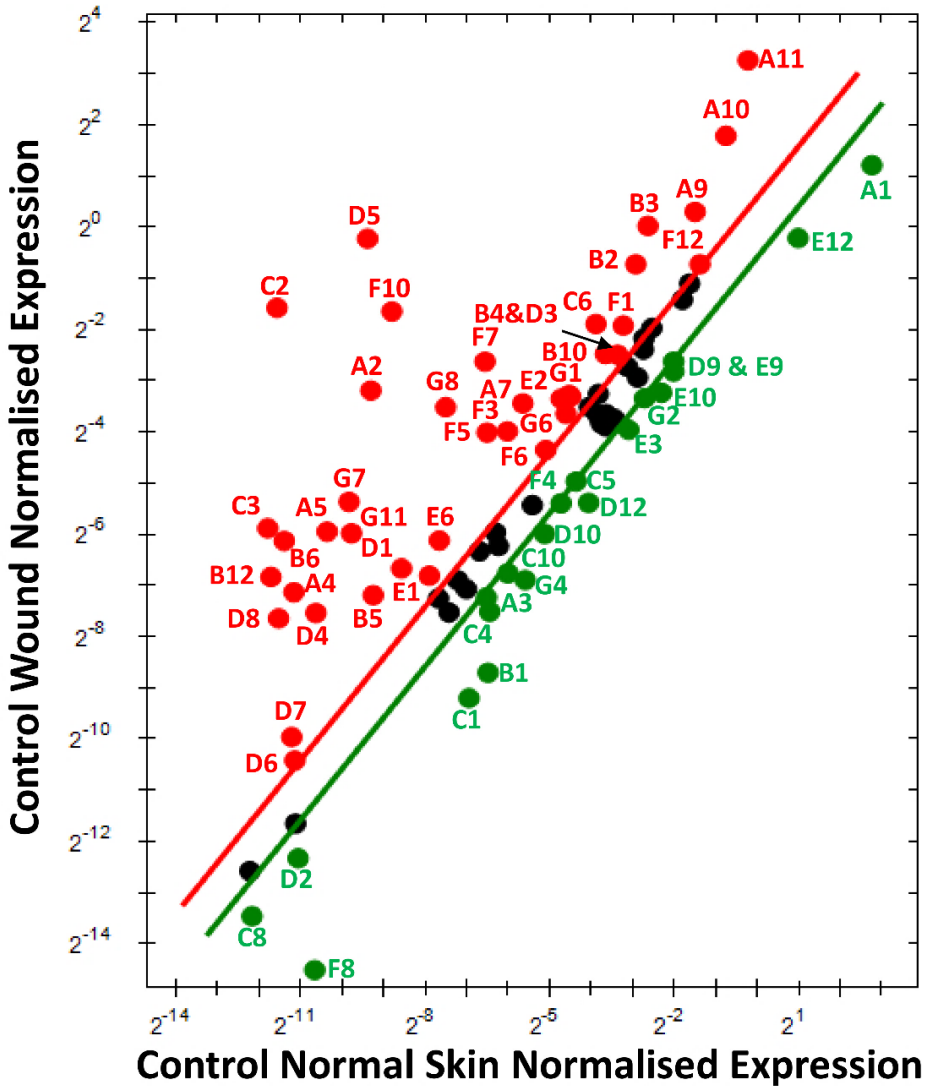

	1	2	3	4	5	6	7	8	9	10	11	12
A	*Acta2*	*Actc1* *	*Angpt1*	*Ccl12* *	*Cd7* **	*Cd40lg*	*Cdh1*	*Col14a1*	*Col1a1* ***	*Col1a2* ***	*Col3a1* **	*Col4a1*
B	*Col4a3*	*Col5a1* ***	*Col5a2* **	*Col5a3* **	*Csf2*	*Csf3* **	*Ctgf*	*Ctnnb1*	*Ctsg*	*Ctsk* **	*Ctsl*	*Cxcl1* **
C	*Cxcl11*	*Cxcl3* **	*Cxcl5*	*Egf* **	*Egfr*	*F13a1* *	*F3*	*Fga*	*Fgf10*	*Fgf2*	*Fgf7*	*Hbegf*
D	*Hgf*	*Ifng*	*Igf1*	*Il10* **	*Il1b* *	*Il2*	*Il4*	*Il6*	*Il6st*	*Itga1*	*Itga2*	*Itga3*
E	*Itga4*	*Itga5* *	*Itga6*	*Itgav*	*Itgb1*	*Itgb3* **	*Itgb5*	*Itgb6*	*Mapk1*	*Mapk3*	*Mif*	*Mmp1a*
F	*Mmp2* *	*Mmp7*	*Mmp9* *	*Pdgfa*	*Plat* **	*Plau* *	*Plaur* *	*Plg*	*Pten*	*Ptgs2* **	*Rac1*	*Rhoa*
G	*Serpine1*	*Stat3*	*Tagln*	*Tgfa* *	*Tgfb1*	*Tgfbr3*	*Timp1* **	*Tnf*	*Vegfa*	*Vtn*	*Wisp1* ***	*Wnt5a*

Figure 3.28. Comparison of the gene expression profiles of skin and wounds from vehicle-treated diabetic mice. Diabetic skin and wounds treated with a vehicle control were collected at day 7 post-injury for qRT-PCR. Red = higher expression in control wounds. Green = higher expression in control skin. Threshold = 1.5-fold change in expression. Black points = no change between groups. Table of genes tested. Significance shown as asterisks. * = $P < 0.05$, ** = $P < 0.01$, *** = $P < 0.001$, deduced via *t* tests. Data normalised to *Actb*, *B2m*, *Gapdh*, *Gusb* and *Hsp90ab1*. n = 3 mice per group.

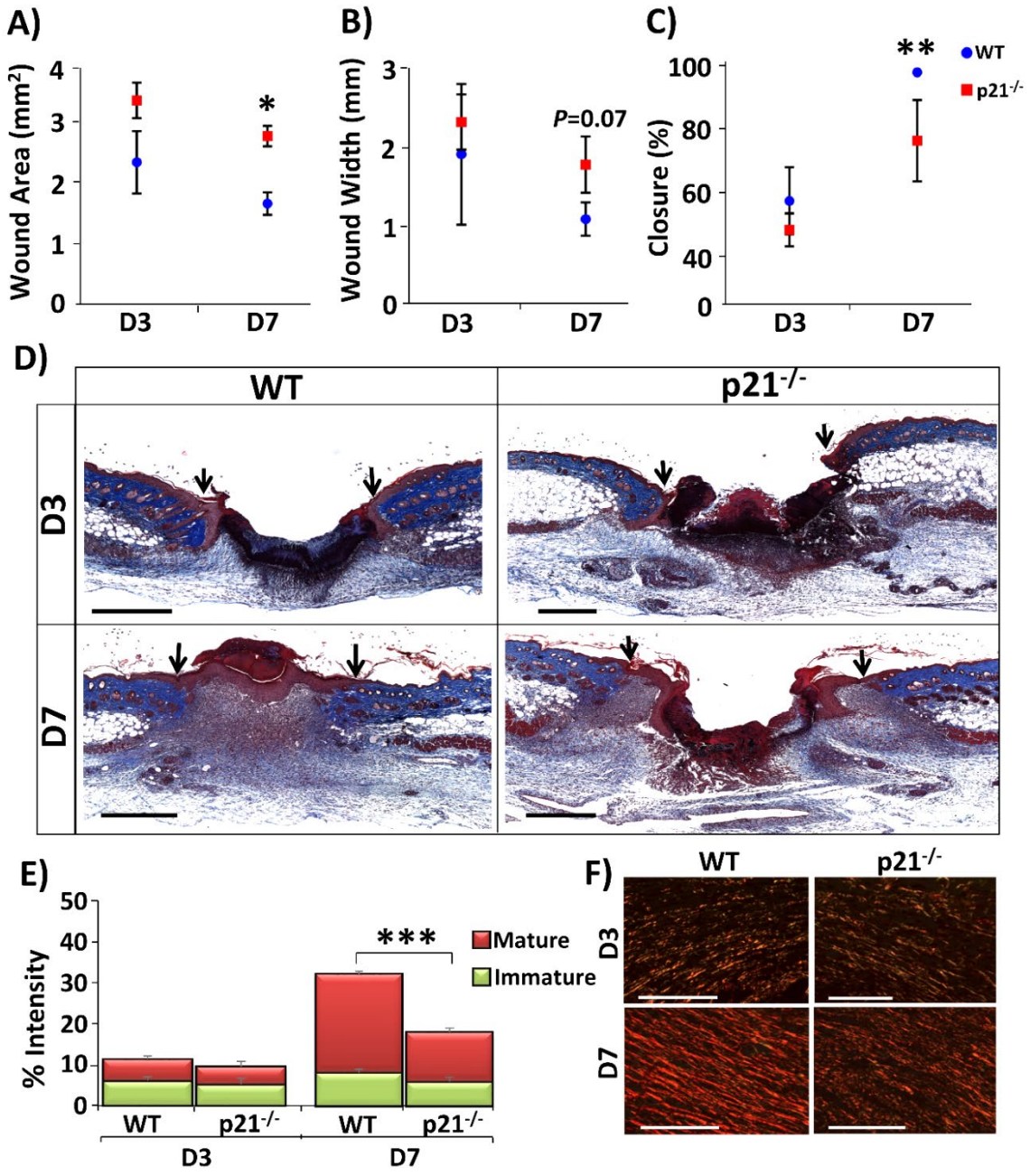

Figure 3.29. Attenuation of p21 leads to delayed healing during late-stage wound repair. Wound area (**A**) and wound width (**B**) are larger in p21$^{-/-}$ wounds at D7 (day 7) post-injury (compared to wild type, WT). Epidermal closure (% closure, **C**) is substantially impaired in D7 p21$^{-/-}$ wounds. Wounds were measured via Masson's Trichrome staining (**D**). Arrows depict wound edges. Bar = 500 μm. Matrix deposition (**E**) was assessed by measuring red (mature) and green (immature) birefringence from picrosirius red staining (**F**, bar = 100 μm). n = 4-6 animals per group. Data show mean + SEM. * = $P < 0.05$, ** = $P < 0.01$, *** = $P < 0.001$. Two-way ANOVA with Sidak's correction.

3.4.11. p21 attenuation alters inflammatory aspects of wound healing.

Although neutrophil and Mφ wound infiltration was unaltered at D3 (**Figure 3.30A-C**), by D7 post-injury p21$^{-/-}$ wounds contained significantly higher numbers of Mφs (P < 0.05; **Figure 3.30B-C**). As Mφ polarisation is an important determinant of wound repair (Campbell et al., 2014), with crucial roles in senescence (Mauer et al., 2014), the levels of Nos-2 (M1) and Arginase-1 (M2) expression were measured in Mφs in p21$^{-/-}$ and WT wounds. No difference was observed in Arginase-1 at D3, while a slight reduction in Nos-2 was seen in p21$^{-/-}$ wounds (P < 0.05; **Figure 3.31A-C**). By D7, a marginal rise in Nos-2 (**Figure 3.31A, C**) and a significant increase in Arginase-1 were observed in p21$^{-/-}$ wounds (**Figure 3.31B-C**; P < 0.05).

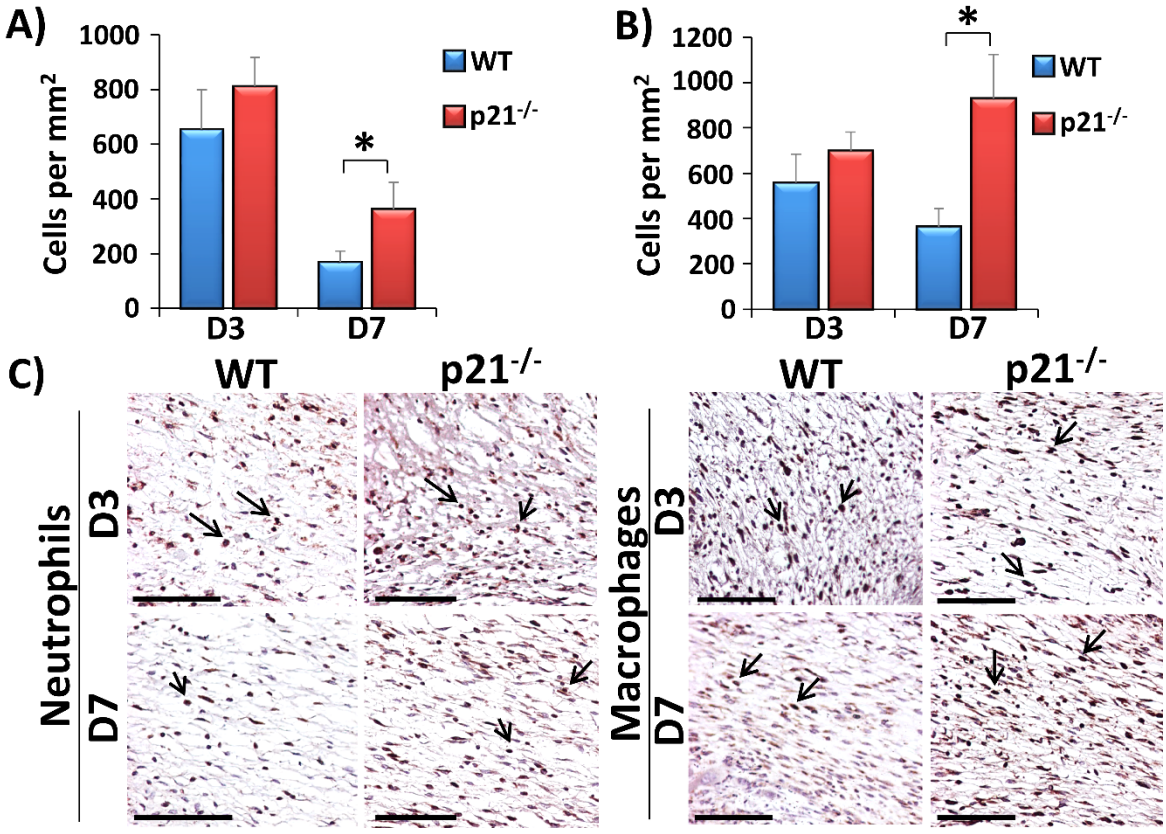

Figure 3.30. Lack of p21 modulates wound immune cell composition. Infiltrating neutrophils (**A**) and macrophages (**B**) were measured in wild type (WT) and p21$^{-/-}$ wounds at D3 (day 3) and D7 (day 7) post-injury. At D7, p21-/- wounds retain significantly more immune cells. Representative staining (**C**) demonstrates immune cells (brown-red, black arrows). Bar = 50 µm. n = 4-6 per group. Data show mean + SEM. * = P < 0.05. Two-way ANOVA with Sidak correction.

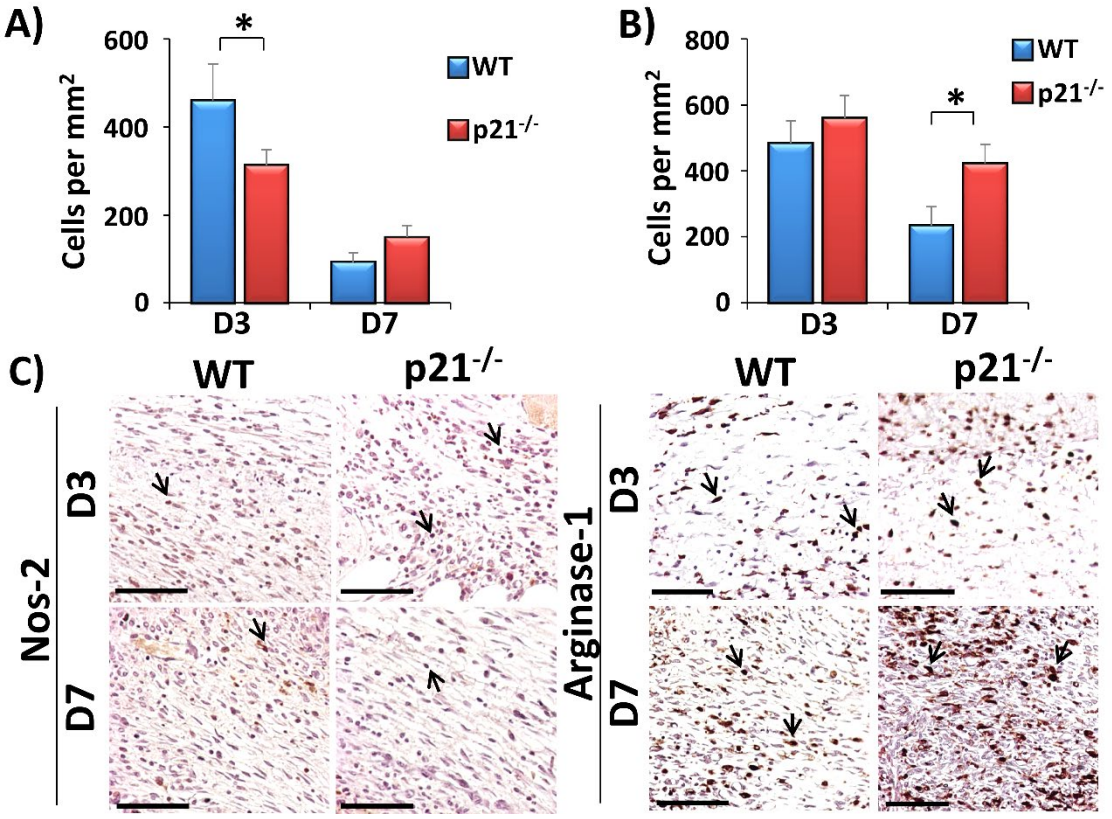

Figure 3.31. Macrophage polarisation is altered by p21 depletion. Macrophage polarisation was assessed in wound tissue from wild type (WT) and p21$^{-/-}$ mice at day 3 (D3) and day 7 (D7) post-injury. Here, M1 (pro-inflammatory) cells are positive for Nos-2 (**A**) and M2 (anti-inflammatory cells) are positive for Arginase-1 (**B**). Representative images are provided in **C**, where black arrows depict positively-stained (brown-red) cells. Bar = 50 µm. n = 4-6 per group. Data show mean + SEM. * = P < 0.05. Two-way ANOVA with Sidak's *post-hoc* analysis.

3.4.12. Removal of p21 heightens proliferation and induces an alternative senescence pathway.

Excessive cellular proliferation (Ki67^{+ve} cells) was apparent in the epidermis (P < 0.05; **Figure 3.32A, C**) and granulation tissue (P = 0.06; **Figure 3.32B-C**) of D7 p21$^{-/-}$ wounds. Further analysis also demonstrated impaired fibroblast differentiation (α-Sma, P < 0.05, **Figure 3.32A, C**) and a significant reduction in Pdgfa^{+ve} cells (P < 0.05, **Figure 3.32B-C**). α-Sma and Pdgfa are important in promoting fibroblast differentiation (Demaria et al., 2014), confirming that D7 p21$^{-/-}$ wounds lacked appropriate fibroblast function. D7 p21$^{-/-}$ wounds displayed increased levels of Mif in the granulation tissue (P < 0.05; **Figure 3.33D, F**), thus were less resolved than WT control wounds (Hardman et al., 2005). Intriguingly, p21$^{-/-}$ D7 wounds showed heightened p16^{+ve} cell infiltration (P < 0.05; **Figure 3.33E-F**), suggesting that p21 attenuation may induce a compensatory mechanism of senescence induction.

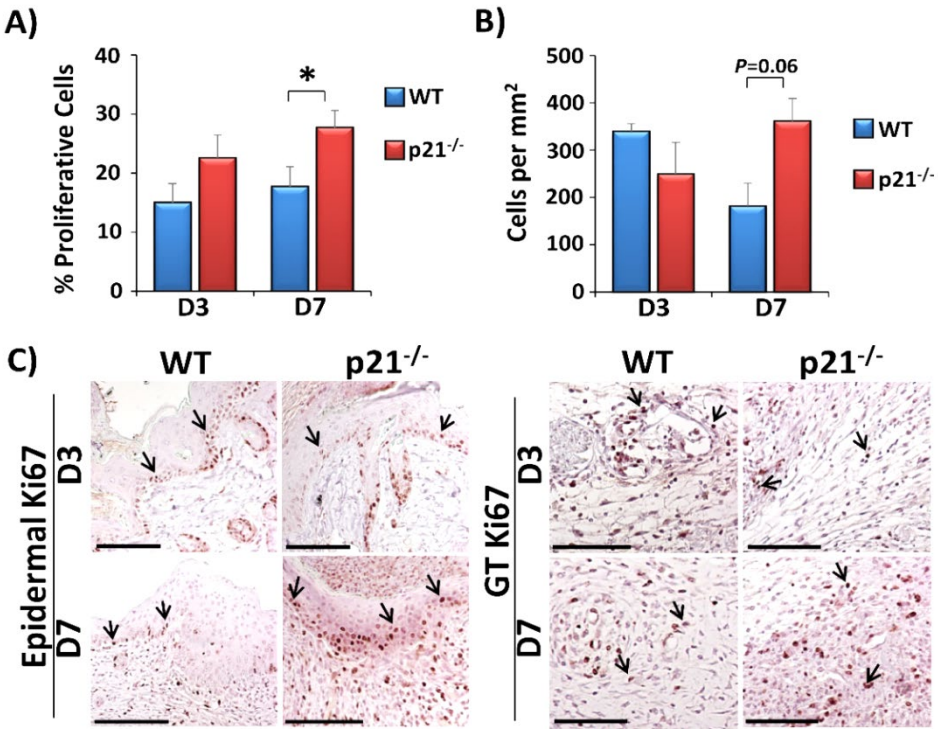

Figure 3.32. p21$^{-/-}$ wounds possess altered proliferation in the dermis and granulation tissue. Epidermal proliferation (% Ki67^{+ve} cells) is significantly increased at D7 (day 7) post-injury in p21$^{-/-}$ wounds (compared to wild type, WT; **A**), with an increased trend in granulation tissue proliferation (**B**). Representative staining (brown-red cells, black arrows; **C**). Bar = 50 µm. n = 4-6 animals per group. Data show mean + SEM. * = $P < 0.05$. Two-way ANOVA with Sidak's multiple hypothesis testing.

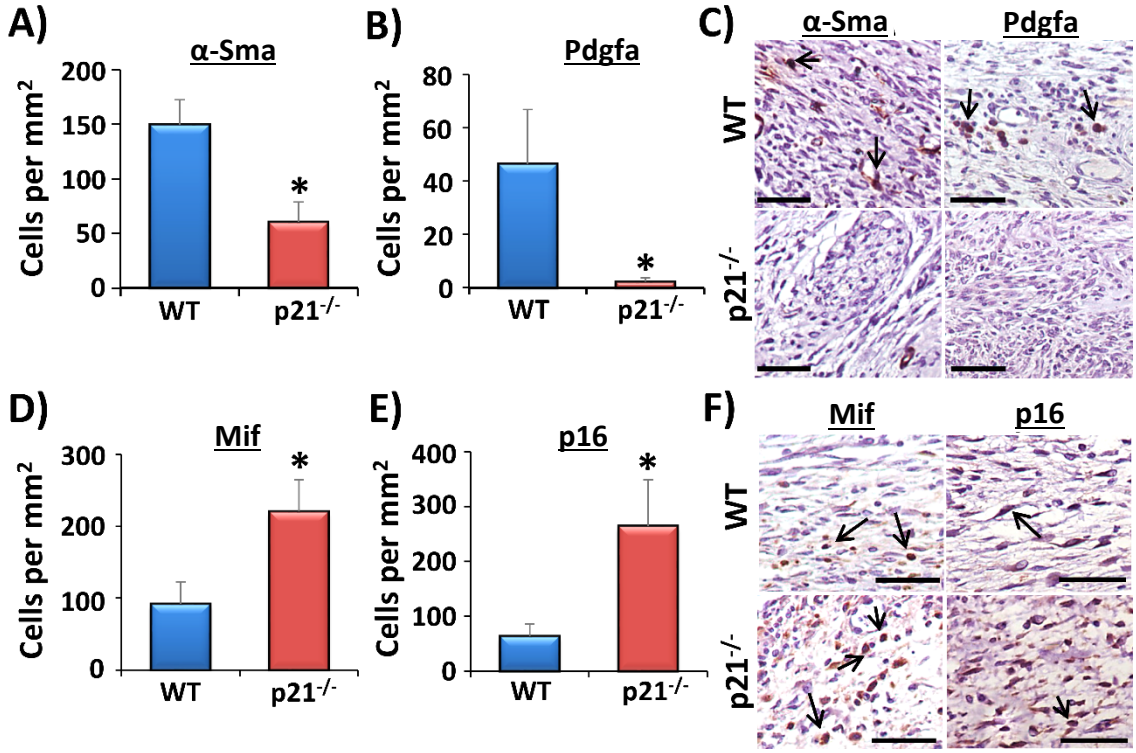

Figure 3.33. Fibrogenesis, inflammatory cytokines, and cell cycle progression are aberrantly affected by p21 attrition. Levels of α-Sma (**A, C**) and Pdgfa (**B-C**) are significantly lower in D7 (day 7 post-injury) p21$^{-/-}$ wounds, compared to WT (wild type), while Mif^{+ve} (**D**, **F**) and p16^{+ve} cells (**E-F**) are higher in p21$^{-/-}$ wounds. Representative staining = red-brown cells (black arrows). Bar = 50 µm. n = 4-6 animals per group. Mean + SEM. * = $P < 0.05$. Independent two-tailed Student's *t* tests.

3.5. Discussion

The phenomenon of cellular senescence has been extensively characterised in a myriad of *in vitro* environments (reviewed in Matjusaitis et al., 2016), yet the mechanisms underlying its correlation with age-related tissue dysfunction are not fully understood. Senescence is believed to contribute to ageing and associated disease states, partly through regulation of the SASP (Coppe et al., 2008). Additional roles for the SASP are emerging in embryogenesis (Storer et al., 2013), liver regeneration (Krizhanovsky et al., 2008; Yosef et al., 2017) and cutaneous wound repair (Demaria et al., 2014; Jun & Lau, 2010; Jun & Lau, 2017).

This chapter aimed to establish how the senescent secretome contributes to wound healing. Previous work has highlighted a central role for PDGFA, a newly characterised SASP component, in governing fibroblast phenotype (Demaria et al., 2014). Pdgfa, expressed by mesenchymal cells, stimulated fibroblast differentiation (by increasing α-Sma^{+ve} cells). However, in this landmark paper, the specific identity of the wound mesenchymal cells was not known, and although the p16/p21 DKO mice possessed significantly reduced wound collagen, the link between Pdgfa and fibroplasia was not mechanistically determined. Nevertheless, the authors did reveal that senescence is fundamentally required for wound resolution and matrix deposition. New data presented in this chapter reveal a direct relationship between senescence, fibroblast function and pathological wound repair. As Demaria et al. (2014) demonstrated peak senescent cell infiltration around 7 days post-injury, senescence in aged and Db wounds was assessed at this time point. However, further investigation will be required to fully elucidate the temporal regulation of senescence during pathological wound repair.

Unsurprisingly, aged murine skin possessed significantly greater numbers of SA-βGAL^{+ve} (**Figure 3.7**), p16^{+ve} and p21^{+ve} cells (**Figure 3.8**) than young skin. Of particular interest was the very high level of SA-βGAL in Db wounds (**Figure 3.11**) accompanied by increased *Cdkn1a* transcription (**Figure 3.12**). Indeed, previous authors have identified the presence of senescent fibroblasts in chronic venous leg ulcers (Agren et al., 1999; Mendez et al., 1998; Stanley & Osler, 2000; Vande Berg et al., 1998). The novel data presented suggested that: (a) senescence may be a correlative marker of impaired wound healing; but crucially (b) senescence is induced in Db wounds in the absence of a chronological ageing phenotype.

Previous studies have already uncovered a central connection between senescence and Db pathology, where Db mice (induced via a high-fat diet) displayed high SA-βGAL^{+ve} and reduced Ki67^{+ve} islet β cells (Sone H & Kagawa, 2005), and greater SA-βGAL staining in adipose tissue (Minamino et al., 2009). It has also been suggested that a Db SASP originating from the circulation or adipose tissue may cause loss of function in nearby organs that lack high levels of senescence (Palmer et al., 2015).

Here it is interesting to note that diabetes shares many common features with ageing, such as accumulation of AGEs (Goova et al., 2001) and heightened ER stress (reviewed in Naidoo & Brown, 2012), which demonstrably promote premature senescence (Liu et al., 2014a). Along with being linked to T2DM, senescence has been shown in T1DM. Here, STZ-induced diabetes elevated rat kidney senescence, measured via upregulation of p16, p21 and p27 proteins and SA-βGAL in tissue (Satriano et al., 2010). Interestingly, removal of p16^{+ve} cells may attenuate the decline in islet repair associated with STZ-induced diabetes, while increasing survival in aged STZ-induced mice (Krishnamurthy et al., 2006). Thus, these data validate a strong feedback loop between diabetes and senescence.

To delve deeper into the link between diabetic pathological wound repair and induction of senescence, Mφs were isolated from the bone marrow of NDb and Db mice. Mφs govern the switch between inflammation and wound resolution (Mantovani et al., 2013), where M1-polarised Mφs mediate inflammation and M2 Mφs promote tissue repair (reviewed in Ferrante & Leibovich, 2012). Contrasting findings are reported for the consequences of Mφ-specific ablation, which is detrimental to healing in adult mice (F4/80^{+ve} ablation only; Goren et al., 2009; Mirza et al., 2009). However, healing in the PU. 1 null mouse, which lacks both neutrophils and Mφs, is scar-free and not impaired (Martin et al., 2003). Mφs exhibit cross-talk behaviours that promote fibroplasia (reviewed in Novak & Koh, 2013; Wynn, 2004), often through cytokine production (Murray et al., 2011; Vidal et al., 2008). Nonetheless, diabetic Mφs display impaired behaviours, including delayed initial wound infiltration through defective chemotaxis and migration (Bannon et al., 2013), prolonged inflammation (Wood et al., 2014), and reduced M2-polarisation (e.g. reduced peroxisome proliferator-activated receptor gamma activity, Mirza et al., 2015).

As in previous work, the diabetic model used in this chapter presented with aberrant wound repair and excessive inflammation (**Figure 3.10**). Db wound tissue Mφs were highly senescent (**Figure 3.13**), and Mφs isolated from the bone marrow of Db mice exhibited reduced retention of polarisation state (**Figure 3.14**). Here, *Nos2* (M1) and *Ym1* (M2) mRNA was significantly reduced (compared to NDb Mφs) at 72 hours post-stimulation. Db Mφs also retained increased expression of the prominent CDKIs, *Cdkn1a* and *Cdkn2a*, suggesting they were highly senescent and less functional than NDb Mφs. As the SASP is an important characteristic of the senescent phenotype, and a potent paracrine mediator of senescence, a cytokine array was performed on CM from NDb and Db Mφs. Here, Db Mφs produced a number of conserved SASP factors, including Cxcl1, Rantes, Mcp-1 and Cxcl2 (**Figure 3.15**; Coppe et al., 2008; Coppe et al., 2010).

Indeed, a short-term hyperglycaemic environment promotes SASP production in human THP-1-derived Mφs, which show increased SA-βGAL^{+ve} staining and elevated production of SASP factors (PAI-1, MCP-1, IL-6, TNF-α and others; Prattichizzo et al., 2018). On the contrary, glucose restriction can extend human fibroblast lifespan *in vitro* (Jin & Zhang, 2013; Li & Tollefsbol, 2011), suggesting a correlation between glucose metabolism and senescence induction. Additionally, the antidiabetic drug, metformin, reduces SASP (e.g. *IL-6* and *CXCL1* mRNA) in human diploid fibroblasts following oncogene-induced senescence, and dampens pro-inflammatory cytokine production in mouse RAW264.7 cells (Moiseeva et al., 2013). Thus, it is clear that the diabetic environment is associated with heightened senescence and a characteristic senescence-based secretome.

As aforementioned, Cxcl1 and Cxcl2 were identified as having the largest fold change differences between Db and NDb Mφ CM (**Figure 3.15**), and *Cxcl1*, *Cxcl2* and their common receptor, *Cxcr2*, were upregulated in Db Mφs (**Figure 3.17**). Intriguingly, the CXCR2 receptor has previously been linked to senescence (Acosta et al., 2008). Here, ectopic expression of CXCR2 induced senescence via a p53-dependent mechanism in MEFs, and shRNA targeting of CXCR2 ameliorated replicative, oncogenic and DNA damage-induced senescence in IMR-90 cells. Db wounds also exhibited significantly elevated levels of *Cxcr2* and its ligands, corroborating previous work showing prolonged Mip-2 (Cxcl2) expression in Db wounds (Wetzler et al., 2000). Furthermore, recent findings demonstrated excessive CXCR2

expression in T cells from T2DM patients, which were highly senescent compared to healthy controls (Lau et al., 2019). Accordingly, these data provide evidence that upregulation of CXCR2 is a common feature of diabetic pathology that may contribute to senescence.

Other authors have demonstrated the importance of CXCR2 signalling in potentiating the diabetic condition. For example, circulating levels of CXCR1/2 ligands are increased in human T1DM blood (Hakimizadeh et al., 2013), while inhibition of Cxcr1/2 prevents the onset of T1DM in preclinical (STZ-induced and NOD) models by blocking inflammation-mediated damage to pancreatic islets (Citro et al., 2015). Amplified expression of *CXCR1* and *CXCR2* is also observed in T1DM rabbits (ear skin; Pradhan et al., 2011) and STZ-induced (male and female) mice (pancreas; Aseer et al., 2015). Of note, Cxcl1 is upregulated in the white adipose tissue of genetically and diet-induced T2DM mice (Neels et al., 2009).

A fundamental role for the SASP is its paracrine "bystander" influence on the local microenvironment. Positive and negative effects of the SASP have been examined, including promoting tumour growth (e.g. chemerin in squamous cell carcinoma, Farsam et al., 2016) and aiding in wound repair (Demaria et al., 2014). Of course, the influence of immune cells on fibroblast behaviour has been characterised in multiple scenarios. For example, Muller et al. (2000) demonstrated that NK cells promoted pro-inflammatory cytokine production in HDFs, while fibroblasts may play an active role in aiding the persistence of wound inflammation (Buckley, 2011). As a result, the role of the Db SASP in mediating wound repair was assessed through modulation of fibroblast behaviour (**Figure 3.17**). Interestingly, significant upregulation of *SERPINE1* (the gene encoding the well-known senescence marker, PAI-1; Kortlever et al., 2006) was observed in young HDFs following Db CM treatment, while aged HDFs showed *SERPINE1* upregulation following M1 CM treatment. Further, expression of *CXCL1* and *CXCL2* was elevated in HDFs following treatment with Db CM from M1-stimulated Mφs. Therefore, these data reveal a hitherto unappreciated role for the Db Mφ secretome in regulating HDF senescence.

As discussed, Acosta et al. (2008) determined a potent role for CXCR2 and its ligands in inducing senescence in murine fibroblasts and immortalised cell lines, yet the authors did not consider the possible effects of the SASP on the local environment. Data in this chapter for the first time elucidated the role of CXCL2 and a CXCL2-

driven SASP in HDFs transfected with a CXCL2 plasmid (**Figure 3.18**). Staining verified that transfected cells produced CXCL2 (2 days post-transfection), while longer culture (6 days) amplified CXCL2 expression, suggesting that the CXCL2-containing SASP potentiated CXCL2 expression in neighbouring cells. HDFs transfected with CXCL2 showed higher nuclear p21, cytoplasmic p16 and increased SA-βGAL, and produce SASP-related cytokines. Indeed, nuclear p21 staining (e.g. in endothelial cells, Matthaei et al., 2012), cytoplasmic p16 (IMR90 fibroblasts, Acosta et al., 2013) and SA-βGAL (in human fibroblasts, Dimri et al., 1995) are associated with cellular senescence. Hence, these data provide evidence that a CXCL2-rich SASP promotes senescence in primary human dermal fibroblasts.

Pathological murine wounds (aged and Db) are characterised by elevated senescence, but fibroblast senescence may also be deemed a contributing factor to poor healing outcome in human leg ulcers (Harding et al., 2005). Chronic wound fibroblasts display high senescence (Agren et al, 1999; Mendez et al, 1998; Vande Berg et al, 1998; Wall et al., 2008), and a correlation exists between fibroblast senescence and time to heal in leg ulcers (Stanley & Osler, 2001). As signalling through CXCR2 is a recognised mediator of senescence, a CXCR2 antagonist (SB265610, Bradley et al., 2009) was used to treat human keratinocytes *in vitro* and human skin wounds *ex vivo* (**Figure 3.20**, **Figure 3.21** and **Figure 3.22**). Intriguingly, SB265610 treatment accelerated scratch wound closure at 8 hours and 24 hours, suggesting blockade of CXCR2 to aid keratinocyte migration. This finding was supported by *ex vivo* wound experiments, where CXCR2 antagonism improved epidermal migration at day 1 and day 3 post-injury, while ligand treatment delayed both *in vitro* and *ex vivo* epidermal migration. Intriguingly, CXCR2 inhibition rescued the effects of CXCL2 *in vitro* and *ex vivo*, yet failed to negate the inhibitory effects of CXCL1 or combinatory ligand treatment. This likely reflects the fact that CXCL1, but not CXCL2, displays promiscuous receptor activation activity (reviewed in Balkwill et al., 2012), and suggests these alternative receptors are active in skin wounds. Consequently, blocking with SB265610 alone is insufficient to prevent the CXCL1-induced delay in epidermal migration.

Curiously, it has previously been shown that CXCR2 activation (through CXCL1 treatment) may promote keratinocyte migration and proliferation (Kroeze et al., 2011), although this effect occurs in a dose-dependent manner. Further, mice

ubiquitously lacking Cxcr2 exhibit delayed re-epithelialisation, less wound granulation, impaired neovascularisation (Devalaraja et al., 2000), diminished neutrophil influx and less monocyte recruitment to wounds (Milatovic et al., 2003). The significance of Cxcr2 antagonism was finally demonstrated in Db wounds, where SB265610 treatment dampened neutrophil influx and reduced Mφ senescence. Consequently, it is clear that CXCR2 signalling must be tightly regulated for optimum wound repair.

Despite senescence being a potential contributor to delayed healing, a short-term transient senescence response is required for wound repair. In fact, $p21^{-/-}$ mice show a marked delay in healing at day 7 post-injury (**Figure 3.29**), which correlates with the timing of senescence induction in normal wounds (Demaria et al., 2014). At D7, significant reduction in matrix deposition, and reduced α-Sma^{+ve} and $Pdgfa^{+ve}$ cells (**Figure 3.33**), confirmed impaired fibrogenesis following p21 attenuation. Previous findings using these mice support these data, where $p21^{-/-}$ livers possessed delayed ECM deposition (Yosef et al., 2017).

Heightened neutrophil and Mφ infiltration were present in $p21^{-/-}$ mouse wounds at D7 (**Figure 3.30**), along with increased expression of the pro-inflammatory cytokine, Mif (**Figure 3.33**), known to contribute to delayed healing in a context-dependent manner (Gilliver et al., 2010). Prolonged inflammation undeniably contributes to poor healing outcome (Lohmann et al., 2017), suggesting one reason for delayed repair in $p21^{-/-}$ wounds. Interestingly, p21 has been shown to centrally regulate immune cell function (Rackov et al., 2016). Ablation of p21 causes murine and human monocyte-derived Mφs to over-secrete IL-1β (Scatizzi et al., 2009), and promotes the activation of murine peritoneal Mφs following LPS stimulation (Trakala et al., 2009). Neutrophil influx is also observed in $p21^{-/-}$ mouse lung tissue (Martin et al., 2016), thus it clear that p21 mediates immune cell function by preventing excessive inflammation.

Inhibition of the p21/p53 senescence pathway is associated with increased proliferation in the liver (Krizhanovsky et al., 2008) and hair follicle stem cells (Lee et al., 2013), known to have vital roles in wound resolution (Ansell et al., 2011; Ito et al., 2005). Indeed, heightened proliferation was observed in the epidermis and dermis of $p21^{-/-}$ wounds (**Figure 3.32**), yet, this was accompanied by a delay in wound closure. As a result, it is clear that senescence induction and wound repair

are both multifactorial and complex processes, signifying that the $p21^{-/-}$ mouse delayed healing phenotype cannot be explained by one feature alone.

Intriguingly, $p21^{-/-}$ wounds possessed more $p16^{+ve}$ cells (**Figure 3.33**), suggesting a compensatory senescence mechanism might be at play. In a model of progeroid aging, Baker et al. (2013) demonstrated increased $p16^{+ve}$ cells in $p21^{-/-}$ mice, thus elucidating an important role for p21 in controlling p16-mediated senescence. Hence, the authors suggested that p21 might cause temporary quiescence to relieve stress that would otherwise stimulate induction of the p16-pRb pathway. It is important to note, however, that induction of $p16^{+ve}$ cells may not directly result in elevated tissue senescence. For example, $p21^{-/-}$ human diploid fibroblasts bypassed senescence induction despite accumulation of p16 (Brown et al., 1997). Therefore, further wound profiling studies will be required to elucidate how p21 attenuation influences senescence in wound healing.

Overall, it is clear that senescence contributes to delayed wound repair through excessive senescent cell accumulation, senescence potentiation and loss of cellular function (summarised in **Figure 3.34**). On the other side of the wound healing "coin", attenuation of p21 leads to impaired fibroplasia, highlighting the importance of a transient, wound-induced senescence response in promoting ECM deposition. Of particular interest, data presented in this chapter explicitly link Db healing and localised wound senescence, modulated in part through Cxcr2 activation. Indeed, CXCR2-activating SASP mediated the function of human fibroblasts, while blockade of the CXCR2 receptor promoted healing during human *ex vivo* and *in vivo* Db murine wound repair. These data not only suggest that excessive CXCR2 may contribute to the Db wound healing phenotype, but that treatment with selective antagonists may promote wound healing. Collectively, these results provide a basis for the development of new wound therapies targeting the CXCR2 receptor and, consequently, wound-induced cellular senescence.

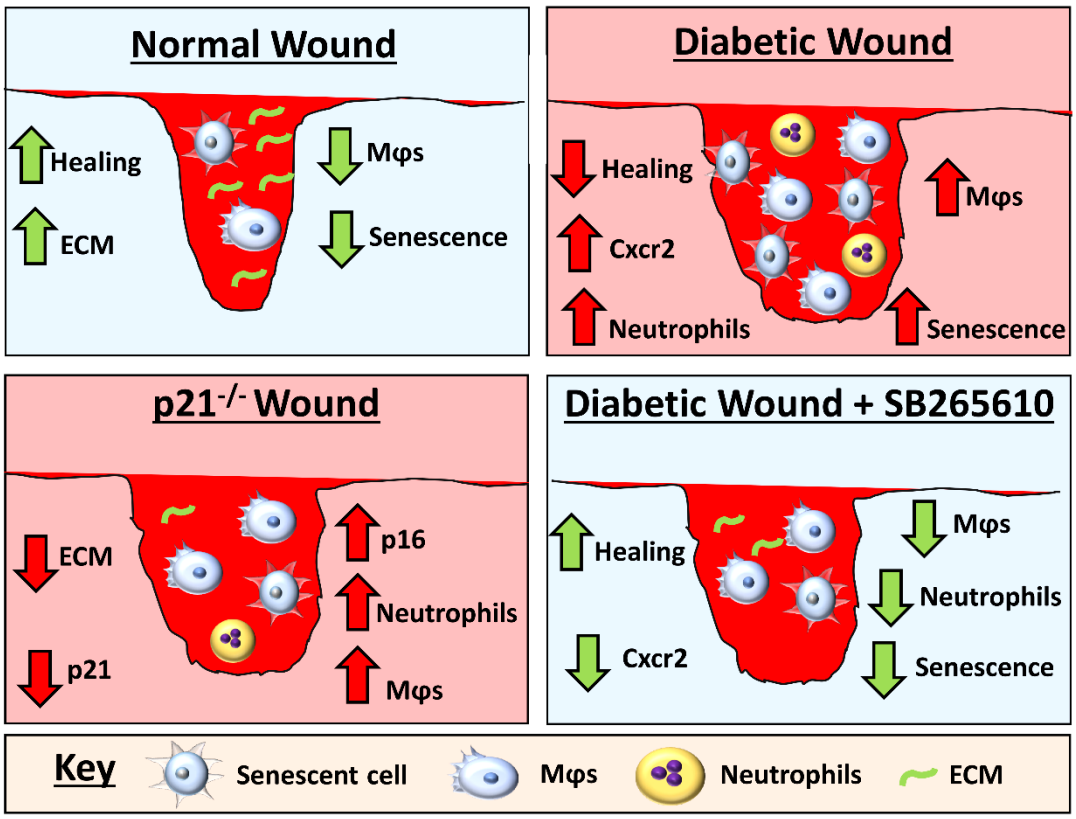

Figure 3.34. Overview of the potential links between senescence and wound repair. Transient senescence occurs during normal wound healing and strongly correlates with fibroplasia, extracellular matrix (ECM) deposition and wound resolution. Lack of p21 ($p21^{-/-}$) delays wound healing by increasing $p16^{+ve}$ senescence and inflammation. In diabetic murine wounds, too much inflammation and a Cxcr2-driven senescent phenotype contributes to delayed repair. Blockade of Cxcr2 (SB265610) dampens inflammation and reduces macrophage (Mφ) senescence to improve murine diabetic wound healing. *Image produced by the author (HNW).*

Chapter 4: lobal Profiling of the Metallome in Wound Repair

Data presented in this chapter has been prepared for publication:

Global metallomics and transcriptomics reveals new roles for multiple metals in normal and pathological wound repair.

Authors: Holly N. Wilkinson[1], Anna Bird[2], Robert Knight[2], Barbara A. Guinn[3] and Matthew J. Hardman[1*]

Diabetes (in preparation)

Affiliations:

[1]Centre for Atherothrombosis and Metabolic Disease, Hull York Medical School; [2]Department of Chemistry, Faculty of Science and Engineering; [3]Department of Biomedical Sciences, Faculty of Health Sciences, University of Hull, HU6 7RX, UK.

Author contributions: All *in vitro*, *in vivo* and *ex vivo* work was carried out by HNW. LA-ICP-MS was carried out with AB, while ICP-MS was performed by RK with additional analysis by HNW. RNA-Seq data was analysed and interpreted by HNW, with the supervision of BAG and MJH. HW and MJH were involved in study concept and design, as well as manuscript preparation.

4.1. Introduction

Metallomics, the global characterisation of metals and metalloids in biological systems, is a rapidly emerging life sciences field, anticipated to complement proteomics, genomics and metabolomics in the integrated, systematic understanding of biology (Sun & Chai, 2010; Zierer et al., 2015). Metals are fundamental for almost all biological processes in eukarya, archaea and bacteria including metabolism, energy transduction, gene expression and cell signalling (Säbel et al., 2009). Some of these metals are required in large quantities (e.g. calcium and sodium), but most are trace elements (e.g. zinc, copper, manganese, iron) needed at more minute levels (Gladyshev & Zhang, 2012). Almost half of all enzymes contain a transition metal core (e.g. copper, zinc or iron), necessary for proper enzymatic function (Andreini et al., 2008; Ascone & Strange, 2009). Even non-essential metals have found their uses in medicine, where they are used in the treatment (e.g. platinum) or diagnosis (e.g. gadolinium and technetium) of disease (Sun & Chai, 2010). Despite their clear importance, current understanding of the temporal and spatial distribution of metals in organic processes, and their biological integration with other omics data, remains limited.

4.1.1. Measuring Metals in Biological Samples

Quantification and functional characterisation of metals in biology is challenging as techniques must be sensitive enough to measure trace metals in very low abundance, yet also be able to distinguish these from non-metal elements. Flame atomic absorption spectroscopy (FAAS) was traditionally used to measure metals in biological and non-biological substrates (Landown et al., 1999), but offers less sensitivity than contemporary approaches. The current gold standard method used to measure metals in inorganic and organic materials is inductively coupled plasma mass spectrometry (ICP-MS). This technique is capable of identifying individual elements by mass, down to one part per quadrillion (reviewed in Liu et al., 2014b). As described in **Section 2.5**, biological samples are digested, vaporised, atomised and ionised through a stream of argon plasma. These ions are then collected and interpreted via mass spectrometry (Montaño et al., 2016).

A limitation of standard ICP-MS is that used alone, it does not provide information about the spatial distribution of elements under study, as whole samples are digested and ablated. To overcome this, many researchers isolate specific tissue

regions via crude physical methods, or use laser-capture microdissection, prior to ICP-MS (Becker et al., 2010). The laser ablation ICP-MS (LA-ICP-MS) technique circumvents this problem to allow sensitive, spatial characterisation of metals *in situ*. First used by Wang et al. (1994) to image strontium and calcium in fish scales, LA-ICP-MS allows ablation of specific tissue regions, which are ionised, separated and detected as per ICP-MS (Becker, 2005).

Other techniques used to assess regional metal distribution include scanning electron microscopy with energy-dispersive X-ray analysis (Zvyagin et al., 2008), energy-filtering transmission electron microscopy (Reimer, 1991), and secondary ion mass spectrometry, each with advantages and disadvantages (Smart et al., 2010; Wu & Becker, 2011). Synchrotron radiation X-ray fluorescence is a more sophisticated technique that shows the 3D tomography of metal distribution at high resolution (to 0.1 μm), allowing spatial determination down to subcellular compartments (Kim et al., 2006b; Ortega et al., 2009; Yang et al., 2005).

Histological staining, while considerably less sensitive than elemental analysis, offers a more affordable and readily available approach to assessing the regional distribution of metals in tissue sections (Danscher, 1984). These stains include: Perl's Prussian blue (Sindrilaru et al., 2011) and Turnbull's staining for non-heme iron (Hansen, 1969); Von Kossa (Rungby et al., 1993) and Alizarin Red staining for calcium deposits (Gilmore et al., 1986); magnesium-dithizonate silver-dithizonate staining for copper (Szerdahelyi & Kása, 1986) and; Timm's method for zinc (Chafetz, 1986). However, many stains are limited to binding labile metal ions, and accordingly, are often not sensitive enough to detect endogenous metals in normal homeostatic tissue (McRae et al., 2009).

Of more biological relevance, antibody staining may be used to detect specific metal-associated proteins and receptors (Bekircan-Kurt et al., 2014). Autometallography techniques, whereby ions are autocatalytically amplified with silver, have also been shown to detect metals, such as zinc, with more sensitivity than traditional methods (Danscher & Stoltenberg, 2006). The development of metal-specific fluorescent probes and probe-based colorimetric assays has allowed direct determination of the location and concentration of active metals in biological tissues (Dlouhy & Outten, 2013; Price et al., 2018; Säbel et al., 2009). These probes, however, require consideration of metal binding kinetics, chelator dissociation constants and metal

availability in the sampled tissue (Tsien et al., 1984). Of note, if protein binding affinity supplants that of the chelator, then minimal chelator binding will occur, leading to false negative results (Dlouhy & Outten, 2013).

Traditional metallomics studies do not generally consider the biological status of the metals in question, including their oxidative state and whether they are bound to specific protein complexes. Indeed, a third of all proteins are associated with metals and the biological state of the metal confers its properties and functions (Da Silva & Williams, 2001). Thus, elemental analysis alone does not fully appreciate the role of metals in biological contexts (reviewed in Yannone et al., 2012). Recently, researchers have acknowledged this limitation and have begun to employ methods to combine ICP-MS with other, more informative, techniques. For example, combining ICP-MS with electrophoresis or chromatography allows specific separation of molecules (McSheehy et al., 2001), and combining ICP-MS with sophisticated proteomic approaches permits identification of metal-containing species in samples (reviewed in Bettmer et al., 2009; Wang et al., 2010). More recently still, an x-ray crystallography technique has been developed to characterise metal binding sites of proteins (Handing et al., 2018). Despite these developments, it remains clear that no single method can fully capture native metal status *in vivo*, and a unifying approach to this problem has yet to be developed.

4.1.2. Bodily Distribution of Metals

Elegant regulatory mechanisms have evolved to tightly control the interplay between metals and DNA, proteins and biomolecules (McRae et al., 2009). Despite their crucial roles in maintaining body function, accumulation of metals can cause severe toxicity. In fact, imbalances in metal homeostasis are linked to wide-ranging degenerative pathologies. One example is Parkinson's disease, which is characterised by accumulation of zinc and iron, and dissipation of copper, in the substantia nigra (Barnham & Bush, 2008). Although it is acknowledged that abnormal metal accretion and loss leads to disease, the cellular and molecular causes are still unclear in many settings. Therefore, the priority should be to identify the subcellular distribution and function of metals in various biological contexts to understand how homeostatic aberrations in the metallome can manifest in disease.

Metals are heterogeneously distributed, both at the tissue level and within cells. Metal abundance usually correlates with function, with metals found concentrated

at the site where they are most highly used (e.g. iron in spleen, Arezes & Nemeth, 2015; calcium in bone, Pozzan et al., 1994). At the cellular level, metals are also distributed based on their role. High amounts of iron are found in mitochondria, where it is required for heme synthesis and iron-sulphur cluster formation (Lill & Kispal, 2000). Zinc concentration is greatest in the cellular nucleus, where it is bound to zinc finger proteins for transcription (Nieto, 2002), while the Golgi apparatus contains high amounts of copper (copper ATPases; Festa & Thiele, 2011). The cellular distribution of metals species is summarised in **Figure 4.1**.

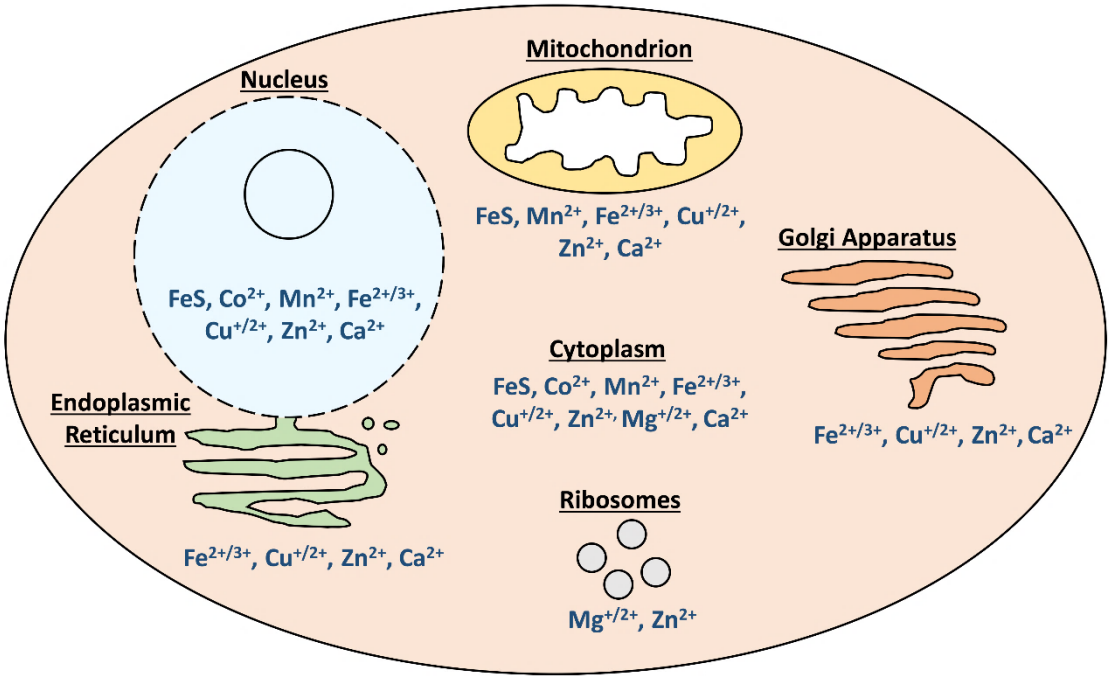

Figure 4.1. Intracellular localisation of metals based on their major cellular functions. Metals are associated with the nucleus (transcription), endoplasmic reticulum (protein and lipid synthesis), Golgi apparatus (protein trafficking) and mitochondria (metabolism). Metals in the cytoplasm are found in free form, bound to metal transport proteins, or incorporated into cytoplasmic structures (e.g. ribosomes). *Image modified from Hare et al. (2015).*

4.1.3. Calcium in the Body

Calcium is the most abundant element in the body, found as a major constituent of bone (as hydroxyapatite) and present in every cell to orchestrate signalling activities (Moe et al., 2015). Calcium drives cellular processes through tight regulation of its storage and release, where its intracellular concentration is 1000-fold lower than in the blood (Berridge et al., 2003). Extracellular calcium is maintained by intestinal absorption, reabsorption from the kidney, and resorption from bone (Peacock, 2010). In the intestine, calcium is absorbed via transcellular or

paracellular uptake (illustrated in **Figure 4.2**). Transcellular uptake occurs at the duodenum brush border via transient receptor potential vanilloid type 6 (TRPV6), a TRP channel regulated by vitamin D, calcium deficiency (van de Graaf et al., 2004) and intracellular calcium binding proteins such as calmodulin (Lambers et al., 2004). The importance of TRPV6 in regulating dietary calcium uptake and availability becomes apparent in genetic knockdown experiments, where *Trpv6* null mice develop osteopenia (Chen et al., 2014a).

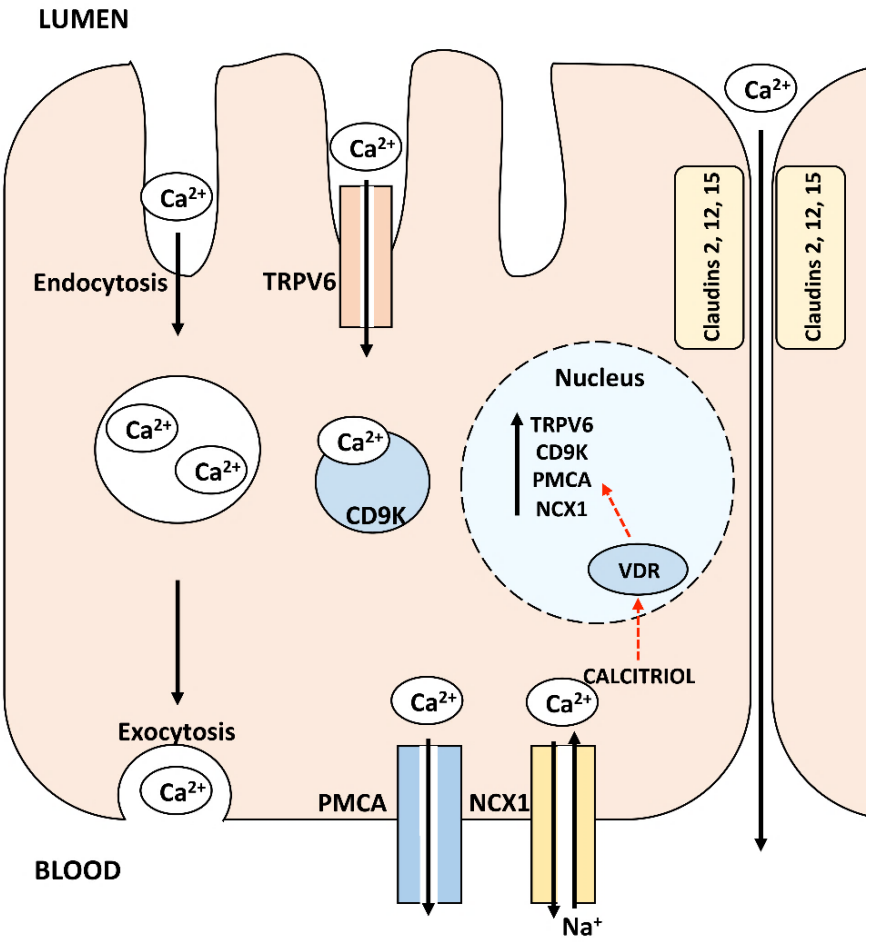

Figure 4.2. Calcium uptake and transport in the body. Calcium is absorbed into the body via transcellular and paracellular transport. Transcellular transport occurs at the apical surface of the duodenum brush border via transient receptor potential vanilloid type 6 (TRPV6). Ionic calcium (Ca^{2+}) then binds to calbindin-D9k (CD9K) and is transported into the blood via plasma membrane calcium ATPase (PMCA) 1b and sodium-calcium exchangers (e.g. NCX1) at the basolateral membrane. Transcellular transport may also ensue via vesicle trafficking (endocytosis and exocytosis). Paracellular transport occurs between adjacent cells via transepithelial electrochemical gradients modulated through tight junction proteins (claudins 2, 12, and 15). Intestinal calcium absorption requires calcitriol, which signals through the vitamin D receptor (VDR) to regulate TRPV6, CD9K, PMCA and NCX1 transcription. *Image produced by the author (HNW).*

Once intracellular, ionic calcium (Ca^{2+}) binds to the buffering protein calbindin-D9k, which is also modulated by vitamin D and calcium availability (Lambers et al., 2006). Ca^{2+} is then transported into the blood via plasma membrane calcium ATPase 1b (PMCA1b) and a sodium-calcium exchanger (NCX) at the basolateral membrane of the enterocyte (Khanal & Nemere, 2008). Intriguingly, knockdown of calbindin-D9k did not affect serum calcium levels in mice (Kutuzova et al., 2006), which was likely compensated for by induction of other calcium transport genes (e.g. *Trpv6*, Lee et al., 2009). Vesicle trafficking was recently proposed as another method of transcellular transport (DiMeglio & Imel, 2019). Unlike transcellular transport, paracellular transport is an energy-independent uptake mechanism that occurs between adjacent cells on the enterocyte membrane. This process is driven by transepithelial electrochemical gradients, through tight junctions consisting of claudins 2, 12, and 15 (Diaz de Barboza et al., 2015; Moor & Bonny, 2016). These claudins are regulated by calcitriol (1, 25-dihydroxyvitamin D3) and calcium binding proteins (e.g. sorcin; Emkey & Emkey, 2012; Meyers et al., 1998).

Plasma calcium is sensed by the calcium sensing receptor (CaSR) and regulated by three calciotropic hormones: parathyroid hormone (PTH), calcitonin, and calcitriol (Zhang et al., 2015a). Ca^{2+} is the primary ligand for CaSR, but it also senses other metal ions (e.g. Mg^{2+} and Be^{2+}; Chakravarti et al., 2012), changes in pH, peptides, amino acids and antibiotics (Hofer & Brown, 2003). Under high calcium conditions, or hypophosphatemia, elevated FGF23 and reduced calcitriol (Moe et al., 2015; Rodriguez-Ortiz et al., 2012), chief cells of the parathyroid gland sense calcium (via the CaSR). This causes activation of phopholipases C, A2 and D, release of inositol 1,4,5-trisphosphate (IP3), mobilisation of Ca^{2+} from intracellular stores, and reduced PTH secretion (Loupy et al., 2012). PTH causes calcium resorption in bone and in the renal tubules, and stimulates renal production of calcitriol. Hence, the CasR serves to balance calcium absorption and resorption in the body (Kameda et al., 1998; Toka et al., 2015).

Previtamin D3 is ingested or synthesised in the skin through exposure to sunlight, enters the blood bound to vitamin D binding protein, and undergoes hydroxylation (via CYP27A1) in the liver to form calcidiol. Calcidiol is further hydroxylated (via CYP27B1) in the kidney to form the biologically active calcitriol (Bikle, 2014; Moe et al., 2015). This rise in calcitriol increases calcium absorption in the intestine, and

synergistically promotes PTH activity. Consequently, low PTH and calcitriol reduce calcium uptake (Pu et al., 2016). When PTH is released, its effects are short-lived, as PTH is rapidly cleared from the body via the liver and kidneys (D'Amour, 2012; Moe et al., 2015). On the contrary, calcitonin, produced by the parafollicular parathyroid cells, correlates positively with serum calcium (Chakravarti et al., 2012) to prevent excessive osteoclastic bone resorption.

4.1.4. Regulation of Intracellular Calcium

Calcium is important in starting life at fertilisation, and ending cellular life through apoptosis (Brini & Carafoli, 2009). In fact, this was first shown by Ringer (1883) who made the discovery that frog hearts contracted in tap water containing "inorganic constituents" but not in distilled water. Nowadays, a large body of literature pertains to the importance of Ca^{2+} as a versatile intracellular secondary messenger, capable of operating in multifaceted ways to govern cellular processes including proliferation, differentiation, metabolism, motility and gene transcription (Berridge et al., 2000). Calcium is arguably the most ubiquitous cation in the body (Carafoli et al., 2001), and extracellular concentrations (~1 mM) exceed cytosolic amounts (~100 nM) to allow incremental fluctuations and signal conduction (Uhlén & Fritz, 2010). Maintaining low cytosolic Ca^{2+} is crucial for cell survival, as uncontrolled accumulation of cytosolic Ca^{2+} causes apoptosis and necrosis (Orrenius et al., 2003). Therefore, specialised proteins, buffers and transport systems control intracellular Ca^{2+} in a temporal and spatial-dependent manner to sustain intracellular levels within the nanomolar range (Berridge et al., 2002). These regulatory systems are highly dynamic and sophisticated, comprising hormonally-regulated feedback loops and many pumps, exchangers, channels and buffers (Krebs et al., 2015).

Intracellular Ca^{2+} is regulated by "on" (entry into the cytoplasm) and "off" (sequestration and expulsion from the cytoplasm) reactions. During the "on" reactions, most of the internalised Ca^{2+} is bound to buffers, while a small quantity is free to bind to effectors to actuate cellular responses (Berridge et al., 2003). However, during "off" reactions, Ca^{2+} is removed from effectors and cytoplasmic buffers, and is expelled from the cytoplasm via pumps and exchangers. The NCX, which has high capacity and low affinity for Ca^{2+} (Sharma & O'Halloran, 2014), and plasma-membrane Ca^{2+}-ATPases (PMCA or ATP2B), which have low capacity and high affinity for Ca^{2+} (Brini et al., 2013), extrude Ca^{2+} from the cell. On the contrary,

sarco(endo)plasmic reticulum Ca^{2+}-ATPases (SERCAs, encoded by *ATP2A1*, *ATP2A2*, and *ATP2A3*; Elaïb et al., 2016), with low capacity and high affinity for Ca^{2+} (Toyoshima, 2009), store Ca^{2+} in the endoplasmic reticulum (ER) at a concentration range of 0.1-1mM (Bygrave & Benedetti, 1996). Mitochondria aid this process, rapidly sequestering free cytosolic Ca^{2+} via a mitochondrial uniporter (MCU; Kirichok, 2004; Liu et al., 2017), and slowly releasing it for uptake (SERCA) and export (PMCA) via a mitochondrial NCX (Schwaller, 2012; **Figure 4.3**).

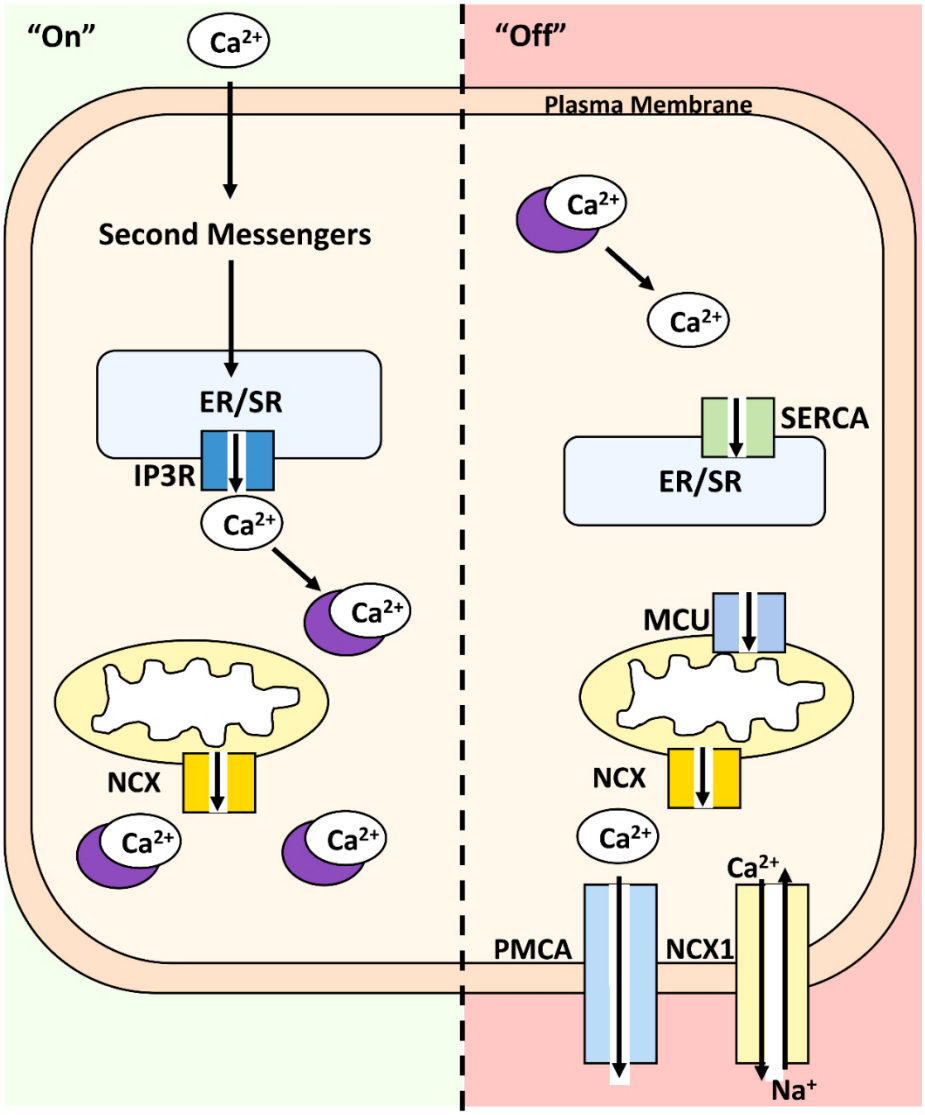

Figure 4.3. Calcium "on" and "off" signalling reactions. During "on" status, calcium enters the cell and causes ionic calcium (Ca^{2+}) release from intracellular stores via second messengers. At the endoplasmic reticulum (ER) or sarcoplasmic reticulum (SR), calcium is released into the cytosol via an inositol 1,4,5-trisphosphate receptor (IP3R). Mitochondrial release of calcium occurs via a mitochondrial sodium-calcium exchanger (NCX). Cytosolic calcium then binds to buffers to actuate cellular responses. During "off" reactions calcium is rapidly sequestered into the ER/SR (SERCA) or mitochondria (MCU) and extruded from the cell via plasma membrane calcium ATPase (PMCA) 1b and the sodium-calcium exchanger (e.g. NCX). SERCA = sarco/endoplasmic reticulum Ca^{2+}-ATPase. MCU = mitochondrial uniporter. *Image produced by the author (HNW).*

Within the lumen of intracellular stores, Ca^{2+} binds to low affinity, high capacity calcium binding proteins (calsequestrin or calreticulin), but in the cytoplasm, Ca^{2+} binds to high affinity, low capacity binding proteins such as the calbindins and the S100 proteins (Krebs et al., 2015). These calcium "buffers" function to fine tune calcium signalling by altering the amplitude of the calcium signal, and the recovery time following signal activation (Berridge et al., 2003). The calcium binding ratio determines the buffering capacity of cells, where low ratios lead to accelerated responses but increase the risk of cytotoxicity (Krebs et al., 2015).

Ca^{2+} enters the cell in response to extrinsic stimuli and loss of intracellular Ca^{2+} stores via an electrochemical gradient through plasma membrane channels (Schwaller, 2012). These include voltage-gated Ca^{2+} channels, receptor-operated Ca^{2+} channels, TRP channels, or store-operated Ca^{2+} entry channels. Release of Ca^{2+} from intracellular organelles (e.g. the ER) occurs against the Ca^{2+} chemical gradient, thus requiring energy from ATP hydrolysis (Toyoshima & Inesi, 2004). When a first messenger binds to a G-protein coupled receptor (GPCR), this causes G-protein activation followed by activation of phospholipase C. Phospholipase C triggers phosphatidylinositol 4,5-bisphosphate hydrolysis, forming diacylglycerol (DAG) and IP3 (Rosenbaum et al., 2009). DAG, which remains bound to the plasma membrane, activates protein kinases (e.g. PKA), leading to protein phosphorylation and functional responses (Wang, 2006). However, IP3 diffuses into the cytoplasm, binds to an IP3 receptor (IP3R) on the ER and causes release of Ca^{2+} into the cytosol (Mikoshiba, 2007). This process is summarised in **Figure 4.4**.

To further convolute matters, there are three IP3Rs (ITPR1, ITPR2 and ITPR3) that can be stimulated by various calcium-binding proteins (e.g. calmodulin; Carafoli et al., 2001; Patterson et al., 2004; Taylor & Laude, 2002) and chemical messengers such as cyclic ADP ribose, nicotinic acid adenine dinucleotide phosphate (NAADP) and sphingosine-1-phosphate (S1P; Bootman et al., 2002; summarised in **Table 4.1**). Ca^{2+} release via NAADP is unaffected by Ca^{2+} depletion from IP3R-regulated stores, hence NAADP serves to liberate Ca^{2+} from intracellular stores separately from IP3R-regulated pathways (Calcraft et al., 2009). Tight control of intracellular Ca^{2+} is important as depletion of ER Ca^{2+}, if persistent, can cause an unfolded protein response in many important proteins (e.g. calreticulin, calsequestrin, calnexin), leading to protein degradation (Arruda & Hotamisligil, 2015).

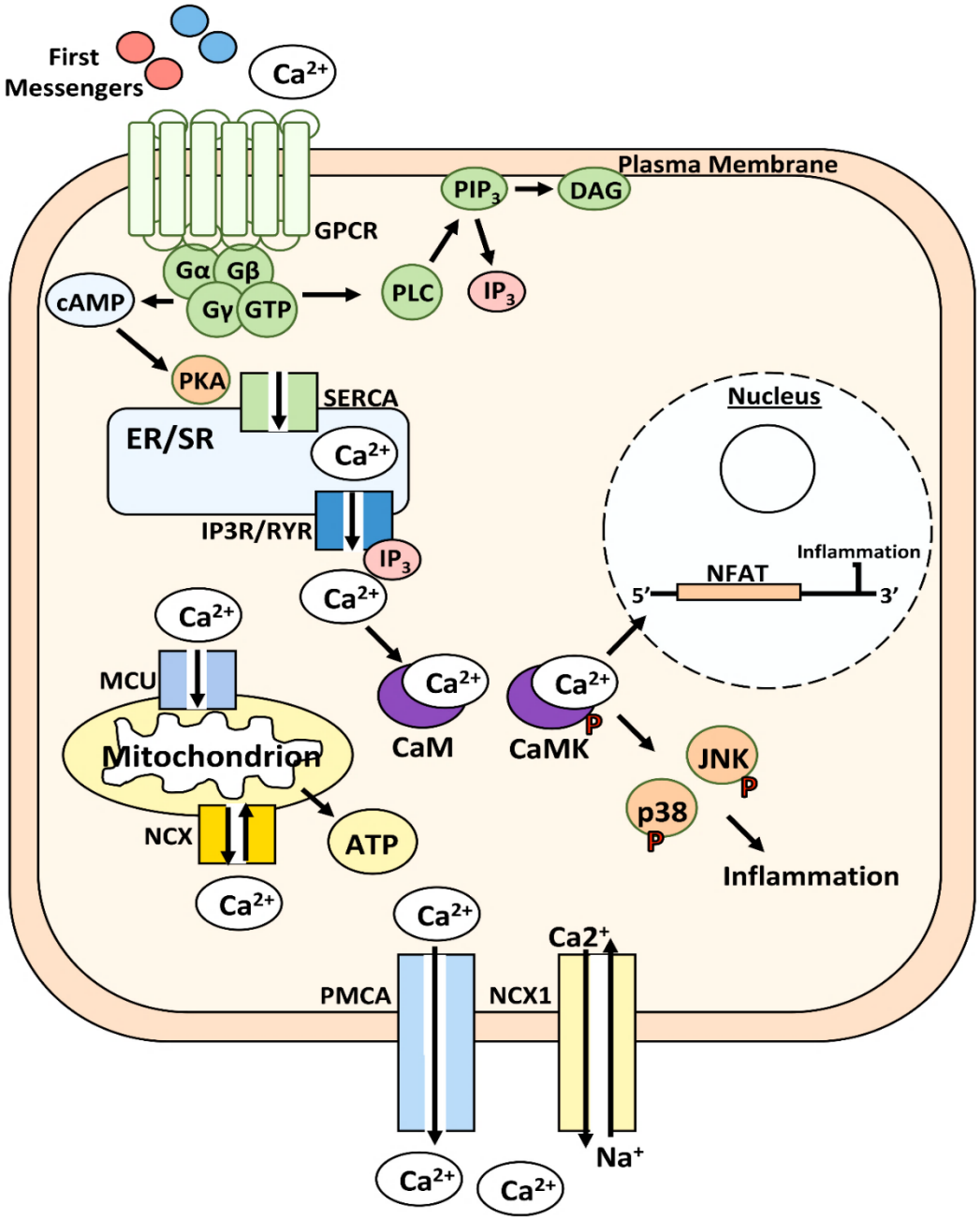

Figure 4.4. Classical intracellular calcium signalling. G-protein coupled receptor (GPCR) activation occurs via first messengers, leading to activation of PLC and hydrolysis of phosphatidylinositol 4,5-bisphosphate (PIP2) into diacylglycerol (DAG) and inositol 1,4,5-trisphosphate (IP3). DAG stimulates protein kinases (e.g. PKA) causing protein phosphorylation. IP3 binds to an IP3 receptor (IP3R) on the sarcoplasmic or endoplasmic reticulum (SR/ER), releasing ionic calcium (Ca^{2+}). GPCR activation additionally leads to cyclic (cAMP) release, PKA production and IP3R stimulation. Ca^{2+} is sequestered in the ER/SR via sarco/endoplasmic reticulum Ca^{2+}-ATPase (SERCA) or in the mitochondria via mitochondrial uniporter (MCU). The sodium-calcium exchanger (NCX) pumps Ca^{2+} from the mitochondria and the cell. Ca^{2+} is also extruded through plasma membrane calcium ATPase (PMCA) 1b. In the cytosol, Ca^{2+} binds to buffers (e.g. calmodulin, CaM), while calcium sensors (calmodulin-dependent protein kinases, CaMKs) phosphorylate proteins to actuate cell responses (e.g. inflammation). NFAT = nuclear factor of activated T cells. JNK = c-Jun N-terminal kinase. *Image produced by the author (HNW).*

Table 4.1. Organelle-based calcium-regulating proteins. *

Name (isoforms)	Tissue and sub-cellular location	Function	Endogenous regulators	References
SERCA (SERCA1a, SERCA1b, SERCA2a, SERCA2b, SERCA3)	Skeletal muscle & non-muscle (SERCA3 only). ER membrane.	Ca^{2+} uptake from the cytosol to ER lumen.	Sarcolipin & Phospholambam.	Meis & Vianna, 1979; Prasad et al., 2004; Toyoshima & Inesi, 2004; Wu et al., 1995; Vandecaetsbeek et al., 2011.
IP3R (IP3R1, IP3R2, IP3R3)	Ubiquitous. ER membrane.	Ca^{2+} release from the ER to cytosol.	IP3, Ca^{2+}, ATP, PKA, PKC, AKT, PKG & CaMK.	Choe & Ehrlich, 2006; Foskett et al., 2007.
RyaR (RyaR1, RyaR2, RyaR3)	Muscle and brain. ER membrane.	Ca^{2+} release from the ER to cytosol.	Ca^{2+}, Mg^{2+}, PKA, PKG & CaMK.	Fill & Copello, 2002; Meissner, 1994; Van Petegem, 2012.
STIM (STIM1, STIM2)	Ubiquitous. ER membrane.	Ca^{2+} entry from extracellular space to cytosol.	Ca^{2+} depletion, ROS, Temperature, Hypoxia, SGK1 & AMPK.	Carrasco & Meyer, 2011; Soboloff et al., 2012.
Orai (Orai1, Orai2, Orai3)	Ubiquitous. Plasma membrane.	Ca^{2+} entry to cytosol, coupled with STIM.	N/A	Cao et al., 2015; Gwack et al., 2008.
Calreticulin	Ubiquitous. ER lumen.	Ca^{2+} chaperone	N/A	Michalak et al., 2009; Prins & Michalak, 2011.
Calnexin	Ubiquitous. ER membrane.	Chaperone	N/A	Caramelo and Parodi, 2008; Prins & Michalak, 2011.
VDAC (VDAC1, VDAC2, VDAC3)	Ubiquitous. Mitochondrial membrane.	Diffusion of Ca^{2+} across mitochondrial membrane.	Hexokinase, Bcl2, PKA, PKCe & ROS.	Colombini, 2012; Messina et al., 2012; Shoshan-Barmatz & Ben-Hail, 2012.
MCU	Ubiquitous. Mitochondrial membrane.	Ca^{2+} uptake into the mitochondria.	MICU1, MICU2, MICUR1 & EMRE.	Chaudhuri et al., 2013; De Stefani et al., 2011; Deluca & Engstrom, 1961; Foskett & Philipson, 2015.
Na^{+}/Ca^{2+} exchanger (NCX)	Ubiquitous. Mitochondrial membrane.	Ca^{2+} efflux from the mitochondria to the cytosol.	K^{+}, Ni^{2+}, Mg^{2+}, Ba^{2+}, La^{3+}, PKC & PINK1.	Chaudhuri et al., 2013; De Stefani et al., 2011; De Stefani & Rizzuto, 2014; Foskett & Philipson, 2015.

**Adapted from Arruda & Hotamisligil (2015).*

Despite all Ca^{2+} signalling pathways relying on Ca^{2+} pulses to potentiate signals, small variations in the spatial and temporal properties of these systems adds to the complexity of studying Ca^{2+}-related networks. The combination of pumps, exchangers and Ca^{2+} binding proteins is unique to each cell, allowing rapid or slow Ca^{2+} transients depending on the cell's major function (Caride et al., 2001). These transients can occur in quick pulses (microseconds to milliseconds) to allow cardiac contraction (Fearnley et al., 2011), or ensue in waves (seconds to minutes) via saltatoric propagation to orchestrate processes from fertilisation (Campbell & Swann, 2006), to gene expression (Di Capite et al., 2009), to wound inflammation (Razzell et al., 2013). Ca^{2+} signalling can also be remodelled, particularly in cancers, to promote tumorigenic behaviours such as proliferation (Monteith et al., 2017). From this, it is clear that the molecular Ca^{2+} toolkit is highly dynamic, adapting to cell death and disease.

4.1.5. Calcium in Pathology

Calcium homeostasis is certainly complex, mediated by a multitude of dynamic, conserved signalling processes and compensatory mechanisms. However, in instances of metabolic dysregulation, the adaptive integrity of Ca^{2+} signalling is lost. Abnormally high (hypercalcemia) and abnormally low (hypocalcemia) calcium indicate serious imbalances in calcium homeostasis (Peacock, 2010). Patients with chronic kidney disease often suffer absorptive hypercalcemia, as they are ill-equipped to deal with excess dietary calcium, or hypocalcemia, as they produce less calcitriol (Gallant & Spiegel, 2017). Hypercalcemia and hypocalcemia can also occur as a result of too much or too little bone resorption, as seen in patients with cancer (hypercalcemia; Goldner, 2016) or following parathyroidectomy (hypocalcemia; Afshan et al., 2017). Calcium deficiency leads to widely acknowledged non-communicable diseases such as osteoporosis (Nordin & Morris, 1989) and rickets (Allgrove & Shaw, 2015), while excessive calcium deposits are found in atheroma plaques (Doherty et al., 1999) and renal calculi (Khan et al., 2016).

Genetic mutations in Ca^{2+} transport proteins, such as SERCA, are associated with increased susceptibility to disease (e.g. certain cancers, Korošec et al., 2006; Korošec et al., 2009; Prasad et al., 2005). Many pathologies are also accompanied by oxidative stress (e.g. obesity), which is known to affect Ca^{2+} transport systems

(Balderas-Villalobos et al., 2013). Thus, it is clear that calcium imbalance within the body is self-perpetuating, both caused by, and exacerbated by, pathology.

4.1.5.1. Calcium and Diabetes

Given the well-defined link between perturbed calcium and body system maintenance, it follows that calcium dysbiosis is associated with many metabolic diseases. One of the most prevalent metabolic disorders is diabetes, which encompasses a number of glucose-mediated subtypes (American Diabetes Association, 2010; **Section 1.3**). Diabetic patients often develop electrolyte disorders, such as diabetic ketoacidosis or nonketotic hyperglycemic hyperosmolar syndrome, and show characteristic deficiencies in magnesium (Ramadass et al., 2015), calcium (Dong & Qin, 2012), phosphate and potassium (Ahn et al., 2017; Liamis et al., 2014). T1DM also poses an increased risk of developing renal failure, leading to hyperphosphatemia, hypocalcemia, and hypoparathyroidism (Liamis et al., 2014). These changes then cause major effects on peripheral tissues, such as altering muscle contraction, and affecting insulin and glucagon secretion in the pancreas (Ahn et al., 2017).

Following stimulation by glucagon or epinephrine, hepatic regulation of glucose is controlled by Ca^{2+}, which modulates gluconeogenesis enzymes and glycogenolysis (Amaya & Nathanson, 2013; Arruda & Hotamisligil, 2015). In the pancreas, elevated intracellular Ca^{2+} causes insulin secretion, mediated in part by calcitriol (Pittas & Dawson-Hughes, 2010). However, in diabetes, pancreatic β cells are subjected to high levels of oxidative stress, which enhances the production of ER chaperone proteins as part of the ER stress response and can lead to apoptosis (Ma et al., 2017; Ron & Walter, 2007). High glucose and excessive inflammation also dampen ER SERCA expression in pancreatic β cells (Cardozo et al., 2005; Hara et al., 2014), while induction of Serca, to increase Ca^{2+} accumulation in the ER, results in improved glucose homeostasis in mice with genetic (*ob/ob*) and diet-induced obesity (Fu et al., 2015). Hence, these findings show the importance of maintaining normal intracellular calcium for natural metabolic function.

Diabetic foot ulcers are a major complication of diabetes, perpetuated by neuropathy and poor tissue perfusion (Tesfaye et al., 2005). Indeed, impairment in Ca^{2+} signalling is known to play a role in neuropathy (Fernyhough & Calcutt, 2010) and endothelial and vascular smooth muscle cell dysfunction related to diabetes

(Tabit et al., 2010), yet the molecular mechanisms contributing to this are not fully understood (Fernández-Velasco et al., 2014). As aforementioned, diabetic tissues are hyperglycaemic, develop insulin resistance, retain reduced endothelial nitric oxide (eNOS) production and are more susceptible to oxidative stress and apoptosis (Fernández-Velasco et al., 2014; Tamareille et al., 2006). eNOS is a Ca^{2+}-dependent enzyme that stimulates SERCA-mediated Ca^{2+} uptake in the sarcoplasmic reticulum to induce vascular smooth muscle cell hyperpolarisation (Fernández-Velasco et al., 2014). Consequently, diminished eNOS is accompanied by reduced Ca^{2+} signalling and increased oxidative stress, which compromises vascular tone and promotes inflammation (Makimattila et al., 1996).

There is a current shift in the focus of research to target the molecular pathways governing this oxidative-stress induced vascular damage to treat vascular complications. For example, overexpression of transcription factor EB has been shown to reduce oxidative stress and attenuate vascular damage in HUVECs and mice (Lu et al., 2017). It is important to note, however, that disparities exist in how diabetes affects Ca^{2+}-dependent vascular function. These reports include data from T1DM (Sheikh et al., 2012; Weber et al., 1996) and T2DM (Bagi et al., 2003; Stalker et al., 2005) rodent models and patients with varying aetiologies (McVeigh et al., 2002; Johnstone et al., 1993). Therefore, although Ca^{2+} is clearly crucial for vascular, hepatic and pancreatic function, development of a unifying hypothesis and treatment modality for calcium perturbations must be approached with caution.

4.1.5.2. Calcium and Ageing

A large body of literature describes the relationship between calcium and chronological ageing, where the expression of a number of calcium-linked genes change with age. One of the most widely known models of premature ageing is the klotho mutant mouse, whose major mutation is in the *α-Klotho* gene (Kuro-o et al., 1997). This mutation leads to many hallmark features of ageing, including arteriosclerosis, skin atrophy, infertility, hypoglycemia, osteoporosis, emphysema and a shortened life span (Nabeshima, 2002). Conversely, overexpression of α-Klotho extends lifespan by 20-30% in mice (Kurosu et al., 2005). Interestingly, α-Klotho protein is expressed in tissues involved in calcium homeostasis, such as the kidney and parathyroid gland (Erben & Andrukhova, 2017; Krajisnik et al., 2010), suggesting a pivotal role for α-Klotho in mediating calcium homeostasis. In fact,

Imura et al., (2007) demonstrated that PTH is rapidly induced in mice in an α-Klotho- and NCX-dependent manner. Fan et al., (2018) showed that Casr and α-Klotho regulate PTH synthesis and growth of the parathyroid glands, where α-Klotho can compensate for Casr deletion. Roles for α-Klotho in attenuating oxidative stress (Wang et al., 2012) and suppressing cancer (Doi et al., 2011) have also been determined.

The link between cellular senescence, ageing and diabetes has already been discussed (**Section 3.1.4**), yet calcium also plays a fundamental role in mediating cellular senescence. Cytoplasmic calcium influx (from the ER or extracellular space) leads to apoptosis, but is also observed in response to senescence-induced stress. Oncogene-induced senescence in mammary epithelial cells is induced by elevated cytosolic Ca^{2+}, and can be prevented by blocking ER Ca^{2+} release (via ITPR1 and ITPR2; Wiel et al., 2014), while depleting ER Ca^{2+} stores prevented H_2O_2-induced senescence in endometrial mesenchymal stem cells (Borodkina et al., 2016). Furthermore, calcium is implicated in mediating SASP production via regulation of the nuclear factor of activated T cells (NFAT) pathway (via calcineurin mediated dephosphorylation, Fric et al., 2014), and is a key regulator of cell cycle, increased during anaphase to speed cell division (Farfariello et al., 2015; Poenie et al., 1986; Tombes & Borisy, 1989). Additionally, CDKIs are modulated by Ca^{2+}, where loss of ER Ca^{2+} stores triggers p16 and p21 activation *in vitro* (Chen et al., 1999). Hence, it is clear that Ca^{2+} modulation is importantly associated with cellular ageing.

4.1.6. Calcium in Skin and Wounds

The epidermal calcium gradient is widely acknowledged, serving to regulate terminal differentiation and thus conserve epidermal barrier integrity (Menon et al., 1985). Interestingly, Ca^{2+} transport to the *stratum granulosum*, and maintenance of the Ca^{2+} gradient, is lost during skin ageing (Rinnerthaler et al., 2013). In skin disorders such as Hailey-Hailey disease (mutated *ATP2C1* encoding the Golgi pump) and Darier's disease (mutated *ATP2A2* encoding the SERCA pump), epidermal calcium balance is disrupted, causing decreased cell adhesion and misexpression of differentiation markers, such as loricrin and involucrin (Dhitavat et al., 2003; Elias et al., 2002; Leinonen et al., 2009; Savignac et al., 2014). A switch from low (0.03 mM) to high (above 0.1 mM) calcium *in vitro* triggers keratinocyte differentiation, characterised by formation of tight junctions (redistribution of claudin and

occludin), adherens junctions (E-cadherin), and the expression of KRT1 and KRT10, involucrin and transglutaminase-I, and loricrin and filaggrin, in sequential order (Bikle et al., 1996; Pillai et al., 1990). Keratinocytes also contain a number of store-operated Ca^{2+} entry channels (including TRPV6 and TRPC1, 3 and 4; Cai et al., 2006; Lehen'kyi et al., 2011; Tu et al., 2005), modulated by phospholipase C and CaSR (Tu et al., 2008).

Skin wound healing is a process that must be initiated rapidly, and tightly controlled by signalling molecules (Fathke et al., 2006; Greaves et al., 2013). Thus, it is unsurprising that calcium plays a major part in orchestrating this cascade, modulating components of each wound repair phase. Proper Ca^{2+}-directed communication is required for activation of platelets in haemostasis, as knockdown of *Atp2a3* leads to delayed thrombosis in mice *in vivo*, and perturbed adhesion and aggregation of platelets *in vitro* (Elaïb et al., 2016). Moreover, intracellular Ca^{2+} directs neutrophil migration (Mandeville & Maxfield, 1997), and activates MCU (Zheng et al., 2017), TRPC1 (Lindemann et al., 2015) and TRPC6 (Damann et al., 2009) to promote neutrophil polarisation and chemotaxis. Inhibition of Ca^{2+} mobilisation with Ca^{2+} channel blockers can prevent Mφ activation (Wright et al., 1985), while a Ca^{2+}-dependent PIP3 gradient is required for Golgi-mediated phagocytosis (Vashi et al., 2017). In later phases of healing, Ca^{2+} is required for cellular proliferation (Berridge, 1995; Schwarz et al., 2006; Zhang et al., 2014b) and the directed migration of fibroblasts (Wei et al., 2009). Ca^{2+} signalling is therefore crucially important for early and late-stage wound repair processes.

4.2. Chapter Aims

Despite relatively detailed understanding of how calcium regulates cell signalling and function, little information is available regarding the temporal, spatial and pathological distribution of calcium and other metals in skin wound repair. It was therefore hypothesised that the metallome would be altered throughout normal and pathological healing in a temporal and spatial manner, which would correlate with metal-linked transcriptional changes and cellular functions. The specific aims of this chapter were to:

1) **Globally characterise endogenous metal levels in skin and determine their temporal profile throughout normal and pathological wound repair.** ICP-MS was used to measure metals in skin and wounds from normal (young and non-diabetic) and pathological (aged and diabetic) healing mice.
2) **Perform comparative analysis of metallome changes (ICP-MS) and gene expression (RNA-Seq) in normal and pathological healing.** This will be the first attempt to perform direct correlative analysis between wound metallomics and transcriptomics.
3) **Explore in detail how changes in a single metallome component (calcium) are linked to functional aspects of wound repair.** Here the contribution to specific aspects of healing will be evaluated using *in vitro* murine and human wound healing models.
4) **Generate pilot data on the spatial distribution of metals in skin and wounds.** The LA-ICP-MS method was optimised and applied to normal mouse wounds.

4.3. Materials and Methods

4.3.1. Animal Experiments

Initially, the study aimed to profile the global distribution of metals in murine tissue across a time course of skin wound healing. Time points were chosen based on their correspondence with the major stages of wound healing (haemostasis, inflammation, proliferation and matrix remodelling; Witte & Barbul, 1997). Two 6mm excisional wounds were created on the dorsum of female wild-type (WT) C57BL/6J mice at 8-10 weeks of age and left open to heal via secondary intention (n = 5 per group). Mice were collected at 1 day (D1), 3 days (D3), 7 days (D7) and 14 days (D14) post-injury. Metal profiling was also undertaken in aged and diabetic murine models of delayed wound healing. Aged (80-90 weeks of age) female WT mice were wounded and collected at D3 (n = 4), diabetic (Db; $Lepr^{-/-}$) young (8-10 weeks of age) female mice were wounded and collected at D3 and D7, along with Non-Db (NDb; $Lepr^{-/+}$) controls (n = 5 per group). All wounding experiments were performed as described in **Section 2.1**.

4.3.2. Wound Processing and Analysis

Wounds were collected from each animal and processed for histology (**Section 2.4.1**), ICP-MS (**Section 2.5**) or qRT-PCR (**Section 2.7**). Calcium-related genes assessed in skin and wound tissue via qRT-PCR were calmodulin 1 (*Calm1*), S100 calcium-binding protein A8 (*S100a8*), *S100a9,* translocating chain-associated membrane protein 2 (*Tram2*), phosphoinositide 3-kinase (*Pi3k*) and the calcium-sensing receptor (*Casr*).

4.3.3. Laser Ablation Inductively Coupled Plasma Mass Spectrometry

To determine how metals changed temporally and spatially throughout normal and pathological repair, laser-ablation ICP-MS (LA-ICP-MS) was performed on a RESOlution-SE instrument (Applied Spectra, California, US). Here, samples are ablated with a focussed laser beam within a laser ablation chamber, and the ablated material is analysed via mass spectrometry (as per ICP-MS; Becker et al., 2010). Methodology was optimised with OCT and paraffin embedded sections of varying thickness. From these optimisation experiments, 8 µm thick paraffin sections were deemed suitable for use in subsequent work. For the generation of pilot data for this thesis, D7 WT samples were processed. LA-ICP-MS laser conditions were set so the energy level was 2.7 mJ, with a fluence of 0.3-0.5 J/cm^{-2}, pulse rate of 20 Hz, spot size

of 200 μm and line scanning at 100 μm/s (as in Hare et al., 2017; Ouypornkochagorn & Feldmann, 2010). The distances between spots were 200 μm and delay times between each analysed spot was 50 seconds. To calibrate the instrument, NIST 612 Trace Elements in Glass (Sigma-Aldrich) were used. Fish liver (DOLT5, **Section 2.5**) was prepared as a reference.

4.3.4. *In Vitro* Analysis

4.3.4.1. Keratinocyte Experiments

WT, NDb and Db MEKs were isolated (**Section 2.2.2**), cultured and scratched upon confluency (**Section 2.6.2**). Calcium was added as calcium chloride up to 5 mM concentration and migration assessed at 24 hours post-scratching. qRT-PCR was used to measure the differentiation markers keratin 14 (*Krt14*), *Krt1*, transglutaminase-1 (*Tsg1*), involucrin (*Ivl*) and small proline-rich protein 2 (*Sprr2*). Calcium markers assessed were *Calm1*, *Casr*, IP3R (*Itpr1*), *Tram2* and *Pi3k*. NHEKs were analysed via qRT-PCR (as above) and immunocytochemistry (**Section 2.6.7.4**) for KRT14, KRT1, Loricrin, CALM1 and CaSR. Positively stained cells were counted or analysed via threshold intensity in ImageJ v.1.8.

4.3.4.2. Fibroblast Assays

WT and Db MDFs, and HDFs, were isolated, cultured and scratched for experiments as described above. HDF migratory behaviours were also determined in real-time using the Livecyte™ (**Section 2.6.10**). qRT-PCR was performed for the matrix markers fibronectin 1 (*FN1*), collagen type 1 alpha chain 1 (*COL1A1*) and collagen type 3 alpha chain 1 (*COL3A1*), and the differentiation marker cadherin 11 (*CDH11*). Immunocytochemistry was performed to measure fibronectin, collagen III, collagen I production following calcium treatment for 11 days. For collagen gel contraction assays, calcium was added to media surrounding collagen-fibroblast gels, left to contract for 48 hours (**Section 2.6.5**). For adhesion assays, HDFs were pre-treated for 24 hours with calcium and seeded onto collagen I-coated plates for 30 minutes (**Section 2.6.3**). Crystal Violet stained cells were counted in Image-Pro.

4.3.4.3. Bone Marrow-Derived Macrophages and THP-1 Cells

NDb and Db BMDMs were differentiated and polarised in the presence of calcium. After 24 hours, polarisation markers (*Nos2*, *Cd86*, *Arg1* and *Ym1*) and calcium-linked genes (*Casr*, *Calm1*, *Tram2*, *Pi3k*, *Itpr1* and S1P Receptor 2, *S1pr2*) were assessed via

qRT-PCR. Phagocytosis was determined using *E. coli* (K-12 strain) BioParticles® following 6 hours of calcium treatment (**Section 2.6.9**).

THP-1 cells (ATCC® TIB-202™, ATCC, Middlesex, UK), used as a model of human monocytes (Bosshart & Heinzelmann, 2016), were grown in RPMI 1640 (Thermo Fisher Scientific) with 10% FBS and 1% penicillin-streptomycin solution. THP-1 cells were treated with or without phorbol 12-myristate 13-acetate (PMA) at the same time as administering calcium. After 3 days, cells were collected for RNA to assess the expression of the differentiation markers, *CD11b*, *CD14*, *CD36* and *CD54* (Michée et al., 2013; Wang et al., 2014) and the calcium-linked genes, *CALM1*, *CASR*, *TRAM2* and *Pi3K*. To measure THP-1 cell adhesion following PMA and FAC stimulation, wells were Crystal Violet stained and counted.

4.3.5. Transcriptional Profiling via RNA-Sequencing

RNA was prepared from skin and wound tissue from WT and Db mice (D0, D3 and D7; n = 3 per group) for RNA-sequencing (RNA-Seq). RNA-Seq offers advantages over DNA-sequencing (e.g. microarray) as it not only allows the investigator to determine changes in the expression of large subsets of genes in a more quantifiable manner with less noise, but it will also identify post-translational modifications of mRNA and alternative splicing events (reviewed in Wang et al., 2009).

RNA-Seq was performed using the paired-end method and Illumina platform. Error rate distribution among reads was <0.04%, while over 90% of reads from each sample were clean and passed quality control. Isolated RNA was enriched for mRNA, fragmented to allow short read (200-300kB) sequencing and cDNA was reverse transcribed from fragmented mRNA. The cDNA 5' and 3' ends were repaired and dA-tailing was performed on blunt 3' ends of the cDNA strands. Adapters were ligated to the 5' ends of each cDNA strand to allow hybridisation to a flow cell and unique identification of each sample. PCR amplification of the cDNA library was then performed to enrich cDNAs containing adapter sequences. Library concentration and fragment lengths were verified, and the library was sequenced. These sequences, or reads, were then aligned to the reference genome (using HISAT2) and assembled to map the transcriptome. Gene expression was determined from number of transcripts, normalised to Fragments per Kilobase Million (FPKM). The full workflow for RNA-Seq is shown in **Figure 4.5**. The above sample – and

bioinformatic – processing was performed by Novogene Ltd. (Cambridge, UK). All subsequent analysis was performed by the author (HNW) as described below.

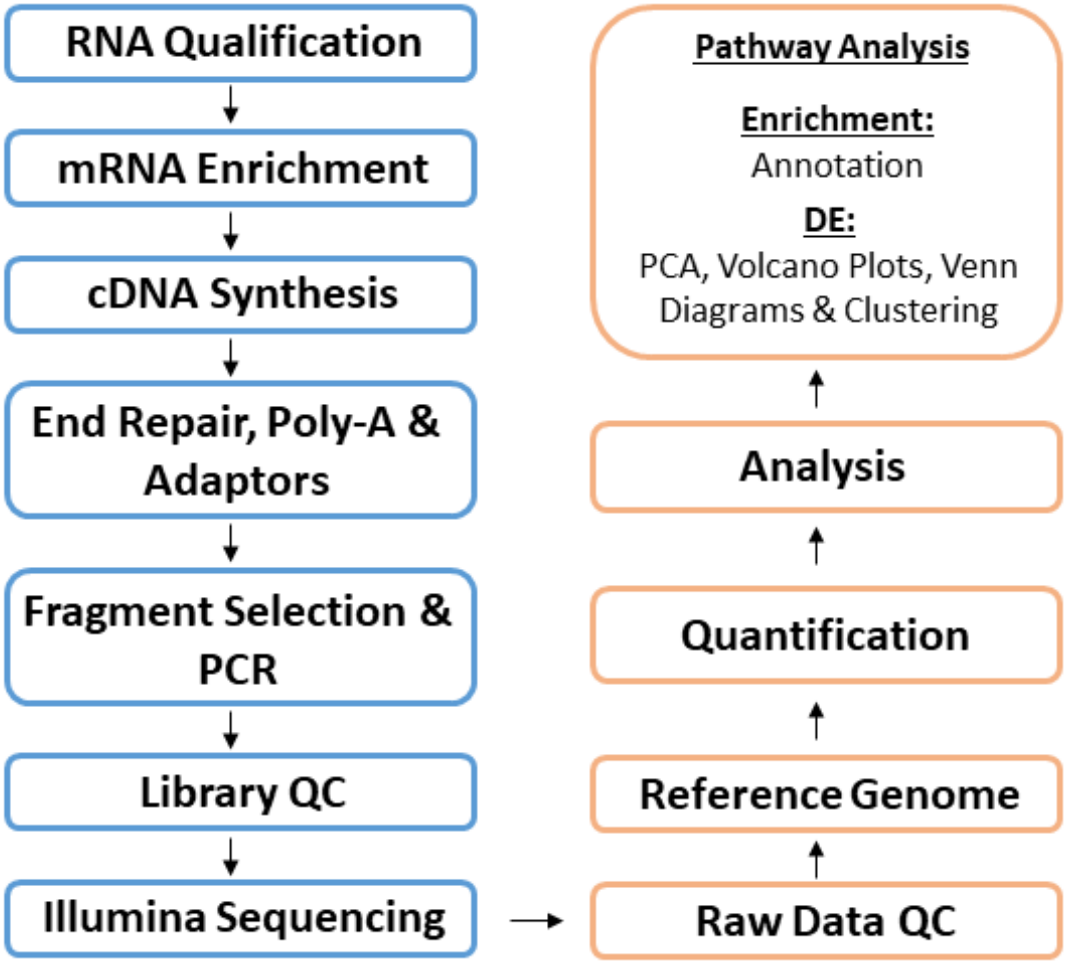

Figure 4.5. Outline of the workflow used for RNA-sequencing and analysis. Quality control (QC) was performed at each major step in the process (RNA, cDNA library and raw data processing) before raw data outputs were mapped onto the reference genome and quantified. Analysis of data was performed using R v.3.6.1, DAVID v.6.8 and ingenuity pathway analysis software. PCA = principal component analysis. DE = differential expression.

4.3.5.1. Multidimensional Scaling of RNA-Sequencing Data

Analyses were performed on differentially expressed (DE) genes. Genes were deemed DE when expression between experimental groups was above 1.5-fold different, with 5% alpha level significance following multiple correction to reduce false discovery rate (Benjamini-Hochberg procedure, shown as P_{adj}). Principal component analysis (PCA) was performed on $\log_2$-transformed FPKM count data from DE genes using R v.3.6.1 (Core Team, 2019) and the 'ggplot2' package (Wickham, 2016). A scree plot was generated to determine the contribution of each PC to the variation in the dataset. From this, PC1, PC2 and PC3 were plotted and the top genes contributing to each PC were determined. For hierarchal clustering, FKPM

counts were log-transformed and scaled prior to clustering using Euclidian distance and Ward D2's method within the R packages 'ISLR' (James et al., 2017), 'RColorBrewer' (Neuwirth & Brewer, 2014) and 'gplots' (Warnes et al., 2016). Heirarchal clusters were generated for the entire DE gene set (10,187 genes), the top 250 most variable genes and DE genes identified from annotated pathways (below). Interactive plots for analysis were prepared in the R packages 'd3heatmap' and 'heatmaply' (Galili et al., 2017).

4.3.5.2. RNA-Sequencing Functional Annotation and Pathway Analysis

Upregulated and downregulated subsets of genes were compared between Db and WT skin and wounds, and between skin and wounds within each genotype (Db or WT). ENSEMBL gene identifiers for DE genes were copied into InteractiVenn (Heberle et al., 2015) to create Venn diagrams. Volcano plots were made using the R Bioconductor package 'EnhancedVolcano' (Blighe, 2019) and allowed visualisation of upregulated and downregulated genes in different comparison groups. Fold change expression was plotted against Benjamini-Hochberg adjusted *P* values. For functional analysis, ENSEMBL gene identifiers were scrutinised in the Database for Annotation, Visualization and Integrated Discovery (DAVID) v.6.8 (Huang et al., 2009), with relevant top annotations (Gene ontology, KEGG pathway or UniProt knowledgebase, UniProtKB) plotted against *P* value (Benjamini-Hochberg false discovery rate). DAVID was also used to find annotations spanning the entire DE data set, thus enabling hierarchal clustering analysis to be performed on chosen significant pathways (metal binding, calcium, aging and iron). Finally, Ingenuity® Pathway Analysis (IPA; Qiagen) was used to generate gene networks with direct interactions and DE data overlays (Db versus WT at D0, D3 and D7). Genes of interest were picked out from the DE data for scatterplots and bar graphs, and analysed via two-way ANOVA with Tukey *post-hoc* analysis in GraphPad Prism v.7.0 (GraphPad Software, California, US).

4.3.6. Data Analysis

All non-RNA-Seq data are presented as mean +/- standard error of the mean. Statistical analysis was performed on these data sets in GraphPad Prism. Livecyte™ analysis was performed in R v.3.6.1 as described in **Section 2.6.10**.

4.4. Results

4.4.1. ICP-MS reveals temporal changes in the metallome across normal wound repair.

Histological analysis confirmed the expected healing profile in WT mouse tissue used in this study (**Appendix Figure 4A.1**). Wound width and area decreased over time, while full closure (re-epithelialisation) was achieved at D7. Neutrophil infiltration was lower at D3 and D7 ($P < 0.001$), and Mφ levels peaked at D3 ($P < 0.05$) before starting to decline. The pro-inflammatory Mφ marker, Nos-2, was highest at D3 ($P < 0.05$), and reduced by D7 ($P < 0.001$), and the pro-healing Mφ marker, Arginase-1, was greatest at D7 ($P < 0.05$).

ICP-MS demonstrated changes in metals throughout normal murine wound repair. A heatmap demonstrates metal abundance as fold change versus D0 normal skin (**Figure 4.6A**). At D1, no significant alterations were observed in the seven elements tested compared to D0. However, by D3 calcium was significantly upregulated ($P < 0.001$), increasing from 381 to 1063 μg/g of tissue (**Figure 4.6B**). At D7 calcium remained significantly higher than D0 ($P < 0.001$; 1222 μg/g). However, calcium was greatly reduced by D14 (61 μg/g; $P < 0.001$). Other metals were also significantly upregulated at D7, compared to D0: Magnesium (215 to 399 μg/g tissue; $P < 0.01$; **Figure 4.6C**); iron (41 to 120 μg/g tissue; $P < 0.001$; **Figure 4.6D**); copper (1.49 to 2.69 μg/g tissue; $P < 0.001$; **Figure 4.6F**) and; manganese (0.19 to 0.47 μg/g tissue; $P < 0.01$; **Figure 4.6G**). At D14, iron (151 μg/g tissue; $P < 0.001$), manganese (0.64 μg/g tissue; $P < 0.001$) and aluminium (14.37 μg/g tissue; $P < 0.001$) were significantly upregulated compared to D0. Collectively, these data highlight clear temporal changes in the wound metallome.

As calcium was the most abundant metal, with the greatest temporal variation during healing, the expression of a number of candidate calcium genes was next assessed in WT wounds. *Casr* ($P < 0.05$ to $P < 0.001$; **Figure 4.6I**), *S100a8* ($P < 0.05$ to $P < 0.001$; **Figure 4.6J**) and *S100a9* ($P < 0.05$; **Figure 4.6K**) were upregulated at D1, D3 and D7, compared to D0, while *Calm1* (**Figure 4.6L**) and *Pi3k* (**Figure 4.6M**) were unchanged throughout healing. On the contrary, *Tram2* expression was downregulated at each post-wound time point ($P < 0.01$; **Figure 4.6N**).

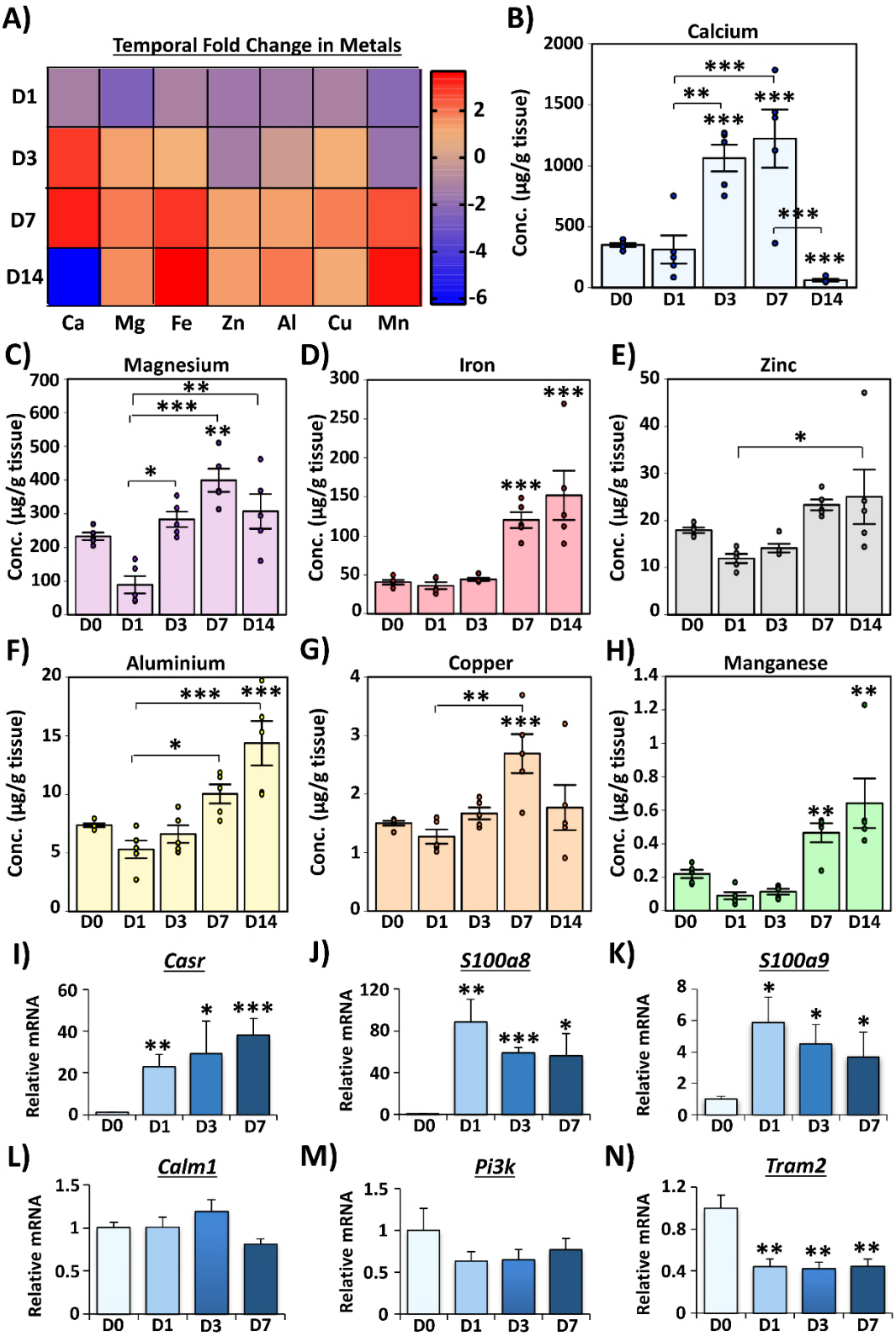

Figure 4.6. ICP-MS reveals temporal alterations in the metallome across normal wound repair. Heat map summary of metal fold changes across healing (versus D0 normal skin; **A**). D = day post-injury. Graphs of abundance (µg/g tissue) for calcium (Ca; **B**), magnesium (Mg; **C**), iron (Fe; **D**), zinc (Zn; **E**), aluminium (Al; **F**), copper (Cu; **G**) and manganese (Mn; **H**). qRT-PCR of calcium-linked genes (**I-N**). Mean +/- SEM. n = 5 mice per group. * = $P < 0.05$, ** = $P < 0.01$, *** = $P < 0.001$. One-way ANOVA with Tukey's *post-hoc* analysis (* alone versus D0).

4.4.2. Pathological wounds display an altered skin and wound metallome.

As with the normal time course tissue, pathological healing was confirmed in aged (**Appendix Figure 4A.2**) and Db (**Appendix Figure 4A.3**) wounds. Aged wounds healed more slowly than young wounds, with reduced wound closure ($P < 0.01$), heightened neutrophil influx ($P < 0.05$) and greater Nos-2 expression ($P < 0.001$) at D3. In Db wounds, wound width was higher ($P < 0.05$) and wound closure was reduced ($P < 0.01$) at D7 compared to NDb. Neutrophil infiltration was increased in Db wounds at D3 ($P < 0.05$) and D7, while Mφs were greatest at D7 in Db wounds ($P < 0.05$). Nos-2 infiltration was higher in Db wounds at D3 ($P < 0.01$) and D7 ($P < 0.05$), whereas Arginase-1 expression was reduced at D7 in the Db model compared to NDb ($P < 0.05$). Taken together, these data confirm significant healing impairment in the aged and Db murine wound tissue used in this study.

Comparisons were first made between the metallome of young versus aged and NDb versus Db skin (**Figure 4.7A**). Here, calcium ($P < 0.001$), aluminium ($P < 0.01$) and copper ($P < 0.001$) were significantly reduced in aged skin, compared to young. Calcium ($P < 0.05$), magnesium ($P < 0.001$), iron ($P < 0.001$), zinc ($P < 0.01$) and copper ($P < 0.05$) were also significantly reduced in Db skin, compared to NDb. In day 3 wounds, calcium was reduced in aged mice ($P < 0.05$), while calcium ($P < 0.05$), magnesium ($P < 0.05$), iron ($P < 0.01$), zinc ($P < 0.01$) and copper ($P < 0.05$) were reduced in Db mouse wounds (**Figure 4.7B** and **Figure 4.8**).

The metallome was also compared at D7 (with D0 and D3) in NDb versus Db mice (**Figure 4.8**). Here, calcium (1308.49 versus 725.15 μg/g; $P < 0.05$), magnesium (350.16 versus 124.23 μg/g; $P < 0.001$), iron (137.11 versus 41.02 μg/g; $P < 0.01$) and zinc (23.94 versus 14.62 μg/g; $P < 0.001$) levels were significantly higher in the NDb group. These findings therefore demonstrate that the normal metallome is greatly perturbed in pathological aged and Db healing, with differential changes in metals observed between the two delayed healing models.

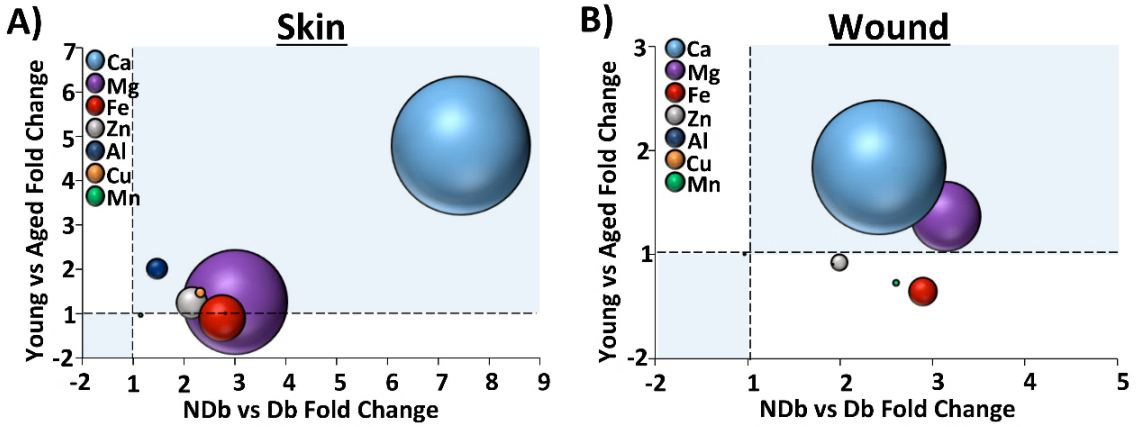

Figure 4.7. The metallome of skin and wounds is crucially altered in pathological healing. Fold change in metals in skin (**A**) and wounds at day 3 post-injury (**B**). Young versus aged fold change plotted against non-diabetic (NDb) versus diabetic (Db) fold change. Sphere size illustrates element abundance in young tissue, where calcium (Ca) was the most abundant metal in skin and wounds. Magnesium (Mg), iron (Fe), zinc (Zn), aluminium (Al), copper (Cu) and manganese (Mn) also shown. Dotted lines = fold change of 1. n = 3-5 mice per group.

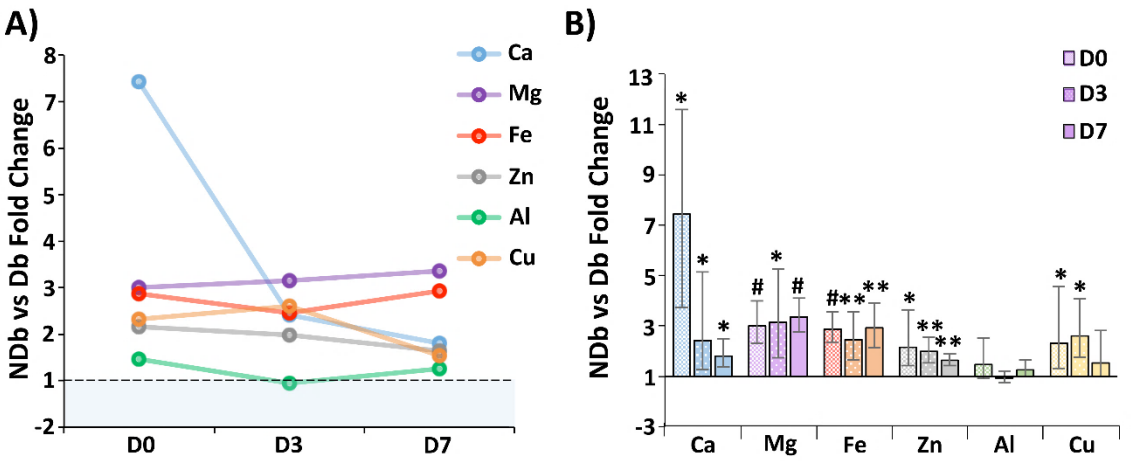

Figure 4.8. Temporal alterations in metals during diabetic healing. Fold change in metals in skin (D0), and wounds at day 3 (D3) and day 7 (D7) post-injury (**A**). Calcium (Ca), magnesium (Mg), iron (Fe), zinc (Zn), aluminium (Al) and copper (Cu). Non-diabetic (NDb) versus diabetic (Db). Dotted line highlights fold change of 1. Values above 1 were upregulated in NDb skin and wounds. Bar graph showing data in **A** plus compound SEM error bars (**B**). n = 3-5 mice per group. * = $P < 0.05$, ** = $P < 0.01$, # = $P < 0.001$. Independent two-tailed Student's *t* tests performed on **B**.

4.4.3. LA-ICP-MS highlights the spatial distribution of metals in skin and wounds.

A pilot study was performed to determine the spatial location of altered metals in D7 normal healing wounds using LA-ICP-MS (**Figure 4.9**). Elemental abundance matched the scales observed in normal ICP-MS, where calcium (**Figure 4.9B**) and

magnesium (**Figure 4.9C**) levels were higher than iron (**Figure 4.9D**), zinc (**Figure 4.9E**), and aluminium (**Figure 4.9F**). Calcium showed regional distribution, where it was over twice as abundant in the granulation tissue and dermis compared to the epidermis. Similarly, the highest amount of iron was exhibited in the granulation tissue of D7 wounds, but was lower in the surrounding dermis and epidermis. By contrast, magnesium and zinc displayed scattered dispersal throughout the entire tissue that was not wound-site specific, which could reflect cell-specific localisation. Aluminium levels appeared more uniform than the other metals tested, but still demonstrated marginal differences in distribution throughout the wound tissue. Together, these preliminary data reveal regional variations in wound metals that may confer their specific roles in modulating wound cell behaviours.

4.4.4. Calcium genes are altered in pathological skin and wounds.

Calcium was highlighted as a key metal decreased in delayed healing wounds. Thus, expression of a number of candidate calcium-linked genes was assessed in normal (young and NDb) and pathological (aged and Db) skin and D3 wounds via qRT-PCR. *Calm1* (**Figure 4.10A**) and *Pi3k* (**Figure 4.10E**) were downregulated in aged wounds compared to aged skin ($P < 0.01$ and $P < 0.001$, respectively) and young wounds ($P < 0.05$). *S100a8* was upregulated following injury in young ($P < 0.001$) and aged ($P < 0.01$) wounds (**Figure 4.10B**), while *S100a9* was only upregulated in young D3 wounds ($P < 0.05$; **Figure 4.10C**). *Tram2* expression was not altered by injury or aged pathology (**Figure 4.10D**), whereas *Casr* was upregulated in young ($P < 0.05$) and aged ($P < 0.01$) wounds, but lower in aged wounds (**Figure 4.10F**).

In the NDb versus Db mice, *Calm1* (**Figure 4.10G**) and *Tram2* (**Figure 4.10J**) were unchanged with injury and showed a non-significant decrease in Db wounds (versus NDb). However, differential effects in other calcium genes were observed. *S100a8* (**Figure 4.10H**) and *S100a9* (**Figure 4.10I**) were significantly higher following injury in NDb ($P < 0.001$ and $P < 0.01$, respectively) and Db ($P < 0.001$ and $P < 0.05$, respectively) mice. *Pi3k* ($P < 0.01$; **Figure 4.10K**) was lower in Db wounds than skin, while *Casr* ($P < 0.05$; **Figure 4.10L**) expression were downregulated in Db wounds compared to NDb. These findings indicate that calcium dysregulation in pathology occurs at both the elemental and molecular level, and correlates with impaired wound healing.

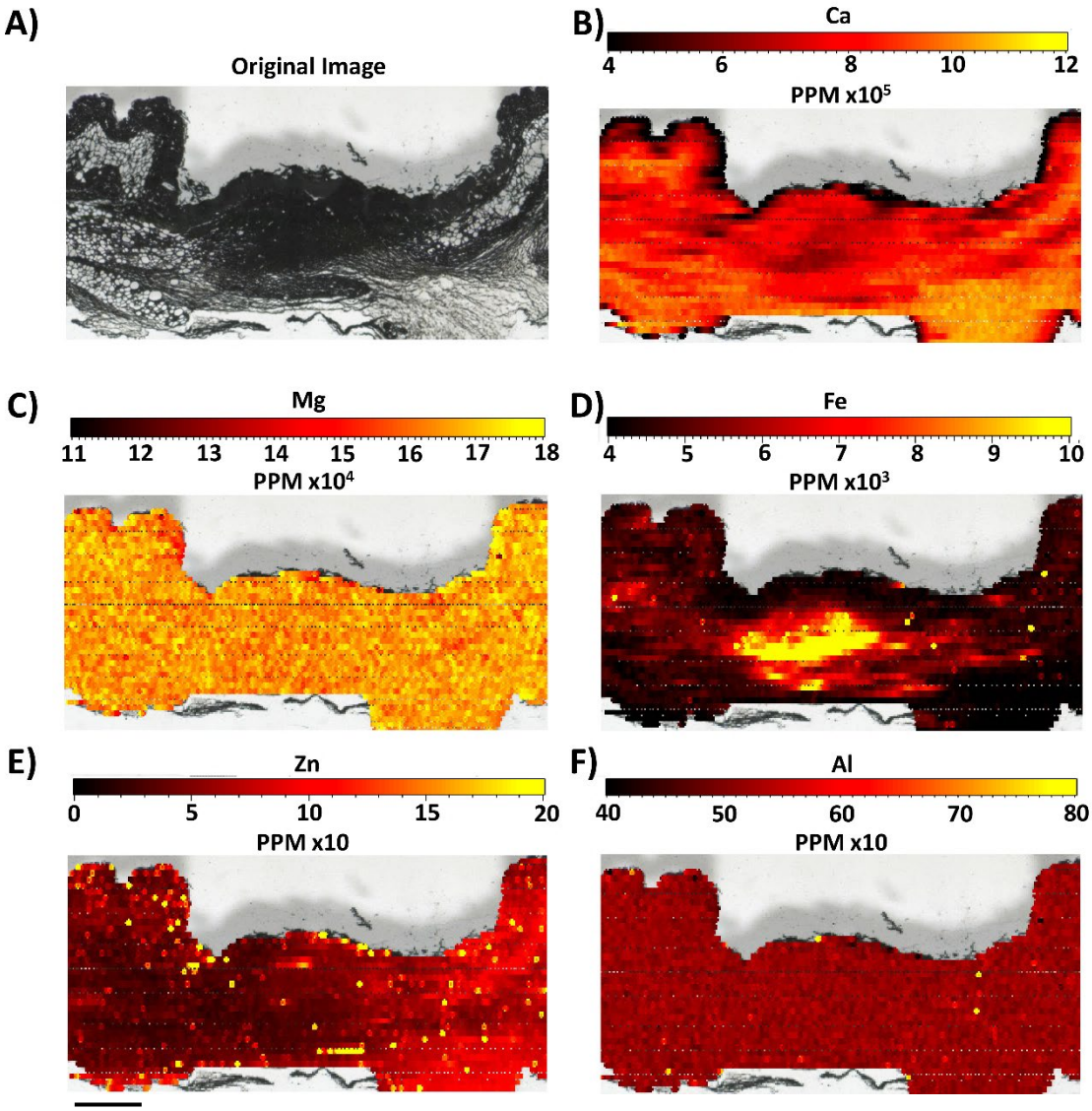

Figure 4.9. Spatial distribution of metals in normal wounds at day 7 post-injury. LA-ICP-MS was used to measure metal distribution spatially in tissue sections. Representative D7 wild-type wound. Original wax section (**A**) and measurements of calcium (Ca, **B**), magnesium (Mg, **C**), iron (Fe, **D**), zinc (Zn, **E**) and aluminium (Al, **F**). PPM = parts per million. Bar = 500 µm.

4.4.5. Calcium intrinsically modulates keratinocyte differentiation and migration, which is perturbed by diabetic pathology.

The functional effects of exogenous calcium were determined using wound-relevant *in vitro* assays. Experiments were first performed on MEKs to assess migration and the expression of differentiation- and calcium-linked genes. MEK migration was highest following 0.1 mM calcium ($P < 0.05$), with 5 mM significantly impairing migration ($P < 0.001$; **Figure 4.11A-B**). By contrast, differentiation markers were significantly altered only following 5 mM calcium treatment, where *Krt14* was reduced ($P < 0.001$; **Figure 4.11C**), and *Krt1* significantly increased ($P < 0.01$; **Figure**

4.11D). *Tsg1* (**Figure 4.11E**) and *Ivl* (**Figure 4.11F**) were modestly elevated with high (1-5mM) calcium, while *Sprr2* was upregulated at all calcium doses ($P < 0.001$; **Figure 4.11G**). High (5mM) calcium upregulated expression of the calcium-linked genes, *Calm1* ($P < 0.01$; **Figure 4.11H**), *Casr* ($P < 0.001$; **Figure 4.11I**) and *Tram2* ($P < 0.05$; **Figure 4.11K**). *Itpr1* was highest following 1 mM calcium ($P < 0.05$; **Figure 4.11J**) and *Pi3k* was elevated at 0.1 mM calcium treatment ($P < 0.05$; **Figure 4.11L**).

As ICP-MS demonstrated calcium perturbation in pathological healing, the effect of calcium on NDb and Db MEKs was next determined. In NDb MEKs, 0.1 mM calcium accelerated scratch closure ($P < 0.05$), yet closure was significantly impaired in Db versus NDb MEKs at 0.1 mM ($P < 0.05$), 1 mM ($P < 0.01$) and 5 mM ($P < 0.001$) calcium (**Figure 4.12A-B**). NDb *Krt1* ($P < 0.01$; **Figure 4.12D**) and *Sprr2* ($P < 0.01$; **Figure 4.12G**) expression were highest at 5 mM calcium, while 1 mM and 5 mM calcium significantly increased *Ivl* expression in NDb MEKs ($P < 0.01$; **Figure 4.12F**). Db MEKs showed significantly reduced *Krt1*, *Ivl* and *Sprr2* expression following 5 mM calcium ($P < 0.05$). Of the calcium-linked genes, *Calm1* expression was modestly reduced in Db MEKs (**Figure 4.12H**) and *Casr* expression was significantly dampened in Db MEKs following 5 mM calcium ($P < 0.05$; **Figure 4.12I**). Collectively, these data establish that calcium influences both migration and differentiation in MEKs, which is impaired in Db pathology.

4.4.6. Calcium induces dose-dependent differential effects on primary human keratinocyte differentiation.

To provide translational relevance, calcium was next added to NHEKs with differentiation marker expression assessed (**Figure 4.13**). *KRT14* and *KRT1* were downregulated in a dose-dependent manner following calcium administration ($P < 0.05$ to $P < 0.01$), while *TSG1* expression was elevated ($P < 0.05$ to $P < 0.001$). *Flg* ($P < 0.001$) was reduced at all quantities assessed (**Figure 4.13A**). Calcium treatment increased *CALM1* ($P < 0.05$ to $P < 0.001$) and *CASR* ($P < 0.01$) expression and reduced *ITPR1* ($P < 0.01$) and *TRAM2* ($P < 0.05$; **Figure 4.13B**). Immunocytochemistry was performed using KRT14, CALM1, KRT1, CaSR and loricrin antibodies to further evaluate NHEK responses to calcium (**Figure 4.13C**). NHEKs were co-stained with KRT14 and CaSR, KRT1 and CALM1, and loricrin and Phalloidin (cytoskeleton stain). Contrary to qRT-PCR, 1 mM and 5 mM calcium increased KRT14 (compared to no calcium; $P < 0.01$ to $P < 0.001$; **Figure 4.13D**). CaSR was elevated at 0.4 mM ($P <$

0.01), 1 mM ($P < 0.05$) and 2 mM ($P < 0.05$) calcium. Protein and transcript levels of KRT1 did not correlate either, as the number of KRT1^{+ve} NHEKs increased at 2mM ($P < 0.01$) and 5 mM ($P < 0.001$) calcium, while CALM1^{+ve} cells were highest following 5 mM calcium ($P < 0.001$). Finally, the cornified envelope marker, loricrin (Mehrel et al., 1990), was increased at 1 mM ($P < 0.01$), 2 mM ($P < 0.01$) and 5 mM ($P < 0.05$) calcium. Together, these results show that NHEK migration and differentiation are dose-dependently affected by calcium treatment.

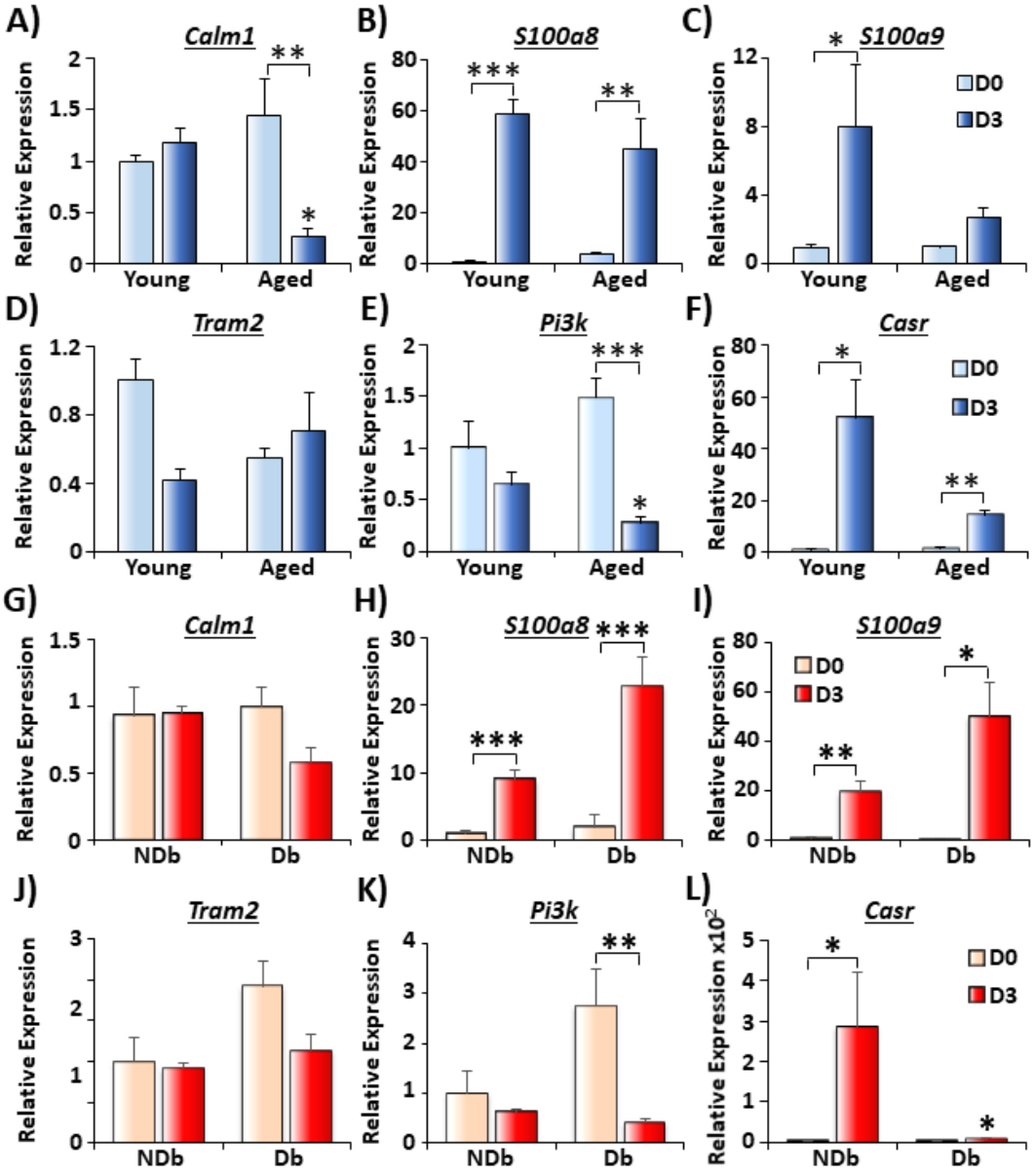

Figure 4.10. Calcium genes are altered in the skin and wounds of pathological healing mice. *Calm1* (**A**), *S100a8* (**B**), *S100a9* (**C**), *Tram2* (**D**), *Pi3k* (**E**) and *Casr* (**F**) expression in young and aged skin (D0) and wounds at day 3 post-injury (D3). *Calm1* (**G**), *S100a8* (**H**), *S100a9* (**I**), *Tram2* (**J**), *Pi3k* (**K**) and *Casr* (**L**) at D0 and D3 in non-diabetic (NDb) and Db mice. Mean + SEM. n = 4-5 mice per group. * = $P < 0.05$, ** = $P < 0.01$, *** = $P < 0.001$. Two-way ANOVA with Tukey's *post-hoc* analysis. * alone versus young/NDb.

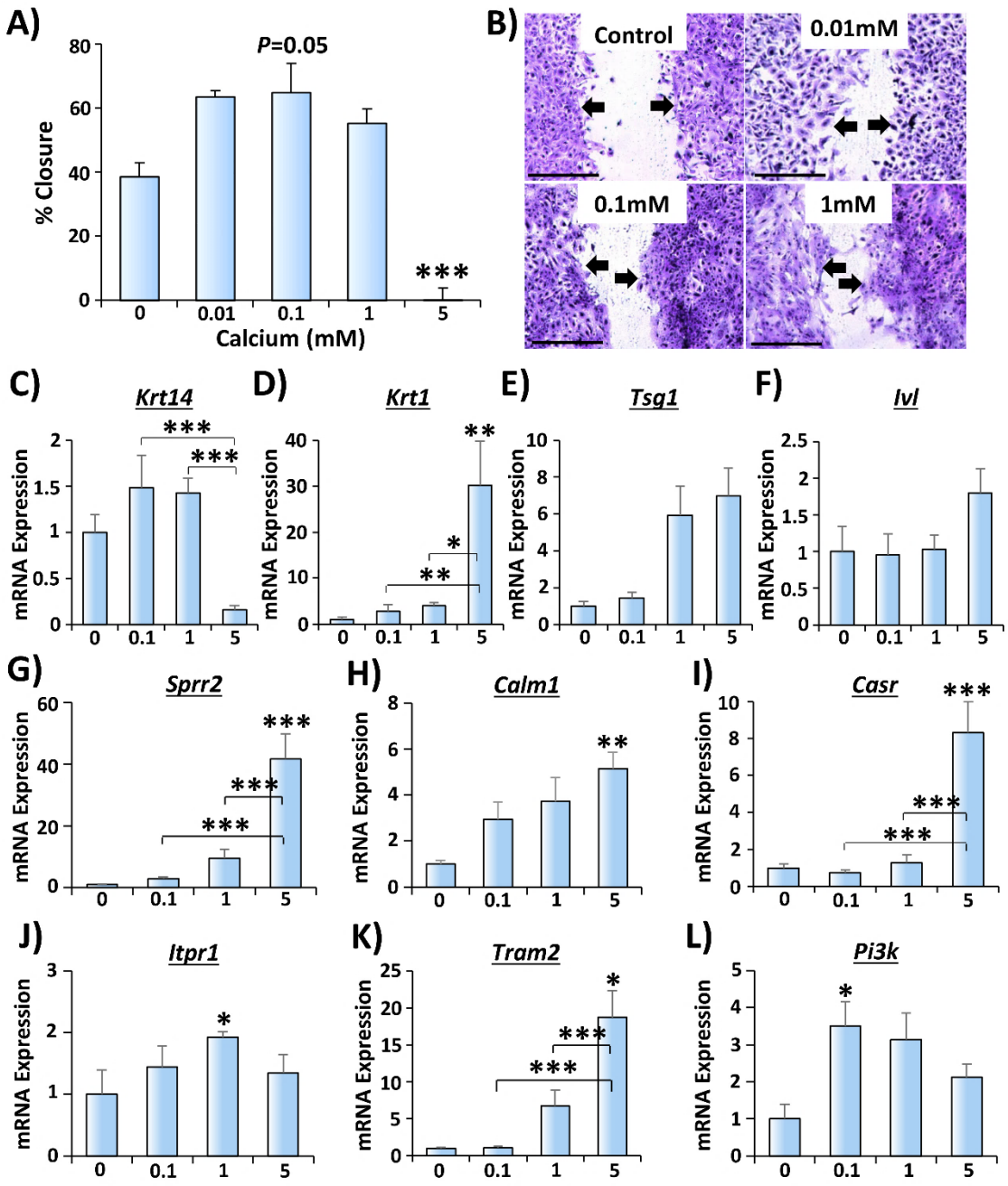

Figure 4.11. Calcium dose-dependently alters murine epidermal keratinocyte migration and differentiation. Murine epidermal keratinocytes (MEKs) were isolated from young mouse skin and treated with calcium. Scratch assays (**A-B**) shows calcium dose-dependently affects MEK migration. Bar = 500 µm. Arrows = wound edges. qRT-PCR demonstrates changes in differentiation markers (**C-G**) and calcium-related genes (**H-L**) following calcium administration. Mean + SEM. n = 4-5 mice. * = $P < 0.05$, ** = $P < 0.01$, *** = $P < 0.001$. One-way ANOVA with Tukey's *post-hoc* analysis. * alone versus control (0 calcium).

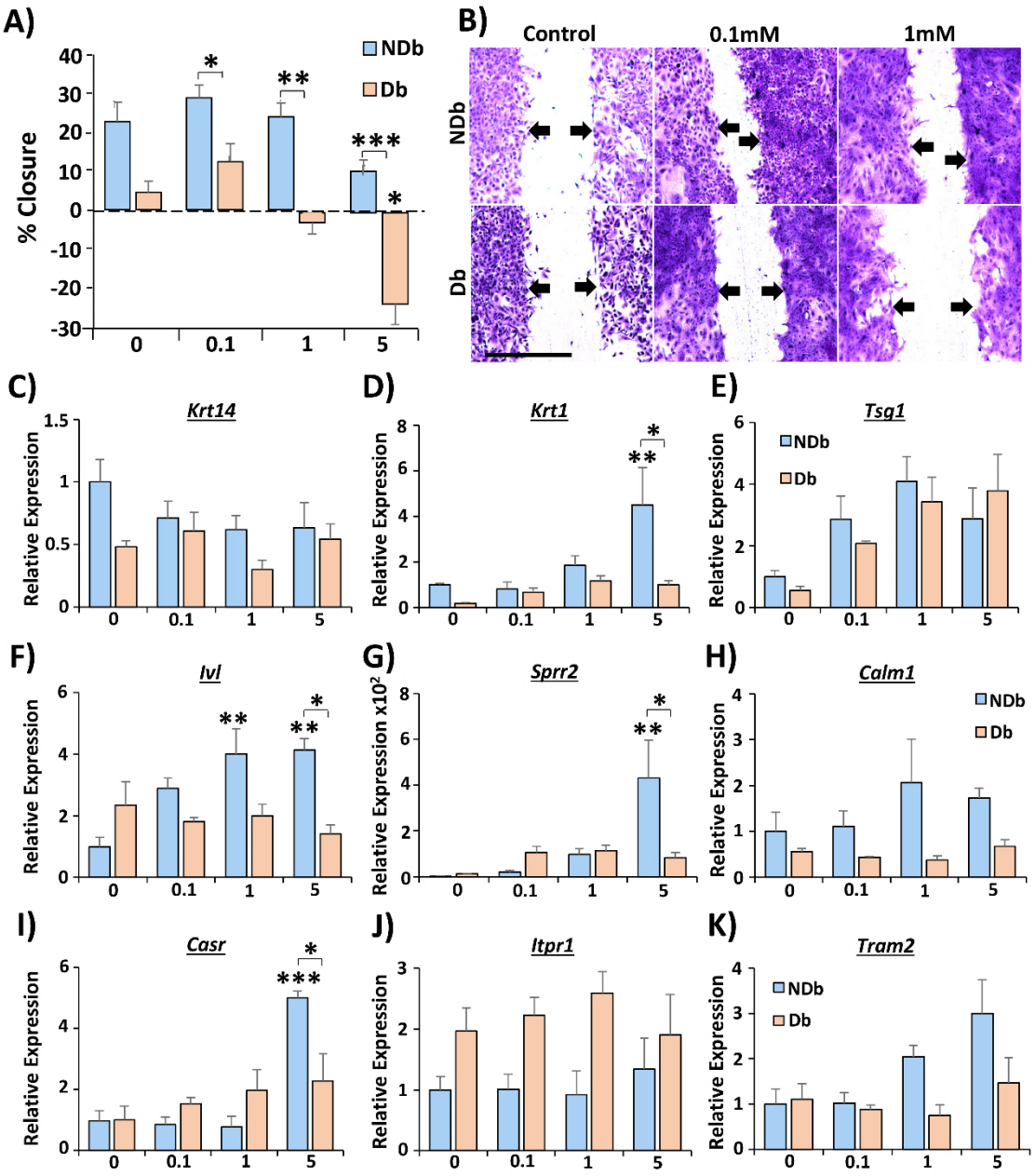

Figure 4.12. Diabetic epidermal keratinocytes show impaired responses to calcium. Murine epidermal keratinocytes (MEKs) were isolated from non-diabetic (NDb) and diabetic (Db) mouse skin and treated with calcium. Scratch assays (**A-B**) demonstrate impaired migration in Db MEKs. Bar = 500 µm. Arrows = wound edges. qRT-PCR of differentiation markers (**C-G**) and calcium-related genes (**H-K**). Mean + SEM. n = 4-5 mice. * = $P < 0.05$, ** = $P < 0.01$, *** = $P < 0.001$. Two-way ANOVA with Tukey's *post-hoc* analysis. * alone versus control (no calcium).

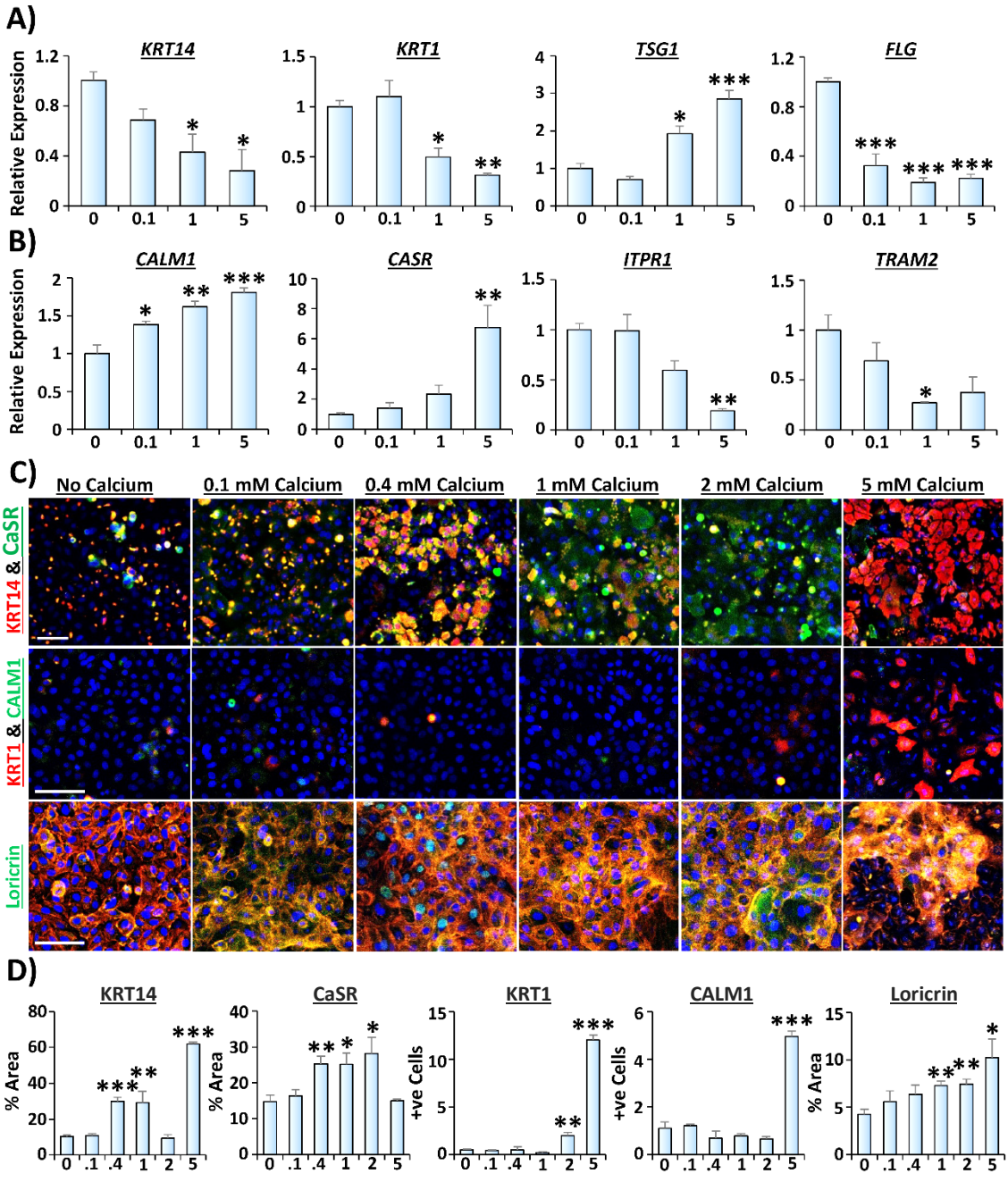

Figure 4.13. Calcium modulates differentiation, calmodulin expression, and the calcium-sensing receptor of human epidermal keratinocytes. Human epidermal keratinocytes (NHEKs) were isolated from human skin and treated with calcium. qRT-PCR demonstrates changes in differentiation markers (**A**) and calcium-related genes (**B**). Immunocytochemistry for keratin 14 (KRT14, red), calcium-sensing receptor (CaSR, green), KRT1 (red), calmodulin 1 (CALM1, green) and loricrin (green; **C**), quantified in **D**. Loricrin staining + Phalloidin (red). DAPI = blue nuclei. Bar = 100 µm. Mean + SEM. Representative of three donors. * = $P < 0.05$, ** = $P < 0.01$, *** = $P < 0.001$. One-way ANOVA with Tukey's *post-hoc* analysis. Significance versus control (no calcium).

4.4.7. Calcium alters migration of murine fibroblasts, independent of diabetic pathology.

Scratch migration assays were performed on WT and Db MDFs (**Figure 4.14**). In WT MDFs, calcium dose-dependently increased migration, leading to accelerated scratch wound closure at 24 hours following 0.4 mM, 1mM and 2 mM treatment ($P < 0.001$; **Figure 4.14A, C**). Although scratch migration was substantially perturbed in Db MDFs, 2 mM calcium significantly improved scratch closure versus no calcium ($P < 0.05$). Intriguingly, 5 mM calcium led to a major delay in scratch closure in Db MDFs ($P < 0.001$; **Figure 4.14B, D**), suggesting that these cells are particularly sensitive to high calcium.

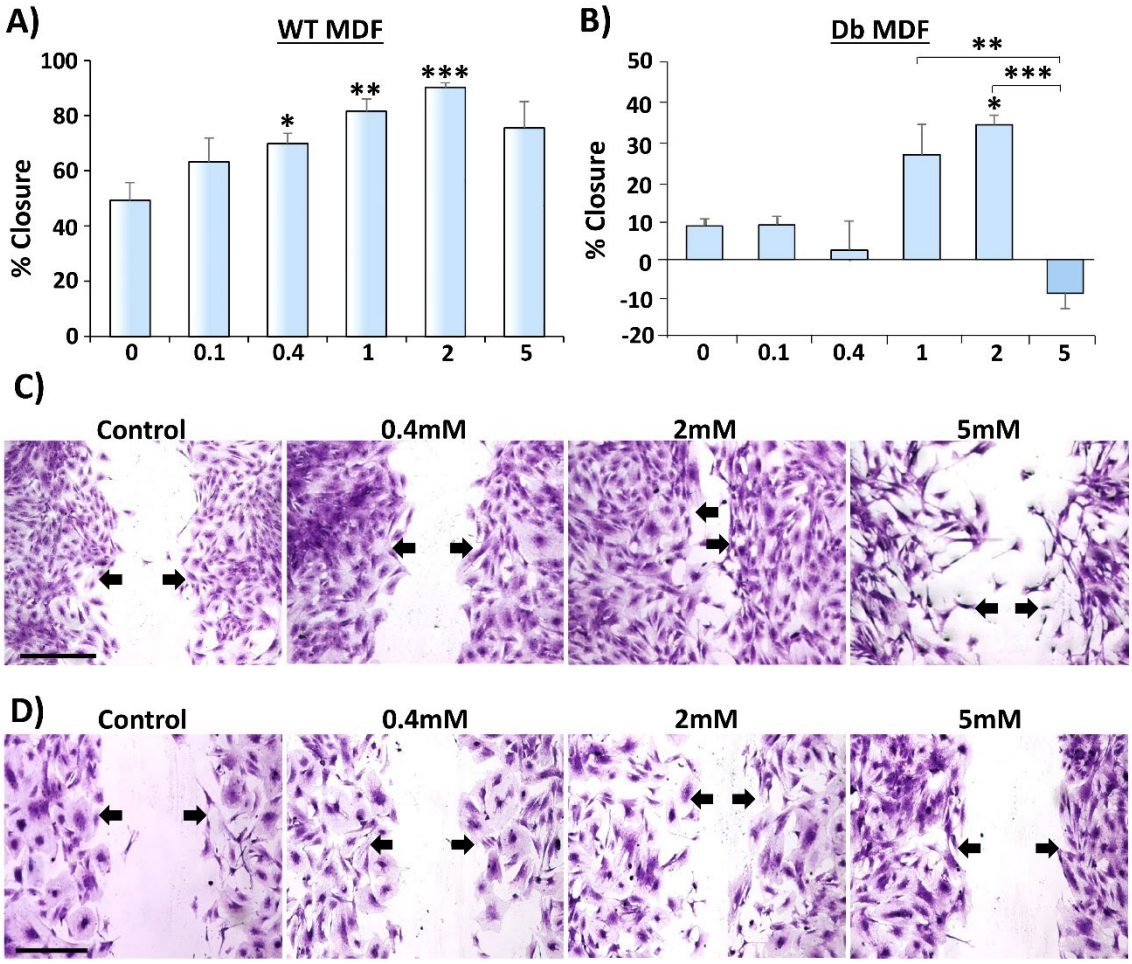

Figure 4.14. Murine dermal fibroblast scratch migration is dose-dependently affected by calcium. Scratch assays were performed on young wild-type (**A, C**) and young diabetic (**B, D**) mouse dermal fibroblasts (MDFs). Representative images (**C-D**). Bar = 500 µm. Arrows = wound edges. Combined 3 donors. Mean + SEM. * = $P < 0.05$, ** = $P < 0.01$, *** = $P < 0.001$. One-way ANOVA with Tukey's *post-hoc* analysis performed on all data sets. * alone versus control (no calcium).

4.4.8. Calcium modulates human dermal fibroblast migration, extracellular matrix production and cellular differentiation.

In human dermal fibroblasts, 1 mM calcium significantly accelerated end-point scratch wound closure as early as 12 hours post-scratching ($P < 0.001$ versus no calcium; **Figure 4.15A-B**). By 48 hours, 0.1 mM, 1 mM and 5 mM calcium significantly increased closure ($P < 0.001$ versus no calcium). Note, HDF migration was minimal in low (0 mM to 0.01 mM) and high (10 mM) calcium, indicating careful modulation of calcium is critical for normal physiological responses.

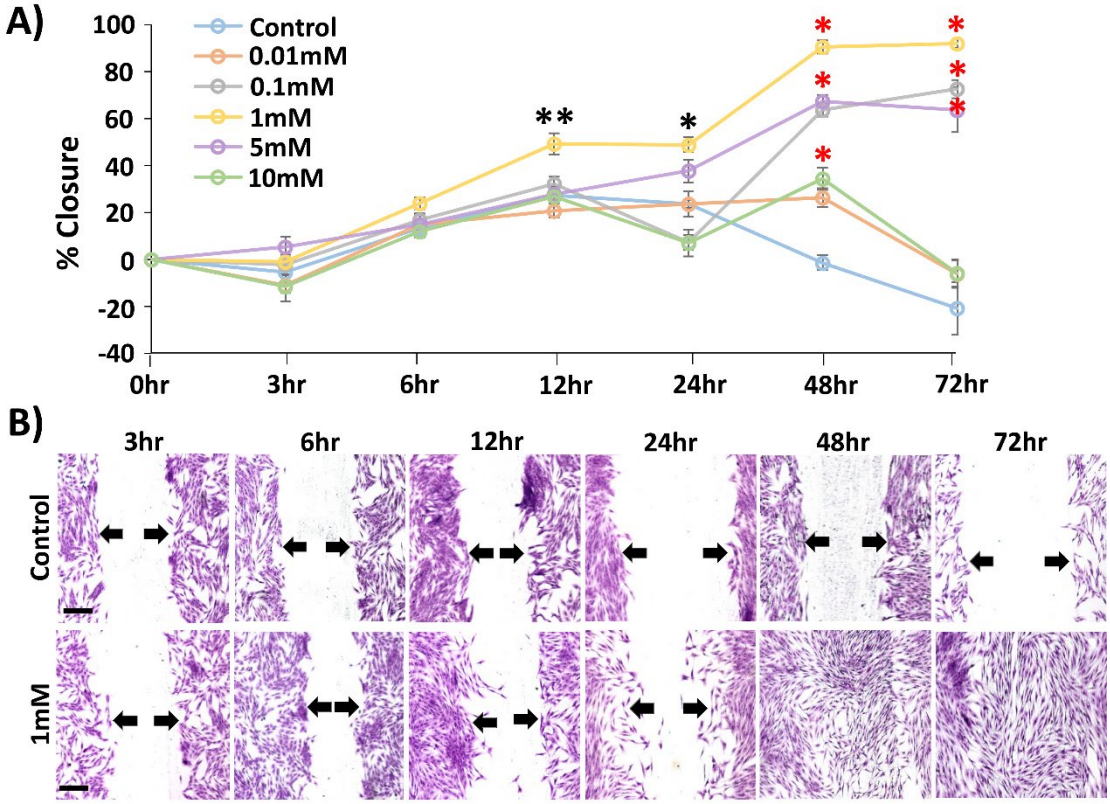

Figure 4.15. Calcium modulates scratch migration in human dermal fibroblasts. Human dermal fibroblasts (HDFs) were isolated from human skin and scratched in confluent monolayers. End-point scratch assay migration data (**A**) and representative crystal violet stained images (**B**). Representative donor. Bar = 300 µm. Mean + SEM. * = $P < 0.05$, ** = $P < 0.01$, red* = $P < 0.001$. One-way ANOVA with Tukey's *post-hoc* analysis performed on all data sets. Significance versus control (no calcium).

End-point migration assays provide limited information about temporal changes in cellular behaviour, therefore the Livecyte™ (ptychographic imaging) was used to monitor HDF scratch migration in real-time. Scratch analysis was first performed to measure track length and scratch area. Track length measures migration distance from the scratch border at time zero, thus increased track length is equivalent to increased scratch migration. Area measures the area of the scratch wound, where

reduced area is equivalent to increased scratch closure. Representative images with scratch overlay demonstrate closure rates at the final imaging frame (24 hours; **Figure 4.16A**). Graphs show track length and area at every 4th frame with error bars (every 1 hour 20 minutes; **Figure 4.16B, D**), and at each frame with linear regression lines (**Figure 4.16C, E**). Over time, track length, and thus scratch migration, increased in all groups, but was highest following 2 mM calcium and lowest following 5 mM calcium. Similarly, the area of scratch closure increased the most following 2 mM calcium, and by 24 hours, this was significantly different to all other treatment groups ($P < 0.001$).

A real advantage of ptychography is the ability to track individual cells in real-time in a non-invasive manner (Suman et al., 2016). Single cell segmentation analysis was therefore performed, where HDFs at the scratch wound edge were individually identified and tracked over time (representative images in **Figure 4.16F**). Data was filtered to include cells tracked for more than four frames, and an average for each parameter (across all tracked cells) was taken for each treatment group. Track length measured the distance travelled by each cell, while displacement determined the distance displaced by each cell (end position divided by starting position; Petrie et al., 2009). Cell speed measured track length over time (μm/min), and instantaneous velocity determined the velocity (μm/s) of a cell between successive frames (Kasprowicz et al., 2017). Single cell segmentation identified greater track length (migration length) at 1 mM ($P < 0.001$) and 2 mM ($P < 0.001$) calcium treatment, which was significantly impaired at 5 mM calcium ($P < 0.001$; **Figure 4.16G**). The same profile was observed for cell displacement ($P < 0.01$ to $P < 0.001$; **Figure 4.16H**), cell speed ($P < 0.05$ to $P < 0.001$; **Figure 4.16I**) and instantaneous velocity ($P < 0.01$; **Figure 4.16J**), showing that cells treated with 1 mM and 2 mM calcium moved the fastest and covered the highest distance.

Meandering index determined the directional persistence of the cells. Meandering index is described as the distance travelled by the cell divided by the cell's displacement, where a higher meandering index demonstrates more directionally persistent migration (Petrie et al., 2009). Meandering index was highest at 1-2 mM, and was significantly reduced at 5 mM calcium ($P < 0.05$; **Figure 4.16K**), showing that migration in cells treated with 1 mM and 2 mM calcium was less random and more directed than in other treatment groups.

The growth and proliferation of cells during scratch wound closure can be determined from cell volume and dry mass measurements (Kasprowicz et al., 2017). Here, cell volume ($P < 0.001$; **Figure 4.16L**) and dry mass ($P < 0.001$; **Figure 4.16M**) were drastically reduced following 5 mM calcium, indicating reduced growth. Finally, cell sphericity was significantly enhanced at 5 mM calcium treatment ($P < 0.001$; **Figure 4.16N**). As migratory cells develop a flattened and elongated appearance (Herant & Dembo, 2010), these data further establish that 5 mM calcium reduces migratory behaviours in HDFs.

Calcium clearly dose-dependently influenced HDF migration. However, another important function of the fibroblast is to deposit ECM and reform the dermis following injury (Frienkel & Woodley, 2001). Thus, qRT-PCR was used to determine expression levels of key matrix-linked (*COL1A1, COL3A1, FN1* and *CDH11*) and calcium-linked (*CALM1* and *CASR*) genes in HDFs treated with calcium (**Figure 4.17**). To mimic pathological calcium conditions in these cells, 0.4 mM Ca (20 % of 2 mM) was used, with 2 mM mimicking normal physiological levels of calcium. Evaluation of higher concentrations of calcium was not possible for ECM assessment, as sustaining (72 hours onwards) calcium >2 mM led to high proportions of cell death in HDF monolayers (*data not shown*). Interestingly, low calcium (0.4 mM) caused the highest expression of *COL1A1* (**Figure 4.17A**), *COL3A1* (**Figure 4.17B**) and *FN1* (**Figure 4.17C**), which were significantly reduced following 1-2 mM calcium treatment. *CDH11* was also highest following 0.4 mM calcium, and reduced at 1 mM ($P < 0.01$) and 2 mM ($P < 0.001$) treatment (**Figure 4.17D**).

By contrast, immunocytochemistry demonstrated that lowered (0.4 mM) calcium did not alter fibronectin accumulation (**Figure 4.17E**), but led to substantially decreased deposition of collagen III ($P < 0.001$; **Figure 4.17F**) and collagen I ($P < 0.001$; **Figure 4.17G**; representative images, **Figure 4.17H**). Low calcium (0 and 0.4 mM) also significantly impaired HDF collagen gel contraction ($P < 0.05$), while HDFs in 1- and 2-mM calcium contracted to a similar extent as TGF-β1 stimulated HDFs (**Figure 4.17J-K**). Further, low calcium (0 and 0.4 mM) greatly reduced the number of adherent cells (to collagen I-coated plates), which were highest at 1 mM ($P < 0.001$) and 2 mM ($P < 0.01$) calcium (**Figure 4.17L-M**). Overall, these data illustrate that abnormal levels of calcium impair fibroblast migration and differentiation-linked behaviours, including ECM production, contraction and cellular adhesion.

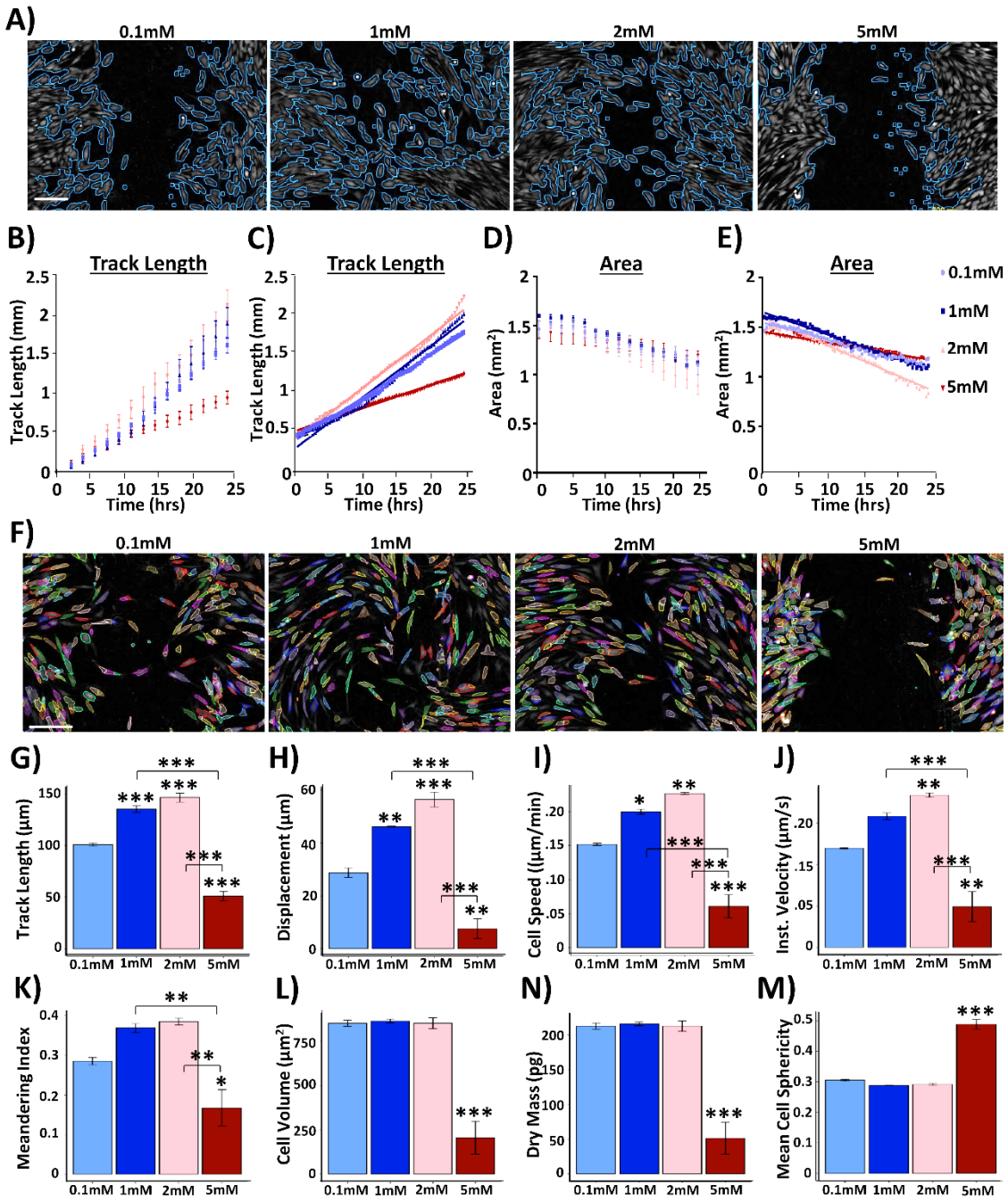

Figure 4.16. Live cell imaging demonstrates calcium-induced modulation of migratory behaviours in human dermal fibroblasts. Live imaging was performed via ptychography. Scratch images from the final frame (24 hours, **A**) with quantification of track length (**B-C**) and area of scratch closure (**D-E**). Single cell segmentation at the final frame (24 hours, **F**) where cells were tracked individually. Mean quantification of single cell parameters (**G-M**). Representative donor. Bar = 200 µm. Mean +/- SEM. * = $P < 0.05$, ** = $P < 0.01$, *** = $P < 0.001$. One-way ANOVA with Tukey's *post-hoc* analysis performed on **G-M**. * alone versus 0.1 mM calcium.

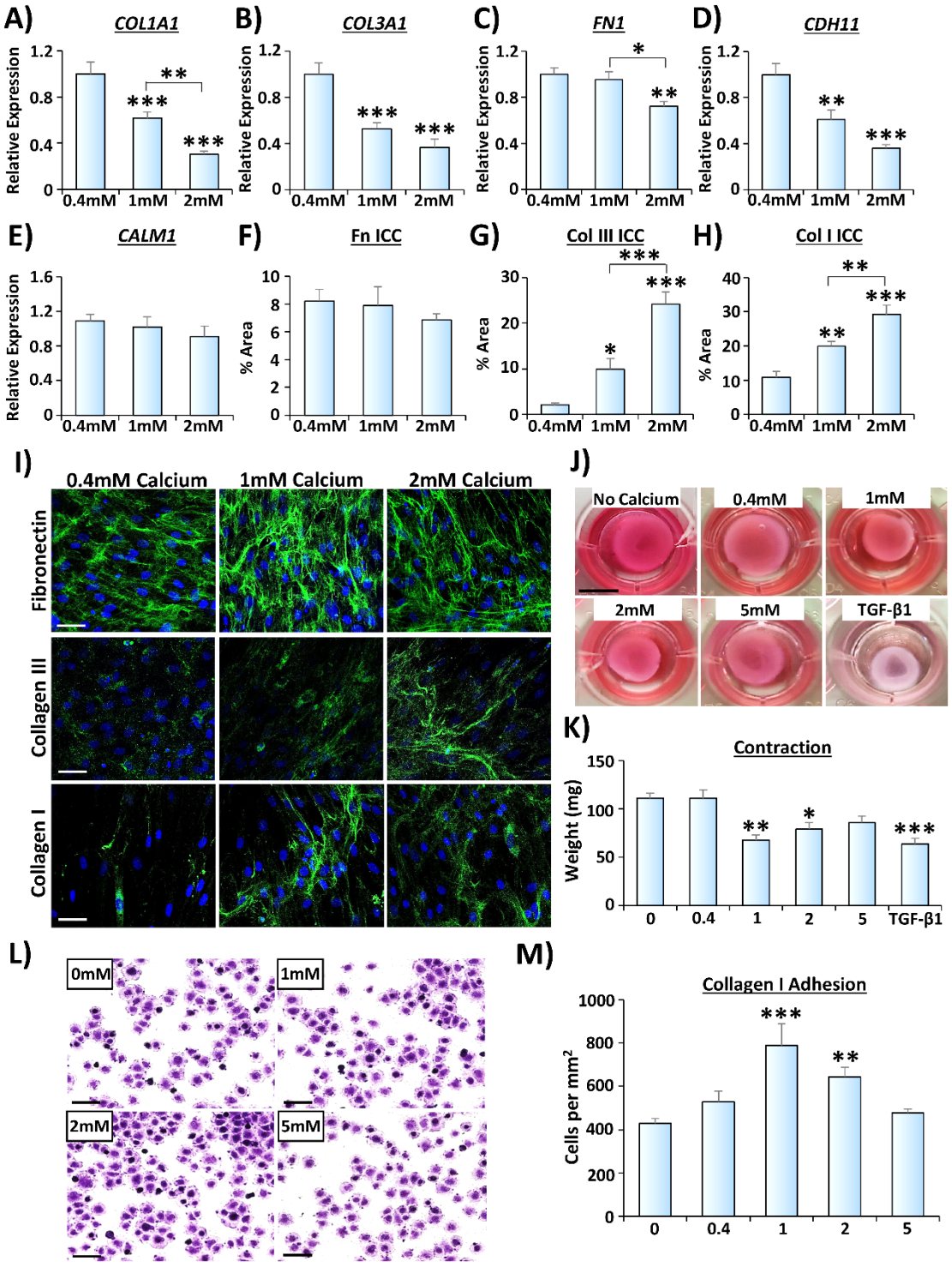

Figure 4.17. Phenotypic behaviours of human dermal fibroblasts are calcium-dependent. qRT-PCR for *COL1A1* (**A**), *COL3A1* (**B**), *FN1* (**C**), *CDH11* (**D**) and *CALM1* (**E**) following two days treatment. Immunocytochemistry for fibronectin (Fn, **F**), collagen III (Col III, **G**) and Col I (**H**) production. DAPI = blue nuclei. Markers = Alexa Fluor® 488. Representative images (**I**). Bar = 50 µm. Collagen contraction gels (**J**) and quantification of gel weights (**K**). Bar = 5 mm. Collagen I adherence assay (**L**) and adherent cell numbers (**M**). Bar = 100 µm. Combined 3 donors. Mean + SEM. * = $P < 0.05$, ** = $P < 0.01$, *** = $P < 0.001$. One-way ANOVA with Tukey's *post-hoc* analyses. * alone versus 0.4mM (**A-H**) or 0 mM (**K, M**) groups.

4.4.9. Diabetic macrophages display intrinsically-altered polarisation and responses to calcium.

Wound Mφs are upregulated at D3 (**Appendix Figure 4A.1**), where calcium levels significantly accumulate (**Figure 4.6**). Transcriptional changes in polarisation and calcium-linked genes were directly assessed between NDb and Db Mφs under different calcium conditions. A heatmap demonstrates Db versus NDb fold change in expression (values above 5 and below -10 are colour saturated, significance not shown, **Figure 4.18A**).

NDb and Db Mφs were compared at 2 mM calcium, where as expected, *Arg1* (**Figure 4.18B**) and *Ym1* (**Figure 4.18C**) were elevated in M2-stimulated Mφs and *Nos2* (**Figure 4.18D**) and *Cd86* (**Figure 4.18E**) were upregulated in M1-stimulated Mφs. Polarisation markers were lower in Db Mφs (**Figure 4.18B-E**), suggesting they were less responsive to stimulation. *Casr* expression was lower in M1 and M2 ($P < 0.01$) Db Mφs (compared to NDb, **Figure 4.18F**). *Tram2* ($P < 0.05$ at M0 and M2; **Figure 4.18G**), *Pi3k* ($P < 0.05$ at M2; **Figure 4.18H**), *Calm1* ($P < 0.001$; **Figure 4.18I**) and *Itpr1* ($P < 0.05$ at M2; **Figure 4.18J**) were higher in NDb than Db Mφs under different polarisation states (full comparisons, **Appendix Figures 4A.4-4A.6**). A phagocytosis assay was also performed using *E. coli* BioParticles™ (**Appendix Figure 4A.7**), where high calcium increased particle uptake in M0 and M1 Mφs.

4.4.10. PMA-induced differentiation in THP-1 cells is calcium-dependent.

THP-1 cells were used as a human monocyte model due to their versatility and availability (Bosshart & Heinzelmann, 2016). As THP-1 cells are immortalised, there were no concerns around maintaining their viability for differentiation experiments. THP-1 cells were stimulated to differentiate into Mφ-like cells with PMA in the presence of calcium, evaluated using qRT-PCR for validated markers and physical assessment of cellular adhesion. *CD11b* expression was unaffected by calcium level (**Figure 4.19A**), while *CD14* expression was highest in THP-1 cells stimulated with PMA under 2mM calcium conditions ($P < 0.001$; **Figure 4.19B**). Similarly, *CD36* expression was only significantly upregulated in PMA-stimulated cells treated with 2 mM calcium ($P < 0.05$; **Figure 4.19C**). *CD54* expression was greatest in THP-1 cells plus PMA (versus no PMA) irrespective of calcium dose (**Figure 4.19D**). The connection to calcium was further assessed by profiling candidate calcium-linked

genes. Here, PMA stimulation significantly increased expression of *Calm1* following 2 mM calcium treatment ($P < 0.05$; **Figure 4.19E**), while *Casr* expression was downregulated following PMA stimulation in 0.4 mM ($P < 0.001$) and 3 mM ($P < 0.001$) calcium (**Figure 4.19F**). PMA stimulation also dampened *Tram2* expression in low (0.4 mM) calcium ($P < 0.01$; **Figure 4.19G**) and *Pi3K* expression in high (3 mM) calcium ($P < 0.05$; **Figure 4.19H**). Finally, the effect of stimulation and calcium administration on THP-1 cell adhesion was explored (**Figure 4.19I**). Here, PMA-stimulated THP-1 cells in 2 mM calcium displayed the greatest adherence ($P < 0.05$; **Figure 4.19J**). Hence, calcium is required to promote differentiation marker expression and adherence in differentiating monocytes.

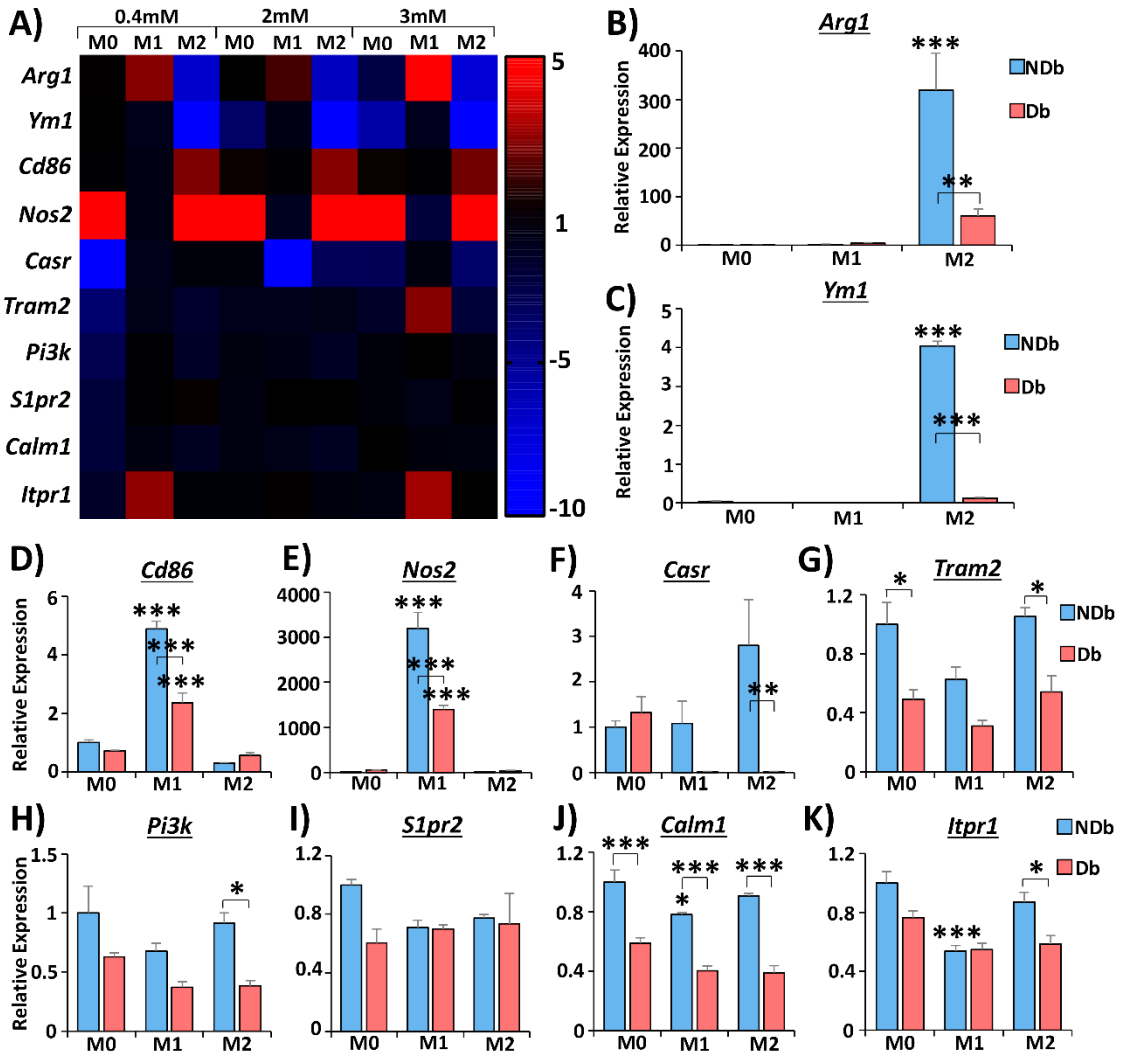

Figure 4.18. Calcium alters transcriptional profiles of bone marrow-derived macrophages. Macrophages were left unstimulated (M0) or stimulated to pro-inflammatory (M1) or anti-inflammatory (M2) states. Heatmap depicting diabetic (Db) versus non-Db (NDb) fold change in expression via qRT-PCR (**A**). Values above 5 and below -10 colour saturated. Individual graphs of expression of M1 (*Cd86* and *Nos2*) and M2 (*Arg1* and *Ym1*) polarisation markers and calcium-linked genes and following 2 mM calcium treatment (**B-K**). n = 4 mice per group. Mean + SEM. ** = $P < 0.01$, *** = $P < 0.001$. Two-way ANOVA with Tukey's *post-hoc* analysis. * alone versus M0 group.

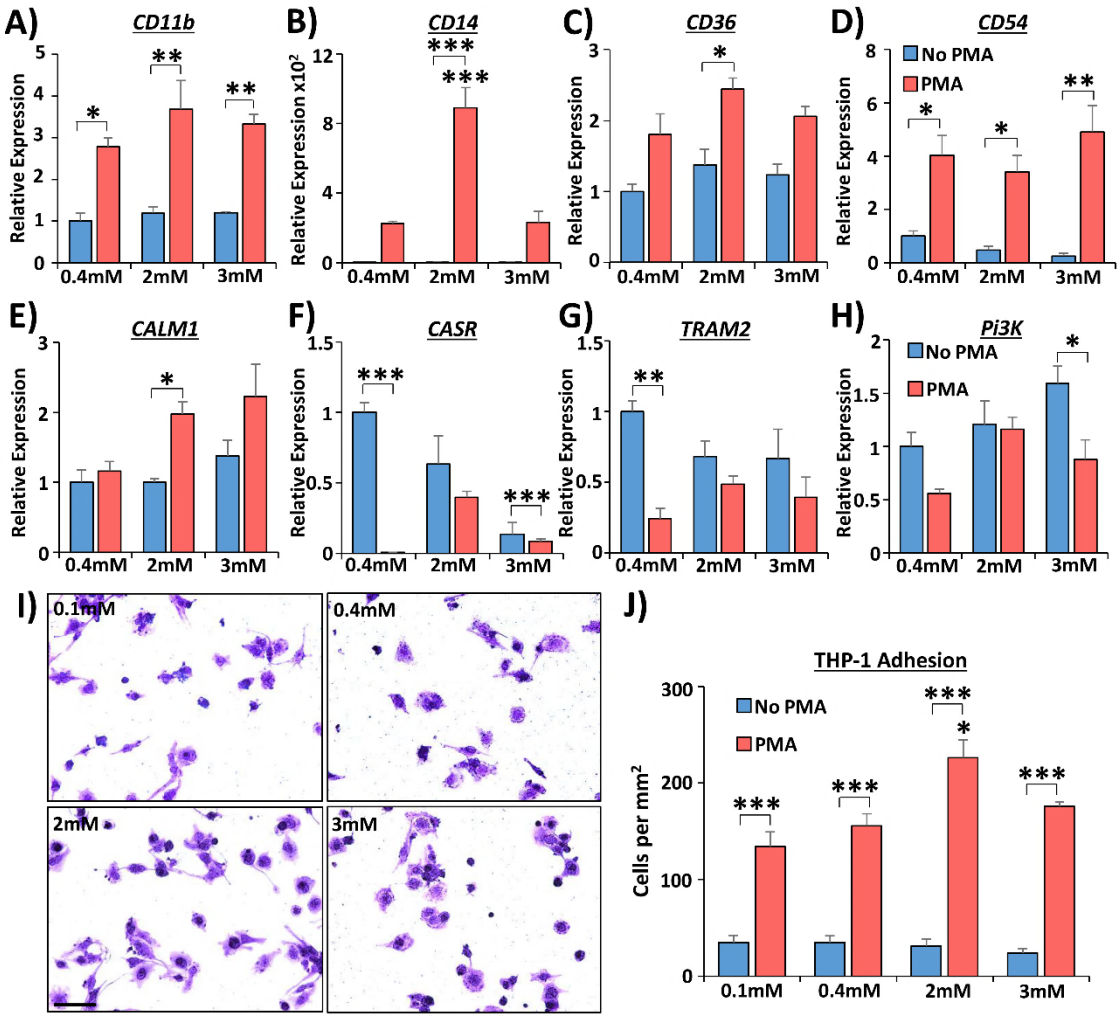

Figure 4.19. PMA-induced THP-1 cell differentiation is governed by calcium. Phorbol 12-myristate 13-acetate (PMA) was used to differentiate THP-1 cells. qRT-PCR assessed differentiation markers in non-stimulated and PMA-stimulated cells (**A-D**). Calcium-linked genes were also assessed (**E-H**). Adhesion was determined by counting adherent crystal violet stained cells (**I**, quantified in **J**). Bar = 100 µm. Three independent experiments. Mean + SEM. ** = $P < 0.01$, *** = $P < 0.001$. Two-way ANOVA with Tukey's *post-hoc* analysis. * alone versus 0.4 mM (**A-H**) or 0.1 mM (**J**) groups.

4.4.11. Transcriptional profiling links metals to wound healing and diabetic pathology at a global level.

The metallome was clearly temporally and spatially altered throughout normal healing and perturbed by pathology. Preliminary investigations also revealed that the expression of a number of candidate calcium-linked genes was dysregulated with healing pathology (**Figure 4.10**), while calcium modulated many wound-relevant cellular functions (**Figure 4.11-4.19**). Thus, a global approach was taken to transcriptionally profile skin and wounds from normal (WT) and pathological (Db) healing mice, and relate transcriptional changes to the metallome.

RNA-Seq identified 10,188 differentially expressed (DE) genes, first visualised via scree plot to determine the contribution of each PC to the variability in the dataset (**Figure 4.20A**). Here, PC1 accounted for over 41.2% of the variability, PC2 for 19.2% and PC3 for 10.9% of the variability. PC1, PC2 and PC3 pair-wise plots revealed inter- and intra-group transcriptional clustering of individual samples. In all cases, sample groups were tightly clustered, with only slight overlap between D3 and D7 Db groups (**Figure 4.20B**). The top 10 genes contributing to each PC was based on determining the genes with the highest loading scores (**Figure 4.20E**).

Hierarchal clustering analysis of the entire DE dataset showed WT and Db skin transcriptional profiles were more similar to each other than wounds. WT wounds (D3 and D7) also retained a higher degree of similarity, and were independent of Db wounds (D3 and D7; **Figure 4.21**). The top 250 most variable genes formed very similar clusters, confirming conserved grouping of the DE data (**Figure 4.22**). Next, direct comparisons were made between DE genes in Db and WT tissue at D0, D3 and D7. Here, 2,288 genes were upregulated in Db versus WT skin, with 1,403 of these genes specific to Db D0. Large numbers of genes were similarly upregulated in Db D3 (1,191; 259 specific) and D7 (1,300; 419 specific) wounds versus WT counterparts (**Figure 4.23A**). A smaller number of genes were exclusively downregulated in Db skin (360) and D3 wounds (209) versus WT, with many more distinct genes (860) down in Db D7 wounds versus WT (**Figure 4.23B**).

Volcano plots allow the spread of significantly upregulated and downregulated genes at D0, D3 and D7 to be visualised (**Figure 4.23C**). Functional annotation analysis of DE genes highlighted over-representation of key pathways associated with wound healing and the metallome. Genes upregulated in Db tissue (D0, D3 and D7) displayed high enrichment for inflammation (P_{adj} = 1.80E-15, 4.30E-13 and 9.50E-20; Gene Ontology), calcium (P_{adj} = 2.00E-14, 0.036 and 0.006, UniProtKB) and metal binding (P_{adj} = 0.001, 0.002 and 0.02, UniProtKB), respectively (**Figure 4.23D-F**). By contrast, calcium signalling (KEGG pathway) was highly enriched in genes downregulated in Db D0 (P_{adj} = 0.042) and D3 (P_{adj} = 8.10E-05) tissues.

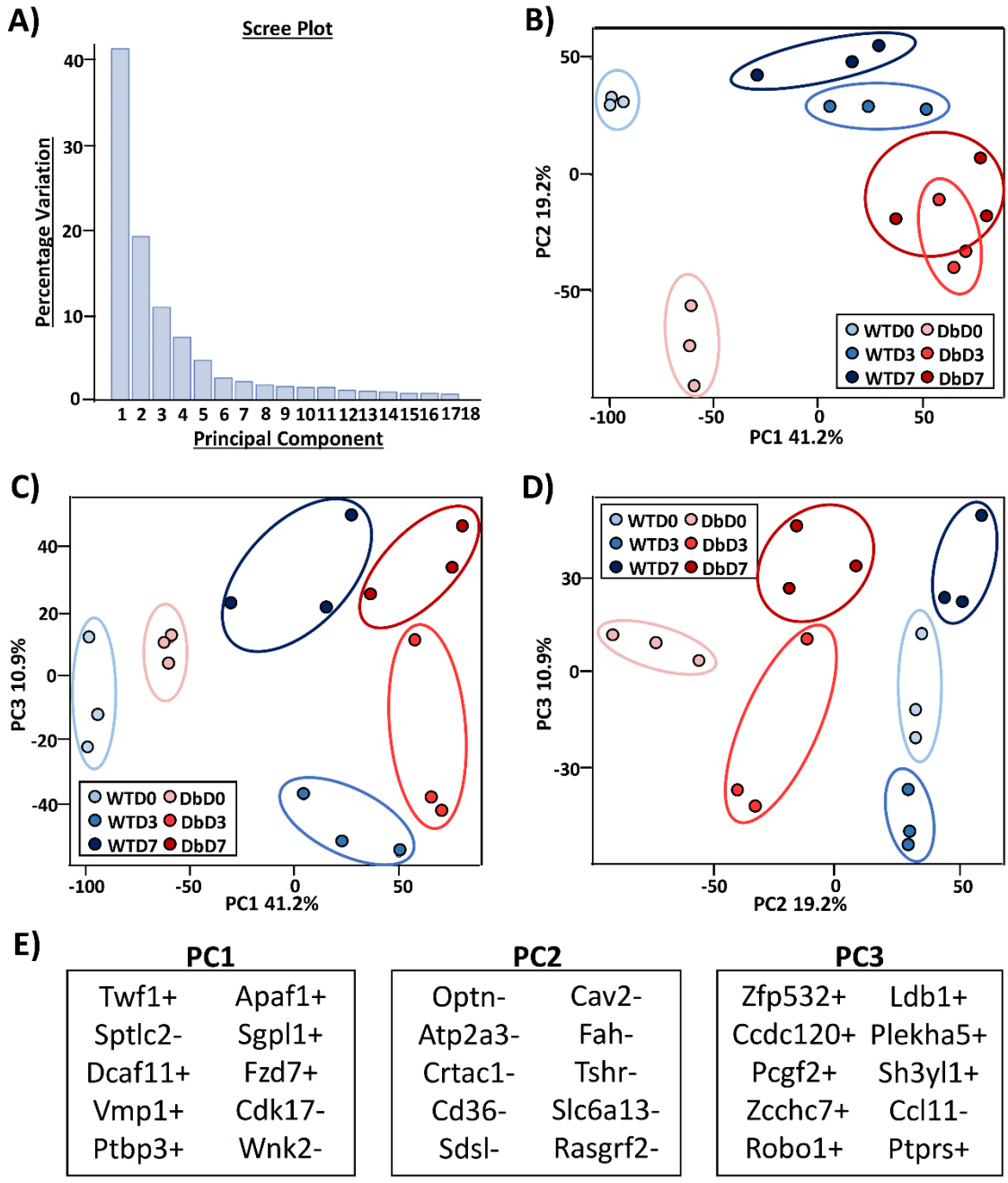

Figure 4.20. Principal component analysis demonstrates tight clustering of skin and wound expression profiles. RNA-sequencing was performed on skin (D0) and wounds at day 3 (D3) and day 7 (D7) post-injury in wild-type (WT) and diabetic (Db) mice. A scree plot shows the contribution of each principal component (PC) to the variability in the dataset (**A**). PC1 versus PC2 (**B**), PC1 versus PC3 (**C**) and PC2 versus PC3 (**D**). Top 10 genes contributing to each PC (**E**), where + = positive effect on PC value and -ve = negative effect on PC value. n = 3 mice per group.

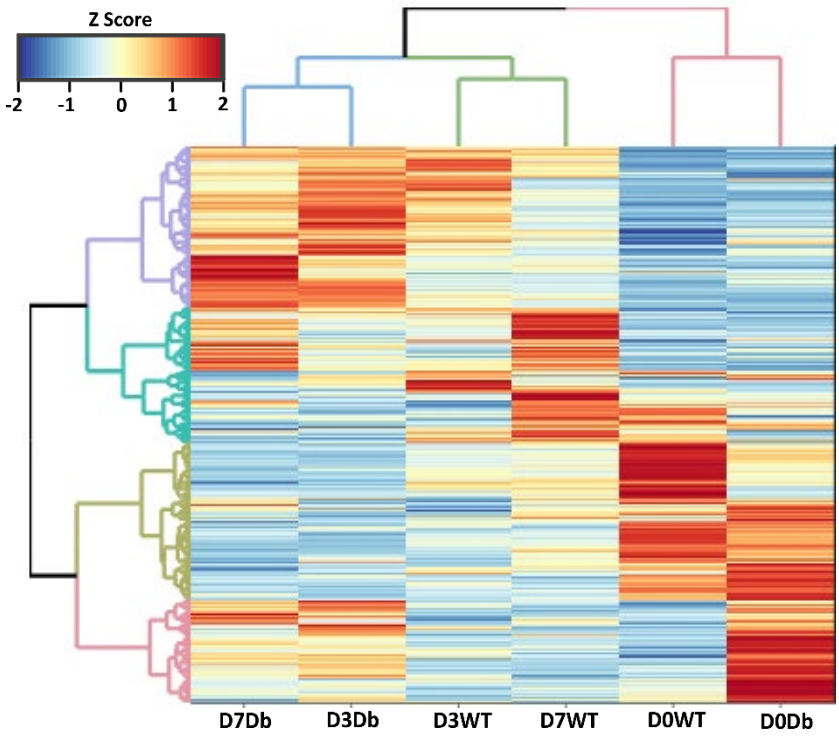

Figure 4.21. Heirarchal clustering of differentially expressed genes by RNA-sequencing. Skin (D0) and wounds at day 3 (D3) and day 7 (D7) post-injury. Wild-type (WT) and diabetic (Db) mice. Clustering of 10,188 differentially expressed genes based on Euclidian distance and Ward D2's method. Distinct clustered branches of dendrograms coloured. n = 3 mice per group.

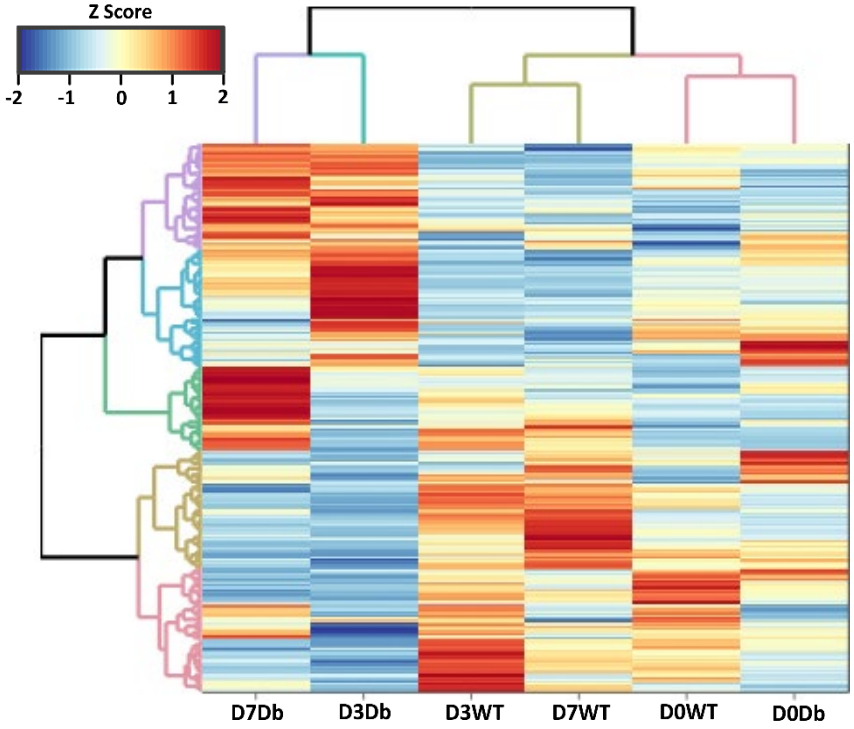

Figure 4.22. Heirarchal clustering of the top 250 differentially expressed genes in the RNA-sequencing dataset. RNA was isolated from WT and Db skin (D0) and wounds (D3 and D7, day post-injury) for transcriptional profiling. Skin clustered more closely than wounds, which clustered based on genotype. Dendrogram branches coloured to indicate distinct clusters. n = 3 mice per group.

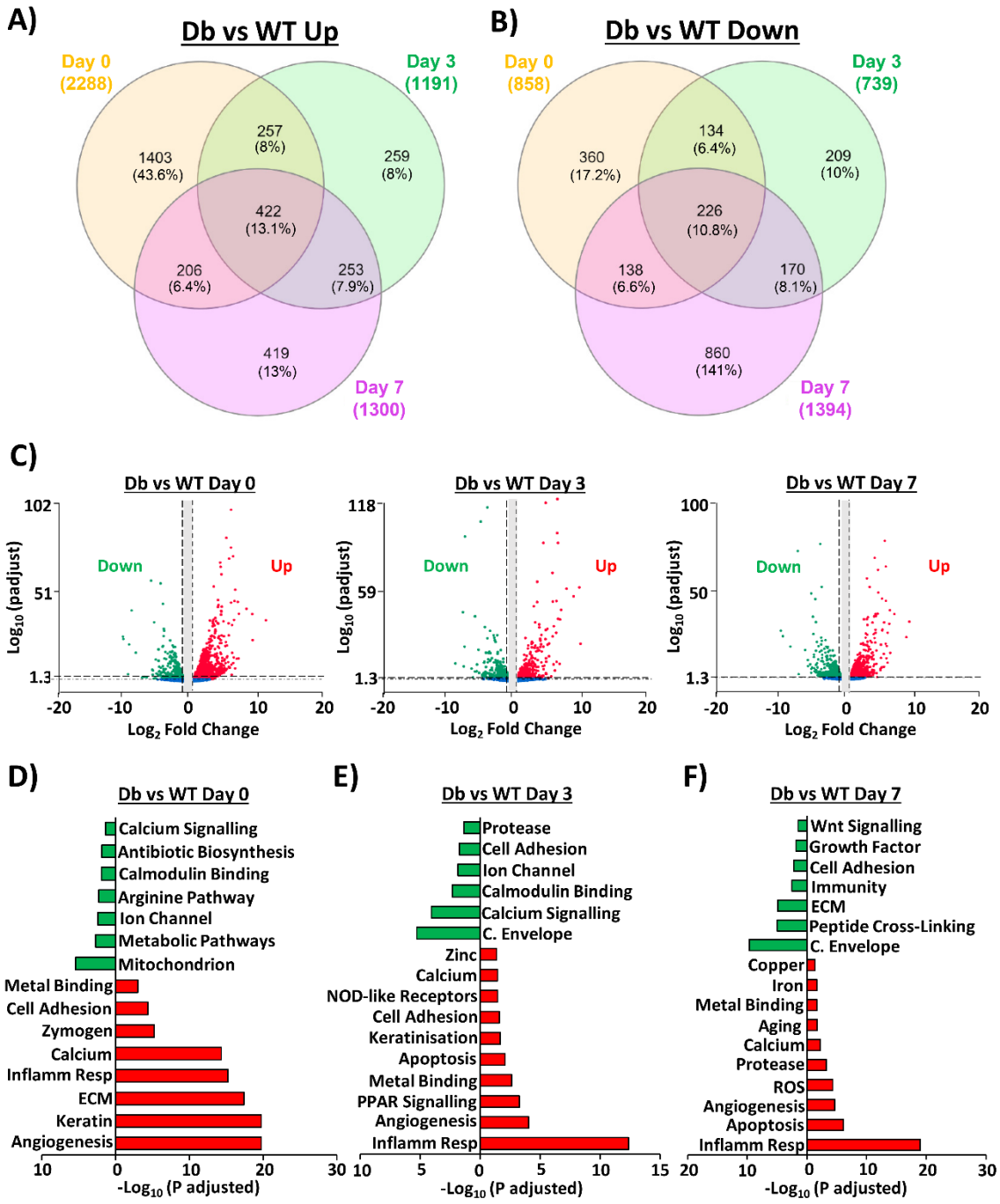

Figure 4.23. Differential expression analysis comparing diabetic and normal murine skin and wounds. Differentially expressed genes in diabetic (Db) versus wild-type (WT) skin (day 0) and wounds (post-injury). Venn diagrams show proportions of genes upregulated (Up, **A**) and downregulated (Down, **B**) in Db tissue, illustrated further by volcano plots (**C**). Cut-off = fold change < 1.5 and $P < 0.05$. Functional annotation analysis revealing significantly annotated pathways in Db versus WT tissue (**D-F**). Red = Up. Green = Down. Inflamm Resp = Inflammatory Response. C. Envelope = Cornified Envelope. Benjamini-Hochberg adjusted *P* value. n = 3 mice per group.

Similar comparisons were made within Db tissues (**Figure 4.24A-C**). Of the genes downregulated in Db wounds at D3 (**Figure 4.24D**) and D7 (**Figure 4.24E**), highly annotated pathways included the calcium signalling KEGG pathway (P_{adj} = 5.00E-07 and P_{adj} = 1.70E-04), and UniProtKB terms metal binding (P_{adj} = 1.20E-06 and P = 2.60E-06) and iron (P_{adj} = 1.60E-04 and P_{adj} = 7.10E-05), respectively. On the other hand, the UniProtKB group calcium was highly enriched in gene subsets upregulated in Db D3 (P_{adj} = 9.60E-06) and D7 (and P_{adj} = 2.10E-10) wounds, and immunity (P_{adj} = 6.50E-46, UniProtKB) was upregulated in D3 Db wounds. Inflammatory response (D7, P_{adj} = 3.30E-37) and aging (D3, P_{adj} = 0.004; D7, P_{adj} = 0.047) Gene Ontology terms were highly enriched in DE genes upregulated in Db wounds. Comparing Db D3 and D7 wounds (**Figure 4.24F**) revealed immunity (UniProtKB) was highly associated with D3 wounds (P_{adj} = 2.20E-22), whereas ECM (P_{adj} = 3.40E-08, Gene Ontology) and calcium (P_{adj} = 4.50E-06, UniProtKB) were more enriched at D7.

Finally, DE genes were compared within WT skin and wounds. Interestingly, although similar numbers of genes were upregulated at D3 versus D0, more genes were upregulated at D7 compared to D0 (**Figure 4.25A-C**). Metal binding (P_{adj} = 1.50E-09, UniProtKB), calcium signalling pathway (P_{adj} = 2.50E-05, KEGG pathway), iron (P_{adj} = 4.50E-04, UniProtKB) and magnesium (P_{adj} = 0.002, UniProtKB) were all annotated in DE genes upregulated at D0 versus D3, whereas calcium (P_{adj} = 6.30E-18, UniProtKB), aging (P_{adj} = 0.003, GO), and copper (P_{adj} = 0.02, UniProtKB) were significantly enriched at D3 (**Figure 4.25D**). In D7 wounds (compared to D0), highly annotated Gene Ontology pathways included ECM (P = 7.00E-32) and cornified envelope (P_{adj} = 5.10E-28), while UniProtKB terms calcium (P_{adj} = 4.00E-18) and copper (P = 0.04; **Figure 4.25E**) were also enriched in D7 wounds. Calcium (P_{adj} = 5.00E-05 and P_{adj} = 1.30E-08, UniProtKB) and ECM (P_{adj} = 0.005 and P_{adj} = 1.90E-16, Gene Ontology) were enriched in genes upregulated at both D3 and D7, respectively, while the UniProtKB term metal binding was specific to D7 (P_{adj} = 0.017; **Figure 4.25F**). Together, these novel findings demonstrate that key metal-linked and ageing-linked pathways are independently identified in global RNA-Seq. These data thus validate the importance of the metallome and senescence in normal and pathological repair.

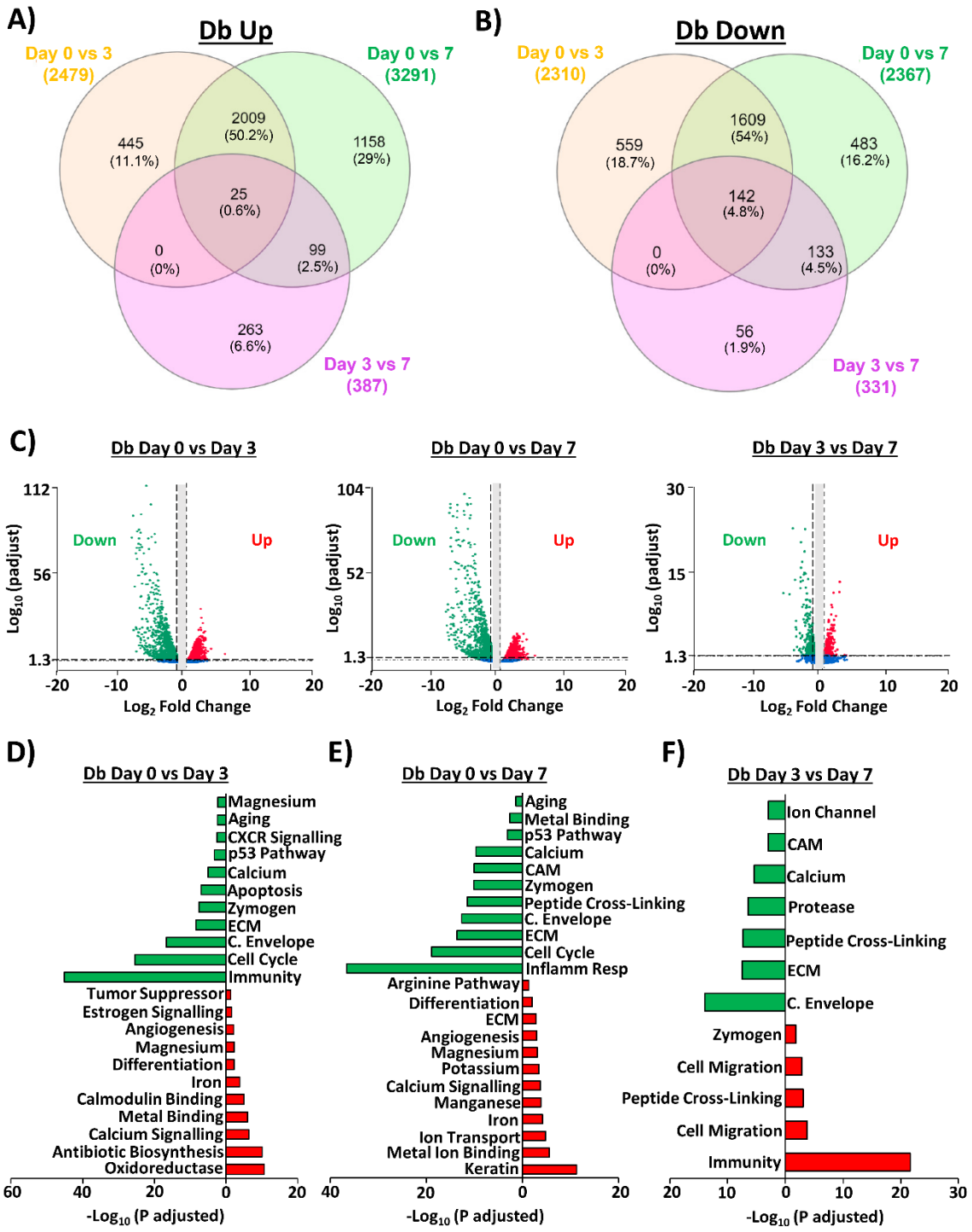

Figure 4.24. Functional annotation analysis comparing differentially expressed genes in diabetic skin and wounds. Differentially expressed genes in diabetic (Db) skin (day 0) versus wounds (day post-injury). Venn diagrams of proportions of genes upregulated (Up, **A**) and downregulated (Down, **B**) in Db tissue. Volcano plots of upregulated and downregulated genes between day 0, day 3 and day 7 (**C**). Cut-off = fold change < 1.5 and $P < 0.05$. Functional annotation analysis showing significantly annotated pathways upregulated (red) and downregulated (green) in Db tissue (**D-F**). C. Envelope = Cornified Envelope. Inflamm Resp = Inflammatory Response. Benjamini-Hochberg adjusted *P* value. n = 3 mice per group.

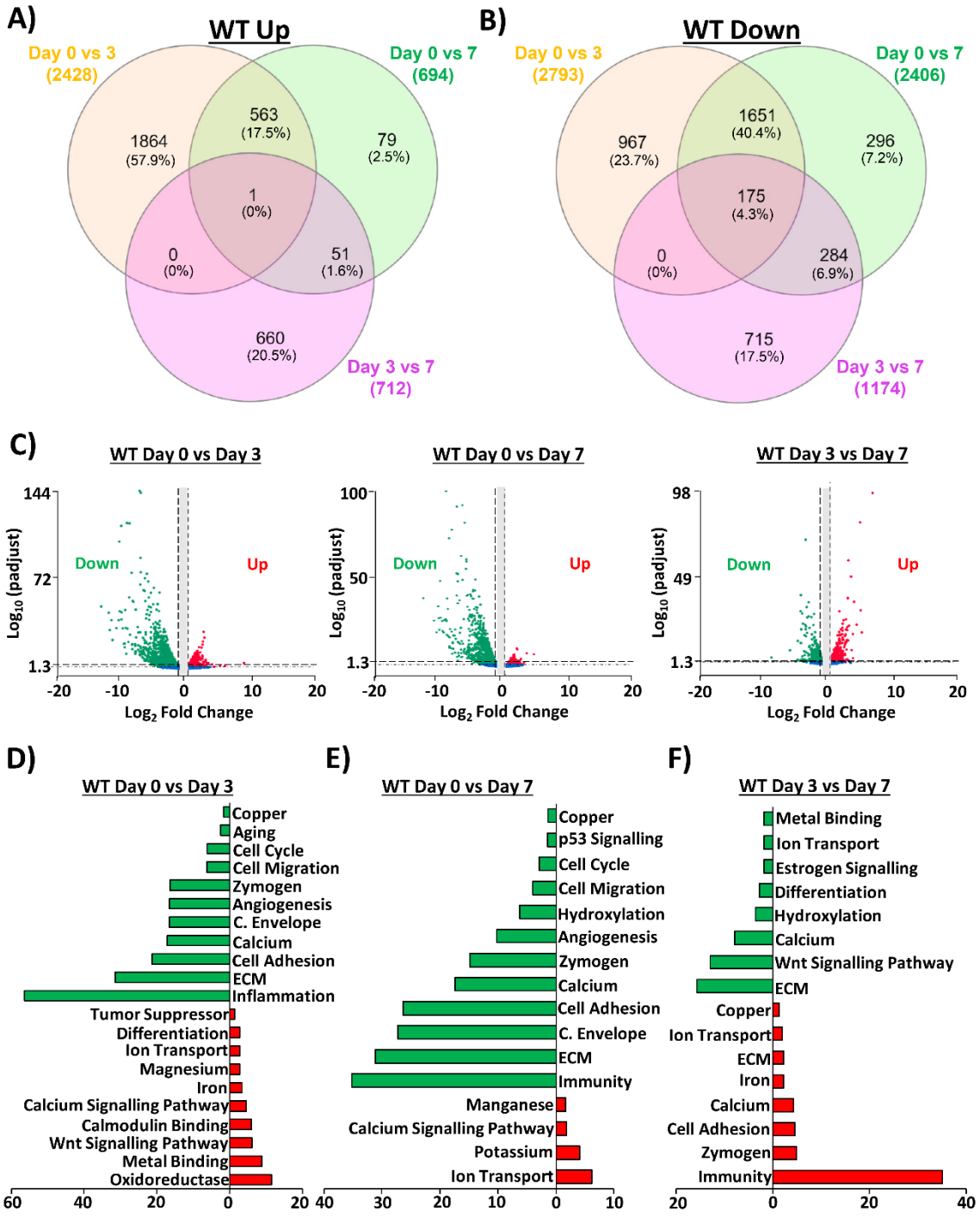

Figure 4.25. Global profiling of differentially expressed genes in normal wound healing. Differentially expressed genes in wild-type (WT) skin (day 0) and wounds (day post-injury). Venn diagrams show proportions of genes upregulated (Up, **A**) and downregulated (Down, **B**) in WT tissue. Volcano plots of upregulated and downregulated genes (**C**). Cut-off at fold change = 1.5 and $P < 0.05$. Functional annotation analysis revealing significantly annotated pathways in WT tissue (**D-F**). Red = upregulated. Green = downregulated. C. Envelope = Cornified Envelope. Benjamini-Hochberg adjusted *P* value. n = 3 mice per group.

4.4.12. RNA-sequencing network analysis confirms altered calcium in diabetic pathology.

To test global association between key biological pathways and healing in WT versus Db tissue, functional annotation was performed on the entire DE data set. Amongst the most highly enriched (UniProtKB) pathways were metal binding (P_{adj} = 1.9E-23; 1609 genes) and calcium (P_{adj} = 2.6E-27; 1607 genes). To explore distribution of these 1607 and 1609 genes across and between experimental groups, hierarchal clustering analysis was repeated using only these genes (**Figure 4.26** and **Figure 4.27**). In the "metal binding" heatmap, wounds and skin clustered into two main independent groups. As with the full data set heatmap (**Figure 4.21**), D3 and D7 WT wounds were clustered, as were D3 and D7 Db (**Figure 4.26**). The "calcium" functional annotation pathway exhibited similar clustering, where skin (WT and Db) clustered more closely than wounds, and wounds clustered by genotype (**Figure 4.27**). Of note, gene clusters revealed co-ordinate regulation of key wound-associated genes. For example, "calcium" cluster 5 contained *Cdkn1a*, *Klf6*, *Klf7, S100a8* and *S100a9,* all highly expressed at Db D3. By contrast, "calcium" cluster 6 contained ECM-linked (*Col1a1*, *Col1a2*, *Mmp14*, *Tgfb1il* and *Col18a1*) and calmodulin-linked (*Calml3* and *Calm4*) genes, all selectively upregulated in D7 WT tissue. Indeed, ECM genes show dampened expression in Db wounds (Bhattacharya et al., 2015) and correlate with reduced ECM deposition (Campbell et al., 2010), while inflammatory mediators (e.g. *S100A8* and *S100A9*) are more highly expressed in diabetes (Jin et al., 2013). Therefore, it is clear that calcium-linked genes cluster based on healing stage and pathology.

To further investigate the association between calcium and the wound transcriptome, pathway analysis was performed using IPA software. Corroborating an important biological role, Ca^{2+} was strongly predicted as an upstream regulator in Db versus WT tissue at D0 (P < 3.36E-4), D3 (P < 1.83E-3) and D7 (P < 1.8E-11). Next, networks were created from the well-documented calcium-linked complexes, Casr and calmodulin (Clapham, 2007; Tu & Bikle, 2013). IPA annotated genes were confirmed as altered in the RNA-Seq data by overlaying DE data sets (Db versus WT at D0, D3 and D7). Complexes upregulated in Db skin with annotated relationship to Casr included Ras homolog (Rho) genes (*Rhob*, *Rhoc*, *Rhof*, *Rhoj*), known to be associated with diabetic complications (e.g. neuropathy; Kolavennu et al., 2008), and von Hippel-Lindau tumour suppressor genes (*Vhl* and *Vhl-ps1*), important for

regulating hypoxia inducible factors (HIFs, Mole et al., 2001). In Db wounds, *Notch1*, *Notch2* and *Nfkbia* were upregulated at D3, and *Hif1a* was highest at D7 (compared to WT). On the contrary, *Casr* expression itself was higher in WT skin (**Figure 4.28A**) and wounds (**Figure 4.29A** and **Figure 4.30A**), confirming its potential dysregulation in diabetic pathology.

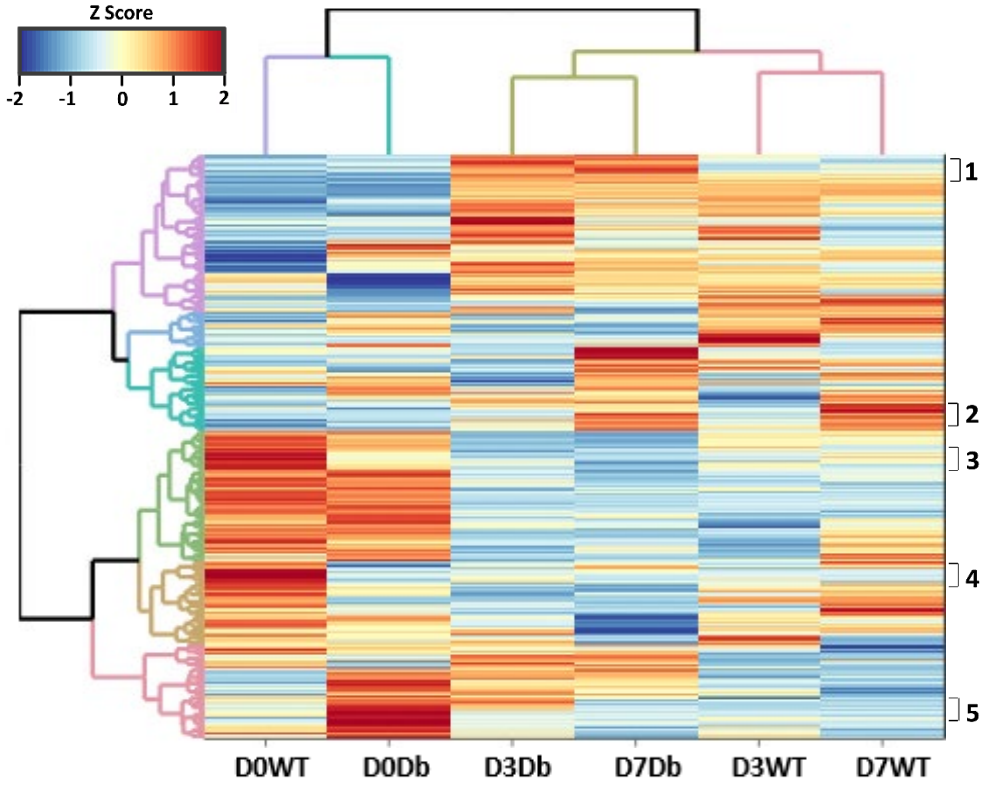

Cluster 1:	Cluster 2:	Cluster 3:	Cluster 4:	Cluster 5:
Atp2b1	*Chys3*	*Adam1a*	*Ap13a5*	*Hpd*
Atp7a	*Spo11*	*Pde4a*	*Pkd2*	*Nrp2*
Prkcd	*Adamts16*	*Nme6*	*Acap2*	*Klf14*
Cdkn1a	*Gm4631*	*Isca1*	*Klf10*	*Alox15*
Klf6	*Cdh2*	*Zfp712 &*	*Smad7*	*Kcnd3*
	Mex3a	*493 & 108*	*Fkbp9*	*Pclo*
	Edil3	*Cacna2d1*		*Atp9a*
	Mmp16	*Cdkal1*		

Figure 4.26. Clustering of differentially expressed genes enriched for metal binding. Clustergram demonstrating similarity between wild-type (WT) and diabetic (Db) skin (D0) and wounds at day 3 (D3) and day 7 (D7) post-injury. Clustering based on a subset of genes significantly annotated as metal binding in enrichment analysis (UniProtKB). Dendrogram branches coloured based on clustering. Selected sub-clusters (based on high differential expression) and their constituent genes also shown. n = 3 mice per group.

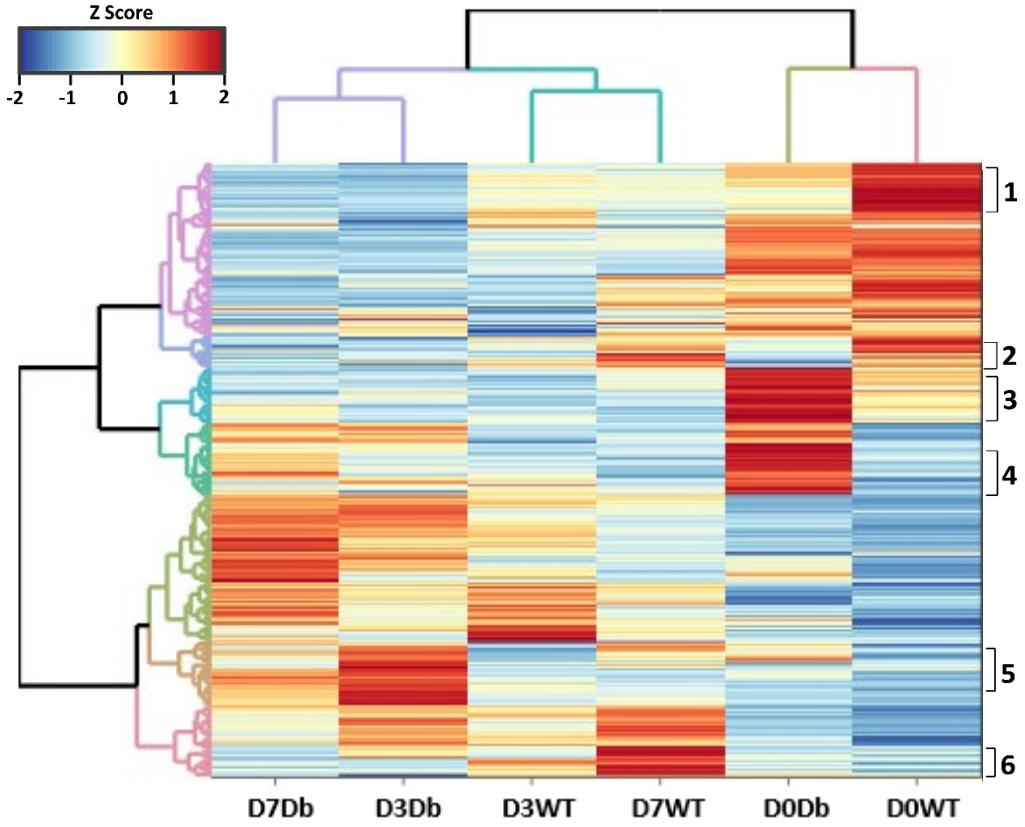

Cluster 1:	Cluster 2:	Cluster 3:	Cluster 4:	Cluster 5:	Cluster 6:
Hif1an	*Micu3*	*Nos1*	*Map3k6*	*Atp2c2*	*Col1a1*
Map3k20 & 12	*Notch1*	*Cyp4b1*	*Prkd1*	*Mmp11*	*Col1a2*
Capn1 & 3	*Klf5*	*Atp1a2*	*Pparg*	*Mmp12*	*Mmp14*
Prkcg	*Cdc42bpg*			*Klf6*	*Tgfb1il*
Camk2a	*Vdr*			*Klf7*	*Calml3*
Casq1	*Capn11*			*Cdkn1a*	*Calm4*
				S100a8	*Col18a1*
				S100a9	*Steap3*

Figure 4.27. Hierarchal clustering analysis of differentially expressed genes associated with calcium annotation. Clustergram demonstrating similarity between wild-type (WT) and diabetic (Db) skin (D0) and wounds at day 3 (D3) and day 7 (D7) post-injury. Clustering based on genes linked to the significantly annotated calcium pathway in enrichment analysis (UniProtKB). Selected sub-clusters (based on high differential expression) of genes also shown. n = 3 mice per group.

In the calmodulin network, Ca^{2+} was revealed as a direct mediator of calmodulin activation (**Figure 4.28B**). *Ryr1*, *Tni* and *Map6* were directly linked to calmodulin, and were more highly expressed in Db skin, while *Pmca* was more highly expressed at WT D0. F actin genes (*Acta1*, *Actn3*, *Actn4* and *Actc1*), shown to have impaired function in diabetic cells previously (Advani et al., 2002), were also upregulated in WT skin. By D3, most complexes directly connected to calmodulin, such as *Ryr1*, were downregulated in Db tissue (**Figure 4.29B**). Calmodulin genes (*Calml3*, *Calm4*

and *Calm5*) were higher in WT than Db tissue regardless of time point, therefore validating its association to the Db model.

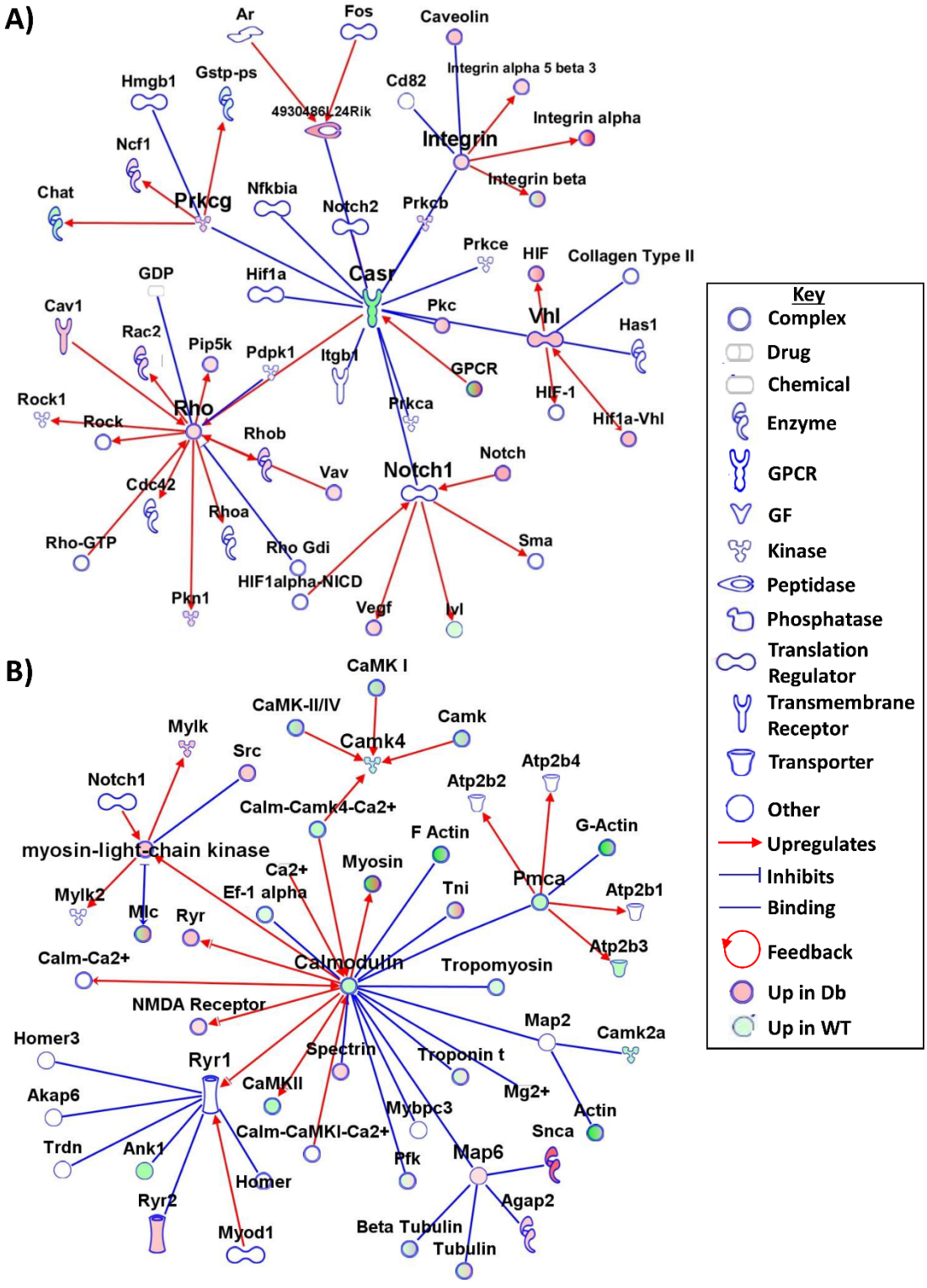

Figure 4.28. Network analysis of calcium-linked complexes demonstrates differential expression of calcium genes in diabetic skin. Ingenuity pathway analysis was used to construct pathways for the calcium-sensing receptor (Casr, **A**) and calmodulin (**B**). Overlays of differentially expressed genes in wild-type (WT) and diabetic (Db) skin also shown. n = 3 mice per group. Complexees, relationships and expression (Db versus WT) described in the key (right).

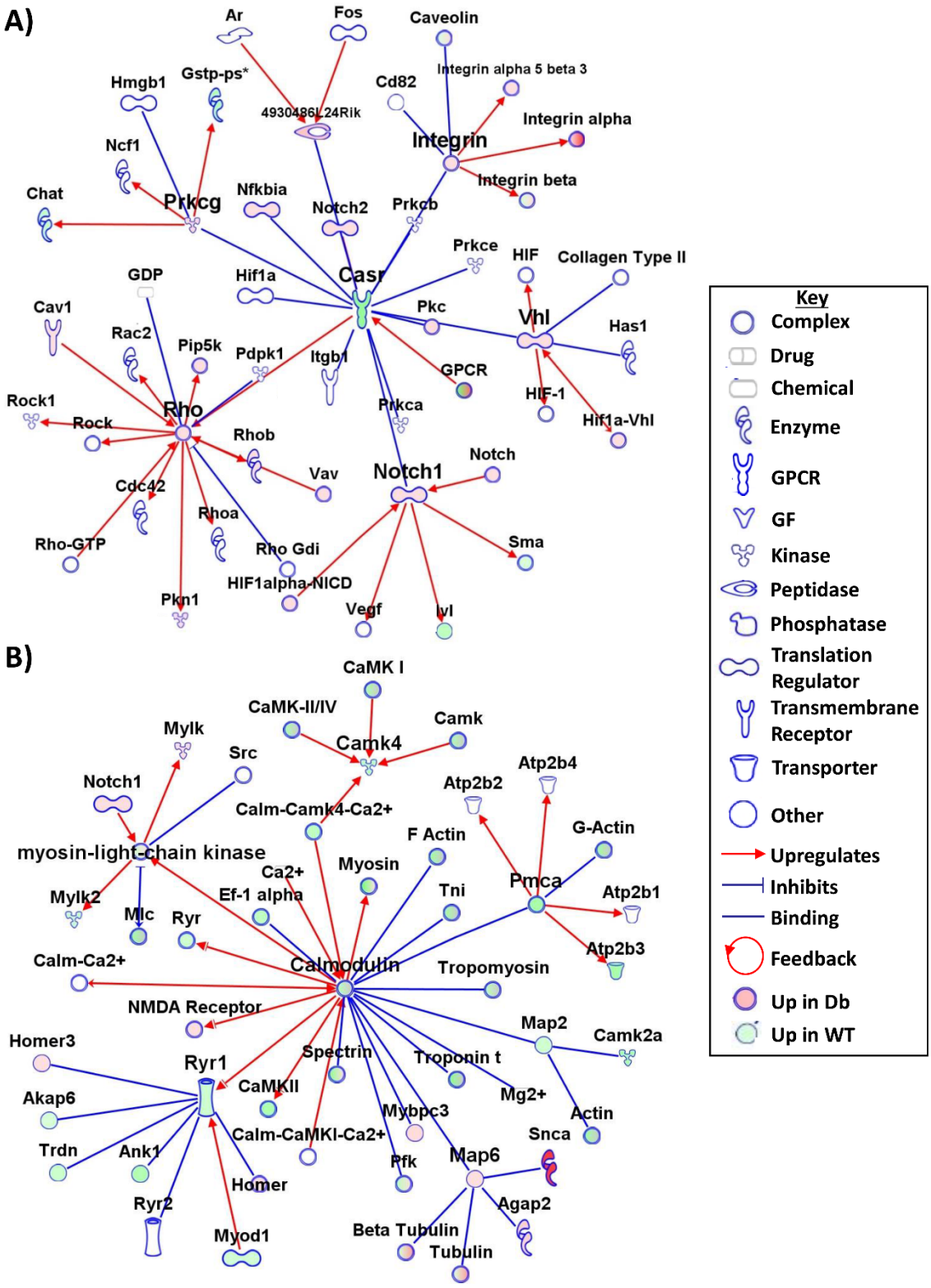

Figure 4.29. Networks illustrating major calcium complexes that are differentially expressed in diabetic wounds. Pathways were built for the calcium-sensing receptor (Casr, **A**) and calmodulin (**B**) using Ingenuity Pathway Analysis. Differentially expressed genes are also shown for diabetic (Db) versus wild-type (WT) wounds at day 3 post-injury. n = 3 mice per group. Key (right) describing complexes, relationships and Db versus WT expression.

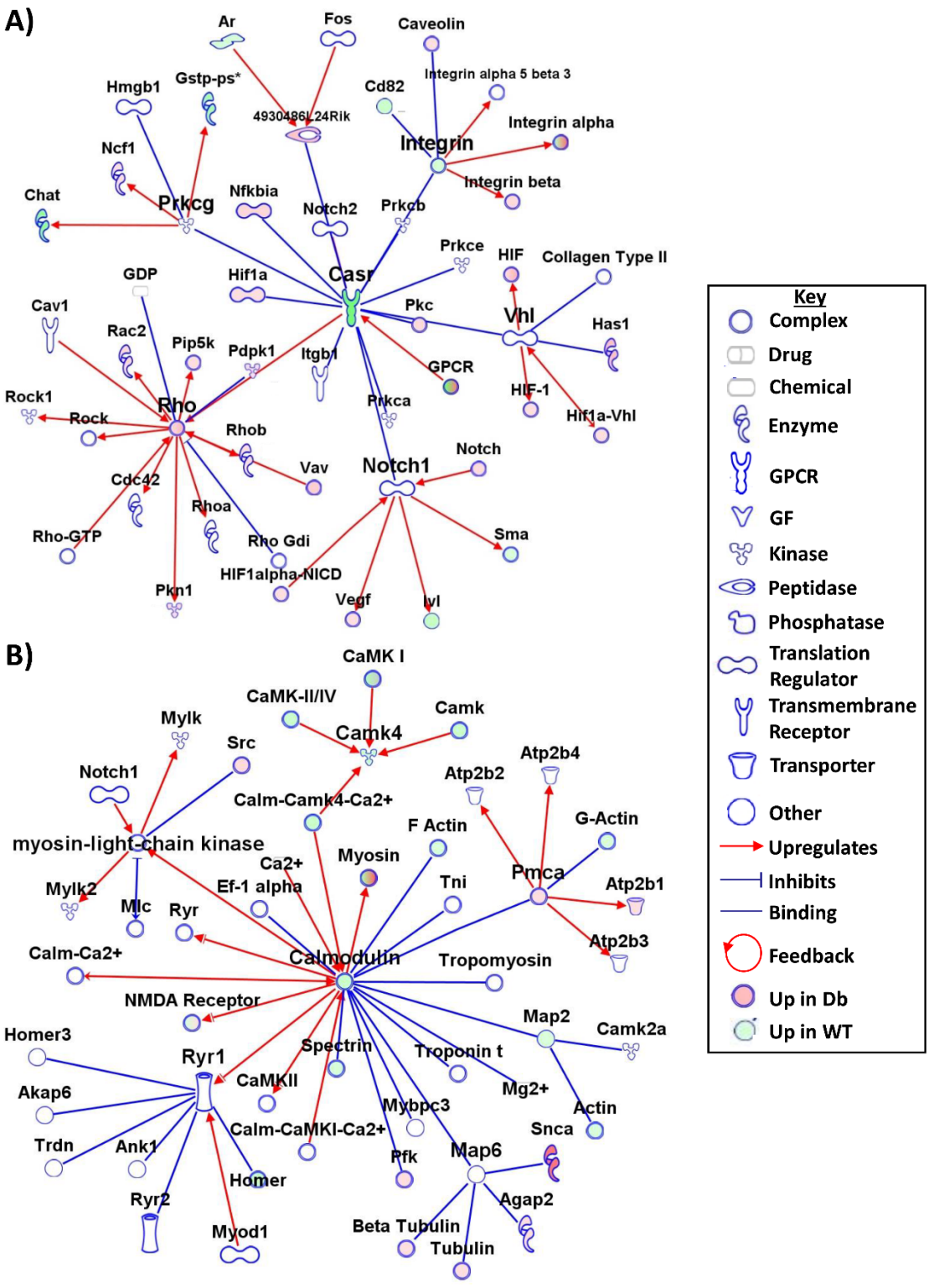

Figure 4.30. Diabetic wounds show altered expression of a number of calcium-linked genes. Networks were built for the calcium-sensing receptor (Casr, **A**) and calmodulin (**B**) using Ingenuity Pathway Analysis, overlaid with differentially expression data from diabetic (Db) versus wild-type (WT) wounds at day 7 post-injury. n = 3 mice per group. Key (right) showing complexes, their relationships and expression (Db versus WT).

A small number of DE genes was picked out from the UniProtKB "calcium" gene list based on their known importance in calcium regulation (summarised in **Section 4.1.4**), and comparisons were made between D0, D3 and D7 WT and Db groups (**Figure 4.31A-C**). Here, *Calm5* (**Figure 4.31E**), *Casr* (**Figure 4.31F**), *Ryr1* (**Figure 4.31G**) and *Vdr* (**Figure 4.31H**) were upregulated at different time points in WT versus Db tissue. Indeed, these genes are vital for calcium uptake and transport, and some have been shown to be downregulated in diabetic pathology previously (Casr in rat eyes, Jiang et al., 2018; Ryr1 in rat hearts, Bidasee et al., 2003). By contrast, *Atp2b1* (**Figure 4.31I**), *S100a8* (**Figure 4.31J**) and *S100a9* (**Figure 4.31K**) were upregulated in Db wounds. S100A8 and S100A9 (the calgranulins) activate the NFκB pathway and drive inflammation in diabetic pathology (Markowitz & Carson III, 2013; Wang et al., 2018d), while inhibition of calgranulin signalling promotes wound repair *in vivo* (in mice, Goova et al., 2001). These findings confirm the metallome and healing profiles observed, whereby calcium genes associated with poor healing are upregulated in Db mice.

4.4.13. Senescence-associated pathways are highly enriched in diabetic wounds.

Novel data presented in **Chapter 3** revealed that diabetic wounds accumulate senescent cells, a hallmark of ageing. The RNA-Seq data set provided an opportunity to independently validate this observation, while delivering additional molecular insight. In fact, ageing (P_{adj} = 1.9E-6) was a top functional annotation identified in the full DE dataset. As in **Section 4.4.13**, hierarchal clustering was performed on the genes within the ageing Gene Ontology grouping to further explore this biological process (**Figure 4.32**). Clustering on "ageing" genes alone led to a quite different heatmap profile to that generated by the entire DE dataset (**Figure 4.21**), top most variable genes (**Figure 4.22**), and metal-based annotations (**Figure 4.26** and **Figure 4.27**). Overall, samples clustered primarily on wound time-point, with a major difference shown between skin and wounds.

The senescence-related factors, Cdkn1a (p21, P < 1.74E-2), Cdkn2b (p27, P < 1.38E-2), Cdkn2a (p16, P < 1.13E-5) were identified as upstream regulators in D7 Db wounds via IPA. Network analysis was performed in IPA on the Cxcr2 pathway, newly identified in **Chapter 3** to play a key role in Db pathological healing. To reinforce this observation, Cxcl1 (P < 8.03E-3 and P < 4.04E-6), Cxcl2 (P < 5.05E-6

and P < 5.47E-11), and Cxcr2 (P < 5.64E-7 and P < 1.21E-8) were independently identified by IPA as upstream regulators in Db skin and D7 wounds, respectively. In the Cxcr2 network, based on direct interactions (IPA) and regulatory predictions (DE dataset), Cdkn2a was shown to activate Cxcr2, and Cxcr2 was able to bind to Cav1 (**Figure 4.33**). Multiple senescence regulators were altered in Db versus WT at D0, D3 and D7 (**Figure 4.34A-C**). For example, *Serpine1*, *Cdkn2b*, *Cav1* and *Cxcl2* were more highly expressed at Db D0 compared to WT (**Figure 4.34A**). By D3, additional complexes were upregulated in Db tissue (e.g. *Cdkn1a*; **Figure 4.34B**), while *Cxcr1* and *Cxcr2* were upregulated in Db wounds versus WT at D7 alone (**Figure 4.34C**). Longitudinal profiles across groups corroborated increased expression of *Cdkn1a* (P < 0.01; **Figure 4.34D**), *Cxcl1* (P < 0.001; **Figure 4.34E**), *Cxcl2* (P < 0.001; **Figure 4.33F**) and *Cxcr2* (P < 0.05; **Figure 4.34G**) in Db D7 wounds, with *Cav1* (P < 0.001 and P < 0.05; **Figure 4.34H**), *Cyr61* (CNN1 gene, P < 0.01; **Figure 4.34I**) and *Serpine1* (P < 0.01; **Figure 4.34K**) upregulated in Db versus WT in at least one time-point. Collectively, this transcriptomics data independently confirms major enrichment of senescence markers in Db skin and wounds.

4.4.14. Iron is transcriptionally distinct between normal healing and diabetic wounds.

Iron abundance is temporally and pathologically altered in wound repair (**Figure 4.6** and **Figure 4.7**). Interestingly, the "iron" UniProtKB group was high overrepresented in the full DE dataset (P_{adj} = 2.7E-7; **Figure 4.23-4.25**). Therefore, the "iron" UniProtKB genes were pulled from the full DE dataset and scrutinised further. Hierarchal clustering of these iron-associated genes demonstrated high similarity in gene expression between Db and WT skin, and separate clustering of WT and Db wounds (**Figure 4.35**).

Returning to the full DE dataset, network analysis identified the transferrin receptor (Tfrc) pathway as a highly predicted upstream regulator in Db versus WT D0 (P < 2.1E-3), D3 (P < 4.7E-4), and D7 (P < 4.86E-11) DE datasets. Tfrc directly binds to iron, Steap3 and Trf (**Figure 4.36**). In Db skin, *Hfe* and *Tfr2* were upregulated (compared to WT; **Figure 4.36A**), while *Slc38a2* was upregulated at Db D3 (**Figure 4.36B**) and D7 (**Figure 4.36C**). *Tfrc* itself was increased in D7 Db wounds versus WT. Finally, *Steap3*, responsible for the conversion of Fe^{3+} to Fe^{2+}, was decreased in Db D7 wounds (versus WT).

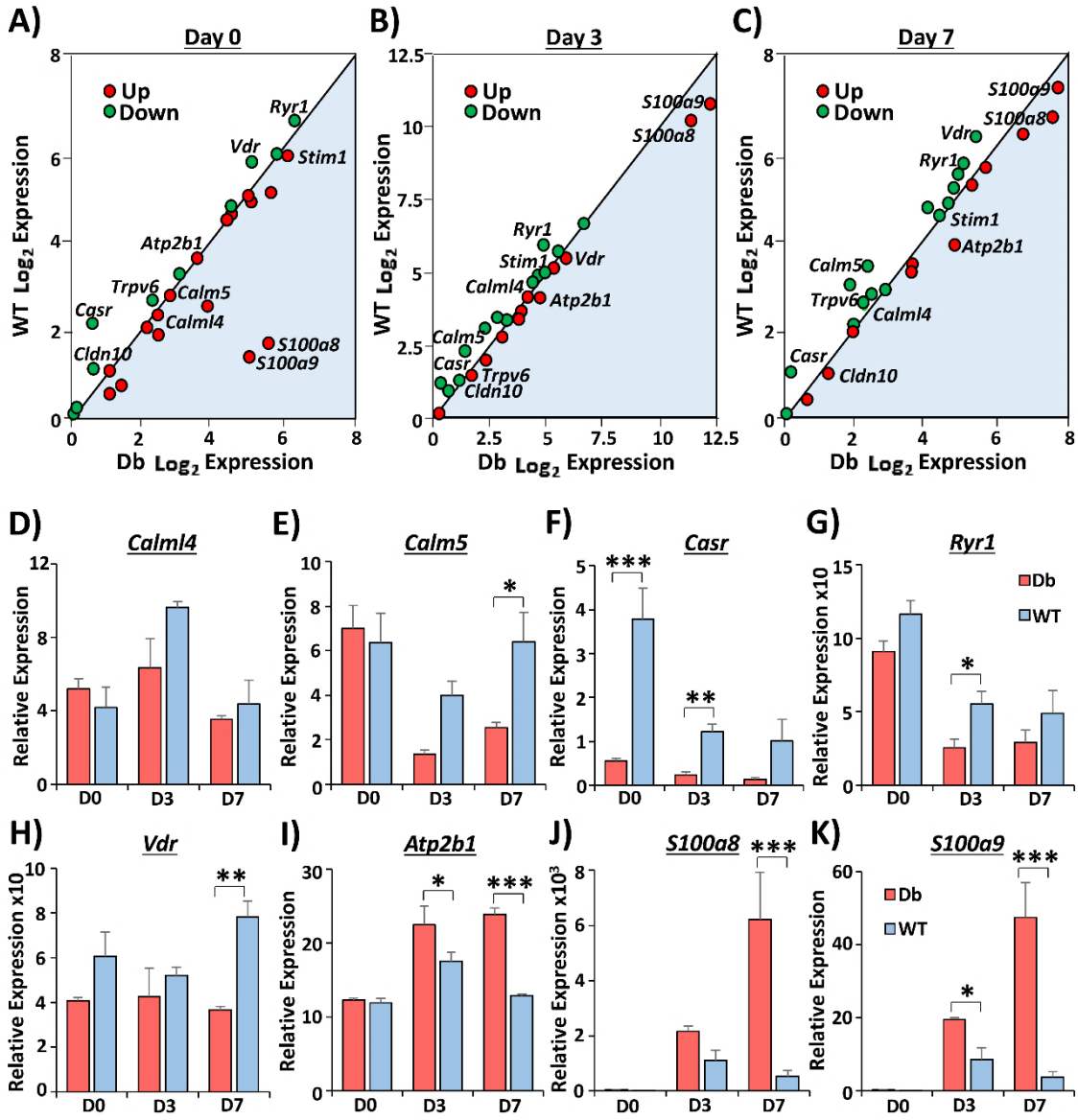

Figure 4.31. Transcriptional profiling reveals alterations in a subset of calcium genes between diabetic and normal healing tissue. Scatterplots show $\log_2$ fold change expression of a number of calcium-linked genes between diabetic (Db) and wild-type (WT) skin (D0, day 0, **A**) and wounds at day 3 (D3, **B**) and day 7 (D7, **C**) post-injury. Up = upregulated in Db. Down = downregulated in Db. Individual genes from RNA-sequencing data (**D-K**). n = 3 mice per group. Mean + SEM. Two-way ANOVA with Tukey's *post-hoc* analysis performed. * = $P < 0.05$, ** = $P < 0.01$, *** = $P < 0.001$.

An important subset of the genes from the UniProtKB "iron" gene list was scrutinised further, based on their importance in regulating the cellular processing of iron (reviewed in Arezes & Nemeth, 2015; Papanikolaou & Pantopoulos, 2017; **Figure 4.37A-C**). Here, *Steap3* was downregulated in D7 Db wounds ($P < 0.01$; **Figure 4.37D**), while *Slc11a1* (**Figure 4.37E**) and *Ftl1* (**Figure 4.37F**) were increased in Db wounds at D3 ($P < 0.01$ and $P < 0.05$) and D7 ($P < 0.01$ and $P < 0.001$). *Slc39a4* ($P < 0.01$; **Figure 4.37G**) and *Tfrc* ($P < 0.01$; **Figure 4.37H**) were similarly upregulated in Db wounds at D7, *Tfr2* expression was higher at Db D0 ($P < 0.001$),

D3 ($P < 0.01$) and D7 ($P < 0.05$; **Figure 4.37I**), and *Hif3a* was increased at Db D0 ($P < 0.001$; **Figure 4.37J**). On the contrary, *Hfe* expression was elevated in WT skin ($P < 0.001$) and D3 wounds ($P < 0.01$; **Figure 4.37K**). Accordingly, these data strongly suggest that the transcriptional regulation of iron is altered across wound healing and perturbed in diabetic repair. A more thorough investigation into the role of iron in normal and pathological (Db) wound healing is provided in **Chapter 5**.

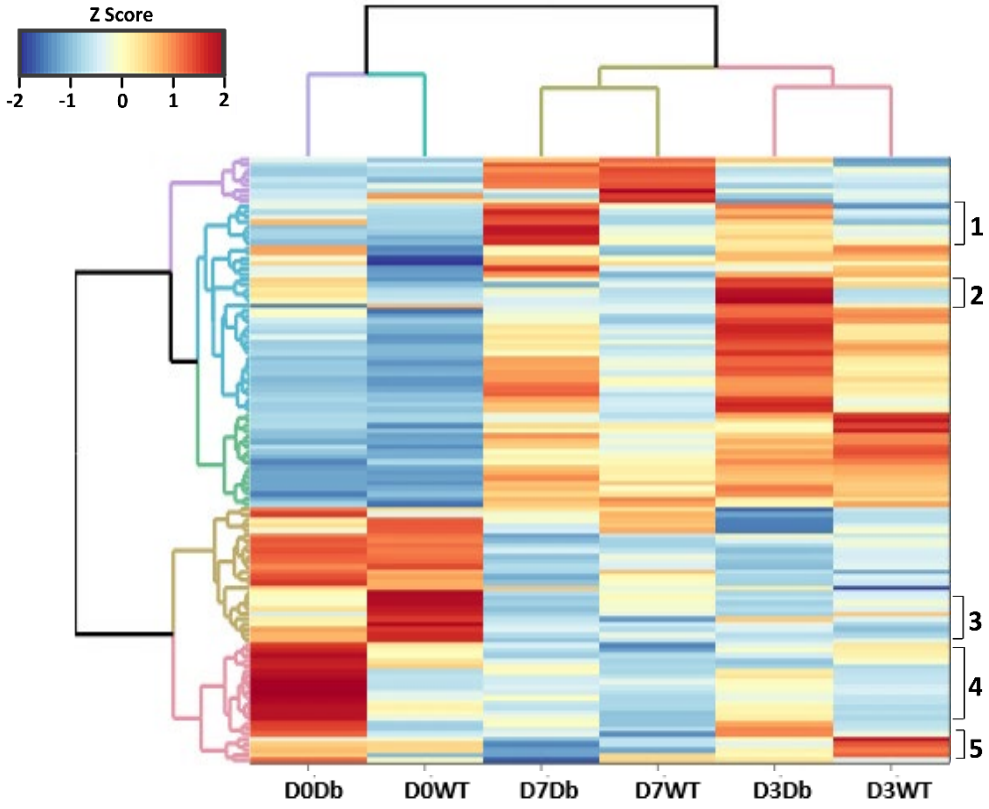

Cluster 1:	Cluster 2:	Cluster 3:	Cluster 4:	Cluster 5:
Tgfb3	*Rpn2*	*Slc12a2*	*Retn*	*Ifi27l2a*
Gclc	*Itgb2*	*P2ry1*	*Pck1*	*Fgf2*
Mpo	*Akt1*	*Eno3*	*Ucp3*	*Sod1*
Madcam1	*Bak1*	*Enog*	*Pde4d*	*Ciita*
Ctc1	*Ccl2*	*Sod2*	*Calca*	*Eef2*
Il15	*Nfkb2*	*mt-Atp6*	*Gsn*	
Jun	*Nfel2l2*	*mt-Co1*	*Agt*	
	Tgfb1	*mt-Nd4*	*Krt83*	

Figure 4.32. Hierarchal clustering analysis of differentially expressed genes that are functionally enriched for ageing processes. Clustering based on differentially expressed genes significantly annotated as part of the ageing Gene Ontology pathway (enrichment analysis). Comparisons made between wild-type (WT) and diabetic (Db) skin (D0) and wounds at day 3 (D3) and day 7 (D7) post-injury (n = 3 per group). Differentially altered sub-clusters also shown.

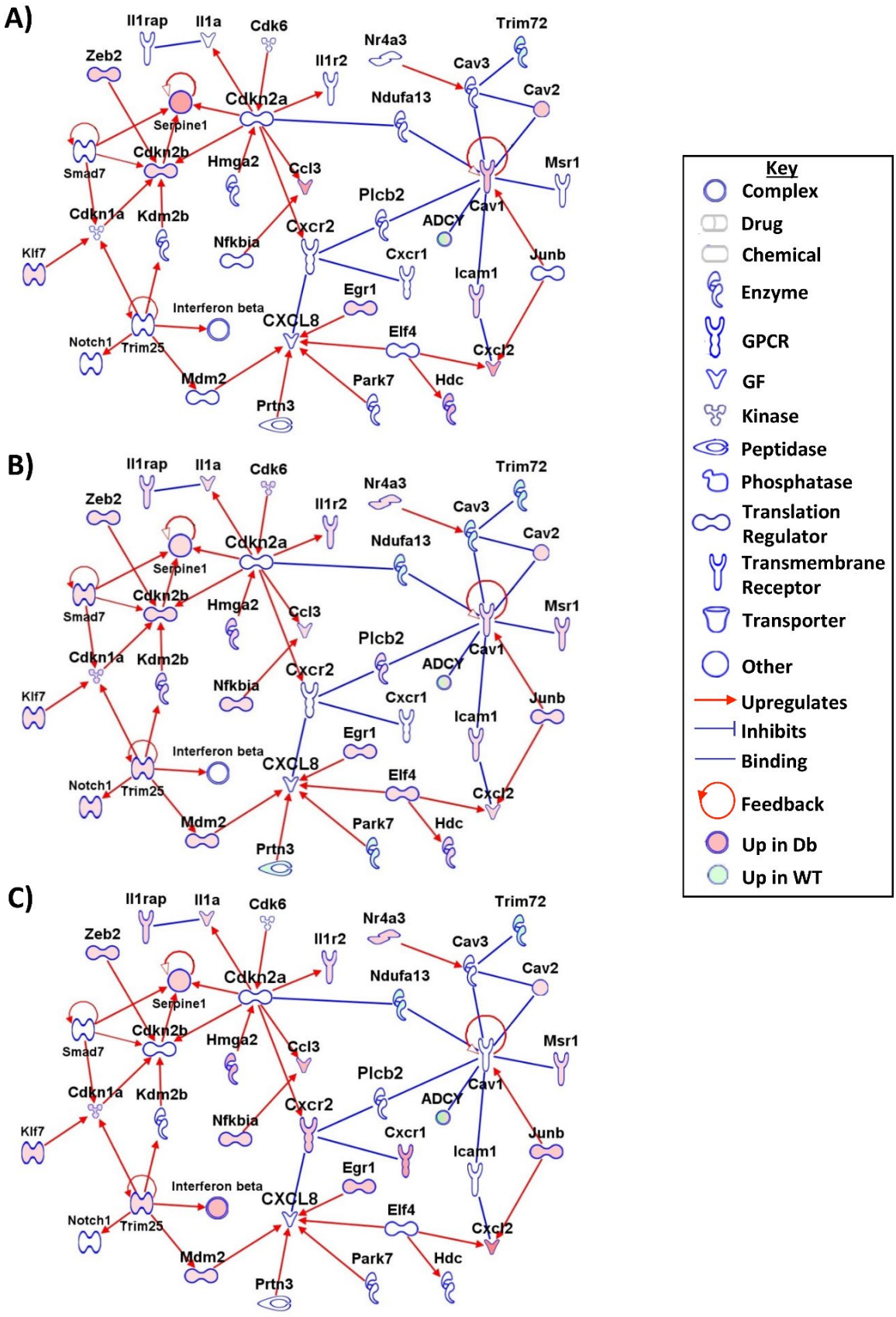

Figure 4.33. Cxcr2 network analysis in diabetic versus normal skin and wounds. Ingenuity Pathway Analysis was used to construct a network around CXCR2. Differential gene expression data was overlaid from skin (**A**), day 3 (**B**) and day 7 (**C**) wounds. Diabetic (Db) versus wild-type (WT) mice. n = 3 mice per group. Key demonstrates complex type, relationship and expression.

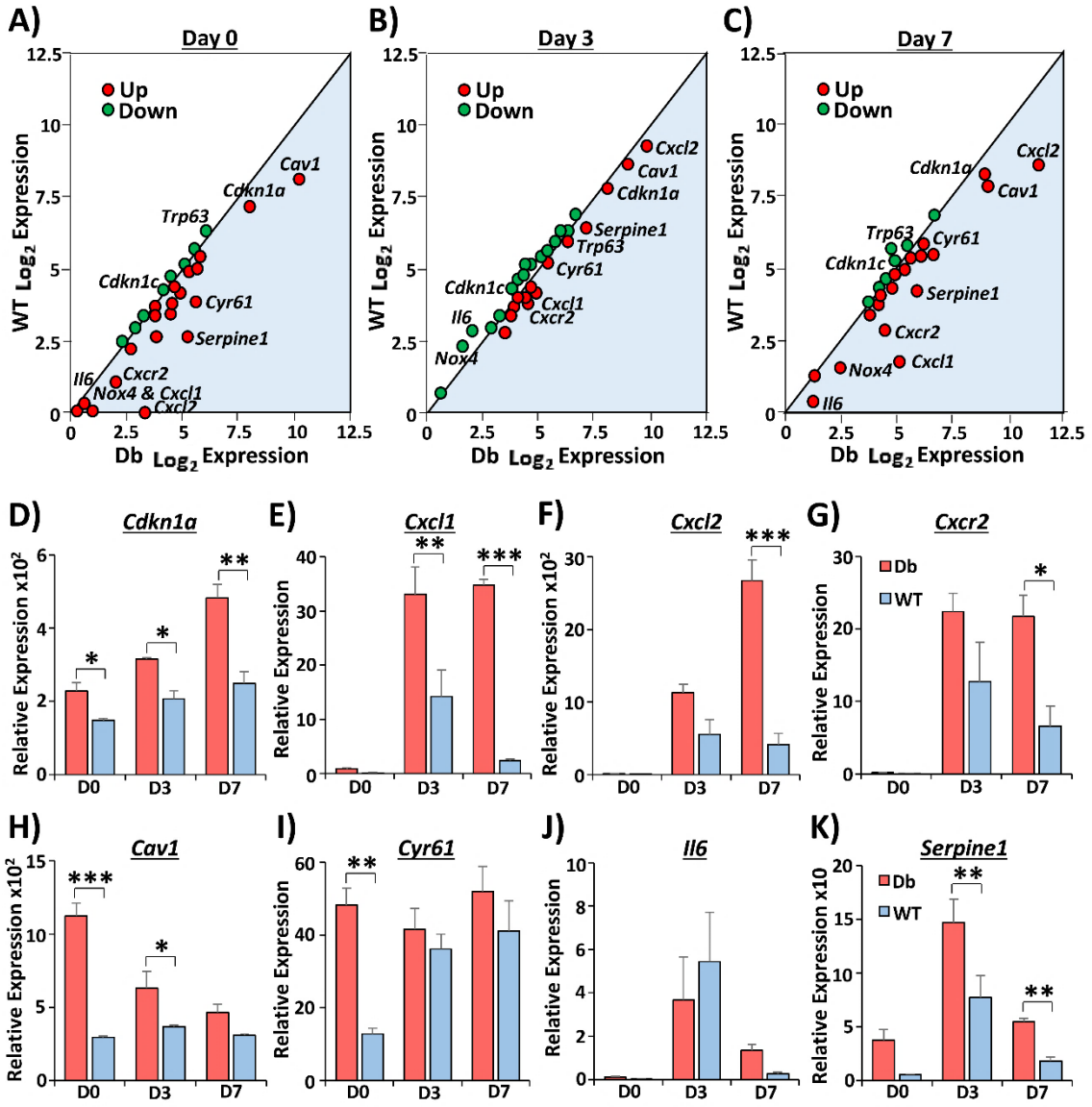

Figure 4.34. Senescence-linked genes are differentially expressed in diabetic and normal skin and wounds. Scatterplots show log_2 fold change expression of a number of senescence genes between diabetic (Db) and wild-type (WT) skin (D0, day 0, **A**) and wounds at day 3 (D3, **B**) and day 7 (D7, **C**) post-injury. Up = upregulated in Db. Down = downregulated in Db. Individual comparisons highlighted from transcriptional profiling data (**D-K**). n = 3 mice per group. Mean + SEM. Two-way ANOVA with Tukey's *post-hoc* analysis performed. * = $P < 0.05$, ** = $P < 0.01$, *** = $P < 0.001$.

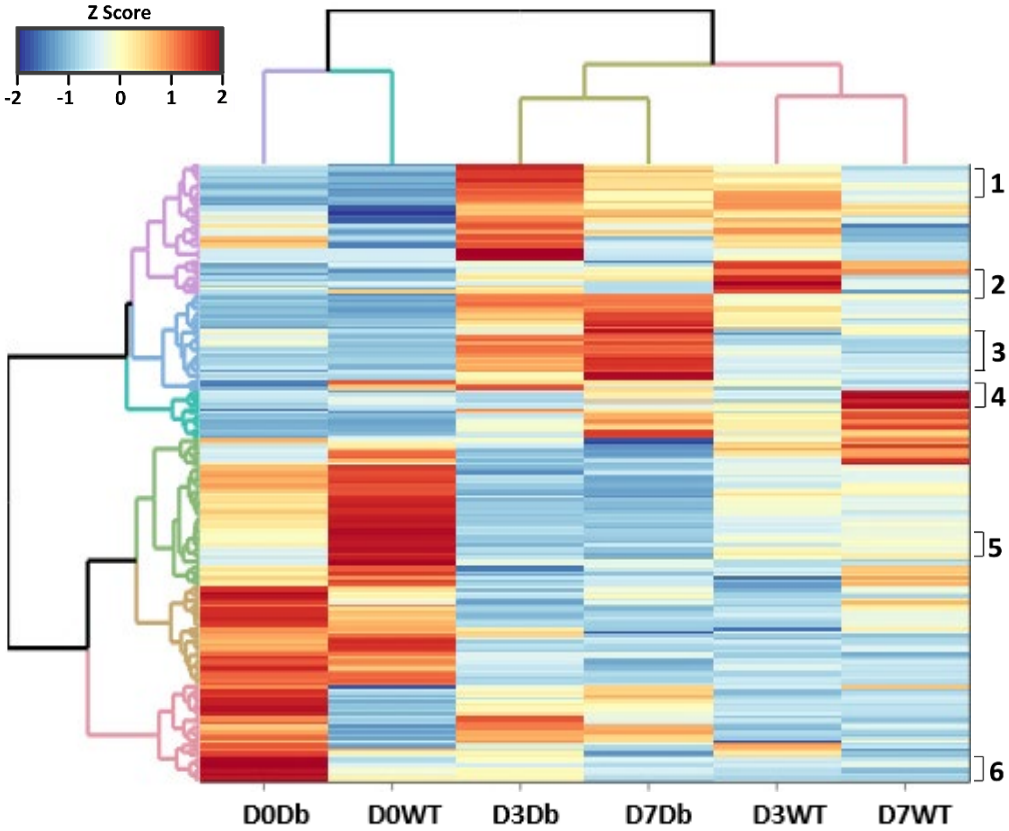

Cluster 1:	Cluster 2:	Cluster 3:	Cluster 4:	Cluster 5:	Cluster 6:
Hmox1	*Steap3*	*Steap2*	*Ido2*	*Cisd1*	*Alox15*
Itgam	*Plod2*	*Cyp2b19*	*Slc22a17*	*Ndufv2*	*Abat*
Hpx	*P4ha2*	*Nos2*	*Slc40a1*	*Cdkal1*	*Hpd*
	Scd1	*Mpo*	*Slc11a2*	*Ppat*	*Cat*
		Alox8	*Scd3*	*Hif1an*	*Heph*
		Ptgs2			

Figure 4.35. Hierarchal clustering of iron-associated genes in diabetic and normal skin and wounds. Clustergrams assembled based on Euclidian distance and Ward's D2 method. Differentially expressed genes from the significantly annotated UniProtKB iron pathway. Comparisons between diabetic (Db) and wild-type (WT) skin (D0) and wounds at day 3 (D3) and day 7 (D7) post-injury (n = 3 per group). Subsets of differential expressed gene clusters presented.

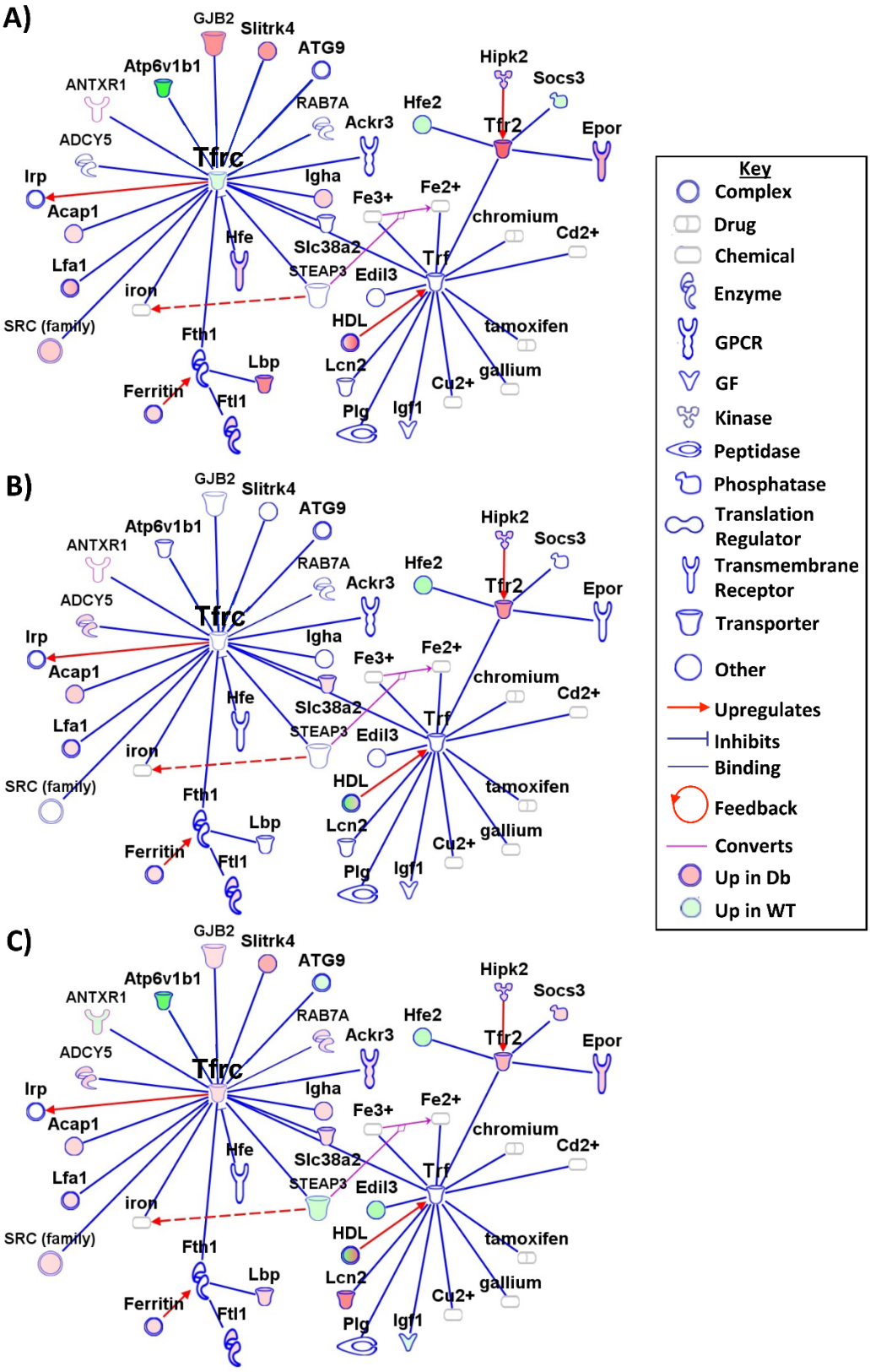

Figure 4.36. Tfrc network analysis illustrates different gene expression profiles in diabetic and normal healing mice. Pathways created in Ingenuity Pathway Analysis, with differential expression datasets overlaid. Diabetic (Db) versus wild-type (WT) comparisons in skin (**A**) and wounds at day 3 (**B**) and day 7 (**C**) post-injury. Key (right) illustrates complex type, relationship and expression (up in Db/WT). n = 3 mice per group.

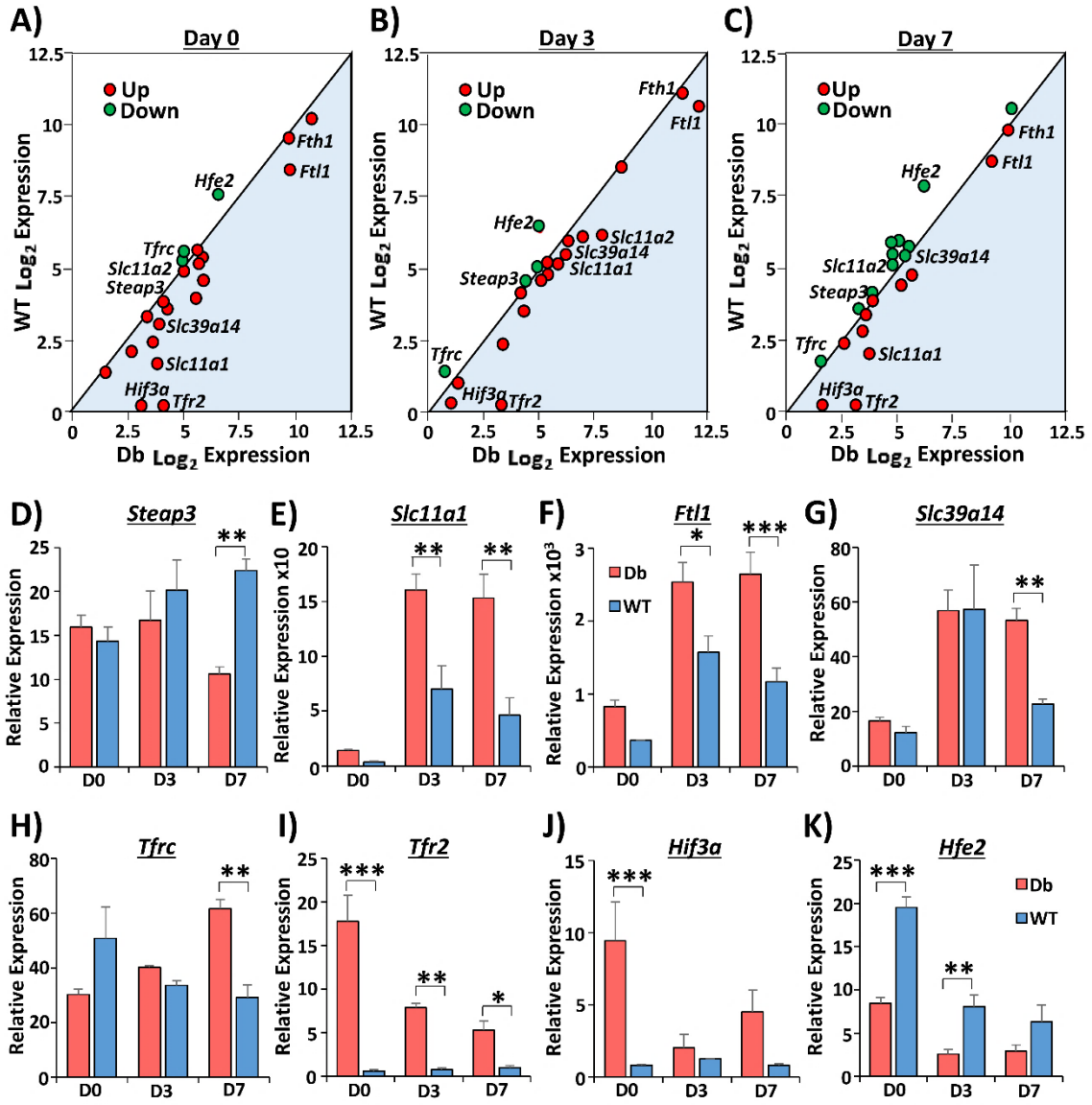

Figure 4.37. Diabetic skin and wounds display temporal changes in genes associated with iron processing. Scatterplots of genes filtered from RNA-sequencing data, depicting log_2 fold change expression between diabetic (Db) and wild-type (WT) skin (day 0, D0; **A**) and wounds at day 3 (D3; **B**) and day 7 (D7; **C**) post-injury. Up = upregulated in Db. Down = downregulated in Db. Individual genes were analysed (**D-K**) with two-way ANOVA and Tukey's *post-hoc* analysis. Mean + SEM. * = $P < 0.05$, ** = $P < 0.01$, ***= $P < 0.001$. n = 3 mice per group.

4.5. Discussion

Endogenous metals are a requirement for all life, and despite obvious applications for metals in biomedicine, the study of metals in biology is a fairly new concept. Emerging evidence is uncovering how specific metals are linked to pathologies such as ageing (Möller et al., 2019) and diabetes (Fernández-Cao et al., 2019). However, understanding of how temporospatial fluctuations in metals may contribute to disease remains limited. The role of the metallome in orchestrating cellular and molecular processes is even more unclear in skin. Here, research is focussed on simple *in vitro* assessments of cellular behaviours following metal administration (e.g. Doyle et al., 1996), or measuring metal bioaccumulation following treatment or occupational exposure (Al-Dayel et al., 2011; Bianco et al., 2015; Lidén et al., 2008). The present work therefore aimed to determine how the principle skin-related endogenous metals were altered temporally and spatially throughout normal and pathological wound repair. Indeed, this information would provide a platform to underpin further studies exploring the mechanistic consequences of skin metallome dysbiosis and addressing clinical translation.

A previous study attempted to characterise endogenous metal abundance in rat skin wound healing (Lansdown et al., 1999). Here the authors used FAAS, a technique up to a thousand times less sensitive than ICP-MS for some of the elements analysed in the present work (Liu et al., 2014b). However, Lansdown et al. (1999) did show that calcium, magnesium, zinc and copper levels fluctuated throughout normal rat wound repair, with calcium and magnesium peaking at day 5 post-injury, when wounds had fully re-epithelialised. Data presented in this thesis confirm similar changes in calcium and magnesium, while significantly extending understanding of time-dependent variations in iron, zinc, aluminium, copper and manganese during normal murine skin healing (**Figure 4.6;** summarised in **Figure 4.38**). Here, calcium abundance peaked at times correlating with inflammation and proliferation, but was significantly downregulated at later-stage healing (D14). Copper and magnesium were elevated at D7, while the transition metals iron, aluminium, and manganese were highest at D7 and D14. Spatial measurements (LA-ICP-MS) provide an additional level of characterisation, clearly demonstrating that metals were differentially localised in late-stage healing wounds (**Figure 4.9**) and thus likely associated with diverse healing processes.

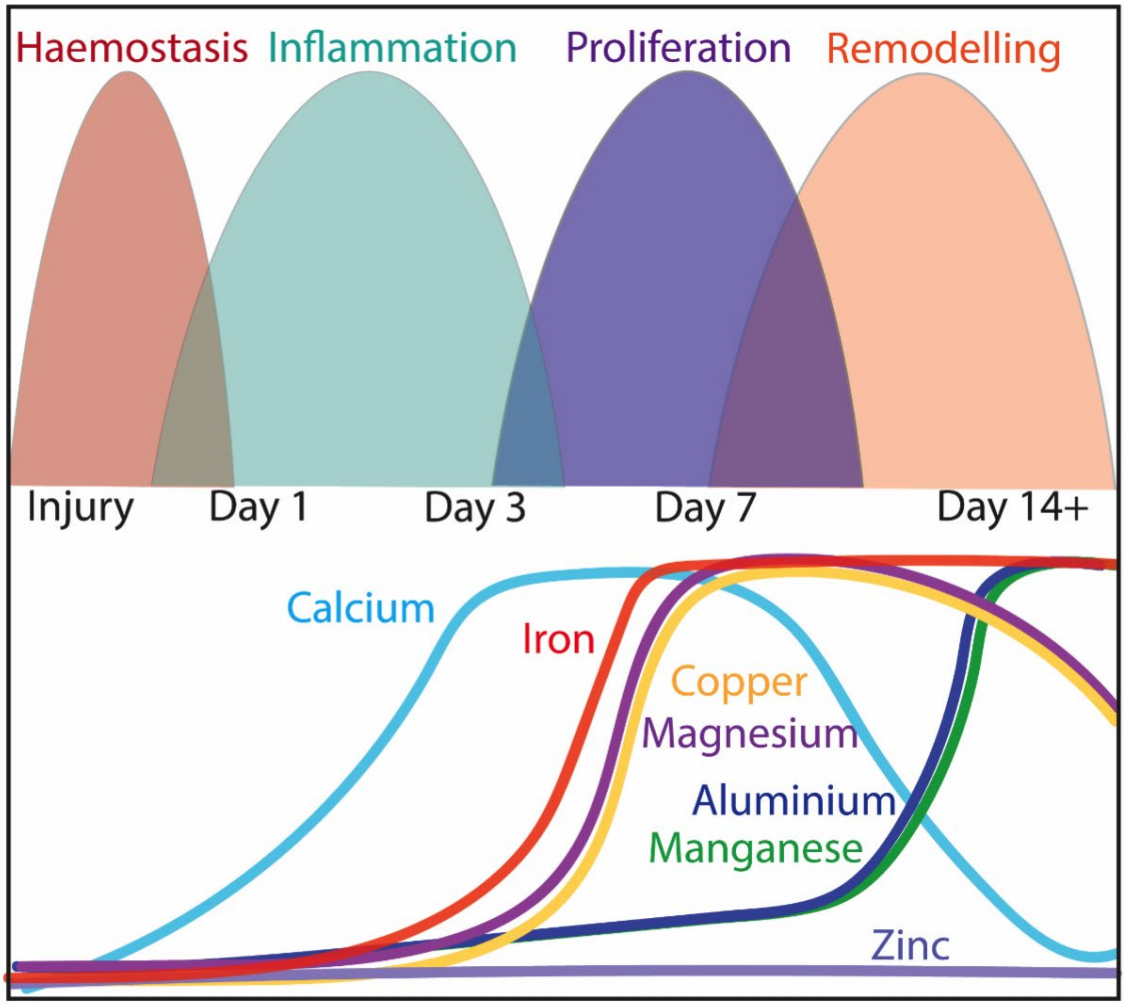

Figure 4.38. Summary of the temporal profile of metals throughout normal healing, and their corresponding wound repair stages. Calcium abundance was greatest at stages correlating with inflammation and repair and was downregulated at later-stage healing. Iron levels were elevated at stages correlating with proliferation and matrix remodelling. Copper and magnesium increased during the proliferative phase, while and aluminium and manganese were highest during remodelling. All changes versus normal skin. *Figure by the author (HNW).*

The relationship between ECM production and transition metals has been confirmed previously in a number of studies. For example, overexpression of manganese superoxide dismutase (MnSOD) caused contraction of collagen gel lattices, and substantially increased TGFβ1 expression and cytoplasmic H_2O_2 production in fibroblasts (Treiber et al., 2009), while overexpression of MnSOD in murine mesangial cells caused accumulation of collagen (hydroxyproline; Craven et al., 2001). Treatment of mice and human airway epithelial (H292) cells with copper nanoparticles led to similar results by increasing production of TGFβ1 (Ko et al., 2018), a potent stimulator of ECM production (Leask, 2010; Ohmaru-Nakanishi et al., 2018). Copper, largely recognised for its role in angiogenesis (Das et al., 2016),

is crucial for the functioning of the collagen-stabilising lysyl oxidase (LOX) enzymes (Csiszar, 2001; Lucero and Kagan, 2006). *LOX* knockdown contributes to impaired collagen production in multiple experimental models (human skin equivalents, Huang et al., 2019; hepatic stellate cells, Ma et al., 2018a), thus demonstrating its significance in ECM maintenance. An additional recent association has been made between iron and ECM deposition and remodelling (Wilkinson et al., 2019c), with a mechanistic explanation for this phenomenon described in detail in **Chapter 5**. Collectively, these data reinforce the importance of preserving timely fluctuations in metals to regulate normal wound-relevant cellular behaviours.

Crucially, novel differential alterations in the metallome were revealed in pathological aged and Db skin and wounds (**Figure 4.7**). A major reduction in calcium was observed, which is consistent with previous analyses of human skin, where decreased epidermal calcium was shown with ageing (FAAS and histology, Rinnerthaler et al., 2013). As the epidermal calcium gradient is vital for normal skin barrier function (reviewed in Feingold & Denda, 2012), the age-related decline in epidermal calcium may contribute to reduced barrier integrity and increased chronic wound susceptibility (reviewed in Sen, 2009). However, it remains difficult to determine from existing data whether pathological alterations in the skin metallome are associated with delayed healing in a correlative or causative manner.

Calcium perturbations are connected to multiple age-associated disorders (e.g. Alzheimer's disease, Mattson, 2007; Simpson et al., 2011) and mutations in Ca^{2+} signalling can cause various pathologies (reviewed in Missiaen et al., 2000). In fact, disturbed modulation of intracellular Ca^{2+} may be linked to diabetes as it is essential for normal glucose metabolism (reviewed in Guerrero-Hernandez & Verkhratsky, 2014). Although direct research relating calcium to pathological skin repair is lacking, some data exists demonstrating links between abnormal calcium and chronic healing environments. During hypoxia for example, cell-cell communication is lost between sensory neurons and epithelial cells, and Ca^{2+} mobilisation and propagation upon epithelial injury is diminished, leading to delayed corneal epithelial repair (in rats, Lee et al., 2014a).

There is already substantial literature demonstrating the role of calcium in keratinocyte differentiation (Bikle et al., 2001), where calcium-induced stratification was described nearly forty years ago (Hennings et al., 1980; Hennings

& Holbrook, 1983). Indeed, many cornified envelope markers are under the control of calcium and calcium response elements, requiring calcium at concentrations above 0.1 mM (Rinnerthaler et al., 2015). It is therefore unsurprising that high calcium led to upregulation of differentiation markers in NHEKs (KRT1 and loricrin, **Figure 4.13**) and normal MEKs (including *Krt1* and *Sprr2*; **Figure 4.11**). Of significant interest was the observation that Db MEKs were intrinsically altered, displaying reduced migratory capacity and perturbed responses to calcium (reduced *Krt1*, *Ivl*, *Sprr2* and *Casr*; **Figure 4.12**). Here, it is known that compromised Ca^{2+} signalling, particularly release of Ca^{2+} from the ER, leads to impaired keratinocyte migration (Trollinger et al., 2002) and improper stratification (Celli et al., 2011; Celli et al., 2016). Hence, these data propose a critical association between reduced responsiveness to calcium and loss of cell function in Db MEKs.

Calcium administration increased *Casr* expression in normal MEKs and NHEKs (**Figure 4.11** and **Figure 4.13**). In tissue, *Casr* expression was induced upon injury during normal healing (**Figure 4.6**), but impaired in the Db model (**Figure 4.10**). In mice, keratinocyte-specific ablation of *Casr* caused loss of the epidermal Ca^{2+} gradient, reduced the expression of terminal differentiation markers, and led to skin barrier defects (Tu et al., 2012). Similarly, loss of CaSR in NHEKs inhibited calcium-induced differentiation (Tu et al., 2008), while overexpression of CaSR in basal keratinocytes enhanced epidermal permeability barrier formation and accelerated hair growth during murine development (Turksen & Troy, 2003). Hence, abnormal CaSR expression may contribute to diabetic cellular defects during wound healing.

Ca^{2+} propagation in epithelial wound healing is a conserved process that occurs following injury in invertebrates (*Drosophila melangaster* embryos, Razzell et al., 2013; *Caenorhabditis elegans*, Xu & Chisholm, 2011), *Xenopus laevis* (Soto et al., 2013), zebrafish (Yoo et al., 2012), murine skin *ex vivo* (Tu et al., 2019), murine epithelial cells (Leiper et al., 2006) and human keratinocytes *in vitro* (Tsutsumi et al., 2013). As reduced calcium and altered expression of calcium genes was observed in Db skin, dysregulated calcium processing may contribute to reduced skin integrity and impaired wound healing in the Db model. Indeed, blocking Ca^{2+} propagation caused delayed re-epithelialisation in murine skin and human keratinocytes (Tu et al., 2019), while keratinocyte-specific ablation of Casr alone (Tu et al., 2019) and in combination with the Vdr (Oda et al., 2017) led to delayed re-

epithelialisation of mouse wounds *in vivo*. Consequently, it is clear that impaired epidermal calcium homeostasis is linked to poor healing.

Most of the literature pertaining to the role of calcium in wound repair relates to the epidermal calcium gradient (described above), while less evidence exists for the role of calcium in dermal reformation and maintenance. Dermal remodelling occurs during development, ageing, and repair (Antonicelli et al., 2007; Haydont et al., 2019). Until recently, collagen fibrils were thought to be relatively static (based on their incredibly long half-lives; Screen et al., 2015). However, new data has challenged this dogma, demonstrating that tendon ECM undergoes daily, homeostatic turnover regulated by circadian rhythm (Chang et al., 2019). This opens up questions about dermal ECM remodelling and whether Ca^{2+}, and other metals, may not only be connected to formation of the dermis during development and repair, but also to these daily oscillations in matrix breakdown.

Preliminary LA-ICP-MS data presented in this thesis reveal, somewhat controversially, that calcium is higher in the dermis than epidermis (**Figure 4.9**). In fact, calcium signalling (e.g. through TRPV4) is involved in myofibroblast differentiation and contributes to fibrosis (Rahaman et al., 2014; Sharma et al., 2017). Thus, it would be fascinating to determine whether exogenous calcium-induced ECM deposition identified in the present work was the result of HDF differentiation. Calcium also clearly dose-dependently altered HDF migratory behaviours and contraction (as shown earlier, Kawai et al., 2011; Navarro-Requena et al., 2018), and led to previously unreported effects on adhesion (**Figure 4.17**).

Calcium maintains the structural integrity of many matrix proteins, such as fibrillin-1 (Handford, 2000) and collagen I (Cabral et al., 2016), while MMPs, required for ECM remodelling, are calcium- and zinc-dependent (reviewed in Singh et al., 2015). Likewise, laminins, thrombospondins and proteoglycans possess calcium binding sites, as they can be extracted using the Ca^{2+} chelator EDTA (Foulcer et al., 2015; Glasgow et al., 2016). Mutations in the calcium binding sites of these structural proteins leads to a plethora of connective tissue disorders (reviewed in Maurer & Hohenester, 1997; Sherratt et al., 2007; Thur et al., 2001).

The role of calcium in modulating ECM becomes even more apparent in mechanistic knockdown experiments. Pharmacological inhibition of calcium influx decreased angiotensin II-induced collagen I, fibronectin and CTGF protein expression in

cardiac fibroblasts (Chen et al., 2017). Genetic knockdown of the calcium binding protein, calreticulin (Bedard et al., 2005), dampened collagen transcription and deposition (Graham et al., 2010b) and reduced Tgfβ1-dependent collagen I synthesis, which was rescued by calreticulin treatment (in MEFs; Zimmermann et al., 2013). In murine wound healing, intravenous administration of calcium chloride or calcium nanoparticles improved re-epithelialisation and reduced scarring (Kawai et al., 2011), while calreticulin treatment accelerated wound closure and granulation tissue formation in Db mouse wounds, and dose-dependently improved MEF scratch wound closure (Greives et al., 2012). As aged (Peterson et al., 1989) and diabetic (Husni et al., 2014) fibroblasts show impaired Ca^{2+} signalling and reduced ECM production (aged, Cole et al., 2018; Db, Maione et al., 2016), this research suggests that calcium and calcium-regulated proteins are required for ECM production, remodelling and maintenance.

Calcium is important for orchestrating cell migration (reviewed in Minton, 2014), in part through calcium flickers at the leading edge of migrating cells, modulated via the stretch-activated calcium channel, TRPM7 (Wei et al., 2009) and others. Wei et al. (2009) further hypothesised that calcium flickers may control cell steering and chemotaxis. As calcium was the only metal under study to significant accumulate in early repair, it was suggested to be important in early wound signalling events. Indeed, the Ca^{2+} flashes observed upon injury are not only critical for adequate re-epithelialisation, but act as a cue to draw inflammatory cells to the site of injury (Razzell et al., 2013; reviewed in Wood & Martin, 2017). Ca^{2+} signalling in leukocytes is also vital for inflammatory purposes, as calcium directly modulates the NLRP3 inflammasome pathway, where it increases ROS production (Murakami et al., 2012) and promotes assembly of NLRP3 components (Lee et al., 2012). Moreover, store-operated calcium entry is importantly linked to ROS production in neutrophils (Clemens et al., 2017) and Mφs (Jin et al., 2006).

The importance of calcium on immunological function is further demonstrated through calcium inhibition, where calcium chelation prevents Rankl-induced differentiation in BMDMs (Zhou et al., 2010) and genetic knockdown of important calcium signalling factors impairs chemokine production (Trpm2 in monocytes, Wehrhahn et al., 2010) and phagocytosis (Trpv2 in murine peritoneal Mφs, Link et al., 2010). Of note, altered Ca^{2+} signalling is observed in Mφs from *ob/ob* mice (Liang

et al., 2012; Li et al., 2009). These studies are in keeping with the current work revealing that low calcium reduced differentiation in THP-1 cells (**Figure 4.19**) and hindered phagocytosis in murine BMDMs (**Appendix 4A.7**). Bone marrow-mediated calcium influx also promotes Mφ-driven angiogenesis in ischemic sites *in vivo* (Wu et al., 2009), hence identifying an additional wound-relevant benefit of calcium-mediated governance of immune cell function.

Of the candidate calcium genes assessed, *Calm1*, a gene encoding the cytosolic Ca^{2+}-binding protein calmodulin (Edsberg et al., 2012), displayed one of the most interesting profiles. Although its transcription was unaltered throughout normal repair, *Calm1* was downregulated in aged and Db wounds (**Figure 4.10**) and lower in M0, M1 and M2-stimulated Db Mφs (**Figure 4.18**). Calmodulin-linked genes were also DE in RNA-Seq analysis (**Figure 4.27** and **Figure 4.31**). In keratinocytes, *Calm1* expression was induced upon calcium administration (**Figure 4.11** and **Figure 4.13**). It follows that calmodulin, and other calcium-binding proteins, regulate epidermal differentiation (Fairley et al., 1985). Despite these data demonstrating clear perturbations in *Calm1* in ageing and diabetes, little evidence exists linking calmodulin to these pathologies. In fact, the relationship between calmodulin and diabetes is controversial. Calmodulin is implicated in driving the pathogenesis of diabetes by upregulating Ca^{2+} signalling in pancreatic β cells (Epstein et al., 1989; Epstein et al., 1992), and genetically obese mice possess increased calmodulin expression in kidney and heart tissue (Morley et al., 1982). Yet others have shown that streptozocin induction of diabetes leads to significant loss of calmodulin expression (Öztürk et al., 1994), thus demonstrating the importance of evaluating studies in a context-dependent manner.

A transcriptomic approach allowed the direct identification of key gene expression signatures in normal and pathological skin and wounds. Numerous DE genes were identified and multiple annotated pathways significantly enriched. Within the analysis of this plethora of information, the DE data set was found be enriched for the UniProtKB pathways “calcium” and “metals”, and the Gene Ontology pathway “aging”. Of interest, transcriptional profiling demonstrated high annotation of iron, calcium and copper in normal wounds at the same time as their elemental levels accumulated (**Figure 4.25**). Hierarchal clustering analysis of the subsets of DE genes annotated in calcium and metal-based pathways provided additional insight into the

global ties between the metallome and transcriptome, revealing a number of key, metal-linked genes that are differentially expressed between WT and Db tissues.

IPA network analysis expanded the DE gene data, constructing gene networks around calcium, CaSR and calmodulin (**Figure 4.28-4.30**). Here, magnesium, the second most abundant metal in the body, was shown to directly bind calmodulin. Magnesium is pivotal in the regulation and function of many enzymes and channels (Luo et al., 2012), with calcium and magnesium playing combinatorial and antagonistic roles in different cellular contexts. Magnesium alone is antithrombotic, but when combined with calcium, promotes calcium-dependent thrombin production and coagulation (reviewed in Tavoosi & Morrissey, 2014). On the contrary, magnesium prevents calcification in many pathologies (reviewed by Floege, 2015; Villa-Bellosta, 2017). Interestingly, magnesium deficiency has long been associated with T2DM, where magnesium is crucial for glucose and insulin metabolism (Gröber et al., 2015), and reduced serum magnesium is seen in diabetic patients (Resnick et al., 1993; Song et al., 2005). Of note, ICP-MS confirmed that magnesium levels were reduced in murine Db skin and wounds.

RNA-Seq analysis also focussed on senescence, as work in this thesis established that Db wound healing is heavily influenced by senescence and the senescence-associated receptor, CXCR2 (**Chapter 3**). One particularly exciting observation came from the hierarchal clustering analysis of highly enriched pathways. In most cases, D3 and D7 wounds clustered more closely to each other within genotype, but when hierarchal clustering was performed on genes from the "ageing" Gene Ontology pathway, D3 Db and WT, and D7 Db and WT profiles were more similar (**Figure 4.32**). It is known that senescence is induced in normal healing wounds at D7 to aid myofibroblast differentiation (Demaria et al., 2014) and proper tissue resolution (Jun & Lau, 2010), while senescent cells accumulate in Db wounds and exacerbate pathology (**Chapter 3**). This is interesting, and demonstrates that although WT and Db wound "ageing" profiles show a high degree of similarity, that senescence induction can lead to opposing tissue outcomes in different cellular environments. An example of this is with cancer, whereby senescence terminates uncontrolled cell growth and prevents neoplastic transformation (Campisi & Robert, 2014), yet accumulation of senescent cells and their SASP can drive tumour formation in nearby tissues (Farsam et al., 2016).

IPA pathways were also constructed to determine the associations between senescence markers. RNA-Seq confirmed previous findings in **Chapter 3**, demonstrating upregulation of key senescence markers in Db skin and wounds (*Cdkn1a*, *Cxcl1*, *Cxcl2* and *Cxcr2*) and pathway analysis revealed new links between *Cxcr2* and transcription factors such as *Klf7* (**Figure 4.33**). The Krüppel-like factor (KLF) family of transcription factors are important in cell development and differentiation (Ghaleb & Yang, 2017), and appear to play pivotal roles in adipogenesis (Moreno-Navarrete et al., 2017). KLF7 in particular has been suggested to confer susceptibility to the development of T2DM through impaired insulin biosynthesis and secretion (Kanazawa et al., 2006), and through its role in modulating IL-6 (Zhang et al., 2018). An association has also been made between the major A-allele of rs2302870 in *KLF7* and diabetes in a Japanese population (Kanazawa et al., 2005). By contrast, no correlations were made between *KLF7* and T2DM during screening of a Danish population (Zobel et al., 2009). Therefore, currently no robust data exists to demonstrate a fervent connection between *KLF7* and T2DM. Other interesting observations included the specific upregulation of a number of senescence-linked genes in WT wounds only. One such factor was *Cav3*, important for calcium channel activity (Garcia-Caballero et al., 2018) and the regulation of cell proliferation (Hu et al., 2018). Interestingly, siRNA silencing of *CAV3* upregulated p21 in *vitro* (Li et al., 2011). These data propose that the transcriptional control of these senescence-linked factors, and their relationships to metals such as calcium, may be key in understanding the functional differences between normal and diabetic-induced senescence in wound healing.

Another metal-based pathway that was highly enriched in functional annotation analysis was iron, a metal with high dermal wound accumulation (**Figure 4.9**). Pathways were developed in IPA to determine the links between major iron processing components (described in **Chapter 5**), which were temporally and pathologically altered. For example, *Steap3* was upregulated in WT wounds, while *Steap2* was more highly expressed in Db wounds (**Figure 4.35**), and *Tfrc*, although higher in WT skin, was elevated in Db D7 wounds (**Figure 4.37**). The role of iron in wound repair will been explored in depth in **Chapter 5**.

In conclusion, the results obtained in this chapter show that metal abundance is altered spatially and temporally in normal and pathological healing wounds. Metals orchestrate many aspects of the dynamic healing process in a conserved manner by centrally controlling wound-relevant cellular behaviours. Transcriptional profiling elucidated a novel link between the genome and metallome, where a large subset of genes DE during healing were connected to essential, metal-regulated processes (summarised in **Figure 4.39**). Indeed, these data establish a fundamental, exciting new role for metals in normal and pathological repair, highlighting a timely need to explore the metallome in acute and chronic wounds in the clinical setting.

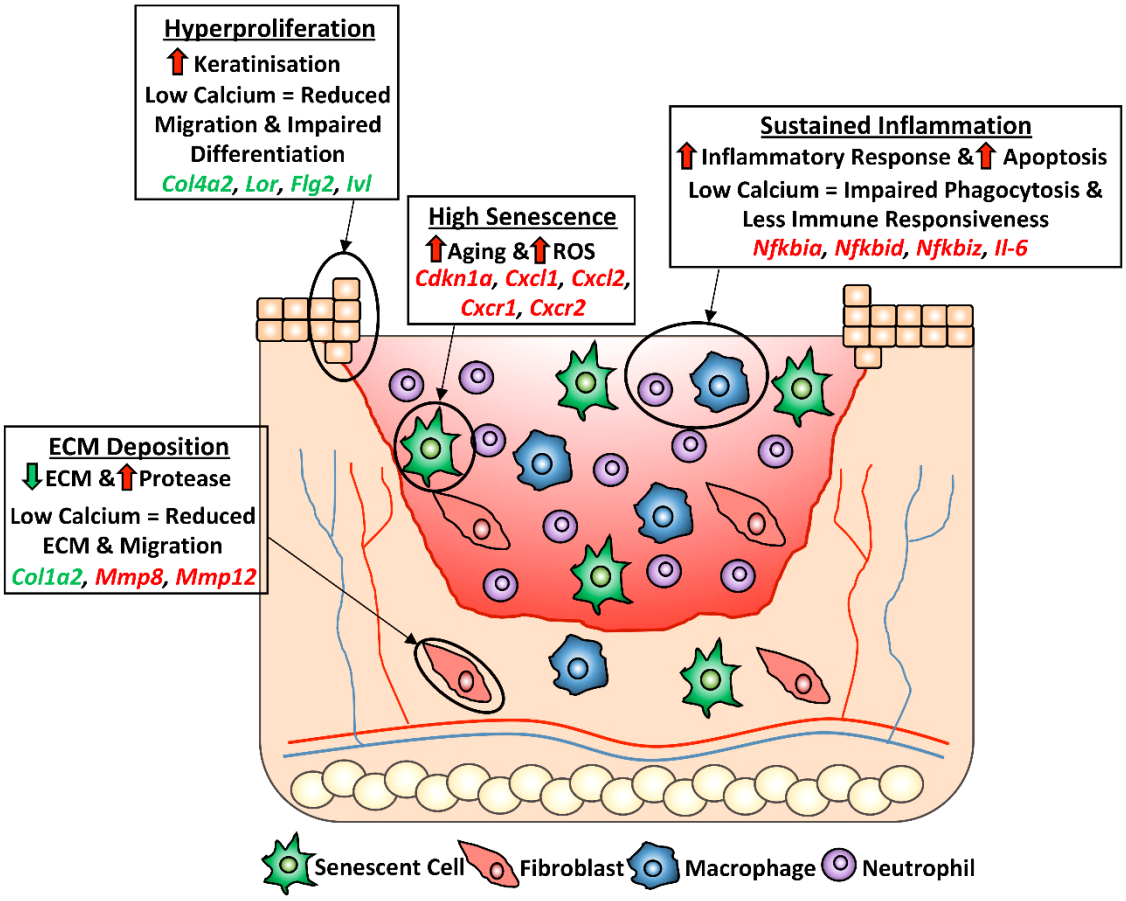

Figure 4.39. Linking the metallome, transcriptome and senescence to known mechanisms of pathological diabetic wound repair. Diabetic (Db) pathological healing wounds show hyperproliferation at the wound edge, high levels of senescence, sustained inflammation and reduced extracellular matrix (ECM) deposition (underlined). Highly annotated RNA-sequencing (RNA-Seq) pathways associated with each pathological healing process shown in each box (first). Cellular effect of low calcium correlated highly with functional process defects (second). A small subset of RNA-Seq genes specific to each process and altered in Db wounds also shown (final). Green arrows/genes = downregulated in diabetic. Red arrows/genes = upregulated in diabetic. *Figure by the author (HNW).*

Chapter 5: Iron Influences Macrophage and Fibroblast Behaviour to Promote Late-Stage Wound Repair

Data presented in this chapter also appears in the following publications:

Reduced iron in diabetic wounds: An oxidative stress-dependent role for STEAP3 in extracellular matrix deposition and remodelling.

Authors: Holly N. Wilkinson[1], Sophie E. Upson[1], Kayleigh L. Banyard[1], Robert Knight[2], Kimberly A. Mace[3] and Matthew J. Hardman[1*]

2019 J Invest Dermatol

139, Issue 11, Pages 2368–2377. DOI: 10.1016/j.jid.2019.05.014

Affiliations: [1]Centre for Atherothrombosis and Metabolic Disease, Hull York Medical School, The University of Hull, HU6 7RX, United Kingdom. [2]Faculty of Science and Engineering, The University of Hull, HU6 7RX, United Kingdom. [3]Faculty of Biology, Medicine and Health, The University of Manchester, M13 9PT, United Kingdom.

Tissue iron promotes wound repair via M2 macrophage polarisation and the chemokines CCL17 and CCL22.

Authors: Holly N. Wilkinson[1], Elizabeth R. Roberts[1], Amber R. Stafford[1], Kayleigh L. Banyard[1], Paolo Matteucci[2], Kimberly A. Mace[3] and Matthew J. Hardman[1].

2019 Am J Pathol

189, Issue 11, Pages 2196-2208. DOI: 10.1016/j.ajpath.2019.07.015

Affiliations: [1]Centre for Atherothrombosis and Metabolic Disease, Hull York Medical School, The University of Hull, HU6 7RX, United Kingdom. [2]Hull University Teaching Hospitals NHS Trust, United Kingdom. [3]Faculty of Biology, Medicine and Health, The University of Manchester, M13 9PT, United Kingdom.

Author contributions: All work presented in this chapter was carried out by HNW. Additional optimisation was carried out by SEU, KLB, ERR and ARS. ICP-MS preparation and interpretation was carried out by HNW, samples were run by RK. PM provided human tissue. HNW performed *in vivo* experiments with KAM. HNW and MJH were involved in study concept and design and manuscript preparation.

5.1. Introduction

Iron is one of the body's most abundant trace elements, responsible for orchestrating a diverse range of cellular functions. The importance of iron pertains to its reactive nature, where it can drive biological processes that require electron transfer, such as oxidative phosphorylation, DNA synthesis and repair (Bogdan et al., 2016). Thus, it is unsurprising that both iron deficiency and accumulation can lead to a range of metabolic abnormalities (e.g. anaemia and hemochromatosis; Bridle et al., 2003). The function of iron in many disease states has been described at length (e.g. chronic inflammation; Cullis, 2011). However, current understanding of how iron interplays with the innate wound healing response is limited. Therefore, this chapter will explore iron in the context of modulating crucial repair processes, with further investigation into its role in pathological diabetic healing.

5.1.1. Iron as a Life-Forming Trace Metal

Iron (chemical symbol Fe, from the latin *ferrum*) is a well-known transition metal. It retains eight oxidative states (-6 to +2) in total, which confer its redox potential (Frey & Reed, 2012). However, only two states are biologically important, ferrous and ferric (Fe^{2+} and Fe^{3+}, respectively; Philpott et al., 2017). The most noted reaction involving Fe^{2+} and Fe^{3+} is the Fenton reaction (Barbusiński et al., 2009; summarised in **Figure 5.1**). Iron can complex with organic compounds, and remains a critical cofactor for a multitude of enzymes (Philpott et al., 2017). Hence it is unsurprising that iron was likely to be central to life's evolutionary advancement, prior to the Great Oxidation Event (2.4 billion years ago, Dupont et al., 2010; Harel et al., 2014). As Fe^{2+} is found in anoxic environments (Hazen & Ferry, 2010), Fe^{3+} enabled redox reactions in Eubacteria and Archeabacteria, forming the basis of cellular metabolism long before oxygen became environmentally available. Today, some microorganisms remain relics of the past, preserving anaerobic iron-regulated respiration (e.g. lithotrophs; Singh et al., 2018).

In higher eukaryotes, the redox potential of iron is utilised in oxygen metabolism, where it can act as an oxygen or electron transporter (Dixon & Stockwell, 2014). Iron is crucially associated with three main protein groups: heme-containing proteins for oxygen metabolism; Fe-sulfur cluster-containing proteins for electron transport and; iron-containing enzymes devoid of sulphur clusters that provide a myriad of functions (Arezes & Nemeth, 2015). As the oxygen-rich environment

favours ferrous iron at neutral pH, Fe^{2+} is reduced to Fe^{3+} to cross the plasma membrane. This occurs through acidification in eukaryotes (Sharp, 2010) and through siderophores in prokaryotes (Neilands, 1995).

$$Fe^{2+} + H_2O_2 \longrightarrow Fe^{3+} + OH^- + OH^\bullet \quad (1)$$

$$OH^\bullet + H_2O_2 \longrightarrow HO_2^\bullet + H_2O \quad (2)$$

$$Fe^{3+} + HO_2^\bullet \longrightarrow Fe^{2+} + H^+ + O_2 \quad (3)$$

$$Fe^{2+} + HO_2^\bullet \longrightarrow Fe^{3+} + HO_2^- \quad (4)$$

$$Fe^{2+} + OH^\bullet \longrightarrow Fe^{3+} + OH^- \quad (5)$$

Figure 5.1. The Fenton chain reaction. Fe^{2+} reacts with H_2O_2 leading to the release of hydroxyl free radicals (OH•), hydroxide ions (OH-) and Fe^{3+} in the typical Fenton reaction (**1**). Steps **2** and **3** then ensue, leading to O_2 and H_2O release, but this also causes the production of hydroperoxyl radicals (HO_2•) and hydrogen ions (H^+). The chain reaction is terminated by steps **4** and **5**. The free radical by-products cause cellular damage; thus, iron is tightly controlled within the body to prevent unwanted oxidative reactions. *Taken from Barbusiński et al. (2009).*

In mammalian physiology, Fe^{3+} is more stable than Fe^{2+}, which reduces O_2 to form free radicals that cause lipid peroxidation, and degradation of proteins and carbohydrates (Ray et al., 2012). As a result, the body has evolved critically sensitive mechanisms that tightly regulate dynamic iron fluxes to prevent cellular toxicity. These include sophisticated coordination between intestinal iron uptake, transport, and cellular sequestration, which will be examined in further detail below.

5.1.2. Iron Uptake and Transport

In healthy individuals, total bodily iron ranges from 3-5 g, yet dietary iron intake only accounts for a minute proportion of the amount necessary to replace small daily losses (urination, bleeding, sweating, skin desquamation; Moll & Davis, 2017). The largest bodily iron demand comes from haemoglobin, whose requirement is met by the reprocessing of ageing erythrocytes by specialised splenic Mφs (Arezes & Nemeth, 2015). Most cell types require very little iron for metabolic processes. Notably, muscles (myoglobin) use approximately 2.5% of the daily iron budget for oxygenation (Papanikolaou & Pantopoulos, 2017). Total body iron is stored in haemoglobin (heme iron; 70%) and in the intracellular stores of hepatocytes (20%) and Mφs (5%; non-heme iron; Arezes & Nemeth, 2015).

Like most nutrients, ingested iron enters the enterocytes of the duodenum lining. At the enterocyte brush border, iron is absorbed as a protein complex (heme, broken down by heme oxygenase 1, HO-1), or as free iron (Fe^{3+}), which is reduced to Fe^{2+} by ascorbic acid and the ferric reductase enzyme, duodenal cytochrome B (Dcytb, Sharp, 2010). Divalent metal transporter 1 (DMT1) then transports iron (plus divalent metals) across the cell membrane and into the enterocyte (Gulec et al., 2014). Intracellular iron is subsequently stored in ferritin or driven to the basolateral membrane for transport into the body via the only known cellular iron exporter, ferroportin (reviewed in Arezes & Nemeth, 2015). The role of ferroportin, a member of the large solute carrier gene family (Drakesmith et al., 2015), was first elucidated in transgenic mice, where exclusive deletion of ferroportin in intestinal cells caused anaemia (Donovan et al., 2005). Additionally, mice with Mφ- (Zhang et al., 2011) and hepatocyte- (Zhang et al., 2012) specific ferroportin deletion became anaemic due to cellular sequestration of iron (Wang et al., 2018b), thus demonstrating the importance of ferroportin in regulating iron availability. The major pathways of intestinal iron absorption are illustrated in **Figure 5.2**.

At the extracellular (bodily) enterocyte surface, Fe^{3+} is oxidised by ferroxidases (hephaestin and ceruloplasmin; Vashchenko & MacGillivray, 2013), rapidly associates with serum transferrin (Tf), and is carried throughout the body to areas of requirement, such as the bone marrow (Papanikolaou & Pantopoulos, 2017). Serum Tf exists in three states to allow the body to respond appropriately to fluctuations in iron uptake. Tf can be iron-free (apo-Tf), bound to one iron molecule (monoferric Tf) or fully saturated (diferric Tf, of holo-Tf; Recalcati et al., 2017). Cellular uptake of Tf-bound iron (TBI) is mediated through the cell surface receptor, Tf receptor 1 (TfR1; Arezes & Nemeth, 2015). The TBI-TfR1 complex is internalised by clathrin-mediated endocytosis (Mayle et al., 2012), the pH of the endosome lowers, and Fe^{3+} is released from the Tf-TfR1 complex (Arezes & Nemeth, 2015). Six-transmembrane epithelial antigen of prostate 3 (STEAP3) reduces Fe^{3+} in the endosome to Fe^{2+}, which is transported to the cytoplasm by DMT1 (Muckenthaler et al., 2017). Meanwhile, the Tf-TfR1 complex returns to the cell surface and apo-Tf is released. Iron chaperones, such as poly (rc) binding protein 2 (PCBP2), exist to aid the transport of Fe^{2+} within the cell. PCBP2 binds to both DMT1 and ferroportin to aid extrication of cellular iron, so has been described as a "gatekeeper" to safely transport iron through the cytoplasm (Yanatori et al., 2017).

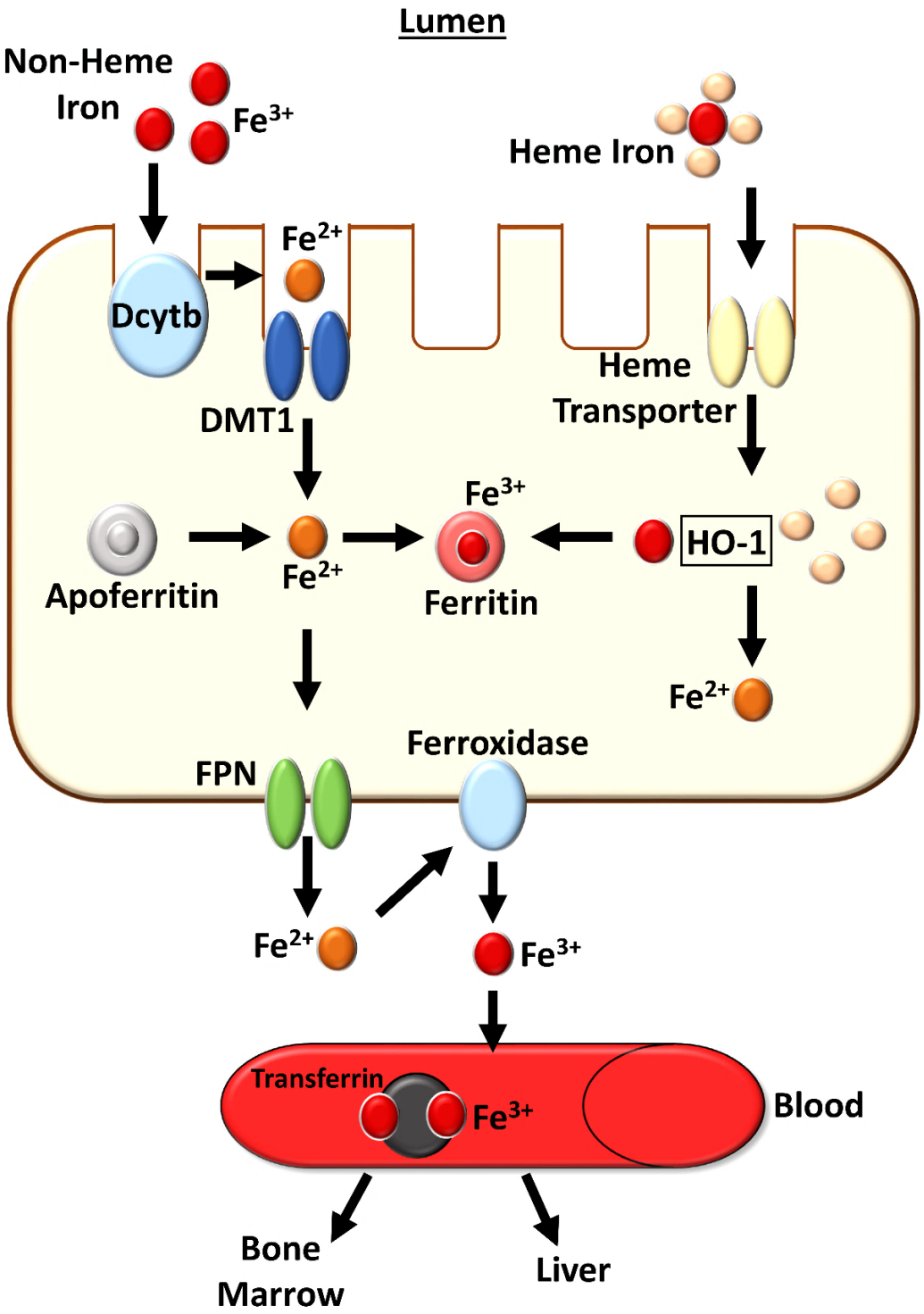

Figure 5.2. Schematic demonstrating the major pathways of iron absorption and transport within the body. Once dietary iron (in non-heme form) reaches the intestinal lumen, it is reduced from its ferric (Fe^{3+}) to ferrous (Fe^{2+}) form by the ferric reductase enzyme, duodenal cytochrome B (Dcytb). Divalent metal transporter 1 (DMT1) transports ferrous iron into the enterocyte, which is stored (in ferritin) or exported (through ferroportin, FPN). For extracellular transport, ferroxidase converts Fe^{2+} to Fe^{3+}, which is safely contained in blood transferrin and transported to required areas (e.g. bone marrow and liver). Alternatively, heme iron enters the enterocyte through a heme transporter and is broken down by heme oxygenase 1 (HO-1) prior to storage or transport. *Image produced by the author (HNW).*

Non-TBI (NTBI) transport only occurs when Tf is fully saturated, allowing a pool of NTBI to form (Recalcati et al., 2017). NTBI can be bound to citrate (rat hepatocytes, Graham et al., 1998), or synthetic iron chelates *in vitro* (e.g. Garrick et al., 1999), while roles for metal transporters in trafficking NTBI have been recently demonstrated. Here, the Zrt/Irt-like protein family member, Zip14, can aid intracellular transport of TBI and NTBI (in mouse cells, Liuzzi et al., 2006). However, as human pancreatic β cells can still uptake NTBI independently of ZIP14 (Coffey & Knutson, 2017), the complete repertoire of NTBI uptake mechanisms remains to be revealed. Cellular iron trafficking and storage is summarised in **Figure 5.3.**

5.1.3. Regulation of Bodily Iron

The body regulates intestinal uptake of iron through multiple mechanisms, fundamentally determined by an individual's requirements. For example, during iron deficiency anaemia, ferroportin, DMT1 and Dcytb are upregulated to aid iron uptake and export from enterocytes, hepatocytes and Mφs (Arezes & Nemeth, 2015). Similarly, expression of the iron-regulating hormone, hepcidin, is repressed during iron deficiency, erythropoiesis and hypoxia (Ganz & Nemeth, 2012). In response to high iron, and/or chronic inflammation and infection, *HAMP* gene expression is upregulated, resulting in hepcidin production by hepatocytes (D'Alessio et al., 2012). Hepcidin prevents iron export by stimulating ferroportin internalisation and degradation (Ganz, 2013). Intriguingly, one of the pathways involved in *HAMP* regulation is the hemojuvelin (HJV)-bone morphogenic protein (BMP) –axis (Babitt et al., 2006). This is important, as BMPs are cytokines within the TGF-β superfamily, playing major roles in fibrosis (Guo & Wang, 2009). Activated HJV-BMP complexes trigger phosphorylation of mothers against decapentaplegic homologs (SMADs) 1, 5 and 8 (Andriopoulos et al., 2009), which complex with SMAD4, and are translocated to the nucleus. Here, the complex binds to two BMP response elements (BMP-RE1 and BMP-RE2) that regulate *HAMP* gene transcription (Papanikolaou & Pantopoulos, 2017; Shi & Massagué, 2003). The most relevant BMP ligand for hepcidin release is iron-regulated BMP6, as revealed *in vivo* (in mice, Andriopoulos et al., 2009).

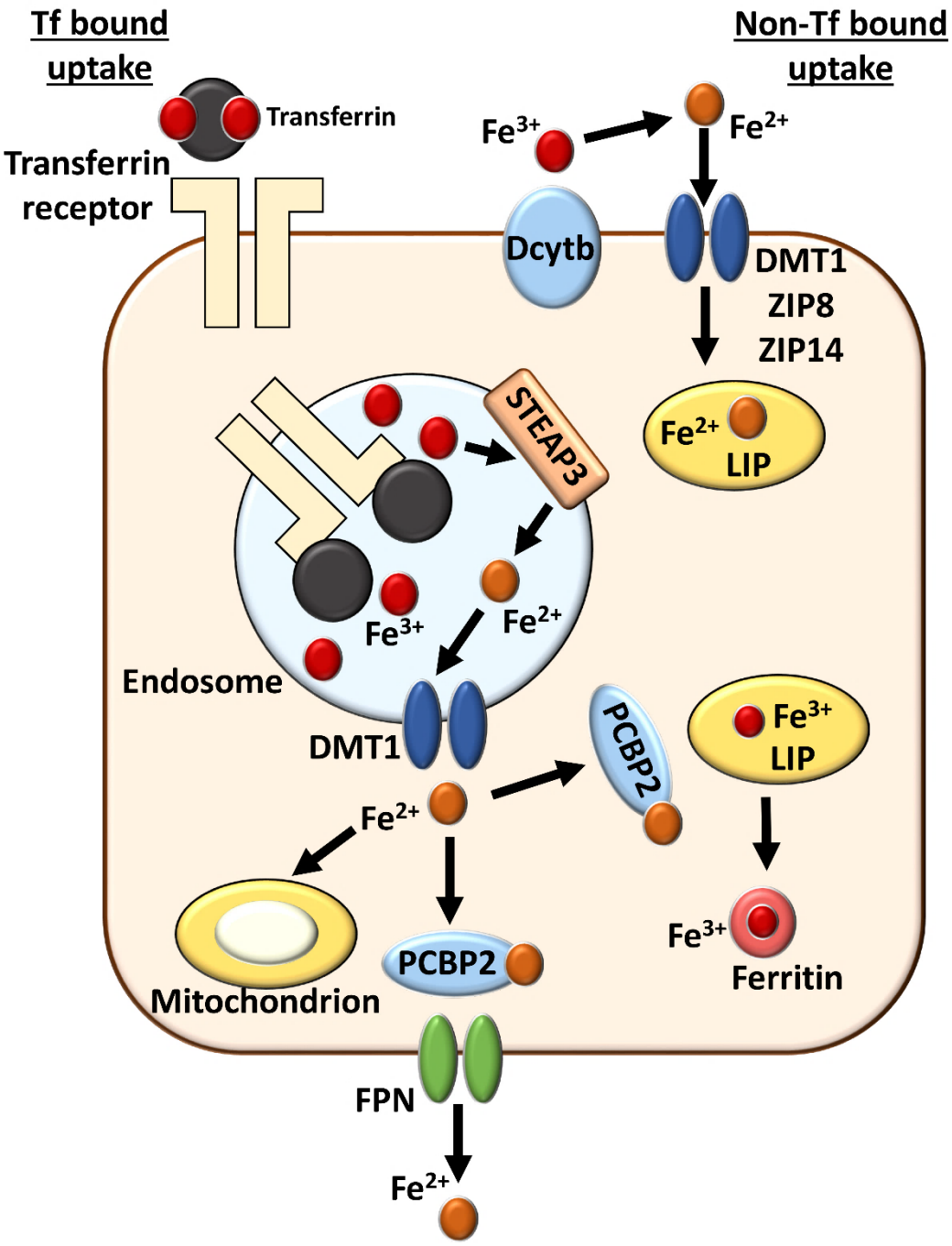

Figure 5.3. Cellular iron uptake and transport. Transferrin (Tf) bound ferric (Fe^{3+}) iron enters the cell through the Tf receptor via endocytosis. Within the endosome, ferric iron is reduced to its ferrous (Fe^{2+}) form by six-transmembrane epithelial antigen of prostate (STEAP3) and transported into the cytosol (via divalent metal transporter 1, DMT1). Ferrous iron is then: a) used by the cell (e.g. in the mitochondria for respiration); b) becomes part of the labile iron pool (LIP); c) is stored in ferritin; or d) is exported via ferroportin (FPN). Transport of Fe^{2+} within the cytoplasm is supported by the iron chaperone, poly (rc)-binding protein 2 (PCBP2). Non-Tf bound iron can also enter the cell through a number of transporters (e.g. DMT1, ZIP8, and ZIP14). *Schematic produced by the author (HNW).*

Hepcidin can be further regulated by human hemochromatosis protein (HFE) binding to TfR2. Under normal iron conditions, HFE binds to hepatic TfR1, but when iron levels increase, holo-Tf has higher affinity for TfR1 than HFE, causing HFE to dissociate and complex with TfR2 (Core et al., 2014; Goswami et al., 2006). This activation leads to *HAMP* expression through the ERK1/2 pathway. The importance of HFE/TfR2 binding has been shown *in vitro* (Gao et al., 2009) and in experimental murine models (e.g. Wallace et al., 2009), where global knockdown of both Hfe and Tfr2 leads to greater iron loading than knockdown of either protein alone. In humans, the significance of HFE and TfR2 is illustrated in patients with hereditary hemochromatosis (HH), who possess mutations in *HFE* or *TFR2* (Camaschella et al., 2000; Del-Castillo-Rueda et al., 2012). To further complicate matters, HFE and TfR2 may interact with the BMP axis, as *Hfe*/*Tfr2* knockout mice possess downregulation of BMPs (Corradini et al., 2009; Wallace et al., 2009), and BMP signalling is impaired in HH patients (Bolondi et al., 2010). Yet, due to the complex nature of iron-regulation, full understanding of the key molecular processes that lead to iron disease pathology have yet to be garnered.

Following release into the cytoplasm, Fe^{2+} is trafficked by iron chaperone proteins towards the major iron-metabolism organelle, the mitochondrion. Within mitochondria, iron is packaged into heme or iron-sulfur clusters for metabolic processes (Muckenthaler et al., 2017). As aforementioned, free iron is highly reactive and must be tightly regulated by the body. If cellular uptake exceeds requirement, or oxidative stress is induced (Cairo et al., 1995), iron is sequestered within a protein cage known as ferritin (Papanikolaou & Pantopoulos, 2017). Intracellular iron storage also allows for iron bioavailability in times of deficiency (discussed below). Ferritin consists of heavy and light polypeptide chains, which self-assemble into a capsule able to retain up to 4, 500 iron atoms (Huard et al., 2013; Wilkinson & Pantopoulos, 2014). The heavy chain acts as a ferroxidase enzyme, while the light chain aids iron transport to the ferritin core (Finazzi & Arosio, 2014). Ferritin can be found in the nucleus, mitochondria, cytoplasm, and even serum, where it acts as an indicator of iron status (Arenzes & Nemeth, 2015).

5.1.3.1. HIFs and Iron Regulation

Hypoxia inducible factors (HIFs) are heterodimeric transcription factors responsible for modulating cellular responses to low oxygen, thus driving angiogenesis and erythropoiesis (Majmundar et al., 2010). HIFs contain an oxygen-dependent α subunit (e.g. HIF-1α, HIF-2α and HIF-3α) and constitutively–expressed β subunit (Suzuki et al., 2017). During normoxia, two proline residues on HIF α subunits undergo prolyl hydroxylation by prolyl hydroxylase domain-containing enzymes (PHDs), bind to von Hippel-Lindau tumour suppressor protein, and are degraded (Ivan et al., 2001). During hypoxia, PHDs are repressed and HIF α subunits are stabilised via dimerisation with β subunits. HIF complexes then interact with hypoxia response elements, cause hypoxia response gene transcription, increase cellular oxygenation, and allow metabolic adaptation to hypoxic stress (Arany et al., 1996). Intriguingly, HIFs can regulate iron metabolism. During hypoxia, HIFs downregulate *Hamp* gene expression (in mice, Nicolas et al., 2002), and during iron depletion, HIFs upregulate DMT1, and HIF-1 alone decreases ferritin (Shah et al., 2009). Cellular iron can also directly affect HIF protein production as under low iron conditions, PHDs are inactive and HIFs are stabilised (Shah & Xie, 2014).

5.1.3.2. The Labile Iron Pool

Despite free iron being a potent oxidant and ROS generator, cells contain a labile iron pool (LIP) of free iron (first described by Jacobs, 1977). The LIP comprises of Fe^{2+} and Fe^{3+} bound to small molecules (nucleic acids, amino acids and glutathione) and serves as an iron store and iron status indicator (Eisenstein, 2000). In general, the LIP contains less than 5% of the cell's iron, but the LIP is dynamic, changing in size in response to iron availability (Kakhlon et al., 2002). Upon TBI uptake, ferritin degradation, and reduced export, the cytosolic LIP enlarges. This increase in LIP size is sensed by iron-responsive element-binding proteins (IRPs), which degrade in iron replete states (Eisenstein, 2000; Kaklon et al., 2002). As a result, the LIP serves as another intricate level of iron regulation.

5.1.3.3. Molecular Iron Regulation

Hormones and receptor binding modulate large-scale regulation of iron, but on a molecular level, individual cells can determine the fate of iron to ensure its tight regulation. For example, post-transcriptional modifications of iron-related mRNAs is controlled largely by the IRP/IRE (iron-responsive element) system. IRP1 and

IRP2, the cytosolic iron sensors, bind to conserved hairpin structures (IREs) in the 5' or 3' direction of untranslated regions (UTRs) of iron-related mRNAs. During low iron, 5'-UTR IREs are translationally repressed, while 3'-UTR IREs mediate mRNA stability (Bogdan et al., 2016). 5'-UTR IREs are present in genes that lower the labile iron pool, such as ferritin and ferroportin, while 3'-UTR IREs are found in DMT1 and TfR1 that enhance iron uptake (Connell et al., 2018). Therefore, during iron deficiency, binding to the 3'-UTR of TfR1 and DMT1 mRNA protects against degradation, while repression of 5'-UTR IREs of ferritin and ferroportin mRNA by a steric hindrance mechanism prevents their translation, thus enhancing cellular iron uptake (Wilkinson & Pantopoulos, 2014).

By contrast, in enterocytes, ferroportin translational is not repressed during iron depletion, as this would prevent intestinal absorption of iron into the blood. It is thought that ferroportin is translated in this context due to splice variants (e.g. *fpn1b*; Zhang et al., 2009a) that lack the 5' IRE, thus evading translational repression. During iron saturation, iron (4Fe-4S) clusters occupy IREs, while IRP1 contains its own iron cluster and is converted to an aconitase-like enzyme that functions in cellular metabolism (e.g. producing NAPDH and acetyl-CoA; Wilkinson & Pantopoulos, 2014). IRP2 is similarly prevented from binding to IREs when intracellular iron is high, but it undergoes ubiquitination and proteosomal degradation (Arenzes & Nemeth, 2015). During iron starvation, iron clusters dissociate from IRP1, and IRP2 is not degraded, allowing binding to IREs. A schematic of IRE/IRP translational regulation is provided in **Figure 5.4**.

5.1.4. Iron disorders

Despite the complex and sophisticated processes that occur to regulate body iron, genetic, physiological and environmental alterations can lead to iron deficiency or iron overload. The most common iron overload disorder is HH, characterised by toxic accumulation of iron in vital organs. HH is driven by abnormally low hepcidin, resulting in high serum iron, Tf saturation and bodily iron accumulation (Bridle et al., 2003). The four main subtypes of the disease are: a) HFE-HH, the most frequent type; b) juvenile hemochromatosis, the deadliest; c) TFR2-associated and; d) ferroportin disease (Arenes & Nemeth, 2015). As aforementioned, iron-loading disorders are characterised by mutations in important iron-regulating genes. For example, inactivation of *HAMP* and *HJV* lead to juvenile hemochromatosis (Lin et al.,

2005; Roetto et al., 2003). Consequently, these mutations cause hyperabsorption of dietary iron and failure of iron-loading cells, such as Mφs, to retain recycled iron. Of note, mouse models that possess targeted deletion of *HFE*, *HAMP* and *TFR2* recapitulate the clinical manifestations of HH (reviewed in Fleming et al., 2011).

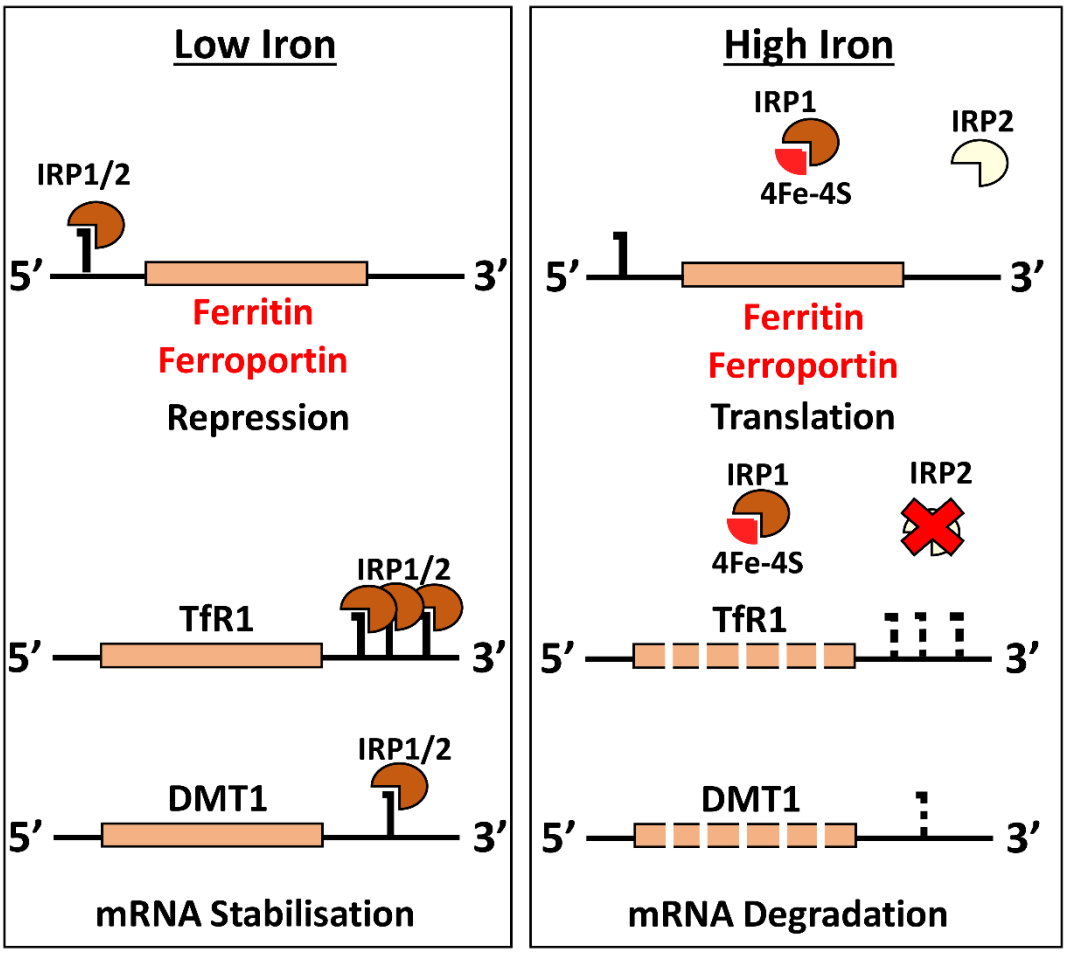

Figure 5.4. Molecular regulation of cellular iron. Under low iron conditions, iron-responsive element-binding protein 1 (IRP1) and IRP2 bind to the 5' end of untranslated regions (UTR) of iron-related mRNAs, which prevents ferritin and ferroportin translation. IRP1 and IRP2 bind to the 3' end of transferrin receptor 1 (TfR1) and divalent metal transporter 1 (DMT1) mRNA, thus stabilising mRNA translation and increasing cytosolic iron uptake. During high iron conditions, IRP1 is bound to cytosolic iron while IRP2 degrades, therefore preventing UTR binding. Hence, ferritin and ferroportin are translated, while TfR1 and DMT1 mRNA degrades. These changes lower cytosolic iron by reducing uptake and increasing storage and export. *Illustration provided by the author (HNW).*

5.1.4.1. Iron Deficiency

Iron deficiency disorders include iron deficiency anaemia, the most common nutritional deficiency worldwide (Miller, 2013). Iron deficiency anaemia is characterised by deficient serum Tf saturation, as well as reduced serum ferritin (Baker, 2000). Iron deficiency anaemia usually develops slowly, except in the case of blood loss, as iron can be released from recycled erythrocytes and iron stores

during urgent requirement (Miller, 2013). Therefore, these sources of iron must become replete before anaemia develops. Genetic mutations may also lead to iron deficiency, such as iron refractory iron deficiency anaemia, caused by inactivation of the hepcidin silencer, *TMPRSS6* (Finberg et al., 2008). As a result, sustained upregulation of hepcidin results in wide scale iron sequestration by Mφs, and ultimately leads to hypoferraemia (Wang & Babitt, 2016).

The second most prevalent form of anaemia, anaemia of chronic diseases, or anaemia of inflammation, results from chronic illness or inflammation that reduces serum iron. It is characterised by low serum iron, reduced Tf saturation and increased storage of iron in the reticuloendothelial system (Cullis, 2011). This reduction in iron is mediated via upregulation of hepcidin, found in patients with multiple myeloma (Sharma et al., 2008), chronic kidney disease (Mercadal et al., 2014) and chronic obstructive pulmonary disease (Tandara et al., 2015).

5.1.4.2. Hepcidin and Inflammation

Inflammation plays an important role in iron regulation, protecting the host from sepsis (Park et al., 2001). Release of hepcidin, a well-known AMP (Michels et al., 2015), causes cellular hoarding of iron, which reduces serum iron availability to extracellular pathogens, dampens inflammation (demonstrated in *Vibrio vulnificus* infection in mice, Arezes et al., 2015), and subsequently protects against sepsis (Chen et al., 2014b). The hepcidin-inflammation link was primarily demonstrated in a murine model of LPS administration, which led to upregulation of hepcidin (Pigeon et al., 2001), later found to be dependent on IL-6 (Nemeth et al., 2004). Furthermore, IL-6 infusion in human volunteers increased urine hepcidin and reduced serum iron (Nemeth et al., 2004), while ablation of Il-6 prevented inflammation-induced hepcidin production (Nicolas et al., 2002). It is now known that hepcidin-mediated inflammation is regulated by both the IL-6/JAK/STAT pathway, and the BMP-SMAD axis (Sangkhae & Nemeth, 2017).

5.1.5. The Role of Iron in Diabetes

Diabetes is a well-known complication of HH as iron loading can cause pancreatic β cell apoptosis and lead to the development of insulin resistance (McClain et al., 2006). Diabetes is also commonly associated with thalassemia (β globin [haemoglobin] subunit deficiency), a disease that causes iron overload due to the frequent requirement of blood transfusions (Simcox et al., 2013; Weatherall, 2001).

However, iron may be additionally linked to the pathogenesis and phenotype of typical T2DM. Patients with T2DM generally retain increased iron stores, characterised by elevated serum ferritin (Eshed & Lishner, 2001; Yeap et al., 2015). Indeed, serum ferritin positively correlates with obesity (a strong risk factor for T2DM onset, Ford & Cogswell, 1999), and insulin and glucose levels (in women, Sheu et al., 2003; in men, Tuomainen et al., 1997).

Raised serum ferritin and increased heme iron uptake have previously been associated with a greater risk of developing T2DM (Jehn et al., 2007; Rajpathak et al., 2006), yet these effects are attenuated when data is adjusted for inflammation markers (Bao et al., 2012). High serum ferritin is also closely coupled to increased central adiposity (Jehn et al., 2004), cardiovascular disease (Qi et al., 2007) and fatty liver disease (Valenti et al., 2012). Consequently, it is difficult to determine whether iron is directly influencing the etiology of diabetes, or whether it is associated with a secondary symptom of the disease.

Elevated iron stores may induce T2DM through a number of mechanisms, including causing oxidative damage and destruction to pancreatic β cells, as observed in HH in humans (Abraham et al., 2006; Fernandez-Real et al., 2002) and mice (Jouihan et al., 2008). Of note, heightened hepatic iron storage impairs glucose metabolism by reducing insulin extraction and the responsiveness of adipocyte insulin receptors (Taylor et al., 1984), while iron loading via a high iron content diet causes insulin resistance and increases glucose uptake in mice (Huang et al., 2013). Rats fed on high fat diets also developed changes in iron metabolism that promoted iron loading, such as elevated hepcidin and reduced ferroportin (Meli et al., 2013). In summary, it is clear that many of the risks that lead to the development of T2DM (e.g. high fat diet) are associated with alterations in iron metabolism.

A clear negative correlation exists between adiponectin, an adipokine causally linked to insulin sensitivity (Kubota et al., 2002), and serum ferritin levels (in humans, Forouhi et al., 2007; Gabrielsen et al., 2012). Changes in iron genes (e.g. increased ferritin and IRP) are also associated with adipocyte differentiation (Festa et al., 2000), while mice with adipocyte-specific deletion of ferroportin display greater iron storage, increased insulin resistance and reduced adiponectin production (Gabrielsen et al., 2012). However, a dichotomy exists between adiponectin and insulin sensitivity in HH patients compared to T2DM patients. In

HH, hepcidin production is impaired, resulting in low cellular iron and high adiponectin levels, while the opposite exists in T2DM alone (Gabrielsen et al., 2012).

As a viable therapeutic option, dietary restriction of iron is associated with improved prognosis. For example, T2DM rats fed on iron-restricted diets displayed improved glycaemia (Minamiyama et al., 2010), while leptin-deficient *ob/ob* mice on iron-restricted diets or iron chelation therapy showed increased insulin sensitivity and improved β cell function, compared to controls (Cooksey et al., 2010). It is clear that dietary iron and iron homeostasis are intimately linked to the diabetic metabolic phenotype, and as impaired wound healing is a major complication of diabetes, this opens up speculation about how local iron levels are affected in diabetic skin, and how this may contribute to wound repair.

5.1.6. Iron in the Skin

The role of iron in modulating metabolism has been explored since before the 1950s (Granick, 1954). Therefore, it is not surprising that researchers have been postulating the relationship between iron in skin pathology and wound healing for decades (Heughan et al., 1974; Jacobson & Vanprohaska, 1965). The skin remains the first barrier against external insult, with crucial mechanisms to protect against chemical-induced and UVR-induced oxidative damage (Applegate et al., 1998). UVA radiation exposure triggers increased fibroblast and keratinocyte labile iron (Pourzand et al., 1999; Reelfs et al., 2010), causes heme iron release from fibroblasts (Kvam et al., 1999), and upregulates ferritin expression in human skin (Applegate et al., 1998). As elevated free iron leads to oxidative damage, this offers one explanation for the predominant role of UVA in ROS generation. Indeed, keratinocytes are more resistant to UVA damage than fibroblasts *in vitro* (in humans, Applegate et al., 1995) and in a human skin equivalent model, partly through upregulation of ferritin (Marionnet et al., 2010). Indeed, overexpression of ferritin protects against UV-induced stress in multiple cell types (HeLa cells, Cozzi et al., 2000; lens epithelial cells, Goralska et al., 2001).

5.1.7. Iron in Wound Healing

5.1.7.1. Haemostasis

In wound healing, iron is most noted for its oxidative function in haemostasis, where ferrous iron is released from haemoglobin (Lipinski & Pretorius, 2012). Although associated with negative consequences, free radical production in this instance acts to promote blood clotting (by polymerising fibrinogen to insoluble fibrin in human blood, Kell & Pretorius, 2015; Pretorius et al., 2013), while ROS production also triggers thrombin release and platelet activation (in mice, Woollard et al., 2009).

5.1.7.2. Inflammation

Chronic wounds contain an abundant source of heme (erythrocytes; Wenk et al., 2001; Yeoh-Ellerton & Stacey, 2003; Zamboni et al., 2006), which sustains wound site neutrophil recruitment through heme-driven release of OH- (Yeoh-Ellerton & Stacey, 2003). Similarly, Fe^{2+} sequestration heightens M1 polarisation via increased Tnf-α and Nos2 (in murine studies, Kroner et al., 2014; Sindrilaru et al., 2011; Sindrilaru & Scharffetter-Kochanek, 2013), and elevates the expression of the M2 markers, *Arg1* and *Ym1*, in splenic and peritoneal Mφs (in iron-loaded mice, Agoro et al., 2018). Indeed, the importance of iron in modulating Mφ function has been discussed at length (e.g. Ganz & Nemeth, 2015; Jung et al., 2015), as iron sequestration is an innate part of the phagocytic anti-infection machinery.

Pro-inflammatory Mφs are directed by cytokines to sequester heme and non-heme iron, thus reducing its availability to extracellular pathogens (Ganz, 2009; Nairz et al., 2008). However, Mφs can alter their iron transport systems depending on whether an infection is extracellular or intracellular. During intra-Mφ *Salmonellae* infection, ferroportin expression is increased (Chlosta et al., 2006) and TfR1 expression (mRNA and protein) is decreased to aid iron secretion (Nairz et al., 2008). This mechanism is driven by the pro-inflammatory phenotype, as Mφs lacking Ifn-γ (Nairz et al., 2008), Nos2 (Nairz et al., 2013) and lipocalin-2 (Nairs et al., 2015) are unable to effectively excrete iron during intracellular infection.

M2-like Mφs primarily act to dampen inflammation and drive wound resolution (Li et al., 2007), and like M1 Mφs, have characteristic iron processing behaviours (Recalcati et al., 2010). Gene ontology analysis has demonstrated substantial differences in iron-regulated genes between M1 and M2 Mφs (Recalcati et al., 2010), which correlates with their opposing functions for iron processing. One key feature

of the M2 Mφ is the overexpression of scavenger receptors, which aid in clearing cell debris and damaging particles (Biswas & Mantovani, 2010), and are required for heme scavenging (e.g. CD163, Bacci et al., 2009; CD91, Maniecki et al., 2006) to dampen inflammatory processes (Cairo et al., 2011). Further, the M2 (IL-10^{high}) phenotype is associated with elevated HO-1 activity (Lee & Chau, 2002), which reduces inflammation by catalysing the breakdown of heme into biliverdin, CO and ferrous iron (Gozzelino et al., 2010). M2 Mφs counteract the damaging effects of HO-1-driven ferrous iron release by increasing ferroportin expression through IRP1 inhibition (Recalcati et al., 2010; Vallelian et al., 2010). The key differences in the iron regulatory mechanisms of M1 and M2 Mφs are summarised in **Figure 5.5**.

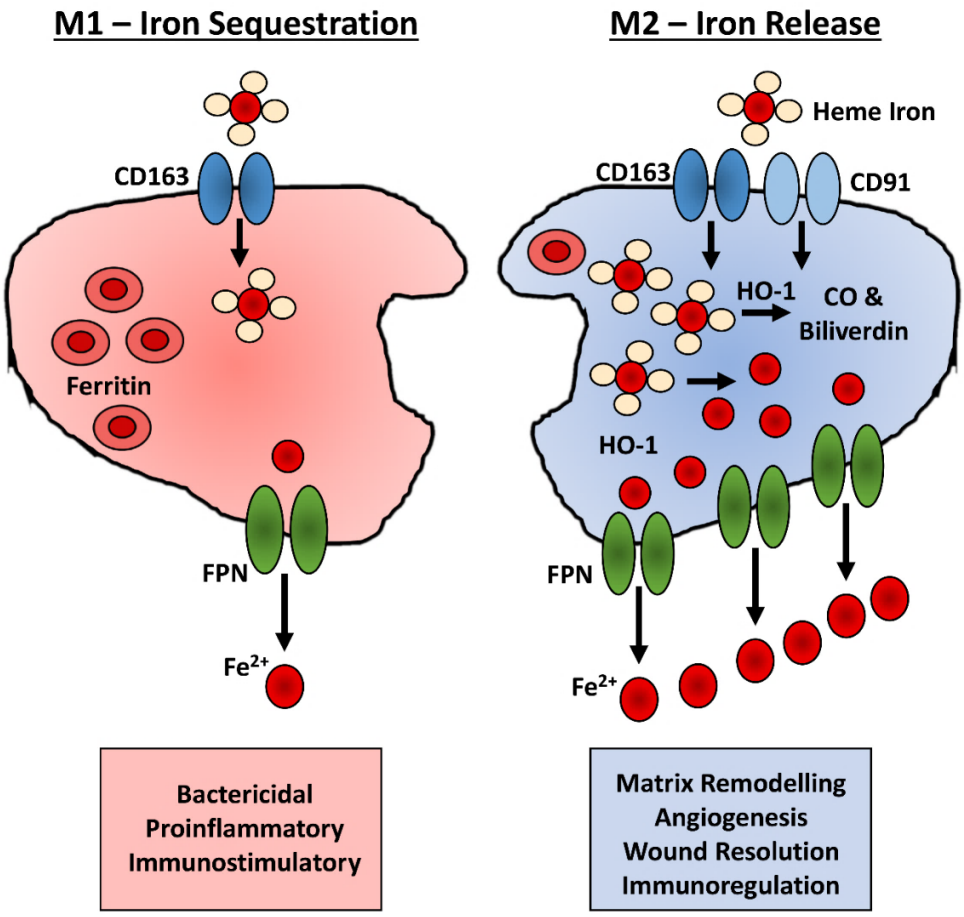

Figure 5.5. Key differences in iron metabolism between M1 and M2 macrophages. M1 (pro-inflammatory) macrophages (Mφs) show an iron sequestration phenotype characterised by high ferritin and low ferroportin (FPN), thus depleting extracellular iron in the microenvironment. By contrast, M2 (anti-inflammatory) Mφs have high levels of scavenger receptors (e.g. CD163 and CD91) and increased heme oxygenase 1 (HO-1) activity. HO-1 breaks down heme into ferrous iron, biliverdin and carbon monoxide (CO), which drives wound resolutory processes (e.g. angiogenesis, Józkowicz et al., 2003). Ferrous iron is then expelled through FPN. The crucial roles of M1 and M2 Mφs are summarised in boxes beneath the schematic. *Image produced by the author (HNW)*

5.1.7.3. Angiogenesis

Oxidative stress can be a detrimental process, yet induction of hypoxia, through iron-dependent enzymes (such as factor inhibiting HIF [FIH]; Lando et al., 2002), is required for the stimulation of angiogenesis (Loenarz & Schofield, 2008; Ozer & Bruick, 2007). Indeed, the functional importance of iron in promoting blood vessel formation has been demonstrated previously. For example, lipocalin-2 administration increased intracellular ferrous iron and ROS, which subsequently improved endothelial cell migration and tubule formation (in rat cells *in vitro*, Wu et al., 2015). However, excessive Fe^{2+} accumulation altered hepcidin function, caused heightened Vegf production and abnormal retinal angiogenesis in $hjv^{-/-}$ mice (Tawfik et al., 2014). Consequently, balancing intracellular free iron is not only important for regulating oxidative stress and inflammatory processes, but also in modulating blood vessel formation.

5.1.7.4. Fibroplasia

Collagen synthesis and stability requires a dynamic series of post-translational modifications (Vasta et al., 2016). Interestingly, Fe^{2+} is vital for formation of 2-oxoglutarate 4-dependent oxygenases, such as prolyl 3-hydroxylase, prolyl 4-hydroxylase (P4H) and LOX3, which modulate post-translational collagen synthesis through catalysis of pro-collagen (Hutton et al., 1967; Markolovic et al., 2015). One of the most prevalent collagen hydroxylation modifications involves P4H (Gorres & Raines, 2010). As mentioned, Fe^{2+} is a vital cofactor for P4H, a non-heme Fe (II)- and α-ketoglutarate-dependent dioxygenase (Vasta & Raines, 2016), and without P4H-mediated hydroxylation, (2S,4R)-4-hydroxyproline would not form stable collagen triple helices (Pihlajaniemi et al., 1991; Sakakibara et al., 1973). Of note, ascorbate (vitamin C) can convert ferric iron into its ferrous form, reactivating P4H and preventing malformation of collagen (as otherwise observed with scurvy, Myllylä et al., 1978). Similarly, iron chelation, through α, α'-dipyridyl, has been shown to disrupt procollagen mRNA stability, leading to increased procollagen I mRNA turnover (IMR-90 fibroblasts, Ikeda et al., 1992). Overall, it is clear that ferrous iron is vital for the formation of stable ECM, yet how this relates to wound-relevant matrix remodelling remains elusive.

5.2. Chapter Aims

Iron plays a fundamental role in orchestrating cellular metabolism, and is implicated in the pathogenesis of chronic disease. Iron has also been linked to Mφ behaviour, and is required for collagen stabilisation, yet its role in cutaneous biology remains tenuous. It was therefore hypothesised that iron would play crucial roles in modulating fibroblast and Mφ behaviour during wound-relevant processes.

Specific aims were to:

1) **Characterise iron abundance in normal and pathological wound healing.** Total wound iron abundance was measured across a time course of acute healing using ICP-MS. Given that iron is linked to diabetes, and diabetes is a major factor for chronic wounds, ICP-MS was used to demonstrate temporal changes in iron during Db murine wound repair.
2) **Profile the functional response(s) of major wound-relevant cells to iron.** Here, matrix production, secretion and remodelling were assessed in HDFs following iron administration. The effects of a high iron environment were determined in murine Mφs and human Mφs to elucidate how iron alters their behaviour to contribute to late-stage wound healing.
3) **Explore the paracrine effects of iron-loaded immune cells on wound relevant fibroblast functions.** Iron-loaded human Mφs were cultured with HDFs to establish the influence of their secretomes on matrix production in HDFs. Characterised secretome components were then assessed in human *ex vivo* wounds to elucidate their role in the context of wound repair.

Considering that little evidence pertains to the actual role of endogenous iron in cutaneous wound biology, the ultimate aim of the chapter was to reveal the importance of iron in regulating cellular behaviour in the wound environment to promote effective repair.

5.3. Materials and Methods

5.3.1. Animal Experiments

Normal skin and excisional wounds were collected from young (8-10 weeks old) female WT (C57BL/6J) mice for a time course healing experiment (day 1, day 3, day 7 and day 14 post-injury, n = 5 per group). NDb heterozygous mice and Db homozygous mice (described in **Section 2.1**) were wounded at 8-10 weeks of age (n = 3-5 per group) and wounds collected at day 3 (D3) and D7 post-injury, along with normal skin (D0). Wounds were left to heal via secondary intention. Wounding procedures and tissue collection are described in **Section 2.1**.

5.3.2. Measuring Iron in Cells and Tissue

ICP-MS was performed as described in **Section 2.5** to determine the relative abundance of iron in wounds throughout a time course of healing, and to elucidate changes in wound iron with Db pathology. Perl's Prussian Blue (PPB) staining (described in **Section 2.4.5**) was used to visualise iron deposition in wound tissue. PPB was also used to demonstrate intracellular and extracellular iron deposits in HDF cultures treated with and without iron. Iron was administered as ferric ammonium citrate (FAC), a highly soluble, biologically available form of NTBI (Wang et al., 2018a). For PPB analysis, the colour deconvolution plugin (as in Zhou et al., 2015) of ImageJ v.1.8 was used. Colour channels were separated based on Alcian Blue and Haematoxylin staining, and the percentage area of blue staining quantified via threshold analysis. To prevent bias, a macro was created by the author (HNW) to ensure the same parameters were applied to all images.

5.3.2.1. Ferrozine Assay

A ferrozine assay was used to elucidate whether HDFs internalised administered iron. Ferrozine is an effective chelator of ferrous iron (Stookey, 1970), but the assay was modified and performed as in Riemer et al. (2004) to allow for the detection of ferrous and ferric iron. HDFs were treated with Minimum Essential Media (MEM; Gibco, Thermo Fisher Scientific) in 2% FBS and FAC where applicable. Cells were incubated for two days, five days and 11 days, with treatment changes performed every three days. Upon collection, media was aspirated and cells were scraped on ice in 50 mM NaOH containing 1% HALT™ protease inhibitor cocktail (Thermo Fisher Scientific). Cell lysates were stored at -80°C until use. Cellular iron concentration (in μM) was determined from a FAC standard curve.

5.3.2.2. Tissue Assessment of Intracellular Iron

To determine the major iron sequestering cell types, skin and wound tissue were stained for ferritin with Mac3 (Mφs) or α-Sma (fibroblasts). Fluorescently conjugated secondary antibodies were used (Alexa Fluor 594, ferritin; Alexa Fluor 488, Mac3 and α-SMA; both Thermo Fisher Scientific) and images obtained via confocal microscopy (**Section 2.6.7.5**). Cell count analysis was performed in ImageJ v.1.8. Tissue infiltration of Nos-2^{+ve} and Arginase-1^{+ve} Mφs was verified via immunoperoxidase staining as described in **Section 2.4.4**.

5.3.3. Collagen Content of Wound Tissue

Matrix remodelling was assessed across the WT, NDb and Db tissue using picrosirius red staining (**Section 2.4.6**) and immunofluorescent staining for rat anti-collagen type I, rat anti-collagen type III (Abcam) and mouse anti-fibronectin (Santa Cruz Biotechnology). Appropriate Alexa Fluor-conjugated secondary antibodies (594 and 488; Thermo Fisher Scientific) were used and images obtained via confocal microscopy. Threshold intensity analysis of tissue staining was performed in ImageJ v.1.8. qRT-PCR was performed on murine tissue for *Fn1*, *Col1a1* and *Col3a1* transcript levels.

5.3.4. Iron-Regulated Matrix Production

HDFs (isolated as described in **Section 2.3.2**), were cultured in MEM containing 2% FBS for all matrix assays (described below). HDFs from three human donors were used for all experiments. Prior to matrix assessment, viability, growth rates and scratch migration experiments were performed as described in **Section 2.6.2**.

5.3.4.1. Hydroxyproline Assay

Collagen content of FAC-treated HDFs was first assessed indirectly using a hydroxyproline assay kit (Abcam) as per manufacturer's instructions. Hydroxyproline is an amino acid exclusively present to collagen, and is extensively used to determine the collagen content of cells and tissues (Cissell et al., 2017). Alkaline hydrolysis was performed using 10N NaOH, which was neutralised with an equal volume of 10N HCl. Samples were dried to remove HCl and hydroxyproline was then detected using p-dimethylaminobenzaldehyde solution. Plates were measured at 560nm and hydroxyproline concentration ascertained from a hydroxyproline standard curve.

5.3.4.2. Immunofluorescence

HDFs were seeded and left to adhere O/N at 37°C and 5% CO_2. The following day, media was changed to MEM (above) with 10 μM FAC, 100 μM FAC or no FAC (control) and changed every three days (up to day 6). Cells were collected at day 5 or day 11 post-first treatment. Immunofluorescent staining was performed on matrix containing cells, or matrix with cells denuded. Images were captured via confocal microscopy and analysed in ImageJ v.1.8 (**Section 2.6.7.5**).

5.3.4.3. Western Blotting

Western blotting was performed on FAC-treated HDFs at day 5 post-initial treatment for anti-mouse PDGFA and anti-mouse ferritin (Santa Cruz Biotechnology). Western blotting was also performed on denuded ECM collected at day 11 post-initial treatment, prior to mass spectrometry analysis. Primary antibodies used for ECM samples were: anti-mouse COL1A1, anti-mouse PDGFA, anti-mouse COL6A1 and anti-mouse vimentin (all Santa Cruz Biotechnology). In-depth western blotting procedures are provided in **Section 2.6.7.6**. Western blots were also performed on THP-1 cells following FAC administration (for ferritin).

5.3.4.4. Conditioned Media Zymography

Conditioned media was taken from matrix plates at day 11. Cell media was collected, sterile-filtered and stored at -80°C until use. Gelatin zymography gels were performed as described in **Section 2.8.7.3**, and protease activity determined relative to the control group.

5.3.4.5. Mass Spectrometry

Label free LC-MS was performed on denuded matrix from HDFs treated with FAC for 11 days. Protein was isolated and analysed as described in **Section 2.6.7.8**.

5.3.4.6. Scanning Electron Microscopy

Scanning electron microscopy (SEM) was performed to assess HDF structural changes following FAC treatment. Full details are provided in **Section 2.6.7.7**.

5.3.5. Fn-488 Remodelling

HDFs were seeded into 12-well μ-slides (Ibidi, Munich, Germany) at 2.5 x 10^5 cells/mL media. After 6 hours adherence, media was aspirated and changed to MEM with 2% FBS and FAC where applicable. At the same time, Fibronectin HiLyte 488 (Cytoskeleton Inc, Colorado, US) was added at 4 μg/mL for 24 hours. HDFs were

fixed in 4% formaldehyde, counterstained with DAPI and imaged on a confocal microscope. Remodelling of the 488-conjugated fibronectin was assessed via fluorescence intensity analysis in ImageJ v.1.8.

5.3.5.1. MMP2 Inhibition

To determine whether MMP2 was involved in FAC-mediated remodelling of fibronectin, the MMP2 inhibitor, ARP101 (Biotechne), was used. ARP101 was added at the same time as FAC at a concentration of 20 μM (as in da Rocha-Azevedo et al., 2015). Fn-488 remodelling was performed as described above.

5.3.5.2. Fibronectin Degradation Assay

MMP2 was treated with or without the protease activator, 4-aminophenylmercuric acetate, at a concentration of 1 mg/mL for 1 hour prior to the assay (as in Hu & Beeton, 2010). MMP2 was then incubated in 600 μg/mL recombinant human fibronectin (Sigma-Aldrich, as in Steffensen et al., 2011) at 37°C for 24 hours in zymography resolving buffer. Fibronectin alone was included as a control. Following incubation, western blot was performed for fibronectin as previously described.

5.3.6. Oxidative Stress

Intracellular ROS were measured using CellROX® Green Reagent (Thermo Fisher Scientific) as per manufacturer's instructions. Briefly, HDFs were seeded and left to adhere O/N before treating with FAC. After 24 hours, CellROX® was added to each well for 30 minutes, aspirated, and HDFs were fixed in 4% formaldehyde solution. Cells were imaged within 24 hours of CellROX® treatment using a confocal microscope (described in **Section 2.6.7.5**). CTCF was determined in ImageJ v.1.8.

A ROS-Glo™ H_2O_2 Assay (Promega) was performed to determine H_2O_2 production. HDFs were seeded into white opaque-walled 96 well plates and left to adhere O/N. FAC, deferoxamine and PMA were added for 8 hours prior to adding H_2O_2 substrate. In contact with H_2O_2, the substrate breaks down into a luciferin precursor, which is converted to luciferin upon D-cysteine addition. The luciferin then reacts with luciferase, resulting in luminescence proportional to the H_2O_2 in culture. Menadione (20 μM, Thermo Fisher Scientific) was included as a control. Luminescence was read on a VICTOR X Multilabel plate reader (PerkinElmer, Buckinghamshire, UK).

5.3.7. Antioxidant Treatments

To ameliorate oxidative stress, antioxidants (ascorbic acid, MnTBAP chloride and mannitol) were screened (using CellROX®) in HDF cultures at the same time as FAC administration. For main text experiments, mannitol was used at 1 mM concentration in combination with 100 μM FAC.

5.3.8. Oxygen Sensing

Oxygen saturation in FAC-treated HDF cultures was assessed using the SDR SensorDish® Reader (Presens, Regensburg, Germany) and accompanying software. The SDR SensorDish® was calibrated as per manufacturer's instructions before adding a sensor plate with seeded HDFs to the reading platform. Measurements were recorded every five minutes and data output analysed using Microsoft Excel.

5.3.9. Iron Gene Regulation

RNA and cDNA were made as described in **Section 2.7**. qRT-PCR was performed to determine relative changes in the expression of iron-related genes throughout a time course of normal (WT) healing, and a time course of pathological (Db) repair. The genes under study were: *Slc11a2* (DMT1), *Irp1*, *Steap3*, *Slc40a1* (ferroportin), *Tf*, *Tfr1* (TfR1), *Ftl* (ferritin light chain) and *Fth* (ferritin heavy chain). HDFs treated with iron were additionally profiled for alterations in *LOX1* and LOX-like genes, *LOXL1* and *LOXL2*, prolyl 4-hydroxylase subunits α1, α2 and β (*P4HA1*, *P4HA2* and *P4HB*, respectively), matrix genes (*COL1A1*, *COL1A2*, *COL3A1*, *COL6A1*, *FN1*, *PDGFA* and *VIM*), *MMP2*, differentiation markers, α-SMA (*ACTA2*) and *CDH11*, and the hypoxia regulators, *HIF1A*, *HIF2A* and *FIH*. Polarisation was assessed in bone marrow derived Mφs (BMDMs; *Nos2*, *Cd86*, *Ym1*, *Arg1*, *Tnf*, *Il1b*, *Ccl17* and *Ccl22*) and THP-1-derived Mφs (TDMs; *TNF*, *IL1B*, *CCL17* and *CCL22*). Mφs were also profiled for iron genes (primer sequences provided in **Appendix 2A.32-2A.33**).

5.3.10. SiRNA Transfection

HDFs were seeded into 24 well plates at a density of $2x10^4$ cells per well without antibiotics. The following day, cells were transfected with two validated Silencer® Select SiRNAs (Thermo Fisher Scientific) targeting *STEAP3* (Si-S3#1 and Si-S3#2). Cationic lipid-based transfection was achieved with Lipofectamine® RNAiMAX in Opti-MEM™ (both Thermo Fisher Scientific) as per manufacturer's guidelines. Silencer® Select Negative Control No. 1 SiRNA (Si-Ctrl) and Silencer® Select

Positive Control GAPDH SiRNA (Si-GAPDH) were used for optimisation experiments, and as internal controls. After six hours, media was replaced with fresh MEM and HDFs were treated with FAC for 5 days. HDFs were analysed via qRT-PCR to determine expression levels of *STEAP3*. CellROX® assay, immunocytochemistry (ICC), zymography and western blot was performed as previously described.

For experimental optimisation, HDFs were treated with control siRNA (Si-Ctrl), GAPDH siRNA (Si-GAPDH) or STEAP3 siRNA (Si-S3#1) for 2 days and 5 days and collected for RNA. qRT-PCR demonstrated significant, stable knockdown of *GAPDH* and *STEAP3* at 2 days and 5 days (**Appendix Figure 5A.6**). Next, HDFs were transfected with or without 100 μM FAC to determine knockdown efficiency, where FAC treatment did not affect *GAPDH* or *STEAP3* knockdown efficiency (**Appendix Figure 5A.6**). Preliminary ICC experiments were carried out in siRNA knockdown cells to assess collagen I and collagen III production (**Appendix Figure 5A.7**), and fibronectin and ferritin expression (**Appendix Figure 5A.8**). Zymography and western blot analysis (**Appendix Figure 5A.9**) was also performed.

5.3.11. Bone Marrow-Derived Macrophages

NDb and Db BMDMs were stimulated to M1 and M2 states as described in **Section 2.6.9**. BMDMs were collected at 24, 48- and 72-hours post-stimulation to assess polarisation via qRT-PCR. Cytokines were added in the presence of FAC to determine how FAC influenced BMDM polarisation and iron processing (qRT-PCR). As a functional readout of Mφ behaviour, phagocytosis assays were performed (below).

5.3.12. THP-1 Cell Culture

THP-1 cells were cultured and differentiated as described in **Section 4.3.4.3**. For polarisation experiments, TDMs were stimulated to M1 (IFN-γ and LPS) and M2 (IL-13 and IL-4) states as in Bi et al., (2016) and Genin et al., (2015). TDMs were treated with FAC at the time of polarisation for qRT-PCR analysis and western blotting, or treated with FAC for 6 hours post-stimulation prior to phagocytosis experiments.

5.3.12.1. Phagocytosis Experiments

NDb BMDMS, Db BMDMs, and TDMs, were tested for their ability to phagocytose *E. coli* (K-12 strain) BioParticles®, with CTCF used to measure particle uptake (**Section 2.6.9.3**). Polarised TDMs were also incubated with live *E. coli* (ATCC® 25922) at a MOI of 10 for two hours at 37°C and 5% CO_2. Media was plated on MHA

to determine CFU/mL of non-internalised bacteria. TDMs were next incubated in gentamicin for one hour to kill any remaining external *E. coli*, lysed with 0.1% triton X-100 and plated on MHA to count the number of internalised bacterial colonies.

5.3.12.2. THP-1 Differentiation Experiments

THP-1 cells were treated with or without PMA at the same time as administering FAC. After 3 days, cells were collected for RNA to assess differentiation marker expression (**Section 4.3.4.3**). THP-1 adhesion was measured using CellTiter 96® AQueous One Solution (**Section 2.6.4**). Zymography and Proteome Profiler™ chemokine arrays (Biotechne) were also performed (described in **Section 3.3.3.1**) on CM collected from TDMs.

5.3.13. Transwell Co-Culture

THP-1 cells were differentiated and polarised in transwell inserts (0.4 μm; Corning, Flintshire, UK), washed in DPBS to remove exogenous cytokines, and transferred to plates seeded with HDFs. TDM inserts were replaced after 3 days of culture. On day 9, HDFs were fixed and stained for collagen type I, illustrated in **Figure 5.6**.

5.3.14. Human *Ex Vivo* Wounding

Human skin was collected and wounded as described in **Section 2.3.1**. Wounds were treated with a vehicle, CCR4 antagonist (C021), CCL17 and/or CCL22 (R&D Systems, Oxford, UK), applied topically every 2 days (**Table 5.1**). Wounds were collected at 3 days post-wounding for histological analysis.

5.3.15. Statistical Analysis

All data is presented as mean +/- standard deviation of the mean (SEM). Appropriate statistical tests and *post-hoc* analyses were performed as described in **Section 2.9**.

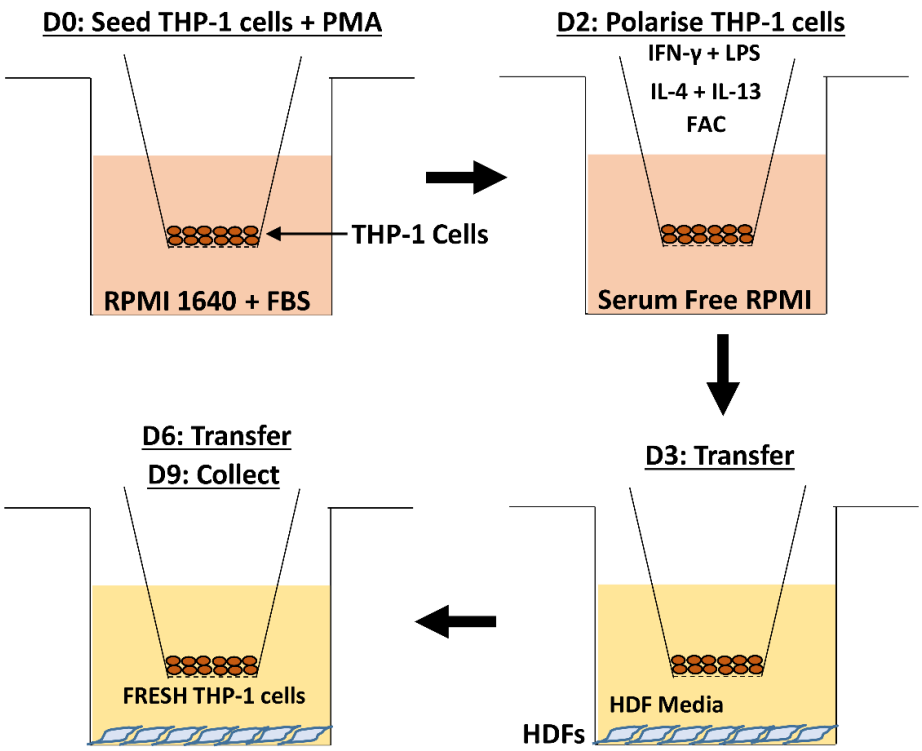

Figure 5.6. Schematic of the macrophage-fibroblast transwell set-up. THP-1 cells were seeded into transwell inserts and differentiated with phorbol 12-myristate 13-acetate (PMA) in RPMI media containing foetal bovine serum (FBS). On day 2 (D2), THP-1 cells were polarised to M1 or M2 macrophage (Mφ) states in serum free RPMI with ferric ammonium citrate (FAC). On day 3, transwell inserts containing polarised THP-1 Mφs were rinsed in human dermal fibroblast (HDF) media and added to HDFs. HDFs were collected for analysis on day 9. *Image by the author (HNW).*

Table 5.1. Treatments used for *ex vivo* human wound experiments.

Treatment Group	Concentration
Vehicle	1% BSA + 0.002% DMSO
CCL17	50 ng/mL
CCL22	50 ng/mL
CCL17 + CCL22	25 ng/mL & 25 ng/mL
C021	100 nM
CCL17 + C021	50 ng/mL & 100 nM
CCL22 + C021	50 ng/mL & 100 nM
CCL17 + CCL22 + C021	25 ng/mL & 25 ng/mL & 100 nM

5.4. Results

5.4.1. Iron accumulates during late-stage wound repair and correlates with extracellular matrix deposition.

ICP-MS, the gold standard technique for measuring metal abundance (Lee et al., 2014b), was used to determine the total concentration of iron within wounds across a time course of normal healing. Wounds were collected at day 1 (D1), D3, D7 and D14 post-injury and iron abundance was compared to D0 (normal skin; **Figure 5.7A**). Here, iron accumulated significantly in D7 and D14 wounds, compared to D0 ($P < 0.001$). PPB staining was used to confirm the ICP-MS data via histological visualisation (**Figure 5.7B**), where D7 ($P < 0.001$) and D14 ($P < 0.001$) wounds displayed increased iron deposits, confirmed via quantification (**Figure 5.7C**).

As late-stage wound healing is associated with ECM remodelling (Li et al., 2007), ECM deposition was characterised in murine wound tissue. Immunofluorescent staining (**Figure 5.7D**) showed fibronectin was highest at D3 ($P < 0.01$) and significantly reduced by D14 ($P < 0.05$; **Figure 5.7E**). Collagen III (**Figure 5.7F**) and collagen I (**Figure 5.7G**) staining was significantly greater at D7 than D1 (Collagen III, $P < 0.001$; Collagen I, $P < 0.01$), D3 (Collagen III, $P < 0.001$; Collagen I, $P < 0.01$) and D14 (Collagen III, $P < 0.05$; Collagen I, $P < 0.01$). Thus, iron accumulation in normal healing correlated strongly with wound collagen deposition.

5.4.2. Diabetic wounds display impaired iron accretion and delayed extracellular matrix deposition.

As Db wounds display significantly delayed healing (**Chapters 3**, **4** and reviewed in Ansell et al., 2012), a further aim was to characterise iron accumulation in pathological Db healing. Total wound iron was compared between NDb and Db skin and excisional wounds at D3 and D7 post-injury (**Figure 5.8A**). NDb wounds displayed significantly elevated iron at D7 (compared to D0, $P < 0.01$), comparable to the levels shown in WT mice (**Figure 5.7A**). Iron in Db wounds was also upregulated at D7 ($P < 0.01$), yet Db skin ($P < 0.001$) and wounds (D3, $P < 0.01$; D7, $P < 0.001$) possessed significantly reduced iron compared to NDb. PPB histology confirmed reduced iron in Db wounds at D3 ($P < 0.001$) and D7 ($P < 0.001$; **Figure 5.8B-C**). As expected, NDb wounds acquired significant iron deposits at D3 ($P < 0.001$) and D7 ($P < 0.001$, compared to D0).

ECM deposition was impaired in Db wound healing (**Figure 5.8D**), where fibronectin was substantially increased at D7 ($P < 0.001$) (**Figure 5.8E**), and collagen III (**Figure 5.8F**) and collagen I (**Figure 5.8G**) deposition were impaired compared to NDb (representative images in **Figure 5.9B-C**). Further, mRNA assessment showed upregulation of *Col3a1* ($P < 0.01$) and *Col1a1* ($P < 0.001$) in normal healing (**Figure 5.9D**), while levels of *Col3a1* and *Col1a1* (**Figure 5.9E**) were not altered in Db wounds. Impaired matrix remodelling was confirmed via picrosirius red staining, used to assess immature and mature fibre composition from birefringence excited via polarised light microscopy (Junqeira et al., 1978). In normal healing, D7 and D14 wounds possessed significantly greater overall collagen content ($P < 0.001$), and more mature fibres than at D1 ($P < 0.001$) and D3 ($P < 0.01$; **Figure 5.10A-B**). NDb D7 tissue also possessed greater collagen content compared to D3, while immature ($P < 0.001$) and mature ($P < 0.05$) fibre deposition was significantly reduced in Db D7 wounds compared to NDb (**Figure 5.10C-D**). Together, these data demonstrated that Db pathological healing wounds possessed reduced iron and impaired ECM deposition.

5.4.3. Fibroblasts sequester administered iron, which has no detrimental effects on cell viability.

As wound iron accumulation correlates strongly with ECM deposition, the effects of iron (as FAC) were determined on fibroblasts *in vitro*. A ferrozine assay demonstrated that 100 μM FAC increased intracellular iron storage at 5 days (D5, $P < 0.001$) and 11 days (D11, $P < 0.01$; **Figure 5.11A**). Western blot confirmed intracellular iron storage via increased ferritin expression in HDFs treated with 100 μM FAC ($P < 0.05$; **Figure 5.11B**). ICC allowed visualisation of elevated cytoplasmic ferritin stores following 100 μM FAC ($P < 0.001$; **Figure 5.11C-D**). Treatment with deferoxamine plus 100 μM FAC significantly reduced ferritin stores, directly showing that deferoxamine chelated FAC. Finally, high iron was observed in HDFs cultured with 100 μM FAC at 5 days ($P < 0.001$; **Figure 5.11F**) and 11 days ($P < 0.001$; **Figure 5.11G**), which was both internalised (inset, **Figure 5.11E**) and associated with deposited ECM (PPB staining). Hence, it is clear that FAC administration leads to excessive internalisation and storage of iron in HDFs.

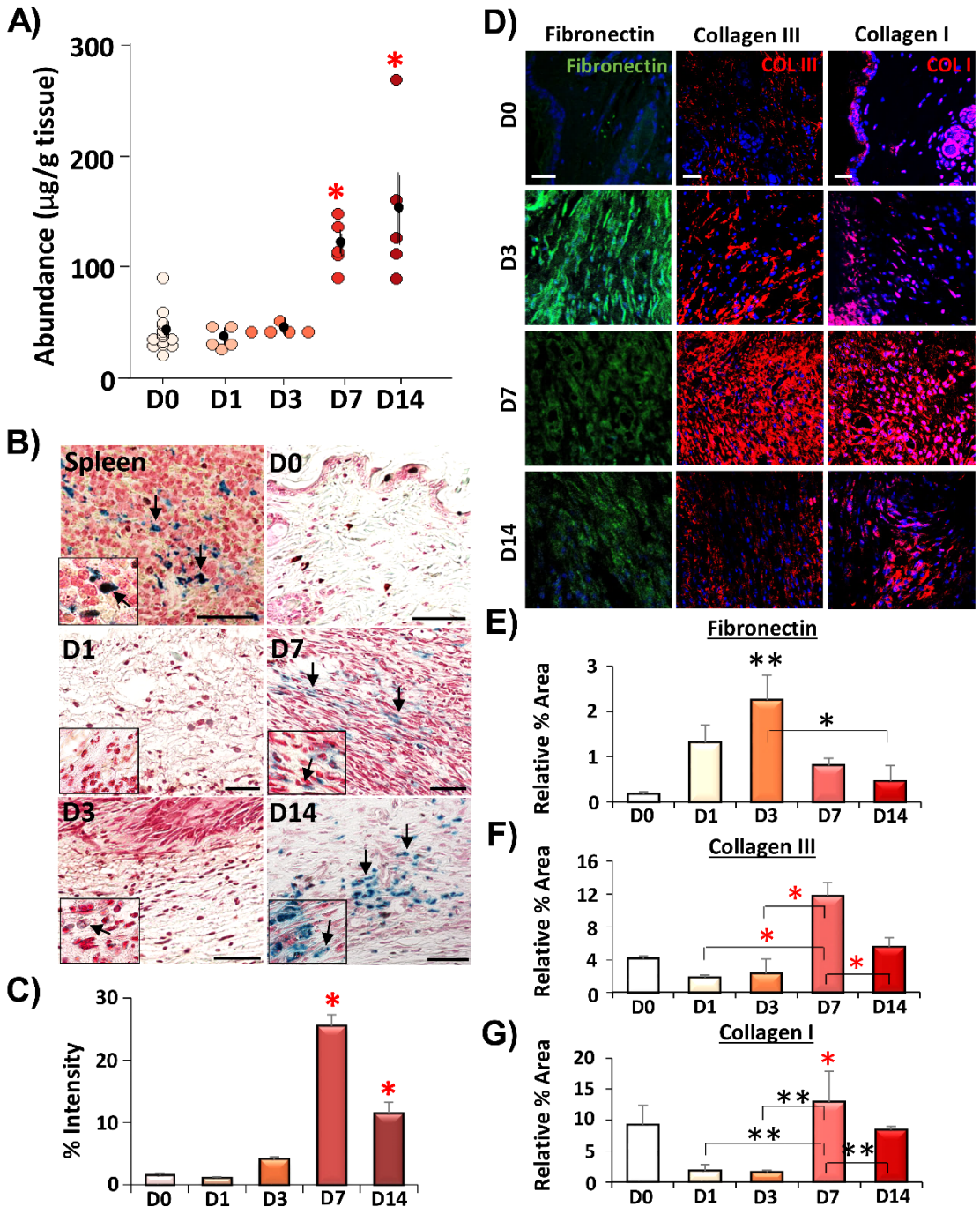

Figure 5.7. ICP-MS demonstrates abundant accumulation of iron during late-stage healing, which correlates with extracellular matrix deposition. Iron abundance is upregulated at day 7 (D7) and D14 post-injury in normal healing (**A**). Perl's Prussian blue staining confirms increased iron deposition at D7 and D14 (**B**), quantified in **C**. Black arrows = blue iron deposits. Spleen = positive control. Inset = high magnification. Bar = 50 µm (10 µm inset). Immunofluorescent staining (**D**) and quantification of fibronectin (**E**), collagen III (COL III; **F**) and collagen I (COL I; **G**). Bar = 50 µm. n = 5 mice per group. Mean +/- SEM. * = $P < 0.01$, ** = $P < 0.01$, red* = $P < 0.001$. One-way ANOVA with Tukey's *post-hoc* test performed on all data. * alone versus D0.

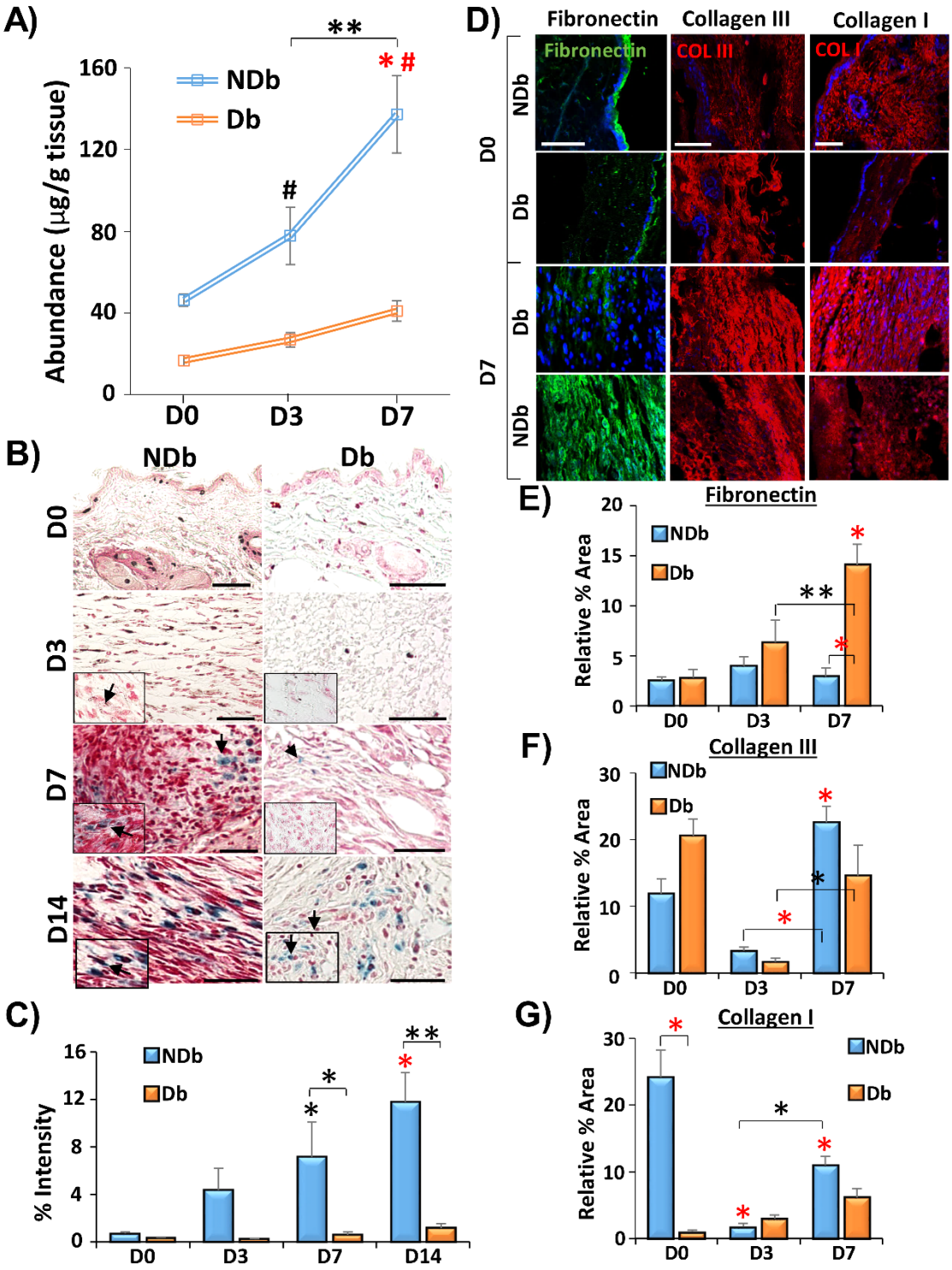

Figure 5.8. Diabetic wounds display significantly reduced wound iron correlating with impaired extracellular matrix deposition. ICP-MS demonstrates reduced iron in diabetic (Db) skin (D0) and wounds (day post-injury; **A**). Perl's Prussian Blue staining (**B**), quantified in **C**. Black arrows = blue iron deposits. Spleen = positive control. Inset = high magnification. Bar = 50 µm (inset 10 µm). Immunofluorescence (**D**) of fibronectin (**E**), collagen III (COL III; **F**) and collagen I (COL I; **G**). Bar = 50 µm. n = 3-5 mice per group. Mean +/- SEM. * = $P < 0.01$, ** = $P < 0.01$, red* or # = $P < 0.001$. # in **A** = NDb versus Db. Two-way ANOVA with Tukey's *post-hoc* test analysis. * alone versus D0.

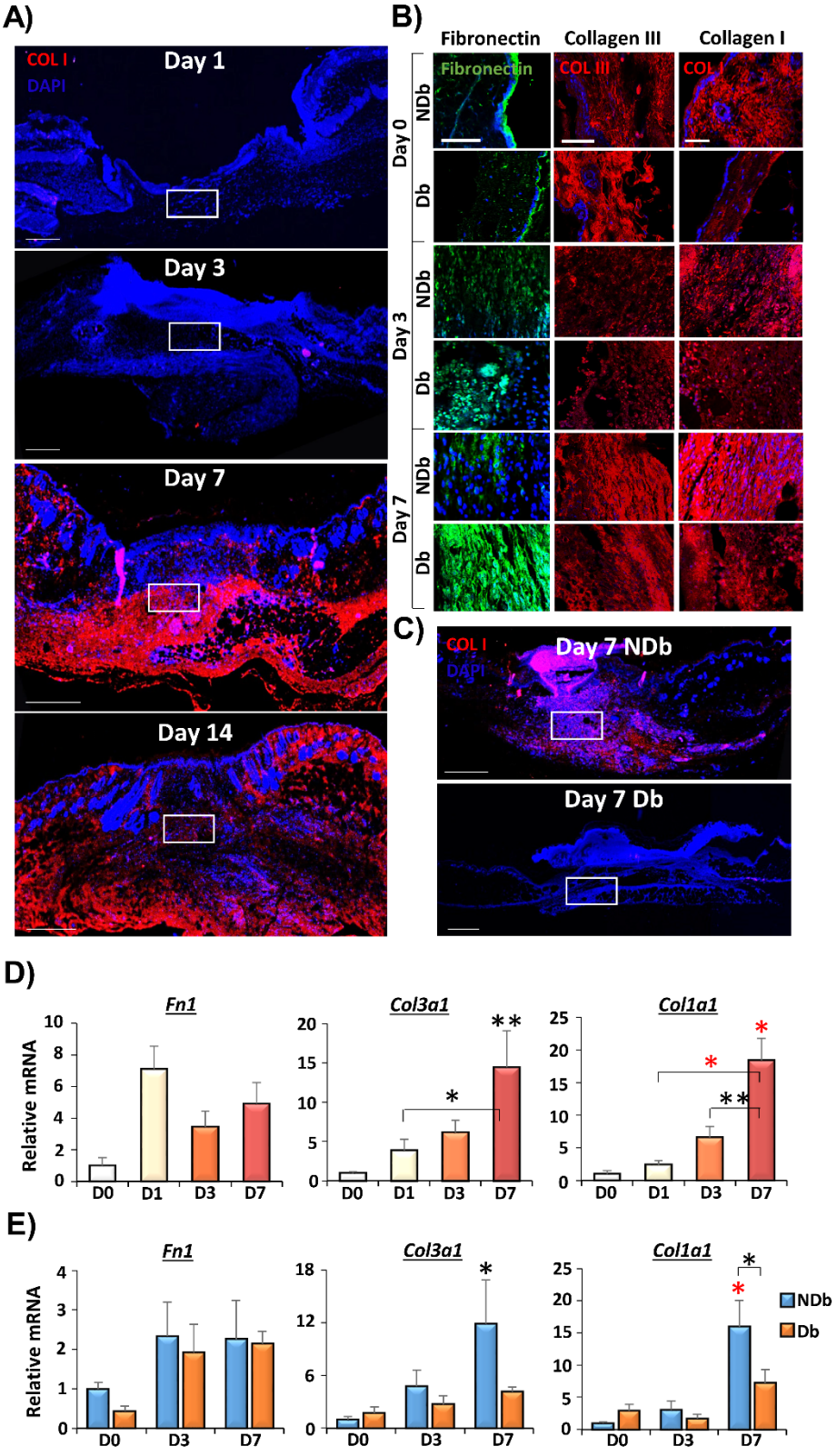

Figure 5.9. Diabetic wounds show altered collagen deposition during late-stage wound repair. Time course wounds with representative regions in white boxes (collagen I; **A**). NDb (non-diabetic) and Db wounds at high (**B**) and low (**C**, collagen I) magnification. Bar on **A** and **C** = 200 µm. Bar on **B** = 50 µm. qRT-PCR of *Fn1*, *Col3a1* and *Col1a1* in wild-type (WT, **D**) and NDb versus Db (**E**) wounds. D0 = normal skin. D = day post-injury. Mean + SEM. n = 3-5 mice per group. * = $P < 0.05$, ** = $P < 0.01$, red* = $P < 0.001$. One-way ANOVA was performed on WT time course data. Two-way ANOVA was performed on NDb versus Db data. Tukey's *post-hoc* analysis where applicable. * alone versus D0.

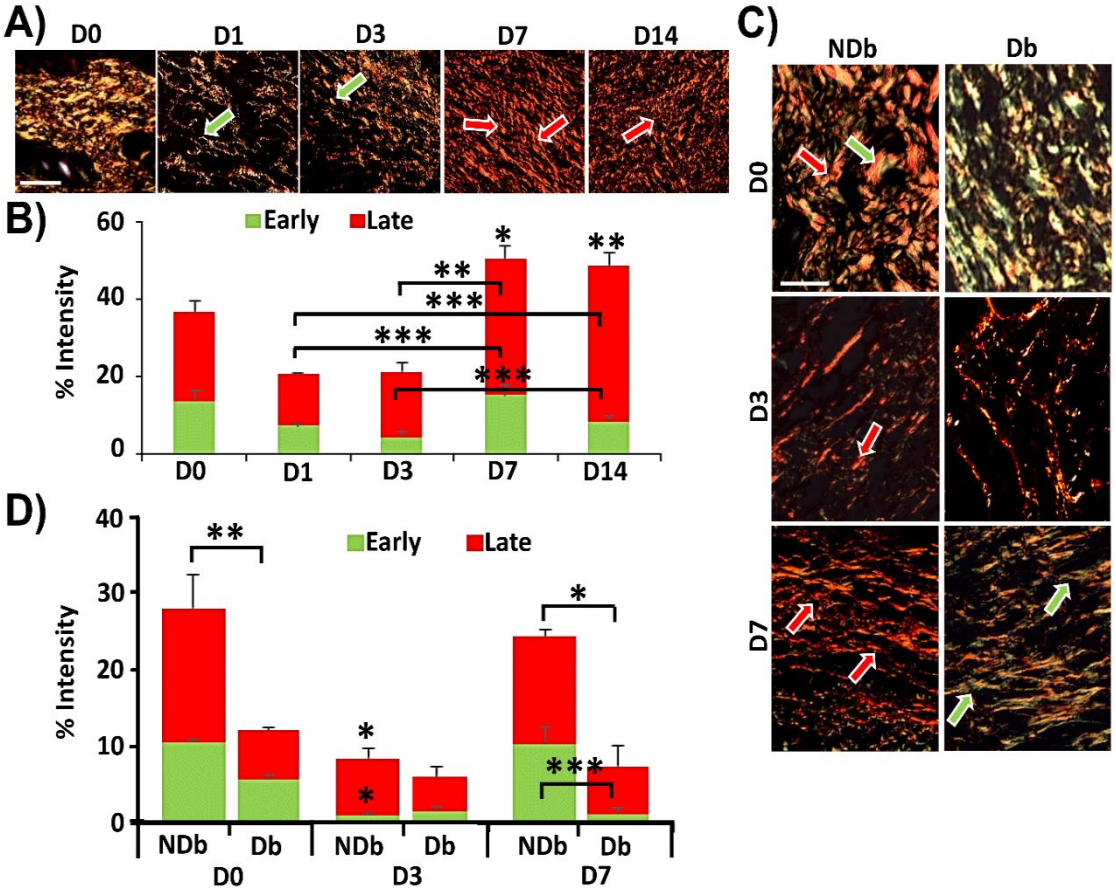

Figure 5.10. Picrosirius red staining demonstrates altered dermal matrix in diabetic wounds. Normal skin (D0) and wounds at day 1 (D1), D3, D7 and D14 post-injury were collected from wild-type mice (n = 5 per group). Picrosirius red staining illustrates changes in early (green-yellow birefringence, green arrows) and late (red-orange birefringence, red arrows) extracellular matrix (ECM) fibres via polarising light microscopy. Representative images are shown in **A** and quantified in **B**. One-way ANOVA for time course data, comparing early and late fibres separately. Diabetic (Db) mice (n = 3 per group), showed delayed ECM deposition (images, **C**; quantified, **D**) compared to non-Db (NDb). Bar = 50 μm. Mean + SEM. Two-way ANOVA for Db data, comparing early and late fibres separately. Tukey's *post-hoc* analysis was performed where applicable. * alone compared to D0 (time course) or NDb to Db within each time point. * = $P < 0.05$, ** = $P < 0.01$, *** = $P < 0.001$.

As iron is a highly reactive metal, the effects of FAC on cellular viability and function were next ascertained. Propidium iodide (PI) uptake was used to assess cell death via flow cytometry (read in the FL-2 and FL-3 channels; see **Chapter 2** for description). Here, 100 μM FAC did not significantly increase cell death following 5 days (**Figure 5.12A-C**) and 11 days (**Figure 5.12D-F**) of treatment, while ethanol-treated cells (positive control) were over 90% positive for PI ($P < 0.001$). Histograms with overlays demonstrated the peak shift for ethanol-treated cells, absent in control and FAC-treated cells (**Figure 5.12C, E**). FAC-treated cells showed a modest reduction in calcein AM uptake at 5 days ($P < 0.001$; **Figure 5.12G**) and 11

days (**Figure 5.12H-I**), but viability was significantly higher than in the ethanol controls ($P < 0.001$). Examples of scatter plots and histograms with markers are provided in **Appendix Figures 5A.1-5A.4**.

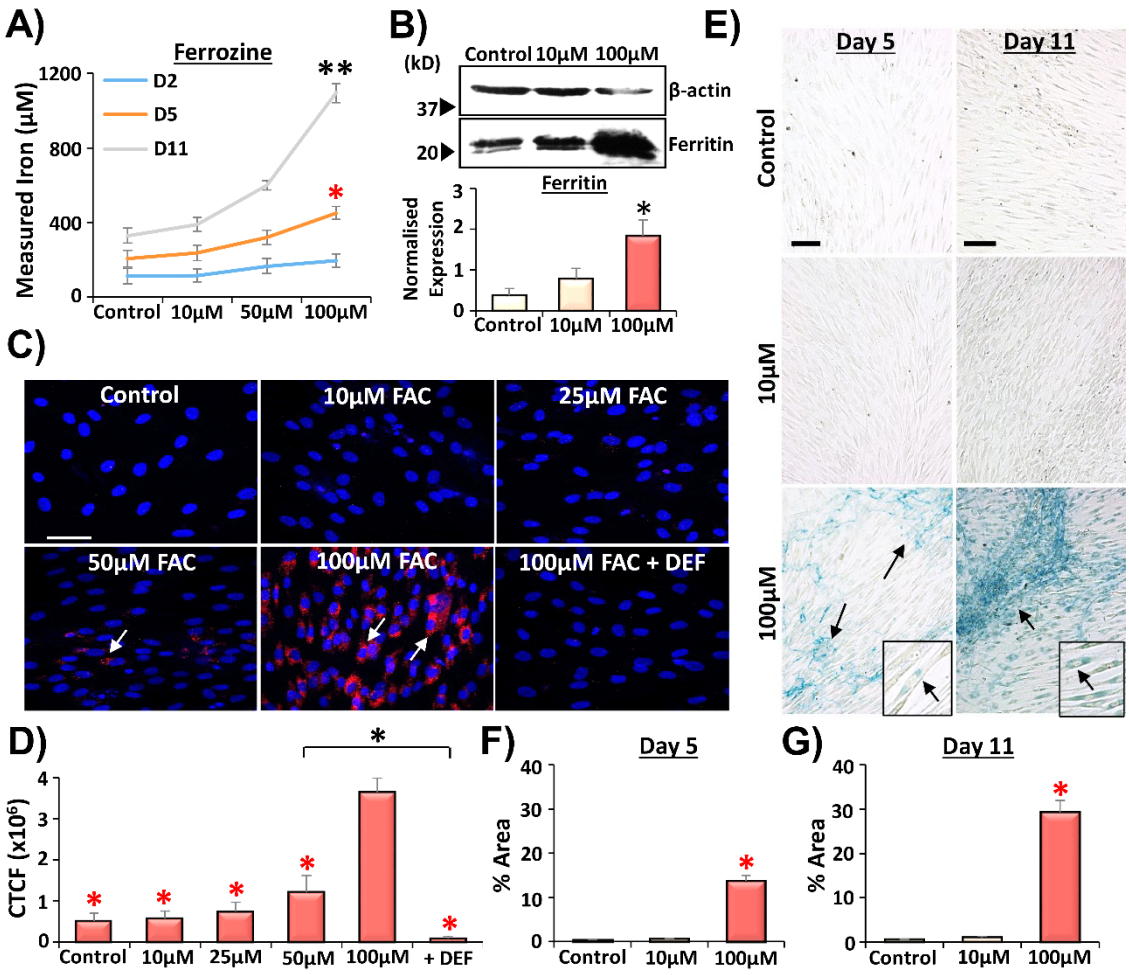

Figure 5.11. Human dermal fibroblasts sequester administered iron. A ferrozine assay demonstrates accumulation of intracellular iron over time (**A**). D2 = day 2 post-initial treatment. Western blot (**B,** β-actin loading control) and ferritin immunocytochemistry (**C**, quantified, **D**). FAC = ferric ammonium citrate. CTCF = corrected total cell fluorescence. Bar = 50 µm. Arrows = ferritin (red). DAPI = nuclei (blue). DEF = 100 µM FAC plus 100 µM deferoxamine. Perl's Prussian blue staining (arrows, blue staining) shows iron deposits (**E**), quantified in **F** and **G**. Bar = 100 µm. n = 3 donors. Mean +/- SEM. * = $P < 0.05$, ** = $P < 0.01$, red* = $P < 0.001$. Two-way ANOVA performed on **A**. One-way ANOVA performed on all other data. Tukey's *post-hoc* tests where applicable.

FAC led to a significant increase in HDF proliferation from D2 onwards ($P < 0.001$; **Figure 5.12J**), while migration was only impaired at 1 mM concentration in young HDFs ($P < 0.001$; **Figure 5.12K, M**). However, in aged HDFs, migration was significant reduced at 100 µM ($P < 0.05$) and 1 mM ($P < 0.001$; **Figure 5.12L-M**), suggesting increased susceptibility to iron treatment. Collectively, these data show

that FAC does not alter young HDF viability or migration up to 100 μM, indicating that 100 μM FAC was suitable for use in subsequent experiments on young HDFs.

5.4.4. qRT-PCR elucidates changes in fibroblast gene expression following iron treatment.

HDFs treated with or without FAC were collected 48 hours post-treatment for qRT-PCR analysis. Data was pooled from three individual donors. Genes assessed included those important for matrix protein translation, iron transport regulation, oxygen sensing and differentiation (**Figure 5.13**). Matrix genes significantly downregulated by FAC treatment included *COL1A1* (100 μM, $P < 0.001$; **Figure 5.13A**), *COL3A1* ($P < 0.001$, **Figure 5.13B**), *FN1* ($P < 0.01$, **Figure 5.13C**) and *PDGFA* (10 μM, $P < 0.05$; 100 μM, $P < 0.01$; **Figure 5.13D**). Intriguingly, expression of *VIM* was significantly increased (100 μM, $P < 0.05$; **Figure 5.13E**). Of the iron-regulating genes, *TFR1* (10 μM, $P < 0.05$; 100 μM, $P < 0.05$; **Figure 5.13F**), *FHC* (10 μM, $P < 0.01$; 100 μM, $P < 0.001$; **Figure 5.13G**), *SLC11A2* (100 μM, $P < 0.05$; **Figure 5.13H**) and *SLC40A1* (10 μM, $P < 0.01$; 100 μM, $P < 0.001$; **Figure 5.13I**) were significantly dampened following FAC treatment.

Expression of hypoxia inducible factors, *HIF1A* ($P < 0.05$; **Figure 5.13K**) and *HIF2A* ($P < 0.05$; **Figure 5.13L**), were decreased following 100 μM FAC, while no change in *FIH* (**Figure 5.13M**) expression was found. Furthermore, a modest reduction in the differentiation markers, *ACTA2* (**Figure 5.13N**) and *CDH11* (**Figure 5.13O**) was observed following 100 μM FAC administration. As ECM and iron gene transcription was altered by FAC treatment, genes important for modulating ECM stability were also assessed (**Figure 5.14**). LOX is one such enzyme, required for collagen crosslinking (Markolovic et al., 2015). Here, *LOX* and the functionally similar, *LOXL1*, were unaltered by FAC treatment while *LOXL2* was downregulated following 100 μM FAC ($P < 0.05$, **Figure 5.14C**). Another enzyme crucial for ECM maintenance was P4H, required to catalyse the synthesis of hydroxyproline. As hydroxyproline increases the melting temperature of collagen, it is fundamental in allowing collagen to remain stable at body temperature (Gorres & Raines, 2010). Here, *P4HA1* was not significantly altered by FAC treatment, while *P4HA2* (**Figure 5.14E**) was significantly reduced by 10 μM ($P < 0.05$) and 100 μM ($P < 0.05$) FAC treatment. FAC administration did not alter *P4HB* expression (**Figure 5.14F**).

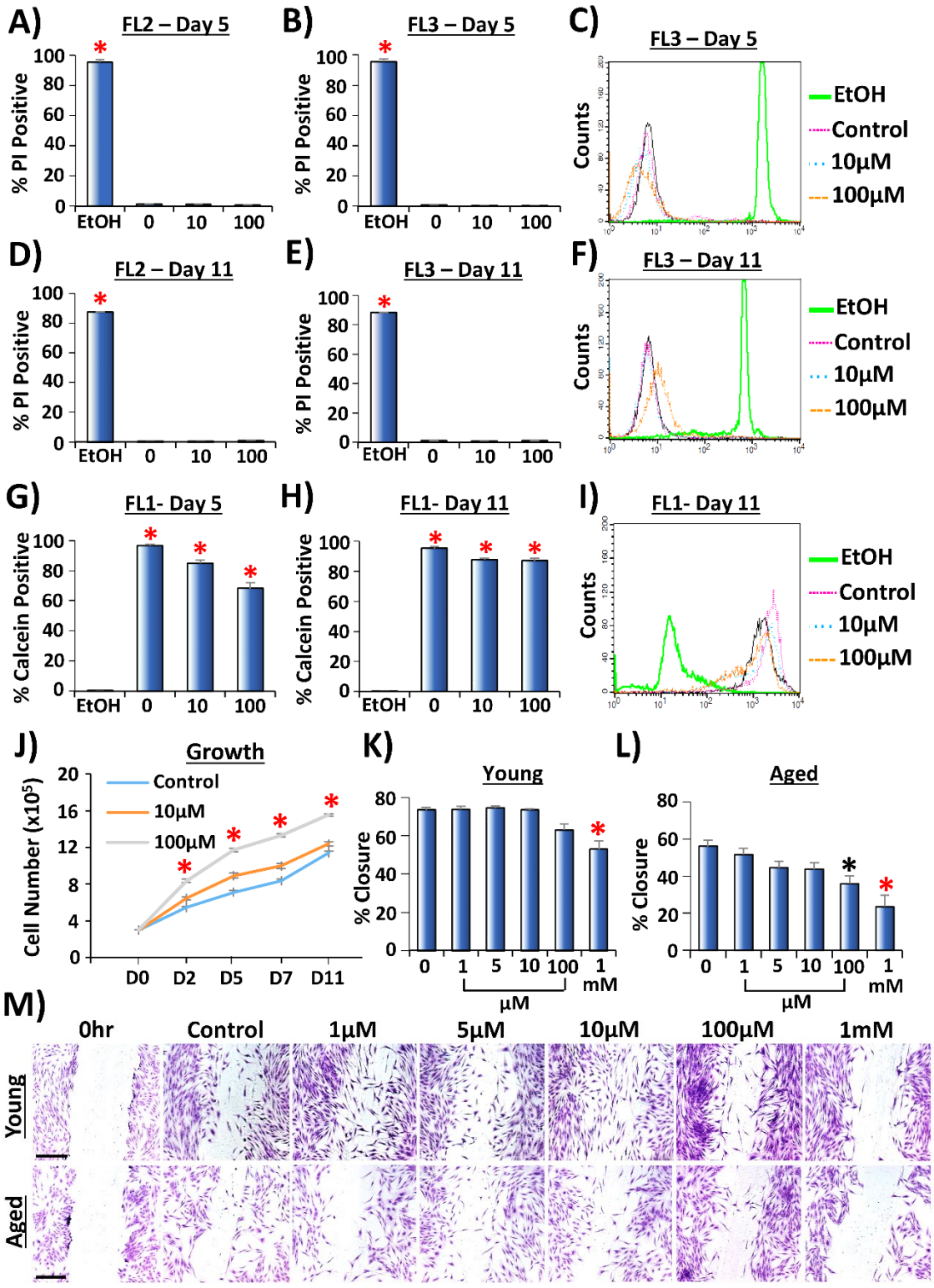

Figure 5.12. Viability, growth and migration of human dermal fibroblasts following iron treatment. Flow cytometry assessed human dermal fibroblast (HDF) viability using propidium iodide (PI; **A-F**) and calcein AM (**G-I**) after 5 days (**A-C**, **G**, **I**) and 11 days (**D-F**, **H-I**) of culture. Ethanol (EtOH) included as a control. Histograms with overlays (**C**, **F**, **I**). Growth kinetics following iron treatment (**J**). HDFs from young (<40 years of age, **K**) and aged (>65 years of age, **L**) donors. Crystal violet staining at 24 hours (**M**). Bar = 500 µm. n = 3 donors. Data represent mean +/- SEM. * = $P < 0.05$, red* = $P < 0.001$. One-way ANOVA and Dunnett's test for multiple hypotheses on data sets **A-I** and **K-M** (versus control). Two-way ANOVA and Tukey's *post-hoc* analysis performed on **J**.

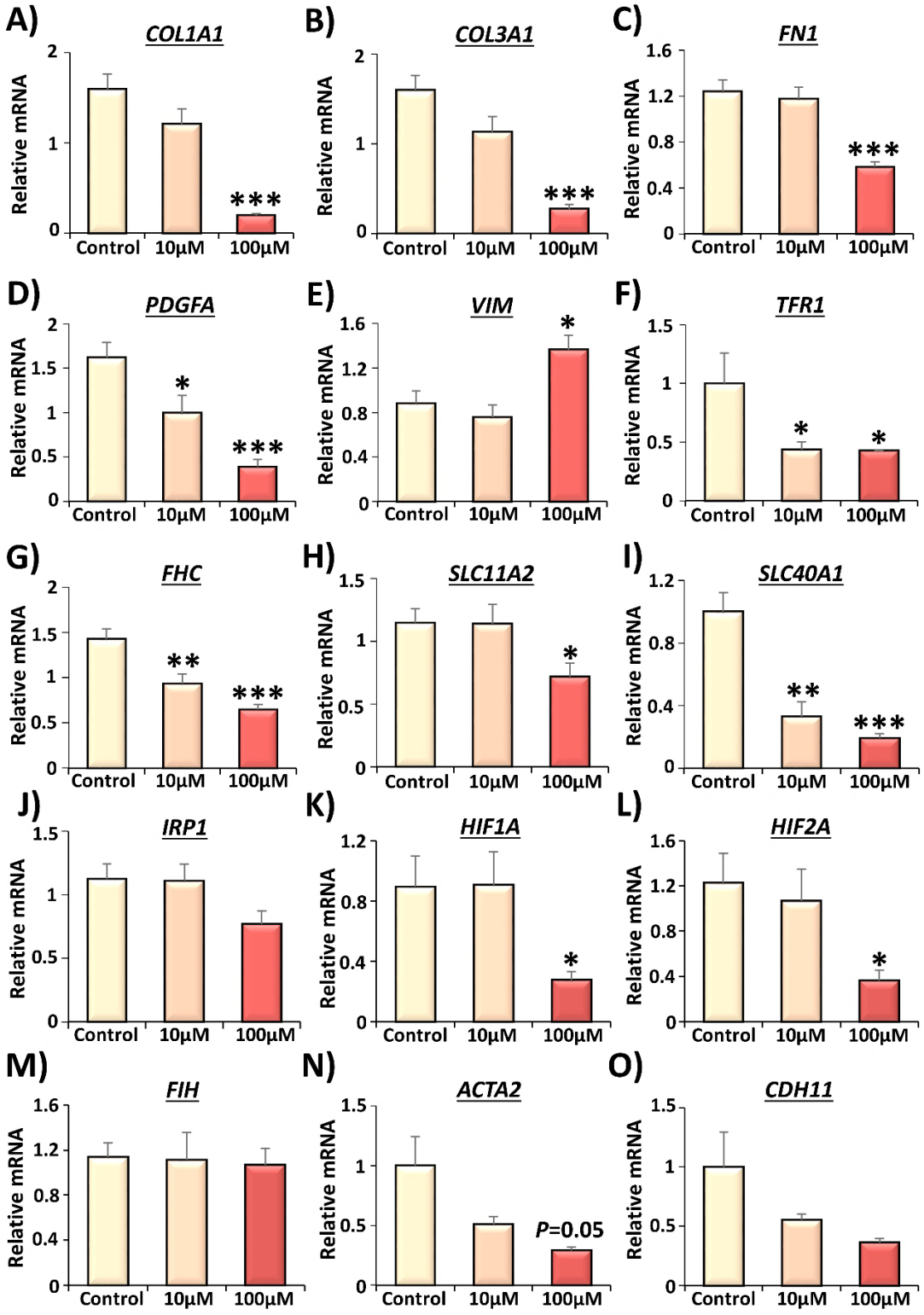

Figure 5.13. Iron alters gene expression in human dermal fibroblasts. qRT-PCR showing changes in human dermal fibroblast gene expression following 72 hours of ferric ammonium citrate treatment. Matrix genes analysed were *COL1A1* (**A**), *COL3A1* (**B**), *FN1* (**C**), *PDGFA* (**D**), *VIM* (**E**). Iron genes analysed were *TFR1* (**F**), *FHC* (**G**), *SLC11A2* (**H**), *SLC40A1* (**I**), *IRP1* (**J**), *HIF1A* (**K**), *HIF2A* (**L**) and *FIH* (**M**) by RT-qPCR. The differentiation markers, *ACTA2* (**N**) and *CDH11* (**O**), were also assessed. Mean + SEM. Combined from 3 donors. * = $P < 0.05$, ** = $P < 0.01$, *** = $P < 0.001$. Significance deduced via one-way ANOVA and Dunnett's *post-hoc* analysis (compared to control).

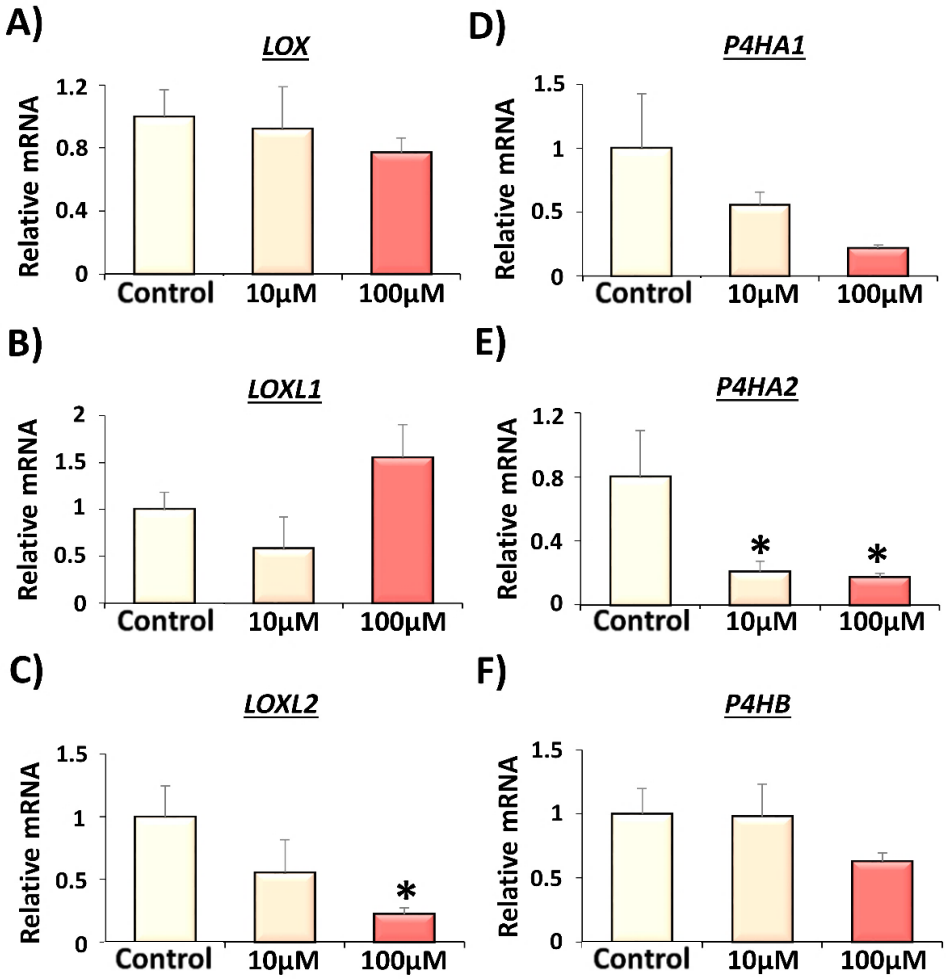

Figure 5.14. Iron administration alters the expression of matrix stabilising genes *in vitro*. qRT-PCR analysis demonstrates changes in human dermal fibroblast matrix gene expression following 72 hours of ferric ammonium citrate treatment. Genes analysed were *LOX* (**A**), *LOXL1* (**B**), *LOXL2* (**C**), *P4HA1* (**D**), *P4HA2* (**E**) and *P4HB* (**F**). Data show mean + SEM. Combined from 3 donors. * = $P < 0.05$. Significance deduced via one-way ANOVA and Dunnett's *post-hoc* analysis (compared to control).

5.4.5. Administration of iron heightens PDGFA expression.

The next aim was to determine how FAC treatment modulated matrix production at the protein level. The first protein of interest was PDGFA, a potent inducer of connective tissue remodelling (Horikawa et al., 2015). PDGFA expression was verified via ICC on cells treated with iron for five days (**Figure 5.15B**) and 11 days (**Figure 5.15C**), with representative staining (**Figure 5.15A**). FAC treatment significantly increased PDGFA expression at day 5 ($P < 0.001$) and day 11 (10 μM, $P < 0.01$; 100 μM, $P < 0.05$). Western blot analysis on cells at day 5 confirmed the elevated PDGFA expression following 100 μM FAC treatment ($P < 0.001$; **Figure 5.15D-E**). As iron clearly modulated PDGFA protein levels in HDFs, the effects of iron administration on major ECM proteins was subsequently assessed.

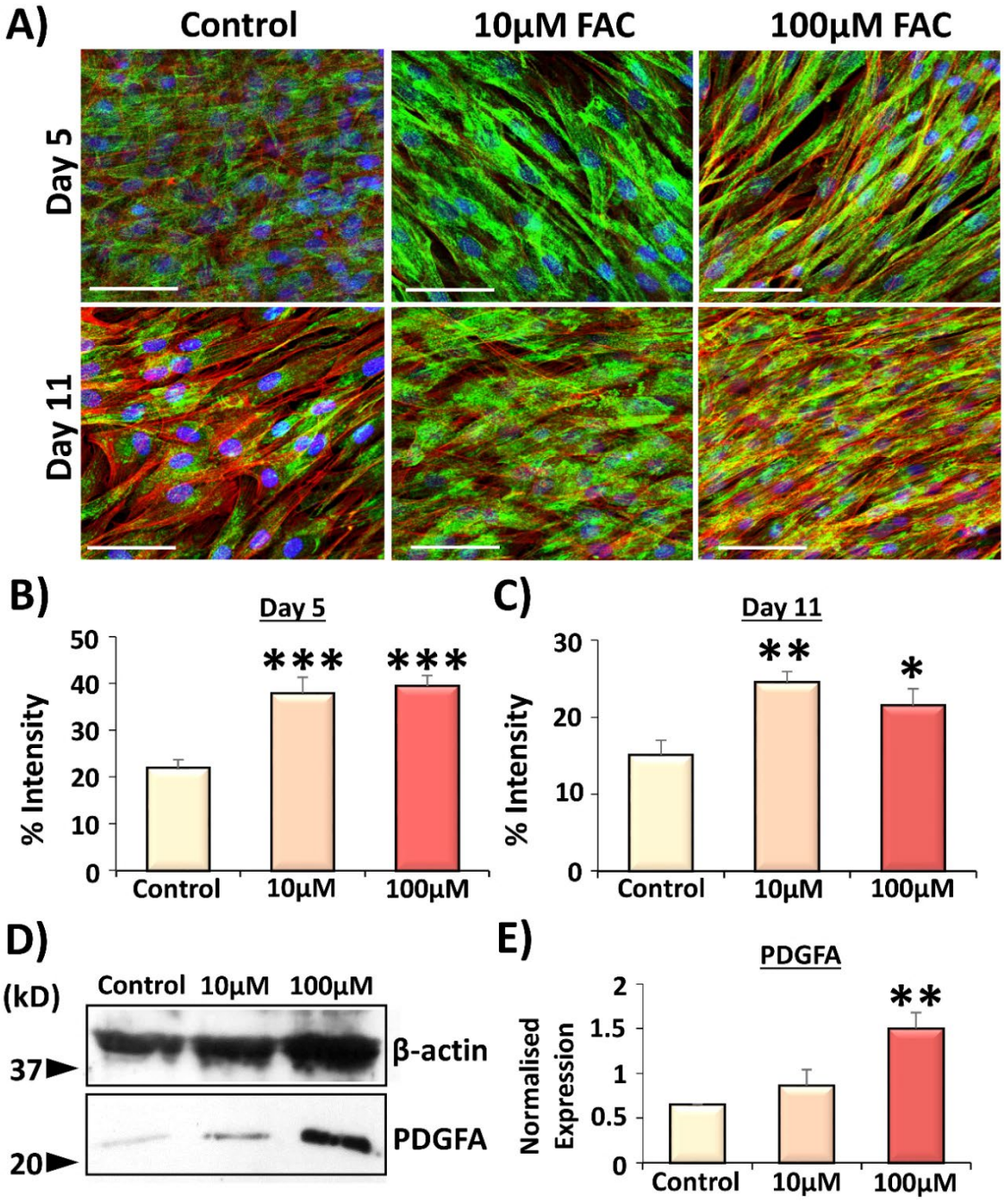

Figure 5.15. The expression of platelet-derived growth factor subunit A is modulated by iron. Human dermal fibroblasts treated with ferric ammonium citrate (FAC) displayed greater PDGFA expression at day 5 (**A-B**) and day 11 (**A, C**) post-initial iron exposure. Data combined from 3 experiments in 3 donors. Representative images of PDGFA (green) are shown in **A** (phalloidin, red; DAPI, blue nuclei). Bar = 50 µm. Western blot at day 5 confirms increased PDGFA expression with FAC (representative blot, **D**, normalised to β actin, **E**). Mean + SEM. * = $P < 0.05$, ** = $P < 0.01$, *** = $P < 0.001$. One-way ANOVA with Dunnett's multiple comparisons analysis (versus control).

5.4.6. Iron accelerates fibronectin remodelling *in vitro* in an MMP2-dependent manner.

An important aspect of wound repair is ECM deposition (Gurtner et al., 2008). Therefore, the next objective was to establish whether iron affected ECM production. At day 5, fibronectin was significantly increased with 10 μM FAC treatment ($P < 0.01$), and decreased to control levels with 100 μM FAC (**Figure 5.16A-B**). By day 11, levels of fibronectin were not significantly different between control and 10 μM FAC, but HDFs treated with 100 μM FAC still showed significantly less fibronectin compared to 10 μM FAC-treated cells ($P < 0.01$; **Figure 5.16C**).

FAC treatment altered the abundance of deposited fibronectin, therefore the ability of HDFs to remodel exogenous fibronectin was determined using an Fn-488 assay (as in Torr et al., 2015). Here, 488-conjugated fibronectin was introduced to naïve HDF cultures at the same time as FAC (**Figure 5.16D-E**). When HDFs cleaved the exogenous fibronectin, this resulted in release of the 488 conjugate, therefore fluorescent intensity was measured as a readout of fibronectin remodelling. FAC treatment increased fibronectin cleavage in a dose-dependent manner (100 μM, $P < 0.001$). To elucidate whether MMP2 was involved in FAC-mediated remodelling of fibronectin, a potent MMP2 inhibitor (ARP101) was added to HDFs treated with 100 μM FAC (**Figure 5.16F**). FAC-induced fibronectin remodelling was significantly reduced in the presence of ARP101 ($P < 0.01$; **Figure 5.16G**), suggesting that FAC-mediated MMP2 production may aid fibronectin remodelling *in vitro*.

In concurrence, CM from HDF cultures treated with 100 μM FAC showed higher MMP2 activity on gelatin zymograms ($P < 0.05$; **Figure 5.16H-I**). To determine whether iron directly altered the activity of MMPs, MMP2 and MMP9 protease standards were incubated with FAC alone (**Figure 5.16J-L**). Zymography revealed that FAC did not significantly alter the activity of MMP2 and MMP9 proteases, thus the effect of FAC on MMP2 expression was HDF-dependent. Finally, exogenous fibronectin was incubated with recombinant MMP2 to directly demonstrate that MMP2 cleaves fibronectin (**Figure 5.16M**). Overall, it was clear that FAC treatment accelerated fibronectin remodelling, in part via upregulation of MMP2.

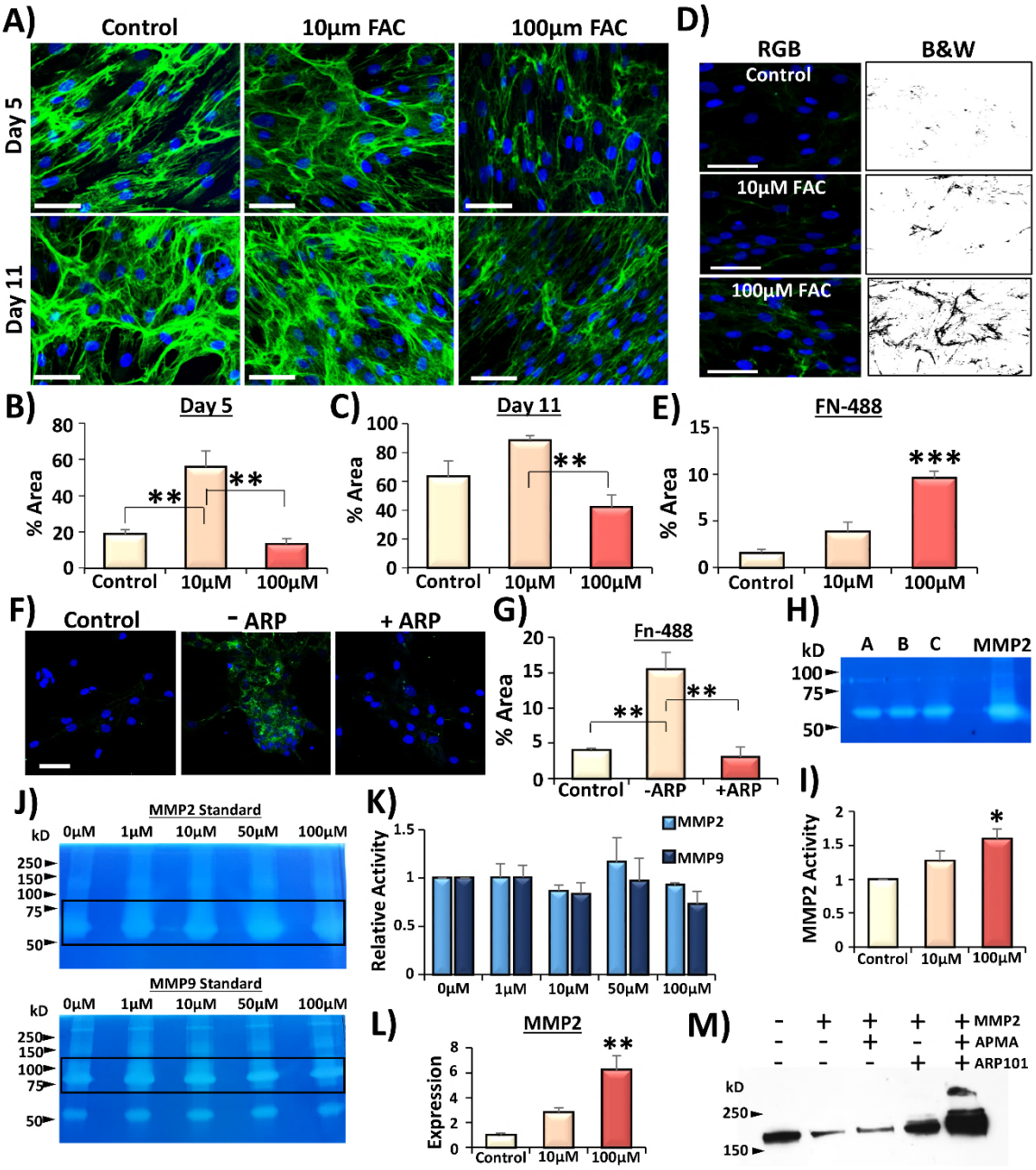

Figure 5.16. Iron loading causes rapid fibronectin remodelling in human dermal fibroblasts *in vitro*. Human dermal fibroblasts (HDFs) were treated with FAC (ferric ammonium citrate), stained for fibronectin (**A**) and quantified (**B-C**). DAPI = blue nuclei. 488 = fibronectin. Fn-488 remodelling (**D**), quantified in **E**. ARP101 (MMP2 inhibitor) remodelling with 100 µM FAC (**F-G**). Bar = 50 µm. Zymography on HDF conditioned media (**H-I**). A= 0 FAC, B = 10 µM FAC, C = 100 µM FAC. MMP2 and MMP9 standards plus FAC (**J-K**). Black boxes = bands measured. *MMP2* expression increases following 100 µM FAC treatment (qRT-PCR, **L**). Western blot demonstrating that MMP2 degrades human fibronectin (**M**). 4-aminophenylmercuric acetate (APMA) = MMP2 activator. n = 3 donors. Mean + SEM. * = $P < 0.05$, * = $P < 0.01$, *** = $P < 0.001$. Significance determined via one-way ANOVA with Tukey's multiple comparisons test (versus control).

5.4.7. Elevated iron causes accelerated extracellular secretion of collagen type III and collagen type I.

Collagens are the major structural protein of the dermis and their deposition and remodelling is vital for proper skin reformation following injury (Bainbridge, 2013). Collagen content of FAC-treated HDFs was first assessed indirectly by measuring their hydroxyproline content. Indeed, 100 μM FAC significantly increased hydroxyproline ($P < 0.001$), which was attenuated in the presence of the iron chelator, deferoxamine ($P < 0.001$; **Figure 5.17A**).

Subsequently, HDFs were treated with or without FAC for 11 days and stained for collagen type III and collagen type I via immunofluorescence. Collagen III ($P < 0.001$; **Figure 5.17B-C**) and collagen I ($P < 0.001$; **Figure 5.17B, D**) deposition were not only significantly higher following 100 μM FAC treatment, but were only visible as extracellular fibres following 100 μM FAC administration. When HDFs were denuded from their ECM, the same result was observed whereby collagen III ($P < 0.001$; **Figure 5.17E-F**) and collagen I ($P < 0.001$; **Figure 5.17E, G**) deposition were much greater following 100 μM FAC administration. Immunofluorescence for collagen III (**Figure 5.17H**) and collagen I (**Figure 5.17I**) was also performed at a range of FAC doses to determine whether a dose-dependent effect could be seen. However, only 100 μM FAC led to significant extracellular collagen deposition ($P < 0.001$). Treatment with the iron chelator, deferoxamine, prevented FAC-induced collagen deposition, while treatment with an iron-independent oxidant (PMA) did not increase collagen deposition. These results demonstrated that high iron administration induced the extracellular deposition of collagen III and collagen I matrix *in vitro*.

5.4.8. Profiling of denuded extracellular matrix confirms that iron induces hypersecretion of matrix proteins.

The protein content of deposited ECM was further characterised from denuded plates following 11 days of FAC treatment. Western blot of denuded ECM showed that 100 μM FAC treatment lead to significantly greater expression of COL1A1 ($P < 0.05$; **Figure 5.18A-B**), COL6A1 ($P < 0.001$; **Figure 5.18A, C**), PDGFA ($P < 0.001$; **Figure 5.18, D**) and vimentin ($P < 0.001$; **Figure 5.18A, E**). Western blot analysis only allows targeted monitoring of a small group of proteins with limited sensitivity (Naba et al., 2015). Thus, mass spectrometry was employed as a non-directed

approach, and also demonstrated that high FAC treatment increased extracellular deposition of collagen-rich ECM (**Appendix Table 5A.1**).

Previous analyses focussed on assessing protein expression via western blot and low-power fluorescent visualisation (ICC). Scanning electron microscopy (SEM) allowed for the determination of cellular structural changes following FAC treatment at higher magnification and resolution. Limited structural alterations were evident in 10 μM FAC-treated fibroblasts versus control (**Figure 5.18F**). By contrast, following 100 μM FAC treatment HDFs displayed large microvesicles (white arrows) and an increase in extracellular secretions (grey arrows). Together, these data show that treatment with high FAC promoted ECM secretion and deposition in HDFs.

5.4.9. Naïve fibroblasts respond to extracellular matrix deposited by iron-treated cells.

Naïve HDFs were exposed to denuded ECM from FAC-treated HDFs to determine whether the FAC-deposited ECM could influence gene expression in non-FAC stimulated HDFs. After 48 hours, the naïve HDFs were collected to assess changes in gene transcription (schematic of the experiment in **Figure 5.19A**). Intriguingly, naïve HDFs showed the same responses as seen in iron treated cells. For example, naïve HDFs cultured on matrix from 100 μM FAC-stimulated HDFs retained significantly dampened mRNA levels of *COL1A1* ($P < 0.01$; **Figure 5.19B**), *COL3A1* ($P < 0.001$; **Figure 5.19C**), *FN1* ($P < 0.05$; **Figure 5.19D**) and *COL6A1* ($P < 0.01$; **Figure 5.19E**), and modest reductions in *PDGFA* (**Figure 5.19F**) and *ACTA2* (**Figure 5.19G**). Significant reductions in of *P4HA2* ($P < 0.001$; **Figure 5.20B**), *LOX* ($P < 0.01$; **Figure 5.20D**), *LOXL1* ($P < 0.01$; **Figure 5.20E**) and *SLC40A1* ($P < 0.05$; **Figure 5.20H**) were also observed. These results demonstrated that exposure to ECM produced by FAC-loaded HDFs, and not direct FAC administration, induced gene expression changes in naïve HDFs comparable to those shown in FAC-treated HDFs.

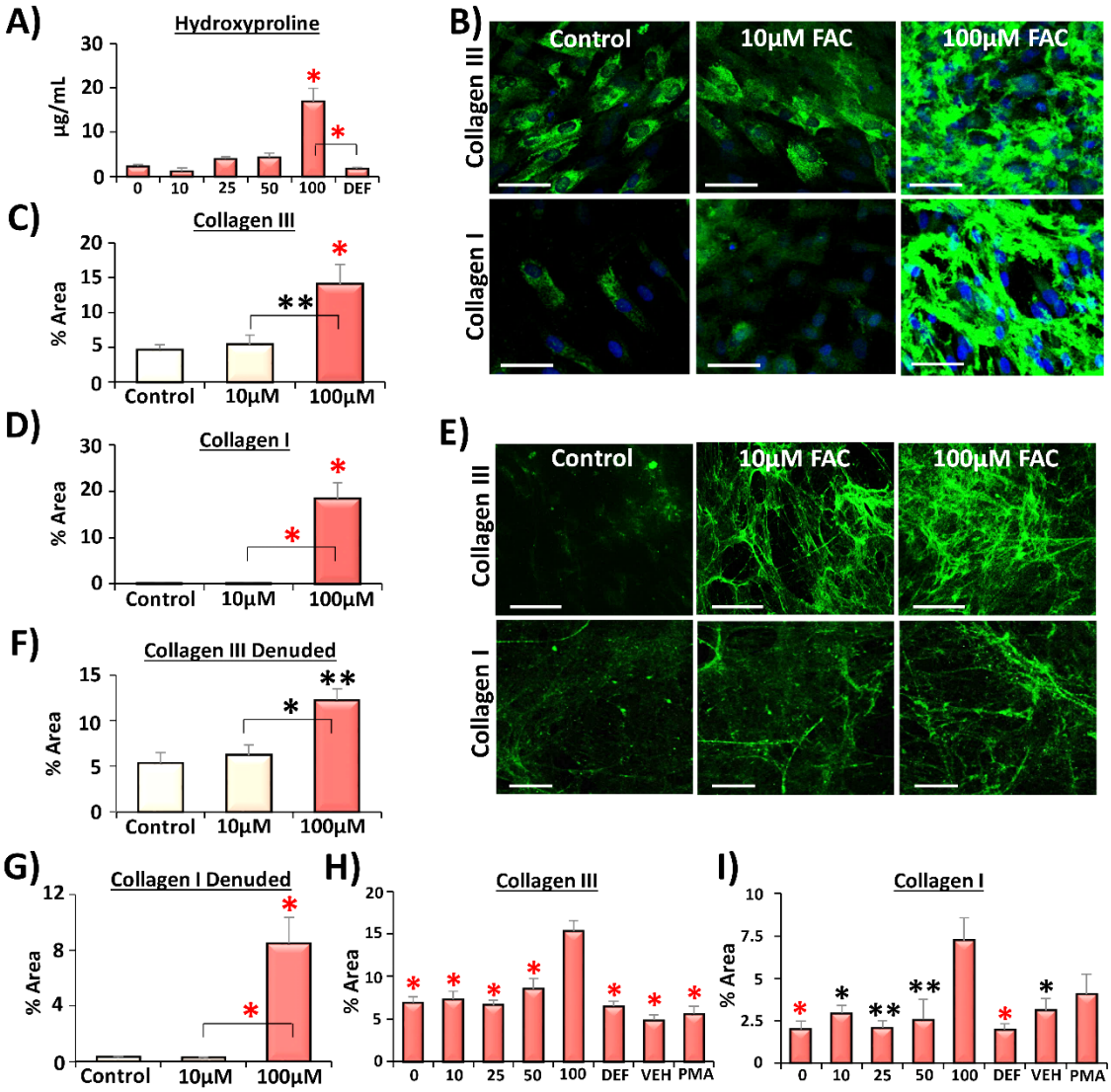

Figure 5.17. Iron supplementation promotes extracellular deposition of collagen. Hydroxyproline content was measured in human dermal fibroblasts following 11 days of ferric ammonium citrate (FAC) treatment (**A**). Extracellular production of collagen III (**C**) and I (**D**) increases following 100 µM FAC. Images in **B**. Collagens = green. DAPI = blue nuclei. Cells were removed (denuded) from extracellular matrix (**E**) and extracellular collagen III (**F**) and I (**G**) assessed. Dose-dependent analysis of collagen III (**H**) and collagen I (**I**). DEF = 100 µM FAC plus 100 µM deferoxamine (iron chelator). VEH = vehicle for phorbol 12-myristate 13-acetate (PMA). Bar = 50 µm. Representative of 3 donors. Mean + SEM. * = $P < 0.05$, ** = $P < 0.01$, red* = $P < 0.001$. Data in **H** and **I** compared to 100 µM FAC. One-way ANOVA and Tukey's *post-hoc* analysis.

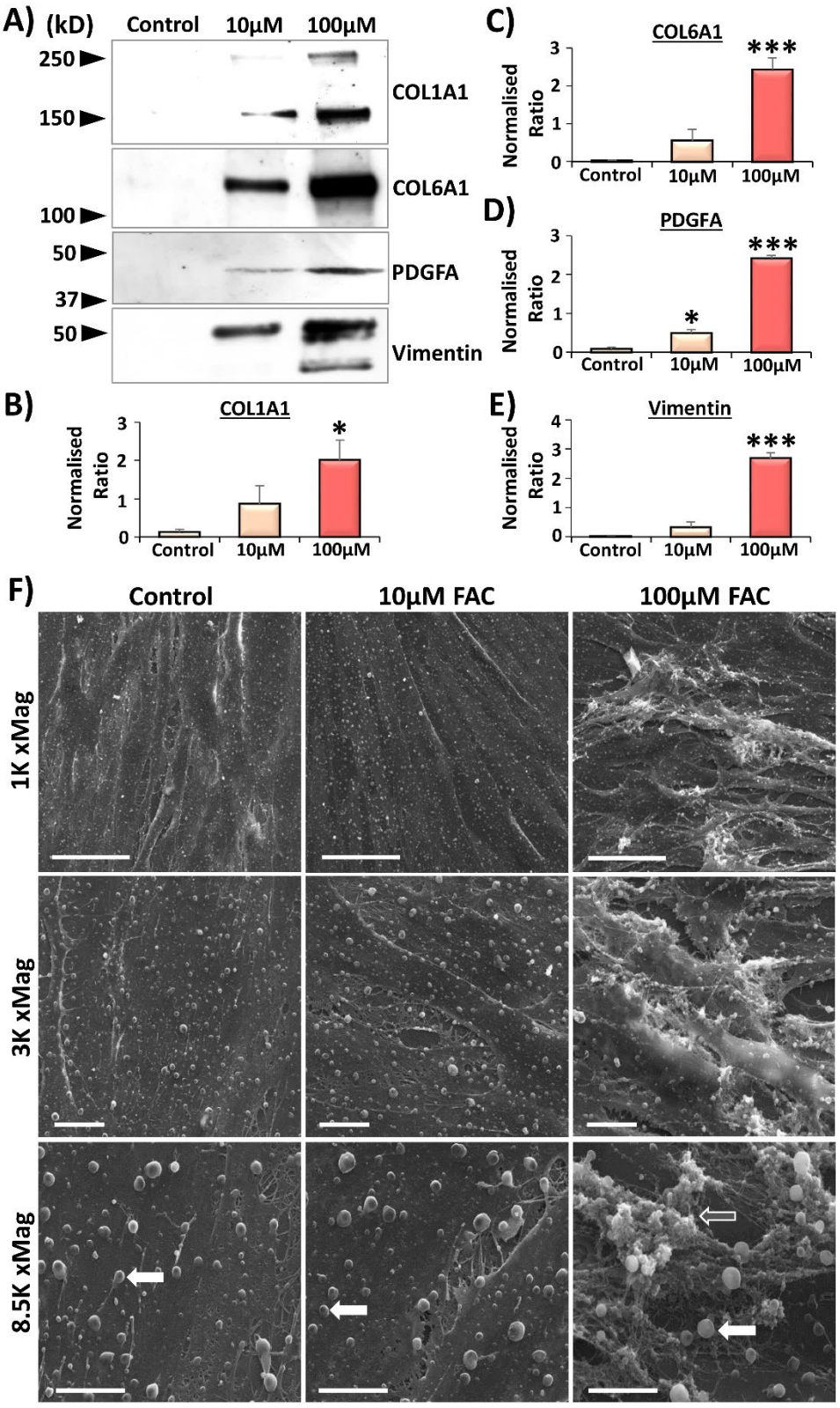

Figure 5.18. Iron treatment enhances extracellular matrix secretion *in vitro*. Representative western blots of denuded ECM (**A**). Quantification of COL1A1 (**B**), COL6A1 (**C**), PDGFA (**D**) and Vimentin (**E**). n = 3 donors. FAC = ferric ammonium citrate. Mean + SEM. * = $P < 0.05$, *** = $P < 0.001$. One-way ANOVA with Dunnett's multiple comparisons test (versus control). High FAC treatment increased extracellular secretions (grey arrows) and caused larger microvesicle formation (white arrows), as demonstrated by scanning electron microscopy (**F**). 1K magnification bar = 50 nm. 3K magnification bar = 10 nm. 8.5K magnification bar = 5 nm.

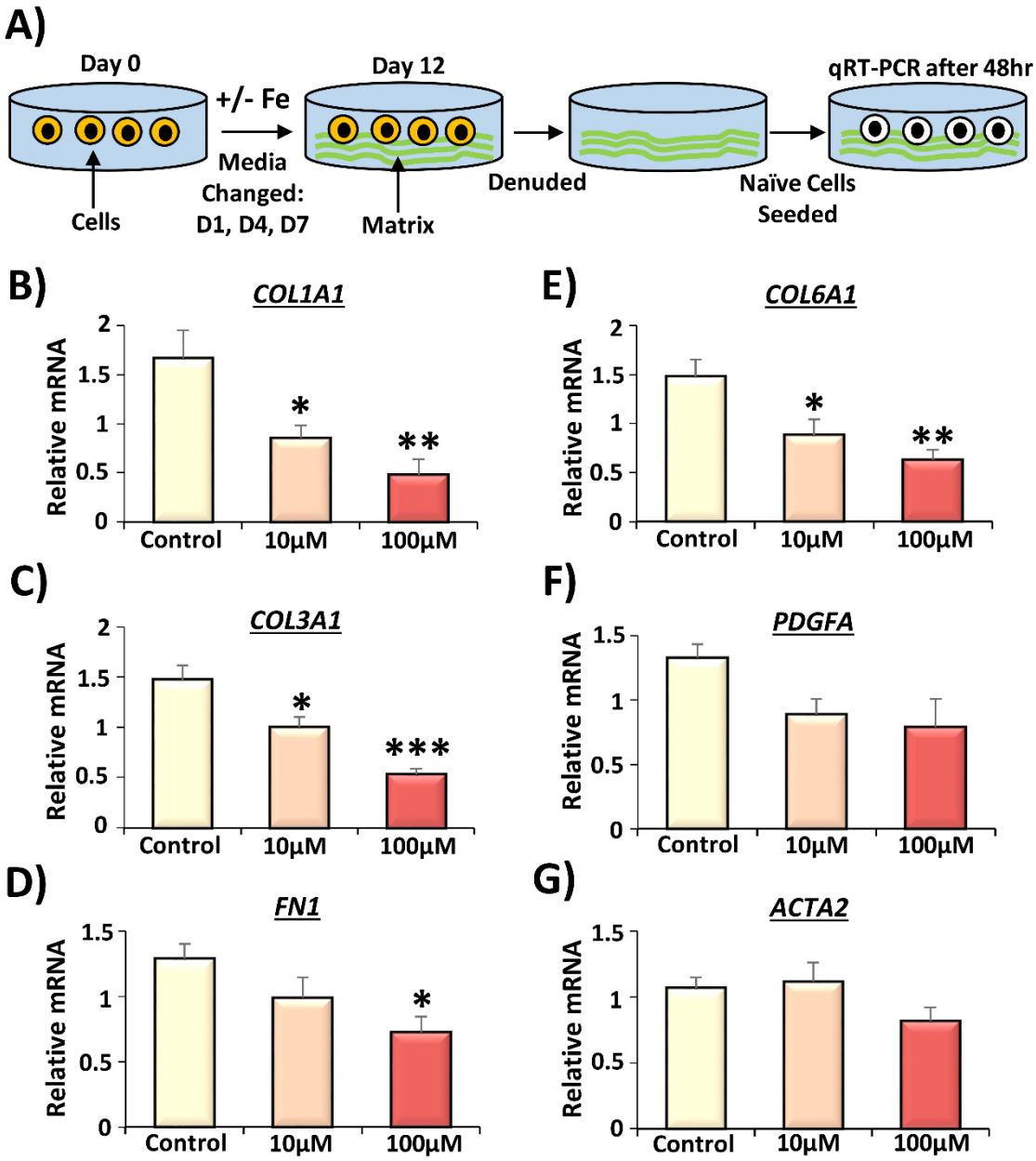

Figure 5.19. Naïve human dermal fibroblasts are influenced by extracellular matrix produced by iron-loaded cells. Human dermal fibroblasts (HDFs) were treated with or without ferric ammonium citrate (FAC) for 11 days and denuded from their deposited extracellular matrix. Donor matched naïve cells were deposited onto the denuded ECM without iron supplementation. After 48 hours, HDFs were collected for qRT-PCR (schematic, **A**). Gene expression for *COL1A1* (**B**), *COL3A1* (**C**), *FN1* (**D**), *COL6A1* (**E**), *PDGFA* (**F**) and *ACTA2* (**G**). Data pooled from 3 donors. Mean + SEM. * = $P < 0.05$, ** = $P < 0.01$, *** = $P < 0.001$. One-way ANOVA with Dunnett's *post-hoc* analysis (versus control).

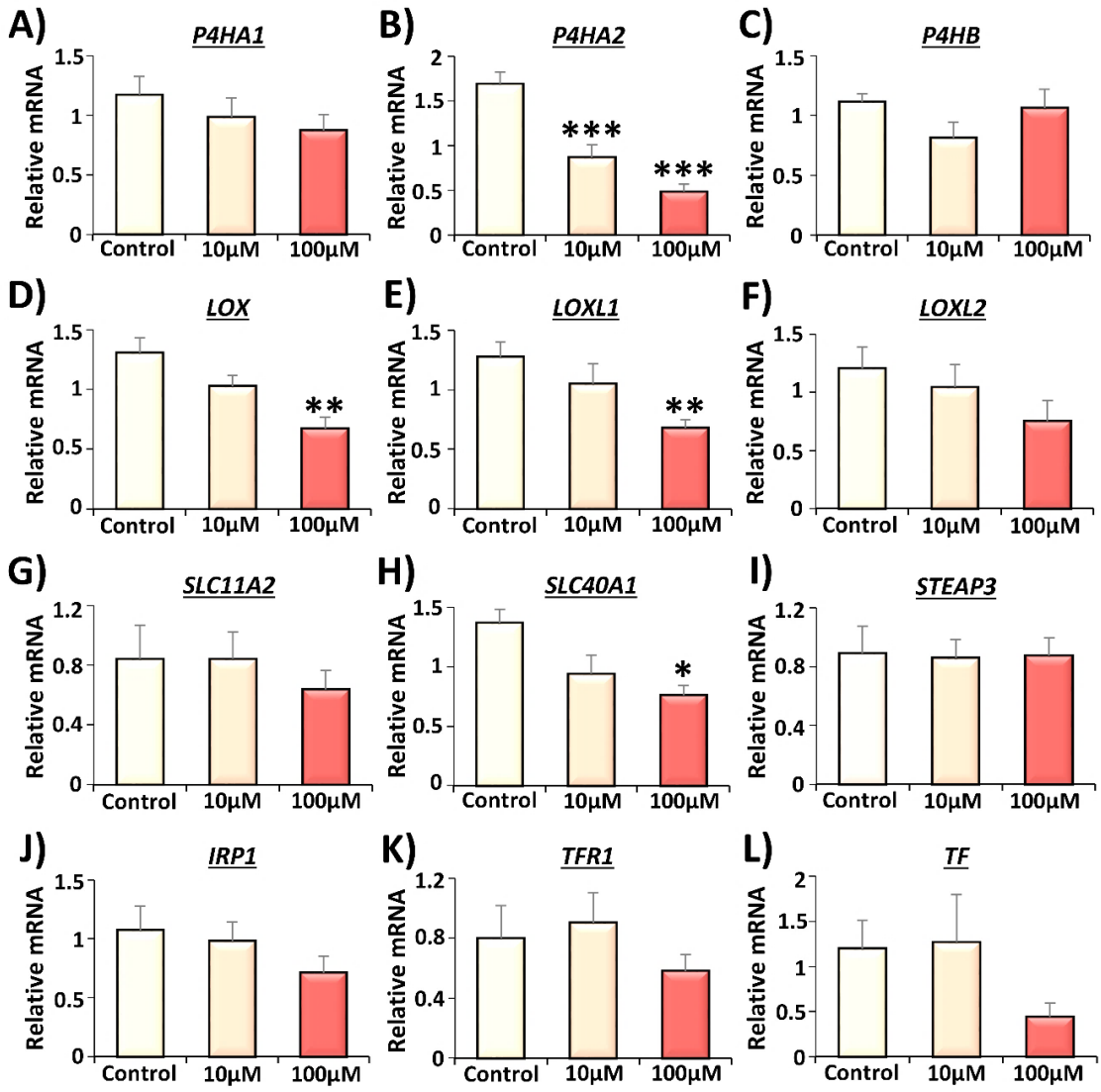

Figure 5.20. Iron-loaded extracellular matrix influences enzyme expression in naïve human dermal fibroblasts. Naïve human dermal fibroblasts (HDFs) were seeded onto denuded extracellular matrix from cells treated with or without ferric ammonium citrate. HDFs were collected after 48 hours exposure and profiled via qRT-PCR for changes in prolyl 4 hydroxylase (P4H) and lysyl oxidase (LOX) gene expression and iron-regulatory genes. *P4HA1* (**A**), *P4HA2* (**B**), *P4HB* (**C**), *LOX* (**D**), *LOXL1* (**E**), *LOXL2* (**F**), *SLC11A2* (**G**), *SLC40A1* (**H**), *STEAP3* (**I**), *IRP1* (**J**), *TFR1* (**K**) and *TF* (**L**). Data pooled from 3 donors. Mean +/- SEM. * = $P < 0.05$, ** = $P < 0.01$, *** = $P < 0.001$. One-way ANOVA performed on all data sets with Dunnett's *post-hoc* analysis (compared to control).

5.4.10. Iron induces extracellular matrix deposition via an oxidative stress-dependent mechanism.

To elucidate whether oxidative stress was involved in FAC-mediated deposition of ECM, a CellROX® assay was performed. Here, FAC caused a dose-dependent increase in intracellular ROS (**Figure 5.21A-B**), where 100 μM FAC led to the most significant effect ($P < 0.001$), attenuated by deferoxamine treatment ($P < 0.001$).

Oxygen content was also measured in HDF cultures, but was not altered by FAC administration (**Appendix Figure 5A.5**). A number of antioxidants were screened to determine whether they could inhibit FAC-mediated oxidative stress (**Appendix Figure 5A.5**). Only mannitol, a hydroxyl radical scavenger (Shen, 1997), effectively and consistently dampened ROS production in 100 μM FAC-treated HDFs ($P < 0.05$; **Figure 5.21C-D**). Interestingly, FAC-treated HDFs supplemented with mannitol showed reduced collagen III ($P < 0.001$; **Figure 5.21C, E**) and collagen I ($P < 0.01$; **Figure 5.21C, F**) production, and decreased cytoplasmic ferritin stores ($P < 0.001$; **Figure 5.21G**). Hence, it is clear that FAC induced ECM deposition occurred via an oxidative stress-dependent mechanism.

5.4.11. *STEAP3* is required for FAC-induced oxidative stress-dependent extracellular matrix deposition.

To determine a molecular link between FAC-induced ECM deposition and wound repair, a wound tissue screen of iron-related genes was performed via qRT-PCR (**Figure 5.22A**). Data are depicted as heat maps showing fold change in expression. The left panel demonstrates fold change differences in normal healing WT wounds (versus skin). The right panel shows fold change differences in Db wounds (versus NDb). In normal healing, *Steap3* ($P < 0.05$; **Figure 5.22B**), *Slc40a1* ($P < 0.05$) and *Slc11a2* ($P < 0.05$) were significantly upregulated at D7 post-injury, *Ftl* was elevated at D1 post-injury ($P < 0.05$), and *Fth* was modestly higher at D1. In Db wounds, *TfR1* ($P < 0.05$) was upregulated at D7, while *Irp1* ($P < 0.001$), *Fth* ($P < 0.01$) and *Ftl* ($P < 0.001$) were increased at D3 post-injury. Of note, *Steap3* was significantly downregulated at D7 post-injury in Db versus NDb wounds ($P < 0.001$; **Figure 5.22C**). In HDFs, 100 μM FAC led to *STEAP3* upregulation ($P < 0.05$; **Figure 5.22D**), which was attenuated by mannitol treatment ($P < 0.05$; **Figure 5.22E**), suggesting a potential link between *STEAP3* and FAC-induced oxidative stress.

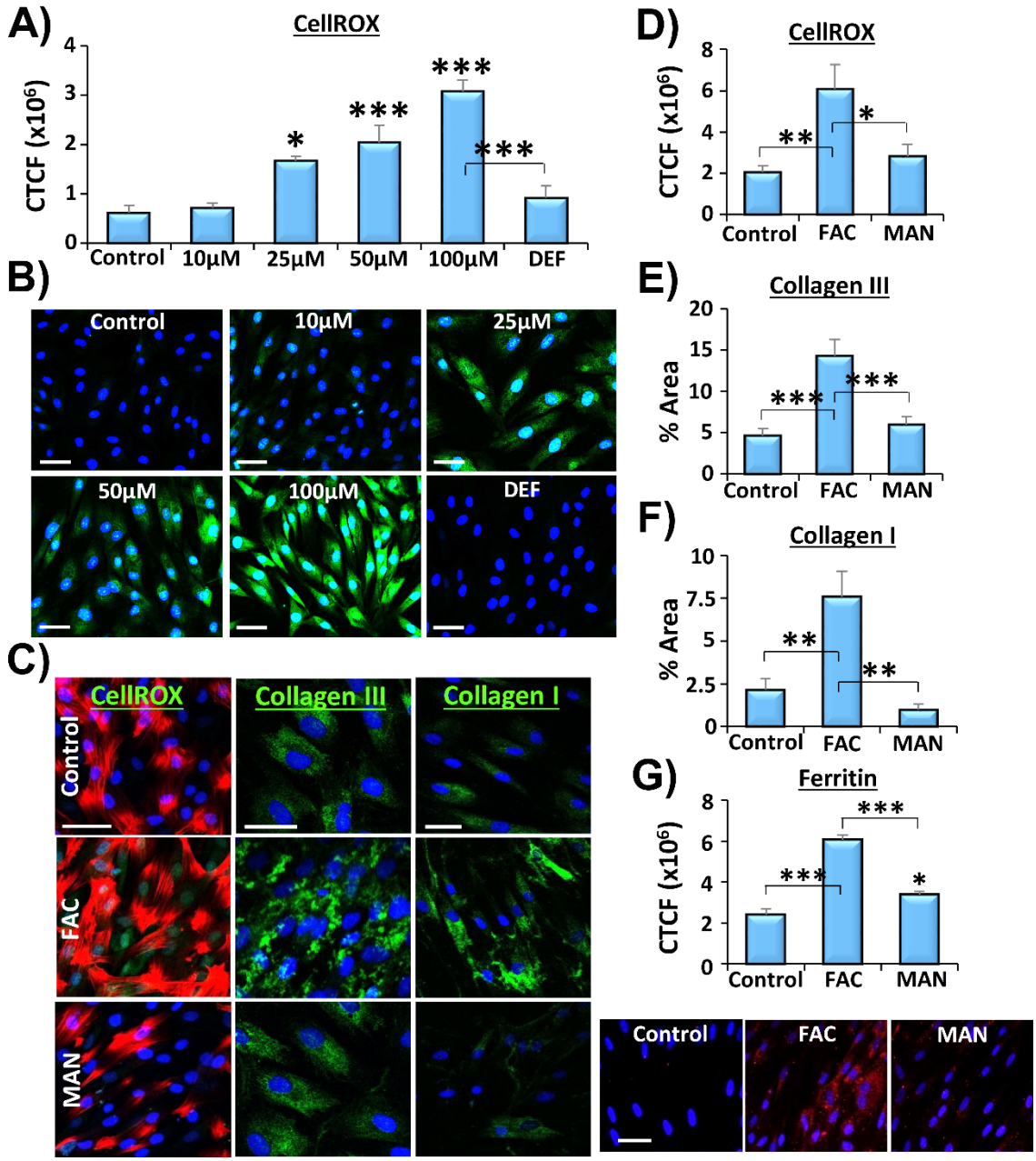

Figure 5.21. Iron induces collagen deposition via oxidative stress, which is attenuated by mannitol. Ferric ammonium citrate (FAC) treatment leads to a dose-dependent increase in oxidative stress (CellROX®, **A-B**). CellROX® =green. DAPI = blue nuclei. Phalloidin = red cytoskeleton. Mannitol (MAN) attenuates FAC (100 µM) induced oxidative stress (**C-D**) and reduces collagen III (**C, E**) and collagen I deposition (**C, F**). MAN also reduces ferritin storage (**G**). Ferritin = red. Bar = 50 µm. CTCF = corrected total cell fluorescence. n = 3 donors per experiment. Data show mean + SEM. * = $P < 0.05$, ** = $P < 0.01$, *** = $P < 0.001$. One-way ANOVA with Tukey's *post-hoc* analysis (versus control).

Targeted knockdown of *STEAP3* was optimised (**Appendix Figures 5A.6-5A.9**) and performed with two validated siRNAs (Si-S3#1 and Si-S3#2; **Figure 5.22F**), leading to a significant reduction in collagen I ($P < 0.001$; **Figure 5.22G-H**) and collagen III production ($P < 0.001$; **Figure 5.22I-J**) compared to control siRNA (Si-Ctrl). Finally, as mannitol treatment dampened *STEAP3* in HDFs, a CellROX® assay was performed on siRNA treated cells (**Figure 5.22K-L**). Here, ROS production was significantly reduced in no FAC ($P < 0.01$; $P < 0.05$) and 100 μM FAC-treated ($P < 0.001$) HDFs following siRNA knockdown. Taken together, these findings suggested that HDFs require *STEAP3* for FAC-mediated oxidative stress-induced extracellular deposition of collagen I and collagen III.

5.4.12. Macrophages are major iron sequestering cells in late-stage wound healing.

So far this chapter has focussed on the role of iron in modulating HDF behaviour, yet other cell types are present and required for adequate late-stage wound repair. To establish the co-interaction between iron and other wound-relevant cells, immunofluorescent staining was performed on WT mouse wound time course tissue. The overall percentage of ferritin^{+ve} cells increased throughout healing, and was significantly higher at day 3 ($P < 0.001$) and day 7 ($P < 0.001$) post-injury versus normal skin (day 0; **Figure 5.23A-C**). A proportion of wound Mφs (Mac3) co-stained for ferritin (**Figure 5.23A, B**). Quantification revealed a significant accumulation of sequestered ferritin in Mφs at day 3 ($P < 0.05$) and day 7 ($P < 0.001$**; Figure 5.23B, D**) post-injury. Note, α-Sma^{+ve} fibroblasts accrued ferritin only at day 7 post-injury ($P < 0.05$; **Figure 5.23B, E**). By day 7 post-injury, tissue infiltrating Mφs were largely anti-inflammatory, characterised by reduced Nos-2 ($P < 0.001$ versus day 3; **Figure 5.24A-B**) and increased Arginase-1 ($P < 0.05$ versus day 3 post-injury; **Figure 5.24A, C**). These results suggest that wound iron preferentially accumulated in Mφs, temporally correlating with tissue infiltration of pro-healing (M2) Mφs.

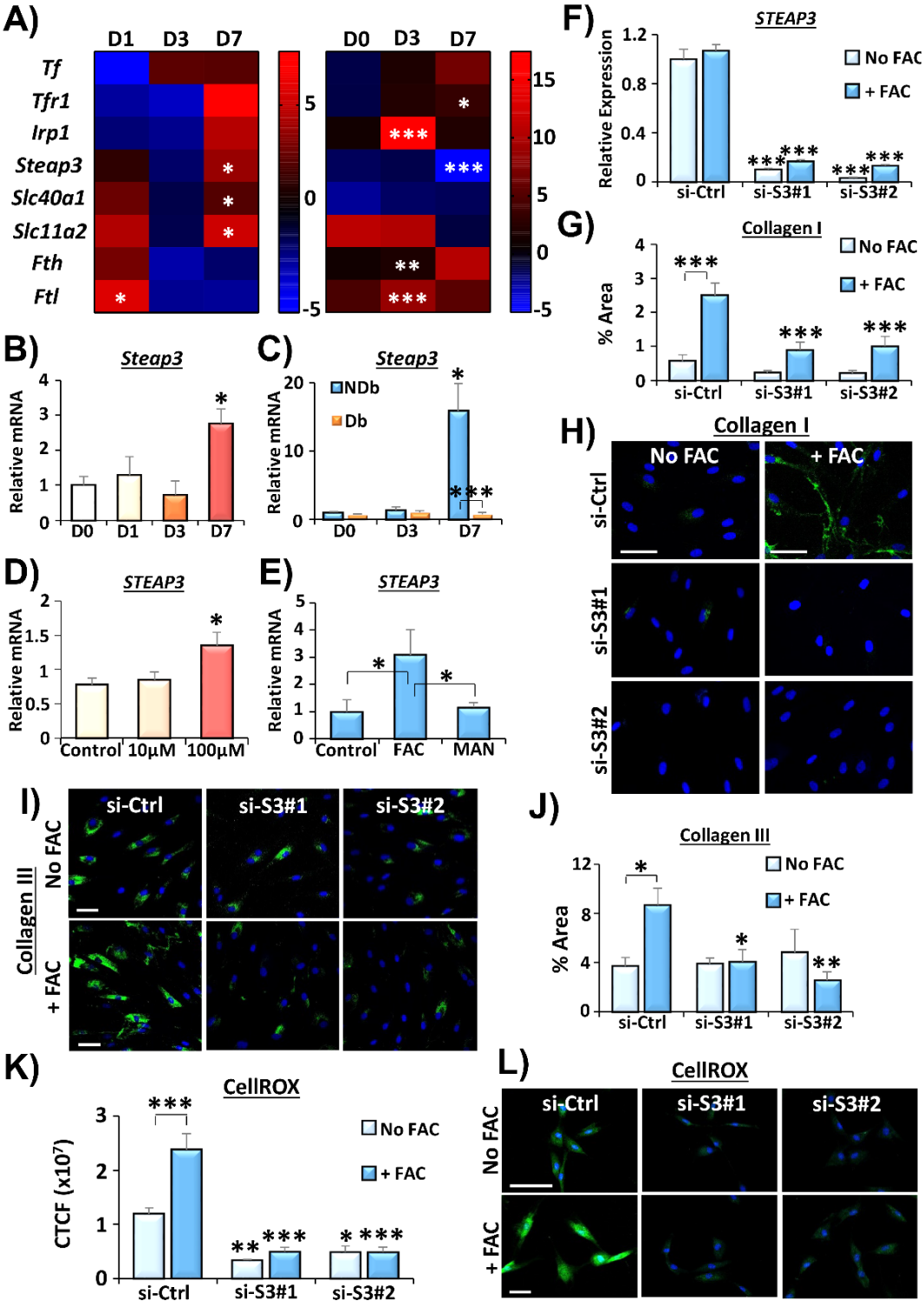

Figure 5.22. Oxidative stress-induced collagen deposition requires STEAP3. Iron genes across normal (**A**, left panel) and diabetic (Db) healing (**A**, right panel). Fold change expression versus normal skin (D0) or Non-Db (NDb). D3 = day 3 post-injury. *Steap3* in normal (**B**) and Db wounds (**C**). n = 3-4 mice per group. Human dermal fibroblasts treated with ferric ammonium citrate (FAC) show increased *STEAP3* (**D**), attenuated by mannitol (MAN, plus 100 μM FAC; **E**). *STEAP3* knockdown via siRNA (**F**). FAC-mediated collagen I (**G-H**) and collagen III (**I-J**) deposition and stress (**K-L**). si-Ctrl = validated siRNA control. si-S3 = *STEAP3* siRNA. n = 3 human donors. Bar = 50 μm. Mean + SEM. * = $P < 0.05$, ** = $P < 0.01$, *** = $P < 0.001$. One-way ANOVA with Tukey's *post-hoc* test was performed on **A** (left panel), **B**, **D** and **E**. Two-way ANOVA was performed on other data sets.

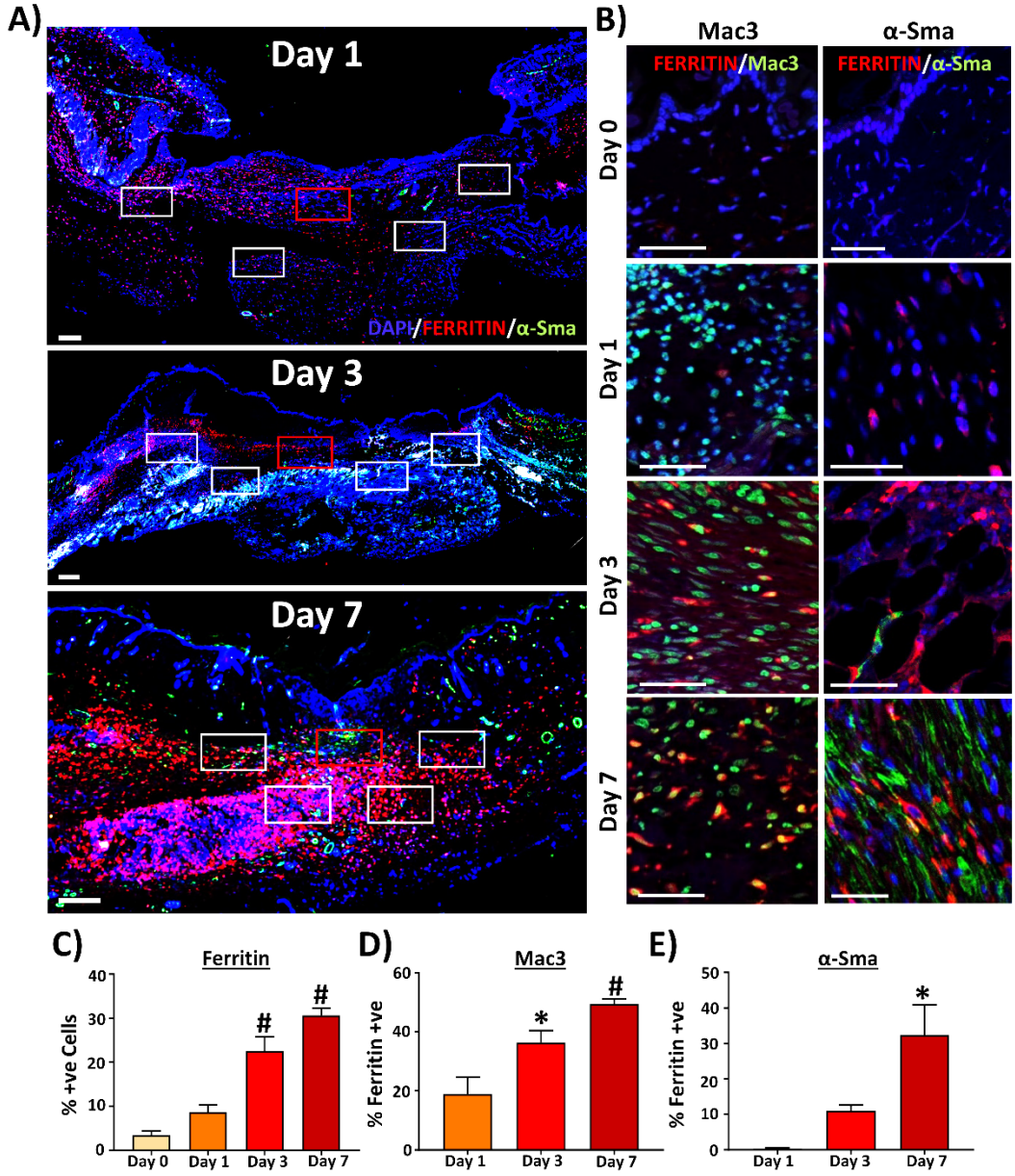

Figure 5.23. Wound cells sequester iron during late-stage wound healing. Full wound images demonstrating ferritin (red) and α-Sma (green) staining (**A**). DAPI = blue nuclei. Five regions in the granulation tissue were analysed (white boxes). Representative images in **B** from red boxes in **A**. Ferritin^{+ve} cells accumulate at day 3 and day 7 post-injury (**C**). Ferritin^{+ve} macrophages (Mac3; **D**) and fibroblasts (α-Sma; **E**) also increase in late-stage repair. Bar in **A** = 100 μm. Bar in **B** = 50 μm. n = 5 per group. Mean + SEM. * = $P < 0.05$, # = $P < 0.001$. n = 5. One-way ANOVA with Tukey's *post-hoc* analysis (versus day 0 in **C** or day 1 in **D-E**).

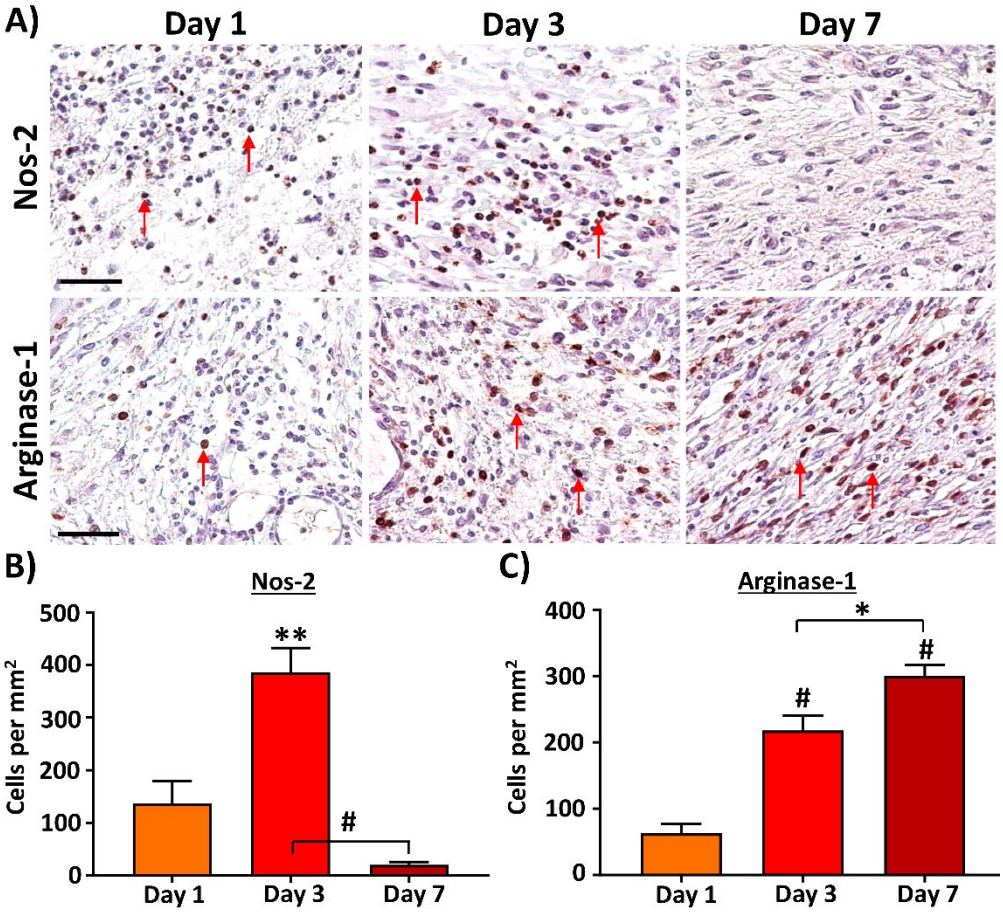

Figure 5.24. Temporal changes in macrophage polarisation throughout normal wound repair. Representative staining of Nos-2 and Arginase-1 positive macrophages (Mφs) in normal wounds (**A**). Nos-2 Mφs reach peak infiltration at day 3 (**B**) and Arginase-1 Mφs reach peak infiltration at day 7 post-injury (**C**). Arrows = positive staining. Bar = 50 µm. Mean + SEM. * = $P < 0.05$, ** = $P < 0.01$, # = $P < 0.001$. n = 5 per group. One-way ANOVA with Tukey's *post-hoc* analysis. */# alone versus day 1.

In both NDb and Db mouse wounds, ferritin was increased at day 3 ($P < 0.01$ versus $P < 0.05$) and day 7 post-injury ($P < 0.001$ versus $P < 0.01$; **Figure 5.25A-B**). However, absolute ferritin levels were reduced in Db wounds ($P < 0.05$ at day 7 post-injury). At day 3, NDb and Db wounds displayed approximately equal ferritin^{+ve} Mφs, however, by day 7 Mφ iron sequestration was clearly reduced in Db wounds (**Figure 5.25A, C**). This reduced proportion of ferritin^{+ve} Mφs in day 7 Db wounds was observed in the context of increased total Mφs ($P < 0.01$; **Figure 5.25E**) and Nos2^{+ve} cells (M1 Mφ marker; **Figure 5.25D, F**). By contrast, and in agreement with published literature (Bannon et al., 2014), wound Arginase-1^{+ve} cells (M2 Mφ marker) were reduced in day 7 Db versus NDb wounds ($P < 0.05$; **Figure 2D, G**), mirroring total ferritin^{+ve} Mφs (**Figure 5.25C**). Collectively, these data revealed altered Mφ iron sequestration and polarisation in Db wounds.

5.4.13. Diabetic macrophages show altered profiles to non-diabetic counterparts when stimulated with cytokines and iron.

In vitro studies were performed to further explore the effect of iron on Mφ function. Murine Mφs were isolated from bone marrow and stimulated to M1 and M2 states with cytokines (**Section 2.6.9**). In NDb Mφs, M1 (*Nos2* and *Cd68*) and M2 (*Ym1* and *Arg1*) polarisation markers were assessed 24 hours, 48 hours and 72 hours post-stimulation. Each marker was upregulated as expected (i.e. M1 markers with M1 polarisation) at each time point, but expression of *Nos2* ($P < 0.001$; **Figure 5.26A**), *Cd86* ($P < 0.05$; **Figure 5.26B**), and *Arg1* ($P < 0.001$; **Figure 5.26D**) was reduced by 72 hours, suggesting reduced retention of polarisation by this time. Therefore, Mφs were subsequently stimulated and used at 24- and 48-hours post-stimulation.

To examine key markers of polarisation and iron regulation (via qRT-PCR), NDb Mφs were treated with FAC at the time of cytokine stimulation and collected after 24 hours. Data were represented as a heatmap (**Figure 5.26E**) to demonstrate fold change differences between the no FAC and FAC (10 μM or 100 μM) treatment groups. As expected, M1-polarised Mφs possessed higher levels of *Nos2* ($P < 0.01$) while *Ym1* ($P < 0.01$) was upregulated in M2-polarised Mφs (**Figure 5.26E** and **Appendix Figure 5A.10**). Profiling of iron-related genes revealed a number of key observations. Firstly, M1-stimulated Mφs showed reduced expression of *Steap3*, *Slc40a1*, *Tf* ($P < 0.05$) and *Tfr1* compared to unstimulated Mφs. Secondly, M2-stimulated Mφs retained heightened *Slc11a2* ($P < 0.05$) and *TfR1* ($P < 0.001$) versus unstimulated Mφs. Finally, FAC treatment led to a significant reduction in *Slc11a2* ($P < 0.05$) and *Tfr1* ($P < 0.001$) in M2 Mφs.

The same analysis (polarisation, iron treatment and qRT-PCR) was performed in Db Mφs. Data were presented as a heatmap comparing FAC-treated to control (no FAC) Db Mφs (**Figure 5.27A**). *Slc40a1* expression was downregulated in M1 and M2-stimulated Db Mφs compared to M0, regardless of FAC treatment ($P < 0.001$; **Figure 5.27B**). *Steap3* expression was lower in M0 Mφs treated with 100 μM FAC ($P < 0.01$; **Figure 5.27C**), while M1-stimulated Db Mφs possessed reduced *Steap3* expression compared to M0 Mφs ($P < 0.001$). FAC significantly dampened *Tf* expression in M0 Db Mφs at 10 μM ($P < 0.001$) and 100 μM ($P < 0.05$) concentrations (**Figure 5.27D**), while *Tf* expression was dampened in M1 ($P < 0.001$) and M2-stimulated ($P < 0.01$) Db Mφs compared to M0. Finally, *TfR1* expression was upregulated in M2-

stimulated Mφs compared to M0 ($P < 0.01$) and M1 ($P < 0.001$) states, while 100 μM FAC reduced *TfR1* expression in M2-stimulated Db Mφs (**Figure 5.27E**). Collectively, these data show that FAC treatment differentially alters NDb and Db BMDM iron-related transcriptional profiles.

5.4.14. Iron skews human THP-1 cytokine expression towards a pro-healing state.

THP-1 cells were used as a human monocyte model that, although limited, recapitulates many of the responses of true primary human monocytes (reviewed in Qin, 2012). The effects of FAC on human TDM differentiation and stimulation were thus investigated. Human THP-1 cells were differentiated into Mφs using PMA, and stimulated with cytokines in the presence of FAC. *STEAP3* expression was reduced in M1 TDMs compared to M0 ($P < 0.01$), while 100 μM FAC downregulated *STEAP3* in M0 ($P < 0.001$) and M2 TDMs ($P < 0.05$; **Figure 5.28A**). *SLC40A1* was upregulated in M0 ($P < 0.001$), M1 ($P < 0.001$) and M2 ($P < 0.001$) TDMs following 100 μM FAC treatment (**Figure 5.28B**). M1-stimulated TDMs also retained higher *FHC* expression than M0 TDMs ($P < 0.001$), which was dampened by FAC treatment (**Figure 5.28C**). However, no differences in *TF* (**Figure 5.28D**), *TFR1* (**Figure 5.28E**) or *SLC11A2* (**Figure 5.28F**) were shown between treatment groups.

FAC treatment led to a significant decrease in the M1 markers *IL1B* ($P < 0.01$; **Figure 5.29A**) and *TNF* ($P < 0.001$; **Figure 5.29B**) in M1-stimulated TDMs, while expression of the M2 markers *CCL17* ($P < 0.001$; **Figure 5.29C**) and *CCL22* ($P < 0.001$; **Figure 5.29D**) were elevated in M2-stimulated TDMs following 100 μM FAC. As alterations in *TNF*, *IL1B*, *CCL17* and *CCL22* were seen in TDMs, the expression of these cytokines was confirmed in NDb and Db BMDMs. Here, similar effects were observed in NDb BMDMs, where *Il1b* expression was reduced at both FAC concentrations ($P < 0.001$; **Figure 5.29E**). Db BMDMs were less responsive to iron with *Il1b* expression only reduced by 100 μM FAC treatment ($P < 0.05$; **Figure 5.29I**). High FAC (100 μM) did not reduce *Tnf* expression in NDb (**Figure 5.29F**) or Db (**Figure 5.29J**) BMDMs. Intriguingly, 100 μM FAC treatment significantly elevated *Ccl17* in M0 ($P < 0.001$) and M1-stimulated ($P < 0.001$) BMDMs (**Figure 5.29G, K**), and *Ccl22* expression in M0 ($P < 0.001$) and M1 ($P < 0.001$) NDb and Db BMDMs (**Figure 5.29H, L**), respectively. Together, these data reveal that iron skews the expression of the pro-inflammatory cytokines in TDMs and BMDMs.

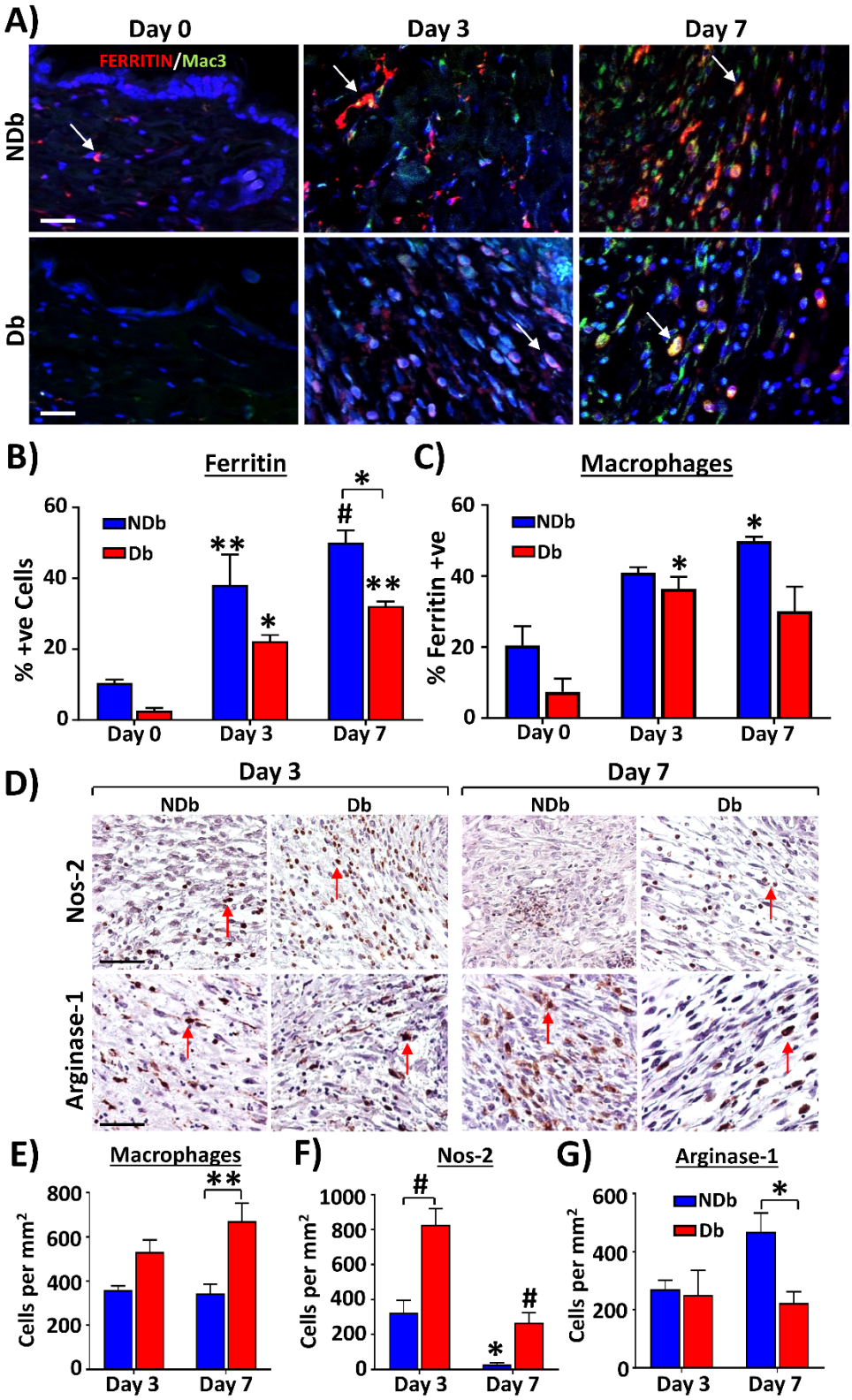

Figure 5.25. Diabetic wound macrophages show impaired ferritin sequestration and altered polarisation. Non-diabetic (NDb) and Db wounds stained for Mac3 (macrophages, green) and ferritin (red; **A**). DAPI = blue nuclei. Quantification of total ferritin^{+ve} cells (**B**) and ferritin^{+ve} macrophages (Mφs, **C**). Immunoperoxidase staining for Nos-2 and Arginase-1 (**D**). Quantification of wound Mφs (**E**), Nos-2^{+ve} (**F**) and Arginase-1^{+ve} (**G**) Mφs. Bar = 50 μm. n = 3-5 mice per group. Mean + SEM. * = $P < 0.05$, ** = $P < 0.01$, # = $P < 0.001$. Two-way ANOVA with Tukey's *post-hoc* analysis. */# alone versus day 3.

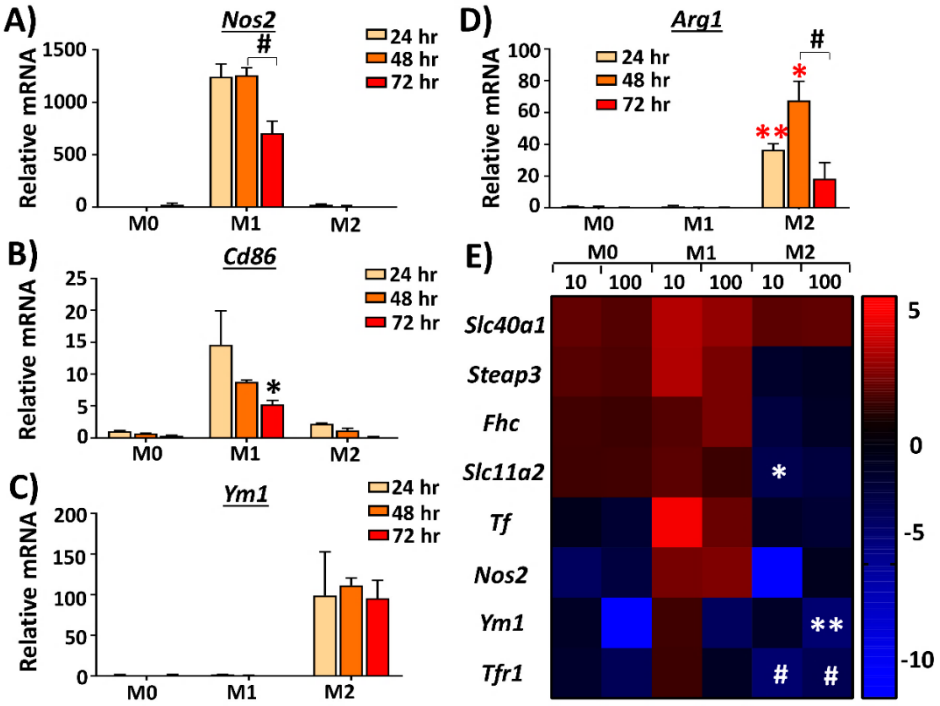

Figure 5.26. Iron alters macrophage gene transcription. Non-diabetic (NDb) macrophages were polarised for 24, 48 and 72 hours and collected for qRT-PCR. Expression of M1 (*Nos2*, **A** and *Cd86*, **B**), and M2 (*Ym1*, **C** and *Arg1*, **D**) markers. Alterations in iron genes were determined following ferric ammonium citrate (FAC, μM) treatment (**E**). Heatmap fold change expression versus control (no FAC). n = 3 donors. Mean + SEM. * = $P < 0.05$, ** = $P < 0.01$, # = $P < 0.001$. Red * versus M0 group. Black * versus 24hr. Two-way ANOVA with Tukey's *post-hoc* analysis.

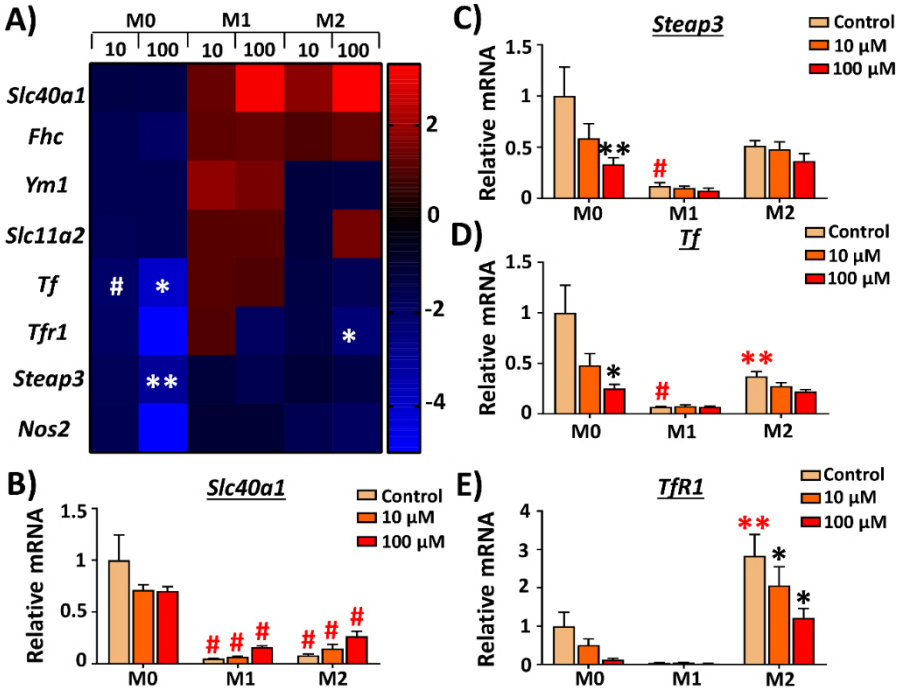

Figure 5.27. Iron gene regulation in diabetic macrophages is altered by iron. Diabetic (Db) macrophages were polarised and treated with ferric ammonium citrate (μM, FAC) for 24 hours prior to qRT-PCR. Heatmap fold change expression versus control (**A**). *Slc40a1* (**B**), *Steap3* (**C**), *Tf* (**D**) and *TfR1* (**E**). n = 3 donors. Mean + SEM. * = $P < 0.05$, ** = $P < 0.01$, # = $P < 0.001$. Red */# versus M0 group. Black * versus control. Two-way ANOVA with Tukey's *post-hoc* analysis.

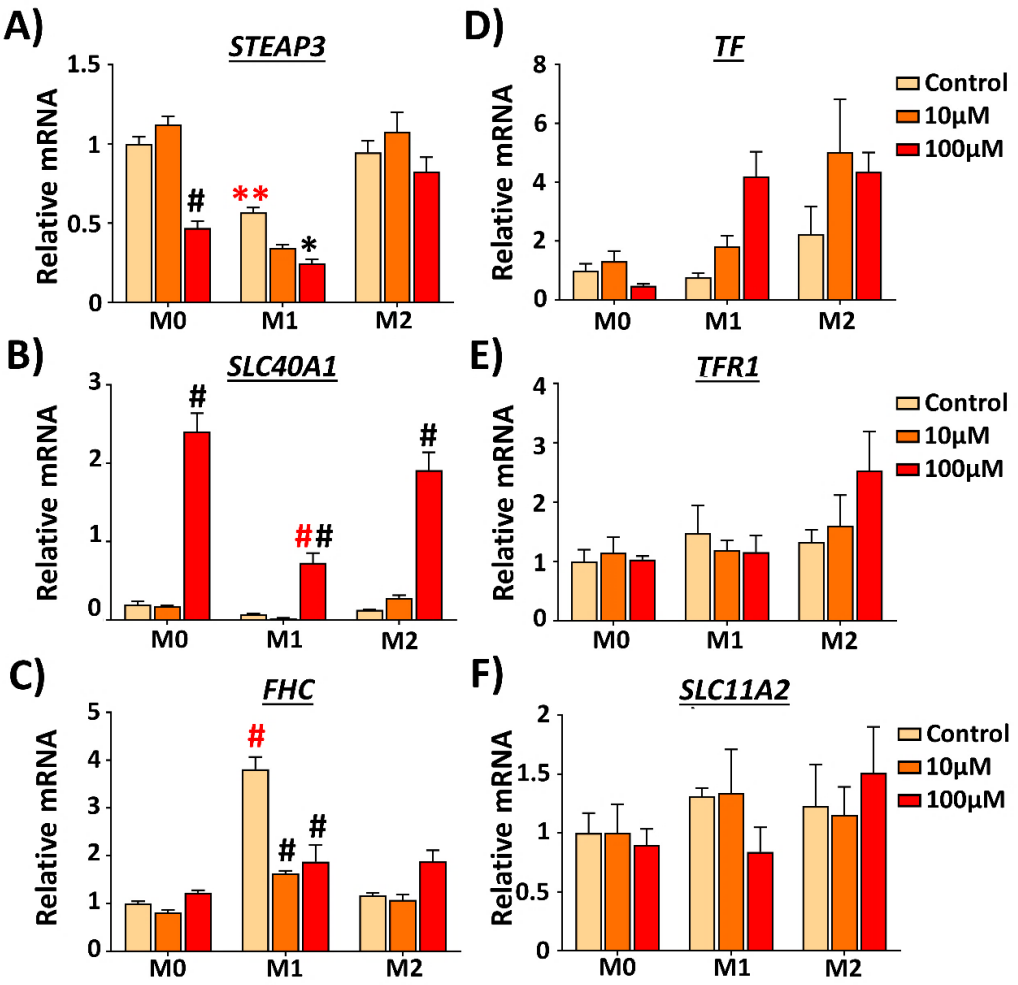

Figure 5.28. Iron-regulated genes are altered in THP-1 macrophages following iron administration. THP-1 macrophages were treated with ferric ammonium citrate (FAC) for 24 hours prior to qRT-PCR. *STEAP3* (**A**), *SLC40A1* (**B**), *FHC* (**C**), *TF* (**D**), *TFR1* (**E**) and *SLC11A2* (**F**) were investigated. Mean + SEM. * = $P < 0.05$, ** = $P < 0.01$, # = $P < 0.001$. Red */# versus M0 group. Black */# versus control. Two-way ANOVA with Tukey's *post-hoc* analysis.

As a functional readout of Mφ behaviour, phagocytic ability of *E. coli* Bioparticles™ was determined in NDb (**Figure 5.30A-B**) and Db (**Figure 5.30C-D**) BMDMs. In NDb BMDMs, M2 stimulation increased *E. coli* uptake ($P < 0.05$), while uptake was not altered by polarisation state in Db BMDMs. In NDb M2-stimulated BMDMs, 100 μM FAC reduced phagocytic ability ($P < 0.05$), while FAC treatment reduced *E. coli* uptake in Db BMDMs regardless of stimulation state (M0, $P < 0.01$; M2, $P < 0.01$). qRT-PCR was performed in BMDMs following phagocytosis, which showed similar gene responses to FAC-treated BMDMs without *E. coli* (**Appendix Figure 5A.11**). Phagocytic ability in TDMs was also reduced by FAC (**Appendix Figure 5A.12**).

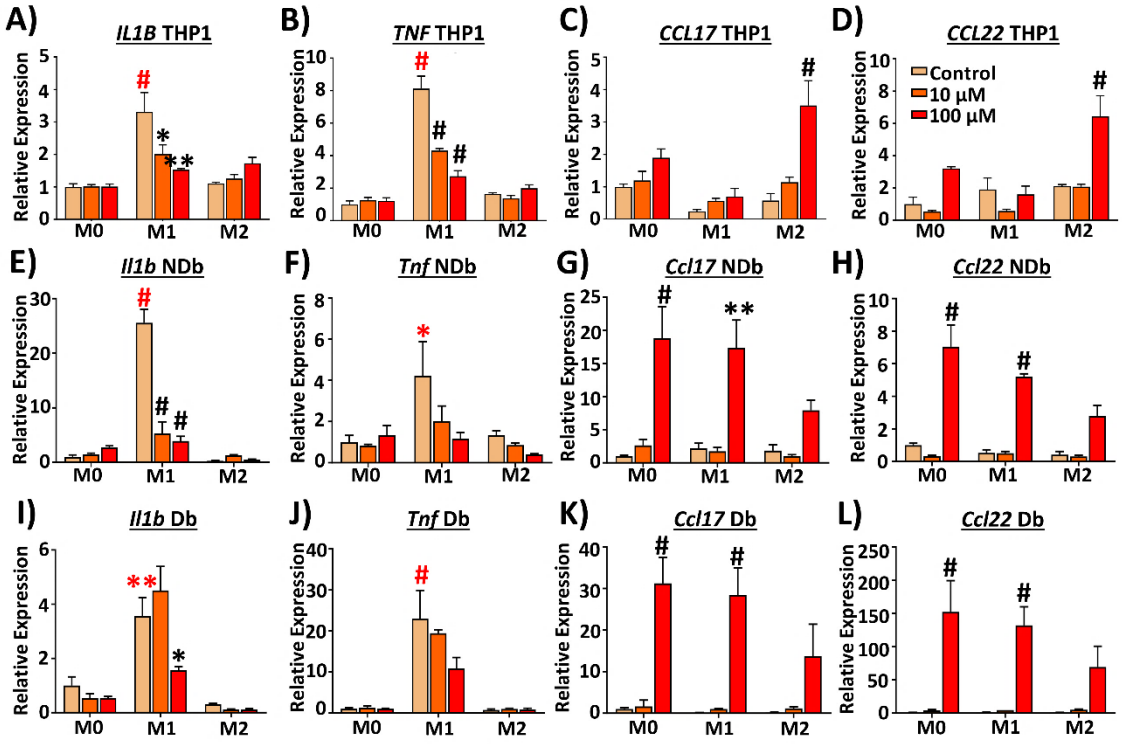

Figure 5.29. Iron administration crucially alters macrophage polarisation and phagocytosis. THP-1 macrophages (Mφs) were treated with ferric ammonium citrate (FAC) for 24 hours prior to qRT-PCR for M1 (*IL1B* and *TNF*; **A-B**) and M2 (*CCL17* and *CCL22*, **C-D**) markers. Non-diabetic (NDb) and Db Mφ expression of *Il1b* (**E, I**), *Tnf* (**F, J**), *Ccl17* (**G, K**) and *Ccl22* (**H, L**). n = 3 donors/experiments. Mean + SEM. * = $P < 0.05$, ** = $P < 0.01$, # = $P < 0.001$. Red */# versus M0 group. Black */# versus control. Two-way ANOVA with Tukey's *post-hoc* analysis.

5.4.15. Exposure to an iron-rich environment increases macrophage differentiation.

The tissue microenvironment drives monocyte to Mφ differentiation (reviewed in Lawrence, 2016), thus the next aim was to investigate the influence of exogenous iron on the differentiation of THP-1 Mφs *in vitro*. Here, FAC (100 µM) administration significantly potentiated THP-1 monocyte differentiation in response to PMA treatment, marked by enhanced expression of the differentiation markers *CD11b* ($P < 0.001$), *CD14* ($P < 0.001$), *CD36* and *CD54* ($P < 0.001$; **Figure 5.31A-D**). FAC also increased cellular adhesion, a phenotypic marker of differentiation ($P < 0.001$; **Figure 5.31E**) and significantly induced MMP-9 activity ($P < 0.001$; **Figure 5.31F-G**). In the wound environment Mφs will be exposed to iron deposited in the ECM, thus THP-1 monocytes were exposed to FAC-treated HDF ECM to determine how this influenced their differentiation. HDFs treated with 100 µM FAC deposited an extensive collagen-rich ECM (see **Figure 5.30H** and **Figure 5.15**) with high iron content, as demonstrated by PPB staining (**Figure 5.31I**) and ferrozine assay

(**Figure 5.31J**). THP-1 monocytes were seeded onto this denuded ECM and stimulated with PMA to induce differentiation. Exposure to the iron-rich ECM upregulated the expression *CD11b* ($P < 0.05$), *CD14* ($P < 0.001$), *CD36* ($P < 0.001$) and *CD54* ($P < 0.01$; **Figure 5.31K-N**). Clearly, both exogenous iron treatment and exposure to iron-rich ECM stimulated Mφ differentiation.

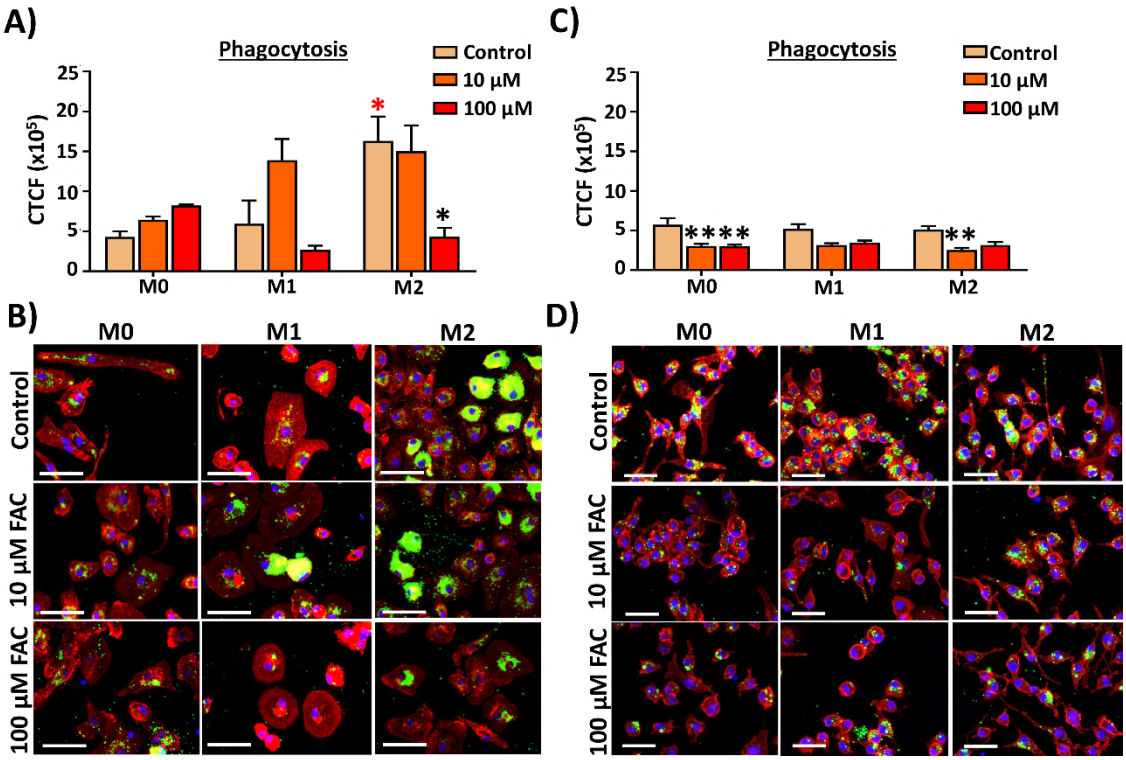

Figure 5.30. Phagocytosis is impaired in diabetic macrophages, and reduced with iron treatment. Non-diabetic (NDb; **A-B**) and Db (**C-D**) bone-marrow derived macrophages were subjected to phagocytosis following ferric ammonium citrate (FAC) treatment. *E. coli* Bioparticles™ = green. Phalloidin = red. DAPI = blue nuclei. CTCF = corrected total cell fluorescence. Bar = 50 µm. n = 3 donors/experiments. Mean + SEM. * = $P < 0.05$, ** = $P < 0.01$. Red * versus M0 group. Black * versus control. Two-way ANOVA with Tukey's *post-hoc* analysis.

5.4.16. M2-stimulated iron-loaded macrophages produce ECM-enhancing soluble factors.

TDMs treated with 100 µM FAC show significantly greater ferritin storage in M0 ($P < 0.001$) and M2 states ($P < 0.001$; **Figure 5.32A-B**) by ICC, and in all three activation states via western blot ($P < 0.01$ to $P < 0.001$; **Figure 5.32C**). For both techniques, the highest levels of ferritin were observed in 100 µM FAC-treated M2-polarised TDMs. As Mφs play a key role in ECM remodelling (Varol & Sagi, 2018), a transwell co-culture approach was used to test the paracrine effects of FAC-stimulated TDMs on HDF ECM production. Transwell co-culture of M2-stimulated FAC-treated TDMs

upregulated *COL1A1* ($P < 0.05$; **Figure 5.32D**), *COL1A2* ($P < 0.001$; **Figure 5.32E**) and *COL3A1* ($P < 0.05$; **Figure 5.32F**) expression in HDFs. Collagen I protein levels were also highest in HDFs co-cultured with M2-stimulated, FAC-treated TDMs ($P < 0.001$; **Figure 5.32G-H**). As M2-stimulated TDM CM enhanced ECM production in HDFs, TDM CM was profiled using chemokine arrays to characterise secreted factors of interest (**Figure 5.32I**). Here, CM from M2-stimulated TDMs treated with 100 μM FAC displayed higher levels of multiple chemokines, including CCL17 and CCL22.

5.4.17. CCL17 and CCL22 promote human wound repair *ex vivo*.

An *ex vivo* wound model was used to test the biological significance of TDM-derived chemokines. Given that the CCL17-CCR4 receptor axis has previously been suggested to be important for healing (Bünemann et al., 2018), CCL17, CCL22 and an antagonist to their common receptor, CCR4 (Yoshie & Matsushima, 2014), were topically applied to human *ex vivo* wounds. Wound closure (re-epithelialisation) was significantly increased following treatment with CCL17 ($P < 0.01$) or CCL22 ($P < 0.05$) in isolation, and to a greater extent by a combination of both ligands ($P < 0.001$; **Figure 5.33A-B**). While the CCR4 antagonist (CO21) had no direct effect on wound closure, it significantly blocked the healing promoting effect of CCL17 ($P < 0.05$) and the effect of the combination of both ligands ($P < 0.01$). Finally, CCL17 and CCL22 effects on ECM production were evaluated. Collagen I and collagen III content were assessed from three regions close to the wound surface (**Figure 5.33C**). Collagen I was significantly increased following treatment with CCL17 ($P < 0.05$) or a combination of both ligands ($P < 0.05$), an effect that was reversed by co-treatment with the antagonist, C021 (**Figure 5.33D-E**). Collagen III was significantly elevated following treatment with each ligand alone or in combination ($P < 0.05$), which was again blocked by the receptor antagonist, CO21 (**Figure 5.33D, F**). Together, these data reveal a novel, previously unappreciated role for the Mφ-derived chemokines, CCL17 and CCL22, in promoting human *ex vivo* wound repair.

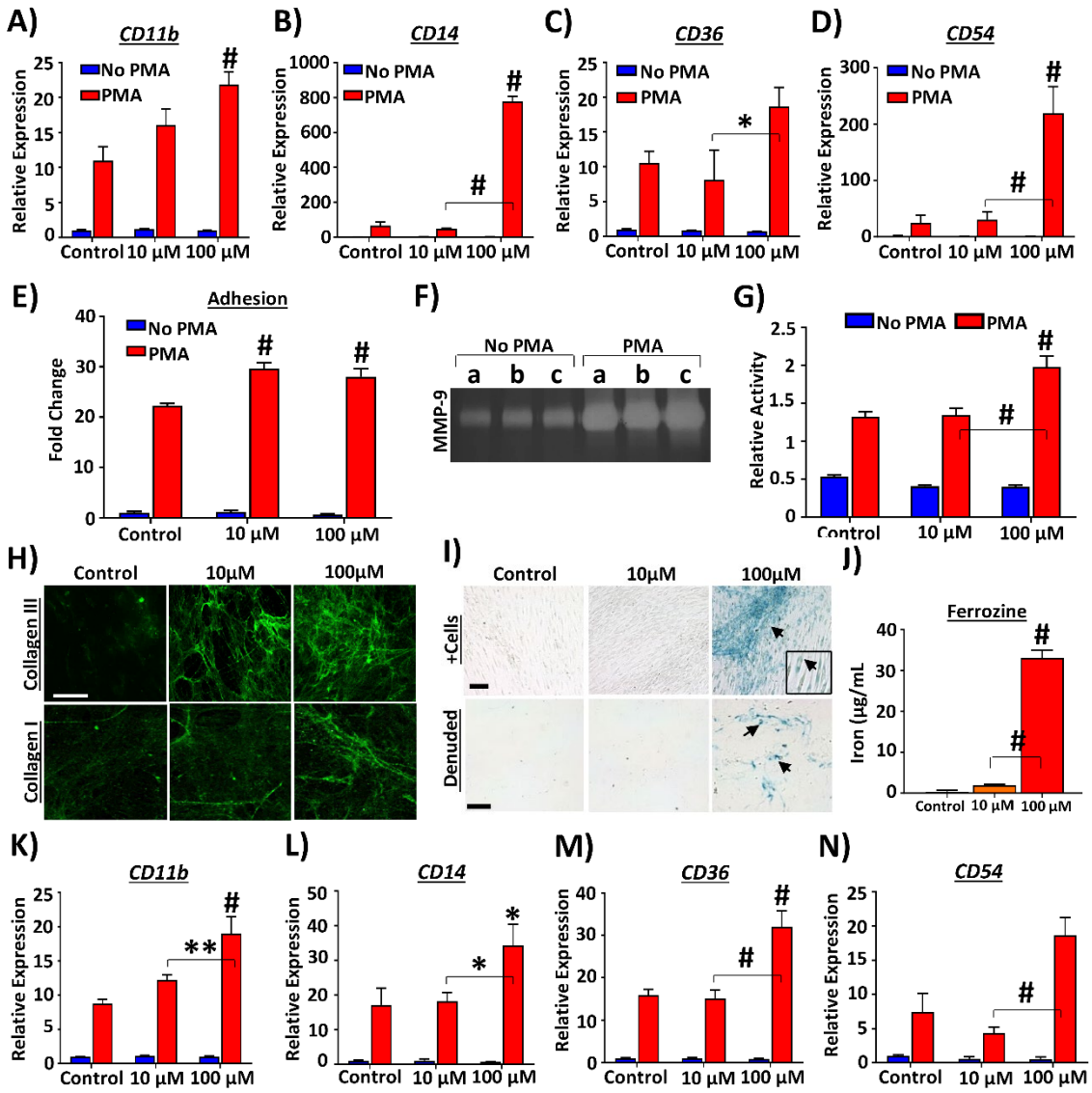

Figure 5.31. A high iron environment enhances PMA-induced differentiation in THP-1 macrophages. THP-1 macrophages (TDMs) were treated with ferric ammonium citrate (FAC) at the same time as phorbol 12-myristate 13-acetate (PMA) for differentiation. *CD11b* (**A**), *CD14* (**B**), *CD36* (**C**), *CD54* (**D**) expression. FAC increases adhesion (**E**) and MMP9 activity (**F-G**). a = control, b = 10 µM FAC, c = 100 µM FAC. Human dermal fibroblasts (HDFs) deposit extracellular matrix (ECM) rich in collagen (green, **H**) and iron, shown by Perl's Prussian blue staining (**I**, arrows for deposits) and ferrozine assay (**J**). TDMs seeded onto FAC-treated HDF ECM show high expression of differentiation markers (**K-N**). Bar = 50 µm. n = 3 donors/3 independent experiments. Mean + SEM. * = $P < 0.05$, ** = $P < 0.01$, # = $P < 0.001$. Two-way ANOVA with Tukey's *post-hoc* analysis. */# alone versus control.

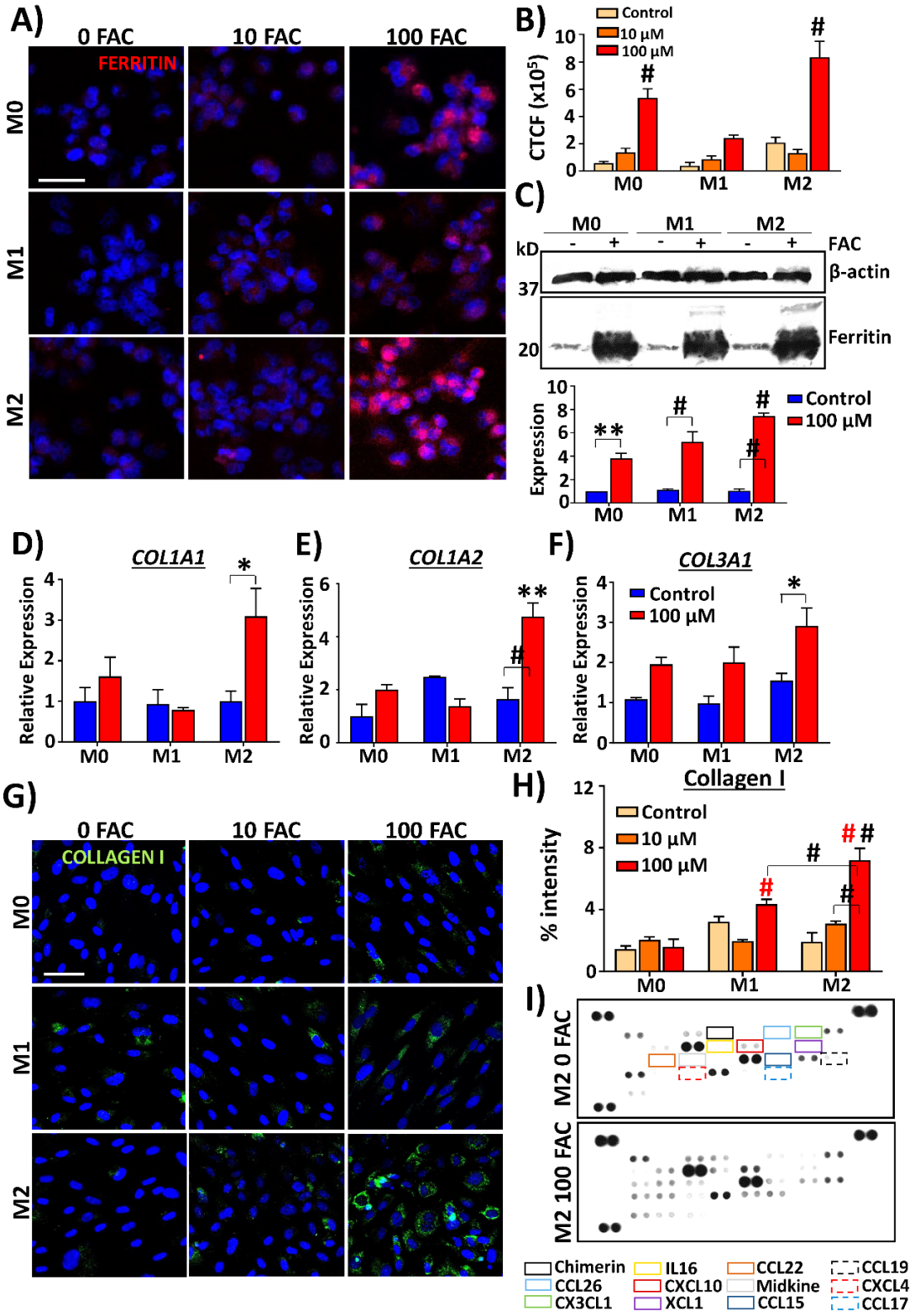

Figure 5.32. Iron-loaded THP-1 macrophages secrete factors that stimulate extracellular matrix production. Ferric ammonium citrate (FAC) treated THP-1 macrophages (TDMs) show high ferritin expression via immunocytochemistry (**A-B**) and western blot (**C**). + FAC = 100 µM. TDM conditioned media (CM) upregulates *COL1A1* (**D**), *COL1A2* (**E**) and *COL3A1* (**F**) in human dermal fibroblasts (HDFs). Transwell co-culture (TDMs + HDFs) increases collagen I production in HDFs (**G-H**). Chemokines in M2 THP-1 CM (**I**). Bar = 50 µm. n = 3 donors. Mean + SEM. * = $P < 0.05$, ** = $P < 0.01$, # = $P < 0.001$. Two-way ANOVA with Tukey's *post-hoc* analysis. # in **B** versus control. */# alone in **C** & **E** versus M0 group. Red # in **H** versus M0 group. Black # alone in **H** versus control.

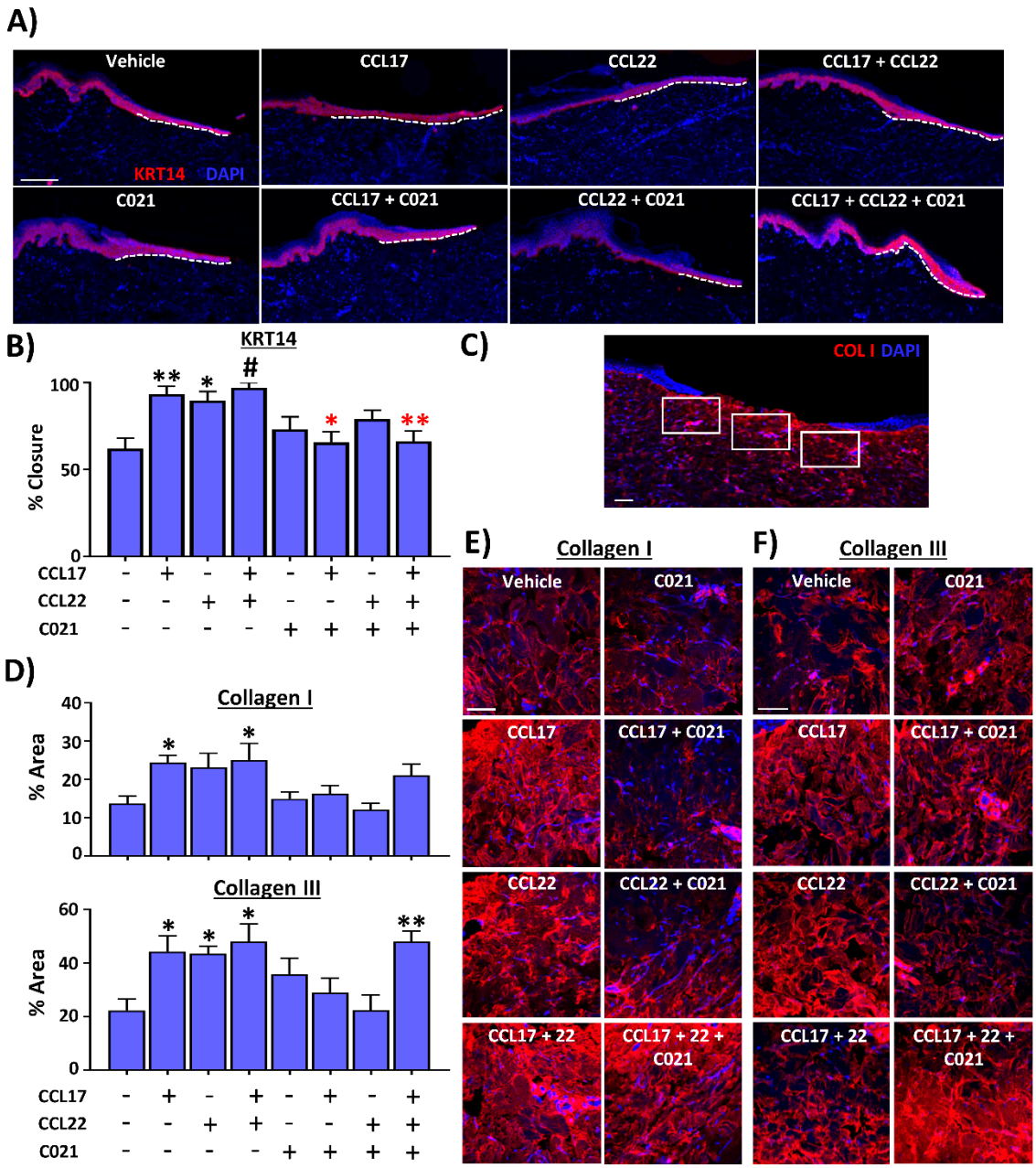

Figure 5.33. CCL17 and CCL22 promote healing during human *ex vivo* wound repair. Keratin 14 staining (KRT14, **A**) and quantification of re-epithelialisation (% closure, **B**). Representative image of collagen quantification from three regions (white boxes, **C**). Collagen I and collagen III immunocytochemistry (**D**) and images (**E**). Bar = 50 µm. n = 3 donors. Mean + SEM. * = $P < 0.05$, ** = $P < 0.01$, # = $P < 0.001$. Significance versus control. Red* in **B** = versus ligand only group. One-way ANOVA with Tukey's *post-hoc* analysis.

5.5. Discussion

Iron is a crucial trace element that has driven organismal life since the dawn of evolutionary time. Its role as a redox active metal is well-known, as is its major function in, and sequestration for, erythropoiesis (Majmundar et al., 2010). The main aim of this chapter was to explore the temporal regulation of iron during wound repair, and elucidate a novel mechanistic function for iron in skin healing. Iron is largely recognised for driving haemostasis (e.g. Lipinski & Pretorius, 2012) and modulating inflammatory cell behaviour (Kroner et al., 2014; Sindrilaru et al., 2011; Sindrilaru & Scharffetter-Kochanek, 2013; Agoro et al., 2018) in early-stage wound healing. Both deficiency (VLUs, Mekkes et al., 2003; Rayner et al., 2009) and excessive (PPB deposits in VLUs, Caggiati et al., 2010; DFU serum, Wenk et al., 2001) iron have also been associated with human wound chronicity. Therefore, manipulation of wound iron to prevent venous insufficiency and dampen inflammation may be a viable future therapeutic option for chronic wounds, but only once the biological roles of iron in late-stage wound healing are better understood.

The present work showed that iron plays a major role in modulating the dermal ECM, a characteristic function of late-stage wound repair. The first line of evidence for this new role came from ICP-MS profiling across a murine acute wound time course (**Figure 5.7**). Unexpectedly, iron levels were upregulated during late-stage wound repair, rather than earlier stages of healing that retain crucial iron-responsive processes, such as blood clotting and inflammation (Lipinski & Pretorius, 2012; Yeoh-Ellerton & Stacey, 2003). Although previous authors have measured metals in experimental rat wounds (using FAAS, Lansdown et al., 1999), and iron in chronic wound exudate (ICP-optical emission spectroscopy, Yeoh-Ellerton & Stacey, 2003), this is the first time the abundance of iron has been measured in murine wound tissue using the more sensitive and accurate technique of ICP-MS (Liu et al., 2014b). Pathological Db wounds displayed significantly aberrant iron levels (**Figure 5.8**) suggesting that iron may be crucial for regulating late-stage healing processes known to be impaired in diabetic healing, such as angiogenesis (Icli et al., 2016) and ECM deposition and remodelling (reviewed in Schultz & Wysocki, 2009; **Figure 5.8**).

The resolution state of acute wounds was characterised by focussing on ECM formation and remodelling. Picrosirius red staining allowed for the visualisation of immature and mature ECM fibres via histology (Junqueira et al., 1979). Substantial

matrix deposition occurred in late-stage healing and was impaired in Db wounds (**Figure 5.10**). The use of picrosirius red staining to demonstrate differences in collagen type I and collagen type III has come under scrutiny in recent years, where it has been suggested that changing the orientation of the imaging stage alters tissue fibre birefringence (Lattouf et al., 2014). In the present study, picrosirius red staining was useful to assess the overall abundance of matrix fibres, but to fully distinguish between collagen I and collagen III, more direct techniques were used. As expected, acute wounds displayed significant upregulation of *Col1a1* and *Col3a1* mRNA, and heightened deposition of collagen III and collagen I (ICC) at day 7 post-injury. However, diabetic wounds showed impaired fibroplasia, with reduced deposition of red birefringent fibres and collagen I, and dampened expression of *Col1a1* and *Col3a1*, at day 7 post-injury (shown previously, Hsu et al., 2014).

In wound tissue, iron deposits appeared to be associated with the dermal matrix (**Figure 5.7** and **Section 4.4.3** LA-ICP-MS), while ferritin stores were apparent in both Mφs and fibroblasts (**Figure 5.23**). Combined with the late-stage iron profile shown via ICP-MS, these data suggested Mφs and fibroblasts to be intimately linked to the wound iron response. HDFs readily uptake and store administered FAC, which aids cellular proliferation (reviewed in Le & Richardson, 2002; **Figure 5.11**). Along with significantly increased ferritin storage, HDFs treated with FAC displayed higher intracellular and extracellular PDGFA expression (**Figure 5.15** and **Figure 5.18**). Indeed, overexpression of *Pdgfa* in cardiac myocytes contributes to fibrosis (Gallini et al., 2016), and PDGFA has long been associated with late-stage wound healing (humans, Pierce et al., 1995) and proper connective tissue formation during development (mice, Olson & Soriano, 2009). As this suggested that FAC treatment stimulated pro-fibrotic behaviour in HDFs, the effects of FAC on fibronectin remodelling, and collagen III and collagen I production, were next ascertained.

The immature matrix protein fibronectin was first assessed due to its early and selective abundance in cell culture (Greiling & Clark, 1997). Fibronectin, a large glycoprotein associated with the ECM, is important for binding platelets during haemostasis and forming granulation tissue for epithelial migration and cellular adhesion (Barker & Engler, 2017; Leiss et al., 2008). Despite its crucial function in early repair, fibronectin is replaced by stronger and more stable collagen fibres during late-stage dermal remodelling (reviewed in Lenselink, 2015). Intriguingly,

under higher iron conditions, HDFs deposited less fibronectin due to increased remodelling via MMP2 (**Figure 5.16**). Previous work has also demonstrated that MMP2 cleaves fibronectin *in vitro* (Jiao et al., 2012).

On the contrary, high intracellular iron loading led to greater deposition of collagen-rich ECM, and increased microvesicles and secretions were observed via SEM (**Table 5A.1, Figure 5.17-5.18**). Early studies have illustrated that iron deficiency leads to the formation of weakened scar tissue (Bains et al., 1966; Jacobson & Vanprohaska, 1965). Concurrently, delivery of iron *in vitro* aids spheroid growth and ECM production in rat aortic smooth muscle cells (Casco et al., 2017), proliferation in human myeloid progenitor cells (Pourcelot et al., 2015), and fibrogenesis in murine hepatic stellate cells (Mehta et al., 2018). A number of studies have also shown iron-loading, as a result of HH, to coincide with inflammation and fibrosis (reviewed in Wood et al., 2008), or correlate with serum fibrosis markers (Wang et al., 2017b). Yet, HH patients often present with comorbities known to contribute to fibrosis (e.g. alcohol consumption, Bataller et al., 2003) and fibrosis in a cohort of HH patients was not associated with TGF-β (Wood et al., 2013), a potent fibrotic stimulant (reviewed in Penn et al., 2012). This fits with experimental data comparing mouse models of HH where iron-loading occurs in the liver, but is not correlated to increased ECM production (picrosirius red staining), or upregulation of *Col1a1* or *Acta2* mRNA (Subramaniam et al., 2012). Therefore, it is difficult to determine whether iron is directly linked to fibrosis in iron-loading pathologies.

Accumulation of iron may drive liver fibrosis through increased free radical production (Lunova et al., 2014). As oxidative stress induces fibroblast senescence (Volonte et al., 2015), and knockdown of senescent pathways (e.g. p21) alleviates liver fibrosis (Yosef et al., 2017), it can be assumed that iron plays a key role in modulating collagen deposition through its redox potential. Iron causes oxidative stress through the release of OH- (Gao et al., 2009), which promotes collagen production in cardiac rat fibroblasts via NADPH oxidase (Wang et al, 2013), and induces fibrosis in human hepatic stellate cells *in vitro* (Zhan et al., 2006). More recently, high levels of protein oxidation have been linked to idiopathic pulmonary fibrosis, and bleomycin and TGFβ-induced fibrosis in mice, which can be attenuated by antioxidant administration (Anathy et al, 2018). Finally, excessive production of dermal ECM and heightened ROS is characteristic of systemic sclerosis skin

fibroblasts (from patients and mice; Sambo et al., 2001; Kavian et al., 2010), and can be downregulated by the antioxidant stimulator, nuclear factor-like 2 (Kavian et al., 2018). Together, these findings suggest a potential contributor to ECM deposition in FAC-treated HDFs is oxidative stress.

Dermal wound healing is subject to redox control, where oxidative stress, caused by an excess of oxidants (e.g. ROS and RNS), is useful in early wound repair to combat infection. However, if wound oxidants are not effectively scavenged by antioxidants, inflammation persists and wound tissue breakdown exceeds repair (Schäfer & Werner, 2008). Antioxidant enzymes, such as SODs, catalase and glutathione peroxidases, and non-enzymatic oxidants, such as ascorbic acid, α-tocopherol and glutathione, are key in this oxidant scavenging (Koskenkorva-Frank et al., 2013). Despite ROS production often being negatively associated with driving persistent inflammation in chronic wounds (reviewed in Schafer & Werner, 2008), ROS are vital wound signal transducers, attracting leukocytes to injured sites in zebrafish (Niethammer et al., 2009) and *Drosophila* (Razzell et al., 2013), and stimulating regeneration in amphibians (Love et al., 2013). ROS also play an important role in mammalian wound healing responses, where impaired NADPH oxidase signalling delays healing (Lévigne et al., 2016; reviewed in André-Lévigne et al., 2017).

As expected, FAC treatment heightened ROS production in HDFs (**Figure 5.21**), which was first dampened by iron chelation. Indeed, iron chelation can accelerate wound closure in normal (Mohammadpour et al., 2012) and pathological aged and diabetic murine wounds by reducing ROS and inflammation (Duscher et al., 2017). The OH- scavenger, mannitol (Shen, 1997), also inhibited FAC-induced ROS production, leading to reduced ECM deposition. This suggested a direct association between FAC-mediated ECM production and oxidative stress. To investigate the mechanistic link between FAC-induced oxidative stress and ECM deposition further, a tissue screen of iron genes was performed. *Slc11a2*, *Slc40a1* and *Steap3* were elevated in normal healing at day 7 post-injury, suggesting there may be increased endosomal conversion of Fe^{3+} and Fe^{2+} (Muckenthaler et al., 2017), combined with higher extracellular export of iron once it becomes available in the cytosol (Yanatori et al., 2017). Nevertheless, it was difficult to discern from this data whether iron-loaded wound cells were contributing to extracellular iron deposition in wounds, or internalising and processing iron deposits already present in the granulation tissue.

Db wounds displayed an altered profile of iron gene expression with significant downregulation of *Steap3* compared to NDb, while *Slc11a2* and *Slc40a1* were not upregulated (**Figure 5.22**). Accordingly, these findings suggest an altered wound iron response, whereby Db wound cells sequester iron (increased *Tfr1*, *Fth*, *Ftl*; as observed in iron-loaded Mφs previously, Philippot et al., 2014) but fail to efficiently convert ferric iron to its biologically available state, or export excess iron. Direct targeting of *STEAP3* with two validated siRNAs reduced collagen deposition *in vitro*. *In silico*, Han et al. (2018) recently demonstrated that *STEAP3*-associated genes are linked to cellular functions including ECM organisation. Crucially, antioxidant treatment *in vitro* dampened *STEAP3* in FAC-stimulated HDFs, while siRNA targeting of *STEAP3* reduced oxidative stress, implying a direct role for *STEAP3* in FAC-mediated oxidative stress-induced ECM deposition (summarised in **Figure 5.34**).

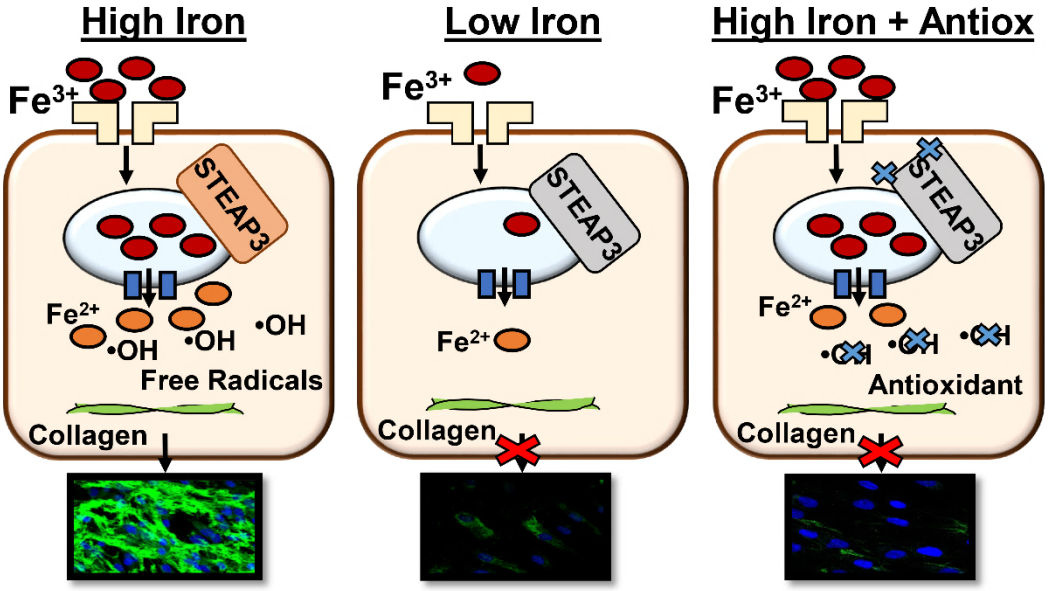

Figure 5.34. Iron induces oxidative stress which leads to collagen deposition in fibroblasts. High iron uptake and endosomal conversion from Fe^{3+} to Fe^{2+} (via STEAP3) increases hydroxyl radical production (OH) in fibroblasts, which promotes extracellular collagen deposition. Under low iron conditions, endosomal iron uptake and oxidative stress are reduced, resulting in low collagen deposition. Antioxidant treatment reduces *STEAP3* activity and attenuates oxidative stress under high iron conditions, thus preventing collagen deposition. Further, siRNA targeting of *STEAP3* prevents endosomal conversion of iron in iron-loading conditions, therefore mitigating FAC-mediated oxidative stress and reducing collagen deposition *in vitro*. *Image by the author (HNW).*

In wound healing, Mφs are able to perform versatile functions with high plasticity to allow effective repair. Functionally, Cd11b-specific (Mirza et al., 2009), and arginase-specific (Campbell et al., 2013) ablation leads to delayed healing and excessive inflammation. This illustrates not only the importance of the presence of

Mφs, but also effective temporal modulation of Mφ phenotype in wound healing. As Mφs in day 7 wounds were largely of the M2 phenotype (Krzyszczyk et al., 2018; **Figure 5.24**), M2 Mφs may be intricately involved in the deposition and sequestration of iron during late-stage repair and linked to pathology. Indeed, it was previously suggested that heme clearance (i.e. increased iron sequestration) by Mφs could aid healing. Here, wounds treated with chemerin15 possessed higher levels of Mφ iron sequestration, increased Arginase-1^{+ve} Mφs and healed faster than vehicle-treated wounds (Cash et al., 2014). In the present work, the number of ferritin^{+ve} Mφs increased in normal healing (**Figure 5.23**), while Mφ infiltration and sequestration of iron was impaired in Db wounds (**Figure 5.25**).

Circulating monocytes differentiate into wound site Mφs in response to environmental cues (Das et al., 2015), potentially including iron. Iron deficiency reduced CD14 expression in blood monocyte-derived Mφs (Kramer et al., 2002) and heme iron mediated *Spic*-induced Mφ differentiation in mice (Haldar et al., 2014). In concurrence, the present work revealed that exposure to high iron increased Mφ differentiation (**Figure 5.30**), but also significantly extended this observation to demonstrate a role for iron in modulating Mφ polarisation and chemokine secretion.

Mφs have gained much press regarding their iron-modulating roles and were first classified as cells of the reticuloendothelial system before later being assigned to their true monocyte lineage (van Furth, 1972). Mφs not only modulate bodily heme storage and erythrocyte recycling (Arezes & Nemeth, 2015), but as discussed above, are also responsible for engulfing damaged erythrocytes in the wound bed (Sindrilaru et al., 2011). M1- and M2-like Mφs display opposite iron-dependent functional phenotypes, where M1 Mφs sequester iron and M2 Mφs return iron to the extracellular environment (Jung et al., 2015). It is important to note, however, that the traditional dichotomous classification of Mφ polarisation is becoming outdated as human (Xue et al., 2014) and murine (Lavin et al., 2014) Mφs show diverse transcriptional and phenotypic responses to different stimuli (reviewed in Ginhoux et al., 2016). Future work investigating iron processing in Mφs should be extended to include tissue-specific and pathology-specific differences.

In the present work, NDb M1-stimulated Mφs showed increased *Fhc* and lowered *Fpn* and *TfR1*, whereas M2-stimulated Mφs possessed higher levels of *TfR1* (as in Corna et al., 2010; Recalcati et al 2010), reduced by FAC treatment (as in microglia,

Mairuae et al., 2011; **Figure 5.26**). M1 and M2 Mφs demonstrated reduced *Fpn* mRNA compared to non-stimulated cells (as in Recalcati et al., 2010). However, the effect of iron on Mφ phenotype appears to be context dependent. Heme uptake by Mφs in the damaged spinal cord promoted an M1 phenotype in mice (Kroner et al., 2014), while iron sequestration induced an M1 phenotype in raw264.7 Mφs (Zhou et al., 2018b). It has even been suggested that sustained, iron-induced, pro-inflammatory Mφs may contribute to poor healing via triggering fibroblast senescence (Sindrilaru & Scharffetter-Kochanek, 2013; Wlaschek et al., 2019).

On the contrary, in atherosclerotic plaques, haemoglobin-haptoglobin complexes shifted Mφs towards an M2 phenotype both *in vivo* (higher CD163) and *in vitro* (increased IL-10 and IL-1RA; Finn et al., 2012). Likewise, high iron also upregulated M2 marker expression (*Arg1*, *Ym1* and *Il-10*) and reduced pro-inflammatory cytokines, in LPS-stimulated Mφs (Agoro et al., 2018). Thus, it is clear that iron loading can switch Mφs to a pro-healing state in the right environmental context, reinforcing that Mφs retain extensive functional plasticity.

Although not widely characterised, the late-stage M2 switch may be driven by degradation of M1 receptors (Lin et al., 2016) and activation of STAT6 and PPARγ (Nelson et al., 2011). The present work also revealed that iron may critically promote alternative activation by reducing the expression of *TNF-α* and *IL-1β* and upregulating *CCL17* and *CCL22* (**Figure 5.29**). M2 Mφs release a myriad of factors (e.g. TGFβ1) to promote re-epithelialisation, fibroplasia, fibroblast differentiation (Li et al., 2007) and ECM remodelling (Varol & Sagi, 2018). In the current study, iron treatment of Mφs significantly potentiated the release of a range of chemokines, which promoted collagen production by HDFs (**Figure 5.32**). M2 Mφ CM is known to stimulate collagen 1 and collagen 3 production in fibroblasts *in vitro* (Ploeger et al., 2013), but direct application of M2-stimulated BMDMs did not alter diabetic healing *in vivo* (Jetten et al., 2014). Nevertheless, these novel data suggest that iron indirectly stimulates HDF ECM deposition via modulation of Mφ behaviour, with potential therapeutic application in pathological healing.

A chemokine screen of the iron-treated M2 TDMs identified CCL17 and CCL22, which directly promoted re-epithelialisation and collagen deposition in human *ex vivo* wound repair (**Figure 5.33**). This is in line with previous work in HaCaTs (Nakahigashi et al., 2011), fibroblasts (Buskermolen et al., 2017), and during fibrosis

in vivo (Belperio et al., 2004). *Ccl17* overexpression promoted wound closure and granulation tissue formation in murine wounds (Kato et al., 2011). Curiously, Barros et al. (2019) demonstrated improved healing in aloxan-induced CCR4$^{-/-}$ T1DM mice and in WT T1DM mice treated with anti-CCL17 and anti-CCL22.

In summary, data presented in this chapter reveal a previously unappreciated role for iron during the remodelling phase of wound repair *in vivo*, which was impaired in pathological Db healing. Both fibroblasts and Mφs were crucially modulated by a high iron environment, which stimulated ECM deposition *in vitro* (summarised in **Figure 5.35**). Iron-mediated collagen production was further shown to be dependent on oxidative stress and *STEAP3*. Iron promoted Mφ differentiation and skewed Mφs towards an M2-like state that produced a secretome highly enriched with ECM-stimulating factors. Finally, two identified factors, CCL17 and CCL22, promoted re-epithelialisation and collagen deposition in human *ex vivo* wounds. It is tempting to speculate that local iron administration, perhaps targeted to the latter stages of wound repair, could deliver clinical benefit. Further studies are now essential to explore the feasibility of directly manipulating tissue iron and iron-regulated factors as a conduit to improving healing pathology.

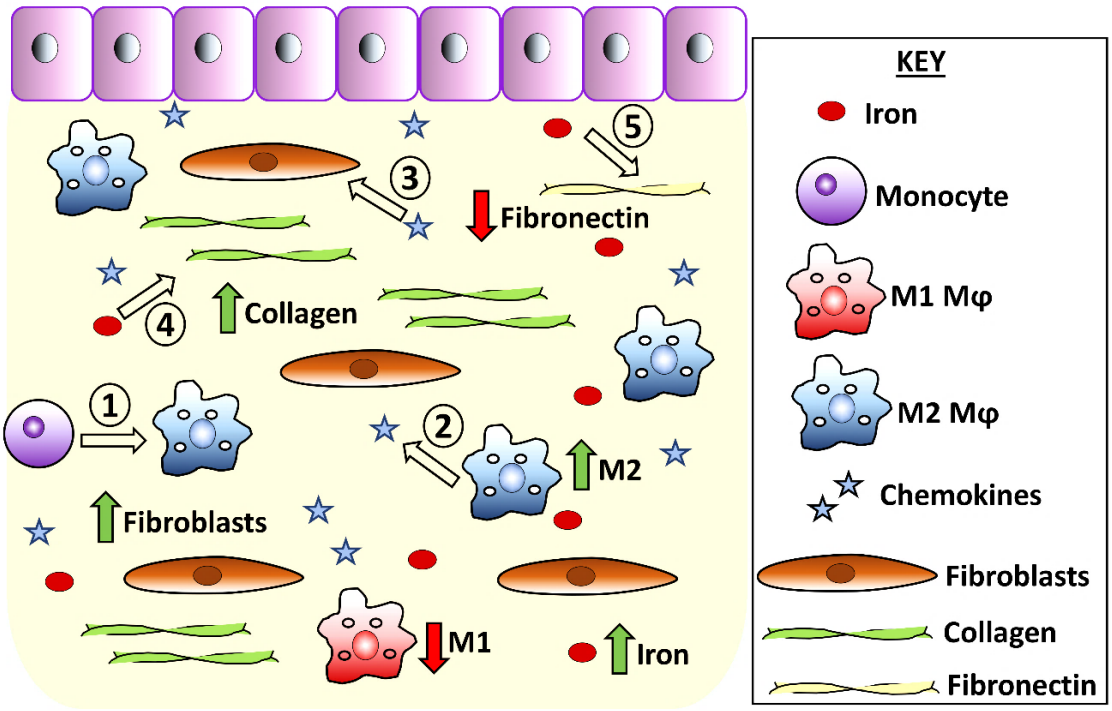

Figure 5.35. Iron stimulates late-stage healing by altering macrophage and fibroblast behaviours. High iron promotes macrophage (Mφ) differentiation (**1**) and skews Mφs towards a pro-healing M2 phenotype (**2**). Iron-stimulated M2 Mφs release chemokines that upregulate extracellular collagen deposition in fibroblasts (**3**). Iron independently increases fibroblast extracellular collagen deposition (**4**) and promotes fibronectin remodelling (**5**). *Image by HNW.*

Chapter 6: Exploring the Wound Healing Potential of Bioactive lass

Selected results presented in this chapter also appear in the following publication:

A Novel Silver Bioactive Glass Elicits Antimicrobial Efficacy against *Pseudomonas aeruginosa* and *Staphylococcus aureus* in an *Ex Vivo* Skin Wound Biofilm Model.

Authors: Holly N. Wilkinson[1], Sammi Iveson[1], Paul Catherall[2] and Matthew J. Hardman[1]

2018 Front Microbiol.

Affiliations:

[1]The School of Life Sciences, The University of Hull, Hull, HU6 7RX, United Kingdom.
[2]Theraglass Ltd., London, United Kingdom.

Author contributions: All *in vitro* and *ex vivo* work was carried out by HNW. Additional microbiological analysis, that is not in included in this chapter, was carried out by SI. PC, the industrial supervisor, was involved in final drafting of the manuscript. HNW and MJH were involved in study concept and design and manuscript preparation.

6.1. Introduction

The integumentary system provides a physical barrier against the external environment while performing an array of vital physiological functions (Hardman et al., 1998). Hence, breaches to the skin barrier must be repaired in a timely and efficient manner to prevent infection and wound persistence (Bjarnsholt et al., 2008). Sadly, non-healing, chronic wounds affect millions of patients each year and incur substantial healthcare costs worldwide (Posnett et al., 2008, Gould et al., 2015). For many years, one of the most discussed contributing factors to wound chronicity has been critical colonisation by pathogenic organisms (infection), present in the form of biofilms (Dow et al., 1999; James et al., 2008; Wilkinson et al., 2016; Wolcott et al., 2015). Biofilms are aggregates of bacteria that evade extrinsic stressors and develop rapid pathogenicity due to their multi-faceted, adaptable features (reviewed in Flemming et al., 2016; see **Figure 6.1**). They are encapsulated in self-produced EPS, which provides a protective barrier against host defences and systemic antibiotics (Flemming & Wingender, 2010).

The heterogeneity of biofilm communities confers increased virulence through the inter-specific transfer of metabolites and antimicrobial-resistance genes (Mah et al., 2012; Parsek & Greenberg, 2005). Despite improved healthcare and the widespread availability of antimicrobial therapies, wound infection remains a key driver in the recalcitrant nature of chronic wounds (Velnar et al., 2009). These pervasive wound infections persist largely due to the prevalence of antibiotic-resistant bacterial strains and the presence of biofilms (reviewed in Percival, 2018). Therefore, there remains significant need to develop novel treatments that will provide consistent antimicrobial effectiveness while also aiding in tissue repair.

6.1.1. Metals as Therapeutic Agents

6.1.1.1. Antimicrobial Properties of Metals

Metals have long been known to be potent antimicrobials, with silver and copper used since ancient times to disinfect water and preserve food (reviewed in Alexander, 2009). In the 1880's, copper was incorporated into fungistatic agents to prevent crop infections (Ayres, 2004), paving the way towards the agricultural practices maintained today. In medicine, ancient Egyptians used copper as astringents (Lemire et al., 2013), while the use of silver in historic medical practices is far reaching, including treating polyps of the larynx (Bedingfield, 1849), as sutures

for vaginal tears (Sims, 1852), and in child eye infections (Credé, 1881). Metal preparations have even been used to treat a number of communicable diseases, including tuberculosis (gold in guinea pigs, Dewitt, 1918) and syphilis (reviewed in De Medina, 1922). With the prominent discovery of antibiotics by Sir Alexander Fleming in the 1920's, the application of metals in medicine greatly diminished (Lemire et al., 2013). However, with the advent of antibiotic resistance (e.g. methicillin-resistant *S. aureus*, MRSA), the use of metals in medicine is undergoing a renaissance (Lemire et al., 2013), and in today's clinics formulations of copper and silver can be found in abundance (Hodgkinson & Petris, 2012).

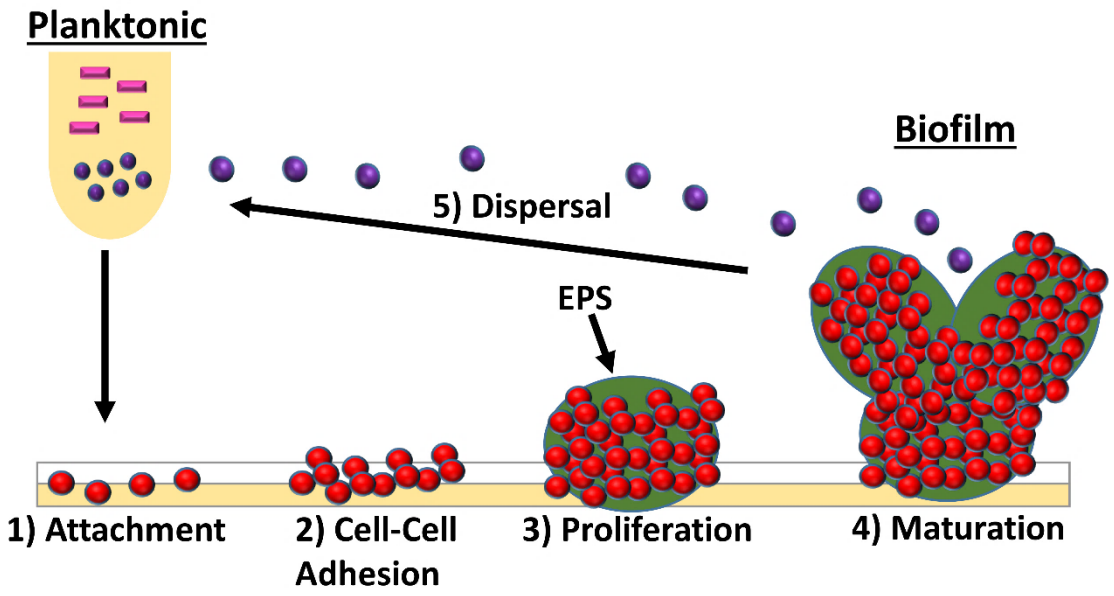

Figure 6.1. Main stages of biofilm formation. Planktonic bacteria form biofilms in response to specific environment cues. Firstly, planktonic bacteria attach to a surface (**1**), and then attach to each other via adhesion proteins (**2**). Next, adhered bacteria start to proliferate and produce extracellular polymeric substances (EPS; **3**). Once matured (**4**), encapsulated bacteria within a biofilm are protected from the environment, and planktonic bacteria are dispersed for new colony formation (**5**; Vogeleer et al., 2014). *Image based on O'Toole et al. (2000).*

Silver is particularly toxic to bacteria, even at incredibly low (µM) concentrations (Harrison et al., 2004). Independent of hyperosmotic shock, the underlying mechanisms of metal antimicrobial efficacy have been discussed and illustrated at length, where their activities have been termed "oligodynamic" (Marx & Barillo, 2014). The main actions by which metals exert their antimicrobial effects are: (1) by replacing hydrogen and creating metal-sulphur and metal-disulphide bonds, thus inhibiting oxidase enzymes and altering protein structure and; (2) replacing hydrogen bonds between DNA strands and interfering with DNA replication (Klueh et al., 2000; Percival et al., 2005). The reductive activity of metals leads to loss of the

bacterial cell envelope, damage to the cell membrane and cell wall, inhibition of electron-transport driven respiration, and ultimately cell death (reviewed in Mijnendonckx et al., 2013; illustrated in **Figure 6.2**).

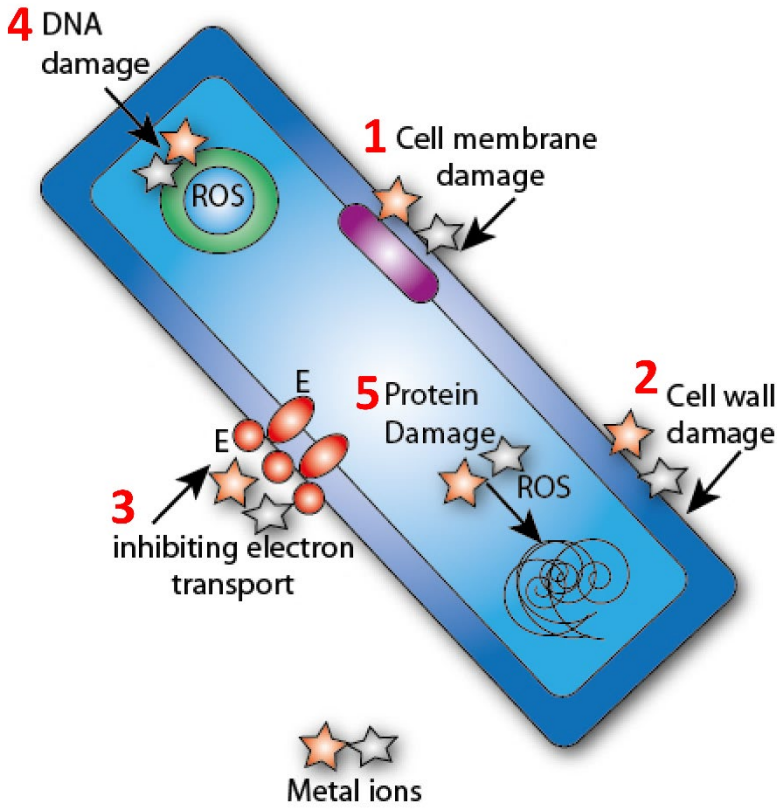

Figure 6.2. The major antibacterial mechanisms of metal ions. In summary, metal ions cause damage to cell membranes (**1**) and cell walls (**2**), inhibit electron transport-driven respiration (**3**), and produce toxic levels of intracellular reactive oxygen species (ROS). High ROS leads to lipid peroxidation, DNA damage (**4**), protein damage (**5**) and loss of function. *From Wilkinson et al. (2016).*

Metals also exert their effects through their ROS-generating capabilities, causing DNA, lipid and protein damage to cells. This was revealed in cultures of *S. aureus* and *E. coli*, where addition of silver ions led to increased expression of ROS-sensitive *sox* genes (Park et al., 2009). Morones-Ramirez et al. (2013) visibly demonstrated that silver administration increased hydroxyl free radicals (using 3'-[p-hydroxyphenyl] fluorescein dye) in *E. coli*. Anaerobic organisms, although less susceptible (Mijnendonckx et al., 2013), can be killed by higher concentrations of silver combined with other factors (e.g. UVR; Kim & An, 2012). As silver enters the cell through transmembrane transport, it has been suggested that Gram-negative bacteria may be more susceptible than Gram-positive bacteria, by virtue of their peptidoglycan cell wall (Morones et al., 2005).

As more metal-containing treatments are emerging, metal resistant strains of common bacteria, such as *Pseudomonas aeruginosa* (*P. aeruginosa*), *S. aureus* and *E. coli*, are emerging (Percival et al., 2005; Randall et al., 2015). Bacterial resistance mechanisms can be intrinsic, or acquired through exposure to an antimicrobial agent. Therefore, bacteria inherit or develop (through horizontal gene transfer) plasmid-resistance genes and metal ion efflux systems, or lack metal-membrane binding sites altogether (e.g. outer membrane porins; Mijnendonckx et al., 2013). For example, a specific *E. coli* strain resistant to copper and silver presents a cusCFBARS gene cluster containing heavy metal-sequestering MTT-like proteins, and a sophisticated efflux system involving P-type ATPase heavy metal pumps (Franke et al., 2003). In this strain, copper and silver are rapidly sequestered and expelled from the cells before they can cause irreversible damage. Development of resistance to one type of metal can also confer protection against others; copper resistance, for example, is often accompanied by resistance to silver and zinc (Mijnendonckx et al., 2013). Metal resistance occurs less frequently than antibiotic resistance as metals target multiple bacterial processes, making it more difficult to acquire resistance (Percival et al., 2005; Percival et al., 2012). Moreover, as metals specifically damage bacterial cell walls, they may present an attractive co-treatment to improve overall bacterial susceptibility to antibiotics (as demonstrated *in vitro* with copper, aluminium and zinc; Goh et al., 2008; Panáček et al., 2018).

Despite current knowledge of the antimicrobial capacity of metals, and evidence of how microbes develop resistance, few studies have addressed the specific biochemical and biophysical mechanisms by which metals exert their effects. This is likely due to the difficulty in pinpointing a single metal-driven bactericidal process within the diverse, sophisticated and adaptable metabolism of microorganisms. Nevertheless, determining the intricacies in metal functionality is crucial for development of novel and efficacious metal-based therapies.

6.1.1.2. Anti-Inflammatory Properties of Metals

Endogenous metals are carefully balanced to prevent excessive inflammation and toxicity. Clinically, the potential effects of metals on the host inflammatory response are secondary to their antimicrobial efficacy. Yet, both pro-inflammatory and anti-inflammatory effects of metals (e.g. copper, zinc and silver) have been observed experimentally. Zinc, for example, plays a potent role in inflammation, where it

rapidly accumulates in renewing tissues (e.g. bone marrow) and affects the function of polymorphonuclear leukocytes and Mφs (Wellinghausen et al., 1997). Zinc can dampen LPS and IL-1β-induced inflammation via the uncoupling of eNOS (in rats, Abou-Mohamed et al., 1998; Förstermann & Münzel, 2006), and protect against oxidation of enzyme sulfhydryl groups (*in vivo*, Lim et al., 2004; Zhou et al., 2005) to inhibit nitric oxide synthesis.

By contrast, silver and copper are most prominently known for their oxidant activities, where they stimulate pro-inflammatory activities at high concentrations (Bonham et al., 2002). However, many authors have argued that the inflammatory effects of metals are largely dependent on their delivery mechanism. In one study of mouse burn wounds, the use of silver nanoparticles dampened inflammation by reducing neutrophil infiltration and Il-6 levels (Tian et al., 2007). Moreover, inhalation of silver nanoparticles did not cause an inflammatory response in rodent lungs (Braakhuis et al., 2014), thus suggesting silver nanoparticles to be a viable option for treating infection without being detrimental to the host. Intriguingly, copper and zinc complexes are often included in non-steroidal anti-inflammatory drug preparations to increase their antioxidant activity (via increasing SODs; Dimiza et al., 2011). As a result, there is clear scope to develop novel metal-based treatments for many anti-inflammatory applications.

6.1.1.3. Metals Promoting Wound Repair

In both experimental and clinical studies, a number of metal complexes have demonstrated promising effects in wound restoration (e.g. in mice, Borkow et al., 2010; Rakhmetova et al., 2010; in human burns, Atiyeh et al., 2007). The mechanisms underlying the regenerative capabilities of metals are largely undefined, but likely include: (a) metal-mediated pro-angiogenic effects via increased vascular endothelial growth factor, Vegf (e.g. γ-Fe_2O_3 nanoparticles in rat wounds, Ziv-Polat et al., 2010); (b) stimulating keratinocyte and fibroblast migration via increased cytokine and growth factor (GF) release (Sen et al., 2002) and; (c) regulating the balance between fibrosis and apoptosis during ECM remodelling (Sarsour et al., 2008). It is therefore not surprising that a large number of wound care products incorporate metal modulating complexes in the hope of improving chronic wound outcome.

6.1.1.4. Traditional Metal Therapies

The simplest mode to deliver therapeutics is topically, and traditionally, metal salts such as silver sulphadiazine have been incorporated into creams for wound surface application (Toy & Macera, 2011). In the wound care industry today, metal salt emollients are viewed as a crude application as this treatment modality does not allow for metal delivery in a biologically active (ionic) form. It is also difficult to accurately manage silver sulphadiazine concentration and subsequent sequestration of silver by tissues. Therefore, a number of complications, including cytotoxicity (Toy & Macera, 2011) and argyria (silver staining of tissues, Marx & Barillo, 2014) can arise. One example of the pitfalls of using metal salts is evident from a study in 1993 (Ågren, 1993), where application of zinc sulphate caused delayed re-epithelialisation of porcine wounds. When zinc was applied in a more controlled manner as zinc oxide in the same study, wound healing was greatly improved. Another important consideration for metal-based therapies is the possibility of interaction of exogenous metal ions with endogenous biological ions. For example, metal ions bind to halide ions (e.g. chloride ions) to form salt complexes. In wound fluid, excess chloride ions are found which could therefore affect metal ion availability (Percival et al., 2005). Consequently, delivery systems and metal formulations must be engineered to regulate their bioavailability and treatment suitability.

6.1.1.5. Current Metal Preparations

A multitude of metal incorporated dressings are currently commercially available, including metal nanoparticles which oxidise upon contact with wound fluid, thus aiding ionic metal delivery (Rai et al., 2009). However, a crucial requirement of dressings is to remove excess wound exudate while preventing extreme drying (Boateng et al., 2008). Highly exuding wounds require absorbent dressings such as alginates, hydrogels and hydrocolloids (Jones, 2013). Alginates in particular have been combined with metals, such as silver (e.g. Aquacel® Ag, Convatec, Flintshire, UK) and zinc (Zinc Alginate®, Covidien, Medtronic Ltd, Watford, UK; reviewed in Klinkajon & Supaphol, 2014) for their antimicrobial properties. Nanoparticle preparations (e.g. ACTICOAT, Smith and Nephew Ltd) are often used as they increase bioactive surface area and thus allow reduced heavy metal incorporation (reviewed in Rai et al., 2009). Utilising nanoparticles permits control over particle size and metal oxidative state, while nanoparticles also demonstrate a larger

antimicrobial effect (than traditional preparations) during *in vitro* assays (Lu et al., 2013; Martinez-Castanon et al., 2008). Despite the plethora of metal-containing topical wound products, their bioactive effects during *in vivo* wound repair remain contentious. Thus, there is a current shift towards developing novel systems for metal-based therapies.

6.1.2. Novel Delivery Systems

6.1.2.1. Biological Scaffolds

In chronic wound pathophysiology, ECM degradation prevents adequate migration by endothelial cells, fibroblasts and keratinocytes (Demidova-Rice et al., 2012). One exciting avenue of pre-clinical wound healing research is therefore the use of scaffolds to promote cellular migration (Boateng et al., 2008). Incorporation of the ECM components, collagen and hyaluronic acid (Koria et al., 2011), is popular in cellular and acellular biological scaffolds. Cellular scaffolds integrate recombinant and patient-derived cells and ECM, which is advantageous for enhancing the half-life of growth factors (GFs) and controlling of the kinetics of GF delivery (Lee et al., 2011). In wound healing, evidence exists to show that cellular scaffolds promote re-epithelialisation and dermal remodelling (in rat wounds, Tan et al., 2014; Zeinali et al., 2014). Acellular ECM scaffolds maintain the correct tissue architecture for the host (as they are made of endogenous matrix) but retain none of the complications associated with cell seeding (Boateng et al., 2008; Nichols et al., 2012). Empirical studies also use acellular scaffolds extensively to determine their effects on cellular migration *in vivo* (mice, Kobsa et al., 2013; pigs, Adolph et al., 2015) and *in vitro* (human dermal fibroblasts, and mesenchymal stem cells, Griffin et al., 2015).

Despite the numerous advances of using ECM scaffolds in wound healing, there remains an ethical stigma around the use of stem cells to create biological scaffolds, with biological risks including antigenicity and infection (Boateng et al., 2008). Host complications can arise through use of the wrong source material, inefficient decontamination processes, and lack of full consideration of the host environment (Keane et al., 2012). To counteract any adverse effects, stringent decontamination methods are regulated by the US Food and Drug Administration Agency. However, these harsh purifying processes can damage the ECM and reduce functionality (Keane et al., 2015), meaning non-biological scaffolds, such as polymers, are often favoured (Bose et al., 2012).

6.1.2.2. Non-Biological Scaffolds

Non-biological scaffolds are usually applied to tissues with high collagen content, such as bone. Common non-biological scaffolds include porous ceramics (e.g. incorporating calcium phosphate), synthetic polymers (e.g. graphene, Goenka et al., 2014) and composites with metallic matrices (Bose et al., 2012), each conferring their own advantages and disadvantages. As with all matrices, the mechanical properties of the scaffold must be matched to the intended tissue (Bose et al., 2012), and the porosity and shape manipulated correctly to facilitate cell seeding, cellular migration and nutrient diffusion (Walthers et al., 2014). Non-biological scaffolds, like biological scaffolds, should also be properly sterilised prior to application to prevent infection (Daghighi et al., 2013). Indeed, non-biological scaffolds have shown promise in facilitating wound repair *in vivo*, promoting migration, cell attachment and proliferation (in mice, Babaeijandaghi et al., 2010; in rats, Rho et al., 2006; in guinea pigs, Khil et al., 2003).

6.1.2.3. Electrospinning

Electrospinning is one of many techniques available to produce 3D non-biological scaffolds with adequate porosity for tissue integration. Electrospinning was developed in the 1930's, where it was particularly useful in the textile industry (Khil et al., 2003) and in filtration (producing parts for gas masks, Persano et al., 2013). It is now used extensively in tissue engineering (Sill & von Recum, 2008). Although electrospinning processes are widespread and variable, they all follow the same basic approach (**Figure 6.3**). First, a scaffold solution (e.g. polymer) is fed through a syringe and spinneret (Sarsour et al., 2005). At the same time, an electrical field is generated, causing the scaffold solution in the syringe to deform and stream out of the syringe as a rectilinear jet (Persano et al., 2013; Poologasundarampillai et al., 2014). The charged jet of scaffold solution is subjected to strong electrostatic forces that cause it to bend and stretch towards the counter electrode at the opposite end of the machinery. Fibres elongate from the liquid, which straightens and solidifies as it is deposited on the target electrode/substrate.

The resultant product is a scaffold of nanoparticle fibres that can be uniaxial, cross-linked, non-woven or layered (Sarsour et al., 2005; Persano et al., 2013; Poologasundarampillai et al., 2014). Fibre structure, porosity and diameter can be manipulated via changing the voltage, composition, concentration and viscosity of

the solution (Khil et al., 2003). Of interest, electrospinning incorporates therapeutic agents into scaffolds more efficiently than other methods (e.g. covalent bonding), demonstrated when electrospinning poly (ι-lactic acid) with laminin (Koh et al., 2008). Electrospun scaffolds are ideal matrices for regenerative purposes, due to their high porosity and large surface area to aid cell attachment (Poologasundarampillai et al., 2014).

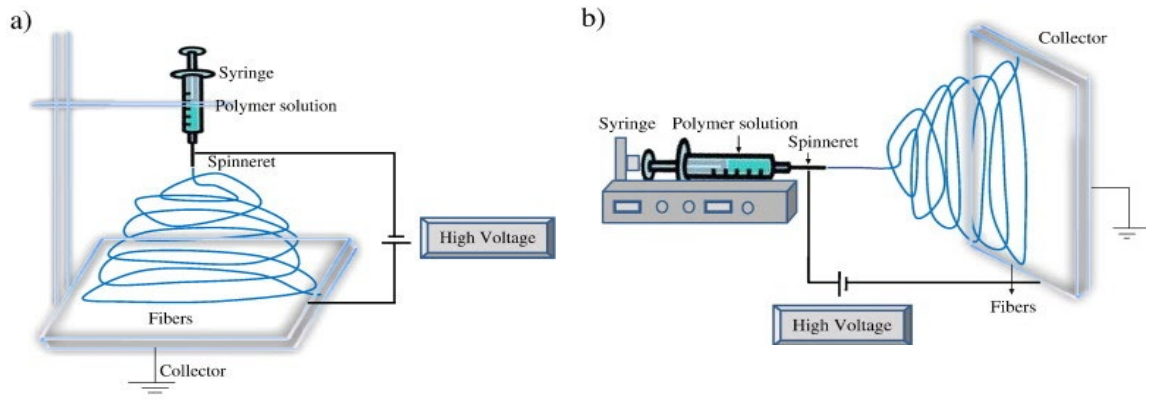

Figure 6.3. An illustration of the electrospinning technique. A jet of charged solution leaves the syringe spinneret and stretches towards the opposite electrode/collector, resulting in a number of identical fibres with large surface area for bioactivity. The diagram shows typical vertical (**a**) and horizontal (**b**) apparatus. *Taken from Bardwaj & Kundu (2010).*

6.1.2.4. Bioactive Glass

Base materials for most scaffolds include polyglycolic acid, poly (ι-lactic acid) and polylactide (Venugopal & Ramakrishna, 2005). However, bioactive glass (BG) is a silicon-based alternative to other scaffolds, first proposed in a seminal report where it was used to heal rat femurs (reviewed in Bose et al., 2012; Hench, 2006). BG is now available in an array of different forms, and is categorised into two main types: borate-based BGs and silicon-based BGs, with the former displaying faster biodegradability (Liu et al., 2014c). Conventional BG preparations are used in dentistry and bone repair, where their composition includes compounds with known pro-healing effects (e.g. CaO, SiO_2, P_2O_5 and MgO; Lin et al., 2012; see **Table 6.1**). In fact, the most extensively researched BG (Miguez-Pacheco et al., 2015), 45S5 Bioglass™, has lower amounts of silicon dioxide than more recent formulations. BGs bond compatibly to tissues via dissolution and precipitation reactions that actuate surface ion exchange. In damaged bone tissue, BG ion release (usually silicon and calcium) increases pH, causing the formation of a hydroxycarbonate apatite interface layer between the host tissue and BG, usually via damaged collagen fibres

(Jones, 2013). This interface is thought to form rapid, stable conduits for cell migration. Indeed, BG has been shown to promote cell migration, osteoprogenitor differentiation and ultimately accelerate bone reformation (reviewed in Kargozar et al., 2018; Miguez-Pacheco et al., 2015; see **Figure 6.4**).

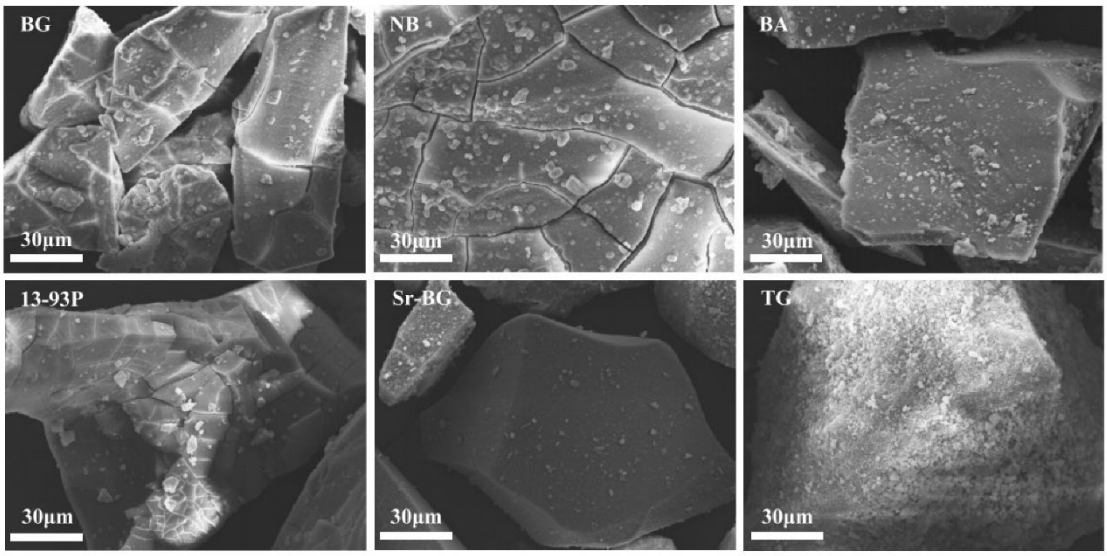

Figure 6.4. Scanning electron micrographs of six commercially available bioactive glasses following 24-hour immersions in simulated body fluid. Light particles on the bioactive glass exteriors are hydroxycarbonate apatite. BG, Bioglass®; NB, Novabone™; BA, BonAlive™; traditional, 13-93P; Sr-BG, Strontium Bioglass®; TG, Theraglass™. *From Maçon et al. (2015*).

Table 6.1. Compositions of widely studied bioactive glass. *

Composition (Mol%)	Common Bioactive Glass Formulations		
	45S5	**13-93**	**S53P4**
SiO_2	45	53	53
CaO	24.5	20	20
P_2O_5	6	4	4
K_2O	0	12	0
Na_2O	24.5	6	23
MgO	0	5	0

**Data from Miguez-Pacheco et al. (2015).*

Of note, the increased alkalinity provided by BG may have antibacterial effects (Zehnder et al., 2006). BG components can also be used as a substrate for incorporating known antimicrobials, such as metal nanoparticles (Gholipourmalekabadi et al., 2016; Kaya et al., 2018). Despite its main therapeutic application being bone restoration, BG may retain efficacy in soft tissue research. These potential effects include promoting cell adhesion and migration (human lung epithelial cells, Verrier et al., 2004) and increasing epidermal and fibroblast GF

expression (Keshaw et al., 2005; Yang et al., 2015). In experimental studies on rats, BG has also demonstrated efficacy in normal and diabetic healing, via upregulation of Vegf and Fgf2 (Lin et al., 2012).

The first electrospun BG, a sol-gel derived BG (Lu et al., 2009), showed large bioactivity, fast degradability and versatility (Liu et al., 2014c). Since then, BG electrospun scaffolds have become increasingly more favourable in soft tissue studies, incorporating anything from matrix components (e.g. gelatin), to cells (Fu et al., 2010; Jones, 2013; Wang et al., 2018c), to inorganic metals (Liu et al., 2014c; Moura et al., 2017). One advantage of using electrospun BG for metal incorporation is the release of metals at non-cytotoxic levels as the BG degrades (Liu et al., 2014c). Interestingly, metal integration into mesoporous borate BG nanofibers has previously resulted in pro-angiogenic responses in wounds (copper, Zhao et al., 2015) and bone (Cobalt, Wu et al., 2012). In wound healing, the use of copper did not adversely impact the structure and function of BG, yet copper was released at a therapeutic rate, stimulating human umbilical vein endothelial cell migration and the production of βFGF and PDGF in human dermal fibroblasts (Zhao et al., 2015).

Assessment of metal ion release (copper, zinc, iron and strontium) from BG into simulated body fluid further corroborated that BG degradability was not altered with metal incorporation. However, metal ion release was dependent on the composition of the metal investigated (Liu et al., 2009). Other studies have considered the effects of zinc-BG on osteoblast proliferation (Du et al., 2006), silver and calcium incorporated BG in angiogenesis (in rabbits, Dai et al., 2011), and strontium oxide-BG to promote re-epithelialisation (in rats, Jebahi et al., 2013). BG-supported regeneration has even been assessed in cardiovascular, nervous and gastrointestinal repair (reviewed Miguez-Pacheco et al., 2015). Despite the promising implications of BG, to date, only a handful of case studies exist for the use of BG for wound-related complications (e.g. charcot foot, Godoy-Santos et al., 2019).

Along with its effects on host tissue function, the antimicrobial efficacy of BG preparations incorporating known antimicrobial agents has been investigated in multiple studies (Moghaddam et al., 2018; Munukka et al., 2008; Tejido-Rastrilla et al., 2019). However, these have all focussed solely on *in vitro* effects against planktonic bacterial viability and have not considered clinically relevant models such as biofilms or infected host systems (e.g. cells or tissue). Further, determination

of other measures of antimicrobial efficacy, such as reducing bacterial pathogenicity and virulence, have been greatly understudied. As a result, there is clear need to assess how both BG, and BG incorporating known antimicrobials (e.g. silver), influence bacterial pathogenic modalities in more sophisticated models of infection.

6.1.3. Theraglass™

Theraglass™ (TG, Theraglass Ltd., London, UK) is a novel, highly bioactive, binary sol-gel derived BG (Maçon et al., 2015) composed of $70SiO_2$: 30CaO by mol% (Bellantone et al., 2002; Poologasundarampillai et al., 2014; Saravanapavan & Hench, 2001). Sol-gel BGs maintain advantages over melt-derived glasses as they have fewer manufacturing steps and consequently less potential for contamination. Melt-derived glasses are also subjected to extremely large temperatures, thus limiting their composition (Li et al., 1991). Further, the high content of silicon and calcium in sol-gel BGs increases the formation of a hydroxycarbonate apatite interface allowing for increased bioactivity (Bellantone et al., 2002; Poologasundarampillai et al., 2014; Saravanapavan & Hench, 2001). Other advantages of TG manufacture include the ability to prepare electrospun 3D cotton wool-like matrices incorporating 2 mol% silver oxide (AgO) for increased therapeutic action (Hack, 2014). Although AgO is added to the TG solution prior to manufacture, electrospun TG matrices may be functionalised by dipping the engineered mesh into a therapeutic agent, which is taken up into the TG matrix due to the tailored nanoporous size (Lin et al., 2010).

6.2. Aims of the Chapter

TG is a novel, sol-gel derived AgO functionalised BG (Maçon et al., 2015; Poologasundarampillai et al., 2014), used in bone regeneration and oral repair. The research hypothesis of this chapter was that AgO functionalised TG would beneficially influence multiple aspects of skin wound healing.

Specific aims were to:

1) **Assess the beneficial effects of Theraglass™** (AgO-functionalised TG, and non-functionalised TG) **on *in vivo* murine wound repair**.
2) **Elucidate the antimicrobial and anti-biofilm effectiveness of AgO-functionalised TG, and non-functionalised TG**, against two well-known opportunistic wound pathogens, *P. aeruginosa* and *S. aureus.*

Current BG studies are limited to simple *in vitro* assays. Here single-and mixed-species biofilm models, as well as *ex vivo* models of porcine and human wound infection, were employed.

6.3. Materials and Methods

6.3.1. Theraglass™ Formulations

TG is composed of 70 mol% SiO_2 and 30 mol% CaO, with one formulation functionalised further with 2 mol% AgO. Commercially available emollients used in this study contained 20% ("Tg20") and 40% ("Tg40") TG with AgO. Freshly prepared powder-cream preparations were manufactured by mixing TG powder ("Tg"), and TG containing AgO ("Tg^{Ag}"), with a vehicle (NIVEA, Beiersdorf Global AG, Germany) to produce fresh 20% (w/w) creams. NIVEA was used as the vehicle as it most closely matched the commercial TG base cream. A 2% (w/w) silver (AgO) control ("Ag") was prepared in NIVEA, and included at the equimolar concentration of AgO in Bg^{Ag}. NIVEA alone was used as a vehicle only control ("Vehicle" or "Veh").

6.3.2. Animal Experiments

Initially, the effects of TG were assessed using a murine excisional wounding model. Female (C57BL/6J) mice were wounded at 8-10 weeks of age as described in **Section 2.1** and split into treatment groups (**Table 6.2**). Treatments were applied topically to wounds immediately after excision, and daily until collection (3 days post-injury). Wounds were left open to heal and were collected as outlined in **Section 2.2**.

Table 6.2. Theraglass™ treatments used for murine excisional wound healing experiments.

Treatment	Animals used	Composition
Vehicle	6	NIVEA
Tg20	6	20% Theraglass™ Ag
Tg40	6	40% Theraglass™ Ag
Tg	6	NIVEA + 20% Theraglass™
Tg^{Ag}	6	NIVEA + 20% Theraglass™ Ag

6.3.2.1. Wound Processing and Histology

Wounds were excised and bisected at their midpoint and fixed in saline buffered formalin. The fixed tissue was processed, embedded and stained as described in **Section 2.4**. H&E stained sections were used to determine wound width and area; Krt14 IHC was used to assess wound closure (re-epithelialisation) and; Mac3 and Ly-6G IHC was used for wound Mφs and neutrophils, respectively. All other methods, including in-depth microbiological assays, are provided in **Chapter 2**.

6.4. Results

6.4.1. Topical Theraglass™ application does not substantially alter the inflammatory phase of acute murine wound repair.

TG formulations or vehicle controls were topically administered to excisional mouse wounds and re-administered daily throughout the three-day treatment period. The efficacy of commercial (cream) TG incorporating silver (20%, Tg20; 40%, Tg40) was compared to freshly prepared TG (powder mixed with NIVEA vehicle immediately prior to administration) with (Tg^{Ag}) or without (Tg) silver at 20% concentration. These treatment groups allowed direct comparison of the efficacy of fresh versus shelved TG, and comparison of formulations with and without silver. Macroscopic and histological analysis was performed to determine whether TG altered the rate of repair in a model of normal murine wound healing. Overall wound area was quantified from macroscopic images, histological wound area and wound width were quantified from H&E stained images, and percentage wound closure (re-epithelialisation) was measured via Krt14 IHC. Macroscopically, wound area was significantly reduced by Tg40 and Tg^{Ag} treatment ($P < 0.05$; **Figure 6.5A**). However, histological assessment failed to reveal any significant effects of TG on wound area, wound width or percentage re-epithelialisation (**Figure 6.5B-D**).

Neutrophils arrive at the wound site from the peripheral blood during the first stage of inflammation, and despite their importance in triggering a wound repair response, excessive neutrophil infiltration can cause impaired healing (Ashcroft et al., 1997; Baltzis et al., 2014). In the present work, neutrophils, detected with Ly6-G, were only elevated following Tg40 treatment ($P < 0.05$; **Figure 6.6A-B**), although there was also a strong trend towards increase with Tg20 treatment.

Like neutrophils, Mφs play a large role in the innate immune response and wound repair, yet excessive inflammation can lead to poor healing outcome (Ashcroft et al., 2003). Assessment of wound Mφs (Mac3) demonstrated that Tg20 treatment caused an overall reduction in infiltrating Mφs ($P < 0.05$; **Figure 6.6A**, **C**), with a trend towards reduced Mφs with Tg40 and Tg^{Ag} treatment also observed. Given the limited effects observed for TG of non-infected wounds *in vivo*, the next aim was to assess the antimicrobial efficacy of TG treatments, as multiple authors have suggested BG to hold antimicrobial efficacy (e.g. Jiang-Chang et al., 2009). The

antimicrobial effects of TG were assessed against two wound-relevant pathogens, *S. aureus* and *P. aeruginosa* (Price et al., 2009).

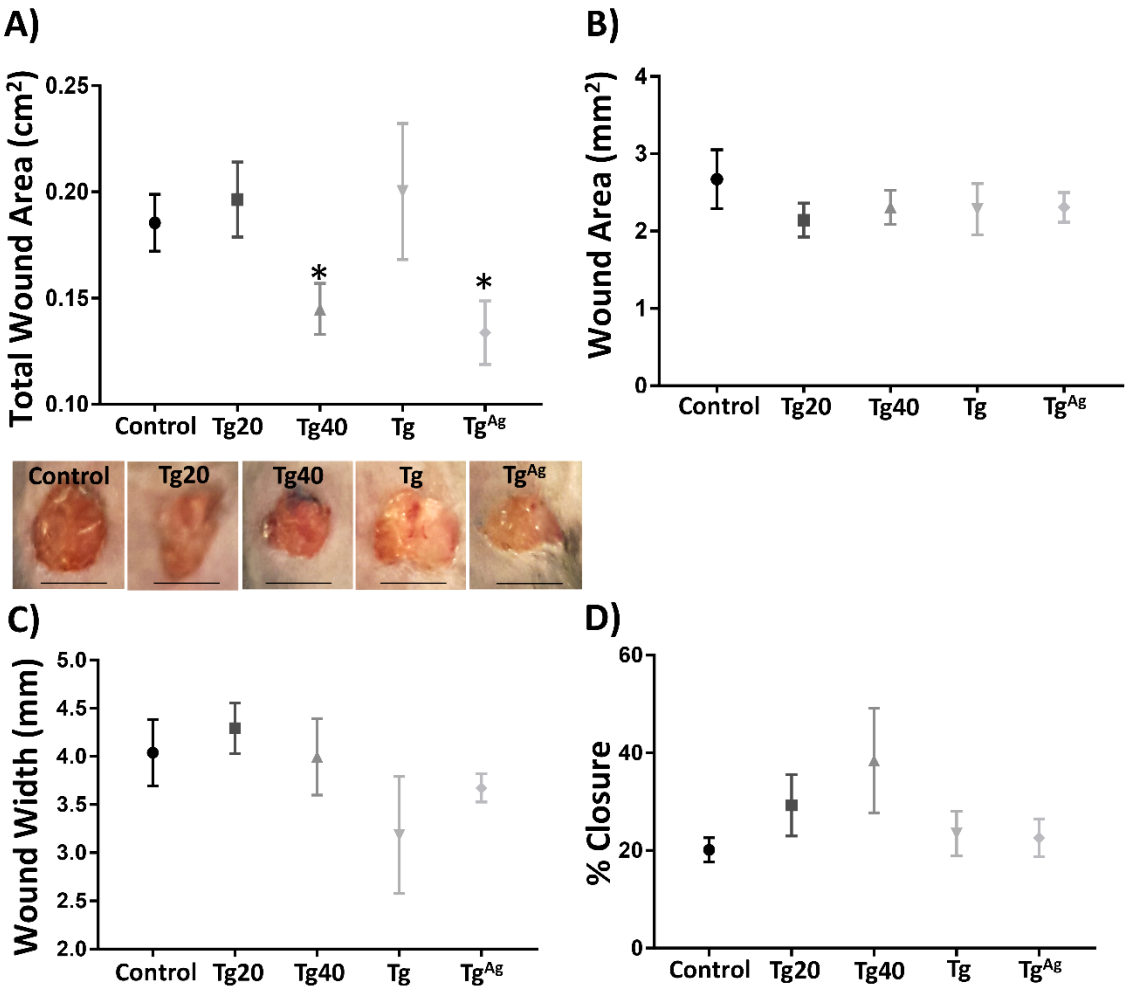

Figure 6.5. Theraglass™ does not substantially alter macroscopic wound closure. Total wound area was measured from macroscopic images (**A**, bar = 0.5 cm). Wound area (**B**), wound width (**C**) and percentage epidermal closure (% Closure, **D**) were measured from histological images. n = 5 mice per group. Veh = vehicle. Tg20 = 20% commercial Theraglass™. Tg40 = 40% commercial Theraglass™. Tg = Theraglass™ in vehicle. Tg^{Ag} = Theraglass™ with silver oxide in vehicle. Mean +/- SEM. * = $P < 0.05$. One-way ANOVA with Dunnett's *post-hoc*, comparing treatment to control group.

6.4.2. Tg^{Ag} elicited potent antimicrobial effects against planktonic cultures of *P. aeruginosa* and *S. aureus*.

Growth inhibition following TG treatment was determined using planktonic agar diffusion assays. Here, potent yet differential effects of Tg and Tg^{Ag} against *P. aeruginosa* (*P. aer*) and *S. aureus* (*S. aur*) at 24 and 48 hours were revealed. Interestingly, Tg^{Ag} elicited the greatest antimicrobial effect, producing the largest inhibition zones in agar diffusion assays against *P. aer* and *S. aur* at both 24 hours ($P < 0.001$) and 48 hours ($P < 0.001$; **Figure 6.7A-D**). Tg also significantly inhibited *P.*

aer growth at 24 ($P < 0.05$) and 48 ($P < 0.05$) hours, but failed to inhibit *S. aur* growth (**Figure 6.7B, D**). By contrast, AgO alone (Ag), at equimolar concentration to that of Tg^{Ag}, caused only modest, non-significant inhibition of *P. aer* and *S. aur*.

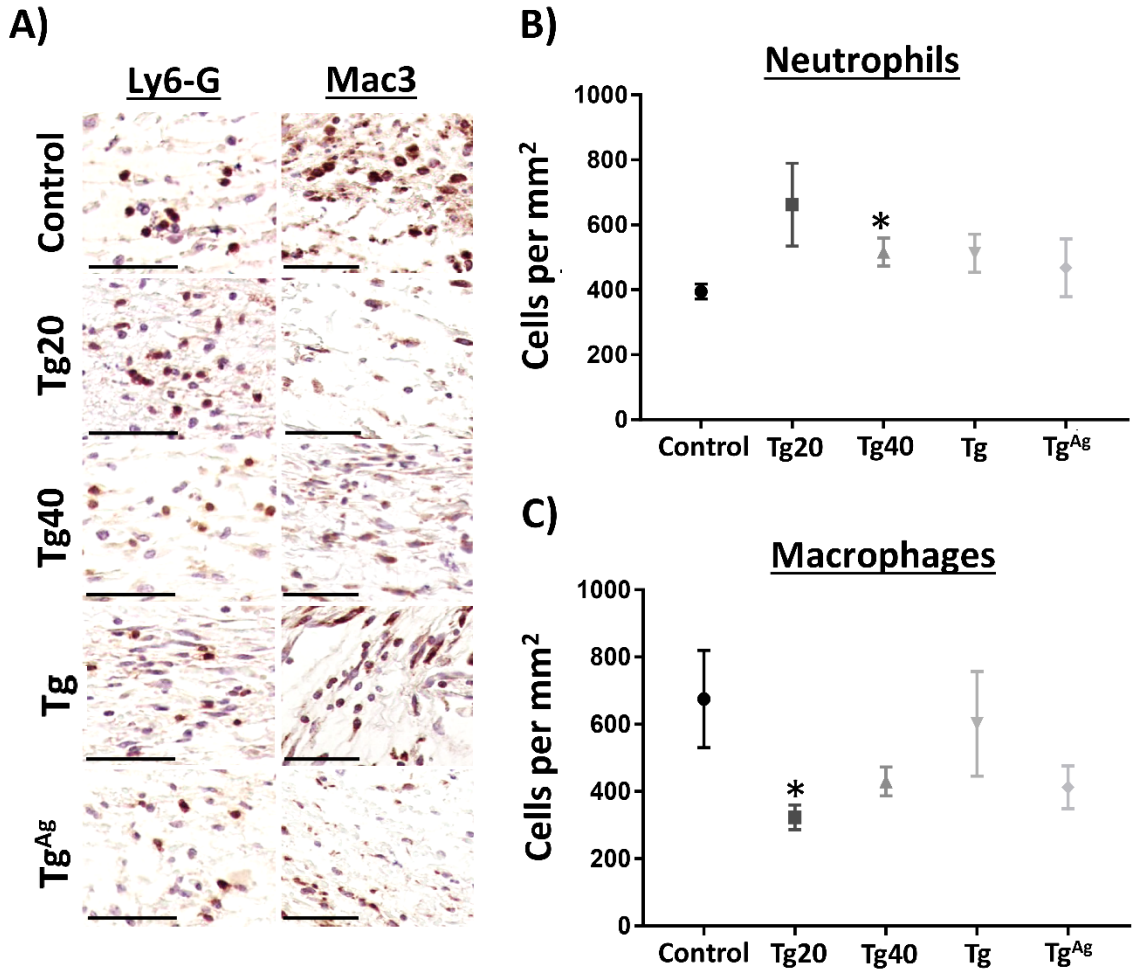

Figure 6.6. Wound inflammatory cell infiltration is disparately altered by Theraglass™. Wound site neutrophils (Ly6-G immunohistochemistry [IHC], **A**) are not dampened by any Theraglass™ formulation (**B**). Wound site macrophages (measured by Mac3 IHC, **A**) are only reduced following Tg20 treatment (**C**). n = 5 mice per group. Bar = 50 µm. Veh = vehicle. Tg20 = 20% commercial Theraglass™. Tg40 = 40% commercial Theraglass™. Tg = Theraglass™ in vehicle. Tg^{Ag} = Theraglass™ with silver oxide in vehicle. Data show mean +/- SEM. * = $P < 0.05$. One-way ANOVA with Dunnett's multiple comparisons was performed (versus Veh).

Next, the temporal bactericidal activity of TG was assessed via time-kill assays. Here, all treatments maintained potent, statistically significant ($P < 0.001$), antimicrobial efficacy, causing over a 6-log reduction in *P. aer* and *S. aur* within 2 hours (**Figure 6.7E-F**). Again, disparate yet interesting results were observed between the two bacterial species. Tg^{Ag} and Tg caused a 6-log reduction in *P. aer* within 30 minutes ($P < 0.001$), while Ag took twice as long to induce this effect ($P < 0.001$; **Figure 6.7E**). Tg^{Ag} ($P < 0.001$) caused a 6-log reduction in *S. aur* within one hour, but Tg and Ag

took two hours to confer this level of viable colony reduction (**Figure 6.7F**). In summary, both agar diffusion and time-kill assays revealed *P. aer* to be more susceptible to both Tg and Tg^{Ag} than *S. aur*, while Tg^{Ag} was significantly more effective than Tg or Ag alone.

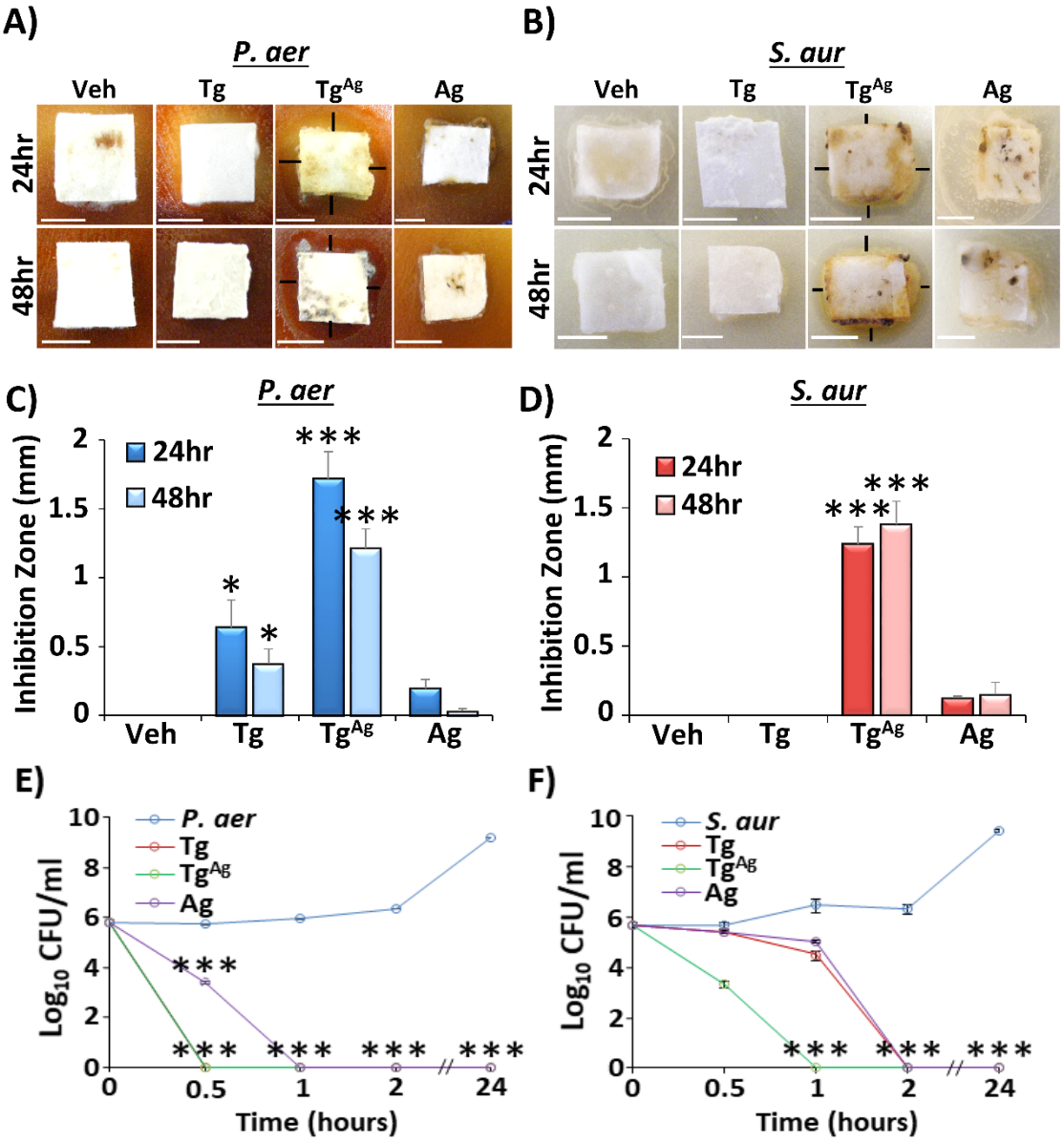

Figure 6.7. Differential antimicrobial efficacy of Theraglass™ against planktonic *P. aeruginosa* and *S. aureus*. Zones of inhibition (illustrated by black lines) from agar diffusion assays against *P. aeruginosa* (*P. aer*, **A, C**) and *S. aureus* (*S. aur*, **B, D**). Time kill assays of *P. aer* (**E**) and *S. aur* (**F**). Bar = 5 mm. Three independent experiments for each data set. Ag = silver oxide alone. Tg = Theraglass™. Tg^{Ag} = Theraglass™ with silver oxide. Data show the mean +/- SEM. * = $P < 0.05$, ** = $P < 0.01$, *** = $P < 0.001$. Two-way ANOVA with Tukey's *post-hoc* test (Veh/bacteria only).

6.4.3. Tg^{Ag}, but not Tg, maintains antimicrobial efficacy over a clinically meaningful time frame.

To determine the stability of the TG and Ag treatments, formulations were freshly mixed and pre-incubated at 4°C, RT or 37°C for 24-120 hours before performing 24hr agar diffusion assays. When Tg^{Ag} and Ag were pre-incubated at 4°C and RT, significant efficacy was maintained against *P. aer* over the full 120-hour period (**Figure 6.8A-B**). On the other hand, Tg maintained statistically significant efficacy for only 72 hours at 4°C and exhibited little to no inhibitory effect following pre-incubation at RT. Following pre-incubation at 37°C, all three treatments lost their effectiveness against *P. aer* (**Figure 6.8C**). Pre-incubation of Tg at 4°C, RT and 37°C fully abrogated inhibition of *S. aur* growth (**Figure 6.9A-C**). This differed largely to Tg^{Ag}, which maintained statistically significant efficacy against *S. aur* over the full 120 hours at both 4°C and RT (**Figure 6.9A-B**). Ag, although more efficacious than Tg alone, was less effective than Tg^{Ag} against both bacterial species.

An alternative measure of treatment effectiveness is the capacity of a compound or dressing to release antimicrobial over time (Anguita-Alonso et al., 2006). Here, the kinetics of TG release were measured by serially incubating Tg, Tg^{Ag} and Ag powders in sterile DPBS over six consecutive days. Every 24 hours, the PBS supernatant was removed and used in agar diffusion assays. In this model, Tg and Ag maintained no antimicrobial efficacy against *P. aer* or *S. aur* at any time point (**Figure 6.8D** and **Figure 6.9D**, respectively), indicating that no antimicrobial factors were released from the Ag-free TG compound or Ag alone. By contrast, Tg^{Ag} strongly inhibited the growth of *P. aer* over the first 96 hours before losing efficacy. Against *S. aur*, Tg^{Ag} exhibited a strong inhibitory effect for the first 96 hours, with subsequent antimicrobial activity rapidly declining. Collectively, these data show that Tg^{Ag} maintains antimicrobial efficacy over a clinically meaningful period when stored at 4°C and RT, and is able to release soluble antimicrobial factors consecutively over four days. Wound dressings are typically replaced every two days or longer to reduce wound disruption and cut nurse time and associated costs (Lindholm & Searle, 2016). Thus, maintaining efficacy over four days would suitably fit with, and reduce the cost of, clinical wound management.

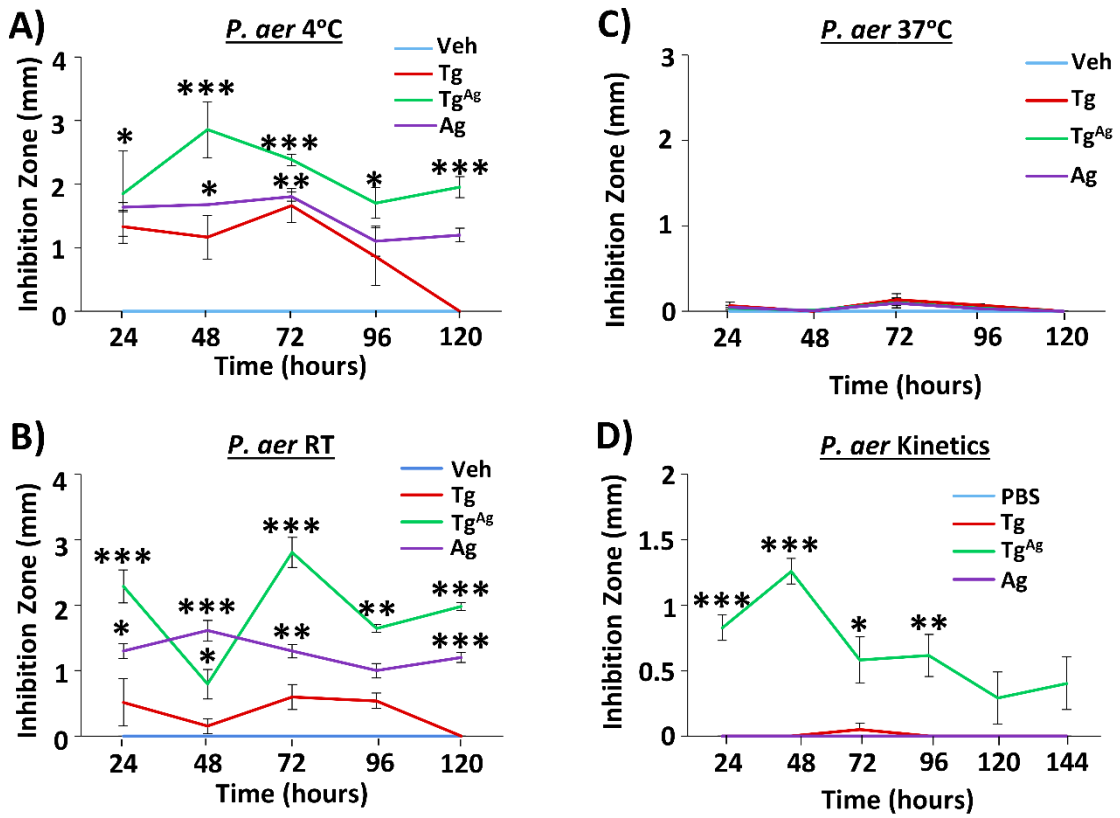

Figure 6.8. Theraglass™ incorporating silver maintains stability and releases soluble antimicrobial factors over a clinically relevant period against *P. aeruginosa*. Tg, Tg^{Ag} and Ag, pre-incubated at 4°C (**A**), room temperature (RT, **B**), and 37°C (**C**) prior to 24-hour agar diffusion assays. Veh = vehicle. Kinetic testing reveals release of soluble antimicrobial factors from Tg^{Ag}, with potent antimicrobial effectiveness over 4 days against *P. aeruginosa* (*P. aer*; **D**). PBS = phosphate buffered saline. Three independent experiments. Mean +/- SEM. * = $P < 0.05$, ** = $P < 0.01$, *** = $P < 0.001$. Two-way ANOVA with Tukey's *post-hoc* analysis (versus Veh/PBS).

6.4.4. Theraglass™ antimicrobial efficacy is different for single-species and co-cultured planktonic bacteria.

The above data clearly indicated that 20% TG maintained potent antimicrobial effectiveness against planktonic forms of *P. aer* and *S. aur*. The next step was to determine the minimum concentration of each TG formulation required to maintain an inhibitory and bactericidal effect. To do this, minimum inhibitory concentration (MIC) and minimum bactericidal concentration (MBC) testing was used (**Table 6.3**). In time-kill assays (**Figure 6.7**), Tg^{Ag} showed the greatest effect against *P. aer*. This was mirrored in MIC and MBC assays, where lower concentrations of Tg^{Ag} were able to inhibit (6.25 mg/mL) and kill (12.5 mg/mL) *P. aer* than *S. aur* (both 100 mg/mL). Interestingly, while Tg conferred a reduced effect against *S. aur* in previous susceptibility tests, the MIC of Tg was identical for both species (50 mg/mL) and the MBC was higher for *P. aer* (100 mg/mL) than *S. aur* (50 mg/mL). In summary, these

data reveal that *S. aur* is more resistant to the inhibitory and bactericidal effects of Tg^{Ag} than *P. aer*, while *P. aer* can maintain viability against Tg at higher concentrations than *S. aur*. Ag alone showed greater efficacy against *P. aer* than Tg^{Ag}, but was relatively less efficacious against *S. aur*.

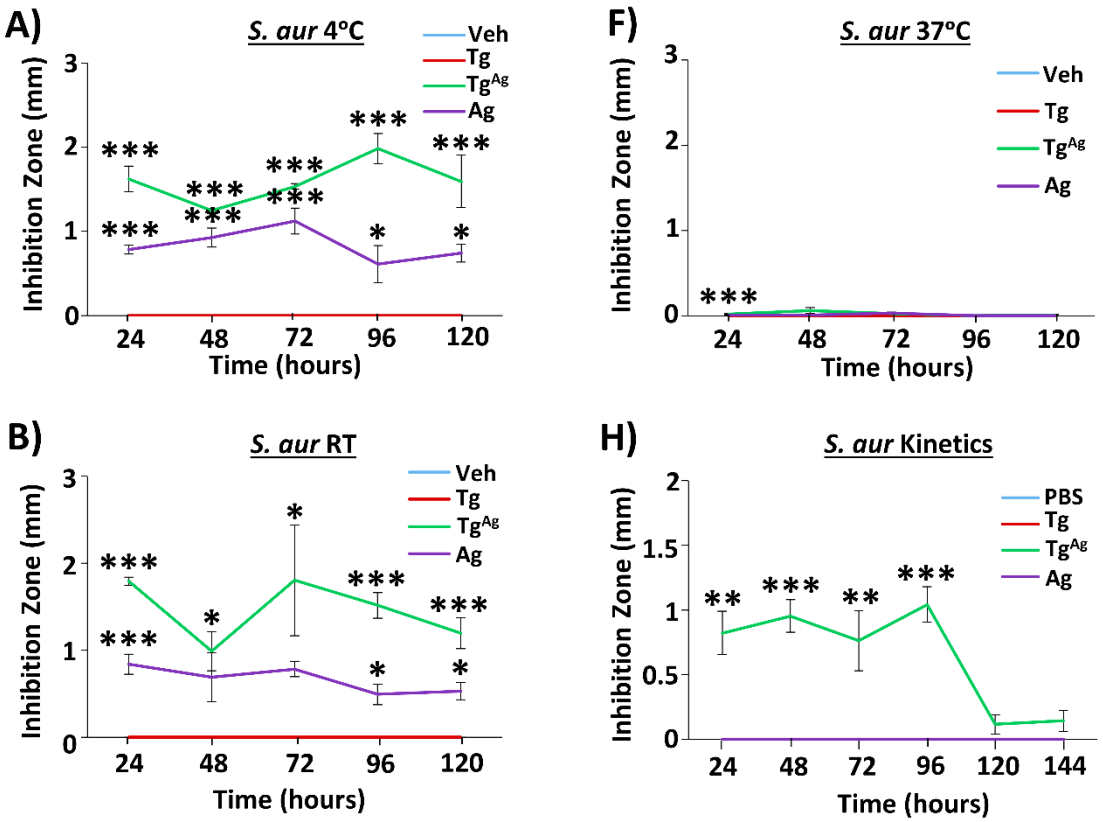

Figure 6.9. Theraglass™ incorporating silver maintains stability and releases soluble antimicrobial factors over a clinically relevant period against *S. aureus*. Tg, Tg^{Ag} and Ag incubated at 4°C (**A**), room temperature (RT, **B**) and 37°C (**C**). Veh = vehicle. Kinetic testing reveals release of soluble antimicrobial factors from Tg^{Ag}, with potent antimicrobial effectiveness over 4 days against *S. aur* (**D**). PBS = phosphate buffered saline. n = 3 experiments. Mean +/- SEM. * = $P < 0.05$, ** = $P < 0.01$, *** = $P < 0.001$. Two-way ANOVA with Tukey's *post-hoc* (versus Veh/PBS).

Next, *P. aer* and *S. aur* cultures were mixed in a 50:50 ratio to give co-culture suspensions. Intriguingly, co-culture existence conferred increased bacterial resistance to Tg^{Ag} versus *P. aer* alone, but decreased resistant versus *S. aur* alone (**Table 6.3**). Further, co-culture bacteria displayed decreased resistance to Tg than single-species bacteria (via MIC), and enhanced susceptibility to Ag (MIC and MBC). Together, these results demonstrate that in co-culture, planktonic bacteria are more susceptible to growth inhibition caused by Tg and Ag, potentially reflecting accumulative toxicity induced by competition for resources (Rendueles et al., 2014).

Table 6.3. Minimum inhibitory concentration (MIC) and minimum bactericidal concentration (MBC) of Theraglass™ (Tg), Theraglass™ with silver (Tg^{Ag}), and silver (Ag).

Treatment	*S. aureus* NCTC 13297		*P. aeruginosa* NCTC 10781		Co-culture	
	MIC 90	MBC	MIC 90	MBC	MIC 90	MBC
Tg^{Ag}	100 mg/mL	100 mg/mL	6.25 mg/mL	12.5 mg/mL	31.25 mg/mL	125 mg/mL
Tg	50 mg/mL	50 mg/mL	50 mg/mL	100 mg/mL	15.63 mg/mL	125 mg/mL
Ag	3.13 µg/mL	6.25 µg/mL	12.5 µg/mL	25 µg/mL	31.25 µg/mL	125 µg/mL

6.4.5. Biofilm formation in *P. aeruginosa* and *S. aureus* is differentially affected by Theraglass™ treatment.

Given the potent effects of Tg and Tg^{Ag} against planktonic bacteria, the next query was whether the treatments altered the ability of planktonic cultures to form biofilms. This was assessed via the Crystal Violet microtiter method, where the strength of biofilm formation was categorised via measurement of dye uptake (OD values at 495nm; **Table 6.4**). Here, *S. aur* and co-cultured bacteria were less able to form adherent biofilms than *P. aer* alone, which was categorised as a strong biofilm producer (**Table 6.5**). At 0.625%, Tg^{Ag} caused *S. aur* to become non-adherent, and reduced biofilm formation by *P. aer* and co-cultures from strong to weak. However, at 0.15%, *S. aur*, *P. aer* and co-culture biofilm formation was unaffected by Tg^{Ag} treatment. Interestingly, Tg had little effect on *S. aur* and co-culture biofilm formation at 0.625%, yet inhibited *P. aer* biofilm formation at this concentration. Ag alone was less effective against *S. aur* than Tg^{Ag}, but reduced *P. aer* and co-culture biofilm formation equally. Overall, *S. aur* and co-culture biofilm formation was less affected by Tg treatment than *P. aer* biofilm formation.

Table 6.4. Classifications used to determine biofilm production in biofilm formation assays.

OD_{495nm} Value	Classification
≤0.04	Non-adherent
>0.04 and ≤0.08	Weak biofilm
>0.08 and ≤0.16	Moderate biofilm
>0.16	Strong biofilm

Table 6.5. Concentrations ("Conc") of Theraglass™ (Tg), Tg with silver (Tg^{Ag}) and silver (Ag) required to inhibit biofilm formation. *

	S. aureus NCTC 13297			*P. aeruginosa* NCTC 10781			Co-culture		
	Conc	**OD**	**Biofilm**	**Conc**	**OD**	**Biofilm**	**Conc**	**OD**	**Biofilm**
+ve		0.1	Moderate		0.54	Strong		0.14	Moderate
Tg^{Ag}	.625%	0.04	Non-adherent	.625%	0.08	Weak	.625%	0.06	Weak
	.15%	0.1	Moderate	.15%	0.23	Strong	.15%	.09	Moderate
Tg	.625%	0.11	Moderate	.625%	0.07	Moderate	.625%	0.09	Moderate
	.15%	0.1	Moderate	.15%	0.5	Strong	.15%	0.11	Moderate
Ag	.625%	0.07	Weak	.625%	0.07	Weak	.625%	0.07	Weak
	.15%	0.08	Weak	.15%	0.24	Strong	.15%	0.1	Moderate

**+ve = bacteria only control. Optical density (OD) at 495nm.*

6.4.6. Tg^{Ag} reduces biofilms of both *P. aeruginosa* and *S. aureus* in an *ex vivo* porcine wound model.

To more accurately model *in vivo* biofilm infection, an *ex vivo* porcine skin/bacterial biofilm model was previously developed by the author (Wilkinson et al., 2016). Established 72-hour biofilms of *P. aer* and *S. aur* were applied to the apical surface of porcine wound explants, cultured at 37°C and 5% CO_2 for 24 hours to allow biofilm adherence. Treatments were added to biofilms for 24 hours. In this model, treatment with Tg, Tg^{Ag} and Ag alone led to a visible reduction in biofilm thickness via histology (**Figure 6.10**). Representative images illustrate biofilms stained via Gram-Twort (*P. aer*, pink; *S. aur*, purple; **Figure 6.10A, D)**, Concanavalin A (**Figure 6.10B, E**) and Acridine Orange (**Figure 6.10C, F**). Gram-Twort stained skin tissue appears green (Fast Green), while Gram-negative bacteria appear pink (Neutral Red), and Gram-positive bacteria are purple (Crystal Violet; Cunningham et al., 2014). Here, *P. aer*, a Gram-negative rod-shaped bacterium, displays a pink biofilm, and *S. aur*, a Gram-positive coccus, stains purple (Inzana et al., 2015; Saraswathi & Beuerman, 2015). Concanavalin A, a carbohydrate conjugate used to illustrate the presence of lectins (green; Howard et al., 1981), stained porcine tissue green, while the DAPI counterstain (blue) showed biofilm cell aggregates.

Quantification of biofilm thickness demonstrated that Tg^{Ag} treatment alone led to a statistically significant reduction in *P. aer* and *S. aur* ($P < 0.05$) biofilm thickness, reducing thickness from 30 μm to less than 10 μm in both species (**Figure 6.10G-H**). Viable colony enumeration (CFU/mL) was performed on dissociated biofilms post-treatment to confirm biofilm reduction. Here, Tg, Tg^{Ag} and Ag significantly ($P < 0.001$) reduced the number of viable colonies (*P. aer* and *S. aur*; **Figure 6.10I-J**), causing over a 2-log reduction in biofilm bacteria. However, Tg^{Ag} was considerably more effective than Tg or Ag alone, leading to a 3-log reduction in *S. aur* biofilms. Together, these data provide direct evidence that TG functionalised with silver maintains antimicrobial efficacy against established *ex vivo* wound biofilms.

6.4.7. *P. aeruginosa* biofilm virulence factors are influenced by Theraglass™.

Bacterial colony enumeration alone does not directly convey bacterial pathogenicity, as invasion and adherence are fundamental for establishing tissue infection (reviewed in Percival et al., 2015). Thus, biofilm virulence was investigated by evaluating protease activity (zymography; **Figure 6.11**) and candidate virulence factors (qRT-PCR; **Figure 6.12**). *P. aer* virulence factors include elastase (*lasA* and *lasB*), alkaline protease (*aprA*), alginate (*algD*), toxin A (*toxA*), and the exotoxin, *exoS* (Badamchi et al., 2017; Goodman & Lory, 2004; Khosravi et al., 2016). On gelatin zymogram, *P. aer* biofilm supernatant gave a range of bands, indicating high and varied protease activity. Quantification was performed for the principle bands (~70KDa and ~50KDa) and the total protease activity in each lane. Protease activity depicted by band 1 (~70KDa), described as a distinct version of elastase (Lomholt et al., 2001), was significantly ($P < 0.01$) inhibited by Tg^{Ag} compared to vehicle (**Figure 6.11A, B**), but not Tg or Ag alone. For band 2 (~50KDa), corresponding to the molecular mass of alkaline protease activity (Caballero et al., 2001; Lomholt et al., 2001), a different pattern of activity was observed, where both Tg and Tg^{Ag} reduced expression ($P < 0.05$) compared to the vehicle (**Figure 6.11A, C**). Tg^{Ag} and Tg concurrently ($P < 0.01$) inhibited total protease activity (**Figure 6.11A, D**). An independent colorimetric protease assay (the Azocasein method; Andrejko et al., 2013) was performed (**Figure 6.12A**) and also illustrated that total protease activity was significantly reduced following Tg^{Ag} treatment ($P < 0.05$, compared to vehicle).

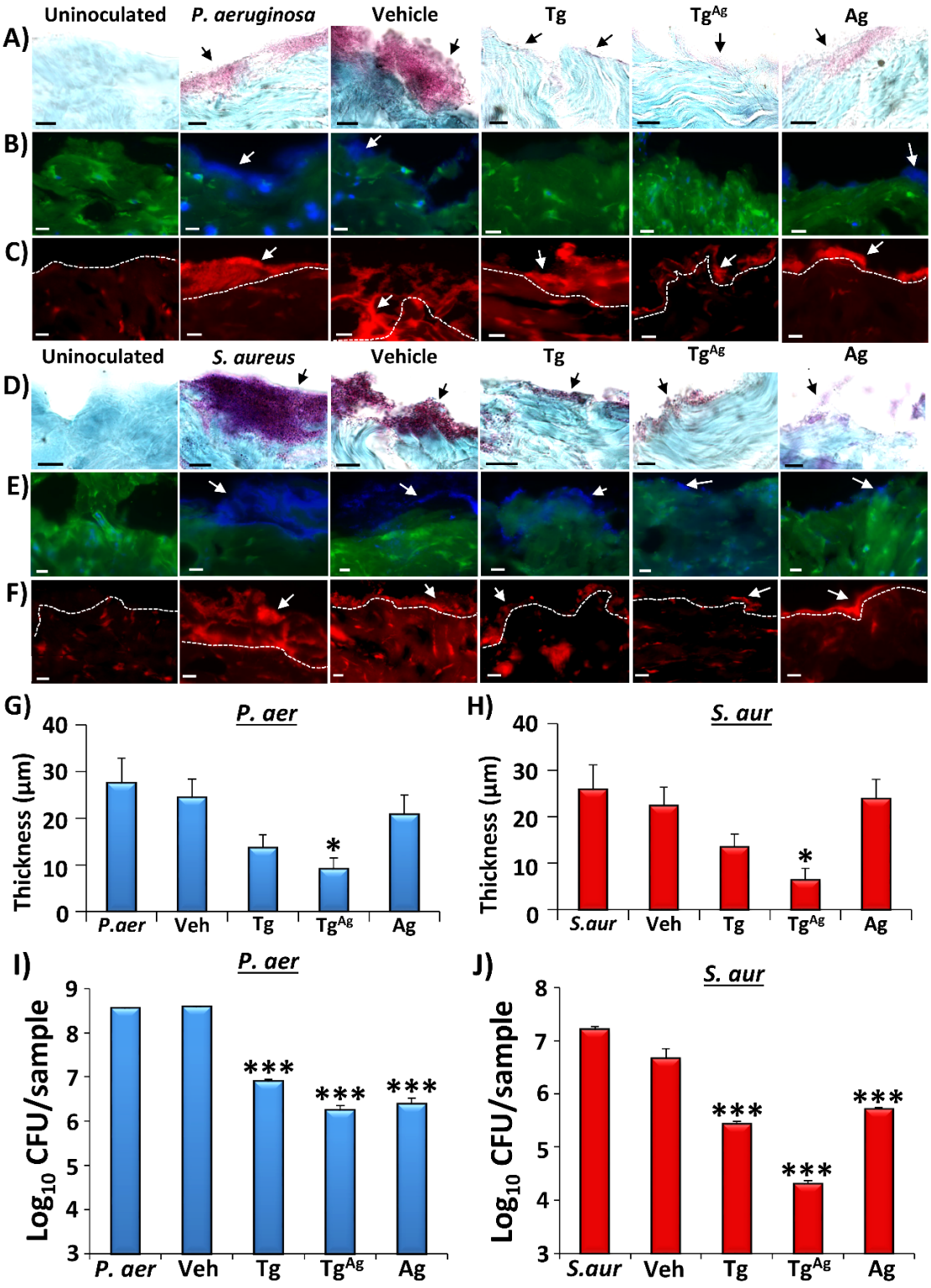

Figure 6.10. Theraglass™ reduces biofilm load in *ex vivo* porcine wounds. Modified Gram-Twort staining for *P. aeruginosa* (*P. aer*; pink; **A**) and *S. aureus* (*S. aur*; purple; **D**) biofilm (black arrows) on porcine skin (blue) following Tg, Tg^{Ag} and Ag treatment. Quantification of Gram-Twort *P. aer* (**G**) and *S. aur* (**H**) biofilm thickness following Tg^{Ag} treatment. Concanavalin A (blue biofilm, **B**, **E**) and Acridine Orange (red biofilm, **C**, **F**) staining of *P. aer* (**B**, **C**) and *S. aur* (**E**, **F**) biofilm (white arrows). Biofilm is not apparent on uninoculated porcine wounds. Colony forming units (CFU)/sample of *P. aer* (**I**) and *S. aur* (**J**) biofilms. n = 3 biopsies per treatment. Black bar = 10 µm, white bar = 20 µm. Mean + SEM. * = $P < 0.05$, *** = $P < 0.001$. One-way ANOVA with Dunnett's *post-hoc* analysis (versus *P. aer*).

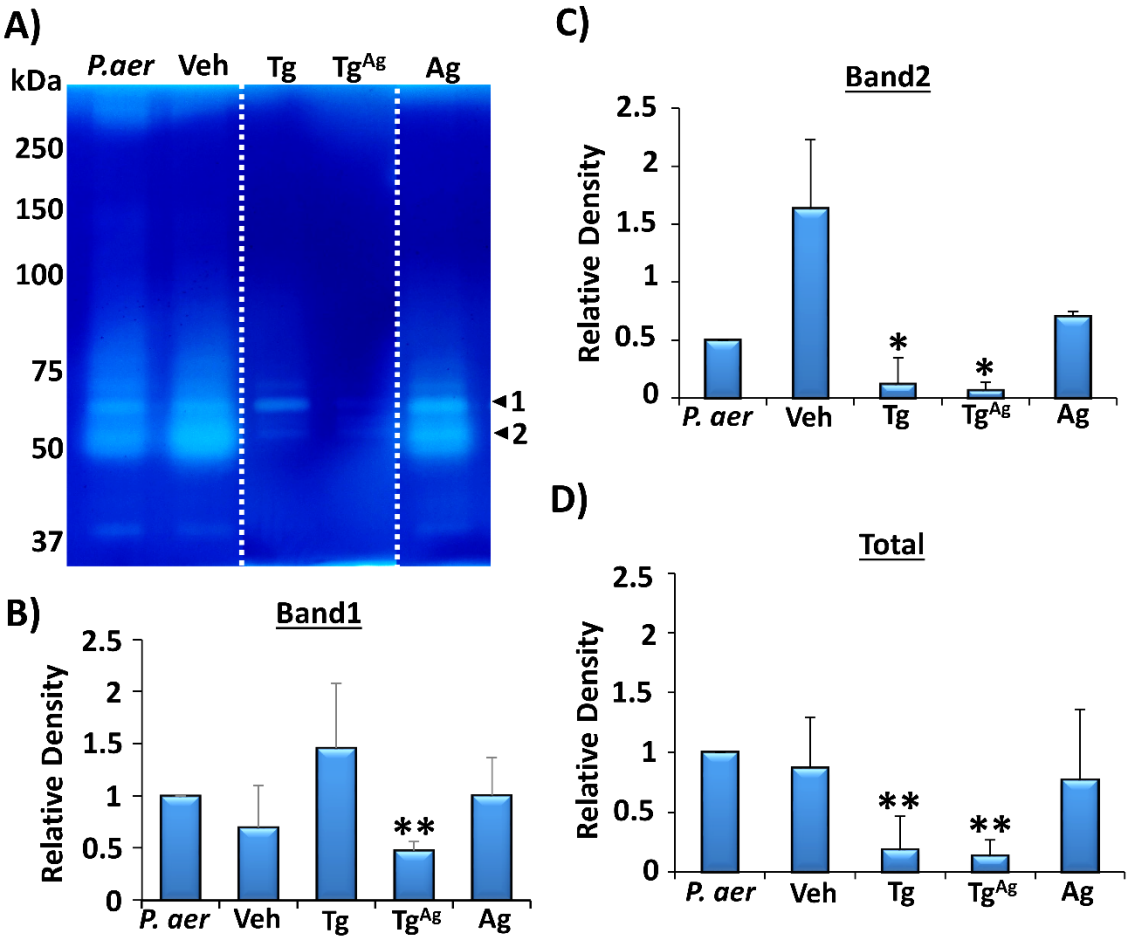

Figure 6.11. Extracellular protease activity from *P. aeruginosa* biofilms is differentially altered by Theraglass™ treatment. Zymography analysis (**A**-**D**) illustrated changes in protease activity, where each lane showed *P. aer* biofilm (*P. aer*), vehicle (Veh), Tg, Tg^{Ag} and Ag treatments, respectively (lanes were cut and placed in this order, white dotted lines). Significantly dampened activity in band 1 protease (~70kDa; **A**, **B**) was demonstrated following Tg^{Ag} treatment, while both Tg and Tg^{Ag} significantly reduced band 2 protease activity (~50kDa, **A**, **C**), and overall protease action (**D**), compared to Veh. Proteases were pooled from three biopsies per treatment and run on three separate gels. Mean + SEM. * = P< 0.05, ** = P < 0.01. One-way ANOVA with Dunnett's *post-hoc* performed (versus *P. aer*).

A number of virulence factors are specifically associated with biofilm formation. qRT-PCR analysis of *P. aer* biofilms revealed that Tg, Tg^{Ag} and Ag significantly reduced expression of the gene *lasB* (P < 0.05; **Figure 6.12B**), important in encoding elastase B production (Casilag et al., 2016). Similarly, all three treatments severely dampened *aprA* expression (a gene encoding alkaline protease, Lomholt et al., 2001; **Figure 6.12C**), but this effect was more considerable following Tg and Tg^{Ag} treatment. Tg and Tg^{Ag} showed a trend towards reduced *algD* (important for alginate biosynthesis, Wiens et al., 2014; **Figure 6.12D**). Other virulence factors unaffected by Theraglass™ treatment include *toxA* and *lasA* (data not shown).

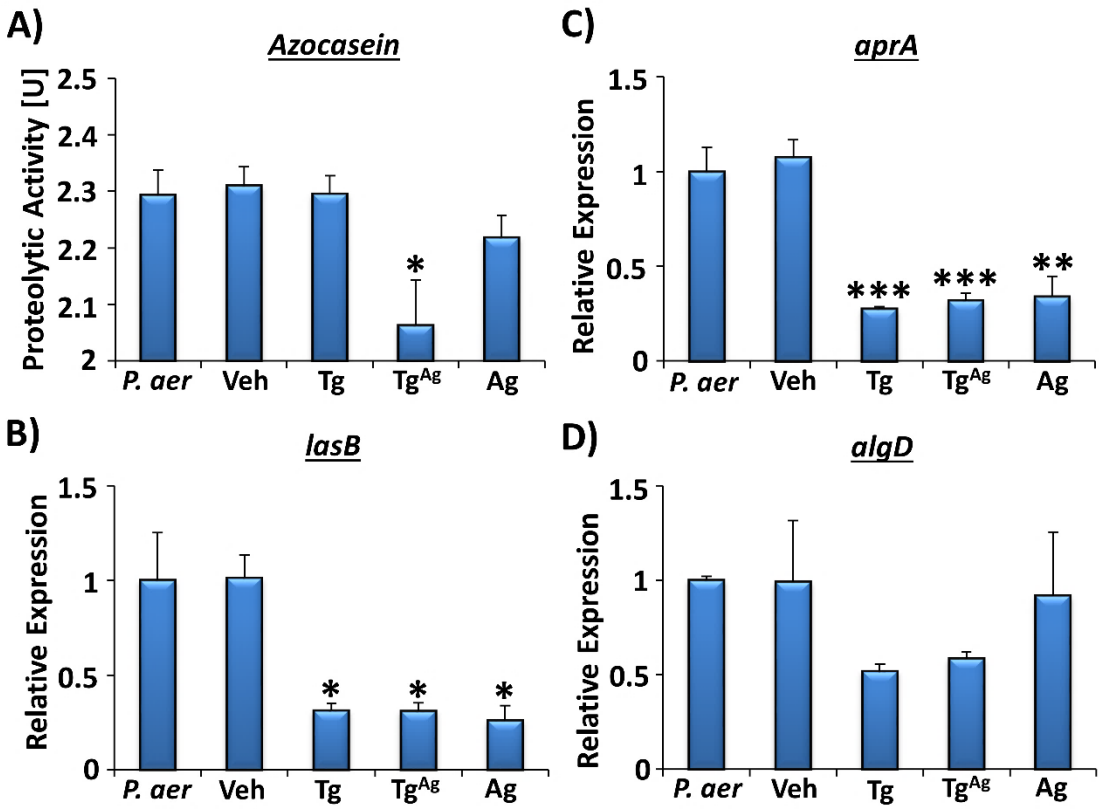

Figure 6.12. Virulence factors from *P. aeruginosa* biofilms are reduced by Theraglass™ treatment. Colorimetric analysis (Azocasein, **A**) illustrated a reduction in proteolytic activity with Tg^{Ag} compared to Vehicle (Veh). Significant reductions were also observed in expression of the virulence genes *lasB* (**B**) and *aprA* (**C**), while no significant changes were shown in *algD* (**D**), illustrated via qRT-PCR. Mean +/- SEM. * = $P < 0.05$, ** = $P < 0.01$. Three independent experiments. One-way ANOVA with Dunnett's *post-hoc* analysis for multiple comparisons (versus *P. aer*).

6.4.8. *S. aureus* virulence factor production is unaffected by Theraglass™.

The invasive mechanisms of *S. aur* differ considerably to those of *P. aer*, also involving coordinated production of multiple virulence factors (Chen et al., 2013). Although *S. aur* is a lesser biofilm producer than *P. aer* (**Table 6.5**), it still produces a potent biofilm. On a gelatin zymogram, gelatinase activity of *S. aur* biofilms was only detected in two bands (37-50kDa), and the activity of these gelatinases was unaffected by any topical treatment (**Figure 6.13A-C**). Concurrently, colorimetric protease analysis (Azocasein method, above) confirmed this observation (**Figure 6.13D**). Some of the most discussed virulence factors of *S. aur* are the fibronectin binding proteins, which allow *S. aur* to adhere strongly to wound substrates (Sinha et al., 2000). In the present work, TG failed to dampen expression of the fibronectin binding protein genes, *fnbpA* and *fnbpB* (**Figure 6.13E-F**).

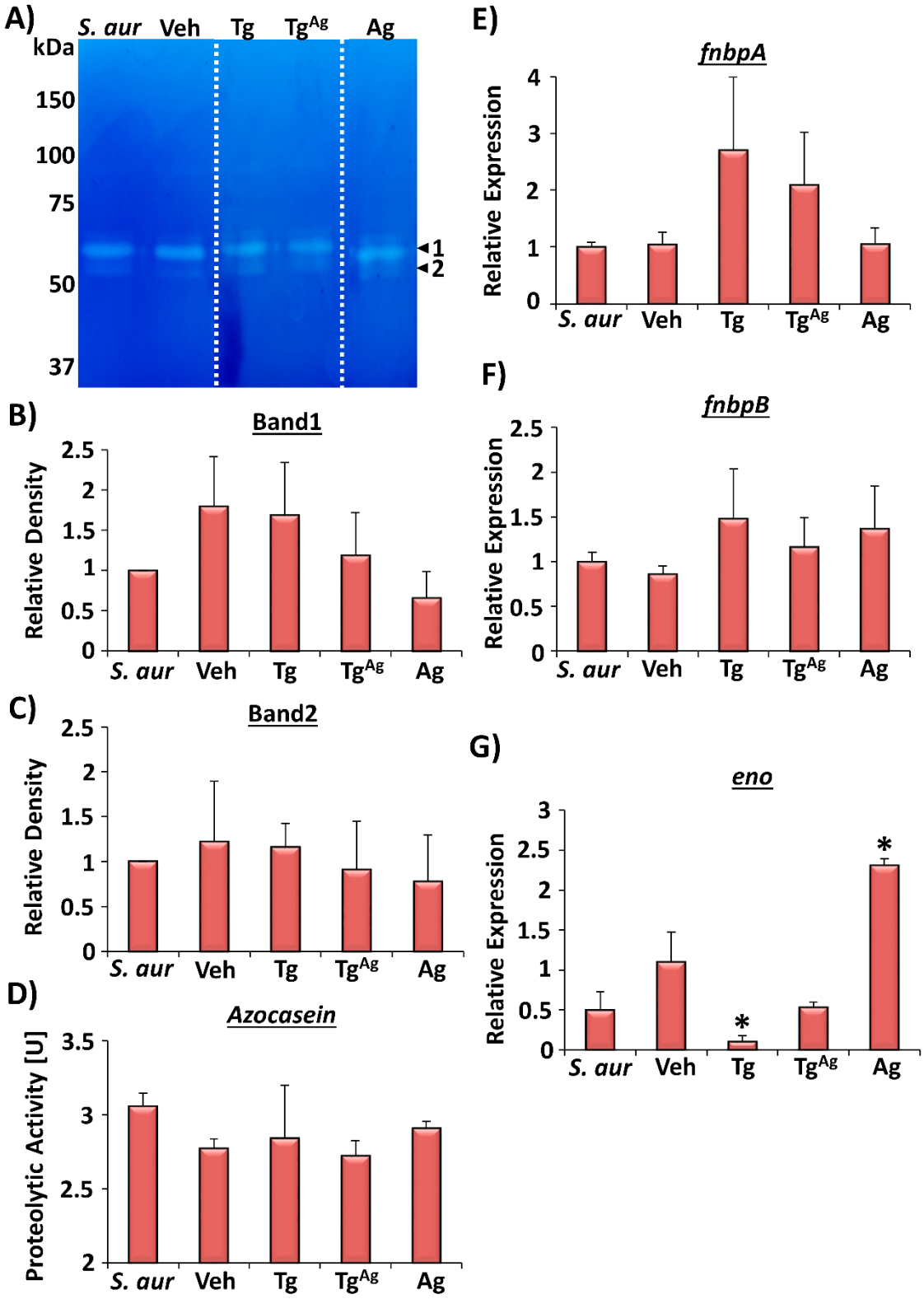

Figure 6.13. Extracellular protease activity from *S. aureus* biofilms is unaffected by Theraglass™ treatment. Zymography analysis (**A-C**) illustrated that Theraglass™ did not alter *S. aur* protease activity in band 1 (~50kDa; **B**) or band 2 (~60kDa; **C**), where each lane showed *S. aur* biofilm (*S. aur*), vehicle (Veh), Tg, Tg^{Ag} and Ag treatments, respectively (lanes were cut, white dotted lines). Azocasein assay of total extracellular protease (**D**) and expression of the virulence genes *fnbpA* (**E**), *fnbpB* (**F**) and *eno* (**G**). Mean + SEM. Three independent experiments. * = $P < 0.05$. One-way ANOVA with Dunnett's *post-hoc* analysis (versus *S. aur*).

Another *S. aur* attachment factor, which associates with the bacterial cell surface, is enolase, or *eno* (Foulston et al., 2014). Here, Tg and Tg^{Ag} reduced *eno* expression in *S. aur* biofilms (compared to the vehicle), reaching significance with Tg treatment ($P < 0.05$; **Figure 6.13G**). Intriguingly, Ag caused upregulation of *eno* ($P < 0.05$). Expression of other virulence factors, such as the sialoprotein-binding protein, *sdrE*, and the staphylococcal accessory regulator, *sarA*, remained unchanged by treatment (data not shown). Therefore, although TG reduces *S. aur* biofilm viability, protease activity and virulence factor expression are largely unaffected.

6.4.9. Administration of Bg^{Ag} provides host protection from biofilm-induced dermal apoptosis and ECM degradation.

P. aer and *S. aur* biofilms produce a number of proteases and virulence factors (discussed above), therefore the direct consequences of bacterial biofilm exposure on host tissue was next assessed. Firstly, porcine wound viability was determined histologically in non-biofilm inoculated samples (**Figure 6.14**). Here, comparable levels of cell proliferation (via Ki67 staining) were observed in freshly collected (4%; pre-culture) tissue versus tissue cultured *ex vivo* for 48 hours (3%; post-culture; **Figure 6.14D**), agreeing with previous work (Yeung et al., 2016). Similarly, TUNEL staining and caspase 3 IHC demonstrated only a marginal increase in cell death following culture, where 20% of cells were $TUNEL^{+ve}$ (**Figure 6.14B, E**) and 5% of cells were in early apoptosis (caspase 3^{+ve}; **Figure 6.14C, F**). By contrast, wounds maintained *ex vivo* for 48 hours with *P. aer* and *S. aur* biofilms displayed significantly increased de-cellularity compared to pre-cultured tissue ($P < 0.01$ and $P < 0.001$, respectively; **Figure 6.14G-H**). In *P. aer* wounds, Tg administration reduced biofilm-induced cellular lysis, while Tg^{Ag}-treated explants maintained higher cellularity compared to *P.* aer and *S. aur* biofilm controls.

Given that TG treatment significantly reduced bacterial protease production, biofilm-induced ECM degradation was determined (**Figure 6.15**). In this model, biofilm infection increased collagen turnover at the biofilm-wound interface (illustrated by an increase in green birefringent fibres). Interestingly, treatment with Tg ($P < 0.05$), Tg^{Ag} (non-significant) and Ag ($P < 0.05$) decreased ECM turnover in wounds inoculated with *P. aer* biofilms, thus reducing breakdown of early wound matrix (**Figure 6.15A, C**). In *S. aur* wounds, Tg^{Ag} alone ($P = 0.05$) maintained a protective effect against biofilm-induced collagen degradation (**Figure 6.15B-C**).

Collectively, these results illustrate that Tg treatment, particularly Tg^{Ag}, is not only effective at killing biofilm bacteria, but also demonstrably reduces the detrimental tissue degrading consequences of biofilm infection.

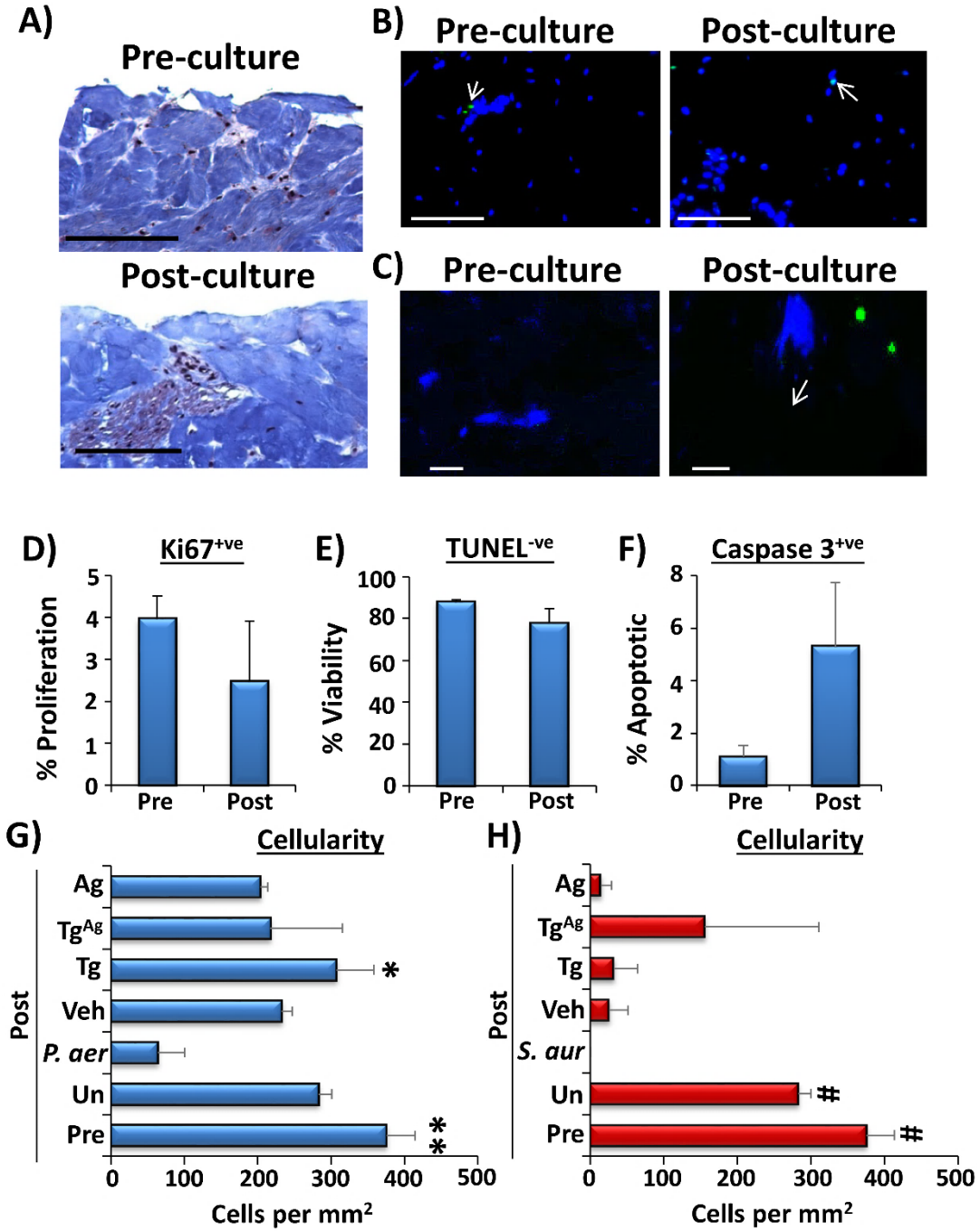

Figure 6.14. Biofilm inoculation drastically reduces porcine explant viability, yet Theraglass™ protects against biofilm-induced de-cellularisation. Viability of porcine wounds was determined via structural assessment (**A**, Masson's Trichrome staining), cell proliferation ($Ki67^{+ve}$ staining, **D**), cell viability ($TUNEL^{-ve}$ cells, blue, **B** and **E**) and apoptosis (Caspase 3^{+ve} cells, green, **C** and **F**). Independent two-tailed Student's *t* tests on data sets **D-F**. n = 3 biopsies per treatment. Cell death following biofilm exposure was determined as tissue cellularity (number of DAPI stained cells per mm^2) in *P. aeruginosa* (*P. aer*, **G**) and *S. aureus* (*S. aur*, **H**) biofilm explants. Mean + SEM. One-way ANOVA with Dunnett's *post-hoc* analysis on **G-H** (versus *P. aer* and *S. aur*). Black bar = 100 µm, white bar = 20 µm. White arrows = apoptotic (green) cells. * = $P < 0.05$, ** = $P < 0.01$, # = $P < 0.001$.

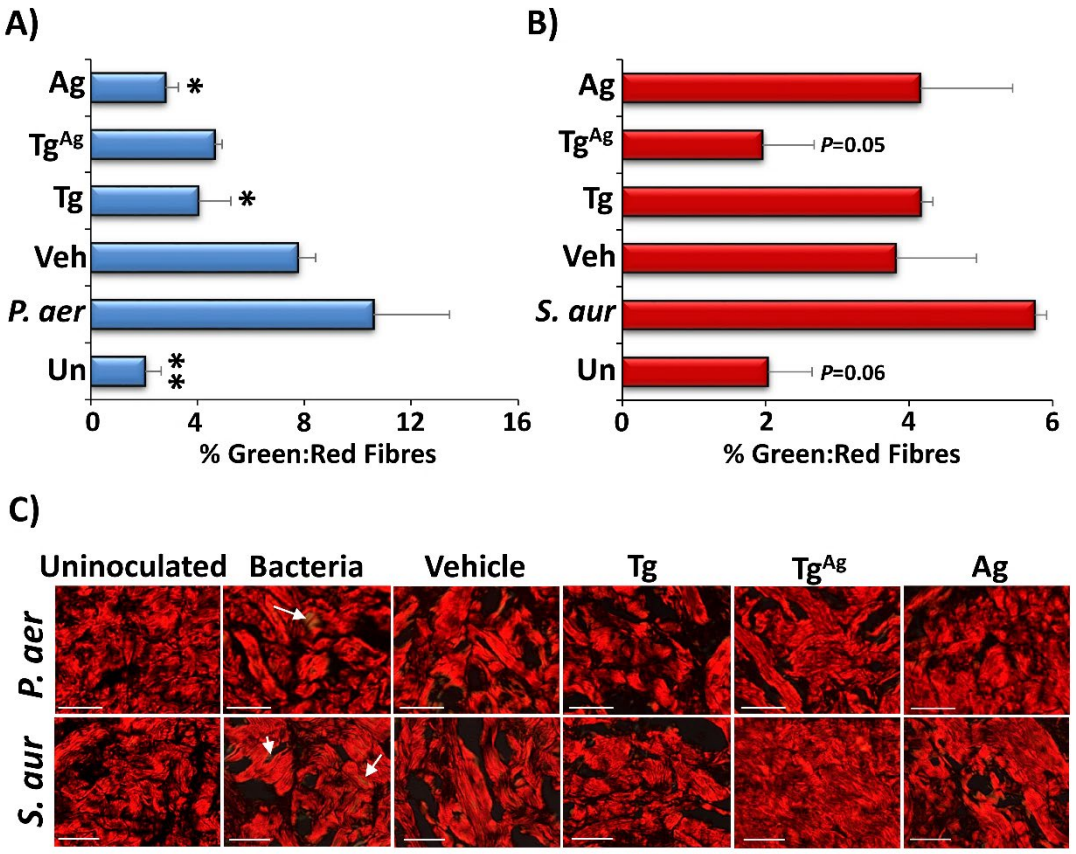

Figure 6.15. Theraglass™ protects against biofilm-induced extracellular matrix turnover. Picrosirius red staining of biofilm-loaded porcine wound tissue revealed changes in collagen III turnover via measurement of % green: red fibres (green birefringence = white arrows). Significantly more collagen III turnover was demonstrated in *P. aeruginosa* (*P. aer*, **A**, **C**) biofilms. *S. aureus* (*S. aur*, **B**, **C**) biofilms increased collagen III turnover compared to Tg^{Ag} and uninoculated porcine explants. Bar = 100 µm. n = 3 biopsies per treatment. Mean + SEM. * = $P < 0.05$, ** = $P < 0.01$. One-way ANOVA was performed with Dunnett's *post-hoc* analysis (versus *P. aer* and *S. aur*).

6.4.10. Theraglass™ reduces co-culture porcine wound biofilm load and the relative contribution of *P. aeruginosa* and *S. aureus*.

The prevalence of polymicrobial infections is a major clinical problem, contributing to the intransigent nature of chronic wounds (Pastar et al., 2013; Fleming et al., 2017). Therefore, to begin to mimic the polymicrobial wound biofilm environment, a co-culture porcine wound biofilm model was established. In this model, all three treatments were less effective against co-culture than single-species biofilms (**Figure 6.16**). Here, direct quantification of Gram-Twort stained biofilms showed Bg^{Ag} to cause a modest, non-significant reduction in biofilm thickness (**Figure 6.16A-B**). Similarly, Concanavalin A and Acridine Orange staining demonstrated that Tg, Ag and Tg^{Ag} only mildly reduced visual biofilm load. However, a statistically significant 1-log reduction in viable co-cultured bacteria was revealed following Tg,

Tg^{Ag} and Ag treatment (P < 0.001; **Figure 6.16C**). Taken together, these data illustrate that TG is less effective against co-cultured than single-species biofilms.

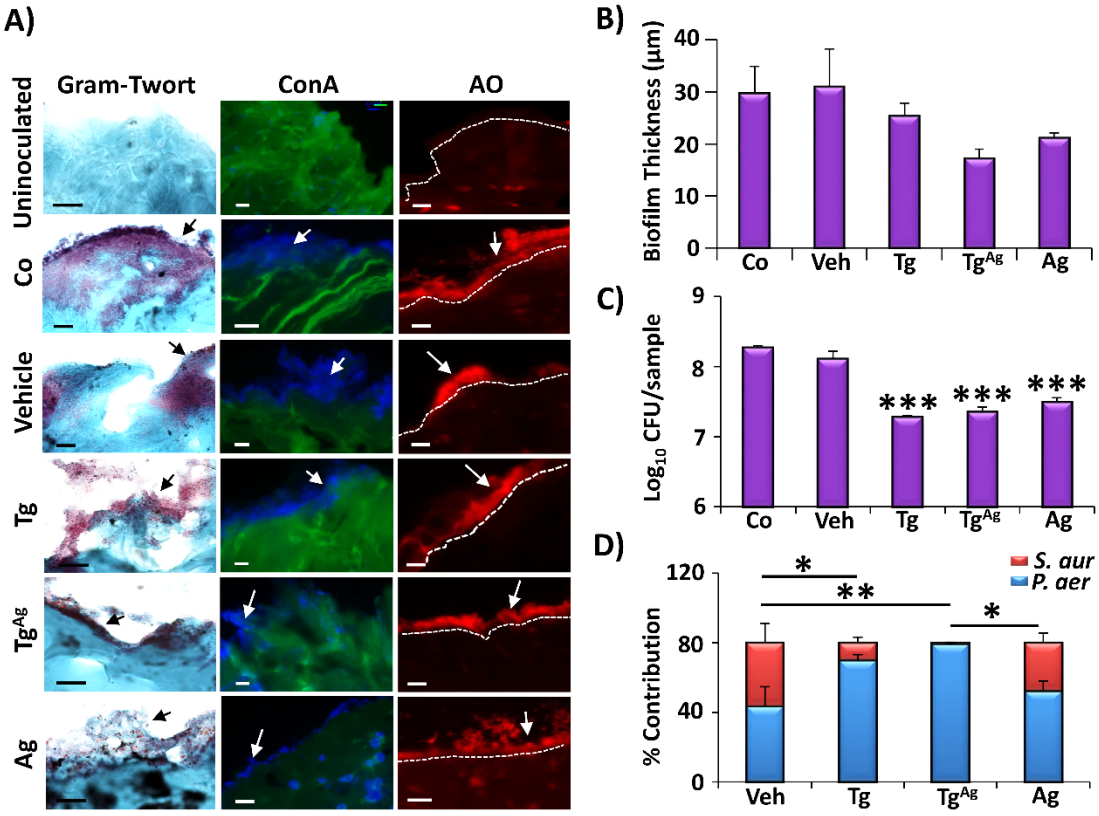

Figure 6.16. Co-culture biofilms of *P. aeruginosa* and *S. aureus* appear more resistant to Theraglass™ than single-species biofilms. Gram-Twort staining (black arrows), Concanavalin A (ConA, blue biofilms, white arrows) and Acridine Orange (AO, red biofilms, above the white-dotted line, depicted by white arrows; **A**). Biofilm thickness (**B**, quantified by Gram-Twort) and biofilm load (colony forming units, CFU/sample; **C**). Percentage contribution of *P. aer* and *S. aur* to the co-culture biofilms (**D**). Black bar = 10 µm, white bar = 20 µm. n = 3 biopsies per treatment. Mean + SEM. * = P < 0.05, ** = P < 0.01, *** = P < 0.001. One-way ANOVA with Dunnett's *post-hoc* analysis.

In polymicrobial communities, a dynamic equilibrium is formed between component species to allow co-existence (Gabrilska & Rumbaugh, 2015). These relationships can involve cooperative behaviours, such as syntrophy, where one organism produces a metabolite that benefits the growth of another (Ramsey et al., 2011). However, when pathogenic infections arise, these are often a result of competitive behaviour, where one potentially pathogenic species may outcompete more commensal species for resources through highly antagonistic mechanisms (reviewed in Gabrilska & Rumbaugh, 2015). As a co-culture system was employed, the relative proportion of *P. aer* and *S. aur* in co-cultured biofilms was determined via enumeration on selective agars (**Figure 6.16D**). Following 72 hours of co-culture, membrane biofilms were transferred to porcine wounds for a further 48

hours of culture. After this time, vehicle-treated biofilms were quantified as 55:45 *P. aer* to *S. aur*, while Ag application caused a non-significant shift in these proportions to approximately 65:35. By contrast, Tg treatment led a much larger, statistically significant shift to almost 90:10 *P. aer* to *S. aur* ($P < 0.05$). However, the greatest effect was observed following Tg^{Ag} treatment, where virtually no *S. aur* could be recovered ($P < 0.01$). Collectively, these data mirror the disparate efficacy of TG against single-species biofilms, while also illustrating the extent to which topical wound treatment can alter the dynamic synergy/antibiosis between bacterial species.

6.4.11. Theraglass™ elicits disparate effects on protease production and virulence factors in co-culture biofilms.

Congruous to single-species assessment, co-culture virulence was assessed via gelatin zymography and analysis of candidate virulence genes. In a zymogram, co-culture biofilms produced greater extracellular protease profile activity compared to single *S. aur* biofilms, yet showed reduced activity compared to *P. aer* biofilms (**Figure 6.17A**). Remarkably, however, additional bands were observed, including aggregates above 250kDa and bands between 100-150kDa which were not visualised in single-species biofilms. Despite the wide profile of proteases in untreated co-cultured biofilms, treatment diminished these bands. The band observed between 50-75kDa was quantified, illustrating that even the vehicle reduced co-culture protease activity ($P < 0.001$; **Figure 6.17B**). However, no significant differences were found between the vehicle and Tg or Ag treatments, proving that the reduction in protease profile was TG-independent. Total protease was also determined via the colorimetric Azocasein assay (**Figure 6.17C**), where an intriguing reduction in protease activity was again observed following vehicle treatment ($P < 0.05$). These observations are likely due to methodological pitfalls of analysing supernatant proteases from samples containing viscous substances.

Virulence factors related to *P. aer* and *S. aur* were next screened in co-culture biofilms (**Figure 6.18A-C**). Here, expression of *aprA* (**Figure 6.18A**) was not affected by treatment (compared to Veh), while *lasB* (**Figure 6.18B**) and *algD* (**Figure 6.18C**) were modestly (non-significantly) reduced following Tg and Tg^{Ag}. No significant effect of TG was observed on *fnbpA* or *fnbpB* compared to the vehicle (**Figure 6.18D-F**; respectively). Further, Tg and Tg^{Ag} dampened *eno* expression,

although this effect failed to reach significance (**Figure 6.18F**). Together, these data show that only modest changes in viability and virulence are observed in co-cultures following TG treatment, and that these effects are less substantial than those observed in single-species biofilms.

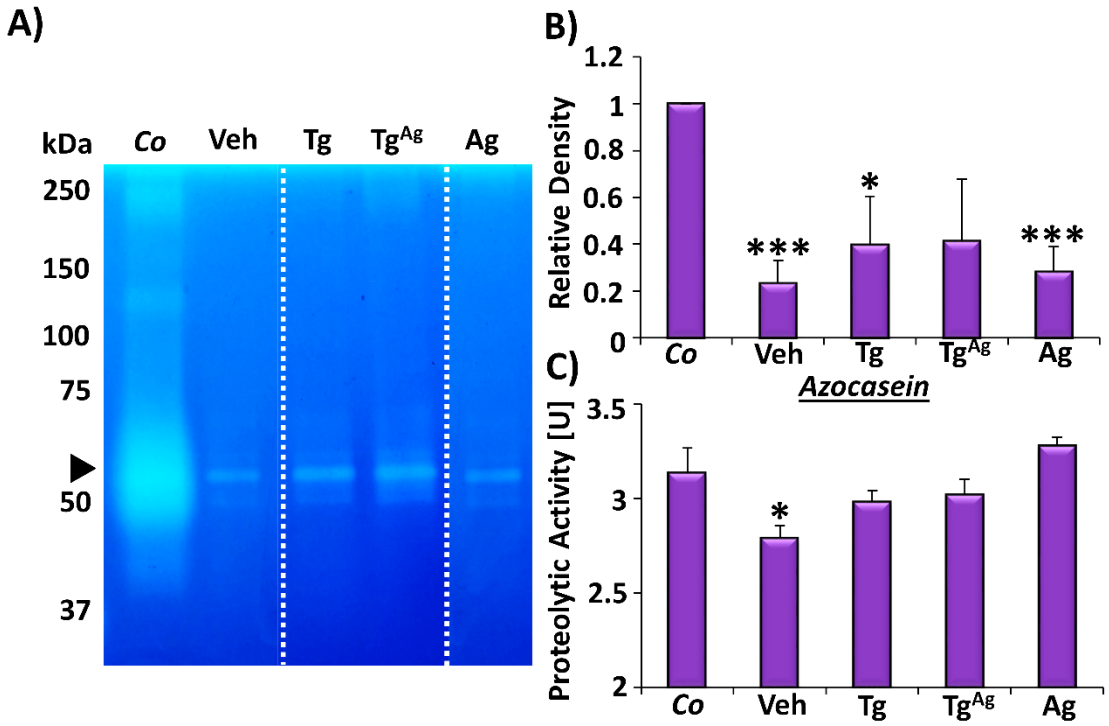

Figure 6.17. Theraglass™ disparately affects protease production in co-culture biofilms. Zymography analysis (**A-B**) showing *P. aeruginosa: S. aureus* co-culture biofilm (*Co*), vehicle (Veh), Tg, Tg^{Ag} and Ag treatments, respectively (lanes were cut and placed in order, white dotted lines). Colorimetric Azocasein (**C**) for protease activity. Proteases were pooled from each treatment and run via gelatin zymogram in three independent experiments. Mean + SEM. * = $P < 0.05$, *** = $P < 0.001$, deduced via one-way ANOVA and Dunnett's *post-hoc* analysis (versus Co).

6.4.12. Theraglass™ eliminates biofilm and protects host tissue in a human *ex vivo* wound biofilm model.

The antimicrobial effects of TG were assessed in a more translational model of human *ex vivo* wound biofilms (**Figure 6.19A**). Here, Tg and Tg^{Ag} treatment caused a 2-log reduction in *P. aer*, *S. aur* and co-culture biofilms, achieving significance in *P. aer* ($P < 0.001$) and co-culture ($P < 0.05$) groups (**Figure 6.19B-D**). Interestingly, post-culture quantification of relative *P.aer* and *S. aur* in co-culture biofilms revealed differential effects to those observed in porcine wounds (**Figure 6.19E**). Veh-treated biofilms were 35:65 *P. aer* to *S. aur*, and 45:55 following Tg^{Ag} treatment. Yet in this model, Tg and Ag alone significantly shifted the proportions to <90% *P. aer*.

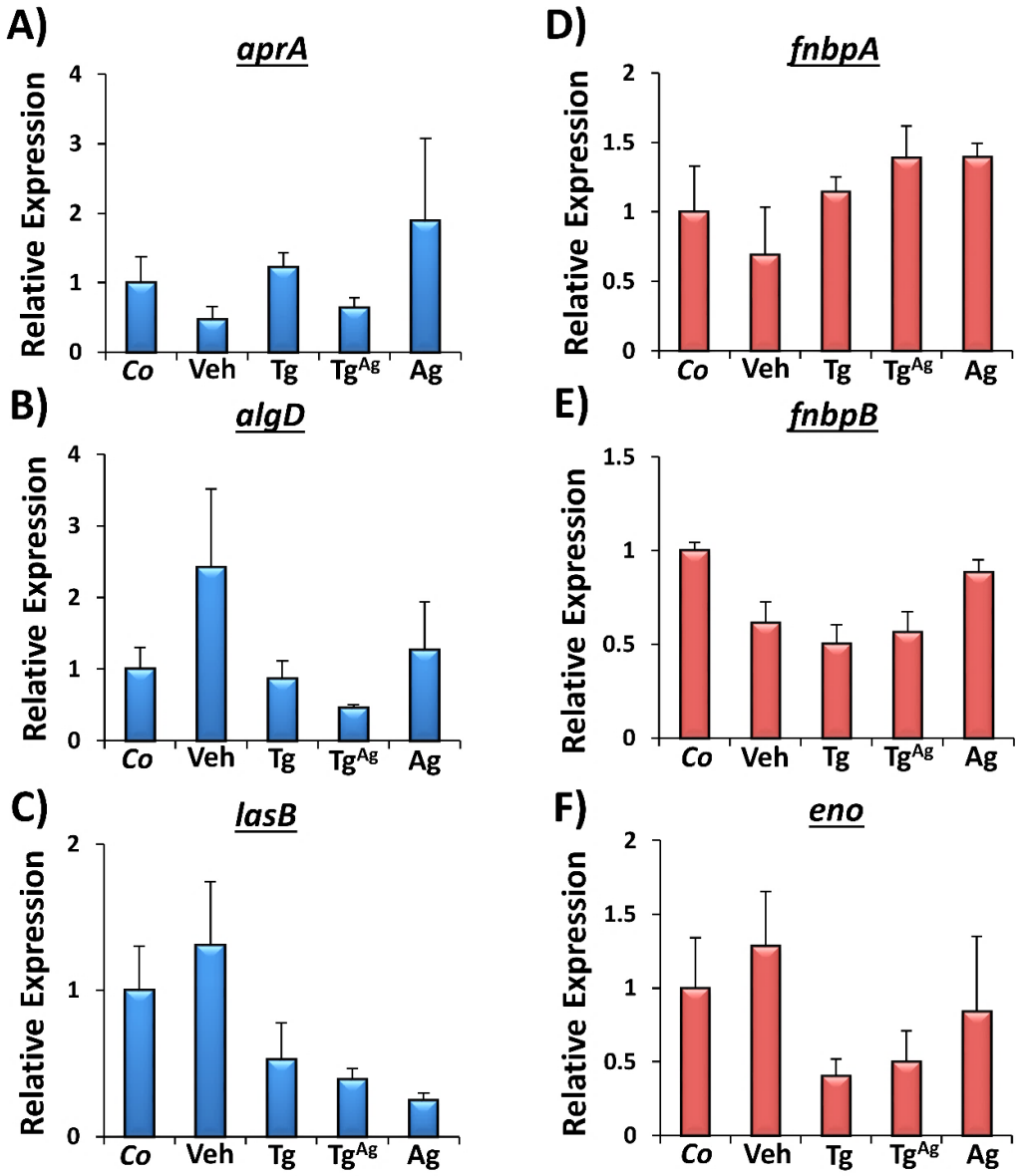

Figure 6.18. Virulence factor expression in co-culture biofilms is unaffected by Theraglass™. Relative expression of *P. aeruginosa* genes *aprA* (**A**), *algD* (**B**) and *lasB* (**C**), and *S. aureus* virulence genes *fnbpA* (**D**), *fnbpB* (**E**), and *eno* (**F**) is not significantly altered by Theraglass™ treatment. n = 3. Mean + SEM. One-way ANOVA was performed on each data set (versus Co).

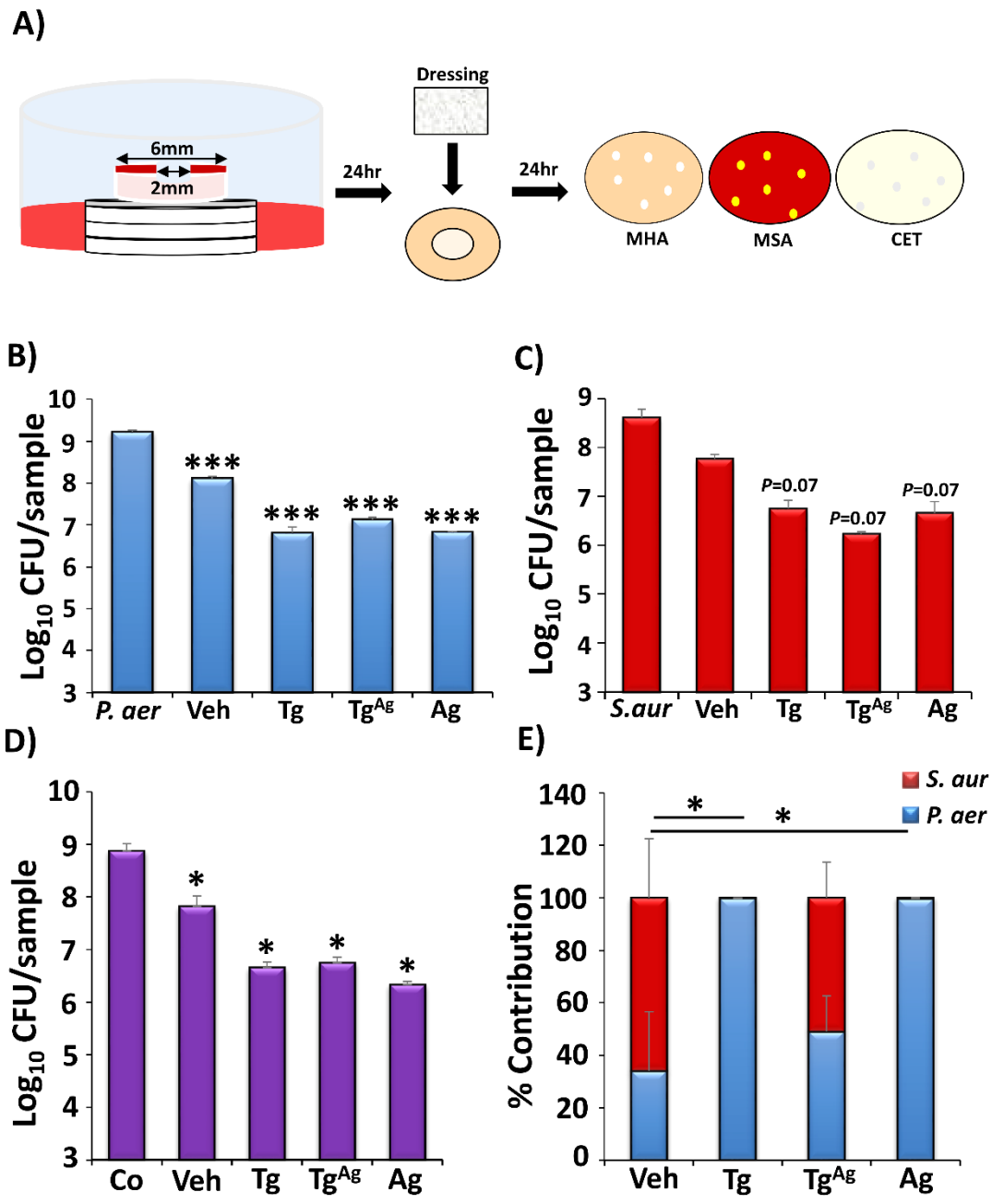

Figure 6.19. Theraglass™ reduces biofilm load in human *ex vivo* wounds. A human *ex vivo* wound biofilm model was employed (schematic, **A**) to assess the efficacy of Theraglass™ in a translationally relevant construct. Enumeration of viable colonies was performed on Mueller Hinton (MHA; both species), mannitol salt (MSA; *S. aureus*-specific) and cetrimide (CET; *P. aeruginosa*-specific) agar. Tg, Tg^{Ag} and Ag significantly reduces *P. aeruginosa* (*P. aer*) biofilm load (colony forming units, CFU/sample; **B**), but has less effect on *S. aureus* (*S. aur*; **C**). Tg, Tg^{Ag} and Ag also significantly reduce *P.aer*: *S. aur* co-culture biofilms (**D**), while Tg alters the relative contribution of *P. aer* and *S. aur* to co-culture biofilms (**E**). n = 3 biopsies per treatment. Mean + SEM. * = $P < 0.05$, *** = $P < 0.001$, deduced via one-way ANOVA and Dunnett's *post-hoc* analysis (versus bacteria only).

6.5. Discussion

It is axiomatic that silver maintains potent antimicrobial efficacy against a wide range of bacterial species (e.g. Gholipourmalekabadi et al., 2016; Drago et al., 2014). However, the effects of silver in wound repair remain controversial, promoting cellular migration and repair in some contexts, while causing eukaryotic cytotoxicity in others (reviewed in Marx & Barillo, 2014). Similarly, very few studies have addressed how BG alters *in vivo* wound repair, and fewer still have determined how BG may influence complex models of infection, focussing only on *in vitro* planktonic assays (e.g. Cunha et al., 2018) and single-species *in vitro* biofilm cultures (e.g. Siqueira et al., 2017). Therefore, the aim of this chapter was to elucidate how a novel BG (TG) functionalised with silver affects both *in vivo* murine wound repair and bacterial viability in models of *ex vivo* skin wound infection.

Although numerous *in vitro* studies have characterised the reparative effects of BG (Keshaw et al., 2005; Verrier et al., 2004; Yang et al., 2015), they cannot be directly compared as BG compositions and cell-based assays vary considerably from study to study. Furthermore, reports assessing how BG may influence *in vivo* wound repair are few and far between. In one example, BG promoted angiogenesis in rat excisional wounds, but this BG formulation contained no silicon dioxide, was doped with copper, and was applied beneath an occlusive pressure dressing (Zhao et al., 2015). In a second investigation, rat wounds were again occluded, and assessed over a period of 16 days (Lin et al., 2012). As the model employed in the current work used a non-occlusive treatment and assessed early stage healing (day 3 post-injury), it is difficult to compare the potential wound-reparative effects of TG to previous work.

In the literature, positive wound healing effects of BG treatment appear to pertain to angiogenesis, matrix restoration and re-epithelialisation, which all correlate with healing stages later than 3 days (in mice; Ansell et al., 2014). Therefore, future studies should aim to assess the efficacy of TG across a time course of wound healing. As murine wounds heal primarily via contraction (Wong et al., 2010), application of an occlusive dressing may also unmask the possible impact of TG on re-epithelialisation. Furthermore, it is difficult to promote acute wound healing in a WT mouse, as cellular functions are already occurring at near optimal rates. Testing TG in models where re-epithelialisation, collagen deposition and angiogenesis are

substantially delayed, such as in aged and Db mice, may therefore reveal the potential functional benefits of TG in repair.

Few studies have addressed the antimicrobial and anti-biofilm efficacy of BG formulations (Galarraga-Vinueza et al., 2017) and their functionalisation with silver (Gholipourmalekabadi et al., 2016), while those that have demonstrate limited efficacy. Data presented in this study has directly assessed TG bactericidal activity against planktonic and biofilm forms of wound-relevant bacteria (*P. aer* and *S. aur*). These findings reveal that TG incorporating silver (Tg^{Ag}) is more potently bactericidal against planktonic *P. aer* and *S. aur* than Tg alone. A key novel observation was that Tg conferred species-specific efficacy, maintaining higher effectiveness against *P. aer* than *S. aur* (**Figure 6.7**). In fact, in agar diffusion tests, Tg alone failed to inhibit *S. aur* growth. This may be due to *S. aur* metabolism (acid production) circumventing increased pH associated with BG, hence reducing the diffusibility of TG into agar (Martins et al., 2011; Stoor et al., 1998).

More likely, the observed differences in the present study most likely reflect the differing cell-wall structure between the two bacterial species. The gram-positive *S. aur* is encapsulated by a thickened peptidoglycan cell wall, which is crucial for maintenance of cell integrity (Zoeiby et al., 2001) and may convey enhanced resistance (McCallum et al., 2010). Indeed, a number of antibiotic-tolerant *S. aur* strains maintain resistance via cell wall-related mechanisms (Utaida et al., 2003; Dengler et al., 2011). *P. aer* also produces antibiotic resistance through evolved cell wall mechanisms, where the outer membrane has low permeability to limit the rate of transport of substances into the cells, while secondary efflux mechanisms expel toxic substances (Breidenstein et al., 2011). The less substantial *P. aer* cell wall structure could confer susceptibility to the increased pH caused by BG ion dissolution (e.g. Ca2+ and Na+ release; Stoor et al., 1998), altering bacterial membrane potential (Munukka et al., 2008) and inducing osmotic stress (Van der Waal et al., 2011). In the present work, testing of pH from microtiter assays revealed that Tg and Tg^{Ag} dissolution raised the pH of MHB to ~10 (data not shown).

Regional variation in skin pH is reported to influence spatial localisation of skin bacteria (reviewed in Schreml et al., 2009), where *S. aur* favours more acidic conditions than *P. aer* (Ushijima et al., 1984). If altered pH were the sole reason for the differential results obtained with TG treatment, then Ag alone would convey

similar effects against *S. aur* as Tg^{Ag}. The antimicrobial efficacy of TG could therefore be substantiated through its relative components, such as silicon dioxide (Maçon et al., 2017; Siqueira et al., 2017).

Of more physiological relevance, TG significantly reduced biofilm load in an *ex vivo* porcine wound model, albeit less effectively than against planktonic species (**Figure 6.10**). Interestingly, Tg^{Ag} led to a greater reduction in *S. aur* than *P. aer* biofilm, which could be a consequence of the species-specific differences observed in biofilm formation. *P. aer* is a notoriously strong biofilm-producer (Harrison-Balestra et al., 2003), as shown via biofilm formation assays in the present study (**Table 6.5**), and established previously by its ability to produce a multitude of extracellular proteases (Andrejko et al., 2013). By contrast, *S. aur* forms weaker initial biofilms, heavily relying on adhesion proteins and autolysin production for its virulence and biofilm generation (Bose et al., 2012; Foulston et al., 2014; Rice et al., 2007).

As aforementioned, *S. aur* favours acidic conditions in the clinical setting (Weinrick et al., 2004), therefore it is likely that low physiological pH aids biofilm growth. Indeed, this was demonstrated *in vitro*, where *S. aur* biofilm matrix is strongly induced by a drop in pH, and can be reversed by increasing alkalinity (Foulston et al., 2014). As TG treatment increases pH, it is postulated that alkaline stress could contribute to reduced biofilm load. However, this assumption does not fit with one particular study where increasing pH with calcium hydroxide did not affect biofilm viability (Van der Waal et al., 2011), thus other factors are likely to be contributing to the observed anti-biofilm effects.

The most common method for determining bacterial load in samples is through assessing colony viability (Buysschaert et al., 2016). However, recent evidence suggests some bacteria, including *P. aer* and *S. aur*, can enter a viable but not culturable state, where they are unable to grow, but maintain metabolic activity that may contribute to biofilm virulence (Pasquaroli et al., 2014; Zhang et al., 2015b). Further, as alterations in exogenous stimuli are known to modify virulence factor expression (*P. aer*; Rumbaugh et al., 1999; Shigematsu et al., 2001; Breidenstein et al., 2011), bacterial virulence was quantified via analysis of protease and cell-host matrix binding genes. In fact, effective invasion and adherence are fundamental in establishing tissue infection (reviewed in Percival et al., 2015).

Tg^{Ag} and Tg significantly reduced expression of *lasB* and *aprA*, while causing a modest reduction in *algD* (**Figure 6.12**). Examination of *P. aer* gelatinases confirmed these effects (**Figure 6.11**), demonstrating that Tg and Tg^{Ag} substantially reduced activity corresponding to elastase (~37kDa; Miyajima et al., 2001) and alkaline protease (50-75kDa; Engel et al., 1997; Schmidtchen et al., 2003), confirmed via colorimetric analysis. LasB is particularly interesting as it exhibits potent widespread proteolytic activity, causing excessive wound proteolysis which inhibits repair (Kessler et al., 1998) and prevents normal dermal fibroblast growth (Schmidtchen et al., 2003). LasB has also been shown to degrade antimicrobial peptides (AMPs; Schmidtchen et al., 2002), and prevent host inflammatory responses via peptide cleavage (Van Der Plas et al., 2016).

Tg caused a significant reduction in the *S. aur* virulence factor enolase (*eno*; **Figure 6.13**), which binds plasminogen, fibrinogen and laminin to aid bacterial virulence (*in vitro*, Carneiro et al., 2004; Furuya & Ikeda, 2011). Interestingly, TG did not affect gelatinase activity (**Figure 6.13**; ~55kDa aureolysin and ~50kDa enolase; Beenken et al., 2010; Furuya & Ikeda, 2011; Shaw et al., 2004), or the expression of any other *S. aur* virulence genes under study. Previous authors have demonstrated that infection type and duration can alter extracellular protease production (Lomholt et al., 2001; Rumbaugh et al., 1999). Therefore, future work will aim to address how proteolytic activity is temporally altered following TG treatment.

As TG substantially reduced protease and virulence in *P. aer* biofilms; the effects of dampening bacterial proteases were next assessed on host tissue. Here, *P. aer* and *S. aur* caused reduced cellularity (**Figure 6.14**) and increased matrix turnover (**Figure 6.15**), while Tg^{Ag} substantially ameliorated this effect in *P. aer*, directly protecting porcine tissue from bacterial degradation.

Chronic wounds are home to diverse microbial communities (Gardner et al., 2013; Kalan et al., 2016) and it is this polymicrobial nature of infection that can profoundly affect clinical outcome (Baldan et al., 2014; Loesche et al., 2017; Wolcott et al., 2015). Indeed, it was recently shown that bacterial abundance is not only linked to poor healing in DFUs, but that microbial diversity profiling following debridement can be used to predict healing outcome (Kalan et al., 2019). Although the exact consequences of interspecies interactions on wound pathogenesis remain to be elucidated, in experimental studies, multi-species biofilms elicit major influences on

host tissue responses, such as inflammation (Pastar et al., 2013). In this regard, a co-culture porcine biofilm model, incorporating both *S. aur* and *P. aer*, was developed to further investigate the intricacies of clinical infection. In co-culture, biofilm bacteria appeared more resistant to TG than single-species biofilms (**Figure 6.16**). Experimental fabrication of biofilm communities can be difficult as one species often predominates (Dalton et al., 2011; Malic et al., 2009). Interestingly, in the present work, a stable ratio of 60:40 *P. aer*: *S. aur* was adopted, in line with the potentially synergistic relationship observed between the two species (Dalton et al., 2011; Korgaonkar et al., 2013 Pastar et al., 2013). However, following TG treatment, *P. aer* became more dominant. This result reflects previous studies demonstrating that *P. aer* may outcompete *S. aur* when resources are limited (Mashburn et al., 2005), in part by sequestering vital cofactors and producing metabolites toxic to *S. aur* (Biswas et al., 2009; DeLeon et al., 2014; Hazan et al., 2016).

Many authors have speculated that infection arises when commensal flora is outcompeted by a pathogenic species with a highly virulent response (Rendueles et al., 2014; reviewed in Tlaskalová-Hogenová et al., 2011). As a result, the dynamic interplay between *S. aur* and *P. aer* in the co-culture model could possibly be influencing TG resistance, potentially through virulent mechanisms. Assessing virulence via protease production revealed that the protease profile (zymogram) of co-culture biofilms was different to those produced by single-species biofilms. Alterations in exogenous stimuli are known to modify *P. aer* virulence, particularly *LasB* (Breidenstein et al., 2011; Pearson et al., 1997; Rumbaugh et al., 1999; Shigematsu et al., 2001), largely through quorum-sensing systems (Dong & Zhang, 2005). Topical treatment, even with the vehicle, dampened protease activity drastically, making it difficult to deduce TG-specific effects. Expression of the *P. aer* virulence factors *algD* and *lasB*, and the *S. aur* virulence factor *eno*, was slightly reduced following TG application (**Figure 6.18**). By contrast, the vehicle was the only treatment to affect total protease activity (**Figure 6.17**), where the contribution of *S. aur* was at its highest (~50%; **Figure 6.16**). It may therefore be stipulated that in co-culture, *P. aer* contributes more to the measurable proteases.

Human and porcine skin, although similar, exhibit subtle differences in structure (reviewed in Summerfield et al., 2015) and immunology (e.g. alterations in dendritic cell subsets, Marquet et al., 2011; discussed in **Chapter 1**). As a result, a more

translationally relevant human *ex vivo* biofilm experiment was performed to fully confirm the antimicrobial efficacy of TG. Here, TG significantly reduced *P. aer* and co-culture biofilm load, while a more modest reduction in *S. aur* biofilm was observed (**Figure 6.19**). The relative contribution of *S. aur* and *P. aer* to biofilms differed in the human model, with the vehicle-treated biofilms comprising of 35: 65 *S. aur*: *P. aer*. The ratio in Tg^{Ag}-treated biofilms was moderately altered (~50:50), and in Tg and Ag treatments, *S. aur* was almost entirely absent.

One potential reason for this shift could be the presence of a host response, mediated through the epidermis. For example, broad-range AMPs, such as β-defensins and LL-37, are produced by epidermal keratinocytes and act directly or via immune modulation (Clausen et al., 2015). AMP production is also locally increased by skin barrier disruption to prime the skin antimicrobial defences (Harder et al., 2010). Previously, it has been shown that silver treatment (Duan et al., 2018), and BG treatment (Zhou et al., 2017) alone can promote epidermal proliferation, however evidence for their combined effects, and/or efficacy in infection models is lacking.

Furthermore, although the present work used *ex vivo* models, which better mimic the bacterial-host interactions than *in vitro* models, they do not necessarily reflect the dynamic interactions observed during *in vivo* infection (Andrejko et al., 2013; Gardette et al., 2019). Recently, diverse spatial and temporal differences in virulence factor expression have been elucidated during *in vivo* infection (Rozemeijer et al., 2015), thus it is becoming increasingly difficult to fully characterise host-pathogen relationships *in vitro* and *ex vivo*. Future work with therefore aim to fully determine the TG-specific effects on the host response by observing changes in epidermal proliferation, inflammation and AMPs in an *ex vivo* and *in vivo* context.

Collectively, this work demonstrates clear potential for Tg and Tg^{Ag} as wound-relevant antimicrobials. Exploration of novel antimicrobial agents, especially for indications where mechanisms of antibiotic resistance and silver resistance are of concern, is crucial (Dalton et al., 2011; Su et al., 2011; Randall et al., 2015). Although not currently addressed, TG presents an attractive opportunity for future functionalisation with a variety of compounds designed to promote wound repair (Bonvallet et al., 2015). Combining both the versatility of TG with its clear antimicrobial efficacy offers exciting prospects for future wound management.

Chapter 7: Discussion and Future Work

Age-related disease is a problem of population dynamics. Life expectancy continues to increase at an exponential rate, and although this is an existential achievement for the human race, numerous societal burdens are associated with an ageing population. One such example is the expansion of individuals suffering from non-healing chronic wounds (Guest et al., 2015), which becomes even more problematic due to the inadequacies of current wound care treatments. Consequently, there is an urgent requirement to understand the molecular and cellular correlates associated with poor healing in order to develop viable new therapies. Together, mechanistic data presented in this thesis has elucidated novel senescence-linked and metal-linked characteristics of pathological healing that confer therapeutic potential. These areas should be explored further in basic research and in the clinic.

7.1. Senescence is an intrinsic ageing mechanism linked to diabetes and wound repair via CXCR2 (Chapter 3).

Cellular senescence evolved as an anti-tumour mechanism (van Deursen, 2014), and is a hallmark feature of ageing. Senescent cells accumulate with age due to extrinsic stress, repeated mitotic division, and prolonged intrinsic oxidative damage (Campisi & d'Adda di Fagagna, 2007). More recently, the focus has shifted to assessing the contribution of senescence to chronic disease, including the group of pathologies encompassed by the term diabetes (Prattichizzo et al., 2016; Spazzafumo et al., 2013). Similar to ageing tissues, diabetic hyperglycaemia causes excessive AGEs and sterile inflammation that are thought to underpin replicative exhaustion, cellular stress and senescence (Coughlan et al., 2011; Ott et al., 2014). Despite this known correlation, little research has scrutinised the mechanistic link between senescence and diabetes in detail. Findings presented in this thesis now strongly implicate senescence may be a common feature of diabetic and aged wound pathology.

Indeed, the prevailing hypothesis is that senescence has negative consequences on tissue repair, due to its association to ageing and diabetes (Baker et al., 2011; Moura et al., 2019, Waaijer et al., 2012), yet curiously, transient induction of senescence

following injury may actually be a key driver of adequate tissue resolution. Burton & Faragher (2018) even recently stated that senescent cells "mimic a wound healing response" by virtue of their morphogenic and hypersecretory changes. Indeed, Krizhanovsky et al. (2008) first related senescence to tissue repair using a murine model of damage-induced senescence during liver fibrosis, which was attenuated by genetic knockdown of p53. Of direct relevance, senescence is induced in dermal fibroblasts following skin injury, requiring the matricellular proteins, CCN1 (Jun & Lau, 2010) and CCN2 (Jun & Lau, 2017). This data contrasted with the work of Krizhanovsky et al. (2008), as CCN1 and CCN2-induced senescence was associated with reduced fibrosis during skin wound repair. These disparities most likely reflect the complexities of the *in vivo* environment, the differences in the models used (e.g. physical injury in skin versus chemical liver damage) and the specific research questions addressed in each study.

The report most relevant to the injury-induced senescence data presented in this thesis came from Demaria et al. (2014), who developed a p16-3MR mouse model to track $p16^{+ve}$ cells via luminescence throughout healing. Using this model, the authors were the first to reveal temporal induction of transient senescence during murine wound repair, which occurred between days 3 and 9 post-injury. Eliminating both $p16^{+ve}$ and $p21^{+ve}$ cells in a DKO mouse both attenuated senescence and delayed healing. Thus, it was crucially established that senescent wound mesenchymal cells are important in driving fibroblast differentiation through the release of SASP factors such as PDGFA. However, many unanswered questions remain, including how these senescent mesenchymal cells appear, in what manner they are induced, and if they can contextually delay healing.

Data presented in **Chapter 3** provides the first direct characterisation of senescence in Db murine wounds, elucidating a causative role for senescence in delayed Db wound healing. These findings, supported by the observation that SA-βGAL^{+ve} cells are apparent in human chronic wound fibroblasts (e.g. Agren et al., 1999; Mendez et al., 1998), suggest that increased wound senescence is a potentially important therapeutic target for chronic wounds. Intriguingly, the present work confirmed that short-term senescence induction is necessary for fibroplasia in late-stage repair (**Section 3.4.10**), opening up speculation as to why Db injury-induced senescence delays healing. Perhaps Db wounds show impaired senescent cell clearance or

produce factors that promote/exacerbate senescence in normal wound cells? These questions directed investigation of both theories, through the assessment of Db Mφs and their communication within the cellular wound environment.

Mφs play critical roles in wound healing (Mirza et al., 2009) and diabetes (reviewed in Wicks et al., 2014). Consequently, it was expected that Mφs would be a key cell-type governing senescence in Db pathology (**Section 3.4.4**). Further analysis demonstrated how the Mφ secretome was directly linked to senescence and Db delayed healing (**Section 3.4.5-3.4.6**), where a novel function for the explicated senescence receptor, CXCR2 (Acosta et al., 2008), was discovered. The effects of CXCR2 appeared conserved across experimental approaches, where its blockade improved human *in vitro* and *ex vivo* healing, and accelerated repair *in vivo* in Db murine wounds (**Section 3.4.7-3.4.8**). These data certainly challenge the outdated dogma that senescent cells, although irreversibly arrested, are non-functional. In fact, they fundamentally modulate the wound environment during normal and pathological repair to promote two very different healing outcomes.

7.2. Global profiling reveals temporospatial changes in the metallome throughout normal and pathological repair (Chapter 4).

Endogenous metals pervade the body, playing necessary roles in transcription, translation and a multitude of cellular functions. A good example is calcium signalling, which controls cell migration (Minton, 2014), proliferation (Pinto et al., 2015) and contraction (Lee & Auersperg, 1980). It is therefore unsurprising that there are scientific journals specifically dedicated to individual metals (e.g. *Cell Calcium*) and more generalised multi-disciplinary metal research (e.g. *Metallome*).

It follows that dysregulation of metal homeostasis will be a major contributor to disease. For instance, abnormal levels of circulating magnesium (Resnick et al., 1993; Wu et al., 2017), calcium (reviewed in Ramadan et al., 2011) and iron (in the form of ferritin, Yeap et al., 2015) have been linked to diabetes and other age-related pathologies. As ageing and diabetes are strong risk factors for developing non-healing wounds (Watson et al., 2011), this led to the hypothesis that the skin metallome would change throughout normal wound healing, and be perturbed in pathological (aged and Db) skin and wounds. New data presented in this thesis directly addressed this hypothesis, identifying substantial temporospatial

variations in the metallome during acute and pathological repair. Indeed, differential changes were also highlighted between aged and Db mice, proposing that the disparate etiology of the models may drive distinct metallome signatures.

A non-biased approach was next taken to explore the global temporal changes in the transcriptome (RNA-Seq) of normal and Db wounds, and determine how these alterations may be linked to the metallome. The findings were profound, where many of the thousands of genes DE in Db wounds were crucially correlated with metal-regulated pathways (**Section 4.4.12**). Hence, these data suggested that numerous metals are temporally, spatially and pathologically altered at the elemental and molecular level. Previous authors have demonstrated direct metal modification of the zebrafish transcriptome (Sonnack et al., 2017), with transcriptional changes associated with metabolism and cell signalling. It would be fascinating to establish: a) how metal treatments transcriptionally and functionally alter Db wound healing and; b) whether genetic manipulation of important metal-regulated genes could restore healing.

RNA-Seq transcriptional profiling independently elucidated a link between diabetic healing and senescence (**Section 4.4.14**). Given that accumulation of senescent cells temporally correlates with changes in wound metals, it would be interesting to define whether wound-induced senescence is metallome regulated. In other context, evidence is emerging to show potential connections between metals and senescence. Elevated intracellular calcium, through release from ER stores (Wiel et al., 2014), has been observed during senescence induction (e.g. via oxidative stress in human stem cells, Borodkina et al., 2016; reviewed in Martin & Bernard, 2018). Calcium is also linked to the inflammatory SASP via modulation of NFκB (Sen et al., 1996; Shatrov et al., 1997) and NFAT (Hogan et al., 2003; Mognol et al., 2016). Finally, mitochondrial accumulation of calcium increases ROS *in vitro*, (Görlach et al., 2015; Ma et al., 2018b). Interaction networks suggested additional associations between diabetes, metals and senescence at the molecular level (**Section 4.4.13-4.4.15**). For example, *Cav3*, downregulated in Db wounds and part of the senescence CXCR2 network, is calcium regulated (Garcia-Caballero et al., 2018; Li et al., 2011).

Moreover, iron is associated with senescence, due to its high oxidative potential (Frey & Reed, 2012). Accumulation of iron causes oxidative stress and senescence (bone marrow stem cells, Yang et al., 2017), while senescent MEFs accumulate large

amounts of intracellular iron (Masaldan et al., 2018). Interestingly, data presented in this thesis demonstrate that senescent cells accumulate when wound iron is elevated, signifying potential causation. Taken together, these findings reveal a novel relationship between the metallome and pathological wound repair, and also imply that temporospatial metallome regulation may be associated with other pathology-related mechanisms, such as senescence.

7.3. Temporal accumulation of iron is required for late-stage healing, governing macrophage behaviour and extracellular matrix turnover (Chapter 5).

Global metallome profiling studies uncovered significant upregulation of iron during late-stage repair. As Db wounds displayed reduced iron and impaired ECM deposition (**Section 5.4.2**), it was hypothesised that a central relationship between iron and ECM remodelling exists. This theory was assessed using *in vitro* assays that measured ECM protein production and remodelling, revealing that iron accelerated deposition of collagen-rich ECM via an oxidative stress-dependent mechanism requiring the metalloreductase, STEAP3 (**Section 5.4.11**).

The deposited ECM from iron-loaded fibroblasts was enriched for collagens, however, further characterisation (e.g. mass spectrometry analysis) is required to fully characterise matrix composition differences between non-treated and iron-loaded fibroblasts. Iron-loaded fibroblasts also exhibited increased secretions (including large microvesicles - via scanning electron microscopy; **Section 5.4.8**). These microvesicles may traffic matrix proteins, or contain interesting molecular components (e.g. miRNA) for uptake by other cells (Turchinovich et al., 2012). Certainly, keratinocyte microvesicles are capable of stimulating fibroblasts (Huang et al., 2015) and have been postulated as an innovative approach for regenerative medicine (Sabin & Kikyo, 2014). A future aim will be to characterise the size, number and components of microvesicles produced by iron-loaded fibroblasts, and explore their mechanistic effects on other wound cells.

Literature measuring iron levels in diabetic patients is controversial, where elevated serum ferritin is observed in diabetic patients (Thomas et al., 2004), elevated serum ferritin is only apparent in certain cohorts of diabetic patients (Fernández-Real et al., 2002), or there is no difference in serum ferritin between non-diabetic and

diabetic subjects (Kazi et al., 2008). Indeed, high iron is seen as a risk factor for developing diabetes-associated perturbations in insulin sensitivity (Gabrielsen et al., 2012), and patients with hereditary hemochromatosis certainly possess increased risk of diabetic complications (McClain et al., 2006) that can be alleviated with phlebotomy and iron chelation therapy (Inoue et al., 1997; reviewed in Kontoghiorghes et al., 2010). By contrast, data in this thesis demonstrated reduced iron in skin and wound tissue of Db mice using the sensitive elemental analysis technique, ICP-MS. Indeed, differences in local skin tissue architecture, such as poor micro-vascular perfusion (Jonasson et al., 2017; Levy et al., 2008), could underlie the reduced iron observed in Db mouse skin and wounds.

There are a number of general caveats to the presented studies. In this thesis, and in most other published studies, cells are grown on tissue culture plastic. Tissue culture plastic is over a thousand times stiffer than native fibroblast matrix (Liu et al., 2015), which will alter fibroblast transcription, proliferation and TGFβ-regulated activation (Hadjipanayi et al., 2009; Hinz, 2015; Karamichos et al., 2007). Therefore, to better mimic natural cellular responses, these experiments should be repeated on matrix that better represents the skin's mechanical properties.

Overall, data in this thesis demonstrate the importance of iron in modulating cellular processes required for wound repair and highlight the significance of assessing these functions in a context-dependent manner. Thus, future studies should focus on exploring the influence of iron across more translationally relevant models and settings, to ultimately support therapeutic evaluation in chronic wounds.

7.4. Bioactive glass offers therapeutic potential to infected non-healing wounds (Chapter 6).

Critical colonisation of wounds by bacterial biofilms is a long-standing problem that contributes to wound persistence and more serious systemic infections (Velnar et al., 2009). Hence, it is unsurprising that the wound care market is dominated by products designed to prevent or kill locally infecting bacteria (Han & Ceilley, 2017). While silver and iodine have been used since ancient times (Alexander, 2009), their wound healing efficacy remains controversial (Marx & Barillo, 2014). The aim of this this chapter was to explore the wound healing and antimicrobial efficacy of a commercial bioactive glass (BG) material (Theraglass™; TG) doped with silver.

Data presented in this thesis show that TG was potently antimicrobial in formulations with and without silver. Previous studies demonstrated benefits of using BG, where BG doped dressings improved wound closure (in rats, Hu et al., 2018; Li et al., 2016). Unfortunately, the TG formulations used in the present work did not beneficially alter normal murine wound healing, reflecting the fact that they need to be assessed in a pathological (aged and Db) wound context. Moreover, the effects of TG on immune cell function during infection remain to be determined. Nevertheless, these data provide convincing evidence that TG can be used in an antimicrobial and anti-biofilm capacity.

As it is now known that metals such as calcium, magnesium and iron are temporally and spatially impaired in pathological healing wounds, a clear next step would be to develop a novel metal-based delivery platform. Indeed, TG could be functionalised for this purpose, following characterisation and tailoring of its metal release kinetics, to therapeutically restore the wound metallome.

7.5. Future work.

Work in this thesis has elucidated previously unknown mechanistic links between senescence, the metallome, and pathological (diabetic) repair (Wilkinson et al., 2019a; Wilkinson et al., 2019b; Wilkinson et al., 2019c). While these findings are fundamentally important, they leave many basic science and clinical questions unanswered. For instance, it is still unknown what drives transient senescence during wound repair (microbiota, metals, host response?), and how pathology causes excessive senescence. In this regard, future studies should aim to temporally profile senescence in pathological repair to understand how senescent cells accumulate, and more significantly, how these cells resolve post-injury. This could be achieved using histological assessments of wounds collected at later stages of healing, utilising previously published reporter models (e.g. p16-3MR mouse; Demaria et al., 2014), or using receptor-directed tracers for positron emission tomography live imaging (as developed to Burke et al., 2019; Vag et al., 2018).

There is evident need to additionally characterise the effects of CXCR2 on senescence in human chronic wounds. Tissues could be first profiled for senescence and CXCR2 levels, with the response of chronic wound-derived cells and *ex vivo* skin to CXCR2 antagonism then assessed. This data would determine whether CXCR2

may be of clinical benefit, and strengthen the case for obtaining ethical approval for a phase I study. As CXCR2 antagonists already possess proven clinical safety from previous clinical trials (Kirsten et al., 2015; O'Byrne et al., 2016; Watz et al., 2017), they should be relatively easy to repurpose for wound healing. Moreover, understanding how metal fluctuations may be linked to the temporal senescence profile, and CXCR2 signalling, is of fervent interest.

Although combining ICP-MS with RNA-Seq allowed correlations to be garnered between metals, healing and senescence, they only gave an indication of the functional relevance of these relationships. To really understand the prominence of metal changes and how this relates to cellular machinery and functional output, metals must be examined at the subcellular compartment level (e.g. using synchrotron radiation X-ray fluorescence; Ortega et al., 2009). This is essential, as high extracellular metal quantities may be irrelevant to cellular concentrations and functions. For example, high influx of calcium from intracellular stores alone can massively impact cellular responses. Thus, extracellular elemental abundance does not necessarily reflect intracellular concentration or cellular output.

Metallome profiling identified elemental fluctuations in a temporospatial manner throughout wound repair. However, one of the major remaining queries concerns how metals enter and leave the wound site. In reality, it is likely that metals arrive at the wound via the blood, and through the influx of metal-containing cells. It was postulated that wound iron may accrue due to accumulation of Mφs that sequestered heme from the wound clot (**Chapter 5**), but another key wound process that was not addressed was angiogenesis. At day 7, the granulation tissue becomes highly vascularised (Gurevich et al., 2018), and the formation of new blood vessels would likely contribute to wound iron abundance. By contrast, Db wounds are poorly perfused (Boyko et al., 1999; Icli et al., 2016) and do not heal at the same rate as NDb wounds. To address this fully, angiogenesis would need to be assessed and correlated with elemental abundance, and *in vitro* investigation of metal functions would need to be extended to endothelial cells. Another option would be to broaden ICP-MS analysis to include measurements of metals in the blood and metal storing organs, such as the spleen and liver. This would determine whether stored elements contribute to skin metallome changes, and vice versa, during wound repair.

Following on from this thesis, it will be essential to verify whether the skin and wound metallome is altered in a temporospatial manner in human acute and chronic wounds. Here, ICP-MS and LA-ICP-MS could be used to accurately measure element quantities, and would be compared to cellular functions and wound repair stage. If a global deficit in metals was confirmed in human chronic wounds then it would be relatively easy to envisage metal-targeted treatment modalities with clinical benefit.

Finally, wound healing research has recently shifted its focus to the microbiome, which is known to be altered by ageing (Jugé et al., 2018) and diabetes (Gardiner et al., 2017) and is associated with chronic wound healing (Kalan et al., 2019; Loesche et al., 2017). In fact, dysbiosis in the microbiome causes delayed wound healing *in vivo* (Williams et al., 2017; Williams et al., 2018). Although the relationship between the transcriptome and metallome is only just beginning to be explored, it would be of fundamental interest to ascertain whether the skin metallome contributes to the bacterial composition of the skin, and vice versa.

7.6. Concluding statement.

Despite constant technological and knowledge-based advancements in wound research, understanding of the underlying biology of poor healing remains limited and current chronic wound therapies are insufficient. Research is now shifting to focus on less well-studied areas in the hope that this may shed light on these long-standing clinical problems. One emerging area is metallomics, where current methodologies open a number of novel capabilities. In this work, ICP-MS profiling of wound tissue has highlighted fascinating spatial and temporal alterations in the metallome throughout normal wound repair, and demonstrated that perturbations in time-dependent metal accumulation are correlated with pathological healing. At a fundamental level, this study provides a new platform for exploration of how metals may transcriptionally regulate conserved wound processes and cellular mechanisms, such as senescence. There is now an unprecedented opportunity to further investigate the crucial relationship between the metallome, transcriptome and microbiome in acute and pathological skin wound repair.

References

Abbas, A. M. & Elsamanoudy, A. Z. (2011) 'Effects of 17β-estradiol & antioxidant administration on oxidative stress & insulin resistance in ovariectomized rats', *Can J Physiol Pharmacol*, 89(7), 497-504.

Abou-Mohamed, G., Papapetropoulos, A., Catravas, J. D. & Caldwell, R. W. (1998) 'Zn 2+ inhibits nitric oxide formation in response to lipopolysaccharides: Implication in its anti-inflammatory activity', *Eur J Pharmacol*, 341(2), 265-272.

Abraham, D., Rogers, J., Gault, P., Kushner, J. P. & McClain, D. A. (2006) 'Increased insulin secretory capacity but decreased insulin sensitivity after correction of iron overload by phlebotomy in hereditary haemochromatosis', *Diabetologia*, 49(11), 2546-2551.

Acosta, J. C., Banito, A., Wuestefeld, T., Georgilis, A., Janich, P., Morton, J. P., Athineos, D., Kang, T.-W., Lasitschka, F. & Andrulis, M. (2013) 'A complex secretory program orchestrated by the inflammasome controls paracrine senescence', *Nat Cell Biol*, 15(8), 978-990.

Acosta, J. C., O'Loghlen, A., Banito, A., Guijarro, M. V., Augert, A., Raguz, S., Fumagalli, M., Da Costa, M., Brown, C. & Popov, N. (2008) 'Chemokine signaling via the CXCR2 receptor reinforces senescence', *Cell*, 133(6), 1006-1018.

Adams, M. P., Mallet, D. G. & Pettet, G. J. (2015) 'Towards a quantitative theory of epidermal calcium profile formation in unwounded skin', *PloS One*, 10(1), e0116751.

Adolph, E. J., Guo, R., Pollins, A. C., Zienkiewicz, K., Cardwell, N., Davidson, J. M., Guelcher, S. A. & Nanney, L. B. (2015) 'Injected biodegradable polyurethane scaffolds support tissue infiltration & delay wound contraction in a porcine excisional model', *J Biomed Mater Res B*, 104(8), 1679-1690

Advani, A., Marshall, S. & Thomas, T. (2002) 'Impaired neutrophil actin assembly causes persistent CD11b expression & reduced primary granule exocytosis in Type II diabetes', *Diabetologia*, 45(5), 719-727.

Afshan, S., Musa, A. R. F., Echols, V., Lerant, A. A. & Fülöp, T. (2017) 'Persisting hypocalcemia after surgical parathyroidectomy: The differential effectiveness of calcium citrate versus calcium carbonate with acid suppression', *Am J Med Sci*, 353(1), 82-86.

Agoro, R., Taleb, M., Quesniaux, V. F. & Mura, C. (2018) 'Cell iron status influences macrophage polarization', *PloS One*, 13(5), e0196921.

Agren, M. S., Steenfos, H. H., Dabelsteen, S., Hansen, J. B. & Dabelsteen, E. (1999) 'Proliferation & mitogenic response to PDGF-BB of fibroblasts isolated from chronic venous leg ulcers is ulcer-age dependent', *J Invest Dermatol*, 112(4), 463-469.

Ahn, C., Kang, J.-H. & Jeung, E.-B. (2017) 'Calcium homeostasis in diabetes mellitus', *J Vet Sci*, 18(3), 261-266.

Al-Dayel, O., Hefne, J. & Al-Ajyan, T. (2011) 'Human exposure to heavy metals from cosmetics', *Orient J Chem*, 27, 1.

Al-Nuaimi, Y., Sherratt, M. J. & Griffiths, C. E. (2014) 'Skin health in older age', *Maturitas*, 79(3), 256-264.

Alexander, J. W. (2009) 'History of the medical use of silver', *Surg Infect*, 10(3), 289-292.

Allen, T. D. & Potten, C. S. (1975) 'Desmosomal form, fate, & function in mammalian epidermis', *J Ultrastruct Res*, 51(1), 94-105.

Allgrove, J. & Shaw, N. J. (2015) 'A practical approach to vitamin D deficiency & rickets', *Endocr Dev*, 28, 119-133.

Allsopp, R. C., Chang, E., Kashefi-Aazam, M., Rogaev, E. I., Piatyszek, M. A., Shay, J. W. & Harley, C. B. (1995) 'Telomere shortening is associated with cell division *in vitro* & *in vivo*', *Exp Cell Res*, 220(1), 194-200.
Almine, J. F., Wise, S. G. & Weiss, A. S. (2012) 'Elastin signaling in wound repair', *Birth Defects Res C Embryo Today*, 96(3), 248-257.
Amadeu, T. P., Braune, A. S., Porto, L. C., Desmoulière, A. & Costa, A. M. (2004) 'Fibrillin-1 & elastin are differentially expressed in hypertrophic scars & keloids', *Wound Repair Regen*, 12(2), 169-174.
Amaya, M. J. & Nathanson, M. H. (2013) 'Calcium signaling in the liver', *Comp Physiol*, 3(1), 515-539.
Anathy, V., Lahue, K. G., Chapman, D. G., Chia, S. B., Casey, D. T., Aboushousha, R., van der Velden, J. L., Elko, E., Hoffman, S. M. & McMillan, D. H. (2018) 'Reducing protein oxidation reverses lung fibrosis', *Nat Med*, 24(8), 1128-1135.
Andrasi, E., Igaz, S., Molnár, Z. & Mako, S. (2000) 'Disturbances of magnesium concentrations in various brain areas in Alzheimer's disease', *Magnes Res*, 13(3), 189-196.
Andreini, C., Bertini, I., Cavallaro, G., Holliday, G. L. & Thornton, J. M. (2008) 'Metal ions in biological catalysis: From enzyme databases to general principles', *J Biol Inorg Chem*, 13(8), 1205-1218.
Andrejko, M., Zdybicka-Barabas, A., Janczarek, M. & Cytryńska, M. (2013) 'Three *Pseudomonas aeruginosa* strains with different protease profiles', *Acta Biochim Pol*, 60(1), 83-90.
Andriopoulos Jr, B., Corradini, E., Xia, Y., Faasse, S. A., Chen, S., Grgurevic, L., Knutson, M. D., Pietrangelo, A., Vukicevic, S. & Lin, H. Y. (2009) 'BMP6 is a key endogenous regulator of hepcidin expression & iron metabolism', *Nat Genet*, 41(4), 482-487.
André-Lévigne, D., Modarressi, A., Pepper, M. & Pittet-Cuénod, B. (2017) 'Reactive oxygen species & NOX enzymes are emerging as key players in cutaneous wound repair', *Int J Mol Sci*, 18(10), e2149.
Anguita-Alonso, P., Rouse, M. S., Piper, K. E., Jacofsky, D. J., Osmon, D. R. & Patel, R. (2006) 'Comparative study of antimicrobial release kinetics from polymethylmethacrylate', *Clin Ortho Rel Res*, 445, 239-244.
Ansell, D. M., Campbell, L., Thomason, H. A., Brass, A. & Hardman, M. J. (2014) 'A statistical analysis of murine incisional & excisional acute wound models', *Wound Repair Regen*, 22(2), 281-287.
Ansell, D. M., Holden, K. A. & Hardman, M. J. (2012) 'Animal models of wound repair: Are they cutting it?', *Exp Dermatol*, 21(8), 581-585.
Ansell, D. M., Kloepper, J. E., Thomason, H. A., Paus, R. & Hardman, M. J. (2011) 'Exploring the "hair growth–wound healing connection": Anagen phase promotes wound re-epithelialization', *J Invest Dermatol*, 131(2), 518-528.
Antonicelli, F., Bellon, G., Debelle, L. & Hornebeck, W. (2007) 'Elastin-elastases & inflamm-aging', *Curr Top Rev Biol*, 79, 99-155.
Applegate, L. & Frenk, E. (1995) 'Oxidative defense in cultured human skin fibroblasts & keratinocytes from sun-exposed & non-exposed skin', *Photodermatol Photoimmunol Photomed*, 11(3), 95-101.
Applegate, L. A., Scaletta, C., Panizzon, R. & Frenk, E. (1998) 'Evidence that ferritin is UV inducible in human skin: Part of a putative defense mechanism', *J Invest Dermatol*, 111(1), 159-163.
Arany, Z., Huang, L. E., Eckner, R., Bhattacharya, S., Jiang, C., Goldberg, M. A., Bunn, H. F. & Livingston, D. M. (1996) 'An essential role for p300/CBP in the cellular response to hypoxia', *Proc Nat Acad Sci*, 93(23), 12969-12973.

Arezes, J., Jung, G., Gabayan, V., Valore, E., Ruchala, P., Gulig, P. A., Ganz, T., Nemeth, E. & Bulut, Y. (2015) 'Hepcidin-induced hypoferremia is a critical host defense mechanism against the siderophilic bacterium *Vibrio vulnificus*', *Cell Host Microbe*, 17(1), 47-57.
Arezes, J. & Nemeth, E. (2015) 'Hepcidin & iron disorders: New biology & clinical approaches', *Int J Lab Hematol*, 37, 92-98.
Argyropoulos, A. J., Robichaud, P., Balimunkwe, R. M., Fisher, G. J., Hammerberg, C., Yan, Y. & Quan, T. (2016) 'Alterations of Dermal Connective Tissue Collagen in Diabetes: Molecular Basis of Aged-Appearing Skin', *PLoS One*, 11(4), e0153806.
Arndt-Jovin, D. J. & Jovin, T. M. (1989) 'Fluorescence labeling & microscopy of DNA', *Methods Cell Biol*, 30, 417-448.
Arpino, V., Brock, M. & Gill, S. E. (2015) 'The role of TIMPs in regulation of extracellular matrix proteolysis', *Matrix Biol*, 44, 247-254.
Arruda, A. P. & Hotamisligil, G. S. (2015) 'Calcium homeostasis & organelle function in the pathogenesis of obesity & diabetes', *Cell Metab*, 22(3), 381-397.
Artandi, S. E., Alson, S., Tietze, M. K., Sharpless, N. E., Ye, S., Greenberg, R. A., Castrillon, D. H., Horner, J. W., Weiler, S. R. & Carrasco, R. D. (2002) 'Constitutive telomerase expression promotes mammary carcinomas in aging mice', *Proc Nat Acad Sci*, 99(12), 8191-8196.
Arthur, A., Cakouros, D., Cooper, L., Nguyen, T., Isenmann, S., Zannettino, A. C., Glackin, C. A. & Gronthos, S. (2016) 'Twist-1 Enhances Bone Marrow Mesenchymal Stromal Cell Support of Hematopoiesis by Modulating CXCL12 Expression', *Stem Cells*, 34(2), 504-509.
Ascone, I. & Strange, R. (2009) 'Biological X-ray absorption spectroscopy & metalloproteomics', *J Synchrotron Radiat*, 16(3), 413-421.
Aseer, K. R., Kim, S. W., Choi, M. S. & Yun, J. W. (2015) 'Opposite expression of Sparc between the liver & pancreas in streptozotocin-induced diabetic rats', *PLoS One*, 10(6), e0131189.
Ashcroft, G. S., Dodsworth, J., Van Boxtel, E., Tarnuzzer, R., Horan, M. A., Schultz, G. S. & Ferguson, M. (1997) 'Estrogen accelerates cutaneous wound healing associated with an increase in TGF-b1 levels', *Nat Med*, 3(11), 1209-1215.
Ashcroft, G. S., Mills, S. J., Lei, K., Gibbons, L., Jeong, M.-J., Taniguchi, M., Burow, M., Horan, M. A., Wahl, S. M. & Nakayama, T. (2003) 'Estrogen modulates cutaneous wound healing by downregulating macrophage migration inhibitory factor', *J Clin Invest*, 111(9), 1309-1318.
Association, A. D. (2010) 'Diagnosis & classification of diabetes mellitus', *Diabetes Care*, 33(1), 62-69.
Atiyeh, B. S., Costagliola, M., Hayek, S. N. & Dibo, S. A. (2007) 'Effect of silver on burn wound infection control & healing: Review of the literature', *Burns*, 33(2), 139-148.
Atkinson, M. A., Eisenbarth, G. S. & Michels, A. W. (2014) 'Type 1 diabetes', *Lancet*, 383(9911), 69-82.
Augusti, D. V., Lago, R. M. & Augusti, R. (2004) 'Quantitative determination of the enantiomeric composition of panthotenic acid solutions: A mass spectrometry experiment', *J Braz Chem Soc*, 15(5), 786-790.
Ayres, P. G. (2004) 'Alexis Millardet: France's forgotten mycologist', *Mycologist*, 18(1), 23-26.
Babaeijandaghi, F., Shabani, I., Seyedjafari, E., Naraghi, Z. S., Vasei, M., Haddadi-Asl, V., Hesari, K. K. & Soleimani, M. (2010) 'Accelerated epidermal regeneration & improved dermal reconstruction achieved by polyethersulfone nanofibers', *Tissue Eng Part A*, 16(11), 3527-3536.

Babitt, J. L., Huang, F. W., Wrighting, D. M., Xia, Y., Sidis, Y., Samad, T. A., Campagna, J. A., Chung, R. T., Schneyer, A. L., Woolf, C. J., Andrews, N. C. & Lin, H. Y. (2006) 'Bone morphogenetic protein signaling by hemojuvelin regulates hepcidin expression', *Nat Genet*, 38(5), 531-539.
Bacci, M., Capobianco, A., Monno, A., Cottone, L., Di Puppo, F., Camisa, B., Mariani, M., Brignole, C., Ponzoni, M. & Ferrari, S. (2009) 'Macrophages are alternatively activated in patients with endometriosis & required for growth & vascularization of lesions in a mouse model of disease', *Am J Pathol*, 175(2), 547-556.
Badamchi, A., Masoumi, H., Javadinia, S., Asgarian, R. & Tabatabaee, A. (2017) 'Molecular detection of six virulence genes in *Pseudomonas aeruginosa* isolates detected in children with urinary tract infection', *Microb Pathog*, 107, 44-47.
Badenhorst, D., Maseko, M., Tsotetsi, O. J., Naidoo, A., Brooksbank, R., Norton, G. R. & Woodiwiss, A. J. (2003) 'Cross-linking influences the impact of quantitative changes in myocardial collagen on cardiac stiffness & remodelling in hypertension in rats', *Cardiovasc Res*, 57(3), 632-641.
Baggiolini, M. (2001) 'Chemokines in pathology & medicine', *J Int Med*, 250(2), 91-104.
Bagi, Z., Koller, A. & Kaley, G. (2003) 'Superoxide-NO interaction decreases flow-& agonist-induced dilations of coronary arterioles in type 2 diabetes mellitus', *Am J Physiol Heart Circ*, 285(4), H1404-H1410.
Bainbridge, P. (2013) 'Wound healing & the role of fibroblasts', *J Wound Care*, 22(8), 407-408.
Bains, J. W., Crawford, D. & Ketcham, A. S. (1966) 'Effect of chronic anemia on wound tensile strength: Correlation with blood volume, total red blood cell volume & proteins', *Ann Surg*, 164(2), 243-246.
Baker, A. H., Edwards, D. R. & Murphy, G. (2002) 'Metalloproteinase inhibitors: Biological actions & therapeutic opportunities', *J Cell Sci*, 115(19), 3719-3727.
Baker, D. J., Childs, B. G., Durik, M., Wijers, M. E., Sieben, C. J., Zhong, J., Saltness, R. A., Jeganathan, K. B., Verzosa, G. C. & Pezeshki, A. (2016) 'Naturally occurring p16 Ink4a-positive cells shorten healthy lifespan', *Nature*, 530(7589), 184-189.
Baker, D. J., Perez-Terzic, C., Jin, F., Pitel, K. S., Niederländer, N. J., Jeganathan, K., Yamada, S., Reyes, S., Rowe, L. & Hiddinga, H. J. (2008) 'Opposing roles for p16 Ink4a & p19 Arf in senescence & ageing caused by BubR1 insufficiency', *Nat Cell Biol*, 10(7), 825-836.
Baker, D. J., Weaver, R. L. & van Deursen, J. M. (2013) 'p21 both attenuates & drives senescence & aging in BubR1 progeroid mice', *Cell Rep*, 3(4), 1164-1174.
Baker, D. J., Wijshake, T., Tchkonia, T., LeBrasseur, N. K., Childs, B. G., Van De Sluis, B., Kirkland, J. L. & van Deursen, J. M. (2011) 'Clearance of p16Ink4a-positive senescent cells delays ageing-associated disorders', *Nature*, 479(7372), 232-236.
Baker, S. A. & Miller-Ihli, N. J. (1999) 'Comparison of a cross-flow & microconcentric nebulizer for chemical speciation measurements using CZE-ICP-MS', *App Spectrosc*, 53(4), 471-478.
Baker, W. F. (2000) 'Iron deficiency in pregnancy, obstetrics, & gynecology', *Hematol Oncol Clin North Am*, 14(5), 1061-1077.
Balaban, R. S., Nemoto, S. & Finkel, T. (2005) 'Mitochondria, oxidants, & aging', *Cell*, 120(4), 483-495.
Baldan, R., Cigana, C., Testa, F., Bianconi, I., De Simone, M., Pellin, D., Di Serio, C., Bragonzi, A. & Cirillo, D. M. (2014) 'Adaptation of *Pseudomonas aeruginosa* in cystic fibrosis airways influences virulence of *Staphylococcus aureus in vitro* & murine models of co-infection', *PLoS One*, 9(3), e89614.

Balderas-Villalobos, J., Molina-Muñoz, T., Mailloux-Salinas, P., Bravo, G., Carvajal, K. & Gómez-Viquez, N. L. (2013) 'Oxidative stress in cardiomyocytes contributes to decreased SERCA2a activity in rats with metabolic syndrome', *Am J Physiol Heart Circ Physiol*, 305(9), 1344-1353.
Balkwill, F. R. (2012) 'The chemokine system & cancer', *J Pathol*, 226(2), 148-157.
Balouiri, M., Sadiki, M. & Ibnsouda, S. K. (2016) 'Methods for *in vitro* evaluating antimicrobial activity: A review', *J Pharm Anal*, 6(2), 71-79.
Baltzis, D., Eleftheriadou, I. & Veves, A. (2014) 'Pathogenesis & treatment of impaired wound healing in diabetes mellitus: New insights', *Adv Ther*, 31(8), 817-836.
Bannon, P., Wood, S., Restivo, T., Campbell, L., Hardman, M. J. & Mace, K. A. (2013) 'Diabetes induces stable intrinsic changes to myeloid cells that contribute to chronic inflammation during wound healing in mice', *Dis Mod Mech*, 6(6), 1434-1447.
Bao, W., Rong, Y., Rong, S. & Liu, L. (2012) 'Dietary iron intake, body iron stores, & the risk of type 2 diabetes: A systematic review & meta-analysis', *BMC Med*, 10(10), e119.
Baran, R., Dawber, R. P. & Haneke, E. (2005) 'Hair & nail relationship', *Skinmed*, 4(1), 18-23.
Baranek, T., Debret, R., Antonicelli, F., Lamkhioued, B., Belaaouaj, A., Hornebeck, W., Bernard, P., Guenounou, M. & Le Naour, R. (2007) 'Elastin receptor (spliced galactosidase) occupancy by elastin peptides counteracts proinflammatory cytokine expression in lipopolysaccharide-stimulated human monocytes through NF-kappaB down-regulation', *J Immunol*, 179(9), 6184-6192.
Barbusiński, K. (2009) 'Fenton reaction-controversy concerning the chemistry', *Ecol Chem Eng*, 16(3), 347-358.
Barker, T. H. & Engler, A. J. (2017) 'The provisional matrix: Setting the stage for tissue repair outcomes', *Matrix Biol*, 60-61, 1-4.
Barnham, K. J. & Bush, A. I. (2008) 'Metals in Alzheimer's & Parkinson's diseases', *Curr Opin Chem Biol*, 12(2), 222-228.
Baroni, A., Buommino, E., De Gregorio, V., Ruocco, E., Ruocco, V. & Wolf, R. (2012) 'Structure & function of the epidermis related to barrier properties', *Clin Dermatol*, 30(3), 257-262.
Barr, A. R., Cooper, S., Heldt, F. S., Butera, F., Stoy, H., Mansfeld, J., Novák, B. & Bakal, C. (2017) 'DNA damage during S-phase mediates the proliferation-quiescence decision in the subsequent G1 via p21 expression', *Nat Commun*, 8, e14728.
Barrientos, S., Stojadinovic, O., Golinko, M. S., Brem, H. & Tomic-Canic, M. (2008) 'Growth factors & cytokines in wound healing', *Wound Repair Regen*, 16(5), 585-601.
Barros, J. F., Waclawiak, I., Pecli, C., Borges, P. A., Georgii, J. L., Ramos-Junior, E. S., Canetti, C., Courau, T., Klatzmann, D. & Kunkel, S. L. (2019) 'Role of Chemokine Receptor CCR4 & Regulatory T Cells in Wound Healing of Diabetic Mice', *J Invest Dermatol*, 139(5), 1161-1170.
Bataller, R., North, K. E. & Brenner, D. A. (2003) 'Genetic polymorphisms & the progression of liver fibrosis: A critical appraisal', *Hepatology*, 37(3), 493-503.
Baum, C. L. & Arpey, C. J. (2005) 'Normal cutaneous wound healing: Clinical correlation with cellular & molecular events', *Dermatol Surg*, 31(6), 674-686.
Beauséjour, C. M., Krtolica, A., Galimi, F., Narita, M., Lowe, S. W., Yaswen, P. & Campisi, J. (2003) 'Reversal of human cellular senescence: Roles of the p53 & p16 pathways', *EMBO J*, 22(16), 4212-4222.
Becker, J., Niehren, S., Matusch, A., Wu, B., Hsieh, H.-F., Kumtabtim, U., Hamester, M., Plaschke-Schlütter, A. & Salber, D. (2010) 'Scaling down the bioimaging of metals by

laser microdissection inductively coupled plasma mass spectrometry (LMD-ICP-MS)', *Int J Mass Spectrom*, 294(1), 1-6.
Becker, J. S. (2005) 'Inductively coupled plasma mass spectrometry (ICP-MS) & laser ablation ICP-MS for isotope analysis of long-lived radionuclides', *Int J Mass Spectrom*, 242(2), 183-195.
Bedard, K., Szabo, E., Michalak, M. & Opas, M. (2005) 'Cellular functions of endoplasmic reticulum chaperones calreticulin, calnexin, & ERp57', *Int Rev Cytol*, 245, 91-121.
Bedingfield, J. (1849) 'Claim to priority of the application of nitrate of silver in ulceration of the larynx', *Prov Med Surg J*, 13(17), 461.
Beenken, K. E., Mrak, L. N., Griffin, L. M., Zielinska, A. K., Shaw, L. N., Rice, K. C., Horswill, A. R., Bayles, K. W. & Smeltzer, M. S. (2010) 'Epistatic relationships between sarA & agr in *Staphylococcus aureus* biofilm formation', *PloS One*, 5(5), e10790.
Begin-Heick, N., Dalpe-Scott, M., Rowe, J. & Heick, H. M. (1985) 'Zinc supplementation attenuates insulin secretory activity in pancreatic islets of the *ob/ob* mouse', *Diabetes*, 34(2), 179-184.
Behm, B., Schreml, S., Landthaler, M. & Babilas, P. (2012) 'Skin signs in diabetes mellitus', *J Eur Acad Dermatol Venereol*, 26(10), 1203-1211.
Bekircan-Kurt, C. E., Üçeyler, N. & Sommer, C. (2014) 'Cutaneous activation of rage in nonsystemic vasculitic & diabetic neuropathy', *Muscle Nerve*, 50(3), 377-383.
Bellantone, M., Coleman, N. J. & Hench, L. L. 2002. *Silver-containing*, *sol/gel derived bioglass compositions*. US Patent US6482444B1. Available online: https://patents.google.com/patent/US6482444 [Accessed 30/8/19].
Belperio, J. A., Dy, M., Murray, L., Burdick, M. D., Xue, Y. Y., Strieter, R. M. & Keane, M. P. (2004) 'The role of the Th2 CC chemokine ligand CCL17 in pulmonary fibrosis', *J Immunol*, 173(7), 4692-4698.
Bengtsson, H., Bravo, H. C., Gentleman, R., Hossjer, O., Jaffee, H., Jiang, D., Langfelder, P., Hickey, P. & Bengtsson, M. H. (2018) 'Package 'matrixStats''. Available online: http://cran.r-project.org [Accessed 30/8/19].
Beringer, A., Gouriou, Y., Lavocat, F., Ovize, M. & Miossec, P. (2018) 'Blockade of store-operated calcium entry reduces IL-17/TNF cytokine-induced inflammatory response in human myoblasts', *Front Immunol*, 9, e3170.
Bermudez, D. M., Herdrich, B. J., Xu, J., Lind, R., Beason, D. P., Mitchell, M. E., Soslowsky, L. J. & Liechty, K. W. (2011) 'Impaired biomechanical properties of diabetic skin: Implications in pathogenesis of diabetic wound complications', *Am J Pathol*, 178(5), 2215-2223.
Bernatchez, S. F., Parks, P. J., Grussing, D. M., Matalas, S. L. & Nelson, G. S. (1998) 'Histological characterization of a delayed wound healing model in pig', *Wound Repair Regen*, 6(3), 223-233.
Bernhagen, J., Krohn, R., Lue, H., Gregory, J. L., Zernecke, A., Koenen, R. R., Dewor, M., Georgiev, I., Schober, A. & Leng, L. (2007) 'MIF is a noncognate ligand of CXC chemokine receptors in inflammatory & atherogenic cell recruitment', *Nat Med*, 13(5), 587-596.
Berridge, M. J. (1995) 'Calcium signalling & cell proliferation', *Bioessays*, 17(6), 491-500.
Berridge, M. J. (2002) 'The endoplasmic reticulum: A multifunctional signaling organelle', *Cell Calcium*, 32(5-6), 235-249.
Berridge, M. J., Bootman, M. D. & Roderick, H. L. (2003) 'Calcium signalling: Dynamics, homeostasis & remodelling', *Nat Rev Mol Cell Biol*, 4(7), 517-529.

Berridge, M. J., Lipp, P. & Bootman, M. D. (2000) 'The versatility & universality of calcium signalling', *Nat Rev Mol Cell Biol*, 1(1), 11-21
Berry, D. C., Jiang, Y., Arpke, R. W., Close, E. L., Uchida, A., Reading, D., Berglund, E. D., Kyba, M. & Graff, J. M. (2017) 'Cellular aging contributes to failure of cold-induced beige adipocyte formation in old mice & humans', *Cell Metab*, 25(1), 166-181.
Besson, A., Dowdy, S. F. & Roberts, J. M. (2008) 'CDK inhibitors: Cell cycle regulators & beyond', *Dev Cell*, 14(2), 159-169.
Bettmer, J., Bayón, M. M., Encinar, J. R., Sánchez, M. L. F. & Medel, A. S. (2009) 'The emerging role of ICP-MS in proteomic analysis', *J Proteom*, 72(6), 989-1005.
Bhardwaj, N. & Kundu, S. C. (2010) 'Electrospinning: A fascinating fiber fabrication technique', *Biotechnol Adv*, 28(3), 325-347.
Bhattacharya, S., Aggarwal, R., Singh, V. P., Ramachandran, S. & Datta, M. (2015) 'Downregulation of miRNAs during delayed wound healing in diabetes: Role of Dicer', *Mol Med*, 21(1), 847-860.
Bi, J., Zeng, X., Zhao, L., Wei, Q., Yu, L., Wang, X., Yu, Z., Cao, Y., Shan, F. & Wei, M. (2016) 'miR-181a induces macrophage polarized to M2 phenotype & promotes M2 macrophage-mediated tumor cell metastasis by targeting KLF6 & C/EBPα', *Mol Ther Nucl Acids*, 5, e368.
Bianco, C., Kezic, S., Visser, M. J., Pluut, O., Adami, G. & Krystek, P. (2015) 'Pilot study on the identification of silver in skin layers & urine after dermal exposure to a functionalized textile', *Talanta*, 136, 23-28.
Bidasee, K. R., Nallani, K., Henry, B., Dincer, U. D. & Besch, H. R. (2003) 'Chronic diabetes alters function & expression of ryanodine receptor calcium-release channels in rat hearts', *Mol Cell Biochem*, 249(1-2), 113-123.
Bikle, D. D. (2014) 'Vitamin D metabolism, mechanism of action, & clinical applications', *Chem Biol*, 21(3), 319-329.
Bikle, D. D., Ng, D., Tu, C.-L., Oda, Y. & Xie, Z. (2001) 'Calcium-& vitamin D-regulated keratinocyte differentiation', *Mol Cell Endocrinol*, 177(1-2), 161-171.
Bikle, D. D., Ratnam, A., Mauro, T., Harris, J. & Pillai, S. (1996) 'Changes in calcium responsiveness & handling during keratinocyte differentiation. Potential role of the calcium receptor', *J Clin Invest*, 97(4), 1085-1093.
Biran, A., Zada, L., Abou Karam, P., Vadai, E., Roitman, L., Ovadya, Y., Porat, Z. & Krizhanovsky, V. (2017) 'Quantitative identification of senescent cells in aging & disease', *Aging Cell*, 16(4), 661-671.
Birk, D. E. & Bruckner, P. (2005) 'Collagen suprastructures', In: Brinckmann J., Notbohm H. & Müller P.K. (eds) *Collagen*. Berlin: Springer, 185-205.
Biswas, L., Biswas, R., Schlag, M., Bertram, R. & Götz, F. (2009) 'Small-colony variant selection as a survival strategy for *Staphylococcus aureus* in the presence of *Pseudomonas aeruginosa*', *App Environ Microbiol*, 75(21), 6910-6912.
Biswas, S. K. & Mantovani, A. (2010) 'Macrophage plasticity & interaction with lymphocyte subsets: Cancer as a paradigm', *Nat Immunol*, 11(10), 889-896.
Bitto, A., Sell, C., Crowe, E., Lorenzini, A., Malaguti, M., Hrelia, S. & Torres, C. (2010) 'Stress-induced senescence in human & rodent astrocytes', *Exp Cell Res*, 316(17), 2961-2968.
Bjarnsholt, T., Kirketerp-Møller, K., Jensen, P. Ø., Madsen, K. G., Phipps, R., Krogfelt, K., Høiby, N. & Givskov, M. (2008) 'Why chronic wounds will not heal: A novel hypothesis', *Wound Repair Regen*, 16(1), 2-10.
Bleaken, B. M., Menko, A. S. & Walker, J. L. (2016) 'Cells activated for wound repair have the potential to direct collective invasion of an epithelium', *Mol Biol Cell*, 27(3), 451-465.

Blecher, K., Martinez, L. R., Tuckman-Vernon, C., Nacharaju, P., Schairer, D., Chouake, J., Friedman, J. M., Alfieri, A., Guha, C. & Nosanchuk, J. D. (2012) 'Nitric oxide-releasing nanoparticles accelerate wound healing in NOD-SCID mice', *Nanomed Nanotechnol Biol Med*, 8(8), 1364-1371.
Blighe, K. 2019. 'EnhancedVolcano: Publication-ready volcano plots with enhanced colouring & labeling' Available online: https://github.com/kevinblighe/EnhancedVolcano [Accessed 30/8/19].
Bloom, B. R. & Bennett, B. (1966) 'Mechanism of a reaction *in vitro* associated with delayed-type hypersensitivity', *Science*, 153(3731), 80-82.
Blume-Peytavi, U., Kottner, J., Sterry, W., Hodin, M. W., Griffiths, T. W., Watson, R. E., Hay, R. J. & Griffiths, C. E. (2016) 'Age-associated skin conditions & diseases: Current perspectives & future options', *Gerontologist*, 56(2), 230-242.
Boateng, J. S., Matthews, K. H., Stevens, H. N. & Eccleston, G. M. (2008) 'Wound healing dressings & drug delivery systems: A review', *J Pharm Sci*, 97(8), 2892-2923.
Bogdan, A. R., Miyazawa, M., Hashimoto, K. & Tsuji, Y. (2016) 'Regulators of iron homeostasis: New players in metabolism, cell death, & disease', *Trends Biochem Sci*, 41(3), 274-286.
Bolondi, G., Garuti, C., Corradini, E., Zoller, H., Vogel, W., Finkenstedt, A., Babitt, J. L., Lin, H. Y. & Pietrangelo, A. (2010) 'Altered hepatic BMP signaling pathway in human HFE hemochromatosis', *Blood Cells Mol Dis*, 45(4), 308-312.
Bonham, M., O'Connor, J. M., Hannigan, B. M. & Strain, J. (2002) 'The immune system as a physiological indicator of marginal copper status?', *Br J Nutr*, 87(05), 393-403.
Bonvallet, P. P., Schultz, M. J., Mitchell, E. H., Bain, J. L., Culpepper, B. K., Thomas, S. J. & Bellis, S. L. (2015) 'Microporous dermal-mimetic electrospun scaffolds pre-seeded with fibroblasts promote tissue regeneration in full-thickness skin wounds', *PloS One*, 10(3), e0122359.
Bootman, M. D., Berridge, M. J. & Roderick, H. L. (2002) 'Calcium signalling: More messengers, more channels, more complexity', *Curr Biol*, 12(16), R563-R565.
Borkow, G., Gabbay, J., Dardik, R., Eidelman, A. I., Lavie, Y., Grunfeld, Y., Ikher, S., Huszar, M., Zatcoff, R. C. & Marikovsky, M. (2010) 'Molecular mechanisms of enhanced wound healing by copper oxide-impregnated dressings', *Wound Repair Regen*, 18(2), 266-275.
Borodkina, A. V., Shatrova, A. N., Deryabin, P. I., Griukova, A. A., Abushik, P. A., Antonov, S. M., Nikolsky, N. N. & Burova, E. B. (2016) 'Calcium alterations signal either to senescence or to autophagy induction in stem cells upon oxidative stress', *Aging*, 8(12), 3400-3418.
Borrás, C., Gambini, J., López-Grueso, R., Pallardó, F. V. & Viña, J. (2010) 'Direct antioxidant & protective effect of estradiol on isolated mitochondria', *Biochim Biophys Acta Mol Bas Dis*, 1802(1), 205-211.
Bose, S., Roy, M. & Bandyopadhyay, A. (2012) 'Recent advances in bone tissue engineering scaffolds', *Trends Biotechnol*, 30(10), 546-554.
Bosshart, H. & Heinzelmann, M. (2016) 'THP-1 cells as a model for human monocytes', *Ann Trans Med*, 4(21), e438.
Bottai, G., Mancina, R., Muratori, M., Di Gennaro, P. & Lotti, T. (2013) '17β-estradiol protects human skin fibroblasts & keratinocytes against oxidative damage', *J Eur Acad Dermatol Venereol*, 27(10), 1236-1243.
Boulton, A. J. (2013) 'The diabetic foot. Preface', *Med Clin North Am*, 97(5), xiii-xiv.
Boyko, E. J., Ahroni, J. H., Stensel, V., Forsberg, R. C., Davignon, D. R. & Smith, D. G. (1999) 'A prospective study of risk factors for diabetic foot ulcer. The Seattle Diabetic Foot Study', *Diabetes Care*, 22(7), 1036-1042.

Braakhuis, H. M., Park, M. V., Gosens, I., De Jong, W. H. & Cassee, F. R. (2014) 'Physicochemical characteristics of nanomaterials that affect pulmonary inflammation', *Particle Fibre Toxicol*, 11(1), e18.
Bradley, M., Bond, M., Manini, J., Brown, Z. & Charlton, S. (2009) 'SB265610 is an allosteric, inverse agonist at the human CXCR2 receptor', *Brit J Pharmacol*, 158(1), 328-338.
Bradshaw, N., Hall, E. F. & Sanderson, N. E. (1989) 'Communication. Inductively coupled plasma as an ion source for high-resolution mass spectrometry', *J Anal Atom Spectrom*, 4(8), 801-803.
Bragulla, H. H. & Homberger, D. G. (2009) 'Structure & functions of keratin proteins in simple, stratified, keratinized & cornified epithelia', *J Anat*, 214(4), 516-559.
Braverman, I. M. (2000) 'The cutaneous microcirculation'. *J Invest Dermatol*, 5(1), 3-9.
Bray, D. (2000) 'Critical point drying of biological specimens for scanning electron microscopy', In: Williams J.R. & Clifford A.A. (eds) *Supercritical Fluid Methods & Protocols*. Berlin: Springer, 235-243.
Breidenstein, E. B., de la Fuente-Núñez, C. & Hancock, R. E. (2011) *'Pseudomonas aeruginosa*: All roads lead to resistance', *Trends Microbiol*, 19(8), 419-426.
Brew, K., Dinakarpandian, D. & Nagase, H. (2000) 'Tissue inhibitors of metalloproteinases: Evolution, structure & function', *Biochim Biophysi Acta Prot Struct Mol Enzymol*, 1477(1-2), 267-283.
Bridle, K. R., Frazer, D. M., Wilkins, S. J., Dixon, J. L., Purdie, D. M., Crawford, D. H., Subramaniam, V. N., Powell, L. W., Anderson, G. J. & Ramm, G. A. (2003) 'Disrupted hepcidin regulation in HFE-associated haemochromatosis & the liver as a regulator of body iron homoeostasis', *Lancet*, 361(9358), 669-673.
Brincat, M., Versi, E., Moniz, C., Magos, A., De Trafford, J. & Studd, J. (1987) 'Skin collagen changes in postmenopausal women receiving different regimens of estrogen therapy', *Obstet Gynecol*, 70(1), 123-127.
Brini, M., Calì, T., Ottolini, D. & Carafoli, E. (2013) 'The plasma membrane calcium pump in health & disease', *FEBS J*, 280(21), 5385-5397.
Brini, M. & Carafoli, E. (2009) 'Calcium pumps in health & disease', *Physiol Rev*, 89(4), 1341-1378.
Brinkmann, V., Reichard, U., Goosmann, C., Fauler, B., Uhlemann, Y., Weiss, D. S., Weinrauch, Y. & Zychlinsky, A. (2004) 'Neutrophil extracellular traps kill bacteria', *Science*, 303(5663), 1532-1535.
Brodsky, S. V., Gealekman, O., Chen, J., Zhang, F., Togashi, N., Crabtree, M., Gross, S. S., Nasjletti, A. & Goligorsky, M. S. (2004) 'Prevention & reversal of premature endothelial cell senescence & vasculopathy in obesity-induced diabetes by ebselen', *Circ Res*, 94(3), 377-384.
Brown, G. L., Nanney, L. B., Griffen, J., Cramer, A. B., Yancey, J. M., Curtsinger III, L. J., Holtzin, L., Schultz, G. S., Jurkiewicz, M. J. & Lynch, J. B. (1989) 'Enhancement of wound healing by topical treatment with epidermal growth factor', *N Eng J Med*, 321(2), 76-79.
Brown, J. P., Wei, W. & Sedivy, J. M. (1997) 'Bypass of senescence after disruption of p21CIP1/WAF1 gene in normal diploid human fibroblasts', *Science*, 277(5327), 831-834.
Broughton, I., Janis, J. E. & Attinger, C. E. (2006) 'Wound healing: An overview', *Plast Reconstr Surg*, 117(7), 1e-S-32e-S.
Buckley, C. D. (2011) 'Why does chronic inflammation persist: An unexpected role for fibroblasts', *Immunol Lett*, 138(1), 12-14.

Buffoli, B., Rinaldi, F., Labanca, M., Sorbellini, E., Trink, A., Guanziroli, E., Rezzani, R. & Rodella, L. F. (2014) 'The human hair: From anatomy to physiology', *Int J Dermatol*, 53(3), 331-341.
Burden, N., Chapman, K., Sewell, F. & Robinson, V. (2015) 'Pioneering better science through the 3Rs: An introduction to the national centre for the replacement, refinement, & reduction of animals in research (NC3Rs)', *J Am Assoc Lab Anim Sci*, 54(2), 198-208.
Burke, B., Miranda, C., Lee, R., Renard, I., Nigam, S., Clemente, G., D'huys, T., Ruest, T., Domarkas, J. & Thompson, J. (2019) 'Copper-64 PET imaging of the CXCR4 chemokine receptor using a cross-bridged cyclam bis-tetraazamacrocyclic antagonist', *J Nucl Med*, jnumed. 118.218008.
Burton, D. G. & Faragher, R. G. (2018) 'Obesity & type-2 diabetes as inducers of premature cellular senescence & ageing', *Biogerontology*, 19(6), 447-459.
Buskermolen, J. K., Roffel, S. & Gibbs, S. (2017) 'Stimulation of oral fibroblast chemokine receptors identifies CCR3 & CCR4 as potential wound healing targets', *J Cell Physiol*, 232(11), 2996-3005.
Bustin, S. A., Benes, V., Garson, J. A., Hellemans, J., Huggett, J., Kubista, M., Mueller, R., Nolan, T., Pfaffl, M. W. & Shipley, G. L. (2009) 'The MIQE guidelines: Minimum information for publication of quantitative real-time PCR experiments', *Clin Chem*, 55(4), 611-622.
Buysschaert, B., Byloos, B., Leys, N., Van Houdt, R. & Boon, N. (2016) 'Reevaluating multicolor flow cytometry to assess microbial viability', *App Microbiol Biotechnol*, 100(21), 9037-9051.
Bygrave, F. L. & Benedetti, A. (1996) 'What is the concentration of calcium ions in the endoplasmic reticulum?', *Cell Calcium*, 19(6), 547-551.
Byrne, C., Tainsky, M. & Fuchs, E. (1994) 'Programming gene expression in developing epidermis', *Development*, 120(9), 2369-2383.
Bünemann, E., Hoff, N.-P., Buhren, B. A., Wiesner, U., Meller, S., Bölke, E., Müller-Homey, A., Kubitza, R., Ruzicka, T. & Zlotnik, A. (2018) 'Chemokine ligand–receptor interactions critically regulate cutaneous wound healing', *Eur J Med Res*, 23(1), e4.
Caballero, A. R., Moreau, J. M., Engel, L. S., Marquart, M. E., Hill, J. M. & O'Callaghan, R. J. (2001) '*Pseudomonas aeruginosa* protease IV enzyme assays & comparison to other *Pseudomonas* proteases', *Anal Biochem*, 290(2), 330-337.
Cabral, W. A., Ishikawa, M., Garten, M., Makareeva, E. N., Sargent, B. M., Weis, M., Barnes, A. M., Webb, E. A., Shaw, N. J. & Ala-Kokko, L. (2016) 'Absence of the ER cation channel TMEM38B/TRIC-B disrupts intracellular calcium homeostasis & dysregulates collagen synthesis in recessive osteogenesis imperfecta', *PLoS Genet*, 12(7), e1006156.
Caggiati, A., Rosi, C., Casini, A., Cirenza, M., Petrozza, V., Acconcia, M. & Zamboni, P. (2010) 'Skin iron deposition characterises lipodermatosclerosis & leg ulcer', *Eur J Vasc Endovasc Surg*, 40(6), 777-782.
Cai, S., Fatherazi, S., Presland, R. B., Belton, C. M., Roberts, F. A., Goodwin, P. C., Schubert, M. M. & Izutsu, K. T. (2006) 'Evidence that TRPC1 contributes to calcium-induced differentiation of human keratinocytes', *Pflügers Archiv*, 452(1), 43-52.
Cairo, G., Recalcati, S., Mantovani, A. & Locati, M. (2011) 'Iron trafficking & metabolism in macrophages: Contribution to the polarized phenotype', *Trends Immunol*, 32(6), 241-247.
Cairo, G., Tacchini, L., Pogliaghi, G., Anzon, E., Tomasi, A. & Bernelli-Zazzera, A. (1995) 'Induction of ferritin synthesis by oxidative stress. Transcriptional & post-transcriptional regulation by expansion of the "free" iron pool', *J Biol Chem*, 270(2), 700-703.

Calcraft, P. J., Ruas, M., Pan, Z., Cheng, X., Arredouani, A., Hao, X., Tang, J., Rietdorf, K., Teboul, L. & Chuang, K.-T. (2009) 'NAADP mobilizes calcium from acidic organelles through two-pore channels', *Nature*, 459(7246), 596-600.
Caley, M. P., Martins, V. L. & O'Toole, E. A. (2015) 'Metalloproteinases & wound healing', *Adv Wound Care*, 4(4), 225-234.
Calvet, H. M. & Yoshikawa, T. T. (2001) 'Infections in diabetes', *Infect Dis Clin North Am*, 15(2), 407-421.
Camaschella, C., Roetto, A., Calì, A., De Gobbi, M., Garozzo, G., Carella, M., Majorano, N., Totaro, A. & Gasparini, P. (2000) 'The gene TFR2 is mutated in a new type of haemochromatosis mapping to 7q22', *Nat Genet*, 25(1), 14-15.
Campbell, L., Emmerson, E., Davies, F., Gilliver, S. C., Krust, A., Chambon, P., Ashcroft, G. S. & Hardman, M. J. (2010) 'Estrogen promotes cutaneous wound healing via estrogen receptor β independent of its antiinflammatory activities', *J Exp Med*, 207(9), 1825-1833.
Campbell, L., Saville, C. R., Murray, P. J., Cruickshank, S. M. & Hardman, M. J. (2013) 'Local arginase 1 activity is required for cutaneous wound healing', *J Invest Dermatol*, 133(10), 2461-2470.
Campisi, J. (2013) 'Aging, cellular senescence, & cancer', *Ann Rev Physiol*, 75, 685-705.
Campisi, J., Andersen, J. K., Kapahi, P. & Melov, S. 'Cellular senescence: A link between cancer & age-related degenerative disease?'. *Semin Cancer Biol*, 21(6), 354-359.
Campisi, J. & di Fagagna, F. d. A. (2007) 'Cellular senescence: When bad things happen to good cells', *Nat Rev Mol Cell Biol*, 8(9), 729-740.
Campisi, J. & Robert, L. (2014) 'Cell senescence: Role in aging & age-related diseases', *Interdiscip Top Gerontol*, 39, 45-61.
Canton, R., Manzanares, J., Alvarez, E. & Zaragoza, F. (1987) '*In vitro* & *in vivo* antiaggregant effects of magnesium halogenates', *Thromb Haemost*, 58(4), 957-959.
Cao, X., Choi, S., Maléth, J. J., Park, S., Ahuja, M. & Muallem, S. (2015) 'The ER/PM microdomain, PI (4, 5) P2 & the regulation of STIM1–Orai1 channel function', *Cell Calcium*, 58(4), 342-348.
Carafoli, E., Santella, L., Branca, D. & Brini, M. (2001) 'Generation, control, & processing of cellular calcium signals', *Crit Rev Biochem Mol Biol*, 36(2), 107-260.
Caramelo, J. J. & Parodi, A. J. (2008) 'Getting in & out from calnexin/calreticulin cycles', *J Biol Chem*, 283(16), 10221-10225.
Cardozo, A. K., Ortis, F., Storling, J., Feng, Y.-M., Rasschaert, J., Tonnesen, M., Van Eylen, F., Mandrup-Poulsen, T., Herchuelz, A. & Eizirik, D. L. (2005) 'Cytokines downregulate the sarcoendoplasmic reticulum pump Ca2+ ATPase 2b & deplete endoplasmic reticulum Ca2+, leading to induction of endoplasmic reticulum stress in pancreatic β-cells', *Diabetes*, 54(2), 452-461.
Caride, A., Filoteo, A., Penheiter, A., Paszty, K., Enyedi, A. & Penniston, J. (2001) 'Delayed activation of the plasma membrane calcium pump by asudden increase in Ca2+: Fast pumps reside in fast cells', *Cell Calcium*, 30(1), 49-57.
Carneiro, C. R., Postol, E., Nomizo, R., Reis, L. F. & Brentani, R. R. (2004) 'Identification of enolase as a laminin-binding protein on the surface of *Staphylococcus aureus*', *Microb Infect*, 6(6), 604-608.
Carrasco, S. & Meyer, T. (2011) 'STIM proteins & the endoplasmic reticulum-plasma membrane junctions', *Ann Rev Biochem*, 80, 973-1000.
Casco, M., Olsen, T., Herbst, A., Evans, G., Rothermel, T., Pruett, L., Simionescu, D., Visconti, R. & Alexis, F. (2017) 'Iron Oxide Nanoparticles Stimulates Extra-Cellular Matrix Production in Cellular Spheroids', *Bioengineering*, 4(1), e4.

Cash, J. L., Bass, M. D., Campbell, J., Barnes, M., Kubes, P. & Martin, P. (2014) 'Resolution mediator chemerin15 reprograms the wound microenvironment to promote repair & reduce scarring', *Curr Biol*, 24(12), 1406-1414.
Casilag, F., Lorenz, A., Krueger, J., Klawonn, F., Weiss, S. & Häussler, S. (2016) 'The LasB elastase of *Pseudomonas aeruginosa* acts in concert with alkaline protease AprA to prevent flagellin-mediated immune recognition', *Infect Immun*, 84(1), 162-171.
Castellanos-Gutiérrez, A., Sánchez-Pimienta, T. G., Carriquiry, A., da Costa, T. H. M. & Ariza, A. C. (2018) 'Higher dietary magnesium intake is associated with lower body mass index, waist circumference & serum glucose in Mexican adults', *Nutr J*, 17(1), e114.
Celli, A., Crumrine, D., Meyer, J. M. & Mauro, T. M. (2016) 'Endoplasmic reticulum calcium regulates epidermal barrier response & desmosomal structure', *J Invest Dermatol*, 136(9), 1840-1847.
Celli, A., Mackenzie, D., Crumrine, D., Tu, C., Hupe, M., Bikle, D., Elias, P. & Mauro, T. (2011) 'Endoplasmic reticulum Ca2+ depletion activates XBP1 & controls terminal differentiation in keratinocytes & epidermis', *Br J Dermatol*, 164(1), 16-25.
Chafetz, M. D. (1986) 'Timm's method modified for human tissue & compatible with adjacent section histofluorescence in the rat', *Brain Res Bull*, 16(1), 19-24.
Chakraborti, S., Chakraborti, T., Mandal, M., Mandal, A., Das, S. & Ghosh, S. (2002) 'Protective role of magnesium in cardiovascular diseases: A review', *Mol Cell Biochem*, 238(1-2), 163-179.
Chakravarti, B., Chattopadhyay, N. & Brown, E. M. (2012) 'Signaling through the extracellular calcium-sensing receptor (CaSR)', *Adv Exp Med Biol*, 740, 103-142.
Chakravarti, S., Magnuson, T., Lass, J. H., Jepsen, K. J., LaMantia, C. & Carroll, H. (1998) 'Lumican regulates collagen fibril assembly: Skin fragility & corneal opacity in the absence of lumican', *J Cell Biol*, 141(5), 1277-1286.
Chandra, T. & Narita, M. (2013) 'High-order chromatin structure & the epigenome in SAHFs', *Nucleus*, 4(1), 23-28.
Chang, J., Garva, R., Pickard, A., Yeung, C.-Y. C., Mallikarjun, V., Swift, J., Holmes, D. F., Calverley, B., Lu, Y. & Adamson, A. (2019) 'Circadian control of the secretory pathway is a central mechanism in tissue homeostasis', *BioRxiv*, e304014.
Chang, K. C., Wang, Y., Oh, I. G., Jenkins, S., Freedman, L. P., Thompson, C. C., Chung, J. H. & Nagpal, S. (2010) 'Estrogen receptor β is a novel therapeutic target for photoaging', *Mol Pharmacol*, 77(5), 744-750.
Chatterjee, M., Rath, D. & Gawaz, M. (2015) 'Role of chemokine receptors CXCR4 & CXCR7 for platelet function', *Biochem Soc Trans*, 43(4), 720-726.
Chaudhuri, D., Sancak, Y., Mootha, V. K. & Clapham, D. E. (2013) 'MCU encodes the pore conducting mitochondrial calcium currents', *Elife*, 2, e00704.
Chen, C., Krishnan, V., Macon, K., Manne, K., Narayana, S. V. & Schneewind, O. (2013) 'Secreted proteases control autolysin-mediated biofilm growth of *Staphylococcus aureus*', *J Biol Chem*, 288(41), 29440-29452.
Chen, F., Ni, B., Yang, Y. O., Ye, T. & Chen, A. (2014a) 'Knockout of TRPV6 causes osteopenia in mice by increasing osteoclastic differentiation & activity', *Cell Physiol Biochem*, 33(3), 796-809.
Chen, Q. X., Song, S. W., Chen, Q. H., Zeng, C. L., Zheng, X., Wang, J. L. & Fang, X. M. (2014b) 'Silencing airway epithelial cell-derived hepcidin exacerbates sepsis induced acute lung injury', *Crit Care*, 18(4), 470.
Chen, S.-r., Zhang, W.-p., Bao, J.-m., Cheng, Z.-b. & Yin, S. (2017) 'Aristoyunnolin H attenuates extracellular matrix secretion in cardiac fibroblasts by inhibiting calcium influx', *Arch Pharmacol Res*, 40(1), 122-130.

Chen, Y.-J., Lin, J.-K. & Lin-Shiau, S.-Y. (1999) 'Proliferation arrest & induction of CDK inhibitors p21 & p27 by depleting the calcium store in cultured C6 glioma cells', *Eur J Cell Biol*, 78(11), 824-831.
Childs, B. G., Baker, D. J., Kirkland, J. L., Campisi, J. & Van Deursen, J. M. (2014) 'Senescence & apoptosis: Dueling or complementary cell fates?', *EMBO Rep*, 15(11), 1139-1153.
Chlosta, S., Fishman, D. S., Harrington, L., Johnson, E. E., Knutson, M. D., Wessling-Resnick, M. & Cherayil, B. J. (2006) 'The iron efflux protein ferroportin regulates the intracellular growth of Salmonella enterica', *Infect Immun*, 74(5), 3065-3067.
Choe, C.-u. & Ehrlich, B. E. (2006) 'The inositol 1, 4, 5-trisphosphate receptor (IP3R) & its regulators: Sometimes good & sometimes bad teamwork', *Sci Signal*, 2006(363), re15.
Choudhury, A. R., Ju, Z., Djojosubroto, M. W., Schienke, A., Lechel, A., Schaetzlein, S., Jiang, H., Stepczynska, A., Wang, C. & Buer, J. (2007) 'Cdkn1a deletion improves stem cell function & lifespan of mice with dysfunctional telomeres without accelerating cancer formation', *Nat Med*, 39(1), 99-105.
Christensen, B. E. (1989) 'The role of extracellular polysaccharides in biofilms', *J Biotechnol*, 10(3-4), 181-202.
Chung, J. H., Yano, K., Lee, M. K., Youn, C. S., Seo, J. Y., Kim, K. H., Cho, K. H., Eun, H. C. & Detmar, M. (2002) 'Differential effects of photoaging vs intrinsic aging on the vascularization of human skin', *Arch Dermatol*, 138(11), 1437-1442.
Cissell, D. D., Link, J. M., Hu, J. C. & Athanasiou, K. A. (2017) 'A modified hydroxyproline assay based on hydrochloric acid in Ehrlich's solution accurately measures tissue collagen content', *Tissue Eng Part C Methods*, 23(4), 243-250.
Citro, A., Cantarelli, E. & Piemonti, L. (2015) 'The CXCR1/2 Pathway: Involvement in Diabetes Pathophysiology & Potential Target for T1D Interventions', *Curr Diabetes Rep*, 15(10), e68.
Clapham, D. E. (2007) 'Calcium signaling', *Cell*, 131(6), 1047-1058.
Clark, R., Ashcroft, G., Spencer, M. J., Larjava, H. & Ferguson, M. (1996) 'Re-epithelialization of normal human excisional wounds is associated with a switch from αvβ5 to αvβ6 integrins', *Br J Dermatol*, 135(1), 46-51.
Clausen, B. E. & Stoitzner, P. (2015) 'Functional Specialization of Skin Dendritic Cell Subsets in Regulating T Cell Responses', *Front Immunol*, 6, e534.
Clegg, D., Hevener, A. L., Moreau, K. L., Morselli, E., Criollo, A., Van Pelt, R. E. & Vieira-Potter, V. J. (2017) 'Sex hormones & cardiometabolic health: Role of estrogen & estrogen receptors', *Endocrinology*, 158(5), 1095-1105.
Clemens, R. A., Chong, J., Grimes, D., Hu, Y. & Lowell, C. A. (2017) 'STIM1 & STIM2 cooperatively regulate mouse neutrophil store-operated calcium entry & cytokine production', *Blood*, 130(13), 1565-1577.
Coffey, R. & Knutson, M. D. (2017) 'The plasma membrane metal-ion transporter ZIP14 contributes to nontransferrin-bound iron uptake by human β-cells', *Am J Physiol Cell Physiol*, 312(2), 169-175.
Cole, M. A., Quan, T., Voorhees, J. J. & Fisher, G. J. (2018) 'Extracellular matrix regulation of fibroblast function: Redefining our perspective on skin aging', *J Cell Commun Signal*, 12(1), 35-43.
Collado, M., Blasco, M. A. & Serrano, M. (2007) 'Cellular senescence in cancer & aging', *Cell*, 130(2), 223-233.
Coller, B. S. (2011) 'Historical perspective & future directions in platelet research', *J Thromb Haemost*, 9(1), 374-395.
Colombini, M. (2012) 'VDAC structure, selectivity, & dynamics', *Biochim Biophys Acta Biomembranes*, 1818(6), 1457-1465.

Connell, G. J., Danial, J. S. & Haastruthers, C. X. (2018) 'Evaluation of the iron regulatory protein-1 interactome', *Biometals*, 31(1), 139-146.
Cooksey, R. C., Jones, D., Gabrielsen, S., Huang, J., Simcox, J. A., Luo, B., Soesanto, Y., Rienhoff, H., Dale Abel, E. & McClain, D. A. (2010) 'Dietary iron restriction or iron chelation protects from diabetes & loss of β-cell function in the obese (*ob/ob* lep−/−) mouse', *Am J Physiol Endocrinol Metab*, 298(6), 1236-1243.
Coppé, J.-P., Desprez, P.-Y., Krtolica, A. & Campisi, J. (2010) 'The senescence-associated secretory phenotype: The dark side of tumor suppression', *Ann Rev Path Mech Dis*, 5, 99-118.
Coppé, J.-P., Kauser, K., Campisi, J. & Beauséjour, C. M. (2006) 'Secretion of vascular endothelial growth factor by primary human fibroblasts at senescence', *J Biol Chem*, 281(40), 29568-29574.
Coppé, J.-P., Patil, C. K., Rodier, F., Sun, Y., Muñoz, D. P., Goldstein, J., Nelson, P. S., Desprez, P.-Y. & Campisi, J. (2008) 'Senescence-associated secretory phenotypes reveal cell-nonautonomous functions of oncogenic RAS & the p53 tumor suppressor', *PLoS Biol*, 6(12), e301.
Coppé, J.-P., Rodier, F., Patil, C. K., Freund, A., Desprez, P.-Y. & Campisi, J. (2011) 'Tumor suppressor & aging biomarker p16INK4a induces cellular senescence without the associated inflammatory secretory phenotype', *J Biol Chem*, 286(42), 36396-36403.
Cordeiro, J. V. & Jacinto, A. (2013) 'The role of transcription-independent damage signals in the initiation of epithelial wound healing', *Nat Rev Mol Cell Biol*, 14(4), 249-262.
Core, A. B., Canali, S. & Babitt, J. L. (2014) 'Hemojuvelin & bone morphogenetic protein (BMP) signaling in iron homeostasis', *Front Pharmacol*, 5, e104.
Core Team (2019) 'R: A language and environment for statistical computing. R Foundation for Statistical Computing', Vienna, Austria. Available online: https://www.R-project.org/ [Accessed 30/8/19].
Corna, G., Campana, L., Pignatti, E., Castiglioni, A., Tagliafico, E., Bosurgi, L., Campanella, A., Brunelli, S., Manfredi, A. A. & Apostoli, P. (2010) 'Polarization dictates iron handling by inflammatory & alternatively activated macrophages', *Haematologica*, 95(11), 1814-1822.
Corradini, E., Garuti, C., Montosi, G., Ventura, P., Andriopoulos, B., Lin, H. Y., Pietrangelo, A. & Babitt, J. L. (2009) 'Bone morphogenetic protein signaling is impaired in an HFE knockout mouse model of hemochromatosis', *Gastroenterology*, 137(4), 1489-1497.
Coughlan, M. T., Yap, F. Y., Tong, D. C., Andrikopoulos, S., Gasser, A., Thallas-Bonke, V., Webster, D. E., Miyazaki, J.-i., Kay, T. W. & Slattery, R. M. (2011) 'Advanced glycation end products are direct modulators of β-cell function', *Diabetes*, 60(10), 2523-2532.
Coulombe, P. A. & Lee, C.-H. (2012) 'Defining keratin protein function in skin epithelia: Epidermolysis bullosa simplex & its aftermath', *J Invest Dermatol*, 132, 763-775.
Cozzi, A., Corsi, B., Levi, S., Santambrogio, P., Albertini, A. & Arosio, P. (2000) 'Overexpression of wild type & mutated human ferritin H-chain in HeLa cells *in vivo* role of ferritin ferroxidase activity', *J Biol Chem*, 275(33), 25122-25129.
Craven, P. A., Phillips, S. L., Melhem, M. F., Liachenko, J. & DeRubertis, F. R. (2001) 'Overexpression of manganese superoxide dismutase suppresses increases in collagen accumulation induced by culture of mesangial cells in high-media glucose', *Metab Clin Exp*, 50(9), 1043-1048.

Craven, P. A., Studer, R. K., Felder, J., Phillips, S. & DeRubertis, F. R. (1997) 'Nitric oxide inhibition of transforming growth factor-beta & collagen synthesis in mesangial cells', *Diabetes*, 46(4), 671-681.
Credé, C. (1881) 'The prevention of eye inflammation in the newborn', *Arch Gynecol Obstet*, 17, 50-53.
Csermely, P. & Somogyi, J. (1989) 'Zinc as a possible mediator of signal transduction in T lymphocytes', *Acta Physiol Hung*, 74(2), 195-199.
Csiszar, K. (2001) 'Lysyl oxidases: A novel multifunctional amine oxidase family', *Prog Nucleic Acid Res Mol Biol*, 70, 1-32.
Cullis, J. O. (2011) 'Diagnosis & management of anaemia of chronic disease: Current status', *Br J Haematol*, 154(3), 289-300.
Cumberbatch, M., Dearman, R. J., Griffiths, C. E. & Kimber, I. (2003) 'Epidermal Langerhans cell migration & sensitisation to chemical allergens', *Apmis*, 111(7-8), 797-804.
Cunha, M. T., Murça, M. A., Nigro, S., Klautau, G. B. & Salles, M. J. C. (2018) '*In vitro* antibacterial activity of bioactive glass S53P4 on multiresistant pathogens causing osteomyelitis & prosthetic joint infection', *BMC Infect Dis*, 18(1), e157.
Cunningham, G., Seghrouchni, K., Ruffieux, E., Vaudaux, P., Gayet-Ageron, A., Cherkaoui, A., Godinho, E., Lew, D., Hoffmeyer, P. & Uçkay, I. (2014) 'Gram & acridine orange staining for diagnosis of septic arthritis in different patient populations', *Int Orthop*, 38(6), 1283-1290.
D'Alessio, A., Esposito, B., Giampietri, C., Ziparo, E., Pober, J. S. & Filippini, A. (2012) 'Plasma membrane microdomains regulate TACE-dependent TNFR1 shedding in human endothelial cells', *J Cell Mol Med*, 16(3), 627-636.
D'Amour, P. (2012) 'Acute & chronic regulation of circulating PTH: Significance in health & in disease', *Clin Biochem*, 45(12), 964-969.
D'Orazio, J., Jarrett, S., Amaro-Ortiz, A. & Scott, T. (2013) 'UV radiation & the skin', *Int J Mol Sci*, 14(6), 12222-12248.
da Rocha-Azevedo, B., Ho, C.-H. & Grinnell, F. (2015) 'PDGF-stimulated dispersal of cell clusters & disruption of fibronectin matrix on three-dimensional collagen matrices requires matrix metalloproteinase-2', *Mol Biol Cell*, 26(6), 1098-1105.
Da Silva, J. F. & Williams, R. J. P. (2001) *The biological chemistry of the elements: the inorganic chemistry of life.* Oxford: Oxford University Press.
Daghighi, S., Sjollema, J., van der Mei, H. C., Busscher, H. J. & Rochford, E. T. (2013) 'Infection resistance of degradable versus non-degradable biomaterials: An assessment of the potential mechanisms', *Biomaterials*, 34(33), 8013-8017.
Dai, C., Guo, H., Lu, J., Shi, J., Wei, J. & Liu, C. (2011) 'Osteogenic evaluation of calcium/magnesium-doped mesoporous silica scaffold with incorporation of rhBMP-2 by synchrotron radiation-based μCT', *Biomaterials*, 32(33), 8506-8517.
Dai, Q., Huang, J., Klitzman, B., Dong, C., Goldschmidt-Clermont, P. J., March, K. L., Rokovich, J., Johnstone, B., Rebar, E. J. & Spratt, S. K. (2004) 'Engineered Zinc Finger–Activating Vascular Endothelial Growth Factor Transcription Factor Plasmid DNA Induces Therapeutic Angiogenesis in Rabbits With Hindlimb Ischemia', *Circulation*, 110(16), 2467-2475.
Dalton, T., Dowd, S. E., Wolcott, R. D., Sun, Y., Watters, C., Griswold, J. A. & Rumbaugh, K. P. (2011) 'An *in vivo* polymicrobial biofilm wound infection model to study interspecies interactions', *PloS One*, 6(11), e27317.
Damann, N., Owsianik, G., Li, S., Poll, C. & Nilius, B. (2009) 'The calcium-conducting ion channel transient receptor potential canonical 6 is involved in macrophage inflammatory protein-2-induced migration of mouse neutrophils', *Acta Physiol*, 195(1), 3-11.

Danielson, K. G., Baribault, H., Holmes, D. F., Graham, H., Kadler, K. E. & Iozzo, R. V. (1997) 'Targeted disruption of decorin leads to abnormal collagen fibril morphology & skin fragility', *J Cell Biol*, 136(3), 729-743.
Danscher, G. (1984) 'Autometallography', *Histochemistry*, 81(4), 331-335.
Danscher, G. & Stoltenberg, M. (2006) 'Silver enhancement of quantum dots resulting from (1) metabolism of toxic metals in animals & humans,(2) *in vivo*, *in vitro* & immersion created zinc–sulphur/zinc–selenium nanocrystals,(3) metal ions liberated from metal implants & particles', *Prog Histochem Cyto*, 41(2), 57-139.
Das, A., Sinha, M., Datta, S., Abas, M., Chaffee, S., Sen, C. K. & Roy, S. (2015) 'Monocyte & macrophage plasticity in tissue repair & regeneration', *Am J Pathol*, 185(10), 2596-2606.
Das, A., Sudhahar, V., Chen, G.-F., Kim, H. W., Youn, S.-W., Finney, L., Vogt, S., Yang, J., Kweon, J. & Surenkhuu, B. (2016) 'Endothelial antioxidant-1: A key mediator of copper-dependent wound healing *in vivo*', *Sci Rep*, 6, e33783.
David, J. R. (1966) 'Delayed hypersensitivity *in vitro*: Its mediation by cell-free substances formed by lymphoid cell-antigen interaction', *Proc Nat Acad Sci*, 56(1), 72-77.
Davidson, J. M. (1998) 'Animal models for wound repair', *Arch Dermatol Res*, 290 (1), 1-11.
Diaz de Barboza, G. D., Guizzardi, S. & de Talamoni, N. T. (2015) 'Molecular aspects of intestinal calcium absorption', *World J Gastroenterol*, 21(23), 7142-7154.
DE MEDINA, J. B. (1922) 'Silver arsphenamin in the treatment of syphilis', *Arch Dermatol Syphilol*, 5(3), 321-324.
De Stefani, D., Raffaello, A., Teardo, E., Szabò, I. & Rizzuto, R. (2011) 'A forty-kilodalton protein of the inner membrane is the mitochondrial calcium uniporter', *Nature*, 476(7360), 336-340.
De Stefani, D. & Rizzuto, R. (2014) 'Molecular control of mitochondrial calcium uptake', *Biochem Biophys Res Commun*, 449(4), 373-376.
Debacq-Chainiaux, F., Ameur, R. B., Bauwens, E., Dumortier, E., Toutfaire, M. & Toussaint, O. (2016) 'Stress-induced (premature) senescence', In: Rattan S. & Hayflick L. (eds) *Cellular ageing & replicative senescence*. Berlin: Springer, 243-262.
Debacq-Chainiaux, F., Erusalimsky, J. D., Campisi, J. & Toussaint, O. (2009) 'Protocols to detect senescence-associated beta-galactosidase (SA-βgal) activity, a biomarker of senescent cells in culture & *in vivo*', *Nat Prot*, 4(12), 1798-1806.
Debeer, S., Le Luduec, J.-B., Kaiserlian, D., Laurent, P., Nicolas, J.-F., Dubois, B. & Kanitakis, J. (2013) 'Comparative histology & immunohistochemistry of porcine versus human skin', *Eur J Dermatol*, 23(4), 456-466.
Defloor, T. (1999) 'The risk of pressure sores: A conceptual scheme', *J Clin Nurs*, 8(2), 206-216.
Del-Castillo-Rueda, A., Moreno-Carralero, M. I., Cuadrado-Grande, N., Alvarez-Sala-Walther, L. A., Enríquez-de-Salamanca, R., Méndez, M. & Morán-Jiménez, M. J. (2012) 'Mutations in the HFE, TFR2, & SLC40A1 genes in patients with hemochromatosis', *Gene*, 508(1), 15-20.
DeLeon, S., Clinton, A., Fowler, H., Everett, J., Horswill, A. R. & Rumbaugh, K. P. (2014) 'Synergistic interactions of *Pseudomonas aeruginosa* & *Staphylococcus aureus* in an *in vitro* wound model', *Infect Immun*, 82(11), 4718-4728.
DeLuca, H. F. & Engstrom, G. (1961) 'Calcium uptake by rat kidney mitochondria', *Proc Nat Acad Sci*, 47(11), 1744-1750.
Demaria, M., Ohtani, N., Youssef, S. A., Rodier, F., Toussaint, W., Mitchell, J. R., Laberge, R.-M., Vijg, J., Van Steeg, H. & Dollé, M. E. (2014) 'An essential role for

senescent cells in optimal wound healing through secretion of PDGF-AA', *Dev Cell*, 31(6), 722-733.
Demidova-Rice, T. N., Hamblin, M. R. & Herman, I. M. (2012) 'Acute & impaired wound healing: Pathophysiology & current methods for drug delivery, part 2: Role of growth factors in normal & pathological wound healing: Therapeutic potential & methods of delivery', *Adv Skin Wound Care*, 25(8), 349-370.
Dengler, V., Meier, P. S., Heusser, R., Berger-Bächi, B. & McCallum, N. (2011) 'Induction kinetics of the *Staphylococcus aureus* cell wall stress stimulon in response to different cell wall active antibiotics', *BMC Microbiol*, 11, 16.
Denney, H., Clench, M. R. & Woodroofe, M. N. (2009) 'Cleavage of chemokines CCL2 & CXCL10 by matrix metalloproteinases-2 & -9: Implications for chemotaxis', *Biochem Biophys Res Commun*, 382(2), 341-347.
Detwiler, T. C., Charo, I. & Feinman, R. (1978) 'Evidence that calcium regulates platelet function', *Thromb Haemost*, 40(2), 207-211.
Devalaraja, R. M., Nanney, L. B., Qian, Q., Du, J., Yu, Y., Devalaraja, M. N. & Richmond, A. (2000) 'Delayed wound healing in CXCR2 knockout mice', *J Invest Dermatol*, 115(2), 234-244.
Devy, J., Duca, L., Cantarelli, B., Joseph-Pietras, D., Scandolera, A., Rusciani, A., Parent, L., Thevenard, J., Pasco, S. B., Tarpin, M., Martiny, L. & Debelle, L. (2010) 'Elastin-derived peptides enhance melanoma growth *in vivo* by upregulating the activation of Mcol-A (MMP-1) collagenase', *Br J Cancer*, 103(10), 1562-1570.
DeWitt, L. M. (1918) 'The use of Gold Salts in the Treatment of Experimental Tuberculosis in Guinea-Pigs: XVIII. Studies on the Biochemistry & Chemotherapy of Tuberculosis', *J Infect Dis*, 426-437.
Di Capite, J., Ng, S. W. & Parekh, A. B. (2009) 'Decoding of cytoplasmic Ca2+ oscillations through the spatial signature drives gene expression', *Curr Biol*, 19(10), 853-858.
Di Micco, R., Fumagalli, M., Cicalese, A., Piccinin, S., Gasparini, P., Luise, C., Schurra, C., Nuciforo, P. G., Bensimon, A. & Maestro, R. (2006) 'Oncogene-induced senescence is a DNA damage response triggered by DNA hyper-replication', *Nature*, 444(7119), 638-642.
Diegelmann, R. F. & Evans, M. C. (2004) 'Wound healing: An overview of acute, fibrotic & delayed healing', *Front Biosci*, 9(1), 283-289.
Dieu-Nosjean, M.-C., Massacrier, C., Homey, B., Vanbervliet, B., Pin, J.-J., Vicari, A., Lebecque, S., Dezutter-Dambuyant, C., Schmitt, D. & Zlotnik, A. (2000) 'Macrophage inflammatory protein 3α is expressed at inflamed epithelial surfaces & is the most potent chemokine known in attracting Langerhans cell precursors', *J Exp Med*, 192(5), 705-718.
Dikovskaya, D., Cole, J. J., Mason, S. M., Nixon, C., Karim, S. A., McGarry, L., Clark, W., Hewitt, R. N., Sammons, M. A. & Zhu, J. (2015) 'Mitotic stress is an integral part of the oncogene-induced senescence program that promotes multinucleation & cell cycle arrest', *Cell Rep*, 12(9), 1483-1496.
DiMeglio, L. A. & Imel, E. A. (2019) 'Calcium & phosphate: Hormonal regulation & metabolism', In: *Basic & applied bone biology*. Elsevier, 257-282.
Dimiza, F., Perdih, F., Tangoulis, V., Turel, I., Kessissoglou, D. P. & Psomas, G. (2011) 'Interaction of copper (II) with the non-steroidal anti-inflammatory drugs naproxen & diclofenac: Synthesis, structure, DNA-& albumin-binding', *J Inorg Biochem*, 105(3), 476-489.
Dimova, D. K. & Dyson, N. J. (2005) 'The E2F transcriptional network: Old acquaintances with new faces', *Oncogene*, 24(17), 2810-2826.

Dimri, G. P., Lee, X., Basile, G., Acosta, M., Scott, G., Roskelley, C., Medrano, E. E., Linskens, M., Rubelj, I. & Pereira-Smith, O. (1995) 'A biomarker that identifies senescent human cells in culture & in aging skin *in vivo*', *Proc Nat Acad Sci*, 92(20), 9363-9367.
Dixon, S. J. & Stockwell, B. R. (2014) 'The role of iron & reactive oxygen species in cell death', *Nat Chem Biol*, 10(1), 9-17.
Dlouhy, A. C. & Outten, C. E. (2013) 'The iron metallome in eukaryotic organisms', *Met Ions Life Sci*, 12, 241-278.
Dogra, S. & Rai, R. (2014) 'Venous leg ulcer: Topical treatment, dressings & surgical debridement', *Ind Dermatol Online J*, 5(3), 371-373.
Doherty, T. M., Detrano, R. C., Mautner, S. L., Mautner, G. C. & Shavelle, R. M. (1999) 'Coronary calcium: The good, the bad, & the uncertain', *Am Heart J*, 137(5), 806-814.
Doi, S., Zou, Y., Togao, O., Pastor, J. V., John, G. B., Wang, L., Shiizaki, K., Gotschall, R., Schiavi, S. & Yorioka, N. (2011) 'Klotho inhibits transforming growth factor-β1 (TGF-β1) signaling & suppresses renal fibrosis & cancer metastasis in mice', *J Biol Chem*, 286(10), 8655-8665.
Dong, J. & Qin, L. (2012) 'Dietary calcium intake & risk of type 2 diabetes: Possible confounding by magnesium', *Eur J Clin Nutr*, 66(3), 408-410.
Dong, Y.-H. & Zhang, L.-H. (2005) 'Quorum sensing & quorum-quenching enzymes', *J Microbiol*, 43(1), 101-109.
Dongiovanni, P., Lanti, C., Gatti, S., Rametta, R., Recalcati, S., Maggioni, M., Fracanzani, A. L., Riso, P., Cairo, G. & Fargion, S. (2015) 'High fat diet subverts hepatocellular iron uptake determining dysmetabolic iron overload', *PloS One*, 10(2), e0116855.
Donlin, L. T., Jayatilleke, A., Giannopoulou, E. G., Kalliolias, G. D. & Ivashkiv, L. B. (2014) 'Modulation of TNF-induced macrophage polarization by synovial fibroblasts', *J Immunol*, 193(5), 2373-2383.
Donovan, A., Lima, C. A., Pinkus, J. L., Pinkus, G. S., Zon, L. I., Robine, S. & Andrews, N. C. (2005) 'The iron exporter ferroportin/Slc40a1 is essential for iron homeostasis', *Cell Metab*, 1(3), 191-200.
Dorsett-Martin, W. A. (2004) 'Rat models of skin wound healing: A review', *Wound Repair Regen*, 12(6), 591-599.
Dow, G., Browne, A. & Sibbald, R. (1999) 'Infection in chronic wounds: Controversies in diagnosis & treatment', *Ostomy Wound Manage*, 45(8), 23-27.
Doyle, J. W., Roth, T. P., Smith, R. M., Li, Y. Q. & Dunn, R. M. (1996) 'Effect of calcium alginate on cellular wound healing processes modeled *in vitro*', *J Biomed Mater Res*, 32(4), 561-568.
Drago, L., Vassena, C., Fenu, S., De Vecchi, E., Signori, V., De Francesco, R. & Romanò, C. L. (2014) '*In vitro* antibiofilm activity of bioactive glass S53P4', *Future Microbiol*, 9(5), 593-601.
Drakesmith, H., Nemeth, E. & Ganz, T. (2015) 'Ironing out ferroportin', *Cell Metab*, 22(5), 777-787.
Driskell, I., Oeztuerk-Winder, F., Humphreys, P. & Frye, M. (2015) 'Genetically induced cell death in bulge stem cells reveals their redundancy for hair & epidermal regeneration', *Stem Cells*, 33(3), 988-998.
Driskell, R. R., Lichtenberger, B. M., Hoste, E., Kretzschmar, K., Simons, B. D., Charalambous, M., Ferron, S. R., Herault, Y., Pavlovic, G. & Ferguson-Smith, A. C. (2013) 'Distinct fibroblast lineages determine dermal architecture in skin development & repair', *Nature*, 504(7479), 277-281.
Du, R. L., Chang, J., Ni, S. Y., Zhai, W. Y. & Wang, J. Y. (2006) 'Characterization & *in vitro* bioactivity of zinc-containing bioactive glass & glass-ceramics', *J Biomater Appl*, 20(4), 341-360.

Duan, J., Duan, J., Zhang, Z. & Tong, T. (2005) 'Irreversible cellular senescence induced by prolonged exposure to H2O2 involves DNA-damage-&-repair genes & telomere shortening', *Int J Biochem Cell Biol*, 37(7), 1407-1420.
Duan, X., Peng, D., Zhang, Y., Huang, Y., Liu, X., Li, R., Zhou, X. & Liu, J. (2018) 'Sub-cytotoxic concentrations of ionic silver promote the proliferation of human keratinocytes by inducing the production of reactive oxygen species', *Front Med*, 12(3), 289-300.
Duca, L., Floquet, N., Alix, A. J., Haye, B. & Debelle, L. (2004) 'Elastin as a matrikine', *Crit Rev Oncol Hematol*, 49(3), 235-244.
Dulkys, Y., Buschermöhle, T., Escher, S. E., Kapp, A. & Elsner, J. (2004) 'T-helper 2 cytokines attenuate senescent eosinophil activation by the CXCR4 ligand stromal-derived factor-1alpha (CXCL12)', *Clin Exp Allergy*, 34(10), 1610-1620.
Dungan, C., Kosmac, K., Peck, B., McCarthy, J. & Peterson, C. (2017) 'p16 & γH2AX as markers of cellular senescence in young & old human skeletal muscle', *FASEB J*, 31(Supp), S713.9.
Dupont, J. & Scholten, J. D. (2010) 'On the structural & surface properties of transition-metal nanoparticles in ionic liquids', *Chem Soc Rev*, 39(5), 1780-1804.
Duscher, D., Januszyk, M., Maan, Z. N., Whittam, A. J., Hu, M. S., Walmsley, G. G., Dong, Y., Khong, S. M., Longaker, M. T. & Gurtner, G. C. (2017) 'Comparison of the Hydroxylase Inhibitor DMOG & the Iron Chelator Deferoxamine in Diabetic & Aged Wound Healing', *Plast Reconstr Surg*, 139(3), 695-706.
Dyer, D. P., Salanga, C. L., Johns, S. C., Valdambrini, E., Fuster, M. M., Milner, C. M., Day, A. J. & Handel, T. M. (2016) 'The Anti-inflammatory Protein TSG-6 Regulates Chemokine Function by Inhibiting Chemokine/Glycosaminoglycan Interactions', *J Biol Chem*, 291(24), 12627-12640.
Dyson, M. (1997) 'Advances in wound healing physiology: The comparative perspective', *Vet Dermatol*, 8(4), 227-233.
Eckert, R. L. (1989) 'Structure, function, & differentiation of the keratinocyte', *Physiol Rev*, 69(4), 1316-1346.
Eckert, R. L. & Rorke, E. A. (1989) 'Molecular biology of keratinocyte differentiation', *Environ Health Perspect*, 80, 109-116.
Edsberg, L. E., Wyffels, J. T., Brogan, M. S. & Fries, K. M. (2012) 'Analysis of the proteomic profile of chronic pressure ulcers', *Wound Repair Regen*, 20(3), 378-401.
Eisenstein, R. S. (2000) 'Iron regulatory proteins & the molecular control of mammalian iron metabolism', *Ann Rev Nutr*, 20(1), 627-662.
El Zoeiby, A., Sanschagrin, F., Havugimana, P. C., Garnier, A. & Levesque, R. C. (2001) '*In vitro* reconstruction of the biosynthetic pathway of peptidoglycan cytoplasmic precursor in *Pseudomonas aeruginosa*', *FEMS Microbiol Lett*, 201(2), 229-235.
Elaïb, Z., Adam, F., Berrou, E., Bordet, J.-C., Prévost, N., Bobe, R., Bryckaert, M. & Rosa, J.-P. (2016) 'Full activation of mouse platelets requires ADP secretion regulated by SERCA3 ATPase–dependent calcium stores', *Blood*, 128(8), 1129-1138.
ELDerawi, W. A., Naser, I. A., Taleb, M. H. & Abutair, A. S. (2018) 'The effects of oral magnesium supplementation on glycemic response among type 2 diabetes patients', *Nutrients*, 11(1), e44.
Elias, P. M. (2004) 'The epidermal permeability barrier: From the early days at Harvard to emerging concepts', *J Invest Dermatol*, 122(2), xxxvi-xxxix.
Elias, P. M., Ahn, S. K., Brown, B. E., Crumrine, D. & Feingold, K. R. (2002) 'Origin of the epidermal calcium gradient: Regulation by barrier status & role of active vs passive mechanisms', *J Invest Dermatol*, 119(6), 1269-1274.

Elsholz, F., Harteneck, C., Muller, W. & Friedland, K. (2014) 'Calcium-a central regulator of keratinocyte differentiation in health & disease', *Eur J Dermatol*, 24(6), 650-661.
Elzi, D. J., Lai, Y., Song, M., Hakala, K., Weintraub, S. T. & Shiio, Y. (2012) 'Plasminogen activator inhibitor 1-insulin-like growth factor binding protein 3 cascade regulates stress-induced senescence', *Proc Nat Acad Sci*, 109(30), 12052-12057.
El-Domyati, M., Attia, S., Saleh, F., Brown, D., Birk, D., Gasparro, F., Ahmad, H. & Uitto, J. (2002) 'Intrinsic aging vs. photoaging: A comparative histopathological, immunohistochemical, & ultrastructural study of skin', *Exp Dermatol*, 11(5), 398-405.
Eming, S. A., Krieg, T. & Davidson, J. M. (2007) 'Inflammation in wound repair: Molecular & cellular mechanisms', *J Invest Dermatol*, 127(3), 514-525.
Emkey, R. D. & Emkey, G. R. (2012) 'Calcium metabolism & correcting calcium deficiencies', *Endocrinol Metab Clin North Am*, 41(3), 527-556.
Emmerson, E. & Hardman, M. J. (2012) 'The role of estrogen deficiency in skin ageing & wound healing', *Biogerontology*, 13(1), 3-20.
Emri, E., Miko, E., Bai, P., Boros, G., Nagy, G., Rózsa, D., Juhász, T., Hegedűs, C., Horkay, I., Remenyik, É. & Emri, G. (2015) 'Effects of non-toxic zinc exposure on human epidermal keratinocytes', *Metallomics*, 7(3), 499-507.
Engel, L. S., Hobden, J. A., Moreau, J. M., Callegan, M. C., Hill, J. M. & O'Callaghan, R. J. (1997) '*Pseudomonas* deficient in protease IV has significantly reduced corneal virulence', *Investig Ophthalmol Vis Sci*, 38(8), 1535-1542.
Epstein, P. N., Overbeek, P. A. & Means, A. R. (1989) 'Calmodulin-induced early-onset diabetes in transgenic mice', *Cell*, 58(6), 1067-1073.
Epstein, P. N., Ribar, T. J., Decker, G. L., Yaney, G. & Means, A. (1992) 'Elevated beta-cell calmodulin produces a unique insulin secretory defect in transgenic mice', *Endocrinology*, 130(3), 1387-1393.
Erben, R. G. & Andrukhova, O. (2017) 'FGF23-Klotho signaling axis in the kidney', *Bone*, 100, 62-68.
Erusalimsky, J. D. & Kurz, D. J. (2005) 'Cellular senescence *in vivo*: Its relevance in ageing & cardiovascular disease', *Exp Gerontol*, 40(8-9), 634-642.
Eshed, I., Elis, A. & Lishner, M. (2001) 'Plasma ferritin & type 2 diabetes mellitus: A critical review', *Endocr Res*, 27(1-2), 91-97.
Evans, P., Elahi, S., Lee, K. & Fairman, B. (2003) 'A rapid & accurate method for the determination of plutonium in food using magnetic sector ICP-MS with an ultra-sonic nebuliser & ion chromatography', *J Environ Monitor*, 5(1), 175-179.
Fairley, J. A., Marcelo, C. L., Hogan, V. A. & Voorhees, J. J. (1985) 'Increased calmodulin levels in psoriasis & low Ca++ regulated mouse epidermal keratinocyte cultures', *J Invest Dermatol*, 84(3), 195-198.
Fan, Y., Liu, W., Bi, R., Densmore, M. J., Sato, T., Mannstadt, M., Yuan, Q., Zhou, X., Olauson, H. & Larsson, T. E. (2018) 'Interrelated role of Klotho & calcium-sensing receptor in parathyroid hormone synthesis & parathyroid hyperplasia', *Proc Nat Acad Sci*, 115(16), 3749-3758.
Fang, M., Wang, J., Li, S. & Guo, Y. (2016) 'Advanced glycation end-products accelerate the cardiac aging process through the receptor for advanced glycation end-products/transforming growth factor-β-Smad signaling pathway in cardiac fibroblasts', *Geriatr Gerontol Int*, 16(4), 522-527.
Farage, M. A., Miller, K. W., Elsner, P. & Maibach, H. I. (2008) 'Intrinsic & extrinsic factors in skin ageing: A review', *Int J Cosmet Sci*, 30(2), 87-95.

Farfariello, V., Iamshanova, O., Germain, E., Fliniaux, I. & Prevarskaya, N. (2015) 'Calcium homeostasis in cancer: A focus on senescence', *Biochimi Biophys Acta Mol Cell Res*, 1853(9), 1974-1979.
Farsam, V., Basu, A., Gatzka, M., Treiber, N., Schneider, L. A., Mulaw, M. A., Lucas, T., Kochanek, S., Dummer, R., Levesque, M. P., Wlaschek, M. & Scharffetter-Kochanek, K. (2016) 'Senescent fibroblast-derived Chemerin promotes squamous cell carcinoma migration', *Oncotarget*, 7(50), 83554-83569.
Fathke, C., Wilson, L., Shah, K., Kim, B., Hocking, A., Moon, R. & Isik, F. (2006) 'Wnt signaling induces epithelial differentiation during cutaneous wound healing', *BMC Cell Biol*, 7(1), e4.
Faury, G., Usson, Y., Robert-Nicoud, M., Robert, L. & Verdetti, J. (1998) 'Nuclear & cytoplasmic free calcium level changes induced by elastin peptides in human endothelial cells', *Proc Natl Acad Sci*, 95(6), 2967-2972.
Fearnley, C. J., Roderick, H. L. & Bootman, M. D. (2011) 'Calcium signaling in cardiac myocytes', *CSH Perspect Biol*, 3(11), a004242.
Feingold, K. R. & Denda, M. (2012) 'Regulation of permeability barrier homeostasis', *Clin Dermatol*, 30(3), 263-268.
Feldman, A., Aigner, E., Weghuber, D. & Paulmichl, K. (2015) 'The potential role of iron & copper in pediatric obesity & nonalcoholic fatty liver disease', *BioMed Res Int*, e287401.
Feldmeyer, L., Keller, M., Niklaus, G., Hohl, D., Werner, S. & Beer, H.-D. (2007) 'The inflammasome mediates UVB-induced activation & secretion of interleukin-1β by keratinocytes', *Curr Biol*, 17(13), 1140-1145.
Fernandez-Velasco, M., Ruiz-Hurtado, G., Gomez, A. M. & Rueda, A. (2014) 'Ca2+ handling alterations & vascular dysfunction in diabetes', *Cell Calcium*, 56(5), 397-407.
Fernyhough, P. & Calcutt, N. A. (2010) 'Abnormal calcium homeostasis in peripheral neuropathies', *Cell Calcium*, 47(2), 130-139.
Fernández-Cao, J. C., Warthon-Medina, M., H Moran, V., Arija, V., Doepking, C., Serra-Majem, L. & Lowe, N. M. (2019) 'Zinc intake & status & risk of type 2 diabetes mellitus: A systematic review & meta-analysis', *Nutrients*, 11(5), e1027.
Fernández-Real, J. M., López-Bermejo, A. & Ricart, W. (2002) 'Cross-talk between iron metabolism & diabetes', *Diabetes*, 51(8), 2348-2354.
Ferrante, C. J. & Leibovich, S. J. (2012) 'Regulation of macrophage polarization & wound healing', *Adv Wound Care*, 1(1), 10-16.
Ferrè, S., Baldoli, E., Leidi, M. & Maier, J. A. (2010) 'Magnesium deficiency promotes a pro-atherogenic phenotype in cultured human endothelial cells via activation of NFkB', *Biochim Biophys Acta Mol Basis Dis*, 1802(11), 952-958.
Festa, M., Ricciardelli, G., Mele, G., Pietropaolo, C., Ruffo, A. & Colonna, A. (2000) 'Overexpression of H ferritin & up-regulation of iron regulatory protein genes during differentiation of 3T3-L1 pre-adipocytes', *J Biol Chem*, 275(47), 36708-36712.
Festa, R. A. & Thiele, D. J. (2011) 'Copper: An essential metal in biology', *Curr Biol*, 21(21), 877-883.
Fields, G. B. (2013) 'Interstitial collagen catabolism', *J Biol Chem*, 288(14), 8785-8793.
Fill, M. & Copello, J. A. (2002) 'Ryanodine receptor calcium release channels', *Physiol Rev*, 82(4), 893-922.
Finazzi, D. & Arosio, P. (2014) 'Biology of ferritin in mammals: An update on iron storage, oxidative damage & neurodegeneration', *Arch Toxicol*, 88(10), 1787-1802.

Finberg, K. E., Heeney, M. M., Campagna, D. R., Aydinok, Y., Pearson, H. A., Hartman, K. R., Mayo, M. M., Samuel, S. M., Strouse, J. J., Markianos, K., Andrews, N. C. & Fleming, M. D. (2008) 'Mutations in TMPRSS6 cause iron-refractory iron deficiency anemia (IRIDA)', *Nat Genet*, 40(5), 569-571.
Fine, J. D., Hall, M., Weiner, M., Li, K. P. & Suchindran, C. (2008) 'The risk of cardiomyopathy in inherited epidermolysis bullosa', *Br J Dermatol*, 159(3), 677-682.
Finn, A. V., Nakano, M., Polavarapu, R., Karmali, V., Saeed, O., Zhao, X., Yazdani, S., Otsuka, F., Davis, T. & Habib, A. (2012) 'Hemoglobin directs macrophage differentiation & prevents foam cell formation in human atherosclerotic plaques', *J Am Coll Cardiol*, 59(2), 166-177.
Fitzner, B., Müller, S., Walther, M., Fischer, M., Engelmann, R., Müller-Hilke, B., Pützer, B. M., Kreutzer, M., Nizze, H. & Jaster, R. (2012) 'Senescence determines the fate of activated rat pancreatic stellate cells', *J Cell Mol Med*, 16(11), 2620-2630.
Fleming, D., Chahin, L. & Rumbaugh, K. (2017) 'Glycoside hydrolases degrade polymicrobial bacterial biofilms in wounds', *Antimicrob Agent Chemother*, 61(2), e01998-16.
Fleming, R. E., Feng, Q. & Britton, R. S. (2011) 'Knockout mouse models of iron homeostasis', *Ann Rev Nutr*, 31, 117-137.
Flemming, H.-C. & Wingender, J. (2010) 'The biofilm matrix', *Nat Rev Microbiol*, 8(9), 623-633.
Flemming, H.-C., Wingender, J., Szewzyk, U., Steinberg, P., Rice, S. A. & Kjelleberg, S. (2016) 'Biofilms: An emergent form of bacterial life', *Nat Rev Microbiol*, 14(9), 563-575.
Floege, J. (2015) 'Magnesium in CKD: More than a calcification inhibitor?', *J Nephrol*, 28(3), 269-277.
Fonder, M. A., Lazarus, G. S., Cowan, D. A., Aronson-Cook, B., Kohli, A. R. & Mamelak, A. J. (2008) 'Treating the chronic wound: A practical approach to the care of nonhealing wounds & wound care dressings', *J Am Acad Dermatol*, 58(2), 185-206.
Fontao, L., Stutzmann, J., Gendry, P. & Launay, J. (1999) 'Regulation of the type II hemidesmosomal plaque assembly in intestinal epithelial cells', *Exp Cell Res*, 250(2), 298-312.
Ford, E. S. & Cogswell, M. E. (1999) 'Diabetes & serum ferritin concentration among U.S. adults', *Diabetes Care*, 22(12), 1978-1983.
Forouhi, N., Harding, A., Allison, M., Sandhu, M., Welch, A., Luben, R., Bingham, S., Khaw, K. & Wareham, N. (2007) 'Elevated serum ferritin levels predict new-onset type 2 diabetes: Results from the EPIC-Norfolk prospective study', *Diabetologia*, 50(5), 949-956.
Foskett, J. K. & Philipson, B. (2015) 'The mitochondrial Ca2+ uniporter complex', *J Mol Cell Cardiol*, 78, 3-8.
Foskett, J. K., White, C., Cheung, K.-H. & Mak, D.-O. D. (2007) 'Inositol trisphosphate receptor Ca2+ release channels', *Physiol Rev*, 87(2), 593-658.
Foulcer, S. J., Day, A. J. & Apte, S. S. (2015) 'Isolation & purification of versican & analysis of versican proteolysis', *Methods Mol Biol*, 1229, 587-604.
Foulston, L., Elsholz, A. K., DeFrancesco, A. S. & Losick, R. (2014) 'The extracellular matrix of *Staphylococcus aureus* biofilms comprises cytoplasmic proteins that associate with the cell surface in response to decreasing pH', *MBio*, 5(5), e01667-14.
Fox, J. & Weisberg, S. (2011) 'Multivariate linear models in R'. Available online: http://staff.ustc.edu.cn/~zwp/teach/MVA/Appendix-Multivariate-Linear-Models.pdf [Accessed 30/8/19].

Franke, S., Grass, G., Rensing, C. & Nies, D. H. (2003) 'Molecular analysis of the copper-transporting efflux system CusCFBA of *Escherichia coli*', *J Bacteriol*, 185(13), 3804-3812.
Frantz, C., Stewart, K. M. & Weaver, V. M. (2010) 'The extracellular matrix at a glance', *J Cell Sci*, 123(24), 4195-4200.
Freinkel, R. K. & Woodley, D. T. (2001) *The biology of the skin.* Carnforth: The Parthenon Publishing Group.
Freund, A., Orjalo, A. V., Desprez, P.-Y. & Campisi, J. (2010) 'Inflammatory networks during cellular senescence: Causes & consequences', *Trends Mol Med*, 16(5), 238-246.
Frey, P. A. & Reed, G. H. (2012) 'The ubiquity of iron', *ACS Chem Biol*, 7(9), 1477-1481.
Fric, J., Lim, C. X., Mertes, A., Lee, B. T., Viganò, E., Chen, J., Zolezzi, F., Poidinger, M., Larbi, A. & Strobl, H. (2014) 'Calcium & calcineurin-NFAT signaling regulate granulocyte-monocyte progenitor cell cycle via Flt3-L', *Stem Cells*, 32(12), 3232-3244.
Frykberg, R. G. & Banks, J. (2015) 'Challenges in the Treatment of Chronic Wounds', *Adv Wound Care*, 4(9), 560-582.
Fréchette, J.-P., Martineau, I. & Gagnon, G. (2005) 'Platelet-rich plasmas: Growth factor content & roles in wound healing', *J Dent Res*, 84(5), 434-439.
Fu, Q., Rahaman, M. N., Bal, B. S., Kuroki, K. & Brown, R. F. (2010) '*In vivo* evaluation of 13-93 bioactive glass scaffolds with trabecular & oriented microstructures in a subcutaneous rat implantation model', *J Biomed Mater Res A*, 95(1), 235-244.
Fu, S., Yalcin, A., Lee, G. Y., Li, P., Fan, J., Arruda, A. P., Pers, B. M., Yilmaz, M., Eguchi, K. & Hotamisligil, G. S. (2015) 'Phenotypic assays identify azoramide as a small-molecule modulator of the unfolded protein response with antidiabetic activity', *Sci Trans Med*, 7(292), e292ra98.
Fuente-Martín, E., Argente-Arizón, P., Ros, P., Argente, J. & Chowen, J. A. (2013) 'Sex differences in adipose tissue: It is not only a question of quantity & distribution', *Adipocyte*, 2(3), 128-134.
Fujimaki, Y., Shimoyama, T., Liu, Q., Umeda, T., Nakaji, S. & Sugawara, K. (2003) 'Low-level laser irradiation attenuates production of reactive oxygen species by human neutrophils', *J Clin Laser Med Surg*, 21(3), 165-170.
Fukai, T. & Ushio-Fukai, M. (2011) 'Superoxide dismutases: Role in redox signaling, vascular function, & diseases', *Antioxid Redox Signal*, 15(6), 1583-1606.
Fumagalli, M., Rossiello, F., Clerici, M., Barozzi, S., Cittaro, D., Kaplunov, J. M., Bucci, G., Dobreva, M., Matti, V. & Beausejour, C. M. (2012) 'Telomeric DNA damage is irreparable & causes persistent DNA-damage-response activation', *Nat Cell Biol*, 14(4), 355-365.
Furuse, M., Hata, M., Furuse, K., Yoshida, Y., Haratake, A., Sugitani, Y., Noda, T., Kubo, A. & Tsukita, S. (2002) 'Claudin-based tight junctions are crucial for the mammalian epidermal barrier: A lesson from claudin-1–deficient mice', *J Cell Biol*, 156(6), 1099-1111.
Furuya, H. & Ikeda, R. (2011) 'Interaction of triosephosphate isomerase from *Staphylococcus aureus* with plasminogen', *Microbiol Immunol*, 55(12), 855-862.
Förstermann, U. & Münzel, T. (2006) 'Endothelial nitric oxide synthase in vascular disease from marvel to menace', *Circulation*, 113(13), 1708-1714.
Gabrielsen, J. S., Gao, Y., Simcox, J. A., Huang, J., Thorup, D., Jones, D., Cooksey, R. C., Gabrielsen, D., Adams, T. D. & Hunt, S. C. (2012) 'Adipocyte iron regulates adiponectin & insulin sensitivity', *J Clin Invest*, 122(10), 3529-3540.

Gabrilska, R. A. & Rumbaugh, K. P. (2015) 'Biofilm models of polymicrobial infection', *Future Microbiol*, 10(12), 1997-2015.
Galarraga-Vinueza, M., Mesquita-Guimarães, J., Magini, R., Souza, J., Fredel, M. & Boccaccini, A. (2017) 'Anti-biofilm properties of bioactive glasses embedding organic active compounds', *J Biomed Mater Res A*, 105(2), 672-679.
Gales, C., Zamfir, C., Radulescu, D., Stoica, B. & Nechifor, M. (2014) 'Protective effect of magnesium & metformin on endometrium & ovary in experimental diabetes mellitus', *Magnes Res*, 27(2), 69-76.
Galiano, R. D., Michaels, V., Dobryansky, M., Levine, J. P. & Gurtner, G. C. (2004) 'Quantitative & reproducible murine model of excisional wound healing', *Wound Repair Regen*, 12(4), 485-492.
Galili, T., O'Callaghan, A., Sidi, J. & Sievert, C. (2017) 'heatmaply: An R package for creating interactive cluster heatmaps for online publishing', *Bioinformatics*, 34(9), 1600-1602.
Gallant, K. M. H. & Spiegel, D. M. (2017) 'Calcium balance in chronic kidney disease', *Curr Osteoporos Rep*, 15(3), 214-221.
Gallini, R., Lindblom, P., Bondjers, C., Betsholtz, C. & Andrae, J. (2016) 'PDGF-A & PDGF-B induces cardiac fibrosis in transgenic mice', *Exp Cell Res*, 349(2), 282-290.
Ganz, T. (2009) 'Iron in innate immunity: starve the invaders', *Curr Opin Immunol*, 21(1), 63-67.
Ganz, T. (2013) 'Systemic iron homeostasis', *Physiol Rev*, 93(4), 1721-1741.
Ganz, T. & Nemeth, E. (2012) 'Iron metabolism: Interactions with normal & disordered erythropoiesis', *CSH Perspect Med*, 2(5), a011668.
Gao, J., Chen, J., Kramer, M., Tsukamoto, H., Zhang, A. S. & Enns, C. A. (2009) 'Interaction of the hereditary hemochromatosis protein HFE with transferrin receptor 2 is required for transferrin-induced hepcidin expression', *Cell Metab*, 9(3), 217-227.
Gao, M., Nguyen, T. T., Suckow, M. A., Wolter, W. R., Gooyit, M., Mobashery, S. & Chang, M. (2015) 'Acceleration of diabetic wound healing using a novel protease–anti-protease combination therapy', *Proc Nat Acad Sci*, 112(49), 15226-15231.
Garcia-Caballero, A., Zhang, F.-X., Hodgkinson, V., Huang, J., Chen, L., Souza, I. A., Cain, S., Kass, J., Alles, S. & Snutch, T. P. (2018) 'T-type calcium channels functionally interact with spectrin (α/β) & ankyrin B', *Mol Brain*, 11(24).
Garcin, C. L., Ansell, D. M., Headon, D. J., Paus, R. & Hardman, M. J. (2016) 'Hair follicle bulge stem cells appear dispensable for the acute phase of wound re-epithelialization', *Stem Cells*, 34(5), 1377-1385.
García-Mesa, Y., García-Piqueras, J., García, B., Feito, J., Cabo, R., Cobo, J., Vega, J. & García-Suárez, O. (2017) 'Merkel cells & Meissner's corpuscles in human digital skin display Piezo2 immunoreactivity', *J Anat*, 231(6), 978-989.
Gardette, M., Le Hello, S., Mariani-Kurkdjian, P., Fabre, L., Gravey, F., Garrivier, A., Loukiadis, E. & Jubelin, G. (2019) 'Identification & prevalence of *in vivo*-induced genes in enterohaemorrhagic *Escherichia coli*', *Virulence*, 10(1), 180-193.
Gardiner, M., Vicaretti, M., Sparks, J., Bansal, S., Bush, S., Liu, M., Darling, A., Harry, E. & Burke, C. M. (2017) 'A longitudinal study of the diabetic skin & wound microbiome', *PeerJ*, 5, e3543.
Gardner, S. E., Hillis, S. L., Heilmann, K., Segre, J. A. & Grice, E. A. (2013) 'The neuropathic diabetic foot ulcer microbiome is associated with clinical factors', *Diabetes*, 62(3), 923-930.
Garrick, L. M., Dolan, K. G., Romano, M. A. & Garrick, M. D. (1999) 'Non-transferrin-bound iron uptake in Belgrade & normal rat erythroid cells', *J Cell Physiol*, 178(3), 349-358.

Genin, M., Clement, F., Fattaccioli, A., Raes, M. & Michiels, C. (2015) 'M1 & M2 macrophages derived from THP-1 cells differentially modulate the response of cancer cells to etoposide', *BMC Cancer*, 15, 577.
Ghaleb, A. M. & Yang, V. W. (2017) 'Krüppel-like factor 4 (KLF4): What we currently know', *Gene*, 611, 27-37.
Ghannad-Rezaie, M., Wang, X., Mishra, B., Collins, C. & Chronis, N. (2012) 'Microfluidic chips for *in vivo* imaging of cellular responses to neural injury in Drosophila larvae', *PloS One*, 7(1), e29869.
Ghersetich, I., Lotti, T., Campanile, G., Grappone, C. & Dini, G. (1994) 'Hyaluronic acid in cutaneous intrinsic aging', *Int J Dermatol*, 33(2), 119-122.
Gholipourmalekabadi, M., Sameni, M., Hashemi, A., Zamani, F., Rostami, A. & Mozafari, M. (2016) 'Silver-& fluoride-containing mesoporous bioactive glasses versus commonly used antibiotics: Activity against multidrug-resistant bacterial strains isolated from patients with burns', *Burns*, 42(1), 131-140.
Gill, S. E. & Parks, W. C. (2008) 'Metalloproteinases & their inhibitors: Regulators of wound healing', *Int J Biochem Cell Biol*, 40(6-7), 1334-1347.
Gill, S. E. & Parks, W. C. (2011) 'Matrix metalloproteinases & their inhibitors in turnover & degradation of extracellular matrix', In: Parks W. & Mecham R. (eds) *Extracellular matrix degradation*. Berlin: Springer, 1-22.
Gilliet, M. & Lande, R. (2008) 'Antimicrobial peptides & self-DNA in autoimmune skin inflammation', *Curr Opin Immunol*, 20(4), 401-407.
Gilliver, S. C., Emmerson, E., Campbell, L., Chambon, P., Hardman, M. J. & Ashcroft, G. S. (2010) '17β-Estradiol inhibits wound healing in male mice via estrogen receptor-α', *Am J Pathol*, 176(6), 2707-2721.
Gilmore, S. K., Whitson, S. W. & Bowers, D. E. (1986) 'A simple method using alizarin red S for the detection of calcium in epoxy resin embedded tissue', *Stain Technol*, 61(2), 89-92.
Ginhoux, F., Schultze, J. L., Murray, P. J., Ochando, J. & Biswas, S. K. (2016) 'New insights into the multidimensional concept of macrophage ontogeny, activation & function', *Nat Immunol*, 17(1), 34-40.
Gladyshev, V. N. & Zhang, Y. (2013) 'Comparative genomics analysis of the metallomes', *Met Ions Life Sci*, 12, 529-580.
Glasgow, H. L., Whitney, M. A., Gross, L. A., Friedman, B., Adams, S. R., Crisp, J. L., Hussain, T., Frei, A. P., Novy, K. & Wollscheid, B. (2016) 'Laminin targeting of a peripheral nerve-highlighting peptide enables degenerated nerve visualization', *Proc Nat Acad Sci*, 113(45), 12774-12779.
Godin, B. & Touitou, E. (2007) 'Transdermal skin delivery: Predictions for humans from *in vivo*, *ex vivo* & animal models', *Adv Drug Deliv Rev*, 59(11), 1152-1161.
Godoy-Santos, A. L., Rosemberg, L. A., de Cesar-Netto, C. & Armstrong, D. G. (2019) 'The use of bioactive glass S53P4 in the treatment of an infected Charcot foot: A case report', *J Wound Care*, 28(Supp), S14-S17.
Goenka, S., Sant, V. & Sant, S. (2014) 'Graphene-based nanomaterials for drug delivery & tissue engineering', *J Control Release*, 173, 75-88.
Goh, C. H., Heng, P. W. S., Huang, E. P. E., Li, B. K. H. & Chan, L. W. (2008) 'Interactions of antimicrobial compounds with cross-linking agents of alginate dressings', *J Antimicrob Chemother*, 62(1), 105-108.
Goldner, W. (2016) 'Cancer-related hypercalcemia', *J Oncol Pract*, 12(5), 426-432.
Golebiewska, E. M. & Poole, A. W. (2015) 'Platelet secretion: From haemostasis to wound healing & beyond', *Blood Rev*, 29(3), 153-162.

Gonzalez-Ramos, A., Cooper, K. D. & Hammerberg, C. (1996) 'Identification of a human dermal macrophage population responsible for constitutive restraint of primary dermal fibroblast proliferation', *J Invest Dermatol*, 106(2), 305-311.
González-Suárez, E., Samper, E., Ramírez, A., Flores, J. M., Martín-Caballero, J., Jorcano, J. L. & Blasco, M. A. (2001) 'Increased epidermal tumors & increased skin wound healing in transgenic mice overexpressing the catalytic subunit of telomerase, mTERT, in basal keratinocytes', *EMBO J*, 20(11), 2619-2630.
Goodman, A. L. & Lory, S. (2004) 'Analysis of regulatory networks in *Pseudomonas aeruginosa* by genomewide transcriptional profiling', *Curr Opin Microbiol*, 7(1), 39-44.
Goova, M. T., Li, J., Kislinger, T., Qu, W., Lu, Y., Bucciarelli, L. G., Nowygrod, S., Wolf, B. M., Caliste, X. & Yan, S. F. (2001) 'Blockade of receptor for advanced glycation end-products restores effective wound healing in diabetic mice', *Am J Pathol*, 159(2), 513-525.
Gooyit, M., Peng, Z., Wolter, W. R., Pi, H., Ding, D., Hesek, D., Lee, M., Boggess, B., Champion, M. M. & Suckow, M. A. (2013) 'A chemical biological strategy to facilitate diabetic wound healing', *ACS Chem Biol*, 9(1), 105-110.
Goralska, M., Holley, B. L. & McGahan, M. C. (2001) 'Overexpression of H-& L-ferritin subunits in lens epithelial cells: Fe metabolism & cellular response to UVB irradiation', *Investig Ophthalmol Vis Sci*, 42(8), 1721-1727.
Goren, I., Allmann, N., Yogev, N., Schürmann, C., Linke, A., Holdener, M., Waisman, A., Pfeilschifter, J. & Frank, S. (2009) 'A transgenic mouse model of inducible macrophage depletion: Effects of diphtheria toxin-driven lysozyme M-specific cell lineage ablation on wound inflammatory, angiogenic, & contractive processes', *Am J Pathol*, 175(1), 132-147.
Gorres, K. L. & Raines, R. T. (2010) 'Prolyl 4-hydroxylase', *Crit Rev Biochem Mol Biol*, 45(2), 106-124.
Gosain, A. & DiPietro, L. A. (2004) 'Aging & wound healing', *World J Surg*, 28(3), 321-326.
Goswami, T. & Andrews, N. C. (2006) 'Hereditary hemochromatosis protein, HFE, interaction with transferrin receptor 2 suggests a molecular mechanism for mammalian iron sensing', *J Biol Chem*, 281(39), 28494-28498.
Gould, L., Abadir, P., Brem, H., Carter, M., Conner-Kerr, T., Davidson, J., DiPietro, L., Falanga, V., Fife, C. & Gardner, S. (2015) 'Chronic wound repair & healing in older adults: Current status & future research', *Wound Repair Regen*, 23(1), 1-13.
Gozzelino, R., Jeney, V. & Soares, M. P. (2010) 'Mechanisms of cell protection by heme oxygenase-1', *Ann Rev Pharmacol Toxicol*, 50, 323-354.
Graham, H. K., Hodson, N. W., Hoyland, J. A., Millward-Sadler, S. J., Garrod, D., Scothern, A., Griffiths, C. E., Watson, R. E., Cox, T. R. & Erler, J. T. (2010a) 'Tissue section AFM: In situ ultrastructural imaging of native biomolecules', *Matrix Biol*, 29(4), 254-260.
Graham, L. V. D., Sweetwyne, M. T., Pallero, M. A. & Murphy-Ullrich, J. E. (2010b) 'Intracellular calreticulin regulates multiple steps in fibrillar collagen expression, trafficking, & processing into the extracellular matrix', *J Biol Chem*, 285(10), 7067-7078.
Graham, R. M., Morgan, E. H. & Baker, E. (1998) 'Characterisation of citrate & iron citrate uptake by cultured rat hepatocytes', *J Hepatol*, 29(4), 603-13.
Granick, S. (1954) 'Iron metabolism', *J Urban Health*, 30(2), 81-105.
Graz, H., D'Souza, V. K., Alderson, D. E. & Graz, M. (2018) 'Diabetes-related amputations create considerable public health burden in the UK', *Diabetes Res Clin Pract*, 135, 158-165.

Greaves, N. S., Ashcroft, K. J., Baguneid, M. & Bayat, A. (2013) 'Current understanding of molecular & cellular mechanisms in fibroplasia & angiogenesis during acute wound healing', *J Dermatol Sci*, 72(3), 206-217.
Greiling, D. & Clark, R. (1997) 'Fibronectin provides a conduit for fibroblast transmigration from collagenous stroma into fibrin clot provisional matrix', *J Cell Sci*, 110(7), 861-870.
Greives, M. R., Samra, F., Pavlides, S. C., Blechman, K. M., Naylor, S. M., Woodrell, C. D., Cadacio, C., Levine, J. P., Bancroft, T. A. & Michalak, M. (2012) 'Exogenous calreticulin improves diabetic wound healing', *Wound Repair Regen*, 20(5), 715-730.
Griffin, D. R., Weaver, W. M., Scumpia, P. O., Di Carlo, D. & Segura, T. (2015) 'Accelerated wound healing by injectable microporous gel scaffolds assembled from annealed building blocks', *Nat Mater*, 14, 737-744.
Groenestege, W. M. T., Thébault, S., van der Wijst, J., van den Berg, D., Janssen, R., Tejpar, S., van den Heuvel, L. P., Van Cutsem, E., Hoenderop, J. G. & Knoers, N. V. (2007) 'Impaired basolateral sorting of pro-EGF causes isolated recessive renal hypomagnesemia', *J Clin Invest*, 117(8), 2260-2267.
Gröber, U., Schmidt, J. & Kisters, K. (2015) 'Magnesium in prevention & therapy', *Nutrients*, 7(9), 8199-8226.
Guasch-Ferré, M., Bulló, M., Martínez-González, M. Á., Ros, E., Corella, D., Estruch, R., Fitó, M., Arós, F., Wärnberg, J. & Fiol, M. (2013) 'Frequency of nut consumption & mortality risk in the PREDIMED nutrition intervention trial', *BMC Med*, 11, 164.
Guerrero-Hernandez, A. & Verkhratsky, A. (2014) 'Calcium signalling in diabetes', *Cell Calcium*, 56(5), 297-301.
Guest, J. F., Ayoub, N., McIlwraith, T., Uchegbu, I., Gerrish, A., Weidlich, D., Vowden, K. & Vowden, P. (2015) 'Health economic burden that wounds impose on the National Health Service in the UK', *BMJ Open*, 5(12), e009283.
Gulec, S., Anderson, G. J. & Collins, J. F. (2014) 'Mechanistic & regulatory aspects of intestinal iron absorption', *Am J Physiol Gastrointest Liver Physiol*, 307(4), G397-G409.
Gundry, R. L., White, M. Y., Murray, C. I., Kane, L. A., Fu, Q., Stanley, B. A. & Van Eyk, J. E. (2009) 'Preparation of proteins & peptides for mass spectrometry analysis in a bottom-up proteomics workflow', *Curr Protoc Mol Biol*, 88, 10.25.1-10.25.23.
Gunin, A. G., Petrov, V. V., Golubtzova, N. N., Vasilieva, O. V. & Kornilova, N. K. (2014) 'Age-related changes in angiogenesis in human dermis', *Exp Gerontol*, 55, 143-151.
Guo, Y. N., Zhu, C., Zeng, M., Wang, W. J., Li, J. & Fan, X. M. (2009) 'Effect of aerosolized STAT1 antisense oligonucleotides on the expressions of cytokines & collagens in lung tissue of pulmonary fibrosis rats induced by bleomycin', *Zhonghua Jie He He Hu Xi Za Zhi*, 32(10), 752-756.
Gurevich, D. B., Severn, C. E., Twomey, C., Greenhough, A., Cash, J., Toye, A. M., Mellor, H. & Martin, P. (2018) 'Live imaging of wound angiogenesis reveals macrophage orchestrated vessel sprouting & regression', *EMBO J*, 37(13), e97786.
Gurtner, G. C., Werner, S., Barrandon, Y. & Longaker, M. T. (2008) 'Wound Repair & Regeneration', *Nature*, 453(7193), 314-321.
Gwack, Y., Srikanth, S., Oh-Hora, M., Hogan, P. G., Lamperti, E. D., Yamashita, M., Gelinas, C., Neems, D. S., Sasaki, Y. & Feske, S. (2008) 'Hair loss & defective T-& B-cell function in mice lacking ORAI1', *Mol Cell Biol*, 28(17), 5209-5222.
Gwynne, B. & Newton, M. (2006) 'An overview of the common methods of wound debridement', *Br J Nurs*, 15(4), 4-10.
Görlach, A., Bertram, K., Hudecova, S. & Krizanova, O. (2015) 'Calcium & ROS: A mutual interplay', *Redox Biol*, 6, 260-271.

Hack, G. D. (2014) Treatment & prevention of dental pathology in humans & non-human animals. US Patent US8722080B2. Available online: https://patents.google.com/patent/US8722080B2/en [Accessed 30/8/19].
Hadjipanayi, E., Mudera, V. & Brown, R. (2009) 'Close dependence of fibroblast proliferation on collagen scaffold matrix stiffness', *J Tissue Eng Regen Med*, 3(2), 77-84.
Haertel, E., Werner, S. & Schäfer, M. (2014) 'Transcriptional regulation of wound inflammation', *Semin Immunol*, 26(4), 321-328.
Hakimizadeh, E., Shamsizadeh, A., Nazari, M., Arababadi, M. K., Rezaeian, M., Vazirinejad, R., Jamali, Z., Poor, N. M., Khorramdelazad, H., Darakhshan, S. & Hassanshahi, G. (2013) 'Increased circulating levels of CXC chemokines is correlated with duration & complications of the disease in type-1 diabetes: A study on Iranian diabetic patients', *Clin Lab*, 59(5-6), 531-537.
Haldar, M., Kohyama, M., So, A. Y.-L., Wumesh, K., Wu, X., Briseño, C. G., Satpathy, A. T., Kretzer, N. M., Arase, H. & Rajasekaran, N. S. (2014) 'Heme-mediated SPI-C induction promotes monocyte differentiation into iron-recycling macrophages', *Cell*, 156(6), 1223-1234.
Hall, J., Buckley, H. L., Lamb, K. A., Stubbs, N., Saramago, P., Dumville, J. C. & Cullum, N. A. (2014) 'Point prevalence of complex wounds in a defined United Kingdom population', *Wound Repair Regen*, 22(6), 694-700.
Han, G. & Ceilley, R. (2017) 'Chronic wound healing: A review of current management & treatments', *Adv Ther*, 34(3), 599-610.
Han, M., Xu, R., Wang, S., Yang, N., Ni, S., Zhang, Q., Xu, Y., Zhang, X., Zhang, C. & Wei, Y. (2018) 'Six-Transmembrane Epithelial Antigen of Prostate 3 Predicts Poor Prognosis & Promotes Glioblastoma Growth & Invasion', *Neoplasia*, 20(6), 543-554.
Han, N.-R., Kim, H.-Y., Yang, W. M., Jeong, H.-J. & Kim, H.-M. (2015) 'Glutamic acid ameliorates estrogen deficiency–induced menopausal-like symptoms in ovariectomized mice', *Nutr Res*, 35(9), 774-783.
Hancı, V., Hakimoğlu, S., Özaçmak, H., Bektaş, S., Özaçmak, H. S., Özdamar, Ş. O., Yurtlu, S. & Turan, I. Ö. (2012) 'Comparison of the effects of bupivacaine, lidocaine, & tramadol infiltration on wound healing in rats', *Rev Bras Anestesiol*, 62(6), 804-810.
Handford, P. (2000) 'Fibrillin-1, a calcium binding protein of extracellular matrix', *Biochim Biophys Acta Mol Cell Res*, 1498(2-3), 84-90.
Handing, K. B., Niedzialkowska, E., Shabalin, I. G., Kuhn, M. L., Zheng, H. & Minor, W. (2018) 'Characterizing metal-binding sites in proteins with X-ray crystallography', *Nat Prot*, 13(5), 1062-1090.
Hanlon, C. D. & Andrew, D. J. (2015) 'Outside-in signaling–a brief review of GPCR signaling with a focus on the Drosophila GPCR family', *J Cell Sci*, 128(19), 3533-3542.
Hansen, L. D., Litchman, W. M. & Daub, G. H. (1969) 'Turnbull's blue & Prussian blue: KFe (III)[Fe (II)(CN) 6]', *J Chem Ed*, 46(1), e46.
Haorah, J., Ramirez, S. H., Schall, K., Smith, D., Pandya, R. & Persidsky, Y. (2007) 'Oxidative stress activates protein tyrosine kinase & matrix metalloproteinases leading to blood–brain barrier dysfunction', *J Neurochem*, 101(2), 566-576.
Hara, T., Mahadevan, J., Kanekura, K., Hara, M., Lu, S. & Urano, F. (2014) 'Calcium efflux from the endoplasmic reticulum leads to β-cell death', *Endocrinology*, 155(3), 758-768.
Harder, J., Bartels, J., Christophers, E. & Schröder, J.-M. (1997) 'A peptide antibiotic from human skin', *Nature*, 387(6636), e861.
Harder, J., Dressel, S., Wittersheim, M., Cordes, J., Meyer-Hoffert, U., Mrowietz, U., Fölster-Holst, R., Proksch, E., Schröder, J. M., Schwarz, T. & Gläser, R. (2010)

'Enhanced expression & secretion of antimicrobial peptides in atopic dermatitis & after superficial skin injury', *J Invest Dermatol*, 130(5), 1355-1364.
Harding, C. R. (2004) 'The stratum corneum: Structure & function in health & disease', *Dermatol Ther*, 17(1), 6-15.
Harding, K., Morris, H. & Patel, G. (2002) 'Science, medicine, & the future: Healing chronic wounds', *Br Med J*, 324(7330), 160-163.
Harding, K. G., Moore, K. & Phillips, T. J. (2005) 'Wound chronicity & fibroblast senescence–implications for treatment', *Int Wound J*, 2(4), 364-368.
Hardman, M. J., Ferguson, M. W., Byrne, C. & Moore, L. (1999) 'Barrier formation in the human fetus is patterned', *J Invest Dermatol*, 113(6), 1106-1113.
Hardman, M. J., Sisi, P., Banbury, D. N. & Byrne, C. (1998) 'Patterned acquisition of skin barrier function during development', *Development*, 125(8), 1541-1552.
Hardman, M. J., Waite, A., Zeef, L., Burow, M., Nakayama, T. & Ashcroft, G. S. (2005) 'Macrophage migration inhibitory factor: A central regulator of wound healing', *Am J Pathol*, 167(6), 1561-1574.
Hare D. J., Kysenius K., Paul B., Knauer B., Hutchinson R. W., O'Connor C., Fryer F., Hennessey T. P., Bush A. I., Crouch P. J. & Doble P. A. (2017) 'Imaging metals in brain tissue by laser ablation - inductively coupled plasma - mass spectrometry (LA-ICP-MS)', *J Vis Exp*, 119, 55042.
Hare, D. J., New, E. J., de Jonge, M. D. & McColl, G. (2015) 'Imaging metals in biology: Balancing sensitivity, selectivity & spatial resolution', *Chem Soc Rev*, 44(17), 5941-5958.
Harel, A., Bromberg, Y., Falkowski, P. G. & Bhattacharya, D. (2014) 'Evolutionary history of redox metal-binding domains across the tree of life', *Proc Nat Acad Sci*, 111(19), 7042-7047.
Harjutsalo, V., Sjöberg, L. & Tuomilehto, J. (2008) 'Time trends in the incidence of type 1 diabetes in Finnish children: A cohort study', *Lancet*, 371(9626), 1777-1782.
Harnett, M. J., Datta, S. & Bhavani-Shankar, K. (2001) 'The effect of magnesium on coagulation in parturients with preeclampsia', *Anesth Analg*, 92(5), 1257-1260.
Harper, M. T. & Poole, A. W. (2010) 'Diverse functions of protein kinase C isoforms in platelet activation & thrombus formation', *J Thromb Haemost*, 8(3), 454-462.
Harrison, J. J., Ceri, H., Stremick, C. A. & Turner, R. J. (2004) 'Biofilm susceptibility to metal toxicity', *Environ Microbiol*, 6(12), 1220-1227.
Harrison-Balestra, C., Cazzaniga, A. L., Davis, S. C. & Mertz, P. M. (2003) 'A wound-isolated *Pseudomonas aeruginosa* grows a biofilm *in vitro* within 10 hours & is visualized by light microscopy', *Dermatol Surg*, 29(6), 631-635.
Haydont, V., Bernard, B. A. & Fortunel, N. O. (2019) 'Age-related evolutions of the dermis: Clinical signs, fibroblast & extracellular matrix dynamics', *Mech Ageing Dev*, 177, 150-156.
Hayflick, L. & Moorhead, P. S. (1961) 'The serial cultivation of human diploid cell strains', *Exp Cell Res*, 25(3), 585-621.
Hazan, R., Que, Y. A., Maura, D., Strobel, B., Majcherczyk, P. A., Hopper, L. R., Wilbur, D. J., Hreha, T. N., Barquera, B. & Rahme, L. G. (2016) 'Auto poisoning of the respiratory chain by a quorum-sensing-regulated molecule favors biofilm formation & antibiotic tolerance', *Curr Biol*, 26(2), 195-206.
Hazen, R. M. & Ferry, J. M. (2010) 'Mineral evolution: Mineralogy in the fourth dimension', *Elements*, 6(1), 9-12.
He, L., He, X., Lim, L. P., De Stanchina, E., Xuan, Z., Liang, Y., Xue, W., Zender, L., Magnus, J. & Ridzon, D. (2007) 'A microRNA component of the p53 tumour suppressor network', *Nature*, 447(7148), 1130-1134.

Heberle, H., Meirelles, G. V., da Silva, F. R., Telles, G. P. & Minghim, R. (2015) 'InteractiVenn: A web-based tool for the analysis of sets through Venn diagrams', *BMC Bioinformatics*, 16(1), e169.
Hench, L. L. (2006) 'The story of Bioglass®', *J Mat Sci Mat Med*, 17(11), 967-978.
Heng, M. K., Song, M. K. & Heng, M. C. (1993) 'Reciprocity between tissue calmodulin & cAMP levels: modulation by excess zinc', *Br J Dermatol*, 129(3), 280-285.
Hennings, H. & Holbrook, K. A. (1983) 'Calcium regulation of cell-cell contact & differentiation of epidermal cells in culture: An ultrastructural study', *Exp Cell Res*, 143(1), 127-142.
Hennings, H., Michael, D., Cheng, C., Steinert, P., Holbrook, K. & Yuspa, S. H. (1980) 'Calcium regulation of growth & differentiation of mouse epidermal cells in culture', *Cell*, 19(1), 245-254.
Herant, M. & Dembo, M. (2010) 'Form & function in cell motility: From fibroblasts to keratocytes', *Biophys J*, 98(8), 1408-1417.
Herchenhan, A., Uhlenbrock, F., Eliasson, P., Weis, M., Eyre, D., Kadler, K. E., Magnusson, S. P. & Kjaer, M. (2015) 'Lysyl oxidase activity is required for ordered collagen fibrillogenesis by tendon cells', *J Biol Chem*, 290(26), 16440-16450.
Herrling, T., Jung, K. & Fuchs, J. (2006) 'Measurements of UV-generated free radicals/reactive oxygen species (ROS) in skin', *Spectrochim Acta A Mol Biomol Spectrosc*, 63(4), 840-845.
Heughan, C., Grislis, G. & Hunt, T. (1974) 'The effect of anemia on wound healing', *Ann Surg*, 179(2), 163-167.
Hieda, Y., Nishizawa, Y., Uematsu, J. & Owaribe, K. (1992) 'Identification of a new hemidesmosomal protein, HD1: A major, high molecular mass component of isolated hemidesmosomes', *J Cell Biol*, 116(6), 1497-1506.
Hielscher, A. & Gerecht, S. (2015) 'Hypoxia & free radicals: Role in tumor progression & the use of engineering-based platforms to address these relationships', *Free Radical Bio Med*, 79, 281-291.
Higley, H., Ksander, G., Gerhardt, C. & Falanga, V. (1995) 'Extravasation of macromolecules & possible trapping of transforming growth factor-β in venous ulceration', *Br J Dermatol*, 132(1), 79-85.
Hinz, B. (2015) 'The extracellular matrix & transforming growth factor-β1: Tale of a strained relationship', *Matrix Biol*, 47, 54-65.
Hirsch, T., Spielmann, M., Zuhaili, B., Koehler, T., Fossum, M., Steinau, H. U., Yao, F., Steinstraesser, L., Onderdonk, A. B. & Eriksson, E. (2008) 'Enhanced susceptibility to infections in a diabetic wound healing model', *BMC Surg*, 8, 5.
Ho, E., Quan, N., Tsai, Y. H., Lai, W. & Bray, T. M. (2001) 'Dietary zinc supplementation inhibits NFkappaB activation & protects against chemically induced diabetes in CD1 mice', *Exp Biol Med*, 226(2), 103-111.
Hodgkinson, V. & Petris, M. J. (2012) 'Copper homeostasis at the host-pathogen interface', *J Biol Chem*, 287(17), 13549-13555.
Hofer, A. M. & Brown, E. M. (2003) 'Extracellular calcium sensing & signalling', *Nat Rev Mol Cell Biol*, 4(7), 530-538.
Hogan, P. G., Chen, L., Nardone, J. & Rao, A. (2003) 'Transcriptional regulation by calcium, calcineurin, & NFAT', *Genes Dev*, 17(18), 2205-2232.
Homberg, M. & Magin, T. M. (2014) 'Beyond expectations: Novel insights into epidermal keratin function & regulation', *Int Rev Cell Mol Biol*, 311, 265-306.
Hong, B.-Z., Kang, H.-S., So, J.-N., Kim, H.-N., Park, S.-A., Kim, S.-J., Kim, K.-R. & Kwak, Y.-G. (2006) 'Vascular endothelial growth factor increases the intracellular magnesium', *Biochem Biophys Res Commun*, 347(2), 496-501.

Horikawa, S., Ishii, Y., Hamashima, T., Yamamoto, S., Mori, H., Fujimori, T., Shen, J., Inoue, R., Nishizono, H., Itoh, H., Majima, M., Abraham, D., Miyawaki, T. & Sasahara, M. (2015) 'PDGFRα plays a crucial role in connective tissue remodeling', *Sci Rep*, 5, e17948.
Hotamisligil, G. S. (2006) 'Inflammation & metabolic disorders', *Nature*, 444(7121), 860-867.
Houghton, A. M., Mouded, M. & Shapiro, S. D. (2011) 'Consequences of elastolysis', In: Parks W. & Mecham R. (eds) *Extracellular matrix degradation*. Berlin: Springer, 217-249.
Howard, M. A., Perkin, J., Koutts, J. & Firkin, B. G. (1981) 'Quantitation of binding of factor VIII antigen to concanavalin A', *Br J Haematol*, 47(4), 607-615.
Hozzein, W. N., Badr, G., Al Ghamdi, A. A., Sayed, A., Al-Waili, N. S. & Garraud, O. (2015) 'Topical application of propolis enhances cutaneous wound healing by promoting TGF-beta/Smad-mediated collagen production in a streptozotocin-induced type I diabetic mouse model', *Cell Physiol Biochem*, 37(3), 940-954.
Hruby, A., Meigs, J. B., O'Donnell, C. J., Jacques, P. F. & McKeown, N. M. (2014) 'Higher magnesium intake reduces risk of impaired glucose & insulin metabolism & progression from prediabetes to diabetes in middle-aged americans', *Diabetes Care*, 37(2), 419-427.
Hsu, I., Parkinson, L., Shen, Y., Toro, A., Brown, T., Zhao, H., Bleackley, R. & Granville, D. (2014) 'Serpina3n accelerates tissue repair in a diabetic mouse model of delayed wound healing', *Cell Death Dis*, 5(10), e1458.
Hu, S., Li, L., Huang, W., Liu, J., Lan, G., Yu, S., Peng, L., Xie, X., Yang, L. & Nian, Y. (2018) 'CAV3. 1 knockdown suppresses cell proliferation, migration & invasion of prostate cancer cells by inhibiting AKT', *Cancer Manag Red*, 10, 4603-4614.
Hu, X. & Beeton, C. (2010) 'Detection of functional matrix metalloproteinases by zymography', *J Vis Exp*, 45, e2445.
Huang, D. W., Sherman, B. T. & Lempicki, R. A. (2009) 'Systematic & integrative analysis of large gene lists using DAVID bioinformatics resources', *Nat Prot*, 4(1), 44-57.
Huang, J., Simcox, J., Mitchell, T. C., Jones, D., Cox, J., Luo, B., Cooksey, R. C., Boros, L. G. & McClain, D. A. (2013) 'Iron regulates glucose homeostasis in liver & muscle via AMP-activated protein kinase in mice', *FASEB J*, 27(7), 2845-2854.
Huang, M., Liu, Z., Baugh, L., DeFuria, J., Maione, A., Smith, A., Kashpur, O., Black III, L. D., Georgakoudi, I. & Whitfield, M. L. (2019) 'Lysyl oxidase enzymes mediate TGF-β1-induced ibrotic phenotypes in human skin-like tissues', *Lab Invest*, 99(4), 514-527.
Huang, P., Bi, J., Owen, G. R., Chen, W., Rokka, A., Koivisto, L., Heino, J., Häkkinen, L. & Larjava, H. (2015) 'Keratinocyte microvesicles regulate the expression of multiple genes in dermal fibroblasts', *J Invest Dermatol*, 135(12), 3051-3059.
Huang, W.-C., Ju, T.-K., Hung, M.-C. & Chen, C.-C. (2007) 'Phosphorylation of CBP by IKKα promotes cell growth by switching the binding preference of CBP from p53 to NF-κB', *Mol Cell*, 26(1), 75-87.
Huard, D. J., Kane, K. M. & Tezcan, F. A. (2013) 'Re-engineering protein interfaces yields copper-inducible ferritin cage assembly', *Nat Chem Biol*, 9(3), 169-176.
Hughes, C. E. & Nibbs, R. J. B. (2018) 'A guide to chemokines & their receptors', *FEBS J*, 285(16), 2944-2971.
Hultgårdh-Nilsson, A., Borén, J. & Chakravarti, S. (2015) 'The small leucine-rich repeat proteoglycans in tissue repair & atherosclerosis', *J Int Med*, 278(5), 447-461.

Hummel, K. P., Coleman, D. L. & Lane, P. W. (1972) 'The influence of genetic background on expression of mutations at the diabetes locus in the mouse. I. C57BL/KsJ & C57BL/6J strains', *Biochem Gen*, 7(1), 1-13.
Humphrey, J. D., Dufresne, E. R. & Schwartz, M. A. (2014) 'Mechanotransduction & extracellular matrix homeostasis', *Nat Rev Mol Cell Biol*, 15(12), 802-812.
Husni, N. R., Jones IV, A. R., Simmons, A. L. & Corkey, B. E. (2014) 'Fibroblasts From Type 1 Diabetics Exhibit Enhanced Ca 2+ Mobilization after TNF or Fat Exposure', *PloS One*, 9(1), e87068.
Hutton Jr, J. J., Tappel, A. & Udenfriend, S. (1967) 'Cofactor & substrate requirements of collagen proline hydroxylase', *Arch Biochem Biophys*, 118(1), 231-240.
Hwang, K.-A., Yi, B.-R. & Choi, K.-C. (2011) 'Molecular mechanisms & *in vivo* mouse models of skin aging associated with dermal matrix alterations', *Lab Anim Res*, 27(1), 1-8.
Icli, B., Nabzdyk, C. S., Lujan-Hernandez, J., Cahill, M., Auster, M. E., Wara, A., Sun, X., Ozdemir, D., Giatsidis, G. & Orgill, D. P. (2016) 'Regulation of impaired angiogenesis in diabetic dermal wound healing by microRNA-26a', *J Mol Cell Cardiol*, 91, 151-159.
IJpma, A. S. & Greider, C. W. (2003) 'Short telomeres induce a DNA damage response in Saccharomyces cerevisiae', *Mol Biol Cell*, 14(3), 987-1001.
Ikeda, H., Wu, G. Y. & Wu, C. H. (1992) 'Evidence that an iron chelator regulates collagen synthesis by decreasing the stability of procollagen mRNA', *Hepatology*, 15(2), 282-287.
Imura, A., Tsuji, Y., Murata, M., Maeda, R., Kubota, K., Iwano, A., Obuse, C., Togashi, K., Tominaga, M. & Kita, N. (2007) 'α-Klotho as a regulator of calcium homeostasis', *Science*, 316(5831), 1615-1618.
Ingersoll, M. A., Platt, A. M., Potteaux, S. & Randolph, G. J. (2011) 'Monocyte trafficking in acute & chronic inflammation', *Trends Immunol*, 32(10), 470-477.
Inoue, Y., Hasegawa, S., Ban, S., Yamada, T., Date, Y., Mizutani, H., Nakata, S., Tanaka, M. & Hirashima, N. (2014) 'ZIP2 protein, a zinc transporter, is associated with keratinocyte differentiation', *J Biol Chem*, 289(31), 21451-21462.
Inoue, Y., Nakanishi, K., Hiraga, T., Okubo, M., Murase, T., Kosaka, K., Miyakoshi, S., Mutoh, Y. & Kobayashi, T. (1997) 'Recovery of pancreatic β-cell function in hemochromatosis: Combined treatment with recombinant human erythropoietin & phlebotomy', *Am J Med Sci*, 314(6), 401-402.
Inzana, J. A., Schwarz, E. M., Kates, S. L. & Awad, H. A. (2015) 'A novel murine model of established Staphylococcal bone infection in the presence of a fracture fixation plate to study therapies utilizing antibiotic-laden spacers after revision surgery', *Bone*, 72, 128-136.
Ishihara, J., Ishihara, A., Starke, R. D., Peghaire, C. R., Smith, K. E., McKinnon, T. A., Tabata, Y., Sasaki, K., White, M. J., Fukunaga, K., Laffan, M. A., Lutolf, M. P., Randi, A. M. & Hubbell, J. A. (2019) 'The heparin binding domain of von Willebrand factor binds to growth factors & promotes angiogenesis in wound healing', *Blood*, 133(24), 2559-2569.
Itahana, K., Itahana, Y. & Dimri, G. P. (2013) 'Colorimetric detection of senescence-associated β galactosidase', *Methods Mol Biol*, 965, 143-156.
Ito, M. & Cotsarelis, G. (2008) 'Is the hair follicle necessary for normal wound healing?', *J Invest Dermatol*, 128(5), 1059-1061.
Ito, M., Liu, Y., Yang, Z., Nguyen, J., Liang, F., Morris, R. J. & Cotsarelis, G. (2005) 'Stem cells in the hair follicle bulge contribute to wound repair but not to homeostasis of the epidermis', *Nat Med*, 11(12), 1351-1354.

Itoh, M., Umegaki-Arao, N., Guo, Z., Liu, L., Higgins, C. A. & Christiano, A. M. (2013) 'Generation of 3D skin equivalents fully reconstituted from human induced pluripotent stem cells (iPSCs)', *PLoS One*, 8(10), e77673.
Ivan, M., Kondo, K., Yang, H., Kim, W., Valiando, J., Ohh, M., Salic, A., Asara, J. M., Lane, W. S. & Kaelin Jr, W. G. (2001) 'HIFα targeted for VHL-mediated destruction by proline hydroxylation: Implications for O2 sensing', *Science*, 292(5516), 464-468.
Izumi, T., Tajima, S. & Nishikawa, T. (1995) 'Differential expression of α1 & α2 chains of type VI collagen in the upper, middle, & lower dermal fibroblasts *in vitro*', *J Biochem*, 117(5), 1004-1007.
Jackson, R. L., Greiwe, J. S. & Schwen, R. J. (2011) 'Ageing skin: Oestrogen receptor β agonists offer an approach to change the outcome', *Exp Dermatol*, 20(11), 879-882.
Jacobs, A. (1977) 'Low molecular weight intracellular iron transport compounds', *Blood*, 50(3), 433-439.
Jacobson, M. J. & Van Prohaska, J. (1965) 'The healing of wounds in iron deficiency', *Surgery*, 57(2), 254-258.
James, G., Witten, D., Hastie, T. & Tibshirani, R. (2017) 'Package 'ISLR''. Available online: https://cran.opencpu.org/web/packages/ISLR/ISLR.pdf [Accessed 30/8/19].
James, G. A., Swogger, E., Wolcott, R., Secor, P., Sestrich, J., Costerton, J. W. & Stewart, P. S. (2008) 'Biofilms in chronic wounds', *Wound Repair Regen*, 16(1), 37-44.
Janson, D. G., Saintigny, G., Van Adrichem, A., Mahé, C. & El Ghalbzouri, A. (2012) 'Different gene expression patterns in human papillary & reticular fibroblasts', *J Invest Dermatol*, 132(11), 2565-2572.
Jayaraman, S., Patel, A., Jayaraman, A., Patel, V., Holterman, M. & Prabhakar, B. (2013) 'Transcriptome analysis of epigenetically modulated genome indicates signature genes in manifestation of type 1 diabetes & its prevention in NOD mice', *PLoS One*, 8(1), e55074.
Jebahi, S., Oudadesse, H., Faouzi, F., Elleuch, J., Rebai, T., Keskes, H., Mostafa, A., El Feki, A. & El Feki, H. (2013) 'Osteoinduction & antiosteoporotic performance of hybrid biomaterial chitosan-bioactive glass graft: Effects on bone remodeling', *J Material Sci Eng*, 2, 128.
Jeffcoate, W. J. & van Houtum, W. H. (2004) 'Amputation as a marker of the quality of foot care in diabetes', *Diabetologia*, 47(12), 2051-2058.
Jehn, M., Clark, J. M. & Guallar, E. (2004) 'Serum ferritin & risk of the metabolic syndrome in U.S. adults', *Diabetes Care*, 27(10), 2422-2428.
Jehn, M. L., Guallar, E., Clark, J. M., Couper, D., Duncan, B. B., Ballantyne, C. M., Hoogeveen, R. C., Harris, Z. L. & Pankow, J. S. (2007) 'A prospective study of plasma ferritin level & incident diabetes: The atherosclerosis risk in communities (ARIC) study', *Am J Epidemiol*, 165(9), 1047-1054.
Jenkins, N. C., Liu, T., Cassidy, P., Leachman, S. A., Boucher, K. M., Goodson, A. G., Samadashwily, G. & Grossman, D. (2011) 'The p16 INK4A tumor suppressor regulates cellular oxidative stress', *Oncogene*, 30(3), 265-274.
Jetten, N., Roumans, N., Gijbels, M. J., Romano, A., Post, M. J., de Winther, M. P., van der Hulst, R. R. & Xanthoulea, S. (2014) 'Wound administration of M2-polarized macrophages does not improve murine cutaneous healing responses', *PloS One*, 9(7), e102994.
Jiang, P., Huang, R., Ma, N. & Jiang, F. (2018) 'The expression of calcium sensing receptor in normal & diabetic rat eyes', *Med Sci Monit*, 24, 706-710.
Jiang, R., Diaz-Castro, B., Looger, L. L. & Khakh, B. S. (2016) 'Dysfunctional calcium & glutamate signaling in striatal astrocytes from Huntington's disease model mice', *J Neurosci*, 36(12), 3453-3470.

Jiao, Y., Feng, X., Zhan, Y., Wang, R., Zheng, S., Liu, W. & Zeng, X. (2012) 'Matrix metalloproteinase-2 promotes αvβ3 integrin-mediated adhesion & migration of human melanoma cells by cleaving fibronectin', *PloS One*, 7(7), e41591.
Jin, J. & Zhang, T. (2013) 'Effects of glucose restriction on replicative senescence of human diploid fibroblasts IMR-90', *Cell Physiol Biochem*, 31(4-5), 718-727.
Jin, S.-W., Zhang, L., Lian, Q.-Q., Yao, S.-L., Wu, P., Zhou, X.-Y., Xiong, W. & Ye, D.-Y. (2006) 'Close functional coupling between Ca2+ release-activated Ca2+ channels & reactive oxygen species production in murine macrophages', *Mediators Inflamm*, 2006(6), e36192.
Jin, Y., Sharma, A., Carey, C., Hopkins, D., Wang, X., Robertson, D. G., Bode, B., Anderson, S. W., Reed, J. C. & Steed, R. D. (2013) 'The expression of inflammatory genes is upregulated in peripheral blood of patients with type 1 diabetes', *Diabetes Care*, 36(9), 2794-2802.
Johnstone, M. T., Creager, S. J., Scales, K. M., Cusco, J. A., Lee, B. K. & Creager, M. A. (1993) 'Impaired endothelium-dependent vasodilation in patients with insulin-dependent diabetes mellitus', *Circulation*, 88(6), 2510-2516.
Jonasson, H., Bergstrand, S., Nystrom, F. H., Länne, T., Östgren, C. J., Bjarnegård, N., Fredriksson, I., Larsson, M. & Strömberg, T. (2017) 'Skin microvascular endothelial dysfunction is associated with type 2 diabetes independently of microalbuminuria & arterial stiffness', *Diabetes Vasc Dis Res*, 14(4), 363-371.
Jones, J. R. (2013) 'Review of bioactive glass: From Hench to hybrids', *Acta Biomater*, 9(1), 4457-4486.
Joost, S., Jacob, T., Sun, X., Annusver, K., La Manno, G., Sur, I. & Kasper, M. (2018) 'Single-cell transcriptomics of traced epidermal & hair follicle stem cells reveals rapid adaptations during wound healing', *Cell Rep*, 25(3), 585-597.
Joshi, N., Caputo, G. M., Weitekamp, M. R. & Karchmer, A. (1999) 'Infections in patients with diabetes mellitus', *N Eng J Med*, 341(25), 1906-1912.
Jouihan, H. A., Cobine, P. A., Cooksey, R. C., Hoagland, E. A., Boudina, S., Abel, E. D., Winge, D. R. & McClain, D. A. (2008) 'Iron-mediated inhibition of mitochondrial manganese uptake mediates mitochondrial dysfunction in a mouse model of hemochromatosis', *Mol Med*, 14(3-4), 98-108.
Jugé, R., Rouaud-Tinguely, P., Breugnot, J., Servaes, K., Grimaldi, C., Roth, M. P., Coppin, H. & Closs, B. (2018) 'Shift in skin microbiota of Western European women across aging', *J Appl Microbiol*, 125(3), 907-916.
Juhan-Vague, I., Roul, C., Alessi, M., Ardissone, J., Heim, M. & Vague, P. (1989) 'Increased plasminogen activator inhibitor activity in non insulin dependent diabetic patients--relationship with plasma insulin', *Thromb Haemost*, 61(3), 370-373.
Jun, J.-I. & Lau, L. F. (2010) 'The matricellular protein CCN1 induces fibroblast senescence & restricts fibrosis in cutaneous wound healing', *Nat Cell Biol*, 12(7), 676-685.
Jun, J. I. & Lau, L. F. (2017) 'CCN2 induces cellular senescence in fibroblasts', *J Cell Commun Signal*, 11(1), 15-23.
Jung, M., Mertens, C. & Brüne, B. (2015) 'Macrophage iron homeostasis & polarization in the context of cancer', *Immunobiology*, 220(2), 295-304.
Junqueira, L. & Montes, G. (1983) 'Biology of collagen-proteoglycan interaction', *Arch Histol Cytol*, 46(5), 589-629.
Junqueira, L. C. U., Bignolas, G. & Brentani, R. (1979) 'Picrosirius staining plus polarization microscopy, a specific method for collagen detection in tissue sections', *Histochem J*, 11(4), 447-455.

Józkowicz, A., Huk, I., Nigisch, A., Weigel, G., Dietrich, W., Motterlini, R. & Dulak, J. (2003) 'Heme oxygenase & angiogenic activity of endothelial cells: Stimulation by carbon monoxide & inhibition by tin protoporphyrin-IX', *Antioxid Redox Signal*, 5(2), 155-162.
Kadler, K. E. (2017) 'Fell Muir Lecture: Collagen fibril formation *in vitro* & *in vivo*', *Int J Exp Pathol*, 98(1), 4-16.
Kadler, K. E., Holmes, D. F., Trotter, J. A. & Chapman, J. A. (1996) 'Collagen fibril formation', *Biochem J*, 316(1), 1-11.
Kagan, H. M. & Li, W. (2003) 'Lysyl oxidase: Properties, specificity, & biological roles inside & outside of the cell', *J Cell Biochem*, 88(4), 660-672.
Kakhlon, O. & Cabantchik, Z. I. (2002) 'The labile iron pool: Characterization, measurement, & participation in cellular processes(1)', *Free Radic Biol Med*, 33(8), 1037-1046.
Kalan, L., Loesche, M., Hodkinson, B. P., Heilmann, K., Ruthel, G., Gardner, S. E. & Grice, E. A. (2016) 'Redefining the chronic-wound microbiome: Fungal communities are prevalent, dynamic, & associated with delayed healing', *MBio*, 7(5), e01058-16.
Kalan, L. R., Meisel, J. S., Loesche, M. A., Horwinski, J., Soaita, I., Chen, X., Uberoi, A., Gardner, S. E. & Grice, E. A. (2019) 'Strain-& species-level variation in the microbiome of diabetic wounds is associated with clinical outcomes & therapeutic efficacy', *Cell Host Microbe*, 25(5), 641-655.
Kalebic, T., Garbisa, S., Glaser, B. & Liotta, L. A. (1983) 'Basement membrane collagen: Degradation by migrating endothelial cells', *Science*, 221(4607), 281-283.
Kameda, T., Mano, H., Yamada, Y., Takai, H., Amizuka, N., Kobori, M., Izumi, N., Kawashima, H., Ozawa, H. & Ikeda, K. (1998) 'Calcium-sensing receptor in mature osteoclasts, which are bone resorbing cells', *Biochem Biophys Res Commun*, 245(2), 419-422.
Kamei, N., Tobe, K., Suzuki, R., Ohsugi, M., Watanabe, T., Kubota, N., Ohtsuka-Kowatari, N., Kumagai, K., Sakamoto, K. & Kobayashi, M. (2006) 'Overexpression of monocyte chemoattractant protein-1 in adipose tissues causes macrophage recruitment & insulin resistance', *J Biol Chem*, 281(36), 26602-26614.
Kanavos, P., van den Aardweg, S. & Schurer, W. (2012) *'Diabetes expenditure, burden of disease & management in 5 EU countries*', London: LSE Health, London School of Economics. Available online: http://www.lse.ac.uk/business-and-consultancy/consulting/assets/documents/diabetes-expenditure-burden-of-disease-and-management-in-5-eu-countries.pdf [Accessed 30/8/19].
Kanazawa, A., Kawamura, Y., Sekine, A., Iida, A., Tsunoda, T., Kashiwagi, A., Tanaka, Y., Babazono, T., Matsuda, M. & Kawai, K. (2005) 'Single nucleotide polymorphisms in the gene encoding Krüppel-like factor 7 are associated with type 2 diabetes', *Diabetologia*, 48(7), 1315-1322.
Kanter, J. E., Kramer, F., Barnhart, S., Averill, M. M., Vivekanandan-Giri, A., Vickery, T., Li, L. O., Becker, L., Yuan, W. & Chait, A. (2012) 'Diabetes promotes an inflammatory macrophage phenotype & atherosclerosis through acyl-CoA synthetase 1', *Proc Nat Acad Sci*, 109(12), E715-E724.
Karamichos, D., Brown, R. & Mudera, V. (2007) 'Collagen stiffness regulates cellular contraction & matrix remodeling gene expression', *J Biomed Mater Res A*, 83(3), 887-894.
Karantza, V. (2011) 'Keratins in health & cancer: More than mere epithelial cell markers', *Oncogene*, 30(2), 127-138.
Kargozar, S., Mozafari, M., Hashemian, S. J., Brouki Milan, P., Hamzehlou, S., Soleimani, M., Joghataei, M. T., Gholipourmalekabadi, M., Korourian, A. & Mousavizadeh, K. (2018) 'Osteogenic potential of stem cells-seeded bioactive

nanocomposite scaffolds: A comparative study between human mesenchymal stem cells derived from bone, umbilical cord Wharton's jelly, & adipose tissue', *J Biomed Mater Res B App Biomater*, 106(1), 61-72.
Karsai, S., Abel, U., Roesch-Ely, M., Affolter, A., Hofele, C., Joos, S., Plinkert, P. & Bosch, F. (2007) 'Comparison of p16INK4a expression with p53 alterations in head & neck cancer by tissue microarray analysis', *J Pathol*, 211(3), 314-322.
Kasprowicz, R., Suman, R. & O'Toole, P. (2017) 'Characterising live cell behaviour: Traditional label-free & quantitative phase imaging approaches', *Int J Biochem Cell Biol*, 84, 89-95.
Kavian, N., Mehlal, S., Jeljeli, M., Saidu, N. E. B., Nicco, C., Cerles, O., Chouzenoux, S., Cauvet, A., Camus, C. & Ait-Djoudi, M. (2018) 'The Nrf2-antioxidant response element signaling pathway controls fibrosis & autoimmunity in scleroderma', *Front Immunol*, 9, 1896.
Kavian, N., Servettaz, A., Mongaret, C., Wang, A., Nicco, C., Chéreau, C., Grange, P., Vuiblet, V., Birembaut, P. & Diebold, M. D. (2010) 'Targeting ADAM-17/notch signaling abrogates the development of systemic sclerosis in a murine model', *Arthritis Rheum*, 62(11), 3477-3487.
Kawai, K., Larson, B. J., Ishise, H., Carre, A. L., Nishimoto, S., Longaker, M. & Lorenz, H. P. (2011) 'Calcium-based nanoparticles accelerate skin wound healing', *PloS One*, 6(11), e27106.
Kawamura, Y., Tanaka, Y., Kawamori, R. & Maeda, S. (2006) 'Overexpression of Kruppel-like factor 7 regulates adipocytokine gene expressions in human adipocytes & inhibits glucose-induced insulin secretion in pancreatic β-cell line', *Mol Endocrinol*, 20(4), 844-856.
Kaya, S., Cresswell, M. & Boccaccini, A. R. (2018) 'Mesoporous silica-based bioactive glasses for antibiotic-free antibacterial applications', *Mat Sci Eng C*, 83, 99-107.
Kazi, T. G., Afridi, H. I., Kazi, N., Jamali, M. K., Arain, M. B., Jalbani, N. & Kandhro, G. A. (2008) 'Copper, chromium, manganese, iron, nickel, & zinc levels in biological samples of diabetes mellitus patients', *Biol Trace Elem Res*, 122(1), 1-18.
Keane, T. J., Londono, R., Turner, N. J. & Badylak, S. F. (2012) 'Consequences of ineffective decellularization of biologic scaffolds on the host response', *Biomaterials*, 33(6), 1771-1781.
Keane, T. J., Swinehart, I. T. & Badylak, S. F. (2015) 'Methods of tissue decellularization used for preparation of biologic scaffolds & *in vivo* relevance', *Methods*, 84, 25-34.
Keen, C. L. & Gershwin, M. E. (1990) 'Zinc deficiency & immune function', *Ann Rev Nutr*, 10(1), 415-431.
Kell, D. B. & Pretorius, E. (2015) 'The simultaneous occurrence of both hypercoagulability & hypofibrinolysis in blood & serum during systemic inflammation, & the roles of iron & fibrin (ogen)', *Integr Biol*, 7(1), 24-52.
Kelner, G. S., Kennedy, J., Bacon, K. B., Kleyensteuber, S., Largaespada, D. A., Jenkins, N. A., Copel&, N. G., Bazan, J. F., Moore, K. W. & Schall, T. J. (1994) 'Lymphotactin: A cytokine that represents a new class of chemokine', *Science*, 266(5189), 1395-1399.
Keshaw, H., Forbes, A. & Day, R. M. (2005) 'Release of angiogenic growth factors from cells encapsulated in alginate beads with bioactive glass', *Biomaterials*, 26(19), 4171-4179.
Kessler, E., Safrin, M., Gustin, J. K. & Ohman, D. E. (1998) 'Elastase & the LasA protease of *Pseudomonas aeruginosa* are secreted with their propeptides', *J Biol Chem*, 273(46), 30225-30231.
Khan, S. R., Pearle, M. S., Robertson, W. G., Gambaro, G., Canales, B. K., Doizi, S., Traxer, O. & Tiselius, H.-G. (2016) 'Kidney stones', *Nat Rev Dis Primers*, 2, 16008.

Khanal, R. C. & Nemere, I. (2008) 'Regulation of intestinal calcium transport', *Annu Rev Nutr*, 28, 179-196.
Khanna, S., Biswas, S., Shang, Y., Collard, E., Azad, A., Kauh, C., Bhasker, V., Gordillo, G. M., Sen, C. K. & Roy, S. (2010) 'Macrophage dysfunction impairs resolution of inflammation in the wounds of diabetic mice', *PloS One*, 5(3), e9539.
Khasigov, P., Podobed, O., Ktzoeva, S., Gatagonova, T., Grachev, S., Shishkin, S. & Berezov, T. (2001) 'Matrix metalloproteinases of normal human tissues', *Biochemistry*, 66(2), 130-140.
Khil, M. S., Cha, D. I., Kim, H. Y., Kim, I. S. & Bhattarai, N. (2003) 'Electrospun nanofibrous polyurethane membrane as wound dressing', *J Biomed Mat Res B Appl Biomater*, 67(2), 675-679.
Khosravi, A. D., Shafie, F., Montazeri, E. A. & Rostami, S. (2016) 'The frequency of genes encoding exotoxin A & exoenzyme S in *Pseudomonas aeruginosa* strains isolated from burn patients', *Burns*, 42(5), 1116-1120.
Kielty, C. M. & Grant, M. E. (2002) 'The collagen family: Structure, assembly, & organization in the extracellular matrix', In: Royce, P.M. & Steinmann, B. (eds) *Connective tissue & its heritable disorders: Molecular*, *genetic*, *& medical aspects*, Wiley-Liss, 159-221.
Killilea, D. W. & Ames, B. N. (2008) 'Magnesium deficiency accelerates cellular senescence in cultured human fibroblasts', *Proc Nat Acad Sci*, 105(15), 5768-5773.
Kim, C., Park, H., Kawada, T., Kim, J., Lim, D., Hubbard, N., Kwon, B., Erickson, K. & Yu, R. (2006a) 'Circulating levels of MCP-1 & IL-8 are elevated in human obese subjects & associated with obesity-related parameters', *Int J Obesity*, 30(9), 1347-1355.
Kim, D. J., Mustoe, T. & Clark, R. A. (2015) 'Cutaneous wound healing in aging small mammals: A systematic review', *Wound Repair Regen*, 23(3), 318-339.
Kim, D. J., Xun, P., Liu, K., Loria, C., Yokota, K., Jacobs, D. R. & He, K. (2010) 'Magnesium intake in relation to systemic inflammation, insulin resistance, & the incidence of diabetes', *Diabetes Care*, 33(12), 2604-2610.
Kim, R. H., Kang, M. K., Kim, T., Yang, P., Bae, S., Williams, D. W., Phung, S., Shin, K. H., Hong, C. & Park, N. H. (2015) 'Regulation of p53 during senescence in normal human keratinocytes', *Aging Cell*, 14(5), 838-846.
Kim, S. A., Punshon, T., Lanzirotti, A., Li, L., Alonso, J. M., Ecker, J. R., Kaplan, J. & Guerinot, M. L. (2006b) 'Localization of iron in Arabidopsis seed requires the vacuolar membrane transporter VIT1', *Science*, 314(5803), 1295-1298.
Kim, S. W. & An, Y.-J. (2012) 'Effect of ZnO & TiO2 nanoparticles preilluminated with UVA & UVB light on *Escherichia coli* & *Bacillus subtilis*', *App Microbiol Biotechnol*, 95(1), 243-253.
King, A. J. (2012) 'The use of animal models in diabetes research', *Br J Pharmacol*, 166(3), 877-894.
Kipling, D. & Cooke, H. J. (1990) 'Hypervariable ultra-long telomeres in mice', *Nature*, 347(6291), 400-402.
Kirichok, Y. V. (2014) 'Mitochondrial uncoupling & thermogenesis', *Biophys J*, 106(2), 4a.
Kirsten, A., Förster, K., Radeczky, E., Linnhoff, A., Balint, B., Watz, H., Wray, H., Salkeld, L., Cullberg, M. & Larsson, B. (2015) 'The safety & tolerability of oral AZD5069, a selective CXCR2 antagonist, in patients with moderate-to-severe COPD', *Pulm Pharmacol Ther*, 31, 36-41.
Kiyono, T., Foster, S. A., Koop, J. I., McDougall, J. K., Galloway, D. A. & Klingelhutz, A. J. (1998) 'Both Rb/p16 INK4a inactivation & telomerase activity are required to immortalize human epithelial cells', *Nature*, 396(6706), 84-88.

Klepeis, V. E., Cornell-Bell, A. & Trinkaus-Randall, V. (2001) 'Growth factors but not gap junctions play a role in injury-induced Ca2+ waves in epithelial cells', *J Cell Sci*, 114(23), 4185-4195.
Klinkajon, W. & Supaphol, P. (2014) 'Novel copper (II) alginate hydrogels & their potential for use as anti-bacterial wound dressings', *Biomed Mater*, 9(4), e045008.
Klueh, U., Wagner, V., Kelly, S., Johnson, A. & Bryers, J. (2000) 'Efficacy of silver-coated fabric to prevent bacterial colonization & subsequent device-based biofilm formation', *J Biomed Mater Res*, 53(6), 621-631.
Ko, J.-W., Shin, N.-R., Park, J.-W., Park, S.-H., Lee, I.-C., Kim, J.-S., Kim, J.-C., Ahn, K.-S. & Shin, I.-S. (2018) 'Copper oxide nanoparticles induce collagen deposition via TGF-β1/Smad3 signaling in human airway epithelial cells', *Nanotoxicology*, 12(3), 239-250.
Kobsa, S., Kristofik, N. J., Sawyer, A. J., Bothwell, A. L., Kyriakides, T. R. & Saltzman, W. M. (2013) 'An electrospun scaffold integrating nucleic acid delivery for treatment of full-thickness wounds', *Biomaterials*, 34(15), 3891-3901.
Koebele, S. V. & Bimonte-Nelson, H. A. (2016) 'The endocrine-brain-aging triad where many paths meet: Female reproductive hormone changes at midlife & their influence on circuits important for learning & memory', *Exp Gerontol*, 94, 14-22.
Koh, H., Yong, T., Chan, C. & Ramakrishna, S. (2008) 'Enhancement of neurite outgrowth using nano-structured scaffolds coupled with laminin', *Biomaterials*, 29(26), 3574-3582.
Koh, T. J. & DiPietro, L. A. (2011) 'Inflammation & wound healing: The role of the macrophage', *Expert Rev Mol Med*, 13, e23.
Kolavennu, V., Zeng, L., Peng, H., Wang, Y. & Danesh, F. R. (2008) 'Targeting of RhoA/ROCK signaling ameliorates progression of diabetic nephropathy independent of glucose control', *Diabetes*, 57(3), 714-723.
Kong, R. & Bhargava, R. (2011) 'Characterization of porcine skin as a model for human skin studies using infrared spectroscopic imaging', *Analyst*, 136(11), 2359-2366.
Kontoghiorghes, G. J., Spyrou, A. & Kolnagou, A. (2010) 'Iron chelation therapy in hereditary hemochromatosis & thalassemia intermedia: Regulatory & non regulatory mechanisms of increased iron absorption', *Hemoglobin*, 34(3), 251-264.
Korgaonkar, A., Trivedi, U., Rumbaugh, K. P. & Whiteley, M. (2013) 'Community surveillance enhances *Pseudomonas aeruginosa* virulence during polymicrobial infection', *Proc Nat Acad Sci*, 110(3), 1059-1064.
Koria, P., Yagi, H., Kitagawa, Y., Megeed, Z., Nahmias, Y., Sheridan, R. & Yarmush, M. L. (2011) 'Self-assembling elastin-like peptides growth factor chimeric nanoparticles for the treatment of chronic wounds', *Proc Nat Acad Sci*, 108(3), 1034-1039.
Korns, D., Frasch, S. C., Fernandez-Boyanapalli, R., Henson, P. M. & Bratton, D. L. (2011) 'Modulation of macrophage efferocytosis in inflammation', *Front Immunol*, 2, 57.
Korošec, B., Glavač, D., Rott, T. & Ravnik-Glavač, M. (2006) 'Alterations in the ATP2A2 gene in correlation with colon & lung cancer', *Cancer Genet Cytogenet*, 171(2), 105-111.
Korošec, B., Glavač, D., Volavšek, M. & Ravnik-Glavač, M. (2009) 'ATP2A3 gene is involved in cancer susceptibility', *Cancer Genet Cytogenet*, 188(2), 88-94.
Kortlever, R. M., Higgins, P. J. & Bernards, R. (2006) 'Plasminogen activator inhibitor-1 is a critical downstream target of p53 in the induction of replicative senescence', *Nat Cell Biol*, 8(8), 877-884.

Kosar, M., Bartkova, J., Hubackova, S., Hodny, Z., Lukas, J. & Bartek, J. (2011) 'Senescence-associated heterochromatin foci are dispensable for cellular senescence, occur in a cell type-& insult-dependent manner & follow expression of p16ink4a', *Cell Cycle*, 10(3), 457-468.
Kosikowska, P., Pikula, M., Langa, P., Trzonkowski, P., Obuchowski, M. & Lesner, A. (2015) 'Synthesis & evaluation of biological activity of antimicrobial–pro-proliferative peptide conjugates', *PloS One*, 10(10), e0140377.
Koskenkorva-Frank, T. S., Weiss, G., Koppenol, W. H. & Burckhardt, S. (2013) 'The complex interplay of iron metabolism, reactive oxygen species, & reactive nitrogen species: insights into the potential of various iron therapies to induce oxidative & nitrosative stress', *Free Radical Bio Med*, 65, 1174-1194.
Kramer, J. L., Baltathakis, I., Alcantara, O. S. & Boldt, D. H. (2002) 'Differentiation of functional dendritic cells & macrophages from human peripheral blood monocyte precursors is dependent on expression of p21 (WAF1/CIP1) & requires iron', *Br J Haematol*, 117(3), 727-734.
Kranke, P., Bennett, M. H., Martyn-St James, M., Schnabel, A., Debus, S. E. & Weibel, S. (2015) 'Hyperbaric oxygen therapy for chronic wounds', *Cochrane Database Syst Rev*, 2, CD004123.
Krause, K. & Foitzik, K. 'Biology of the hair follicle: The basics'. *Semin Cutan Med Surg*, 25(1), 2-10.
Krebs, J., Agellon, L. B. & Michalak, M. (2015) 'Ca2+ homeostasis & endoplasmic reticulum (ER) stress: An integrated view of calcium signaling', *Biochem Biophys Res Commun*, 460(1), 114-121.
Krishna, D. R., Sperker, B., Fritz, P. & Klotz, U. (1999) 'Does pH 6 β-galactosidase activity indicate cell senescence?', *Mech Ageing Dev*, 109(2), 113-123.
Krishnamurthy, J., Ramsey, M. R., Ligon, K. L., Torrice, C., Koh, A., Bonner-Weir, S. & Sharpless, N. E. (2006) 'p16 INK4a induces an age-dependent decline in islet regenerative potential', *Nature*, 443(7110), 453-457.
Krishnamurthy, J., Torrice, C., Ramsey, M. R., Kovalev, G. I., Al-Regaiey, K., Su, L. & Sharpless, N. E. (2004) 'Ink4a/Arf expression is a biomarker of aging', *J Clin Invest*, 114(9), 1299-1307.
Krizhanovsky, V., Yon, M., Dickins, R. A., Hearn, S., Simon, J., Miething, C., Yee, H., Zender, L. & Lowe, S. W. (2008) 'Senescence of activated stellate cells limits liver fibrosis', *Cell*, 134(4), 657-667.
Kroeze, K. L., Boink, M. A., Sampat-Sardjoepersad, S. C., Waaijman, T., Scheper, R. J. & Gibbs, S. (2012) 'Autocrine regulation of re-epithelialization after wounding by chemokine receptors CCR1, CCR10, CXCR1, CXCR2, & CXCR3', *J Invest Dermatol*, 132(1), 216-225.
Kroner, A., Greenhalgh, A. D., Zarruk, J. G., dos Santos, R. P., Gaestel, M. & David, S. (2014) 'TNF & increased intracellular iron alter macrophage polarization to a detrimental M1 phenotype in the injured spinal cord', *Neuron*, 83(5), 1098-1116.
Krtolica, A., Parrinello, S., Lockett, S., Desprez, P.-Y. & Campisi, J. (2001) 'Senescent fibroblasts promote epithelial cell growth & tumorigenesis: A link between cancer & aging', *Proc Nat Acad Sci*, 98(21), 12072-12077.
Krzyszczyk, P., Schloss, R., Palmer, A. & Berthiaume, F. (2018) 'The role of macrophages in acute & chronic wound healing & interventions to promote pro-wound healing phenotypes', *Front Physiol*, 9, 419.
Kubisch, H. M., Wang, J., Luche, R., Carlson, E., Bray, T. M., Epstein, C. J. & Phillips, J. P. (1994) 'Transgenic copper/zinc superoxide dismutase modulates susceptibility to type I diabetes', *Proc Natl Acad Sci*, 91(21), 9956-9959.

Kubota, N., Terauchi, Y., Yamauchi, T., Kubota, T., Moroi, M., Matsui, J., Eto, K., Yamashita, T., Kamon, J. & Satoh, H. (2002) 'Disruption of adiponectin causes insulin resistance & neointimal formation', *J Biol Chem*, 277(29), 25863-25866.
Kuilman, T., Michaloglou, C., Mooi, W. J. & Peeper, D. S. (2010) 'The essence of senescence', *Genes Dev*, 24(22), 2463-2479.
Kuo, S., Kim, H. M., Wang, Z., Bingham, E. L., Miyazawa, A., Marcelo, C. L. & Feinberg, S. E. (2018) 'Comparison of two decellularized dermal equivalents', *J Tissue Eng Regen Med*, 12(4), 983-990.
Kuro-o, M., Matsumura, Y., Aizawa, H., Kawaguchi, H., Suga, T., Utsugi, T., Ohyama, Y., Kurabayashi, M., Kaname, T. & Kume, E. (1997) 'Mutation of the mouse klotho gene leads to a syndrome resembling ageing', *Nature*, 390(6655), 45-51.
Kurosu, H., Yamamoto, M., Clark, J. D., Pastor, J. V., Nandi, A., Gurnani, P., McGuinness, O. P., Chikuda, H., Yamaguchi, M. & Kawaguchi, H. (2005) 'Suppression of aging in mice by the hormone Klotho', *Science*, 309(5742), 1829-1833.
Kutuzova, G. D., Akhter, S., Christakos, S., Vanhooke, J., Kimmel-Jehan, C. & Deluca, H. F. (2006) 'Calbindin D(9k) knockout mice are indistinguishable from wild-type mice in phenotype & serum calcium level', *Proc Natl Acad Sci*, 103(33), 12377-12381.
Kvam, E., Noel, A., Basu-Modak, S. & Tyrrell, R. M. (1999) 'Cyclooxygenase dependent release of heme from microsomal hemeproteins correlates with induction of heme oxygenase 1 transcription in human fibroblasts', *Free Radical Bio Med*, 26(5-6), 511-517.
Labat-Moleur, F., Guillermet, C., Lorimier, P., Robert, C., Lantuejoul, S., Brambilla, E. & Negoescu, A. (1998) 'TUNEL apoptotic cell detection in tissue sections: Critical evaluation & improvement', *J Histochem Cytochem*, 46(3), 327-334.
Labrie, F. (2015) 'All sex steroids are made intracellularly in peripheral tissues by the mechanisms of intracrinology after menopause', *J Steroid Biochem Mol Biol*, 145, 133-138.
Labrie, F., Luu-The, V., Labrie, C. & Simard, J. (2001) 'DHEA & its transformation into androgens & estrogens in peripheral target tissues: Intracrinology', *Front Neuroendocrinol*, 22(3), 185-212.
Lai-Cheong, J. E. & McGrath, J. A. (2009) 'Structure & function of skin, hair & nails', *Medicine*, 37(5), 223-226.
Lam, D. W. & LeRoith, D. (2012) 'The worldwide diabetes epidemic', *Curr Opin Endocrinol Diabetes Obes*, 19(2), 93-96.
Lambers, T. T., Mahieu, F., Oancea, E., Hoofd, L., de Lange, F., Mensenkamp, A. R., Voets, T., Nilius, B., Clapham, D. E., Hoenderop, J. G. & Bindels, R. J. (2006) 'Calbindin-D28K dynamically controls TRPV5-mediated Ca2+ transport', *EMBO J*, 25(13), 2978-2988.
Lambers, T. T., Weidema, A. F., Nilius, B., Hoenderop, J. G. & Bindels, R. J. (2004) 'Regulation of the mouse epithelial Ca2(+) channel TRPV6 by the Ca(2+)-sensor calmodulin', *J Biol Chem*, 279(28), 28855-28861.
Lando, D., Peet, D. J., Gorman, J. J., Whelan, D. A., Whitelaw, M. L. & Bruick, R. K. (2002) 'FIH-1 is an asparaginyl hydroxylase enzyme that regulates the transcriptional activity of hypoxia-inducible factor', *Genes Dev*, 16(12), 1466-1471.
Lane, E. & McLean, W. (2004) 'Keratins & skin disorders', *J Pathol*, 204(4), 355-366.
Langton, A. K., Sherratt, M. J., Griffiths, C. E. & Watson, R. E. (2010) 'A new wrinkle on old skin: The role of elastic fibres in skin ageing', *Int J Cosmet Sci*, 32(5), 330-339.
Lansdown, A. (2002) 'Silver. I: Its antibacterial properties & mechanism of action', *J Wound Care*, 11(4), 125-130.

Lansdown, A., Sampson, B. & Rowe, A. (1999a) 'Sequential changes in trace metal, metallothionein & calmodulin concentrations in healing skin wounds', *J Anat*, 195(3), 375-386.
Lansdown, A. B., Mirastschijski, U., Stubbs, N., Scanlon, E. & Ågren, M. S. (2007) 'Zinc in wound healing: Theoretical, experimental, & clinical aspects', *Wound Repair Regen*, 15(1), 2-16.
Larsson, S. C., Orsini, N. & Wolk, A. (2012) 'Dietary magnesium intake & risk of stroke: A meta-analysis of prospective studies', *Am J Clin Nutr*, 95(2), 362-366.
Lattouf, R., Younes, R., Lutomski, D., Naaman, N., Godeau, G., Senni, K. & Changotade, S. (2014) 'Picrosirius red staining: A useful tool to appraise collagen networks in normal & pathological tissues', *J Histochem Cytochem*, 62(10), 751-758.
Lau, E.Y., Carroll, E.C., Callender, L.A., Hood, G.A., Berryman, V., Pattrick, M., Finer, S., Hitman, G.A., Ackland, G.L. & Henson, S.M. (2019) 'Type 2 diabetes is associated with the accumulation of senescent T cells', *Clin Exp Immunol*, 197(2), 205-213.
Lavin, Y., Winter, D., Blecher-Gonen, R., David, E., Keren-Shaul, H., Merad, M., Jung, S. & Amit, I. (2014) 'Tissue-resident macrophage enhancer landscapes are shaped by the local microenvironment', *Cell*, 159(6), 1312-1326.
Lawrence, T. (2016) 'Coordinated regulation of signaling pathways during macrophage activation', *Microbiol Spectr*, 4(5).
Le, N. T. & Richardson, D. R. (2002) 'The role of iron in cell cycle progression & the proliferation of neoplastic cells', *Biochim Biophys Acta*, 1603(1), 31-46.
Leask, A. (2010) 'Potential therapeutic targets for cardiac fibrosis: TGFβ, angiotensin, endothelin, CCN2, & PDGF, partners in fibroblast activation', *Circ Res*, 106(11), 1675-1680.
Leavitt, T., Hu, M. S., Marshall, C. D., Barnes, L. A., Lorenz, H. P. & Longaker, M. T. (2016) 'Scarless wound healing: Finding the right cells & signals', *Cell Tissue Res*, 365(3), 483-493.
Leber, T. M. & Balkwill, F. R. (1997) 'Zymography: A single-step staining method for quantitation of proteolytic activity on substrate gels', *Anal Biochem*, 249(1), 24-28.
Lee, A., Derricks, K., Minns, M., Ji, S., Chi, C., Nugent, M. A. & Trinkaus-Randall, V. (2014a) 'Hypoxia-induced changes in Ca2+ mobilization & protein phosphorylation implicated in impaired wound healing', *Am J Physiol Cell Physiol*, 306(10), C972-C985.
Lee, B. Y., Han, J. A., Im, J. S., Morrone, A., Johung, K., Goodwin, E. C., Kleijer, W. J., DiMaio, D. & Hwang, E. S. (2006) 'Senescence-associated β-galactosidase is lysosomal β-galactosidase', *Aging Cell*, 5(2), 187-195.
Lee, G.-S., Subramanian, N., Kim, A. I., Aksentijevich, I., Goldbach-Mansky, R., Sacks, D. B., Germain, R. N., Kastner, D. L. & Chae, J. J. (2012) 'The calcium-sensing receptor regulates the NLRP3 inflammasome through Ca 2+ & cAMP', *Nature*, 492(7427), 123-127.
Lee, G. S., Jung, E. M., Choi, K. C., Oh, G. T. & Jeung, E. B. (2009) 'Compensatory induction of the TRPV6 channel in a calbindin-D9k knockout mouse: Its regulation by 1,25-hydroxyvitamin D3', *J Cell Biochem*, 108(5), 1175-1183.
Lee, H.-C. & Auersperg, N. (1980) 'Calcium in epithelial cell contraction', *J Cell Biol*, 85(2), 325-336.
Lee, J., Hoi, C. S., Lilja, K. C., White, B. S., Lee, S. E., Shalloway, D. & Tumbar, T. (2013) 'Runx1 & p21 synergistically limit the extent of hair follicle stem cell quiescence *in vivo*', *Proc Nat Acad Sci*, 110(12), 4634-4639.
Lee, K., Silva, E. A. & Mooney, D. J. (2011) 'Growth factor delivery-based tissue engineering: General approaches & a review of recent developments', *J Royal Soc Interface*, 8(55), 153-170.

Lee, S., Bi, X., Reed, R. B., Ranville, J. F., Herckes, P. & Westerhoff, P. (2014b) 'Nanoparticle size detection limits by single particle ICP-MS for 40 elements', *Environ Sci Technol*, 48(17), 10291-10300.
Lee, T.-S. & Chau, L.-Y. (2002) 'Heme oxygenase-1 mediates the anti-inflammatory effect of interleukin-10 in mice', *Nat Med*, 8(3), 240-246.
Lehen'kyi, V. y., Shapovalov, G., Skryma, R. & Prevarskaya, N. (2011) 'Ion channnels & transporters in cancer. 5. Ion channels in control of cancer & cell apoptosis', *Am J Physiol Cell Physiol*, 301(6), C1281-C1289.
Leinonen, P. T., Hägg, P. M., Peltonen, S., Jouhilahti, E.-M., Melkko, J., Korkiamäki, T., Oikarinen, A. & Peltonen, J. (2009) 'Reevaluation of the normal epidermal calcium gradient, & analysis of calcium levels & ATP receptors in Hailey–Hailey & Darier epidermis', *J Invest Dermatol*, 129(6), 1379-1387.
Leiper, L. J., Walczysko, P., Kucerova, R., Ou, J., Shanley, L. J., Lawson, D., Forrester, J. V., McCaig, C. D., Zhao, M. & Collinson, J. M. (2006) 'The roles of calcium signaling & ERK1/2 phosphorylation in a Pax6+/-mouse model of epithelial wound-healing delay', *BMC Biol*, 4, 27.
Leiss, M., Beckmann, K., Girós, A., Costell, M. & Fässler, R. (2008) 'The role of integrin binding sites in fibronectin matrix assembly *in vivo*', *Curr Opin Cell Biol*, 20(5), 502-507.
Lemaître, V., Soloway, P. D. & D'armiento, J. (2003) 'Increased medial degradation with pseudo-aneurysm formation in apolipoprotein E–knockout mice deficient in tissue inhibitor of metalloproteinases-1', *Circulation*, 107(2), 333-338.
Lemire, J. A., Harrison, J. J. & Turner, R. J. (2013) 'Antimicrobial activity of metals: Mechanisms, molecular targets & applications', *Nat Rev Microbiol*, 11(6), 371-384.
Lengyel, I., Fieuw-Makaroff, S., Hall, A. L., Sim, A. T., Rostas, J. A. & Dunkley, P. R. (2000) 'Modulation of the Phosphorylation & Activity of Calcium/Calmodulin-Dependent Protein Kinase II by Zinc', *J Neurochem*, 75(2), 594-605.
Lenselink, E. A. (2015) 'Role of fibronectin in normal wound healing', *Int Wound J*, 12(3), 313-316.
Lenzen, S. (2008) 'The mechanisms of alloxan- & streptozotocin-induced diabetes', *Diabetologia*, 51(2), 216-226.
Leveque, N., Robin, S., Makki, S., Muret, P., Rougier, A., eacute & Humbert, P. (2003) 'Iron & ascorbic acid concentrations in human dermis with regard to age & body sites', *Gerontology*, 49(2), 117-122.
Levy, B. I., Schiffrin, E. L., Mourad, J.-J., Agostini, D., Vicaut, E., Safar, M. E. & Struijker-Boudier, H. A. (2008) 'Impaired tissue perfusion: A pathology common to hypertension, obesity, & diabetes mellitus', *Circulation*, 118(9), 968-976.
Li, C. & Zhou, H.-M. (2011) 'The role of manganese superoxide dismutase in inflammation defense', *Enzyme Res*, 2011(387176).
Li, G., Mongillo, M., Chin, K.-T., Harding, H., Ron, D., Marks, A. R. & Tabas, I. (2009) 'Role of ERO1-α–mediated stimulation of inositol 1, 4, 5-triphosphate receptor activity in endoplasmic reticulum stress–induced apoptosis', *J Cell Biol*, 186(6), 783-792.
Li, J., Chen, J. & Kirsner, R. (2007) 'Pathophysiology of acute wound healing', *Clin Dermatol*, 25(1), 9-18.
Li, M., Carpio, D. F., Zheng, Y., Bruzzo, P., Singh, V., Ouaaz, F., Medzhitov, R. M. & Beg, A. A. (2001) 'An essential role of the NF-κB/Toll-like receptor pathway in induction of inflammatory & tissue-repair gene expression by necrotic cells', *J Immunol*, 166(12), 7128-7135.
Li, R., Clark, A. & Hench, L. (1991) 'An investigation of bioactive glass powders by sol-gel processing', *J App Biomater*, 2(4), 231-239.

Li, W., Zhang, S.-L., Wang, N., Zhang, B.-B. & Li, M. (2011) 'Blockade of T-type Ca2+ channels inhibits human ovarian cancer cell proliferation', *Cancer Invest*, 29(5), 339-346.
Li, Y. & Tollefsbol, T. O. (2011) 'p16INK4a suppression by glucose restriction contributes to human cellular lifespan extension through SIRT1-mediated epigenetic & genetic mechanisms', *PLoS One*, 6(2), e17421.
Liamis, G., Liberopoulos, E., Barkas, F. & Elisaf, M. (2014) 'Diabetes mellitus & electrolyte disorders', *World J Clin Cases*, 2(10), 488–496.
Liang, C.-C., Park, A. Y. & Guan, J.-L. (2007) '*In vitro* scratch assay: A convenient & inexpensive method for analysis of cell migration *in vitro*', *Nat Prot*, 2(2), 329-333.
Liang, C.-P., Han, S., Li, G., Tabas, I. & Tall, A. R. (2012) 'Impaired MEK signaling & SERCA expression promote ER stress & apoptosis in insulin-resistant macrophages & are reversed by exenatide treatment', *Diabetes*, 61(10), 2609-2620.
Libertini, G. (2015) 'Non-programmed versus programmed aging paradigm', *Curr Aging Sci*, 8(1), 56-68.
Lidén, C., Skare, L., Nise, G. & Vahter, M. (2008) 'Deposition of nickel, chromium, & cobalt on the skin in some occupations–assessment by acid wipe sampling', *Contact Dermatitis*, 58(6), 347-354.
Lill, R. & Kispal, G. (2000) 'Maturation of cellular Fe–S proteins: An essential function of mitochondria', *Trends Biochem Sci*, 25(8), 352-356.
Lim, X., Tan, S. H., Koh, W. L. C., Chau, R. M. W., Yan, K. S., Kuo, C. J., van Amerongen, R., Klein, A. M. & Nusse, R. (2013) 'Interfollicular epidermal stem cells self-renew via autocrine Wnt signaling', *Science*, 342(6163), 1226-1230.
Lim, Y., Levy, M. & Bray, T. M. (2004) 'Dietary zinc alters early inflammatory responses during cutaneous wound healing in weanling CD-1 mice', *J Nutr*, 134(4), 811-816.
Lin, C., Mao, C., Zhang, J., Li, Y. & Chen, X. (2012) 'Healing effect of bioactive glass ointment on full-thickness skin wounds', *Biomed Mater*, 7(4), e045017.
Lin, L., Goldberg, Y. P. & Ganz, T. (2005) 'Competitive regulation of hepcidin mRNA by soluble & cell-associated hemojuvelin', *Blood*, 106(8), 2884-2889.
Lin, S., Ionescu, C., Baker, S., Smith, M. E. & Jones, J. R. (2010) 'Characterisation of the inhomogeneity of sol–gel-derived SiO2–CaO bioactive glass & a strategy for its improvement', *J Solgel Sci Technol*, 53(2), 255-262.
Lin, W.-h., Xiang, L.-J., Shi, H.-X., Zhang, J., Jiang, L.-p., Cai, P.-t., Lin, Z.-L., Lin, B.-B., Huang, Y. & Zhang, H.-L. (2015) 'Fibroblast growth factors stimulate hair growth through β-catenin & Shh expression in C57BL/6 mice', *BioMed Res Int*, 2015(730139).
Lin, Y.-W., Lee, B., Liu, P.-S. & Wei, L.-N. (2016) 'Receptor-interacting protein 140 orchestrates the dynamics of macrophage M1/M2 polarization', *J Innate Immun*, 8(1), 97-107.
Lindemann, O., Strodthoff, C., Horstmann, M., Nielsen, N., Jung, F., Schimmelpfennig, S., Heitzmann, M. & Schwab, A. (2015) 'TRPC1 regulates fMLP-stimulated migration & chemotaxis of neutrophil granulocytes', *Biochim Biophys Acta Mol Cell Res*, 1853(9), 2122-2130.
Lindholm, C. & Searle, R. (2016) 'Wound management for the 21st century: Combining effectiveness & efficiency', *Int Wound J*, 13, 5-15.
Link, T. M., Park, U., Vonakis, B. M., Raben, D. M., Soloski, M. J. & Caterina, M. J. (2010) 'TRPV2 has a pivotal role in macrophage particle binding & phagocytosis', *Nat Immunol*, 11(3), 232-239.

Lipinski, B. & Pretorius, E. (2012) 'Novel pathway of ironinduced blood coagulation: Implications for diabetes mellitus & its complications', *Pol Arch Med Wewn*, 122(3), 115-122.
Liu, J., Huang, K., Cai, G.-Y., Chen, X.-M., Yang, J.-R., Lin, L.-R., Yang, J., Huo, B.-G., Zhan, J. & He, Y.-N. (2014a) 'Receptor for advanced glycation end-products promotes premature senescence of proximal tubular epithelial cells via activation of endoplasmic reticulum stress-dependent p21 signaling', *Cell Signal*, 26(1), 110-121.
Liu, J., Zheng, H., Poh, P., Machens, H.-G. & Schilling, A. (2015) 'Hydrogels for engineering of perfusable vascular networks', *Int J Mol Sci*, 16(7), 15997-16016.
Liu, J. C., Parks, R. J., Liu, J., Stares, J., Rovira, I. I., Murphy, E. & Finkel, T. (2017) 'The *in vivo* biology of the mitochondrial calcium uniporter', *Adv Exp Med Biol*, 982, 49-63.
Liu, L., Moody, J. & Gall, A. (2016) 'A Quantitative, Pooled Analysis & Systematic Review of Controlled Trials on the Impact of Electrical Stimulation Settings & Placement on Pressure Ulcer Healing Rates in Persons With Spinal Cord Injuries', *Ostomy Wound Manage*, 62(7), 16-34.
Liu, S.-A., Li, D., Li, S., Teng, F.-Z., Ke, S., He, Y. & Lu, Y. (2014b) 'High-precision copper & iron isotope analysis of igneous rock standards by MC-ICP-MS', *J Anal Anom Spectrom*, 29(1), 122-133.
Liu, X., Huang, W., Fu, H., Yao, A., Wang, D., Pan, H., Lu, W. W., Jiang, X. & Zhang, X. (2009) 'Bioactive borosilicate glass scaffolds: *In vitro* degradation & bioactivity behaviors', *J Mater Sci Mater Med*, 20(6), 1237-1243.
Liu, X., Rahaman, M. N. & Day, D. E. (2014c) '*In vitro* Degradation & Conversion of Melt-Derived Microfibrous Borate (13-93B3) Bioactive Glass Doped with Metal Ions', *J Am Ceram Soc*, 97(11), 3501-3509.
Liuzzi, J. P., Aydemir, F., Nam, H., Knutson, M. D. & Cousins, R. J. (2006) 'Zip14 (Slc39a14) mediates non-transferrin-bound iron uptake into cells', *Proc Nat Acad Sci*, 103(37), 13612-13617.
Loenarz, C. & Schofield, C. J. (2008) 'Expanding chemical biology of 2-oxoglutarate oxygenases', *Nat Chem Biol*, 4(3), 152-156.
Loesche, M., Gardner, S. E., Kalan, L., Horwinski, J., Zheng, Q., Hodkinson, B. P., Tyldsley, A. S., Franciscus, C. L., Hillis, S. L. & Mehta, S. (2017) 'Temporal stability in chronic wound microbiota is associated with poor healing', *J Invest Dermatol*, 137(1), 237-244.
Lohmann, N., Schirmer, L., Atallah, P., Wandel, E., Ferrer, R. A., Werner, C., Simon, J. C., Franz, S. & Freudenberg, U. (2017) 'Glycosaminoglycan-based hydrogels capture inflammatory chemokines & rescue defective wound healing in mice', *Sci Trans Med*, 9(386), eaai9044.
Lomholt, J. A., Poulsen, K. & Kilian, M. (2001) 'Epidemic population structure of *Pseudomonas aeruginosa*: Evidence for a clone that is pathogenic to the eye & that has a distinct combination of virulence factors', *Infect Immun*, 69(10), 6284-6295.
Long, M., de la Vega, M. R., Wen, Q., Bharara, M., Jiang, T., Zhang, R., Zhou, S., Wong, P. K., Wondrak, G. T. & Zheng, H. (2016) 'An essential role of NRF2 in diabetic wound healing', *Diabetes*, 65(3), 780-793.
Lopes-Paciencia, S., Saint-Germain, E., Rowell, M.-C., Ruiz, A. F., Kalegari, P. & Ferbeyre, G. (2019) 'The senescence-associated secretory phenotype & its regulation', *Cytokine*, 117, 15-22.
Loupy, A., Ramakrishnan, S. K., Wootla, B., Chambrey, R., de La Faille, R., Bourgeois, S., Bruneval, P., Mandet, C., Christensen, E. I. & Faure, H. (2012) 'PTH-independent regulation of blood calcium concentration by the calcium-sensing receptor', *J Clin Invest*, 122(9), 3355-3367.

Love, N. R., Chen, Y., Ishibashi, S., Kritsiligkou, P., Lea, R., Koh, Y., Gallop, J. L., Dorey, K. & Amaya, E. (2013) 'Amputation-induced reactive oxygen species are required for successful Xenopus tadpole tail regeneration', *Nat Cell Biol*, 15(2), 222-228.
Lowe, J. M., Menendez, D. & Fessler, M. B. (2014) 'A new inflammatory role for p53 in human macrophages', *Cell Cycle*, 13(19), 2983-2984.
Lu, H., Fan, Y., Qiao, C., Liang, W., Hu, W., Zhu, T., Zhang, J. & Chen, Y. E. (2017) 'TFEB inhibits endothelial cell inflammation & reduces atherosclerosis', *Sci Signal*, 10(464), eaah4214.
Lu, H., Zhang, T., Wang, X. & Fang, Q. (2009) 'Electrospun submicron bioactive glass fibers for bone tissue scaffold', *J Mater Sci Mater Med*, 20(3), 793-798.
Lu, Z., Rong, K., Li, J., Yang, H. & Chen, R. (2013) 'Size-dependent antibacterial activities of silver nanoparticles against oral anaerobic pathogenic bacteria', *J Mater Sci Mater Med*, 24(6), 1465-1471.
Lucas, T., Waisman, A., Ranjan, R., Roes, J., Krieg, T., Müller, W., Roers, A. & Eming, S. A. (2010) 'Differential roles of macrophages in diverse phases of skin repair', *J Immunol*, 184(7), 3964-3977.
Lucero, H. & Kagan, H. (2006) 'Lysyl oxidase: An oxidative enzyme & effector of cell function', *Cell Mol Life Sci*, 63(19-20), 2304-2316.
Lue, H., Kleemann, R., Calandra, T., Roger, T. & Bernhagen, J. (2002) 'Macrophage migration inhibitory factor (MIF): Mechanisms of action & role in disease', *Microbes Infect*, 4(4), 449-460.
Lugović, L., Lipozenočić, J. & Jakić-Razumović, J. (2001) 'Atopic dermatitis: Immunophenotyping of inflammatory cells in skin lesions', *Int J Dermatol*, 40(8), 489-494.
Lujambio, A., Akkari, L., Simon, J., Grace, D., Tschaharganeh, D. F., Bolden, J. E., Zhao, Z., Thapar, V., Joyce, J. A. & Krizhanovsky, V. (2013) 'Non-cell-autonomous tumor suppression by p53', *Cell*, 153(2), 449-460.
Lundblad, R. L., Kingdon, H. S., Mann, K. G. & White, G. C. (2000) 'Issues with the assay of factor VIII activity in plasma & factor VIII concentrates', *Thromb Haemost*, 84(6), 942-948.
Lunova, M., Goehring, C., Kuscuoglu, D., Mueller, K., Chen, Y., Walther, P., Deschemin, J.-C., Vaulont, S., Haybaeck, J. & Lackner, C. (2014) 'Hepcidin knockout mice fed with iron-rich diet develop chronic liver injury & liver fibrosis due to lysosomal iron overload', *Hepatology*, 61(3), 633-641.
Luo, J., Stewart, R., Berdeaux, R. & Hu, H. (2012) 'Tonic Inhibition of TRPV3 by Mg2+ in Mouse Epidermal Keratinocytes', *J Invest Dermatol*, 132(9), 2158-2165.
Lupa, D. M. W., Kalfalah, F., Safferling, K., Boukamp, P., Poschmann, G., Volpi, E., Götz-Rösch, C., Bernerd, F., Haag, L. & Huebenthal, U. (2015) 'Characterization of skin aging–associated secreted proteins (SAASP) produced by dermal fibroblasts isolated from intrinsically aged human skin', *J Invest Dermatol*, 135(8), 1954-1968.
Lévigne, D., Modarressi, A., Krause, K.-H. & Pittet-Cuénod, B. (2016) 'NADPH oxidase 4 deficiency leads to impaired wound repair & reduced dityrosine-crosslinking, but does not affect myofibroblast formation', *Free Radical Bio Med*, 96, 374-384.
López-Otín, C., Blasco, M. A., Partridge, L., Serrano, M. & Kroemer, G. (2013) 'The hallmarks of aging', *Cell*, 153(6), 1194-1217.
Ma, J., Folsom, A. R., Melnick, S. L., Eckfeldt, J. H., Sharrett, A. R., Nabulsi, A. A., Hutchinson, R. G. & Metcalf, P. A. (1995) 'Associations of serum & dietary magnesium with cardiovascular disease, hypertension, diabetes, insulin, & carotid arterial wall thickness: The ARIC study', *J Clin Epidemiol*, 48(7), 927-940.
Ma, L., Zeng, Y., Wei, J., Yang, D., Ding, G., Liu, J., Shang, J., Kang, Y. & Ji, X. (2018a) 'Knockdown of LOXL1 inhibits TGF-β1-induced proliferation & fibrogenesis of

hepatic stellate cells by inhibition of Smad2/3 phosphorylation', *Biomed Pharmacother*, 107, 1728-1735.
Ma, L.-Y., Lv, Y.-L., Huo, K., Liu, J., Shang, S.-H., Fei, Y.-L., Li, Y.-B., Zhao, B.-Y., Wei, M. & Deng, Y.-N. (2017) 'Autophagy-lysosome dysfunction is involved in Aβ deposition in STZ-induced diabetic rats', *Behav Brain Res*, 320, 484-493.
Ma, T., Gutnick, J., Salazar, B., Larsen, M. D., Suenaga, E., Zilber, S., Huang, Z., Huddleston, J., Smith, R. L. & Goodman, S. (2007) 'Modulation of allograft incorporation by continuous infusion of growth factors over a prolonged duration *in vivo*', *Bone*, 41(3), 386-392.
Ma, X., Warnier, M., Raynard, C., Ferrand, M., Kirsh, O., Defossez, P. A., Martin, N. & Bernard, D. (2018b) 'The nuclear receptor RXRA controls cellular senescence by regulating calcium signaling', *Aging Cell*, 17(6), e12831.
Madison, K. C. (2003) 'Barrier function of the skin:"La raison d'etre" of the epidermis', *J Invest Dermatol*, 121(2), 231-241.
Maeda, M., Hayashi, T., Mizuno, N., Hattori, Y. & Kuzuya, M. (2015) 'Intermittent high glucose implements stress-induced senescence in human vascular endothelial cells: Role of superoxide production by NADPH oxidase', *PLoS One*, 10(4), e0123169.
Mah, T.-F. (2012) 'Regulating antibiotic tolerance within biofilm microcolonies', *J Bacteriol*, 194(18), 4791-4792.
Mahl, J. A., Vogel, B. E., Court, M., Kolopp, M., Roman, D. & Nogués, V. (2006) 'The minipig in dermatotoxicology: Methods & challenges', *Exp Toxicol Pathol*, 57(5-6), 341-345.
Maier, J. A., Malpuech-Brugère, C., Zimowska, W., Rayssiguier, Y. & Mazur, A. (2004) 'Low magnesium promotes endothelial cell dysfunction: Implications for atherosclerosis, inflammation & thrombosis', *Biochim Biophys Acta Mol Basis Dis*, 1689(1), 13-21.
Maione, A. G., Smith, A., Kashpur, O., Yanez, V., Knight, E., Mooney, D. J., Veves, A., Tomic-Canic, M. & Garlick, J. A. (2016) 'Altered ECM deposition by diabetic foot ulcer-derived fibroblasts implicates fibronectin in chronic wound repair', *Wound Repair Regen*, 24(4), 630-643.
Mairuae, N., Connor, J. R. & Cheepsunthorn, P. (2011) 'Increased cellular iron levels affect matrix metalloproteinase expression & phagocytosis in activated microglia', *Neurosci Lett*, 500(1), 36-40.
Majmundar, A. J., Wong, W. J. & Simon, M. C. (2010) 'Hypoxia-inducible factors & the response to hypoxic stress', *Mol Cell*, 40(2), 294-309.
Makimattila, S., Virkamaki, A., Groop, P.-H., Cockcroft, J., Utriainen, T., Fagerudd, J. & Yki-Jarvinen, H. (1996) 'Coronary heart disease/myocardial infarction/bypass grafts/endothelial function', *Circulation*, 94(6), 1276-1282.
Malhotra, V. & Erlmann, P. (2015) 'The pathway of collagen secretion', *Ann Rev Cell Dev Biol*, 31, 109-124.
Malic, S., Hill, K. E., Hayes, A., Percival, S. L., Thomas, D. W. & Williams, D. W. (2009) 'Detection & identification of specific bacteria in wound biofilms using peptide nucleic acid fluorescent in situ hybridization (PNA FISH)', *Microbiology*, 155(8), 2603-2611.
Malumbres, M. & Barbacid, M. (2005) 'Mammalian cyclin-dependent kinases', *Trends Biochem Sci*, 30(11), 630-641.
Mancuso, M. E. & Santagostino, E. (2017) 'Platelets: Much more than bricks in a breached wall', *Br J Haematol*, 178(2), 209-219.
Mandeville, J. T. & Maxfield, F. R. (1997) 'Effects of buffering intracellular free calcium on neutrophil migration through three-dimensional matrices', *J Cell Physiol*, 171(2), 168-178.

Maniecki, M. B., Møller, H. J., Moestrup, S. K. & Møller, B. K. (2006) 'CD163 positive subsets of blood dendritic cells: The scavenging macrophage receptors CD163 & CD91 are coexpressed on human dendritic cells & monocytes', *Immunobiology*, 211(6-8), 407-417.
Mann, K. G. 2003. Factor VII-activating protease: Coagulation, fibrinolysis, & atherothrombosis? *Circulation*, 107(5), 654-655.
Mantovani, A., Biswas, S. K., Galdiero, M. R., Sica, A. & Locati, M. (2013) 'Macrophage plasticity & polarization in tissue repair & remodelling', *J Pathol*, 229(2), 176-185.
Mantovani, A., Sica, A. & Locati, M. (2005) 'Macrophage polarization comes of age', *Immunity*, 23(4), 344-346.
Mao, Y. & Schwarzbauer, J. E. (2005) 'Fibronectin fibrillogenesis, a cell-mediated matrix assembly process', *Matrix Biol*, 24(6), 389-399.
Margolis, D. J., Knauss, J. & Bilker, W. (2002) 'Hormone replacement therapy & prevention of pressure ulcers & venous leg ulcers', *Lancet*, 359(9307), 675-677.
Marionnet, C., Pierrard, C., Lejeune, F., Sok, J., Thomas, M. & Bernerd, F. (2010) 'Different oxidative stress response in keratinocytes & fibroblasts of reconstructed skin exposed to non extreme daily-ultraviolet radiation', *PloS One*, 5(8), e12059.
Markolovic, S., Wilkins, S. E. & Schofield, C. J. (2015) 'Protein hydroxylation catalyzed by 2-oxoglutarate-dependent oxygenases', *J Biol Chem*, 290(34), 20712-20722.
Markowitz, J. & Carson III, W. E. (2013) 'Review of S100A9 biology & its role in cancer', *Biochim Biophys Acta-Reviews on Cancer*, 1835(1), 100-109.
Marks, J. & Shuster, S. (1970) 'Anaemia & skin disease', *Postgrad Med J*, 46(541), 659-663.
Marquet, F., Bonneau, M., Pascale, F., Urien, C., Kang, C., Schwartz-Cornil, I. & Bertho, N. (2011) 'Characterization of dendritic cells subpopulations in skin & afferent lymph in the swine model', *PLoS One*, 6(1), e16320.
Martin, C., Ohayon, D., Alkan, M., Mocek, J., Pederzoli-Ribeil, M., C&alh, C., Thevenot, G., Millet, A., Tamassia, N. & Cassatella, M. A. (2016) 'Neutrophil-expressed p21/waf1 favors inflammation resolution in *Pseudomonas aeruginosa* infection', *Am J Resp Cell Mol Biol*, 54(5), 740-750.
Martin, N. & Bernard, D. (2018) 'Calcium signaling & cellular senescence', *Cell Calcium*, 70, 16-23.
Martin, P. (1997) 'Wound healing--aiming for perfect skin regeneration', *Science*, 276(5309), 75-81.
Martin, P., D'Souza, D., Martin, J., Grose, R., Cooper, L., Maki, R. & McKercher, S. R. (2003) 'Wound healing in the PU. 1 null mouse—tissue repair is not dependent on inflammatory cells', *Curr Biol*, 13(13), 1122-1128.
Martin, P. & Leibovich, S. J. (2005) 'Inflammatory cells during wound repair: The good, the bad & the ugly', *Trends Cell Biol*, 15(11), 599-607.
Martin, P. & Nunan, R. (2015) 'Cellular & molecular mechanisms of repair in acute & chronic wound healing', *Br J Dermatol*, 173(2), 370-378.
Martinez, F. O., Gordon, S., Locati, M. & Mantovani, A. (2006) 'Transcriptional profiling of the human monocyte-to-macrophage differentiation & polarization: New molecules & patterns of gene expression', *J Immunol*, 177(10), 7303-7311.
Martinez-Castanon, G., Nino-Martinez, N., Martinez-Gutierrez, F., Martinez-Mendoza, J. & Ruiz, F. (2008) 'Synthesis & antibacterial activity of silver nanoparticles with different sizes', *J Nanoparticle Res*, 10(8), 1343-1348.
Martins, C. H. G., Carvalho, T. C., Souza, M. G. M., Ravagnani, C., Peitl, O., Zanotto, E. D., Panzeri, H. & Casemiro, L. A. (2011) 'Assessment of antimicrobial effect of Biosilicate® against anaerobic, microaerophilic & facultative anaerobic microorganisms', *J Mat Sci Mat Med*, 22(6), 1439-1446.

Martínez, P. & Blasco, M. A. (2011) 'Telomeric & extra-telomeric roles for telomerase & the telomere-binding proteins', *Nat Rev Cancer*, 11(3), 161-176.
Marx, D. E. & Barillo, D. J. (2014) 'Silver in medicine: The basic science', *Burns*, 40(1), 9-18.
Mashburn, L. M., Jett, A. M., Akins, D. R. & Whiteley, M. (2005) *'Staphylococcus aureus* serves as an iron source for *Pseudomonas aeruginosa* during *in vivo* coculture', *J Bacteriol*, 187(2), 554-566.
Masoro, E. J. (2006) 'Dietary restriction-induced life extension: A broadly based biological phenomenon', *Biogerontology*, 7(3), 153-155.
Matjusaitis, M., Chin, G., Sarnoski, E. A. & Stolzing, A. (2016) 'Biomarkers to identify & isolate senescent cells', *Ageing Res Rev*, 29, 1-12.
Matsumoto, D., Shigeura, T., Sato, K., Inoue, K., Suga, H., Kato, H., Aoi, N., Murase, S., Gonda, K. & Yoshimura, K. (2007) 'Influences of preservation at various temperatures on liposuction aspirates', *Plast Reconstr Surg*, 120(6), 1510-1517.
Matthaei, M., Meng, H., Meeker, A. K., Eberhart, C. G. & Jun, A. S. (2012) 'Endothelial Cdkn1a (p21) overexpression & accelerated senescence in a mouse model of Fuchs endothelial corneal dystrophy', *Invest Ophthalmol Vis Sci*, 53(10), 6718-6727.
Mattson, M. P. (2007) 'Calcium & neurodegeneration', *Aging Cell*, 6(3), 337-350.
Mauer, J., Chaurasia, B., Goldau, J., Vogt, M. C., Ruud, J., Nguyen, K. D., Theurich, S., Hausen, A. C., Schmitz, J., Brönneke, H. S., Estevez, E., Allen, T. L., Mesaros, A., Partridge, L., Febbraio, M. A., Chawla, A., Wunderlich, F. T. & Brüning, J. C. (2014) 'Signaling by IL-6 promotes alternative activation of macrophages to limit endotoxemia & obesity-associated resistance to insulin', *Nat Immunol*, 15(5), 423-430.
Maurer, P. & Hohenester, E. (1997) 'Structural & functional aspects of calcium binding in extracellular matrix proteins', *Matrix Biol*, 15(8-9), 569-580.
Mayle, K. M., Le, A. M. & Kamei, D. T. (2012) 'The intracellular trafficking pathway of transferrin', *Biochim Biophys Acta*, 1820(3), 264-281.
Mazio, C., Casale, C., Imparato, G., Urciuolo, F., Attanasio, C., De Gregorio, M., Rescigno, F. & Netti, P. A. (2019) 'Pre-vascularized dermis model for fast & functional anastomosis with host vasculature', *Biomaterials*, 192, 159-170.
Mazur, A., Maier, J. A., Rock, E., Gueux, E., Nowacki, W. & Rayssiguier, Y. (2007) 'Magnesium & the inflammatory response: Potential physiopathological implications', *Arch Biochem Biophys*, 458(1), 48-56.
Maçon, A. L., Kim, T. B., Valliant, E. M., Goetschius, K., Brow, R. K., Day, D. E., Hoppe, A., Boccaccini, A. R., Kim, I. Y. & Ohtsuki, C. (2015) 'A unified *in vitro* evaluation for apatite-forming ability of bioactive glasses & their variants', *J Mat Sci Mat Med*, 26(2), 1-10.
McCallum, N., Berger-Bächi, B. & Senn, M. M. (2010) 'Regulation of antibiotic resistance in *Staphylococcus aureus*', *Int J Med Microbiol*, 300(2-3), 118-129.
McClain, D. A., Abraham, D., Rogers, J., Brady, R., Gault, P., Ajioka, R. & Kushner, J. P. (2006) 'High prevalence of abnormal glucose homeostasis secondary to decreased insulin secretion in individuals with hereditary haemochromatosis', *Diabetologia*, 49(7), 1661-1669.
McCloy, R. A., Rogers, S., Caldon, C. E., Lorca, T., Castro, A. & Burgess, A. (2014) 'Partial inhibition of Cdk1 in G2 phase overrides the SAC & decouples mitotic events', *Cell Cycle*, 13(9), 1400-1412.
McGee, G. S., Davidson, J. M., Buckley, A., Sommer, A., Woodward, S. C., Aquino, A. M., Barbour, R. & Demetriou, A. A. (1988) 'Recombinant basic fibroblast growth factor accelerates wound healing', *J Surg Res*, 45(1), 145-153.

McRae, R., Bagchi, P., Sumalekshmy, S. & Fahrni, C. J. (2009) 'In situ imaging of metals in cells & tissues', *Chem Rev*, 109(10), 4780-4827.
McSheehy, S., Pohl, P., Szpunar, J., Potin-Gautier, M. & Łobiński, R. (2001) 'Analysis for selenium speciation in selenized yeast extracts by two-dimensional liquid chromatography with ICP-MS & electrospray MS-MS detection', *J Anal Atom Spectrom*, 16(1), 68-73.
McVeigh, G., Morgan, D., Allen, P., Trimble, M., Hamilton, P., Dixon, L., Silke, B. & Hayes, J. (2002) 'Early vascular abnormalities & de novo nitrate tolerance in diabetes mellitus', *Diabetes Obes Metab*, 4(5), 336-341.
Mehrel, T., Hohl, D., Rothnagel, J. A., Longley, M. A., Bundman, D., Cheng, C., Lichti, U., Bisher, M. E., Steven, A. C. & Steinert, P. M. (1990) 'Identification of a major keratinocyte cell envelope protein, loricrin', *Cell*, 61(6), 1103-1112.
Mehta, K. J., Coombes, J. D., Briones-Orta, M., Manka, P. P., Williams, R., Patel, V. B. & Syn, W.-K. (2018) 'Iron enhances hepatic fibrogenesis & activates transforming growth factor-β signaling in murine hepatic stellate cells', *Am J Med Sci*, 355(2), 183-190.
Meis, L. d. & Vianna, A. L. (1979) 'Energy interconversion by the Ca2+-dependent ATPase of the sarcoplasmic reticulum', *Ann Rev Biochem*, 48(1), 275-292.
Meissner, G. (1994) 'Ryanodine receptor/Ca2+ release channels & their regulation by endogenous effectors', *Ann Rev Physiol*, 56(1), 485-508.
Mekkes, J., Loots, M., Van Der Wal, A. & Bos, J. (2003) 'Causes, investigation & treatment of leg ulceration', *Br J Dermatol*, 148(3), 388-401.
Meli, R., Raso, G. M., Irace, C., Simeoli, R., Di Pascale, A., Paciello, O., Pagano, T. B., Calignano, A., Colonna, A. & Santamaria, R. (2013) 'High fat diet induces liver steatosis & early dysregulation of iron metabolism in rats', *PLoS One*, 8(6), e66570.
Mendes, A. L., Miot, H. A. & Haddad, V. (2017) 'Diabetes mellitus & the skin', *An Bras Dermatol*, 92(1), 8-20.
Mendez, M. V., Stanley, A., Park, H.-Y., Shon, K., Phillips, T. & Menzoian, J. O. (1998) 'Fibroblasts cultured from venous ulcers display cellular characteristics of senescence', *J Vasc Surg*, 28(5), 876-883.
Menon, G. K., Grayson, S. & Elias, P. M. (1985) 'Ionic calcium reservoirs in mammalian epidermis: Ultrastructural localization by ion-capture cytochemistry', *J Invest Dermatol*, 84(6), 508-512.
Mercadal, L., Mercadel, L., Metzger, M., Haymann, J. P., Thervet, E., Boffa, J. J., Flamant, M., Vrtovsnik, F., Houillier, P., Froissart, M., Stengel, B. & Group, N. S. (2014) 'The relation of hepcidin to iron disorders, inflammation & hemoglobin in chronic kidney disease', *PLoS One*, 9(6), e99781.
Messina, A., Reina, S., Guarino, F. & De Pinto, V. (2012) 'VDAC isoforms in mammals', *Biochim Biophys Acta Biomembranes*, 1818(6), 1466-1476.
Metcalfe, J. A., Parkhill, J., Campbell, L., Stacey, M., Biggs, P., Byrd, P. J. & Taylor, A. M. R. (1996) 'Accelerated telomere shortening in ataxia telangiectasia', *Nat Med*, 13(3), 350-353.
Meyers, M. B., Puri, T. S., Chien, A. J., Gao, T., Hsu, P. H., Hosey, M. M. & Fishman, G. I. (1998) 'Sorcin associates with the pore-forming subunit of voltage-dependent L-type Ca2+ channels', *J Biol Chem*, 273(30), 18930-18935.
Michalak, M., Groenendyk, J., Szabo, E., Gold, L. I. & Opas, M. (2009) 'Calreticulin, a multi-process calcium-buffering chaperone of the endoplasmic reticulum', *Biochem J*, 417(3), 651-666.
Michels, K., Nemeth, E., Ganz, T. & Mehrad, B. (2015) 'Hepcidin & host defense against infectious diseases', *PLoS Pathog*, 11(8), e1004998.

Michée, S., Brignole-Baudouin, F., Riancho, L., Rostene, W., Baudouin, C. & Labbé, A. (2013) 'Effects of benzalkonium chloride on THP-1 differentiated macrophages *in vitro*', *PLoS One*, 8(8), e72459.
Miguez-Pacheco, V., Hench, L. L. & Boccaccini, A. R. (2015) 'Bioactive glasses beyond bone & teeth: Emerging applications in contact with soft tissues', *Acta Biomater*, 13, 1-15.
Mijnendonckx, K., Leys, N., Mahillon, J., Silver, S. & Van Houdt, R. (2013) 'Antimicrobial silver: Uses, toxicity & potential for resistance', *Biometals*, 26(4), 609-621.
Mikoshiba, K. (2007) 'IP3 receptor/Ca2+ channel: from discovery to new signaling concepts', *J Neurochem*, 102(5), 1426-1446.
Milatovic, S., Nanney, L. B., Yu, Y., White, J. R. & Richmond, A. (2003) 'Impaired healing of nitrogen mustard wounds in CXCR2 null mice', *Wound Repair Regen*, 11(3), 213-219.
Miller, J. L. (2013) 'Iron deficiency anemia: A common & curable disease', *CSH Perspect Med*, 3(7), a011866.
Miller, M. & Mayo, K. (2017) 'Chemokines from a structural perspective', *Int J Mol Sci*, 18(10), e2088.
Mills, A. A., Zheng, B., Wang, X.-J., Vogel, H., Roop, D. R. & Bradley, A. (1999) 'p63 is a p53 homologue required for limb & epidermal morphogenesis', *Nature*, 398(6729), 708-713.
Minamino, T., Orimo, M., Shimizu, I., Kunieda, T., Yokoyama, M., Ito, T., Nojima, A., Nabetani, A., Oike, Y. & Matsubara, H. (2009) 'A crucial role for adipose tissue p53 in the regulation of insulin resistance', *Nat Med*, 15(9), 1082-1087.
Minamiyama, Y., Takemura, S., Kodai, S., Shinkawa, H., Tsukioka, T., Ichikawa, H., Naito, Y., Yoshikawa, T. & Okada, S. (2010) 'Iron restriction improves type 2 diabetes mellitus in Otsuka Long-Evans Tokushima fatty rats', *Am J Physiol Endocrinol Metab*, 298(6), E1140-E1149.
Mine, S., Fortunel, N. O., Pageon, H. & Asselineau, D. (2008) 'Aging alters functionally human dermal papillary fibroblasts but not reticular fibroblasts: A new view of skin morphogenesis & aging', *PLoS One*, 3(12), e4066.
Minton, K. (2014) 'Cell migration: Coordinating calcium signalling', *Nat Rev Mol Cell Biol*, 15(3), 152.
Mirza, R., DiPietro, L. A. & Koh, T. J. (2009) 'Selective & specific macrophage ablation is detrimental to wound healing in mice', *Am J Pathol*, 175(6), 2454-2462.
Mirza, R. E., Fang, M. M., Novak, M. L., Urao, N., Sui, A., Ennis, W. J. & Koh, T. J. (2015) 'Macrophage PPARγ & impaired wound healing in type 2 diabetes', *J Pathol*, 236(4), 433-444.
Mishra, A., Oulès, B., Pisco, A. O., Ly, T., Liakath-Ali, K., Walko, G., Viswanathan, P., Tihy, M., Nijjher, J., Dunn, S. J., Lamond, A. I. & Watt, F. M. (2017) 'A protein phosphatase network controls the temporal & spatial dynamics of differentiation commitment in human epidermis', *Elife*, 6.
Missiaen, L., Robberecht, W., Van Den Bosch, L., Callewaert, G., Parys, J., Wuytack, F., Raeymaekers, L., Nilius, B., Eggermont, J. & De Smedt, H. (2000) 'Abnormal intracellular Ca2+ homeostasis & disease', *Cell Calcium*, 28(1), 1-21.
Miyajima, S., Akaike, T., Matsumoto, K., Okamoto, T., Yoshitake, J., Hayashida, K., Negi, A. & Maeda, H. (2001) 'Matrix metalloproteinases induction by pseudomonal virulence factors & inflammatory cytokines *in vitro*', *Microb Pathog*, 31(6), 271-281.
Moe, A. M., Golding, A. E. & Bement, W. M. 'Cell healing: Calcium, repair & regeneration', *Semin Cell Dev Biol*, 45, 18-23.

Moghaddam, M. M., Eftekhary, M., Erfanimanesh, S., Hashemi, A., Omrani, V. F., Farhadihosseinabadi, B., Lasjerdi, Z., Mossahebi-Mohammadi, M., Chauhan, N. P. S. & Seifalian, A. M. (2018) 'Comparison of the antibacterial effects of a short cationic peptide & 1% silver bioactive glass against extensively drug-resistant bacteria, *Pseudomonas aeruginosa* & *Acinetobacter baumannii*, isolated from burn patients', *Amino Acids*, 50(11), 1617-1628.
Mognol, G., Carneiro, F., Robbs, B., Faget, D. & Viola, J. (2016) 'Cell cycle & apoptosis regulation by NFAT transcription factors: New roles for an old player', *Cell Death Dis*, 7(4), e2199.
Mohammadpour, M., Sadeghi, A., Fassihi, A., Saghaei, L., Movahedian, A. & Rostami, M. (2012) 'Synthesis & antioxidant evaluation of some novel ortho-hydroxypyridine-4-one iron chelators', *Research Pharm Sci*, 7(3), 171-179.
Mohseny, A. B., Tieken, C., van der Velden, P. A., Szuhai, K., de &rea, C., Hogendoorn, P. C. & Cleton-Jansen, A. M. (2010) 'Small deletions but not methylation underlie CDKN2A/p16 loss of expression in conventional osteosarcoma', *Gene Chromosome Cancer*, 49(12), 1095-1103.
Moiseeva, O., Deschênes-Simard, X., St-Germain, E., Igelmann, S., Huot, G., Cadar, A. E., Bourdeau, V., Pollak, M. N. & Ferbeyre, G. (2013) 'Metformin inhibits the senescence-associated secretory phenotype by interfering with IKK/NF-κB activation', *Aging Cell*, 12(3), 489-498.
Mole, D., Maxwell, P., Pugh, C. & Ratcliffe, P. (2001) 'Regulation of HIF by the von Hippel-Lindau tumour suppressor: Implications for cellular oxygen sensing', *IUBMB Life*, 52(1), 43-47.
Moll, R. & Davis, B. (2017) 'Iron, vitamin B12 & folate', *Medicine*, 45(4), 198-203.
Mommers, J., Van Rossum, M., Van Erp, P. & Van de Kerkhof, P. (2000) 'Changes in keratin 6 & keratin 10 (co-) expression in lesional & symptomless skin of spreading psoriasis', *Dermatology*, 201(1), 15-20.
Monneau, Y., Arenzana-Seisdedos, F. & Lortat-Jacob, H. (2016) 'The sweet spot: How GAGs help chemokines guide migrating cells', *J Leukoc Biol*, 99(6), 935-953.
Montaño, M. D., Olesik, J. W., Barber, A. G., Challis, K. & Ranville, J. F. (2016) 'Single Particle ICP-MS: Advances toward routine analysis of nanomaterials', *Anal Bioanal Chem*, 408(19), 5053-5074.
Monteith, G. R., Prevarskaya, N. & Roberts-Thomson, S. J. (2017) 'The calcium–cancer signalling nexus', *Nat Rev Cancer*, 17(6), 367-380.
Moor, M. B. & Bonny, O. (2016) 'Ways of calcium reabsorption in the kidney', *Am J Physiol Renal Physiol*, 310(11), F1337-F1350.
Moreno-Navarrete, J. M. & Fernández-Real, J. M. (2017) 'Adipocyte differentiation', In: Symonds M. (ed) *Adipose tissue biology*. New York: Springer, 69-90.
Morley, J., Levine, A. S., Brown, D. & Handwerger, B. (1982) 'Calmodulin levels in diabetic mice', *Biochem Biophys Res Commun*, 108(4), 1418-1423.
Morones, J. R., Elechiguerra, J. L., Camacho, A., Holt, K., Kouri, J. B., Ramírez, J. T. & Yacaman, M. J. (2005) 'The bactericidal effect of silver nanoparticles', *Nanotechnology*, 16(10), 2346-2353.
Morones-Ramirez, J. R., Winkler, J. A., Spina, C. S. & Collins, J. J. (2013) 'Silver enhances antibiotic activity against gram-negative bacteria', *Sci Trans Med*, 5(190), 190ra81.
Mosser, D. M. & Edwards, J. P. (2008) 'Exploring the full spectrum of macrophage activation', *Nat Rev Immunol*, 8(12), 958-969.
Moulik, P. K., Mtonga, R. & Gill, G. V. (2003) 'Amputation & mortality in new-onset diabetic foot ulcers stratified by etiology', *Diabetes Care*, 26(2), 491-494.

Moura, D., Souza, M., Liverani, L., Rella, G., Luz, G., Mano, J. & Boccaccini, A. (2017) 'Development of a bioactive glass-polymer composite for wound healing applications', *Mater Sci Eng C*, 76, 224-232.
Moura, J., Madureira, P., Leal, E.C., Fonseca, A.C. & Carvalho, E. (2019) 'Immune aging in diabetes and its implications in wound healing', *Clin Immunol*, 200, 43-54.
Muckenthaler, M. U., Rivella, S., Hentze, M. W. & Galy, B. (2017) 'A red carpet for iron metabolism', *Cell*, 168(3), 344-361.
Muller, W. A. (2003) 'Leukocyte-endothelial-cell interactions in leukocyte transmigration & the inflammatory response', *Trends Immunol*, 24(6), 327-334.
Munukka, E., Leppäranta, O., Korkeamäki, M., Vaahtio, M., Peltola, T., Zhang, D., Hupa, L., Ylänen, H., Salonen, J. I. & Viljanen, M. K. (2008) 'Bactericidal effects of bioactive glasses on clinically important aerobic bacteria', *J Mat Sci Mat Med*, 19(1), 27-32.
Murad, S., Grove, D., Lindberg, K., Reynolds, G., Sivarajah, A. & Pinnell, S. (1981) 'Regulation of collagen synthesis by ascorbic acid', *Proc Nat Acad Sci*, 78(5), 2879-2882.
Murakami, T., Ockinger, J., Yu, J., Byles, V., McColl, A., Hofer, A. M. & Horng, T. (2012) 'Critical role for calcium mobilization in activation of the NLRP3 inflammasome', *Proc Nat Acad Sci*, 109(28), 11282-11287.
Murray, P. J. & Wynn, T. A. (2011) 'Protective & pathogenic functions of macrophage subsets', *Nat Rev Immunol*, 11(11), 723.
Muñoz-Espín, D., Cañamero, M., Maraver, A., Gómez-López, G., Contreras, J., Murillo-Cuesta, S., Rodríguez-Baeza, A., Varela-Nieto, I., Ruberte, J. & Collado, M. (2013) 'Programmed cell senescence during mammalian embryonic development', *Cell*, 155(5), 1104-1118.
Myllylä, R., Kuutti-Savolainen, E.-R. & Kivirikko, K. I. (1978) 'The role of ascorbate in the prolyl hydroxylase reaction', *Biochem Biophys Res Commun*, 83(2), 441-448.
Möller, H. E., Bossoni, L., Connor, J. R., Crichton, R. R., Does, M. D., Ward, R. J., Zecca, L., Zucca, F. A. & Ronen, I. (2019) 'Iron, myelin, & the brain: Neuroimaging meets neurobiology', *Trends Neurosci*, 42(6), 384-401.
Müller, K. M., Bickel, M., Wiesmann, U. N. & Spörri, B. (2000) 'Natural killer cells activate human dermal fibroblasts', *Cytokine*, 12(12), 1755-1762.
Naba, A., Clauser, K. R. & Hynes, R. O. (2015) 'Enrichment of extracellular matrix proteins from tissues & digestion into peptides for mass spectrometry analysis', *J Vis Exp*, (101), e53057.
Nabeshima, Y.-i. (2002) 'Klotho: A fundamental regulator of aging', *Ageing Res Rev*, 1(4), 627-638.
Nagase, H., Visse, R. & Murphy, G. (2006) 'Structure & function of matrix metalloproteinases & TIMPs', *Cardiovas Res*, 69(3), 562-573.
Nagata, K. 'HSP47 as a collagen-specific molecular chaperone: Function & expression in normal mouse development'. *Semin Cell Dev Biol*, 14(5), 275-282.
Naidoo, N. & Brown, M. (2012) 'The endoplasmic reticulum stress response in aging & age-related diseases', *Front Physiol*, 3, 263.
Naik, S., Bouladoux, N., Linehan, J. L., Han, S.-J., Harrison, O. J., Wilhelm, C., Conlan, S., Himmelfarb, S., Byrd, A. L. & Deming, C. (2015) 'Commensal–dendritic-cell interaction specifies a unique protective skin immune signature', *Nature*, 520(7545), 104-108.
Nairz, M., Fritsche, G., Brunner, P., Talasz, H., Hantke, K. & Weiss, G. (2008) 'Interferon-γ limits the availability of iron for intramacrophage Salmonella typhimurium', *Eur J Immunol*, 38(7), 1923-1936.
Nairz, M., Schleicher, U., Schroll, A., Sonnweber, T., Theurl, I., Ludwiczek, S., Talasz, H., Brandacher, G., Moser, P. L. & Muckenthaler, M. U. (2013) 'Nitric oxide–mediated

regulation of ferroportin-1 controls macrophage iron homeostasis & immune function in Salmonella infection', *J Exp Med*, 210(5), 855-873.
Nairz, M., Schroll, A., Haschka, D., Dichtl, S., Sonnweber, T., Theurl, I., Theurl, M., Lindner, E., Demetz, E. & Aßhoff, M. (2015) 'Lipocalin-2 ensures host defense against Salmonella Typhimurium by controlling macrophage iron homeostasis & immune response', *Eur J Immunol*, 45(11), 3073-3086.
Nakahigashi, K., Kabashima, K., Ikoma, A., Verkman, A. S., Miyachi, Y. & Hara-Chikuma, M. (2011) 'Upregulation of aquaporin-3 is involved in keratinocyte proliferation & epidermal hyperplasia', *J Invest Dermatol*, 131(4), 865-873.
Narita, M., Nuñez, S., Heard, E., Narita, M., Lin, A. W., Hearn, S. A., Spector, D. L., Hannon, G. J. & Lowe, S. W. (2003) 'Rb-mediated heterochromatin formation & silencing of E2F target genes during cellular senescence', *Cell*, 113(6), 703-716.
Nauta, A., Seidel, C., Deveza, L., Montoro, D., Grova, M., Ko, S. H., Hyun, J., Gurtner, G. C., Longaker, M. T. & Yang, F. (2013) 'Adipose-derived stromal cells overexpressing vascular endothelial growth factor accelerate mouse excisional wound healing', *Mol Ther*, 21(2), 445-455.
Navarro-Requena, C., Pérez-Amodio, S., Castaño, O. & Engel, E. (2018) 'Wound healing-promoting effects stimulated by extracellular calcium & calcium-releasing nanoparticles on dermal fibroblasts', *Nanotechnology*, 29(39), e395102.
Naylor, E. C., Watson, R. E. & Sherratt, M. J. (2011) 'Molecular aspects of skin ageing', *Maturitas*, 69(3), 249-256.
Neels, J. G., Badeanlou, L., Hester, K. D. & Samad, F. (2009) 'Keratinocyte-derived chemokine in obesity: Expression, regulation, & role in adipose macrophage infiltration & glucose homeostasis', *J Biol Chem*, 284(31), 20692-20698.
Neeraja, M., Lakshmi, V., Padmasri, C. & Padmaja, K. (2017) 'Utility of Acridine Orange staining for detection of bacteria from positive blood cultures', *J Microb Methods*, 139, 215-217.
Neilands, J. (1995) 'Siderophores: Structure & function of microbial iron transport compounds', *J Biol Chem*, 270(45), 26723-26726.
Nelson, S. M., Lei, X. & Prabhu, K. S. (2011) 'Selenium levels affect the IL-4–induced expression of alternative activation markers in murine macrophages', *J Nutr*, 141(9), 1754-1761.
Nemes, Z. & Steinert, P. M. (1999) 'Bricks & mortar of the epidermal barrier', *Exp Mol Med*, 31(1), 5-19.
Nemeth, E., Rivera, S., Gabayan, V., Keller, C., Taudorf, S., Pedersen, B. K. & Ganz, T. (2004) 'IL-6 mediates hypoferremia of inflammation by inducing the synthesis of the iron regulatory hormone hepcidin', *J Clin Invest*, 113(9), 1271-1276.
Nestle, F. O., Di Meglio, P., Qin, J.-Z. & Nickoloff, B. J. (2009) 'Skin immune sentinels in health & disease', *Nat Rev Immunol*, 9(10), 679-691.
Neuwirth, E. & Brewer, R. C. (2014) 'ColorBrewer palettes'. Available online: http://ftp.auckland.ac.nz/software/CRAN/doc/packages/RColorBrewer.pdf [Accessed 30/8/19].
Nichols, J. E., Niles, J. A. & Cortiella, J. (2012) 'Production & utilization of acellular lung scaffolds in tissue engineering', *J Cell Biochem*, 113(7), 2185-2192.
Nicolas, G., Chauvet, C., Viatte, L., Danan, J. L., Bigard, X., Devaux, I., Beaumont, C., Kahn, A. & Vaulont, S. (2002) 'The gene encoding the iron regulatory peptide hepcidin is regulated by anemia, hypoxia, & inflammation', *J Clin Invest*, 110(7), 1037-1044.
Niessen, C. M. (2007) 'Tight junctions/adherens junctions: Basic structure & function', *J Invest Dermatol*, 127(11), 2525-2532.

Niethammer, P., Grabher, C., Look, A. T. & Mitchison, T. J. (2009) 'A tissue-scale gradient of hydrogen peroxide mediates rapid wound detection in zebrafish', *Nature*, 459(7249), 996-999.
Nieto, M. A. (2002) 'The snail superfamily of zinc-finger transcription factors', *Nat Rev Mol Cell Biol*, 3(3), 155-166.
Nishio, N., Okawa, Y., Sakurai, H. & Isobe, K. (2008) 'Neutrophil depletion delays wound repair in aged mice', *Age*, 30(1), 11-19.
Nishiyama, T., Amano, S., Tsunenaga, M., Kadoya, K., Takeda, A., Adachi, E. & Burgeson, R. E. (2000) 'The importance of laminin 5 in the dermal–epidermal basement membrane', *J Dermatol Sci*, 24, S51-S59.
Noirey, N., Staquet, M.-J., Gariazzo, M.-J., Serres, M., André, C., Schmitt, D. & Vincent, C. (2002) 'Relationship between expression of matrix metalloproteinases & migration of epidermal & *in vitro* generated Langerhans cells', *Eur J Cell Biol*, 81(7), 383-389.
Nordin, B. & Morris, H. A. (1989) 'The calcium deficiency model for osteoporosis', *Nutr Rev*, 47(3), 65-72.
Novak, M. L. & Koh, T. J. (2013) 'Phenotypic transitions of macrophages orchestrate tissue repair', *Am J Pathol*, 183(5), 1352-1363.
O'Brien, J., Morrissey, P. & Ames, J. (1989) 'Nutritional & toxicological aspects of the Maillard browning reaction in foods', *Crit Rev Sci Nutr*, 28(3), 211-248.
O'Brien, P. D., Sakowski, S. A. & Feldman, E. L. (2014) 'Mouse models of diabetic neuropathy', *ILAR J*, 54(3), 259-272.
O'Byrne, P. M., Metev, H., Puu, M., Richter, K., Keen, C., Uddin, M., Larsson, B., Cullberg, M. & Nair, P. (2016) 'Efficacy & safety of a CXCR2 antagonist, AZD5069, in patients with uncontrolled persistent asthma: A randomised, double-blind, placebo-controlled trial', *Lancet Resp Med*, 4(10), 797-806.
O'Shea, M., Teeling, M. & Bennett, K. (2013) 'The prevalence & ingredient cost of chronic comorbidity in the Irish elderly population with medication treated type 2 diabetes: A retrospective cross-sectional study using a national pharmacy claims database', *BMC Health Serv Res*, 13, 23.
O'Toole, G., Kaplan, H. B. & Kolter, R. (2000) 'Biofilm formation as microbial development', *Ann Rev Microbiol*, 54(1), 49-79.
O'Toole, G. A. (2011) 'Microtiter dish biofilm formation assay', *J Vis Exp*, 4, 2437.
Oberleas, D., Seymour, J. K., Lenaghan, R., Hovanesian, J., Wilson, R. F. & Prasad, A. S. (1971) 'Effect of zinc deficiency on wound-healing in rats', *Am J Surg*, 121(5), 566-568.
Ocak, S., Chaurand, P. & Massion, P. P. (2009) 'Mass spectrometry–based proteomic profiling of lung cancer', *Proc Am Thorac Soc*, 6(2), 159-170.
Oda, Y., Hu, L., Nguyen, T., Fong, C., Tu, C.-l. & Bikle, D. D. (2017) 'Combined deletion of the vitamin D receptor & calcium-sensing receptor delays wound re-epithelialization', *Endocrinology*, 158(6), 1929-1938.
Odland, G.F. (1960) 'A submicroscopic granular component in human epidermis', *J Invest Dermatol*, 34(1), 11-15.
Ohmaru-Nakanishi, T., Asanoma, K., Fujikawa, M., Fujita, Y., Yagi, H., Onoyama, I., Hidaka, N., Sonoda, K. & Kato, K. (2018) 'Fibrosis in preeclamptic placentas is associated with stromal fibroblasts activated by the transforming growth factor-β1 signaling pathway', *Am J Pathol*, 188(3), 683-695.
Ohshima, S. (2012) 'Centrosome aberrations associated with cellular senescence & p53 localization at supernumerary centrosomes', *Oxid Med Cell Longev*, 2012, 217594.

Oishi, Y. & Manabe, I. (2016) 'Macrophages in age-related chronic inflammatory diseases', *NPJ Aging Mech Dis*, 2, 16018.
Olivera, S. & Tomic-Canic, M. (2013) 'Human *ex vivo* wound healing model', *Methods Mol Biol*, 1037, 255-264.
Ollett, W. (1947) 'A Method for staining both Gram-Positive & Gram-Negative Baeteria in Sections', *J Pathol Bacteriol*, 59(1/2), 357-358.
Olson, L. E. & Soriano, P. (2009) 'Increased PDGFRα activation disrupts connective tissue development & drives systemic fibrosis', *Dev Cell*, 16(2), 303-313.
Orioli, D. & Dellambra, E. (2018) 'Epigenetic regulation of skin cells in natural aging & premature aging diseases', *Cells*, 7(12), E268.
Orjalo, A. V., Bhaumik, D., Gengler, B. K., Scott, G. K. & Campisi, J. (2009) 'Cell surface-bound IL-1α is an upstream regulator of the senescence-associated IL-6/IL-8 cytokine network', *Proc Nat Acad Sci*, 106(40), 17031-17036.
Orrenius, S., Zhivotovsky, B. & Nicotera, P. (2003) 'Calcium: Regulation of cell death: The calcium–apoptosis link', *Nat Rev Mol Cell Biol*, 4(7), 552-565.
Ortega, R. (2009) 'Synchrotron radiation for direct analysis of metalloproteins on electrophoresis gels', *Metallomics*, 1(2), 137-141.
Ott, C., Jacobs, K., Haucke, E., Santos, A. N., Grune, T. & Simm, A. (2014) 'Role of advanced glycation end products in cellular signaling', *Redox Biol*, 2, 411-429.
Otten, J. V., Hashimoto, T., Hertl, M., Payne, A. & Sitaru, C. (2014) 'Molecular diagnosis in autoimmune skin blistering conditions', *Curr Mol Med*, 14(1), 69-95.
Ouypornkochagorn, S. & Feldmann, J. r. (2010) 'Dermal uptake of arsenic through human skin depends strongly on its speciation', *Environ Sci Technol*, 44(10), 3972-3978.
Ozer, A. & Bruick, R. K. (2007) 'Non-heme dioxygenases: Cellular sensors & regulators jelly rolled into one?', *Nat Chem Biol*, 3(3), 144-153.
O'Brien, M. (2002) 'Exploring methods of wound debridement', *Br J Comm Nurs*, 7(3), 10-18.
O'Day, D. H., Eshak, K. & Myre, M. A. (2015) 'Calmodulin Binding Proteins & Alzheimer's Disease'*J Alzheimers Dis*, 46(3), 553-569.
O'Dell, B. L. (2000) 'Role of zinc in plasma membrane function', *J Nutr*, 130(5), 1432S-1436S.
Paddock, S. W. (1999) 'Confocal laser scanning microscopy', *Biotechniques*, 27(5), 992-1004.
Pajalunga, D., Mazzola, A., Salzano, A. M., Biferi, M. G., De Luca, G. & Crescenzi, M. (2007) 'Critical requirement for cell cycle inhibitors in sustaining nonproliferative states', *J Cell Biol*, 176(6), 807-818.
Pajarinen, J., Tamaki, Y., Antonios, J. K., Lin, T. H., Sato, T., Yao, Z., Takagi, M., Konttinen, Y. T. & Goodman, S. B. (2015) 'Modulation of mouse macrophage polarization *in vitro* using IL-4 delivery by osmotic pumps', *J Biomed Mat Res A*, 103(4), 1339-1345.
Palmer, A. K., Tchkonia, T., LeBrasseur, N. K., Chini, E. N., Xu, M. & Kirkland, J. L. (2015) 'Cellular senescence in type 2 diabetes: A therapeutic opportunity', *Diabetes*, 64(7), 2289-2298.
Panáček, A., Kvítek, L., Smékalová, M., Večeřová, R., Kolář, M., Röderová, M., Dyčka, F., Šebela, M., Prucek, R. & Tomanec, O. (2018) 'Bacterial resistance to silver nanoparticles & how to overcome it', *Nat Nanotechnol*, 13(1), 65-71.
Paolisso, G. & Barbagallo, M. (1997) 'Hypertension, diabetes mellitus, & insulin resistance: The role of intracellular magnesium', *Am J Hypertens*, 10(3), 346-355.
Papanikolaou, G. & Pantopoulos, K. (2017) 'Systemic iron homeostasis & erythropoiesis', *IUBMB Life*, 69(6), 399-413.

Pare, R., Soon, P. S., Shah, A. & Lee, C. S. (2019) 'Differential expression of senescence tumour markers & its implications on survival outcomes of breast cancer patients', *PloS One*, 14(4), e0214604.
Parekh, A. B. & Putney, J. W. (2005) 'Store-operated calcium channels', *Physiol Rev*, 85(2), 757-810.
Park, C. H., Valore, E. V., Waring, A. J. & Ganz, T. (2001) 'Hepcidin, a urinary antimicrobial peptide synthesized in the liver', *J Biol Chem*, 276(11), 7806-10.
Park, H.-J., Kim, J. Y., Kim, J., Lee, J.-H., Hahn, J.-S., Gu, M. B. & Yoon, J. (2009) 'Silver-ion-mediated reactive oxygen species generation affecting bactericidal activity', *Water Res*, 43(4), 1027-1032.
Park, H. Y., Kim, J. H., Jung, M., Chung, C. H., Hasham, R., Park, C. S. & Choi, E. H. (2011) 'A long-standing hyperglycaemic condition impairs skin barrier by accelerating skin ageing process', *Exp Dermatol*, 20(12), 969-974.
Parrinello, S., Samper, E., Krtolica, A., Goldstein, J., Melov, S. & Campisi, J. (2003) 'Oxygen sensitivity severely limits the replicative lifespan of murine fibroblasts', *Nat Cell Biol*, 5(8), 741-747.
Parsek, M. R. & Greenberg, E. (2005) 'Sociomicrobiology: The connections between quorum sensing & biofilms', *Trends Microbiol*, 13(1), 27-33.
Pasquaroli, S., Citterio, B., Cesare, A., Amiri, M., Manti, A., Vuotto, C. & Biavasco, F. (2014) 'Role of daptomycin in the induction & persistence of the viable but non-culturable state of *Staphylococcus aureus* biofilms', *Pathogens*, 3(3), 759-768.
Passos, J. F., Nelson, G., Wang, C., Richter, T., Simillion, C., Proctor, C. J., Miwa, S., Olijslagers, S., Hallinan, J. & Wipat, A. (2010) 'Feedback between p21 & reactive oxygen production is necessary for cell senescence', *Mol Syst Biol*, 6, 347.
Pastar, I., Nusbaum, A. G., Gil, J., Patel, S. B., Chen, J., Valdes, J., Stojadinovic, O., Plano, L. R., Tomic-Canic, M. & Davis, S. C. (2013) 'Interactions of methicillin resistant *Staphylococcus aureus* USA300 & *Pseudomonas aeruginosa* in polymicrobial wound infection', *PloS One*, 8(2), e56846.
Patterson, R. L., Boehning, D. & Snyder, S. H. (2004) 'Inositol 1, 4, 5-trisphosphate receptors as signal integrators', *Ann Rev Biochem*, 73(1), 437-465.
Paus, R. & Cotsarelis, G. (1999) 'The biology of hair follicles', *N Engl J Med*, 341(7), 491-497.
Pazolli, E., Alspach, E., Milczarek, A., Prior, J., Piwnica-Worms, D. & Stewart, S. A. (2012) 'Chromatin remodeling underlies the senescence-associated secretory phenotype of tumor stromal fibroblasts that supports cancer progression', *Cancer Res*, 72(9), 2251-2261.
Peacock, M. (2010) 'Calcium metabolism in health & disease', *Clin J Am Soc Nephrol*, 5(1), 23-30.
Pearson, J. P., Pesci, E. C. & Iglewski, B. H. (1997) 'Roles of *Pseudomonas aeruginosa* las & rhl quorum-sensing systems in control of elastase & rhamnolipid biosynthesis genes', *J Bacteriol*, 179(18), 5756-5767.
Pelle, E., Jian, J., Zhang, Q., Muizzuddin, N., Yang, Q., Dai, J., Maes, D., Pernodet, N., Yarosh, D. B., Frenkel, K. & Huang, X. (2013) 'Menopause increases the iron storage protein ferritin in skin', *J Cosmet Sci*, 64(3), 175-179.
Penn, J. W., Grobbelaar, A. O. & Rolfe, K. J. (2012) 'The role of the TGF-β family in wound healing, burns & scarring: A review', *Int J Burns Trauma*, 2(1), 18-28.
Percival, S., Bowler, P. & Russell, D. (2005) 'Bacterial resistance to silver in wound care', *J Hosp Infect*, 60(1), 1-7.
Percival, S. L., Malone, M., Mayer, D., Salisbury, A. M. & Schultz, G. (2018) 'Role of anaerobes in polymicrobial communities & biofilms complicating diabetic foot ulcers', *Int Wound J*, 15(5), 776-782.

Percival, S. L. & McCarty, S. M. (2015) 'Silver & alginates: Role in wound healing & biofilm control', *Adv Wound Care*, 4(7), 407-414.
Percival, S. L., Thomas, J., Linton, S., Okel, T., Corum, L. & Slone, W. (2012) 'The antimicrobial efficacy of silver on antibiotic-resistant bacteria isolated from burn wounds', *Int Wound J*, 9(5), 488-493.
Permyakov, E. A. & Uversky, V. N. (2013) 'Protein engineering of calcium binding proteins', *Proteom Res J*, 4(1/2), 119-149.
Persano, L., Camposeo, A., Tekmen, C. & Pisignano, D. (2013) 'Industrial upscaling of electrospinning & applications of polymer nanofibers: A review', *Macromol Mater Eng*, 298(5), 504-520.
Peterkofsky, B. & Udenfriend, S. (1965) 'Enzymatic hydroxylation of proline in microsomal polypeptide leading to formation of collagen', *Proc Nat Acad Sci*, 53(2), 335-342.
Peterson, C., Ratan, R., Shelanski, M. & Goldman, J. (1989) 'Changes in calcium homeostasis during aging & alzheimer's disease', *Ann N Y Acad Sci*, 568(1), 262-270.
Petrie, R. J., Doyle, A. D. & Yamada, K. M. (2009) 'Random versus directionally persistent cell migration', *Nat Rev Mol Cell Biol*, 10(8), 538-549.
Philippot, Q., Deslée, G., Adair-Kirk, T. L., Woods, J. C., Byers, D., Conradi, S., Dury, S., Perotin, J. M., Lebargy, F. & Cassan, C. (2014) 'Increased iron sequestration in alveolar macrophages in chronic obtructive pulmonary disease', *PLoS One*, 9(5), e96285.
Philpott, C. C., Ryu, M.-S., Frey, A. G. & Patel, S. (2017) 'Cytosolic iron chaperones: Proteins delivering iron cofactors in the cytosol of mammalian cells', *J Biol Chem*, 292(31), 12764-12771.
Pierce, G. F., Tarpley, J. E., Tseng, J., Bready, J., Chang, D., Kenney, W. C., Rudolph, R., Robson, M. C., Berg, J. V. & Reid, P. (1995) 'Detection of platelet-derived growth factor (PDGF)-AA in actively healing human wounds treated with recombinant PDGF-BB & absence of PDGF in chronic nonhealing wounds', *J Clin Invest*, 96(3), 1336-1350.
Pigeon, C., Ilyin, G., Courselaud, B., Leroyer, P., Turlin, B., Brissot, P. & Loréal, O. (2001) 'A new mouse liver-specific gene, encoding a protein homologous to human antimicrobial peptide hepcidin, is overexpressed during iron overload', *J Biol Chem*, 276(11), 7811-7819.
Pihlajaniemi, T., Myllylä, R. & Kivirikko, K. I. (1991) 'Prolyl 4-hydroxylase & its role in collagen synthesis', *Hepatology*, 13, S2-S7.
Pillai, S., Bikle, D. D., Mancianti, M. L., Cline, P. & Hincenbergs, M. (1990) 'Calcium regulation of growth & differentiation of normal human keratinocytes: Modulation of differentiation competence by stages of growth & extracellular calcium', *J Cell Physiol*, 143(2), 294-302.
Pimienta, G. & Pascual, J. (2007) 'Canonical & alternative MAPK signaling', *Cell Cycle*, 6(21), 2628-2632.
Pinto, M. C. X., Kihara, A. H., Goulart, V. A., Tonelli, F. M., Gomes, K. N., Ulrich, H. & Resende, R. R. (2015) 'Calcium signaling & cell proliferation', *Cell Signal*, 27(11), 2139-2149.
Pittas, A. G. & Dawson-Hughes, B. (2010) 'Vitamin D & diabetes', *J Steroid Biochem Mol Biol*, 121(1-2), 425-429.
Ploeger, D. T., Hosper, N. A., Schipper, M., Koerts, J. A., de Rond, S. & Bank, R. A. (2013) 'Cell plasticity in wound healing: Paracrine factors of M1/M2 polarized macrophages influence the phenotypical state of dermal fibroblasts', *Cell Commun Signal*, 11(1), e29.

Poenie, M., Alderton, J., Steinhardt, R. & Tsien, R. (1986) 'Calcium rises abruptly & briefly throughout the cell at the onset of anaphase', *Science*, 233(4766), 886-889.
Pomerantz, J., Schreiber-Agus, N., Liégeois, N. J., Silverman, A., Alland, L., Chin, L., Potes, J., Chen, K., Orlow, I. & Lee, H.-W. (1998) 'The Ink4a tumor suppressor gene product, p19Arf, interacts with MDM2 & neutralizes MDM2's inhibition of p53', *Cell*, 92(6), 713-723.
Poologasundarampillai, G., Wang, D., Li, S., Nakamura, J., Bradley, R., Lee, P., Stevens, M., McPhail, D., Kasuga, T. & Jones, J. (2014) 'Cotton-wool-like bioactive glasses for bone regeneration', *Acta Biomater*, 10(8), 3733-3746.
Posnett, J. & Franks, P. (2008) 'The burden of chronic wounds in the UK', *Diabet Med*, 14(5), S7-S85.
Pourcelot, E., Lénon, M., Mobilia, N., Cahn, J.-Y., Arnaud, J., Fanchon, E., Moulis, J.-M. & Mossuz, P. (2015) 'Iron for proliferation of cell lines & hematopoietic progenitors: Nailing down the intracellular functional iron concentration', *Biochim Biophys Acta Mol Cell Res*, 1853(7), 1596-1605.
Pourzand, C., Watkin, R. D., Brown, J. E. & Tyrrell, R. M. (1999) 'Ultraviolet A radiation induces immediate release of iron in human primary skin fibroblasts: The role of ferritin', *Proc Nat Acad Sci*, 96(12), 6751-6756.
Pozzan, T., Rizzuto, R., Volpe, P. & Meldolesi, J. (1994) 'Molecular & cellular physiology of intracellular calcium stores', *Physiol Rev*, 74(3), 595-636.
Pradhan, L., Cai, X., Wu, S., Andersen, N. D., Martin, M., Malek, J., Guthrie, P., Veves, A. & Logerfo, F. W. (2011) 'Gene expression of pro-inflammatory cytokines & neuropeptides in diabetic wound healing', *J Surg Res*, 167(2), 336-342.
Pradhan, L., Nabzdyk, C., Andersen, N. D., LoGerfo, F. W. & Veves, A. (2009) 'Inflammation & neuropeptides: The connection in diabetic wound healing', *Expert Rev Mol Med*, 13(11), e2.
Prasad, A. S. (1976) 'Deficiency of zinc in man', *Am J Dis Child*, 130(4), 259-261.
Prasad, N. B., Biankin, A. V., Fukushima, N., Maitra, A., Dhara, S., Elkahloun, A. G., Hruban, R. H., Goggins, M. & Leach, S. D. (2005) 'Gene expression profiles in pancreatic intraepithelial neoplasia reflect the effects of Hedgehog signaling on pancreatic ductal epithelial cells', *Cancer Res*, 65(5), 1619-1626.
Prasad, V., Okunade, G. W., Miller, M. L. & Shull, G. E. (2004) 'Phenotypes of SERCA & PMCA knockout mice', *Biochem Biophy Res Commun*, 322(4), 1192-1203.
Pratsinis, H., Mavrogonatou, E. & Kletsas, D. (2018) 'Scarless wound healing: From development to senescence', *Adv Drug Deliv Rev* [in press] Available online: https://www.sciencedirect.com/science/article/abs/pii/S0169409X18300632 [Accessed 30/8/19].
Prattichizzo, F., De Nigris, V., La Sala, L., Procopio, A. D., Olivieri, F. & Ceriello, A. (2016) '"Inflammaging" as a druggable target: A senescence-associated secretory phenotype—centered view of type 2 diabetes', *Oxid Med Cell Longev*, 2016, 1810327.
Prattichizzo, F., De Nigris, V., Mancuso, E., Spiga, R., Giuliani, A., Matacchione, G., Lazzarini, R., Marcheselli, F., Recchioni, R. & Testa, R. (2018) 'Short-term sustained hyperglycaemia fosters an archetypal senescence-associated secretory phenotype in endothelial cells & macrophages', *Redox Biol*, 15, 170-181.
Pretorius, E., Bester, J., Vermeulen, N. & Lipinski, B. (2013) 'Oxidation inhibits iron-induced blood coagulation', *Curr Drug Targets*, 14(1), 13-19.
Price, L. B., Liu, C. M., Melendez, J. H., Frankel, Y. M., Engelthaler, D., Aziz, M., Bowers, J., Rattray, R., Ravel, J. & Kingsley, C. (2009) 'Community analysis of chronic wound bacteria using 16S rRNA gene-based pyrosequencing: Impact of diabetes & antibiotics on chronic wound microbiota', *PLoS One*, 4(7), e6462.

Price, T. W., Firth, G., Eling, C. J., Kinnon, M., Long, N. J., Sturge, J. & Stasiuk, G. J. (2018) 'A 18 F radiolabelled Zn (ii) sensing fluorescent probe', *Chem Commun*, 54(26), 3227-3230.
Prins, D. & Michalak, M. (2011) 'Organellar calcium buffers', *CSH Perspect Biol*, 3(3), a004069.
Proksch, E., Brandner, J. M. & Jensen, J. M. (2008) 'The skin: An indispensable barrier', *Exp Dermatol*, 17(12), 1063-1072.
Prowse, K. R. & Greider, C. W. (1995) 'Developmental & tissue-specific regulation of mouse telomerase & telomere length', *Proc Nat Acad Sci*, 92(11), 4818-4822.
Pu, F., Chen, N. & Xue, S. (2016) 'Calcium intake, calcium homeostasis & health', *Food Sci Human Wellness*, 5(1), 8-16.
Pászty, K., Kovács, T., Lacabaratz-Porret, C., Papp, B., Enouf, J., Filoteo, A. G., Penniston, J. T. & Enyedi, A. (1998) 'Expression of hPMCA4b, the major form of the plasma membrane calcium pump in megakaryoblastoid cells is greatly reduced in mature human platelets', *Cell Calcium*, 24(2), 129-135.
Qin, Z. (2012) 'The use of THP-1 cells as a model for mimicking the function & regulation of monocytes & macrophages in the vasculature', *Atherosclerosis*, 221(1), 2-11.
Qu, X., Jin, F., Hao, Y., Li, H., Tang, T., Wang, H., Yan, W. & Dai, K. (2013) 'Magnesium & the risk of cardiovascular events: A meta-analysis of prospective cohort studies', *PLoS One*, 8(3), e57720.
Quan, T. & Fisher, G. J. (2015) 'Role of age-associated alterations of the dermal extracellular matrix microenvironment in human skin aging: A mini-review', *Gerontology*, 61(5), 427-434.
Quondamatteo, F. (2014) 'Skin & diabetes mellitus: What do we know?', *Cell Tissue Res*, 355(1), 1-21.
Rackov, G., Shokri, R., Mon, D., Álvarez, M. & Balomenos, D. (2017) 'The role of IFN-β during the course of sepsis progression & its therapeutic potential', *Front Immunol*, 8, 493.
Radenković, M., Stojanović, M. & Prostran, M. (2016) 'Experimental diabetes induced by alloxan & streptozotocin: The current state of the art', *J Pharmacol Toxicol Methods*, 78, 13-31.
Rahaman, S. O., Grove, L. M., Paruchuri, S., Southern, B. D., Abraham, S., Niese, K. A., Scheraga, R. G., Ghosh, S., Thodeti, C. K. & Zhang, D. X. (2014) 'TRPV4 mediates myofibroblast differentiation & pulmonary fibrosis in mice', *J Clin Invest*, 124(12), 5225-5238.
Rahmat, A., Norman, J. N. & Smith, G. (1974) 'The effect of zinc deficiency on wound healing', *Br J Surg*, 61(4), 271-273.
Rai, M., Yadav, A. & Gade, A. (2009) 'Silver nanoparticles as a new generation of antimicrobials', *Biotechnol Adv*, 27(1), 76-83.
Raine-Fenning, N. J., Brincat, M. P. & Muscat-Baron, Y. (2003) 'Skin aging & menopause', *Am J Clin Dermatol*, 4(6), 371-378.
Rajpathak, S., Ma, J., Manson, J., Willett, W. C. & Hu, F. B. (2006) 'Iron intake & the risk of type 2 diabetes in women: A prospective cohort study', *Diabetes Care*, 29(6), 1370-1376.
Rakhmetova, A., Alekseeva, T., Bogoslovskaya, O., Leipunskii, I., Ol'khovskaya, I., Zhigach, A. & Glushchenko, N. (2010) 'Wound-healing properties of copper nanoparticles as a function of physicochemical parameters', *Nanotechnol Russ*, 5(3-4), 271-276.

Ramadan, J. W., Steiner, S. R., O'Neill, C. M. & Nunemaker, C. S. (2011) 'The central role of calcium in the effects of cytokines on beta-cell function: Implications for type 1 & type 2 diabetes', *Cell Calcium*, 50(6), 481-490.
Ramadass, S., Basu, S. & Srinivasan, A. (2015) 'SERUM magnesium levels as an indicator of status of Diabetes Mellitus type 2', *Diabet Metab Syndr Clin Res Rev*, 9(1), 42-45.
Ramsey, M. M., Rumbaugh, K. P. & Whiteley, M. (2011) 'Metabolite cross-feeding enhances virulence in a model polymicrobial infection', *PLoS Pathog*, 7(3), e1002012.
Randall, C. P., Gupta, A., Jackson, N., Busse, D. & O'neill, A. J. (2015) 'Silver resistance in Gram-negative bacteria: A dissection of endogenous & exogenous mechanisms', *J Antimicrob Chemother*, 70(4), 1037-1046.
Randall, V. A. & Botchkareva, N. V. (2009) 'The biology of hair growth', In: Montagna, W. & Ellis, R. (eds) *Cosmetics Applications of Laser & Light-Based Systems*. Amsterdam: Elsevier, 3-35.
Randle, D. H., Zindy, F., Sherr, C. J. & Roussel, M. F. (2001) 'Differential effects of p19Arf & p16Ink4a loss on senescence of murine bone marrow-derived preB cells & macrophages', *Proc Nat Acad Sci*, 98(17), 9654-9659.
Rangasamy, T., Misra, V., Zhen, L., Tankersley, C. G., Tuder, R. M. & Biswal, S. (2009) 'Cigarette smoke-induced emphysema in A/J mice is associated with pulmonary oxidative stress, apoptosis of lung cells, & global alterations in gene expression', *Am J Physiol Lung Cell Mol Physiol*, 296(6), L888-900.
Ravn, H., Vissinger, H., Kristensen, S. & Husted, S. (1996a) 'Magnesium inhibits platelet activity--an *in vitro* study', *Thromb Haemost*, 76(1), 88-93.
Ravn, H., Vissinger, H., Kristensen, S., Wennmalm, A., Thygesen, K. & Husted, S. (1996b) 'Magnesium inhibits platelet activity--an infusion study in healthy volunteers', *Thromb Haemost*, 75(6), 939-944.
Ray, P. D., Huang, B.-W. & Tsuji, Y. (2012) 'Reactive oxygen species (ROS) homeostasis & redox regulation in cellular signaling', *Cell Signal*, 24(5), 981-990.
Rayner, R., Carville, K., Keaton, J., Prentice, J. & Santamaria, N. (2009) 'Leg ulcers: Atypical presentations & associated comorbidities', *Wound Pract Res*, 17(4), 168-185.
Razzell, W., Evans, I. R., Martin, P. & Wood, W. (2013) 'Calcium flashes orchestrate the wound inflammatory response through DUOX activation & hydrogen peroxide release', *Curr Biol*, 23(5), 424-429.
Recalcati, S., Gammella, E., Buratti, P. & Cairo, G. (2017) 'Molecular regulation of cellular iron balance', *IUBMB Life*, 69(6), 389-398.
Recalcati, S., Locati, M., Marini, A., Santambrogio, P., Zaninotto, F., De Pizzol, M., Zammataro, L., Girelli, D. & Cairo, G. (2010) 'Differential regulation of iron homeostasis during human macrophage polarized activation', *Eur J Immunol*, 40(3), 824-835.
Redel, H., Gao, Z., Li, H., Alekseyenko, A. V., Zhou, Y., Perez-Perez, G. I., Weinstock, G., Sodergren, E. & Blaser, M. J. (2013) 'Quantitation & composition of cutaneous microbiota in diabetic & nondiabetic men', *J Infect Dis*, 207(7), 1105-1114.
Reelfs, O., M Eggleston, I. & Pourzand, C. (2010) 'Skin protection against UVA-induced iron damage by multiantioxidants & iron chelating drugs/prodrugs', *Curr Drug Metab*, 11(3), 242-249.
Rees, R. S., Robson, M. C., Smiell, J. M. & Perry, B. H. (1999) 'Becaplermin gel in the treatment of pressure ulcers: A phase II randomized, double-blind, placebo-controlled study', *Wound Repair Regen*, 7(3), 141-147.

Reimer, L. (1991) 'Energy-filtering transmission electron microscopy', In: Hawkes, P. (ed) *Advances in electronics & electron physics*. Amsterdam: Elsevier, 43-126.
Rendueles, O., Beloin, C., Latour-Lambert, P. & Ghigo, J.-M. (2014) 'A new biofilm-associated colicin with increased efficiency against biofilm bacteria', *ISME J*, 8(6), 1275-1288.
Resch, A., Rosenstein, R., Nerz, C. & Götz, F. (2005) 'Differential gene expression profiling of *Staphylococcus aureus* cultivated under biofilm & planktonic conditions', *Appl Environ Microbiol*, 71(5), 2663-2676.
Resnick, L., Altura, B., Gupta, R., Laragh, J., Alderman, M. & Altura, B. (1993) 'Intracellular & extracellular magnesium depletion in type 2 (non-insulin-dependent) diabetes mellitus', *Diabetologia*, 36(8), 767-770.
Ressler, S., Bartkova, J., Niederegger, H., Bartek, J., Scharffetter-Kochanek, K., Jansen-Dürr, P. & Wlaschek, M. (2006) 'p16INK4A is a robust *in vivo* biomarker of cellular aging in human skin', *Aging Cell*, 5(5), 379-389.
Rheinwald, J. G., Hahn, W. C., Ramsey, M. R., Wu, J. Y., Guo, Z., Tsao, H., De Luca, M., Catricalà, C. & O'Toole, K. M. (2002) 'A two-stage, p16INK4A-& p53-dependent keratinocyte senescence mechanism that limits replicative potential independent of telomere status', *Mol Cell Biol*, 22(14), 5157-5172.
Rho, K. S., Jeong, L., Lee, G., Seo, B.-M., Park, Y. J., Hong, S.-D., Roh, S., Cho, J. J., Park, W. H. & Min, B.-M. (2006) 'Electrospinning of collagen nanofibers: Effects on the behavior of normal human keratinocytes & early-stage wound healing', *Biomaterials*, 27(8), 1452-1461.
Rice, K. C., Mann, E. E., Endres, J. L., Weiss, E. C., Cassat, J. E., Smeltzer, M. S. & Bayles, K. W. (2007) 'The cidA murein hydrolase regulator contributes to DNA release & biofilm development in *Staphylococcus aureus*', *Proc Nat Acad Sci*, 104(19), 8113-8118.
Ridiandries, A., Tan, J. & Bursill, C. (2018) 'The role of chemokines in wound healing', *Int J Mol Sci*, 19(10), e3217.
Rieger, A. M., Nelson, K. L., Konowalchuk, J. D. & Barreda, D. R. (2011) 'Modified annexin V/propidium iodide apoptosis assay for accurate assessment of cell death', *J Vis Exp*, 50, e2597.
Riemer, J., Hoepken, H. H., Czerwinska, H., Robinson, S. R. & Dringen, R. (2004) 'Colorimetric ferrozine-based assay for the quantitation of iron in cultured cells', *Anal Biochem*, 331(2), 370-375.
Ringer, S. (1883) 'A further contribution regarding the influence of the different constituents of the blood on the contraction of the heart', *J Physiol*, 4(1), 29-42.
Rinkevich, Y., Walmsley, G. G., Hu, M. S., Maan, Z. N., Newman, A. M., Drukker, M., Januszyk, M., Krampitz, G. W., Gurtner, G. C. & Lorenz, H. P. (2015) 'Identification & isolation of a dermal lineage with intrinsic fibrogenic potential', *Science*, 348(6232), aaa2151.
Rinnerthaler, M., Duschl, J., Steinbacher, P., Salzmann, M., Bischof, J., Schuller, M., Wimmer, H., Peer, T., Bauer, J. W. & Richter, K. (2013) 'Age-related changes in the composition of the cornified envelope in human skin', *Exp Dermatol*, 22(5), 329-335.
Rinnerthaler, M., Streubel, M. K., Bischof, J. & Richter, K. (2015) 'Skin aging, gene expression & calcium', *Exp Gerontol*, 68, 59-65.
Rios, F. J., Touyz, R. M. & Montezano, A. C. (2017) 'Isolation & differentiation of murine macrophages', *Methods Mol Biol*, 1527, 297-309.
Riss, T. L., Moravec, R. A., Niles, A. L., Duellman, S., Benink, H. A., Worzella, T. J. & Minor, L. (2016) 'Cell viability assays', In: Sittampalam GS, Grossman A, Brimacombe K, et al. (eds) *Assay guidance manual.* Bethesda (MD): Eli Lilly & Company & the

National Center for Advancing Translational Sciences. Available online: https://www.ncbi.nlm.nih.gov/books/NBK144065/ [Accessed 30/8/19].
Rittié, L. & Fisher, G. J. (2015) 'Natural & sun-induced aging of human skin', *CSH Perspect Med*, 5(1), a015370.
Robert, C., Lesty, C. & Robert, A. (1988) 'Ageing of the skin: Study of elastic fiber network modifications by computerized image analysis', *Gerontology*, 34(5-6), 291-296.
Robine, J. M. & Cubaynes, S. (2017) 'Worldwide demography of centenarians', *Mech Ageing Dev*, 165(Pt B), 59-67.
Rodgers, K. E., Ellefson, D. D., Espinoza, T., Hsu, Y. H., diZerega, G. S. & Mehrian-Shai, R. (2006) 'Expression of intracellular filament, collagen, & collagenase genes in diabetic & normal skin after injury', *Wound Repair Regen*, 14(3), 298-305.
Rodier, F. & Campisi, J. (2011) 'Four faces of cellular senescence',*J Cell Biol*, 192(4), 547-556
Rodier, F., Coppé, J.-P., Patil, C. K., Hoeijmakers, W. A., Muñoz, D. P., Raza, S. R., Freund, A., Campeau, E., Davalos, A. R. & Campisi, J. (2009) 'Persistent DNA damage signalling triggers senescence-associated inflammatory cytokine secretion', *Nat Cell Biol*, 11(8), 973-979.
Rodriguez-Ortiz, M. E., Lopez, I., Muñoz-Castañeda, J. R., Martinez-Moreno, J. M., Ramírez, A. P., Pineda, C., Canalejo, A., Jaeger, P., Aguilera-Tejero, E., Rodriguez, M., Felsenfeld, A. & Almaden, Y. (2012) 'Calcium deficiency reduces circulating levels of FGF23', *J Am Soc Nephrol*, 23(7), 1190-1197.
Roetto, A., Papanikolaou, G., Politou, M., Alberti, F., Girelli, D., Christakis, J., Loukopoulos, D. & Camaschella, C. (2003) 'Mutant antimicrobial peptide hepcidin is associated with severe juvenile hemochromatosis', *Nat Genet*, 33(1), 21-22.
Rognoni, E. & Watt, F. M. (2018) 'Skin Cell Heterogeneity in Development, Wound Healing, & Cancer', *Trends Cell Biol*, 28(9), 709-722.
Rompolas, P., Mesa, K. R. & Greco, V. (2013) 'Spatial organization within a niche as a determinant of stem-cell fate', *Nature*, 502(7472), 513-518.
Ron, D. & Walter, P. (2007) 'Signal integration in the endoplasmic reticulum unfolded protein response', *Nat Rev Mol Cell Biol*, 8(7), 519-529.
Roper, J. A., Williamson, R. C., Bally, B., Cowell, C. A., Brooks, R., Stephens, P., Harrison, A. J. & Bass, M. D. (2015) 'Ultrasonic stimulation of mouse skin reverses the healing delays in diabetes & aging by activation of RAC1', *J Invest Dermatol*, 135(11), 2842-2851.
Rosenbaum, D. M., Rasmussen, S. G. & Kobilka, B. K. (2009) 'The structure & function of G-protein-coupled receptors', *Nature*, 459(7245), 356-363.
Ross, R., Shaw, K. D., Martel, Y., de Guise, J. & Avruch, L. (1993) 'Adipose tissue distribution measured by magnetic resonance imaging in obese women', *Am J Clin Nutr*, 57(4), 470-475.
Roth, W., Kumar, V., Beer, H.-D., Richter, M., Wohlenberg, C., Reuter, U., Thiering, S., Staratschek-Jox, A., Hofmann, A. & Kreusch, F. (2012) 'Keratin 1 maintains skin integrity & participates in an inflammatory network in skin through interleukin-18', *J Cell Sci*, 125(22), 5269-5279.
Roy, I., Getschman, A. E., Volkman, B. F. & Dwinell, M. B. (2017) 'Exploiting agonist biased signaling of chemokines to target cancer', *Mol Carcinog*, 56(3), 804-813.
Roy, S., Biswas, S., Khanna, S., Gordillo, G., Bergdall, V., Green, J., Marsh, C. B., Gould, L. J. & Sen, C. K. (2009) 'Characterization of a preclinical model of chronic ischemic wound', *Physiol Genomics*, 37(3), 211-224.
Rozemeijer, W., Fink, P., Rojas, E., Jones, C. H., Pavliakova, D., Giardina, P., Murphy, E., Liberator, P., Jiang, Q., Girgenti, D., Peters, R. P., Savelkoul, P. H., Jansen, K. U.,

Anderson, A. S. & Kluytmans, J. (2015) 'Evaluation of approaches to monitor *Staphylococcus aureus* virulence factor expression during human disease', *PLoS One*, 10(2), e0116945.
Ruan, Y., Wu, S., Zhang, L., Chen, G. & Lai, W. (2014) 'Retarding the senescence of human vascular endothelial cells induced by hydrogen peroxide: Effects of 17beta-estradiol (E2) mediated mitochondria protection', *Biogerontology*, 15(4), 367-375.
Rudolph, K. L., Chang, S., Lee, H.-W., Blasco, M., Gottlieb, G. J., Greider, C. & DePinho, R. A. (1999) 'Longevity, stress response, & cancer in aging telomerase-deficient mice', *Cell*, 96(5), 701-712.
Rumbaugh, K. P., Griswold, J. A., Iglewski, B. H. & Hamood, A. N. (1999) 'Contribution of quorum sensing to the virulence of *Pseudomonas aeruginosa* in burn wound infections', *Infect Immun*, 67(11), 5854-5862.
Rungby, J., Kassem, M., Eriksen, E. F. & Danscher, G. (1993) 'The von Kossa reaction for calcium deposits: Silver lactate staining increases sensitivity & reduces background', *Histochem J*, 25(6), 446-451.
Sabin, K. & Kikyo, N. (2014) 'Microvesicles as mediators of tissue regeneration', *Transl Res*, 163(4), 286-295.
Sagiv, A. & Krizhanovsky, V. (2013) 'Immunosurveillance of senescent cells: The bright side of the senescence program', *Biogerontology*, 14(6), 617-628.
Saito, M., Ohyama, M. & Amagai, M. (2015) 'Exploring the biology of the nail: An intriguing but less-investigated skin appendage', *J Dermatol Sci*, 79(3), 187-193.
Saito, Y., Hasegawa, M., Fujimoto, M., Matsushita, T., Horikawa, M., Takenaka, M., Ogawa, F., Sugama, J., Steeber, D. A., Sato, S. & Takehara, K. (2008) 'The loss of MCP-1 attenuates cutaneous ischemia-reperfusion injury in a mouse model of pressure ulcer', *J Invest Dermatol*, 128(7), 1838-1851.
Sakai, L. Y., Keene, D. R., Morris, N. P. & Burgeson, R. E. (1986) 'Type VII collagen is a major structural component of anchoring fibrils', *J Cell Biol*, 103(4), 1577-1586.
Sakai, S., Endo, Y., Ozawa, N., Sugawara, T., Kusaka, A., Sayo, T., Tagami, H. & Inoue, S. (2003) 'Characteristics of the epidermis & stratum corneum of hairless mice with experimentally induced diabetes mellitus', *J Invest Dermatol*, 120(1), 79-85.
Sakai, S., Kikuchi, K., Satoh, J., Tagami, H. & Inoue, S. (2005) 'Functional properties of the stratum corneum in patients with diabetes mellitus: Similarities to senile xerosis', *Br J Dermatol*, 153(2), 319-323.
Sakakibara, S., Inouye, K., Shudo, K., Kishida, Y., Kobayashi, Y. & Prockop, D. J. (1973) 'Synthesis of (Pro-Hyp-Gly) n of defined molecular weights. Evidence for the stabilization of collagen triple helix by hydroxypyroline', *Biochim Biophys Acta Protein Struct*, 303(1), 198-202.
Salminen, A., Hyttinen, J. M. & Kaarniranta, K. (2011) 'AMP-activated protein kinase inhibits NF-κB signaling & inflammation: Impact on healthspan & lifespan', *J Mol Med*, 89(7), 667-676.
Sambo, P., Baroni, S. S., Luchetti, M., Paroncini, P., Dusi, S., Orlandini, G. & Gabrielli, A. (2001) 'Oxidative stress in scleroderma: Maintenance of scleroderma fibroblast phenotype by the constitutive up-regulation of reactive oxygen species generation through the NADPH oxidase complex pathway', *Arthritis Rheum*, 44(11), 2653-2664.
Sangkhae, V. & Nemeth, E. (2017) 'Regulation of the Iron Homeostatic Hormone Hepcidin', *Adv Nutr*, 8(1), 126-136.
Santoro, M. M. & Gaudino, G. (2005) 'Cellular & molecular facets of keratinocyte reepithelization during wound healing', *Exp Cell Res*, 304(1), 274-286.
Saraswathi, P. & Beuerman, R. W. (2015) 'Corneal biofilms: From planktonic to microcolony formation in an experimental keratitis infection with *Pseudomonas aeruginosa*', *Ocul Surf*, 13(4), 331-345.

Saravanapavan, P. & Hench, L. L. (2001) 'Low-temperature synthesis, structure, & bioactivity of gel-derived glasses in the binary CaO-SiO2 system', *J Biomed Mater Res*, 54(4), 608-618.
Sarris, M., Masson, J. B., Maurin, D., Van der Aa, L. M., Boudinot, P., Lortat-Jacob, H. & Herbomel, P. (2012) 'Inflammatory chemokines direct & restrict leukocyte migration within live tissues as glycan-bound gradients', *Curr Biol*, 22(24), 2375-2382.
Sarsour, E. H., Agarwal, M., Pandita, T. K., Oberley, L. W. & Goswami, P. C. (2005) 'Manganese superoxide dismutase protects the proliferative capacity of confluent normal human fibroblasts', *J Biol Chem*, 280(18), 18033-18041.
Sarsour, E. H., Venkataraman, S., Kalen, A. L., Oberley, L. W. & Goswami, P. C. (2008) 'Manganese superoxide dismutase activity regulates transitions between quiescent & proliferative growth', *Aging Cell*, 7(3), 405-417.
Sartipy, P. & Loskutoff, D. J. (2003) 'Monocyte chemoattractant protein 1 in obesity & insulin resistance', *Proc Nat Acad Sci*, 100(12), 7265-7270.
Sato, K., Kang, W.H., Saga, K. & Sato, K.T. (1989) 'Biology of sweat glands & their disorders. I. Normal sweat gland function', *J Am Acad Dermatol*, 20(4), 537-563.
Satriano, J., Mansoury, H., Deng, A., Sharma, K., Vallon, V., Blantz, R. C. & Thomson, S. C. (2010) 'Transition of kidney tubule cells to a senescent phenotype in early experimental diabetes', *Am J Physiol Cell Physiol*, 299(2), C374-C380.
Savignac, M., Simon, M., Edir, A., Guibbal, L. & Hovnanian, A. (2014) 'SERCA2 dysfunction in Darier disease causes endoplasmic reticulum stress & impaired cell-to-cell adhesion strength: Rescue by Miglustat', *J Invest Dermatol*, 134(7), 1961-1970.
Scandolera, A., Rabenoelina, F., Chaintreuil, C., Rusciani, A., Maurice, P., Blaise, S., Romier-Crouzet, B., El Btaouri, H., Martiny, L., Debelle, L. & Duca, L. (2015) 'Uncoupling of elastin complex receptor during *in vitro* aging is related to modifications in its intrinsic sialidase activity & the subsequent lactosylceramide production', *PLoS One*, 10(6), e0129994.
Scatizzi, J. C., Mavers, M., Hutcheson, J., Young, B., Shi, B., Pope, R. M., Ruderman, E. M., Samways, D. S., Corbett, J. A. & Egan, T. M. (2009) 'The CDK domain of p21 is a suppressor of IL-1β-mediated inflammation in activated macrophages', *Eur J Immunol*, 39(3), 820-825.
Schafer, M. J., White, T. A., Evans, G., Tonne, J. M., Verzosa, G. C., Stout, M. B., Mazula, D. L., Palmer, A. K., Baker, D. J. & Jensen, M. D. (2016) 'Exercise prevents diet-induced cellular senescence in adipose tissue', *Diabetes*, 65(6), 1606-1615.
Scherer, S. S., Pietramaggiori, G., Matthews, J., Perry, S., Assmann, A., Carothers, A., Demcheva, M., Muise-Helmericks, R. C., Seth, A. & Vournakis, J. N. (2009) 'Poly-N-acetyl glucosamine nanofibers: A new bioactive material to enhance diabetic wound healing by cell migration & angiogenesis', *Ann Surg*, 250(2), 322-330.
Schieber, M. & Chandel, N. S. (2014) 'ROS function in redox signaling & oxidative stress', *Curr Biol*, 24(10), R453-R462.
Schmidtchen, A., Frick, I. M., Andersson, E., Tapper, H. & Björck, L. (2002) 'Proteinases of common pathogenic bacteria degrade & inactivate the antibacterial peptide LL-37', *Mol Microbiol*, 46(1), 157-168.
Schmidtchen, A., Holst, E., Tapper, H. & Björck, L. (2003) 'Elastase-producing *Pseudomonas aeruginosa* degrade plasma proteins & extracellular products of human skin & fibroblasts, & inhibit fibroblast growth', *Microb Pathog*, 34(1), 47-55.
Schoepe, S., Schäcke, H., May, E. & Asadullah, K. (2006) 'Glucocorticoid therapy-induced skin atrophy', *Exp Dermatol*, 15(6), 406-420.

Schreml, S., Szeimies, R. M., Karrer, S., Heinlin, J., Landthaler, M. & Babilas, P. (2010) 'The impact of the pH value on skin integrity & cutaneous wound healing', *J Eur Acad Dermatol Venereol*, 24(4), 373-378.
Schroeder, P., Schieke, S. M. & Morita, A. (2006) 'Premature skin aging by infrared radiation, tobacco smoke & ozone', In: Gilchrest B.A., Krutmann J. (eds) *Skin aging*. Berlin: Springer, 45-53.
Schultz, G. S. & Wysocki, A. (2009) 'Interactions between extracellular matrix & growth factors in wound healing', *Wound Repair Regen*, 17(2), 153-162.
Schwaller, B. (2012) 'The regulation of a cell's Ca(2+) signaling toolkit: The Ca (2+) homeostasome', *Adv Exp Med Biol*, 740, 1-25.
Schwarz, E. C., Wissenbach, U., Niemeyer, B. A., Strauß, B., Philipp, S. E., Flockerzi, V. & Hoth, M. (2006) 'TRPV6 potentiates calcium-dependent cell proliferation', *Cell Calcium*, 39(2), 163-173.
Schäfer, M. & Werner, S. (2008) 'Oxidative stress in normal & impaired wound repair', *Pharmacol Res*, 58(2), 165-171.
Screen, H. R., Berk, D. E., Kadler, K. E., Ramirez, F. & Young, M. F. (2015) 'Tendon functional extracellular matrix', *J Orthop Res*, 33(6), 793-799.
Seaton, M., Hocking, A. & Gibran, N. S. (2015) 'Porcine models of cutaneous wound healing', *ILAR J*, 56(1), 127-138.
Segel, G. B., Halterman, M. W. & Lichtman, M. A. (2011) 'The paradox of the neutrophil's role in tissue injury', *J Leukoc Biol*, 89(3), 359-372.
Seitz, O., Schürmann, C., Hermes, N., Müller, E., Pfeilschifter, J., Frank, S. & Goren, I. (2011) 'Wound healing in mice with high-fat diet-or ob gene-induced diabetes-obesity syndromes: A comparative study', *Exp Diabetes Res*, 2010, 476969.
Sekiya, F., Yoshida, M., Yamashita, T. & Morita, T. (1996) 'Magnesium (II) is a crucial constituent of the blood coagulation cascade potentiation of coagulant activities of factor IX by Mg ions', *J Biol Chem*, 271(15), 8541-8544.
Sen, C. K., Khanna, S., Gordillo, G., Bagchi, D., Bagchi, M. & Roy, S. (2002) 'Oxygen, oxidants, & antioxidants in wound healing', *Ann N Y Acad Sci*, 957(1), 239-249.
Sen, C. K., Roy, S. & Packer, L. (1996) 'Involvement of intracellular Ca2+ in oxidant-induced NF-κB activation', *FEBS Lett*, 385(1-2), 58-62.
Shah, P. P., Donahue, G., Otte, G. L., Capell, B. C., Nelson, D. M., Cao, K., Aggarwala, V., Cruickshanks, H. A., Rai, T. S. & McBryan, T. (2013) 'Lamin B1 depletion in senescent cells triggers large-scale changes in gene expression & the chromatin landscape', *Genes Dev*, 27(16), 1787-1799.
Shah, Y. M., Matsubara, T., Ito, S., Yim, S. H. & Gonzalez, F. J. (2009) 'Intestinal hypoxia-inducible transcription factors are essential for iron absorption following iron deficiency', *Cell Metab*, 9(2), 152-164.
Shah, Y. M. & Xie, L. (2014) 'Hypoxia-inducible factors link iron homeostasis & erythropoiesis', *Gastroenterology*, 146(3), 630-642.
Shapouri-Moghaddam, A., Mohammadian, S., Vazini, H., Taghadosi, M., Esmaeili, S. A., Mardani, F., Seifi, B., Mohammadi, A., Afshari, J. T. & Sahebkar, A. (2018) 'Macrophage plasticity, polarization, & function in health & disease', *J Cell Physiol*, 233(9), 6425-6440.
Sharma, K., McCue, P. & Dunn, S. R. (2003) 'Diabetic kidney disease in the *db/db* mouse', *Am J Physiol Renal Physiol*, 284(6), F1138-F1144.
Sharma, S., Goswami, R., Merth, M., Cohen, J., Lei, K. Y., Zhang, D. X. & Rahaman, S. O. (2017) 'TRPV4 ion channel is a novel regulator of dermal myofibroblast differentiation', *Am J Physiol Cell Physiol*, 312(5), C562-C572.

Sharma, S., Nemeth, E., Chen, Y. H., Goodnough, J., Huston, A., Roodman, G. D., Ganz, T. & Lichtenstein, A. (2008) 'Involvement of hepcidin in the anemia of multiple myeloma', *Clin Cancer Res*, 14(11), 3262-3267.
Sharma, V. & O'Halloran, D. M. (2014) 'Recent structural & functional insights into the family of sodium calcium exchangers', *Genesis*, 52(2), 93-109.
Sharp, P. A. (2010) 'Intestinal iron absorption: Regulation by dietary & systemic factors', *Int J Vitam Nutr Res*, 80(4-5), 231-242.
Sharpless, N. E. (2004) 'Ink4a/Arf links senescence & aging', *Exp Gerontol*, 39(11-12), 1751-1759.
Shatrov, V. A., Lehmann, V. & Chouaib, S. (1997) 'Sphingosine-1-phosphate mobilizes intracellular calcium & activates transcription factor NF-κB in U937 cells', *Biochem Biophys Res Commun*, 234(1), 121-124.
Shaw, L., Golonka, E., Potempa, J. & Foster, S. J. (2004) 'The role & regulation of the extracellular proteases of *Staphylococcus aureus*', *Microbiology*, 150(1), 217-228.
Shaw, T. J. & Martin, P. (2016) 'Wound repair: A showcase for cell plasticity & migration', *Curr Opin Cell Biol*, 42, 29-37.
Sheehan, P., Jones, P., Caselli, A., Giurini, J. M. & Veves, A. (2003) 'Percent change in wound area of diabetic foot ulcers over a 4-week period is a robust predictor of complete healing in a 12-week prospective trial', *Diabetes Care*, 26(6), 1879-1882.
Sheetz, M. J. & King, G. L. (2002) 'Molecular understanding of hyperglycemia's adverse effects for diabetic complications', *Jama*, 288(20), 2579-2588.
Sheikh, A. Q., Hurley, J. R., Huang, W., Taghian, T., Kogan, A., Cho, H., Wang, Y. & Narmoneva, D. A. (2012) 'Diabetes alters intracellular calcium transients in cardiac endothelial cells', *PloS One*, 7(5), e36840.
Shen, B., Jensen, R. G. & Bohnert, H. J. (1997) 'Mannitol protects against oxidation by hydroxyl radicals', *Plant Physiol*, 115(2), 527-532.
Sherr, C. J. & DePinho, R. A. (2000) 'Cellular senescence', *Cell*, 102(4), 407-410.
Sherr, C. J. & Roberts, J. M. (1999) 'CDK inhibitors: Positive & negative regulators of G1-phase progression', *Genes Dev*, 13(12), 1501-1512.
Sherratt, M. J. (2009) 'Tissue elasticity & the ageing elastic fibre', *Age*, 31(4), 305-325.
Sherratt, M. J., Baldock, C., Morgan, A. & Kielty, C. M. (2007) 'The morphology of adsorbed extracellular matrix assemblies is critically dependent on solution calcium concentration', *Matrix Biol*, 26(3), 156-166.
Sheu, J. R., Hsiao, G., Shen, M. Y., Fong, T. H., Chen, Y. W., Lin, C. H. & Chou, D. S. (2002) 'Mechanisms involved in the antiplatelet activity of magnesium in human platelets', *Br J Haematol*, 119(4), 1033-1041.
Sheu, S.-Y., Wang, W.-L., Fu, Y.-T., Lin, S.-C., Lei, Y.-C., Liao, J.-H., Tang, N.-Y., Kuo, T.-F. & Yao, C.-H. (2014) 'The pig as an experimental model for mid-dermal burns research', *Burns*, 40(8), 1679-1688.
Sheu, W. H., Chen, Y. T., Lee, W. J., Wang, C. W. & Lin, L. Y. (2003) 'A relationship between serum ferritin & the insulin resistance syndrome is present in non-diabetic women but not in non-diabetic men', *Clin Endocrinol*, 58(3), 380-385.
Shi, D. & Gu, W. (2012) 'Dual roles of MDM2 in the regulation of p53: Ubiquitination dependent & ubiquitination independent mechanisms of MDM2 repression of p53 activity', *Genes Cancer*, 3(3-4), 240-248.
Shi, V. Y., Leo, M., Hassoun, L., Chahal, D. S., Maibach, H. I. & Sivamani, R. K. (2015) 'Role of sebaceous glands in inflammatory dermatoses', *J Am Acad Dermatol*, 73(5), 856-863.
Shi, Y. & Massagué, J. (2003) 'Mechanisms of TGF-beta signaling from cell membrane to the nucleus', *Cell*, 113(6), 685-700.

Shibata, S., Tada, Y., Hau, C. S., Mitsui, A., Kamata, M., Asano, Y., Sugaya, M., Kadono, T., Masamoto, Y., Kurokawa, M., Yamauchi, T., Kubota, N., Kadowaki, T. & Sato, S. (2015) 'Adiponectin regulates psoriasiform skin inflammation by suppressing IL-17 production from γδ-T cells', *Nat Commun*, 6, e7687.
Shigematsu, T., Fukushima, J., Oyama, M., Tsuda, M., Kawamoto, S. & Okuda, K. (2001) 'Iron-Mediated regulation of alkaline proteinase production in *Pseudomonas aeruginosa*', *Microbiol Immunol*, 45(8), 579-590.
Shoshan-Barmatz, V. & Ben-Hail, D. (2012) 'VDAC, a multi-functional mitochondrial protein as a pharmacological target', *Mitochondrion*, 12(1), 24-34.
Shoulders, M. D. & Raines, R. T. (2009) 'Collagen structure & stability', *Ann Rev Biochem*, 78, 929-958.
Sigal, S. H., Rajvanshi, P., Gorla, G. R., Sokhi, R. P., Saxena, R., Gebhard Jr, D. R., Reid, L. M. & Gupta, S. (1999) 'Partial hepatectomy-induced polyploidy attenuates hepatocyte replication & activates cell aging events', *Am J Physiol Gastro Liver Physiol*, 276(5), G1260-G1272.
Sill, T. J. & von Recum, H. A. (2008) 'Electrospinning: Applications in drug delivery & tissue engineering', *Biomaterials*, 29(13), 1989-2006.
Simcox, J. A. & McClain, D. A. (2013) 'Iron & diabetes risk', *Cell Metab*, 17(3), 329-341.
Simon, S. F. & Taylor, C. G. (2001) 'Dietary zinc supplementation attenuates hyperglycemia in *db/db* mice', *Exp Biol Med*, 226(1), 43-51.
Simpson, J. E., Ince, P. G., Shaw, P. J., Heath, P. R., Raman, R., Garwood, C. J., Gelsthorpe, C., Baxter, L., Forster, G. & Matthews, F. E. (2011) 'Microarray analysis of the astrocyte transcriptome in the aging brain: Relationship to Alzheimer's pathology & APOE genotype', *Neurobiol Aging*, 32(10), 1795-1807.
Sims, J. M. (1852) 'ART. IV.--On the Treatment of Vesico-Vaginal Fistula', *Am J Med Sci (1827-1924)*, 23(45), A59.
Sindrilaru, A., Peters, T., Wieschalka, S., Baican, C., Baican, A., Peter, H., Hainzl, A., Schatz, S., Qi, Y. & Schlecht, A. (2011) 'An unrestrained proinflammatory M1 macrophage population induced by iron impairs wound healing in humans & mice', *J Clin Invest*, 121(3), 985-997.
Sindrilaru, A. & Scharffetter-Kochanek, K. (2013) 'Disclosure of the culprits: Macrophages—Versatile regulators of wound healing', *Adv Wound Care*, 2(7), 357-368.
Singh, D., Srivastava, S. K., Chaudhuri, T. K. & Upadhyay, G. (2015) 'Multifaceted role of matrix metalloproteinases (MMPs)', *Front Mol Biosci*, 2, 19.
Singh, V. K., Singh, A. L., Singh, R. & Kumar, A. (2018) 'Iron oxidizing bacteria: Insights on diversity, mechanism of iron oxidation & role in management of metal pollution', *Environ Sust*, 1(3), 221–231.
Sinha, B., Francois, P., Que, Y.-A., Hussain, M., Heilmann, C., Moreillon, P., Lew, D., Krause, K.-H., Peters, G. & Herrmann, M. (2000) 'Heterologously Expressed *Staphylococcus aureus* Fibronectin-Binding Proteins Are Sufficient for Invasion of Host Cells', *Infect Immun*, 68(12), 6871-6878.
Siqueira, R. L., Maurmann, N., Burguêz, D., Pereira, D. P., Rastelli, A. N., Peitl, O., Pranke, P. & Zanotto, E. D. (2017) 'Bioactive gel-glasses with distinctly different compositions: Bioactivity, viability of stem cells & antibiofilm effect against Streptococcus mutans', *Mat Sci Eng C*, 76, 233-241.
Sitte, N., Merker, K., Von Zglinicki, T., Grune, T. & Davies, K. J. (2000) 'Protein oxidation & degradation during cellular senescence of human BJ fibroblasts: Part I—effects of proliferative senescence', *FASEB J*, 14(15), 2495-2502.

Skórkowska-Telichowska, K., Czemplik, M., Kulma, A. & Szopa, J. (2013) 'The local treatment & available dressings designed for chronic wounds', *J Am Acad Dermatol*, 68(4), e117-e126.
Smart, K. E., Smith, J. A. C., Kilburn, M. R., Martin, B. G., Hawes, C. & Grovenor, C. R. (2010) 'High-resolution elemental localization in vacuolate plant cells by nanoscale secondary ion mass spectrometry', *Plant J*, 63(5), 870-879.
Smith, A. N., Willis, E., Chan, V. T., Muffley, L. A., Isik, F. F., Gibran, N. S. & Hocking, A. M. (2010) 'Mesenchymal stem cells induce dermal fibroblast responses to injury', *Exp Cell Res*, 316(1), 48-54.
Smith, E. A. & Fuchs, E. (1998) 'Defining the interactions between intermediate filaments & desmosomes', *J Cell Biol*, 141(5), 1229-1241.
Smith, L. T., Holbrook, K. A. & Byers, P. H. (1982) 'Structure of the dermal matrix during development & in the adult', *J Invest Dermatol*, 79, 93-104.
Snyder, R. J., Lantis, J., Kirsner, R. S., Shah, V., Molyneaux, M. & Carter, M. J. (2016) 'Macrophages: A review of their role in wound healing & their therapeutic use', *Wound Repair Regen*, 24(4), 613-629.
Soboloff, J., Rothberg, B. S., Madesh, M. & Gill, D. L. (2012) 'STIM proteins: Dynamic calcium signal transducers', *Nat Rev Mol Cell Biol*, 13(9), 549-565.
Sokol, C. L. & Luster, A. D. (2015) 'The chemokine system in innate immunity', *CSH Perspect Biol*, 7(5), a016303.
Sone, H. & Kagawa, Y. (2005) 'Pancreatic beta cell senescence contributes to the pathogenesis of type 2 diabetes in high-fat diet-induced diabetic mice', *Diabetologia*, 48(1), 58-67.
Song, Y., Ford, E. S., Manson, J. E. & Liu, S. (2005) 'Relations of magnesium intake with metabolic risk factors & risks of type 2 diabetes, hypertension, & cardiovascular disease: A critical appraisal', *Curr Nutr Food Sci*, 1(3), 231-243.
Sonnack, L., Klawonn, T., Kriehuber, R., Hollert, H., Schäfers, C. & Fenske, M. (2017) 'Concentration dependent transcriptome responses of zebrafish embryos after exposure to cadmium, cobalt & copper', *Comp Biochem Physiol D Genom Proteom*, 24, 29-40.
Soriani, A., Zingoni, A., Cerboni, C., Iannitto, M. L., Ricciardi, M. R., Di Gialleonardo, V., Cippitelli, M., Fionda, C., Petrucci, M. T. & Guarini, A. (2009) 'ATM-ATR–dependent up-regulation of DNAM-1 & NKG2D ligands on multiple myeloma cells by therapeutic agents results in enhanced NK-cell susceptibility & is associated with a senescent phenotype', *Blood*, 113(15), 3503-3511.
Sorrell, J. M., Baber, M. A. & Caplan, A. I. (1996) 'Construction of a bilayered dermal equivalent containing human papillary & reticular dermal fibroblasts: Use of fluorescent vital dyes', *Tissue Eng*, 2(1), 39-49.
Sorrell, J. M. & Caplan, A. I. (2004) 'Fibroblast heterogeneity: More than skin deep', *J Cell Sci*, 117(5), 667-675.
Soto, X., Li, J., Lea, R., Dubaissi, E., Papalopulu, N. & Amaya, E. (2013) 'Inositol kinase & its product accelerate wound healing by modulating calcium levels, Rho GTPases, & F-actin assembly', *Proc Nat Acad Sci*, 110(27), 11029-11034.
Sowers, M. R., Zheng, H., McConnell, D., Nan, B., Harlow, S. D. & Randolph Jr, J. F. (2008) 'Estradiol rates of change in relation to the final menstrual period in a population-based cohort of women', *J Clin Endocrinol Metab*, 93(10), 3847-3852.
Spazzafumo, L., Olivieri, F., Abbatecola, A. M., Castellani, G., Monti, D., Lisa, R., Galeazzi, R., Sirolla, C., Testa, R. & Ostan, R. (2013) 'Remodelling of biological parameters during human ageing: Evidence for complex regulation in longevity & in type 2 diabetes', *Age*, 35(2), 419-429.

Spranger, J., Kroke, A., Möhlig, M., Bergmann, M. M., Ristow, M., Boeing, H. & Pfeiffer, A. F. (2003) 'Adiponectin & protection against type 2 diabetes mellitus', *Lancet*, 361(9353), 226-228.
Sproul, E. P. & Argraves, W. S. (2013) 'A cytokine axis regulates elastin formation & degradation', *Matrix Biol*, 32(2), 86-94.
Sricholpech, M., Perdivara, I., Yokoyama, M., Nagaoka, H., Terajima, M., Tomer, K. B. & Yamauchi, M. (2012) 'Lysyl hydroxylase 3-mediated glucosylation in type I collagen: Molecular loci & biological significance', *J Biol Chem*, 287(27), 22998-23009.
Stadelmann, W. K., Digenis, A. G. & Tobin, G. R. (1998) 'Physiology & healing dynamics of chronic cutaneous wounds', *Am J surg*, 176(2), 26S-38S.
Stalker, T. J., Gong, Y. & Scalia, R. (2005) 'The calcium-dependent protease calpain causes endothelial dysfunction in type 2 diabetes', *Diabetes*, 54(4), 1132-1140.
Stanley, A. & Osler, T. (2001) 'Senescence & the healing rates of venous ulcers', *J Vasc Surg*, 33(6), 1206-1211.
Stanley, A. C., Park, H.-Y., Phillips, T. J., Russakovsky, V. & Menzoian, J. O. (1997) 'Reduced growth of dermal fibroblasts from chronic venous ulcers can be stimulated with growth factors', *J Vasc Surg*, 26(6), 994-1001.
Steffensen, B., Chen, Z., Pal, S., Mikhailova, M., Su, J., Wang, Y. & Xu, X. (2011) 'Fragmentation of fibronectin by inherent autolytic & matrix metalloproteinase activities', *Matrix Biol*, 30(1), 34-42.
Stephen-Haynes, J. & Thompson, G. (2007) 'The different methods of wound debridement', *Br J Comm Nurs*, 12(3), 6-16.
Stephens, P., Cook, H., Hilton, J., Jones, C. J., Haughton, M. F., Wyllie, F. S., Skinner, J. W., Harding, K. G., Kipling, D. & Thomas, D. W. (2003) 'An analysis of replicative senescence in dermal fibroblasts derived from chronic leg wounds predicts that telomerase therapy would fail to reverse their disease-specific cellular & proteolytic phenotype', *Exp Cell Res*, 283(1), 22-35.
Stookey, L. L. (1970) 'Ferrozine-a new spectrophotometric reagent for iron', *Anal Chem*, 42(7), 779-781.
Stoor, P., Söderling, E. & Salonen, J. I. (1998) 'Antibacterial effects of a bioactive glass paste on oral microorganisms', *Acta Odont Scand*, 56(3), 161-165.
Storer, M., Mas, A., Robert-Moreno, A., Pecoraro, M., Ortells, M. C., Di Giacomo, V., Yosef, R., Pilpel, N., Krizhanovsky, V. & Sharpe, J. (2013) 'Senescence is a developmental mechanism that contributes to embryonic growth & patterning', *Cell*, 155(5), 1119-1130.
Stott, F. J., Bates, S., James, M. C., McConnell, B. B., Starborg, M., Brookes, S., Palmero, I., Ryan, K., Hara, E. & Vousden, K. H. (1998) 'The alternative product from the human CDKN2A locus, p14ARF, participates in a regulatory feedback loop with p53 & MDM2', *EMBO J*, 17(17), 5001-5014.
Strathmann, M., Wingender, J. & Flemming, H.-C. (2002) 'Application of fluorescently labelled lectins for the visualization & biochemical characterization of polysaccharides in biofilms of *Pseudomonas aeruginosa*', *J Microbiol Methods*, 50(3), 237-248.
Strong, A. L., Bowles, A. C., MacCrimmon, C. P., Lee, S. J., Frazier, T. P., Katz, A. J., Gawronska-Kozak, B., Bunnell, B. A. & Gimble, J. M. (2015) 'Characterization of a murine pressure ulcer model to assess efficacy of adipose-derived stromal cells', *Plast Reconstr Surg Global Open*, 3(3), e334.
Stumvoll, M., Goldstein, B. J. & van Haeften, T. W. (2005) 'Type 2 diabetes: Principles of pathogenesis & therapy', *Lancet*, 365(9467), 1333-1346.

Stücker, M., Esser, M., Hoffmann, M., Memmel, U., Hirschmüller, A., Von Bormann, C., Hoffmann, K. & Altmeyer, P. (2002) 'High-resolution laser Doppler perfusion imaging aids in differentiating between benign & malignant melanocytic skin tumours', *Acta dermato-venereologica*, 82(1), 25-29.
Su, H.-L., Lin, S.-H., Wei, J.-C., Pao, I.-C., Chiao, S.-H., Huang, C.-C., Lin, S.-Z. & Lin, J.-J. (2011) 'Novel nanohybrids of silver particles on clay platelets for inhibiting silver-resistant bacteria', *PLoS One*, 6(6), e21125.
Subramaniam, V. N., McDonald, C. J., Ostini, L., Lusby, P. E., Wockner, L. F., Ramm, G. A. & Wallace, D. F. (2012) 'Hepatic iron deposition does not predict extrahepatic iron loading in mouse models of hereditary hemochromatosis', *Am J Pathol*, 181(4), 1173-1179.
Sugiyama, T., Kohara, H., Noda, M. & Nagasawa, T. (2006) 'Maintenance of the hematopoietic stem cell pool by CXCL12-CXCR4 chemokine signaling in bone marrow stromal cell niches', *Immunity*, 25(6), 977-988.
Sullivan, T. P., Eaglstein, W. H., Davis, S. C. & Mertz, P. (2001) 'The pig as a model for human wound healing', *Wound Repair Regen*, 9(2), 66-76.
Suman, R., Smith, G., Hazel, K. E., Kasprowicz, R., Coles, M., O'Toole, P. & Chawla, S. (2016) 'Label-free imaging to study phenotypic behavioural traits of cells in complex co-cultures', *Sci Rep*, 6, 22032.
Summerfield, A., Meurens, F. & Ricklin, M. E. (2015) 'The immunology of the porcine skin & its value as a model for human skin', *Mol Immunol*, 66(1), 14-21.
Sun, H. & Chai, Z.-F. (2010) 'Metallomics: An integrated science for metals in biology & medicine', *Ann Rep Prog Chem Sect A*, 106, 20-38.
Suzuki, N., Gradin, K., Poellinger, L. & Yamamoto, M. (2017) 'Regulation of hypoxia-inducible gene expression after HIF activation', *Exp Cell Res*, 356(2), 182-186.
Szerdahelyi, P. & Kasa, P. (1986) 'Histochemical demonstration of copper in normal rat brain & spinal cord', *Histochemistry*, 85(4), 341-347.
Szpunar, J. (2004) 'Metallomics: A new frontier in analytical chemistry', *Anal Bioanal Chem*, 378(1), 54-56.
Säbel, C. E., Shepherd, J. L. & Siemann, S. (2009) 'A direct spectrophotometric method for the simultaneous determination of zinc & cobalt in metalloproteins using 4-(2-pyridylazo) resorcinol', *Anal Biochem*, 391(1), 74-76.
Tabit, C. E., Chung, W. B., Hamburg, N. M. & Vita, J. A. (2010) 'Endothelial dysfunction in diabetes mellitus: Molecular mechanisms & clinical implications', *Rev Endocrin Metab Dis*, 11(1), 61-74.
Takahashi, A., Ohtani, N., Yamakoshi, K., Iida, S.-i., Tahara, H., Nakayama, K., Nakayama, K. I., Ide, T., Saya, H. & Hara, E. (2006) 'Mitogenic signalling & the p16 INK4a–Rb pathway cooperate to enforce irreversible cellular senescence', *Nat Cell Biol*, 8(11), 1291-1297.
Takeo, M., Lee, W. & Ito, M. (2015) 'Wound healing & skin regeneration', *CSH Perspect Med*, 5(1), a023267.
Tamareille, S., Mignen, O., Capiod, T., Rücker-Martin, C. & Feuvray, D. (2006) 'High glucose-induced apoptosis through store-operated calcium entry & calcineurin in human umbilical vein endothelial cells', *Cell Calcium*, 39(1), 47-55.
Tan, Q., Chen, B., Yan, X., Lin, Y., Xiao, Z., Hou, X. & Dai, J. (2014) 'Promotion of diabetic wound healing by collagen scaffold with collagen-binding vascular endothelial growth factor in a diabetic rat model', *J Tissue Eng Regen Med*, 8(3), 195-201.
Tandara, L., Grubisic, T. Z., Ivan, G., Jurisic, Z., Tandara, M., Gugo, K., Mladinov, S. & Salamunic, I. (2015) 'Systemic inflammation up-regulates serum hepcidin in exacerbations & stabile chronic obstructive pulmonary disease', *Clin Biochem*, 48(18), 1252-1257.

Tateishi, Y., Matsumoto, A., Kanie, T., Hara, E., Nakayama, K. & Nakayama, K. I. (2012) 'Development of mice without Cip/Kip CDK inhibitors', *Biochem Biophys Res Commun*, 427(2), 285-292.
Tavoosi, N. & Morrissey, J. H. (2014) 'Influence of membrane composition on the enhancement of factor VIIa/tissue factor activity by magnesium ions', *Thromb Haemost*, 111(4), 770772.
Tawfik, A., Gnana-Prakasam, J. P., Smith, S. B. & Ganapathy, V. (2014) 'Deletion of hemojuvelin, an iron-regulatory protein, in mice results in abnormal angiogenesis & vasculogenesis in retina along with reactive gliosis', *Invest Ophthalmol Vis Sci*, 55(6), 3616-3625.
Taylor, C. & Laude, A. (2002) 'IP3 receptors & their regulation by calmodulin & cytosolic Ca2+', *Cell Calcium*, 32(5-6), 321-334.
Taylor, C. G. (2005) 'Zinc, the pancreas, & diabetes: Insights from rodent studies & future directions', *Biometals*, 18(4), 305-312.
Taylor, G., Lehrer, M. S., Jensen, P. J., Sun, T.-T. & Lavker, R. M. (2000) 'Involvement of follicular stem cells in forming not only the follicle but also the epidermis', *Cell*, 102(4), 451-461.
Taylor, K. R., Costanzo, A. E. & Jameson, J. M. (2011) 'Dysfunctional γδ T cells contribute to impaired keratinocyte homeostasis in mouse models of obesity', *J Invest Dermatol*, 131(12), 2409-2418.
Taylor, R., Husband, D., Marshall, S., Tunbridge, W. & Alberti, K. (1984) 'Adipocyte insulin binding & insulin sensitivity in 'brittle'diabetes', *Diabetologia*, 27(4), 441-446.
Tchkonia, T., Zhu, Y., Van Deursen, J., Campisi, J. & Kirkland, J. L. (2013) 'Cellular senescence & the senescent secretory phenotype: Therapeutic opportunities', *J Clin Invest*, 123(3), 966-972.
Tejido-Rastrilla, R., Ferraris, S., Goldmann, W. H., Grünewald, A., Detsch, R., Baldi, G., Spriano, S. & Boccaccini, A. R. (2019) 'Studies on Cell Compatibility, Antibacterial Behavior, & Zeta Potential of Ag-Containing Polydopamine-Coated Bioactive Glass-Ceramic', *Materials*, 12(3), e500.
Tennakoon, S., Aggarwal, A. & Kállay, E. (2016) 'The calcium-sensing receptor & the hallmarks of cancer', *Biochim Biophys Acta*, 1863(6 Pt B), 1398-1407.
Tesfaye, S., Chaturvedi, N., Eaton, S. E., Ward, J. D., Manes, C., Ionescu-Tirgoviste, C., Witte, D. R. & Fuller, J. H. (2005) 'Vascular risk factors & diabetic neuropathy', *N Eng J Med*, 352(4), 341-350.
Thakar, D., Dalonneau, F., Migliorini, E., Lortat-Jacob, H., Boturyn, D., Albiges-Rizo, C., Coche-Guerente, L., Picart, C. & Richter, R. P. (2017) 'Binding of the chemokine CXCL12α to its natural extracellular matrix ligand heparan sulfate enables myoblast adhesion & facilitates cell motility', *Biomaterials*, 123, 24-38.
Thangavel, C., Dean, J. L., Ertel, A., Knudsen, K. E., Aldaz, C. M., Witkiewicz, A. K., Clarke, R. & Knudsen, E. S. (2011) 'Therapeutically activating RB: Reestablishing cell cycle control in endocrine therapy-resistant breast cancer', *Endocr Relat Cancer*, 18(3), 333-345.
Theocharidis, G., Drymoussi, Z., Kao, A. P., Barber, A. H., Lee, D. A., Braun, K. M. & Connelly, J. T. (2016) 'Type VI collagen regulates dermal matrix assembly & fibroblast motility', *J Invest Dermatol*, 136(1), 74-83.
Thomas, M. C., MacIsaac, R. J., Tsalamandris, C. & Jerums, G. (2004) 'Elevated iron indices in patients with diabetes', *Diabetic Med*, 21(7), 798-802.
Thornton, M. J. (2013) 'Estrogens & aging skin', *Dermato-Endocrinol*, 5(2), 264-270.
Thur, J., Rosenberg, K., Nitsche, D. P., Pihlajamaa, T., Ala-Kokko, L., Heinegård, D., Paulsson, M. & Maurer, P. (2001) 'Mutations in cartilage oligomeric matrix protein

causing pseudoachondroplasia & multiple epiphyseal dysplasia affect binding of calcium & collagen I, II, & IX', *J Biol Chem*, 276(9), 6083-6092.
Tian, J., Wong, K. K., Ho, C. M., Lok, C. N., Yu, W. Y., Che, C. M., Chiu, J. F. & Tam, P. K. (2007) 'Topical delivery of silver nanoparticles promotes wound healing', *ChemMedChem*, 2(1), 129-136.
Tiganescu, A., Hupe, M., Jiang, Y. J., Celli, A., Uchida, Y., Mauro, T. M., Bikle, D. D., Elias, P. M. & Holleran, W. M. (2015) 'UVB induces epidermal 11β-hydroxysteroid dehydrogenase type 1 activity *in vivo*', *Exp Dermatol*, 24(5), 370-376.
Tiganescu, A., Tahrani, A. A., Morgan, S. A., Otranto, M., Desmoulière, A., Abrahams, L., Hassan-Smith, Z., Walker, E. A., Rabbitt, E. H., Cooper, M. S., Amrein, K., Lavery, G. G. & Stewart, P. M. (2013) '11β-Hydroxysteroid dehydrogenase blockade prevents age-induced skin structure & function defects', *J Clin Invest*, 123(7), 3051-3060.
Tigges, J., Krutmann, J., Fritsche, E., Haendeler, J., Schaal, H., Fischer, J. W., Kalfalah, F., Reinke, H., Reifenberger, G. & Stuehler, K. (2014) 'The hallmarks of fibroblast ageing', *Mech Ageing Dev*, 138, 26-44.
Tlaskalová-Hogenová, H., Štěpánková, R., Kozáková, H., Hudcovic, T., Vannucci, L., Tučková, L., Rossmann, P., Hrnčíř, T., Kverka, M. & Zákostelská, Z. (2011) 'The role of gut microbiota (commensal bacteria) & the mucosal barrier in the pathogenesis of inflammatory & autoimmune diseases & cancer: Contribution of germ-free & gnotobiotic animal models of human diseases', *Cell Mol Immunol*, 8(2), 110-120.
To, M., Goz, A., Camenzind, L., Oertle, P., Candiello, J., Sullivan, M., Henrich, P. B., Loparic, M., Safi, F., Eller, A. & Halfter, W. (2013) 'Diabetes-induced morphological, biomechanical, & compositional changes in ocular basement membranes', *Exp Eye Res*, 116, 298-307.
Toka, H. R., Pollak, M. R. & Houillier, P. (2015) 'Calcium sensing in the renal tubule', *Physiology*, 30(4), 317-326.
Tomasek, J. J., Haaksma, C. J., Schwartz, R. J. & Howard, E. W. (2013) 'Whole animal knockout of smooth muscle alpha-actin does not alter excisional wound healing or the fibroblast-to-myofibroblast transition', *Wound Repair Regen*, 21(1), 166-176.
Tombes, R. M. & Borisy, G. G. (1989) 'Intracellular free calcium & mitosis in mammalian cells: Anaphase onset is calcium modulated, but is not triggered by a brief transient', *J Cell Biol*, 109(2), 627-636.
Toque, H. A., Fernandez-Flores, A., Mohamed, R., Caldwell, R. B., Ramesh, G. & Caldwell, R. W. (2017) 'Netrin-1 is a novel regulator of vascular endothelial function in diabetes', *PloS One*, 12(10), e0186734.
Torr, E. E., Ngam, C. R., Bernau, K., Tomasini-Johansson, B., Acton, B. & Sandbo, N. (2015) 'Myofibroblasts exhibit enhanced fibronectin assembly that is intrinsic to their contractile phenotype', *J Biol Chem*, 290(11), 6951-6961.
Toso, C., Emamaullee, J., Merani, S. & Shapiro, A. (2008) 'The role of macrophage migration inhibitory factor on glucose metabolism & diabetes', *Diabetologia*, 51(11), 1937-1946.
Tourigny, M. R., Ursini-Siegel, J., Lee, H., Toellner, K.-M., Cunningham, A. F., Franklin, D. S., Ely, S., Chen, M., Qin, X.-F. & Xiong, Y. (2002) 'CDK inhibitor p18INK4c is required for the generation of functional plasma cells', *Immunity*, 17(2), 179-189.
Toutfaire, M., Bauwens, E. & Debacq-Chainiaux, F. (2017) 'The impact of cellular senescence in skin ageing: A notion of mosaic & therapeutic strategies', *Biochem Pharmacol*, 142, 1-12.
Toy, L. W. & Macera, L. (2011) 'Evidence-based review of silver dressing use on chronic wounds', *J Am Acad Nurse Pract*, 23(4), 183-192.
Toyoshima, C. (2009) 'How Ca2+-ATPase pumps ions across the sarcoplasmic reticulum membrane', *Biochim Biophys Acta Mol Cell Res*, 1793(6), 941-946.

Toyoshima, C. & Inesi, G. (2004) 'Structural basis of ion pumping by Ca2+-ATPase of the sarcoplasmic reticulum', *Ann Rev Biochem*, 73(1), 269-292.
Trakala, M., Arias, C. F., García, M. I., Moreno-Ortiz, M. C., Tsilingiri, K., Fernández, P. J., Mellado, M., Díaz-Meco, M. T., Moscat, J. & Serrano, M. (2009) 'Regulation of macrophage activation & septic shock susceptibility via p21 (WAF1/CIP1)', *Eur J Immunol*, 39(3), 810-819.
Tran, P. O. T., Hinman, L. E., Unger, G. M. & Sammak, P. J. (1999) 'A wound-induced [Ca 2+] i increase & its transcriptional activation of immediate early genes is important in the regulation of motility', *Exp Cell Res*, 246(2), 319-326.
Treiber, N., Peters, T., Sindrilaru, A., Huber, R., Kohn, M., Menke, A., Briviba, K., Kreppel, F., Basu, A. & Maity, P. (2009) 'Overexpression of manganese superoxide dismutase in human dermal fibroblasts enhances the contraction of free floating collagen lattice: Implications for ageing & hyperplastic scar formation', *Arch Dermatol Res*, 301(4), 273-287.
Treuting, P., Clifford, C., Sellers, R. & Brayton, C. (2012) 'Of mice & microflora: Considerations for genetically engineered mice', *Vet Pathol*, 49(1), 44-63.
Trollinger, D. R., Rivkah Isseroff, R. & Nuccitelli, R. (2002) 'Calcium channel blockers inhibit galvanotaxis in human keratinocytes', *J Cell Physiol*, 193(1), 1-9.
Tsien, R., Pozzan, T. & Rink, T. (1984) 'Measuring & manipulating cytosolic Ca2+ with trapped indicators', *Trends Biochem Sci*, 9(6), 263-266.
Tsutsumi, M., Goto, M. & Denda, M. (2013) 'Dynamics of intracellular calcium in cultured human keratinocytes after localized cell damage', *Exp Dermatol*, 22(5), 367-369.
Tu, C.-L. & Bikle, D. D. (2013) 'Role of the calcium-sensing receptor in calcium regulation of epidermal differentiation & function', *Best Pract Res Clin Endocrinol Metab*, 27(3), 415-427.
Tu, C.-L., Celli, A., Mauro, T. & Chang, W. (2019) 'Calcium-Sensing Receptor Regulates Epidermal Intracellular Ca2+ Signaling & Re-Epithelialization after Wounding', *J Invest Dermatol*, 139(4), 919-929.
Tu, C.-L., Chang, W. & Bikle, D. D. (2005) 'Phospholipase Cγ1 is required for activation of store-operated channels in human keratinocytes', *J Invest Dermatol*, 124(1), 187-197.
Tu, C.-L., Chang, W., Xie, Z. & Bikle, D. D. (2008) 'Inactivation of the calcium sensing receptor inhibits E-cadherin-mediated cell-cell adhesion & calcium-induced differentiation in human epidermal keratinocytes', *J Biol Chem*, 283(6), 3519-3528.
Tu, C.-L., Crumrine, D. A., Man, M.-Q., Chang, W., Elalieh, H., You, M., Elias, P. M. & Bikle, D. D. (2012) 'Ablation of the calcium-sensing receptor in keratinocytes impairs epidermal differentiation & barrier function', *J Invest Dermatol*, 132(10), 2350-2359.
Tuomainen, T. P., Nyyssönen, K., Salonen, R., Tervahauta, A., Korpela, H., Lakka, T., Kaplan, G. A. & Salonen, J. T. (1997) 'Body iron stores are associated with serum insulin & blood glucose concentrations. Population study in 1,013 eastern Finnish men', *Diabetes Care*, 20(3), 426-428.
Turchinovich, A., Weiz, L. & Burwinkel, B. (2012) 'Extracellular miRNAs: the mystery of their origin & function', *Trends Biochem Sci*, 37(11), 460-465.
Turksen, K. & Troy, T.-C. (2003) 'Overexpression of the calcium sensing receptor accelerates epidermal differentiation & permeability barrier formation *in vivo*', *Mech Dev*, 120(6), 733-744.
Uchida, T., Nakamura, T., Hashimoto, N., Matsuda, T., Kotani, K., Sakaue, H., Kido, Y., Hayashi, Y., Nakayama, K. I. & White, M. F. (2005) 'Deletion of Cdkn1b ameliorates

hyperglycemia by maintaining compensatory hyperinsulinemia in diabetic mice', *Nat Med*, 11(2), 175-182.
Ueck, C., Volksdorf, T., Houdek, P., Vidal-y-Sy, S., Sehner, S., Ellinger, B., Lobmann, R., Larena-Avellaneda, A., Reinshagen, K., Ridderbusch, I. & Kohrmeyer, K., (2017) 'Comparison of *in-vitro* & *ex-vivo* wound healing assays for the investigation of diabetic wound healing & demonstration of a beneficial effect of a triterpene extract', *PloS One*, 12(1), e0169028.
Uhlén, P. & Fritz, N. (2010) 'Biochemistry of calcium oscillations', *Biochem Biophys Res Commun*, 396(1), 28-32.
Untergasser, A., Nijveen, H., Rao, X., Bisseling, T., Geurts, R. & Leunissen, J. A. (2007) 'Primer3Plus, an enhanced web interface to Primer3', *Nucleic Acids Res*, 35(2), 71-74.
Uribarri, J., Cai, W., Peppa, M., Goodman, S., Ferrucci, L., Striker, G. & Vlassara, H. (2007) 'Circulating glycotoxins & dietary advanced glycation endproducts: Two links to inflammatory response, oxidative stress, & aging', *J Gerontol A Biol Sci Med Sci*, 62(4), 427-433.
Ushach, I. & Zlotnik, A. (2016) 'Biological role of granulocyte macrophage colony-stimulating factor (GM-CSF) & macrophage colony-stimulating factor (M-CSF) on cells of the myeloid lineage', *J Leuk Biol*, 100(3), 481-489.
Ushijima, T., Takahashi, M. & Ozaki, Y. (1984) 'Acetic, propionic, & oleic acid as the possible factors influencing the predominant residence of some species of Propionibacterium & coagulase-negative *Staphylococcus* on normal human skin', *Can J Microbiol*, 30(5), 647-652.
Utaida, S., Dunman, P., Macapagal, D., Murphy, E., Projan, S., Singh, V., Jayaswal, R. & Wilkinson, B. (2003) 'Genome-wide transcriptional profiling of the response of *Staphylococcus aureus* to cell-wall-active antibiotics reveals a cell-wall-stress stimulon', *Microbiology*, 149(10), 2719-2732.
Utsal, L., Tillmann, V., Zilmer, M., Mäestu, J., Purge, P., Jürimäe, J., Saar, M., Lätt, E., Maasalu, K. & Jürimäe, T. (2012) 'Elevated serum IL-6, IL-8, MCP-1, CRP, & IFN-γ levels in 10-to 11-year-old boys with increased BMI', *Horm Res Paediatr*, 78(1), 31-39.
Uysal, K. T., Wiesbrock, S. M., Marino, M. W. & Hotamisligil, G. S. (1997) 'Protection from obesity-induced insulin resistance in mice lacking TNF-α function', *Nature*, 389(6651), 610-614.
Vacchini, A., Locati, M. & Borroni, E. M. (2016) 'Overview & potential unifying themes of the atypical chemokine receptor family', *J Leuk Biol*, 99(6), 883-892.
Vag, T., Steiger, K., Rossmann, A., Keller, U., Noske, A., Herhaus, P., Ettl, J., Niemeyer, M., Wester, H.-J. & Schwaiger, M. (2018) 'PET imaging of chemokine receptor CXCR4 in patients with primary & recurrent breast carcinoma', *EJNMMI Res*, 8, 90.
Valenti, L., Dongiovanni, P. & Fargion, S. (2012) 'Diagnostic & therapeutic implications of the association between ferritin level & severity of nonalcoholic fatty liver disease', *World J Gastroenterol*, 18(29), 3782-3786.
Vallee, B. L. & Falchuk, K. H. (1993) 'The biochemical basis of zinc physiology', *Physiol Rev*, 73(1), 79-118.
Vallelian, F., Schaer, C. A., Kaempfer, T., Gehrig, P., Duerst, E., Schoedon, G. & Schaer, D. J. (2010) 'Glucocorticoid treatment skews human monocyte differentiation into a hemoglobin-clearance phenotype with enhanced heme-iron recycling & antioxidant capacity', *Blood*, 116(24), 5347-5356.
van de Graaf, S. F., Boullart, I., Hoenderop, J. G. & Bindels, R. J. (2004) 'Regulation of the epithelial Ca2+ channels TRPV5 & TRPV6 by 1alpha,25-dihydroxy Vitamin D3 & dietary Ca2+', *J Steroid Biochem Mol Biol*, 89-90(1-5), 303-308.

Van Der Plas, M. J., Bhongir, R. K., Kjellström, S., Siller, H., Kasetty, G., Mörgelin, M. & Schmidtchen, A. (2016) '*Pseudomonas aeruginosa* elastase cleaves a C-terminal peptide from human thrombin that inhibits host inflammatory responses', *Nat Commun*, 7, 11567.
Van der Waal, S., Van der Sluis, L., Özok, A., Exterkate, R., van Marle, J., Wesselink, P. & de Soet, J. (2011) 'The effects of hyperosmosis or high pH on a dual-species biofilm of *Enterococcus faecalis* & *Pseudomonas aeruginosa*: An *in vitro* study', *Int Endod J*, 44(12), 1110-1117.
Van Deursen, J. M. (2014) 'The role of senescent cells in ageing', *Nature*, 509(7501), 439-446.
van Furth, R., Cohn, Z., Hirsch, J., Humphrey, J., Spector, W. & Langevoort, H. (1972) 'The mononuclear phagocyte system: A new classification of macrophages, monocytes, & their precursor cells', *Bull World Health Organ*, 46(6), 845-852.
Van Petegem, F. (2012) 'Ryanodine receptors: Structure & function', *J Biol Chem*, 287(38), 31624-31632.
Van Puyvelde, K., Mets, T., Njemini, R., Beyer, I. & Bautmans, I. (2014) 'Effect of advanced glycation end product intake on inflammation & aging: A systematic review', *Nutr Rev*, 72(10), 638-650.
Vande Berg, J. S., Rose, M. A., Haywood-Reid, P. L., Rudolph, R., Payne, W. G. & Robson, M. C. (2005) 'Cultured pressure ulcer fibroblasts show replicative senescence with elevated production of plasmin, plasminogen activator inhibitor-1, & transforming growth factor-β1', *Wound Repair Regen*, 13(1), 76-83.
Vandecaetsbeek, I., Vangheluwe, P., Raeymaekers, L., Wuytack, F. & Vanoevelen, J. (2011) 'The Ca2+ pumps of the endoplasmic reticulum & Golgi apparatus', *CSH Perspect* Biol, 3(5), a004184.
Varga-Szabo, D., Braun, A. & Nieswandt, B. (2009) 'Calcium signaling in platelets', *J Thromb Haemost*, 7(7), 1057-1066.
Varkey, M., Ding, J. & Tredget, E. E. (2014) 'Superficial dermal fibroblasts enhance basement membrane & epidermal barrier formation in tissue-engineered skin: Implications for treatment of skin basement membrane disorders', *Tissue Eng Part A*, 20(3-4), 540-552.
Varol, C. & Sagi, I. (2018) 'Phagocyte—extracellular matrix crosstalk empowers tumor development & dissemination', *FEBS J*, 285(4), 734-751.
Vashchenko, G. & MacGillivray, R. T. (2013) 'Multi-copper oxidases & human iron metabolism', *Nutrients*, 5(7), 2289-2313.
Vashi, N., Andrabi, S. B. A., Ghanwat, S., Suar, M. & Kumar, D. (2017) 'Ca2+-dependent focal exocytosis of Golgi-derived vesicles helps phagocytic uptake in macrophages', *J Biol Chem*, 292(13), 5144-5165.
Vasta, J. D. & Raines, R. T. (2016) 'Human collagen prolyl 4-hydroxylase is activated by ligands for its iron center', *Biochemistry*, 55(23), 3224-3233.
Velander, P., Theopold, C., Hirsch, T., Bleiziffer, O., Zuhaili, B., Fossum, M., Hoeller, D., Gheerardyn, R., Chen, M., Visovatti, S., Svensson, H., Yao, F. & Eriksson, E. (2008) 'Impaired wound healing in an acute diabetic pig model & the effects of local hyperglycemia', *Wound Repair Regen*, 16(2), 288-293.
Velnar, T., Bailey, T. & Smrkolj, V. (2009) 'The wound healing process: An overview of the cellular & molecular mechanisms', *J Int Med Res*, 37(5), 1528-1542.
Venugopal, J. & Ramakrishna, S. (2005) 'Applications of polymer nanofibers in biomedicine & biotechnology', *Appl Biochem Biotechnol*, 125(3), 147-157.
Vermes, I., Haanen, C. & Reutelingsperger, C. (2000) 'Flow cytometry of apoptotic cell death', *J Immunol Methods*, 243(1-2), 167-190.

Vernon, R. B. & Gooden, M. D. (2002) 'An improved method for the collagen gel contraction assay', *In Vitro Cell Dev Biol*, 38(2), 97-101.
Verrier, S., Blaker, J. J., Maquet, V., Hench, L. L. & Boccaccini, A. R. (2004) 'PDLLA/Bioglass® composites for soft-tissue & hard-tissue engineering: an *in vitro* cell biology assessment', *Biomaterials*, 25(15), 3013-3021.
Verschuren, L., Kooistra, T., Bernhagen, J., Voshol, P. J., Ouwens, D. M., van Erk, M., de Vries-van der Weij, J., Leng, L., van Bockel, J. H. & van Dijk, K. W. (2009) 'MIF deficiency reduces chronic inflammation in white adipose tissue & impairs the development of insulin resistance, glucose intolerance, & associated atherosclerotic disease', *Circ Res*, 105(1), 99-107.
Vidal, B., Serrano, A. L., Tjwa, M., Suelves, M., Ardite, E., De Mori, R., Baeza-Raja, B., de Lagrán, M. M., Lafuste, P. & Ruiz-Bonilla, V. (2008) 'Fibrinogen drives dystrophic muscle fibrosis via a TGFβ/alternative macrophage activation pathway', *Genes Dev*, 22(13), 1747-1752.
Villa-Bellosta, R. (2017) 'Impact of magnesium: Calcium ratio on calcification of the aortic wall', *PloS One*, 12(6), e0178872.
Vlassara, H. & Striker, G. E. (2011) 'AGE restriction in diabetes mellitus: A paradigm shift', *Nat Rev Endocrinol*, 7(9), 526-539.
Vogeleer, P., Tremblay, Y. D., Mafu, A. A., Jacques, M. & Harel, J. (2014) 'Life on the outside: role of biofilms in environmental persistence of Shiga-toxin producing *Escherichia coli*', *Front Microbiol*, 5, 317.
Volonte, D., Zou, H., Bartholomew, J. N., Liu, Z., Morel, P. A. & Galbiati, F. (2015) 'Oxidative stress-induced inhibition of Sirt1 by caveolin-1 promotes p53-dependent premature senescence & stimulates the secretion of interleukin 6 (IL-6)', *J Biol Chem*, 290(7), 4202-4214.
Vuerstaek, J. D., Vainas, T., Wuite, J., Nelemans, P., Neumann, M. H. & Veraart, J. C. (2006) 'State-of-the-art treatment of chronic leg ulcers: A randomized controlled trial comparing vacuum-assisted closure (VAC) with modern wound dressings', *J Vasc Surg*, 44(5), 1029-1037.
Waaijer, M. E., Parish, W. E., Strongitharm, B. H., van Heemst, D., Slagboom, P. E., de Craen, A. J., Sedivy, J. M., Westendorp, R. G., Gunn, D. A. & Maier, A. B. (2012) 'The number of p16INK4a positive cells in human skin reflects biological age', *Aging Cell*, 11(4), 722-725.
Walko, G., Castañón, M. J. & Wiche, G. (2015) 'Molecular architecture & function of the hemidesmosome', *Cell Tissue Res*, 360(3), 529-544.
Wall, I. B., Moseley, R., Baird, D. M., Kipling, D., Giles, P., Laffafian, I., Price, P. E., Thomas, D. W. & Stephens, P. (2008) 'Fibroblast dysfunction is a key factor in the non-healing of chronic venous leg ulcers', *J Invest Dermatol*, 128(10), 2526-2540.
Wallace, D. F., Summerville, L., Crampton, E. M., Frazer, D. M., Anderson, G. J. & Subramaniam, V. N. (2009) 'Combined deletion of Hfe & transferrin receptor 2 in mice leads to marked dysregulation of hepcidin & iron overload', *Hepatology*, 50(6), 1992-2000.
Waller, J. M. & Maibach, H. I. (2006) 'Age & skin structure & function, a quantitative approach (II): Protein, glycosaminoglycan, water, & lipid content & structure', *Skin Res Technol*, 12(3), 145-154.
Walsh, J., Hoffstad, O., Sullivan, M. & Margolis, D. (2016) 'Association of diabetic foot ulcer & death in a population-based cohort from the United Kingdom', *Diabet Med*. 33(11), 1493-1498.
Walters, K. A. & Roberts, M. S. (2002) 'The structure & function of skin', *Drug Pharm Sci*, 119, 1-40.

Walthers, C. M., Nazemi, A. K., Patel, S. L., Wu, B. M. & Dunn, J. C. (2014) 'The effect of scaffold macroporosity on angiogenesis & cell survival in tissue-engineered smooth muscle', *Biomaterials*, 35(19), 5129-5137.
Wang, A. S., Ong, P. F., Chojnowski, A., Clavel, C. & Dreesen, O. (2017a) 'Loss of lamin B1 is a biomarker to quantify cellular senescence in photoaged skin', *Sci Rep*, 7, 15678.
Wang, C. Y. & Babitt, J. L. (2016) 'Hepcidin regulation in the anemia of inflammation', *Curr Opin Hematol*, 23(3), 189-197.
Wang, H., An, P., Xie, E., Wu, Q., Fang, X., Gao, H., Zhang, Z., Li, Y., Wang, X., Zhang, J., Li, G., Yang, L., Liu, W., Min, J. & Wang, F. (2017b) 'Characterization of ferroptosis in murine models of hemochromatosis', *Hepatology*, 66(2), 449-465.
Wang, H., Lafdil, F., Wang, L., Yin, S., Feng, D. & Gao, B. (2011) 'Tissue inhibitor of metalloproteinase 1 (TIMP-1) deficiency exacerbates carbon tetrachloride-induced liver injury & fibrosis in mice: Involvement of hepatocyte STAT3 in TIMP-1 production', *Cell Biosc*, 1, 14.
Wang, H., Li, Z., Niu, J., Xu, Y., Ma, L., Lu, A., Wang, X., Qian, Z., Huang, Z. & Jin, X. (2018a) 'Antiviral effects of ferric ammonium citrate', *Cell Discov*, 4, 14.
Wang, L., Fang, B., Fujiwara, T., Krager, K., Gorantla, A., Li, C., Feng, J. Q., Jennings, M. L., Zhou, J. & Aykin-Burns, N. (2018b) 'Deletion of ferroportin in murine myeloid cells increases iron accumulation & stimulates osteoclastogenesis *in vitro* & *in vivo*', *J Biol Chem*, 293(24), 9248-9264.
Wang, M., Feng, W. Y., Zhao, Y. L. & Chai, Z. F. (2010) 'ICP-MS-based strategies for protein quantification', *Mass Spectrom Rev*, 29(2), 326-348.
Wang, P., Zhou, S., Xu, L., Lu, Y., Yuan, X., Zhang, H., Li, R., Fang, J. & Liu, P. (2013) 'Hydrogen peroxide-mediated oxidative stress & collagen synthesis in cardiac fibroblasts: Blockade by tanshinone IIA', *J Ethnopharmacol*, 145(1), 152-161.
Wang, Q. J. (2006) 'PKD at the crossroads of DAG & PKC signaling', *Trends Pharmacol Sci*, 27(6), 317-323.
Wang, S., Brown, R. & Gray, D. (1994) 'Application of laser ablation-ICPMS to the spatially resolved micro-analysis of biological tissue', *Appl Spectrosc*, 48(11), 1321-1325.
Wang, S., Hu, F., Li, J., Zhang, S., Shen, M., Huang, M. & Shi, X. (2018c) 'Design of electrospun nanofibrous mats for osteogenic differentiation of mesenchymal stem cells', *Nanomed Nanotechnol Biol Med*, 14(7), 2505-2520.
Wang, S., Song, R., Wang, Z., Jing, Z., Wang, S. & Ma, J. (2018d) 'S100A8/A9 in Inflammation', *Front Immunol*, 9, 1298.
Wang, X.-F., Wang, H.-S., Wang, H., Zhang, F., Wang, K.-F., Guo, Q., Zhang, G., Cai, S.-H. & Du, J. (2014) 'The role of indoleamine 2, 3-dioxygenase (IDO) in immune tolerance: Focus on macrophage polarization of THP-1 cells', *Cell Immunol*, 289(1-2), 42-48.
Wang, Y., Kuro-o, M. & Sun, Z. (2012) 'Klotho gene delivery suppresses Nox2 expression & attenuates oxidative stress in rat aortic smooth muscle cells via the cAMP-PKA pathway', *Aging Cell*, 11(3), 410-417.
Wang, Z., Gerstein, M. & Snyder, M. (2009) 'RNA-Seq: A revolutionary tool for transcriptomics', *Nature Rev Genet*, 10(1), 57-63.
Ward, D. T. & Riccardi, D. (2012) 'New concepts in calcium-sensing receptor pharmacology & signalling', *Br J Pharmacol*, 165(1), 35-48.
Warnes, G. R., Bolker, B., Bonebakker, L., Gentleman, R., Liaw, W. H. A., Lumley, T., Maechler, M., Magnusson, A., Moeller, S. & Schwartz, M. (2016) 'Package gplots' Available online: http://cran.r-project.org [Accessed 30/8/19].

Watson, J. M., Kang'ombe, A. R., Soares, M. O., Chuang, L.-H., Worthy, G., Bland, J. M., Iglesias, C., Cullum, N., Torgerson, D. & Nelson, E. A. (2011) 'Use of weekly, low dose, high frequency ultrasound for hard to heal venous leg ulcers: The VenUS III randomised controlled trial', *Br Med J*, 342, d1092.
Watt, F. M. (2002) 'Role of integrins in regulating epidermal adhesion, growth & differentiation', *EMBO J*, 21(15), 3919-3926.
Watz, H., Uddin, M., Pedersen, F., Kirsten, A., Goldmann, T., Stellmacher, F., Groth, E., Larsson, B., Böttcher, G. & Malmgren, A. (2017) 'Effects of the CXCR2 antagonist AZD5069 on lung neutrophil recruitment in asthma', *Pulm Pharmacol Ther*, 45, 121-123.
Weatherall, D. J. (2001) 'Phenotype-genotype relationships in monogenic disease: Lessons from the thalassaemias', *Nat Rev Genet*, 2(4), 245-255.
Weber, L. P., Chow, W. L., Abebe, W. & MacLeod, K. M. (1996) 'Enhanced contractile responses of arteries from streptozotocin diabetic rats to sodium fluoride', *Br J Pharmacol*, 118(1), 115-122.
Webster, J., Scuffham, P., Sherriff, K. L., Stankiewicz, M. & Chaboyer, W. P. (2012) 'Negative pressure wound therapy for skin grafts & surgical wounds healing by primary intention', *Cochrane Database Syst Rev*, 18(4), CD009261.
Wehrhahn, J., Kraft, R., Harteneck, C. & Hauschildt, S. (2010) 'Transient receptor potential melastatin 2 is required for lipopolysaccharide-induced cytokine production in human monocytes', *J Immunol*, 184(5), 2386-2393.
Wei, C., Wang, X., Chen, M., Ouyang, K., Song, L.-S. & Cheng, H. (2009) 'Calcium flickers steer cell migration', *Nature*, 457(7231), 901-905.
Weinrick, B., Dunman, P. M., McAleese, F., Murphy, E., Projan, S. J., Fang, Y. & Novick, R. P. (2004) 'Effect of mild acid on gene expression in *Staphylococcus aureus*', *J Bacteriol*, 186(24), 8407-8423.
Wellinghausen, N., Kirchner, H. & Rink, L. (1997) 'The immunobiology of zinc', *Immunol Today*, 18(11), 519-521.
Wenk, J., Foitzik, A., Achterberg, V., Sabiwalsky, A., Dissemond, J., Meewes, C., Reitz, A., Brenneisen, P., Wlaschek, M. & Meyer-Ingold, W. (2001) 'Selective pick-up of increased iron by deferoxamine-coupled cellulose abrogates the iron-driven induction of matrix-degrading metalloproteinase 1 & lipid peroxidation in human dermal fibroblasts *in vitro*: A new dressing concept', *J Invest Dermatol*, 116(6), 833-839.
Werner, S., Krieg, T. & Smola, H. (2007) 'Keratinocyte-fibroblast interactions in wound healing', *J Invest Dermatol*, 127(5), 998-1008.
Wessels, I., Maywald, M. & Rink, L. (2017) 'Zinc as a gatekeeper of immune function', *Nutrients*, 9(12), e1286.
Wetzler, C., Kämpfer, H., Stallmeyer, B., Pfeilschifter, J. & Frank, S. (2000) 'Large & sustained induction of chemokines during impaired wound healing in the genetically diabetic mouse: Prolonged persistence of neutrophils & macrophages during the late phase of repair', *J Invest Dermatol*, 115(2), 245-253.
Wickham, H. (2007) 'Reshaping data with the reshape package', *J Stat Softw*, 21(12), 1-20.
Wickham, H. (2011) 'The split-apply-combine strategy for data analysis', *J Stat Softw*, 40(1), 1-29.
Wickham, H. (2016) *ggplot2: Elegant graphics for data analysis* [ebook]. Berlin: Springer.
Wickham, H., Henry, L. & Wickham, M. H. (2019) 'Package 'tidyr''. Available online: https://mran.revolutionanalytics.com/web/packages/tidyr/tidyr.pdf [Accessed 30/8/19].

Wicks, K., Torbica, T. & Mace, K. A. 'Myeloid cell dysfunction & the pathogenesis of the diabetic chronic wound'. *Sem Immunol*, 26(4), 341-353.
Wiel, C., Lallet-Daher, H., Gitenay, D., Gras, B., Le Calvé, B., Augert, A., Ferr&, M., Prevarskaya, N., Simonnet, H. & Vindrieux, D. (2014) 'Endoplasmic reticulum calcium release through ITPR2 channels leads to mitochondrial calcium accumulation & senescence', *Nat Commun*, 5, e3792.
Wilkinson, H.N., Clowes, C., Banyard, K.L., Matteuci, P., Mace, K.A. & Hardman, M.J. (2019a) 'Elevated local senescence in diabetic wound healing is linked to pathological repair via CXCR2'. *J Invest Dermatol*, 139(5), 1171-1181.
Wilkinson, H. N. & Hardman, M. J. (2017) 'The role of estrogen in cutaneous ageing & repair', *Maturitas*, 103, 60-64.
Wilkinson, H. N., McBain, A. J., Stephenson, C. & Hardman, M. J. (2016) 'Comparing the effectiveness of polymer debriding devices using a porcine wound biofilm model', *Adv Wound Care*, 5(11), 475-485.
Wilkinson, H. N., Roberts, E. R., Stafford, A. R., Banyard, K. L., Matteucci, P., Mace, K. A. & Hardman, M. J. (2019b) 'Tissue iron promotes wound repair via M2 macrophage polarisation and the chemokines CCL17 and CCL22', *Am J Pathol* [in press] Available online: https://ajp.amjpathol.org/article/S0002-9440(19)30671-6/fulltext [Accessed 30/8/19].
Wilkinson, H. N., Upson, S. E., Banyard, K. L., Knight, R., Mace, K. A. & Hardman, M. J. (2019c) 'Reduced iron in diabetic wounds: An oxidative stress-dependent role for STEAP3 in extracellular matrix deposition & remodelling', *J Invest Dermatol* [in press] Available online: https://linkinghub.elsevier.com/retrieve/pii/S0022-202X(19)31633-1 [Accessed 30/8/19].
Wilkinson, N. & Pantopoulos, K. (2013) 'IRP1 regulates erythropoiesis & systemic iron homeostasis by controlling HIF2α mRNA translation', *Blood*, 122(9), 1658-1668.
Williams, H., Campbell, L., Crompton, R. A., Singh, G., McHugh, B. J., Davidson, D. J., McBain, A. J., Cruickshank, S. M. & Hardman, M. J. (2018) 'Microbial host interactions & impaired wound healing in mice & humans: Defining a role for BD14 & NOD2', *J Invest Dermatol*, 138(10), 2264-2274.
Williams, H., Crompton, R. A., Thomason, H. A., Campbell, L., Singh, G., McBain, A. J., Cruickshank, S. M. & Hardman, M. J. (2017) 'Cutaneous Nod2 expression regulates the skin microbiome & wound healing in a murine model', *J Invest Dermatol*, 137(11), 2427-2436.
Witte, M. B. & Barbul, A. (1997) 'General principles of wound healing', *Surg Clin North Am*, 77(3), 509-528.
Witte, M. B. & Barbul, A. (2003) 'Arginine physiology & its implication for wound healing', *Wound Repair Regen*, 11(6), 419-423.
Wlaschek, M., Singh, K., Sindrilaru, A., Crisan, D. & Scharffetter-Kochanek, K. (2019) 'Iron & iron-dependent reactive oxygen species in the regulation of macrophages & fibroblasts in non-healing chronic wounds', *Free Radical Bio Med*, 133, 262-275.
Wolcott, R. D., Hanson, J. D., Rees, E. J., Koenig, L. D., Phillips, C. D., Wolcott, R. A., Cox, S. B. & White, J. S. (2015) 'Analysis of the chronic wound microbiota of 2,963 patients by 16S rDNA pyrosequencing', *Wound Repair Regen*, 24(1), 163-174.
Wolf, F. & Cittadini, A. (2003) 'Chemistry & biochemistry of magnesium', *Mol Aspects Med*, 24(1-3), 3-9.
Wong, V. W., Sorkin, M., Glotzbach, J. P., Longaker, M. T. & Gurtner, G. C. (2010) 'Surgical approaches to create murine models of human wound healing', *BioMed Res Int*, 2011, 969618.

Wood, M. J., Powell, L. W., Dixon, J. L., Subramaniam, V. N. & Ramm, G. A. (2013) 'Transforming growth factor-β & toll-like receptor-4 polymorphisms are not associated with fibrosis in haemochromatosis', *World J Gastroenterol*, 19(48), 9366-9376.
Wood, M. J., Powell, L. W. & Ramm, G. A. (2008) 'Environmental & genetic modifiers of the progression to fibrosis & cirrhosis in hemochromatosis', *Blood*, 111(9), 4456-4462.
Wood, S., Jayaraman, V., Huelsmann, E. J., Bonish, B., Burgad, D., Sivaramakrishnan, G., Qin, S., DiPietro, L. A., Zloza, A. & Zhang, C. (2014) 'Pro-inflammatory chemokine CCL2 (MCP-1) promotes healing in diabetic wounds by restoring the macrophage response', *PLoS One*, 9(3), e91574.
Wood, W. & Martin, P. (2017) 'Macrophage functions in tissue patterning & disease: New insights from the fly', *Dev Cell*, 40(3), 221-233.
Woodley, D. T., Wang, X., Amir, M., Hwang, B., Remington, J., Hou, Y., Uitto, J., Keene, D. & Chen, M. (2013) 'Intravenously injected recombinant human type VII collagen homes to skin wounds & restores skin integrity of dystrophic epidermolysis bullosa', *J Invest Dermatol*, 133(7), 1910-1913.
Woollard, K. J., Sturgeon, S., Chin-Dusting, J. P., Salem, H. H. & Jackson, S. P. (2009) 'Erythrocyte hemolysis & hemoglobin oxidation promote ferric chloride-induced vascular injury', *J Biol Chem*, 284(19), 13110-13118.
Wright, B., Zeidman, I., Greig, R. & Poste, G. (1985) 'Inhibition of macrophage activation by calcium channel blockers & calmodulin antagonists', *Cell Immunol*, 95(1), 46-53.
Wright, J. A., Oddy, M. J. & Richards, T. (2014) 'Presence & Characterisation of Anaemia in Diabetic Foot Ulceration', *Anemia*, 2014, 104214.
Wu, B. & Becker, J. S. (2011) 'Imaging of elements & molecules in biological tissues & cells in the low-micrometer & nanometer range', *Int J Mass Spectrom*, 307(1), 112-122.
Wu, C., Zhou, Y., Fan, W., Han, P., Chang, J., Yuen, J., Zhang, M. & Xiao, Y. (2012) 'Hypoxia-mimicking mesoporous bioactive glass scaffolds with controllable cobalt ion release for bone tissue engineering', *Biomaterials*, 33(7), 2076-2085.
Wu, J., Xun, P., Tang, Q., Cai, W. & He, K. (2017) 'Circulating magnesium levels & incidence of coronary heart diseases, hypertension, & type 2 diabetes mellitus: A meta-analysis of prospective cohort studies', *Nutr J*, 16(1), 60.
Wu, K., Lee, W.-S., Wey, J., Bungard, D. & Lytton, J. (1995) 'Localization & quantification of endoplasmic reticulum Ca (2+)-ATPase isoform transcripts', *Am J Physiol Cell Physiol*, 269(3), C775-C784.
Wu, L., Du, Y., Lok, J., Lo, E. H. & Xing, C. (2015) 'Lipocalin-2 enhances angiogenesis in rat brain endothelial cells via reactive oxygen species & iron-dependent mechanisms', *J Neurochem*, 132(6), 622-628.
Wu, Q., Shao, H., Darwin Eton, D., Li, J., Li, J., Yang, B., Webster, K. A. & Yu, H. (2009) 'Extracellular calcium increases CXCR4 expression on bone marrow-derived cells & enhances pro-angiogenesis therapy', *J Cell Mol Med*, 13(9), 3764-3773.
Wu, X., Quondamatteo, F. & Brakebusch, C. (2006) 'Cdc42 expression in keratinocytes is required for the maintenance of the basement membrane in skin', *Matrix Biol*, 25(8), 466-474.
Wynn, T. A. (2004) 'Fibrotic disease & the T(H)1/T(H)2 paradigm', *Nature Rev Immunol*, 4(8), 583-594.
Xu, H., Barnes, G. T., Yang, Q., Tan, G., Yang, D., Chou, C. J., Sole, J., Nichols, A., Ross, J. S. & Tartaglia, L. A. (2003) 'Chronic inflammation in fat plays a crucial role in the

development of obesity-related insulin resistance', *J Clin Invest*, 112(12), 1821-1830.
Xu, S. & Chisholm, A. D. (2011) 'A gα q-Ca 2+ signaling pathway promotes actin-mediated epidermal wound closure in *C. elegans*', *Curr Biol*, 21(23), 1960-1967.
Xue, J., Schmidt, S. V., Sander, J., Draffehn, A., Krebs, W., Quester, I., De Nardo, D., Gohel, T. D., Emde, M. & Schmidleithner, L. (2014) 'Transcriptome-based network analysis reveals a spectrum model of human macrophage activation', *Immunity*, 40(2), 274-288.
Xue, W., Zender, L., Miething, C., Dickins, R. A., Hernando, E., Krizhanovsky, V., Cordon-Cardo, C. & Lowe, S. W. (2007) 'Senescence & tumour clearance is triggered by p53 restoration in murine liver carcinomas', *Nature*, 445(7128), 656-660.
Yager, D. R., Chen, S. M., Ward, S. I., Olutoye, O. O., Diegelmann, R. F. & Kelman Cohen, I. (1997) 'Ability of chronic wound fluids to degrade peptide growth factors is associated with increased levels of elastase activity & diminished levels of proteinase inhibitors', *Wound Repair Regen*, 5(1), 23-32.
Yanatori, I., Richardson, D. R., Toyokuni, S. & Kishi, F. (2017) 'The iron chaperone poly(rC)-binding protein 2 forms a metabolon with the heme oxygenase 1/cytochrome P450 reductase complex for heme catabolism & iron transfer', *J Biol Chem*, 292(32), 13205-13229.
Yang, F., Yang, L., Li, Y., Yan, G., Feng, C., Liu, T., Gong, R., Yuan, Y., Wang, N. & Idiiatullina, E. (2017) 'Melatonin protects bone marrow mesenchymal stem cells against iron overload-induced aberrant differentiation & senescence', *J Pineal Res*, 63(3), e12422.
Yang, L., McRae, R., Henary, M. M., Patel, R., Lai, B., Vogt, S. & Fahrni, C. J. (2005) 'Imaging of the intracellular topography of copper with a fluorescent sensor & by synchrotron x-ray fluorescence microscopy', *Proc Nat Acad Sci*, 102(32), 11179-11184.
Yang, Q., Chen, S., Shi, H., Xiao, H. & Ma, Y. (2015) '*In vitro* Study of Improved Wound-Healing Effect of Bioactive Borate-Based Glass Nano-/Micro-Fibers', *Mater Sci Eng C Mater Biol Appl*, 55, 105-117.
Yannone, S. M., Hartung, S., Menon, A. L., Adams, M. W. & Tainer, J. A. (2012) 'Metals in biology: Defining metalloproteomes', *Curr Opin Biotechnol*, 23(1), 89-95.
Ye, J., Coulouris, G., Zaretskaya, I., Cutcutache, I., Rozen, S. & Madden, T. L. (2012) 'Primer-BLAST: A tool to design target-specific primers for polymerase chain reaction', *BMC Bioinformatics*, 13, 134.
Ye, X., Cheng, X., Liu, L., Zhao, D. & Dang, Y. (2013) 'Blood glucose fluctuation affects skin collagen metabolism in the diabetic mouse by inhibiting the mitogen-activated protein kinase & Smad pathways', *Clin Exp Dermatol*, 38(5), 530-537.
Yeap, B. B., Divitini, M. L., Gunton, J. E., Olynyk, J. K., Beilby, J. P., McQuillan, B., Hung, J. & Knuiman, M. W. (2015) 'Higher ferritin levels, but not serum iron or transferrin saturation, are associated with Type 2 diabetes mellitus in adult men & women free of genetic haemochromatosis', *Clin Endocrinol*, 82(4), 525-532.
Yeoh-Ellerton, S. & Stacey, M. C. (2003) 'Iron & 8-isoprostane levels in acute & chronic wounds', *J Invest Dermatol*, 121(4), 918-925.
Yeung, C. Y. C., Holmes, D. F., Thomason, H. A., Stephenson, C., Derby, B. & Hardman, M. J. (2016) 'An *ex vivo* porcine skin model to evaluate pressure-reducing devices of different mechanical properties used for pressure ulcer prevention', *Wound Repair Regen*, 24(6), 1089-1096.
Yokoi, T., Fukuo, K., Yasuda, O., Hotta, M., Miyazaki, J., Takemura, Y., Kawamoto, H., Ichijo, H. & Ogihara, T. (2006) 'Apoptosis signal-regulating kinase 1 mediates

cellular senescence induced by high glucose in endothelial cells', *Diabetes*, 55(6), 1660-1665.
Yoo, S. K., Freisinger, C. M., LeBert, D. C. & Huttenlocher, A. (2012) 'Early redox, Src family kinase, & calcium signaling integrate wound responses & tissue regeneration in zebrafish', *J Cell Biol*, 199(2), 225-234.
Yosef, R., Pilpel, N., Papismadov, N., Gal, H., Ovadya, Y., Vadai, E., Miller, S., Porat, Z., Ben-Dor, S. & Krizhanovsky, V. (2017) 'p21 maintains senescent cell viability under persistent DNA damage response by restraining JNK & caspase signaling', *EMBO J*, 36(15), 2280-2295.
Yoshie, O. & Matsushima, K. (2014) 'CCR4 & its ligands: From bench to bedside', *Int Immunol*, 27(1), 11-20.
Yoshimoto, S., Loo, T. M., Atarashi, K., K&a, H., Sato, S., Oyadomari, S., Iwakura, Y., Oshima, K., Morita, H. & Hattori, M. (2013) 'Obesity-induced gut microbial metabolite promotes liver cancer through senescence secretome', *Nature*, 499(7456), 97-101.
Young, A. & McNaught, C.-E. (2011) 'The physiology of wound healing', *Surgery*, 29(10), 475-479.
Zaidi, Z. & Lanigan, S. W. (2010) 'Skin: Structure & function', In: *Dermatology in Clinical Practice*. London: Springer, 1-15.
Zamboni, P., Izzo, M., Tognazzo, S., Carandina, S., De Palma, M., Catozzi, L., Caggiati, A., Scapoli, G. & Gemmati, D. (2006) 'The overlapping of local iron overload & HFE mutation in venous leg ulcer pathogenesis', *Free Radical Bio Med*, 40(10), 1869-1873.
Zehnder, M., Waltimo, T., Sener, B. & Söderling, E. (2006) 'Dentin enhances the effectiveness of bioactive glass S53P4 against a strain of Enterococcus faecalis', *Oral Surgery*, *Oral Surg Oral Med Oral Pathol Oral Radiol Endod*, 101(4), 530-535.
Zeinali, R., Biazar, E., Keshel, S. H., Tavirani, M. R. & Asadipour, K. (2014) 'Regeneration of full-thickness skin defects using umbilical cord blood stem cells loaded into modified porous scaffolds', *ASAIO J*, 60(1), 106-114.
Zhan, S.S., Jiang, J.X., Wu, J., Halsted, C., Friedman, S.L., Zern, M.A. & Torok, N.J. (2006) 'Phagocytosis of apoptotic bodies by hepatic stellate cells induces NADPH oxidase and is associated with liver fibrosis *in vivo*', *Hepatology*, 43(3), 435-443.
Zhang, C., Miller, C. L., Brown, E. M. & Yang, J. J. (2015a) 'The calcium sensing receptor: From calcium sensing to signaling', *Sci China Life Sci*, 58(1), 14-27.
Zhang, D.-L., Hughes, R. M., Ollivierre-Wilson, H., Ghosh, M. C. & Rouault, T. A. (2009a) 'A ferroportin transcript that lacks an iron-responsive element enables duodenal & erythroid precursor cells to evade translational repression', *Cell Metab*, 9(5), 461-473.
Zhang, H., Clemens, R. A., Liu, F., Hu, Y., Baba, Y., Theodore, P., Kurosaki, T. & Lowell, C. A. (2014a) 'STIM1 calcium sensor is required for activation of the phagocyte oxidase during inflammation & host defense', *Blood*, 123(14), 2238-2249.
Zhang, M., Wang, C., Wu, J., Ha, X., Deng, Y., Zhang, X., Wang, J., Chen, K., Feng, J. & Zhu, J. (2018) 'The Effect & Mechanism of KLF7 in the TLR4/NF-κB/IL-6 Inflammatory Signal Pathway of Adipocytes', *Mediator Inflamm*, 2018, 1756494.
Zhang, S., Ye, C., Lin, H., Lv, L. & Yu, X. (2015b) 'UV disinfection induces a VBNC state in *Escherichia coli* & *Pseudomonas aeruginosa*', *Environ Sci Technol*, 49(3), 1721-1728.
Zhang, X., Zhang, T., Wu, J., Yu, X., Zheng, D., Yang, F., Li, T., Wang, L., Zhao, Y. & Dong, S. (2014b) 'Calcium sensing receptor promotes cardiac fibroblast proliferation & extracellular matrix secretion', *Cell Physiol Biochem*, 33(3), 557-568.

Zhang, Y., Li, W., Yan, T., Lu, C., Zhou, X. & Huang, Y. (2009b) 'Early detection of lesions of dorsal artery of foot in patients with type 2 diabetes mellitus by high-frequency ultrasonography', *J Huazhong Univ Sci Technolog Med Sci*, 29(3), 387-390.
Zhang, Y.-J., Gan, R.-Y., Li, S., Zhou, Y., Li, A.-N., Xu, D.-P. & Li, H.-B. (2015c) 'Antioxidant phytochemicals for the prevention & treatment of chronic diseases', *Molecules*, 20(12), 21138-21156.
Zhang, Z., Zhang, F., An, P., Guo, X., Shen, Y., Tao, Y., Wu, Q., Zhang, Y., Yu, Y. & Ning, B. (2011) 'Ferroportin1 deficiency in mouse macrophages impairs iron homeostasis & inflammatory responses', *Blood*, 118(7), 1912-1922.
Zhang, Z., Zhang, F., Guo, X., An, P., Tao, Y. & Wang, F. (2012) 'Ferroportin1 in hepatocytes & macrophages is required for the efficient mobilization of body iron stores in mice', *Hepatology*, 56(3), 961-971.
Zhao, G., Usui, M. L., Underwood, R. A., Singh, P. K., James, G. A., Stewart, P. S., Fleckman, P. & Olerud, J. E. (2012) 'Time course study of delayed wound healing in a biofilm-challenged diabetic mouse model', *Wound Repair Regen*, 20(3), 342-352.
Zhao, S., Li, L., Wang, H., Zhang, Y., Cheng, X., Zhou, N., Rahaman, M. N., Liu, Z., Huang, W. & Zhang, C. (2015) 'Wound dressings composed of copper-doped borate bioactive glass microfibers stimulate angiogenesis & heal full-thickness skin defects in a rodent model', *Biomaterials*, 53, 379-391.
Zheng, Q., Choi, J., Rouleau, L., Leask, R. L., Richardson, J. A., Davis, E. C. & Yanagisawa, H. (2006) 'Normal wound healing in mice deficient for fibulin-5, an elastin binding protein essential for dermal elastic fiber assembly', *J Invest Dermatol*, 126(12), 2707-2714.
Zheng, X., Chen, M., Meng, X., Chu, X., Cai, C. & Zou, F. (2017) 'Phosphorylation of dynamin-related protein 1 at Ser616 regulates mitochondrial fission & is involved in mitochondrial calcium uniporter-mediated neutrophil polarization & chemotaxis', *Mol Immunol*, 87, 23-32.
Zhou, D., Huang, C., Lin, Z., Zhan, S., Kong, L., Fang, C. & Li, J. (2014) 'Macrophage polarization & function with emphasis on the evolving roles of coordinated regulation of cellular signaling pathways', *Cell Signal*, 26(2), 192-197.
Zhou, L., Zhang, X., Paus, R. & Lu, Z. (2018a) 'The renaissance of human skin organ culture: A critical reappraisal', *Differentiation*, 104, 22-35.
Zhou, S., Parham, D. M., Yung, E., Pattengale, P. & Wang, L. (2015) 'Quantification of glypican 3, β-catenin & claudin-1 protein expression in hepatoblastoma & paediatric hepatocellular carcinoma by colour deconvolution', *Histopathology*, 67(6), 905-913.
Zhou, S., Yuan, X., Liu, Q., Zhang, X., Pan, X., Zang, L. & Xu, L. (2010) 'BAPTA-AM, an intracellular calcium chelator, inhibits RANKL-induced bone marrow macrophages differentiation through MEK/ERK, p38 MAPK & Akt, but not JNK pathways', *Cytokine*, 52(3), 210-214.
Zhou, T., Sui, B., Mo, X. & Sun, J. (2017) 'Multifunctional & biomimetic fish collagen/bioactive glass nanofibers: Fabrication, antibacterial activity & inducing skin regeneration *in vitro* & *in vivo*', *Int J Nanomedicine*, 12, 3495-3507.
Zhou, X., Li, J. & Yang, W. (2014) 'Calcium/calmodulin-dependent protein kinase II regulates cyclooxygenase-2 expression & prostaglandin E2 production by activating cAMP-response element-binding protein in rat peritoneal macrophages', *Immunology*, 143(2), 287-299.
Zhou, X., Perez, F., Han, K. & Jurivich, D. A. (2006) 'Clonal senescence alters endothelial ICAM-1 function', *Mech Ageing Dev*, 127(10), 779-785.
Zhou, Y., Que, K. T., Zhang, Z., Yi, Z. J., Zhao, P. X., You, Y., Gong, J. P. & Liu, Z. J. (2018b) 'Iron overloaded polarizes macrophage to proinflammation phenotype through ROS/acetyl-p53 pathway', *Cancer Med*, 7(8), 4012-4022.

Zhou, Z., Wang, L., Song, Z., Saari, J. T., McClain, C. J. & Kang, Y. J. (2005) 'Zinc supplementation prevents alcoholic liver injury in mice through attenuation of oxidative stress', *Am J Pathol*, 166(6), 1681-1690.
Zhu, Z., Mukhina, S., Zhu, T., Mertani, H. C., Lee, K.-O. & Lobie, P. E. (2005) 'p44/42 MAP kinase-dependent regulation of catalase by autocrine human growth hormone protects human mammary carcinoma cells from oxidative stress-induced apoptosis', *Oncogene*, 24(23), 3774-3785.
Zierer, J., Menni, C., Kastenmüller, G. & Spector, T. D. (2015) 'Integration of 'omics' data in aging research: From biomarkers to systems biology', *Aging Cell*, 14(6), 933-944.
Zijl, S., Vasilevich, A. S., Viswanathan, P., Helling, A. L., Beijer, N. R. M., Walko, G., Chiappini, C., de Boer, J. & Watt, F. M. (2019) 'Micro-scaled topographies direct differentiation of human epidermal stem cells', *Acta Biomater*, 84, 133-145.
Zimmermann, D., Dours-Zimmermann, M., Schubert, M., Bruckner-Tuderman, L. & Heitz, P. U. (1994) 'Expression of the extracellular matrix proteoglycan, versican, in human skin', *Verh Dtsch Ges Pathol*, 78, 481-484.
Zirra, A. (1976) 'The functional significance of the skin's stratum lucidum', *Morphol Embryol (Bucur)*, 22(1), 9-12.
Ziv-Polat, O., Topaz, M., Brosh, T. & Margel, S. (2010) 'Enhancement of incisional wound healing by thrombin conjugated iron oxide nanoparticles', *Biomaterials*, 31(4), 741-747.
Zobel, D. P., Andreasen, C. H., Burgdorf, K. S., Andersson, E. A., Sandbæk, A., Lauritzen, T., Borch-Johnsen, K., Jørgensen, T., Maeda, S. & Nakamura, Y. (2009) 'Variation in the gene encoding Krüppel-like factor 7 influences body fat: Studies of 14 818 Danes', *Eur J Endocrinol*, 160(4), 603-609.
Zvyagin, A. V., Zhao, X., Gierden, A., Sanchez, W., Ross, J. & Roberts, M. S. (2008) 'Imaging of zinc oxide nanoparticle penetration in human skin *in vitro* & *in vivo*', *J Biomed Opt*, 13(6), e064031.
Zweemer, A. J., Toraskar, J., Heitman, L. H. & IJzerman, A. P. (2014) 'Bias in chemokine receptor signalling', *Trends Immunol*, 35(6), 243-252.
Ågren, M. (1993) 'Zinc oxide increases degradation of collagen in necrotic wound tissue', *Brit J Dermatol*, 129(2), 221-222.
Çilliler, A. E., Öztürk, Ş. & Özbakır, Ş. (2007) 'Serum magnesium level & clinical deterioration in Alzheimer's disease', *Gerontology*, 53(6), 419-422.
Öztürk, Y., Aydin, S., Altan, V., Yildizoğlu-Ari, N. & Özçelikay, A. (1994) 'Effect of short & long term streptozotocin diabetes on smooth muscle calmodulin levels in the rat', *Cell Calcium*, 16(2), 81-86.

Appendix

Appendix Contents

Chapter 2: Appendix

2A.1. Formalin Fixative

Formalin fixative was prepared as follows:

1. 450 mL dH_2O.
2. 40 mL formaldehyde solution (Thermo Fisher Scientific).
3. 10 mL glacial acetic acid (Thermo Fisher Scientific).
4. 4.5 g sodium chloride (Thermo Fisher Scientific).
5. 0.25 g alkyltrimethylammonium bromide (Sigma-Aldrich).

Fixative was always made fresh and discarded after 24 hours.

2A.2. Collagen IV-Coated Plates

A vial of Collagen IV (Sigma-Aldrich) was defrosted slowly on ice and diluted to 0.5 mg/mL with 0.25% glacial acetic acid. Diluted solution was added to plates and incubated for three hours at RT, or 1 hour at 37°C with 5% CO_2. The remaining solution was aspirated and plates were rinsed with sterile DPBS. Plates were stored at 4°C until use.

2A.3. Dermal Fibroblast Media

High glucose DMEM with no phenol red, 10% FBS, 100 U/mL penicillin (1%), 100 µg/mL streptomycin (1%), 2.5 µg/mL amphotericin B solution and 10 µg/mL gentamicin sulphate solution (all Thermo Fisher Scientific).

2A.4. Bone Marrow Growth Medium

High glucose (for Db Mφs) or low glucose (for all other Mφs) DMEM (Sigma-Aldrich), 10% FBS, 1% penicillin-streptomycin solution and 20% L929 conditioned media. Prior to supplementation, 100 mL DMEM was removed from the bottle of DMEM and stored in separate, sterile falcon tubes (used for serum starvation).

2A.5. L929-Conditioned Media

L929 cells (CCL-1, ATCC, Middlesex, UK) were grown to 80% confluence in 162 cm^2 flasks. Media was changed (high glucose DMEM containing 10% FBS and 1% P/S) and cells were incubated for two days at 37°C and 5% CO_2. At collection, media was collected, sterile-filtered (0.2 μm filter), and stored at -20°C until use.

2A.6. VECTABOND® Coating Slides

1. Clean glass slides were immersed in acetone (Thermo Fisher Scientific) for 5 minutes at RT.
2. VECTABOND® Reagent (7 mL bottle; Vector Laboratories, Ltd.) was added to 350 mL acetone.
3. Slides were transferred to VECTABOND®-acetone for 5 minutes at RT.
4. Slides were rinsed in dH_2O, dried O/N and stored at RT until use.

2A.7. Masson's Trichrome Reagents

2A.7.1. Weigart's Haematoxylin

1. Solution A was prepared by adding 5 g Haematoxylin (Thermo Fisher Scientific) to 500 mL 95% ethanol (in dH_2O).
2. Solution B was prepared by adding 5.8 g ferric chloride (Thermo Fisher Scientific) to 295 mL dH_20, topped up with 5 mL glacial acetic acid.
3. Equal parts of solution A and solution B were mixed immediately prior to use.

2A.7.2. Biebrich Scarlet-Acid Fuschin Solution

1. 3.6 g Biebrich Scarlet was added to 360 mL dH_2O.
2. 0.4 g Acid Fuchsin was added to 40 mL dH_2O.
3. Biebrich Scarlet and Acid Fuchsin (Sigma-Aldrich) were mixed.
4. The solution was topped up with 4 mL glacial acetic acid.

2A.7.3. Phosphomolybdic-Phosphotungstic Acid Solution

25 g phosphomolybdic acid and 25 g phosphotungstic acid (both Sigma-Aldrich) were mixed with 1 litre of dH_2O.

2A.7.4. Analine Blue Solution

25 g Analine Blue (Sigma-Aldrich) was mixed with 20 mL acetic acid in 1L dH_2O.

2A.8. Citrate Buffer Antigen Retrieval Solution

1. 3.8 g citric acid (Thermo Fisher Scientific) was added to 1800 mL dH_20.
2. The buffer was adjusted to pH 6 with NaOH pellets (Thermo Fisher Scientific) and topped up to 2 litres with dH_2O.

2A.9. Phosphate Buffered Saline Solution

1. 150 g sodium chloride (Thermo Fisher Scientific) was added to 2.5 litres 0.1M PBS (Sigma-Aldrich).
2. The buffer was topped up to 25 litres with 22.5 litres dH_2O.

2A.10. VECTASTAIN® ELITE ABC Kit Reagents

1. Block was made by adding 3 drops of animal serum to 10 mL PBS.
2. Seondary antibody solution was made by adding 2 drops biotinylated secondary antibody to 10 mL PBS.
3. ABC reagent was prepared using 2 drops Reagent A and 2 drops Reagent B added to 5 mL PBS, mixed and stored on ice for 30 minutes prior to use.

2A.11. NovaRED™ Substrate Solution

1. 3 drops Reagent 1 was added to 5 mL dH_20 and mixed well.
2. 2 drops Reagent 2 was added and mixed well.
3. 2 drops Reagent 3 was added and mixed well.
4. 2 drops H_2O_2 was added and mixed well.
5. The solution was used immediately and not stored.

2A.12. X-Gal Solution

1. 1 mM $MgCl_2$ (Sigma-Aldrich) was added to 9.5 mL PBS (above).
2. 5 mM potassium ferricyanide and 5 mM potassium ferrocyanide (Sigma-Aldrich) were added to the PBS/$MgCl_2$ solution in step 1.
3. 2 mM additional $MgCl_2$ was then added to the reagent made in step 2.
4. 1.6 mg (16 µL) X-Gal stock (100 mg/mL in N,N-dimethylformamide; both Thermo Fisher Scientific) was added the reagent made in step 3.

2A.13. Proteinase K Solution

1. 1 M Tris-HCl stock (pH 7.5) was prepared by adding 121.14 g Tris base to 1 litre dH_2O, brought to pH 7.5 with hydrochloric acid.
2. Tris-HCl stock was diluted 1:100 in dH_2O to give a 10 mM solution.
3. Proteinase K (Thermo Fisher Scientific) was added to the 10 mM Tris-HCl solution to give a working solution of proteinase K at 20 µg/mL.

2A.14. MOWIOL Mounting Media with DAPI

1. 2.4 g MOWIOL 4-88 (Sigma-Aldrich) was added to 6 g glycerol (Thermo Fisher Scientific) and 6 mL dH_20 and left to mix for several hours at RT on a stirrer.
2. 12 mL 0.2 M Tris base was added and heated to 50°C for 10 minutes with occasional mixing.
3. MOWIOL 4-88 was clarified by centrifuging at 5,000 x g for 15 minutes.
4. 2.5% 1,4-diazabicyclo[2.2.2]octane (Thermo Fisher Scientific) was added to the collected supernatant to reduce fading.
5. DAPI was added at 1 µg/mL concentration (3.6 µL per 18 mL solution) as a counterstain.
6. The mounting media was stored in airtight containers at -20°C in the dark.

2A.15. Collagen I Coating Plates

1. 45.6 µL of 4 mg/mL stock collagen I from rat tail (Sigma-Aldrich) was added to 12 mL acidified water (82.5 µL acetic acid to 34.5 mL dH_2O).
2. Plates were incubated at RT for 3 hours.
3. Excess collagen I was aspirated.
4. Plates were rinsed in DPBS and stored at 4°C in Clingfilm until use.

2A.16. Matrix Denuding Buffer

20 mM ammonium hydroxide (Sigma-Aldrich) in 0.5% Triton X-100 in DPBS.

2A.17 Electrophoresis Sample Loading Buffer

1. 0.08 g Tris base.
2. 0.2 g sodium dodecyl sulphate.
3. 200 µL 10% Bromophenol Blue.
4. 1 mL glycerol.
5. 10 mL 18.2Ω water.
6. Stored in aliquots at -20°C.

2A.18 Western Blot Acrylamide Gel Recipe

Stock Solution	Final Acrylamide Concentration (%)		
	7	**10**	**12**
40% Acrylamide: Bis-Acrylamide 37.5:1	17.5 mL	25 mL	30 mL
1.5M Tris-HCl pH 8.8	25 mL	25 mL	25 mL
18.2Ω H_2O	56 mL	48.5 mL	43.5 mL
10% SDS	1 mL	1 mL	1 mL
10% APS	500 µL	500 µL	500 µL
TEMED	50 µL	50 µL	50 µL

SDS = sodium dodecyl sulphate; APS = ammonium persulphate. All reagents were prepared in 18.2Ω water. APS was aliquoted and stored at -20°C for long term use. APS and TEMED were added immediately prior to use to prevent premature gel polymerisation. Isopropanol was added to the top of the separating gel to level the gel surface while setting. Isopropanol was rinsed off with dH_2O prior to adding the stacking gel.

2A.19. Stacking Polyacrylamide Gel (4%)

40% Acrylamide: Bis-Acrylamide 37.5:1	2.5 mL
0.5 M Tris-HCl pH 6.8	6.3 mL
18.2Ω H_2O	15. 9 mL
10% SDS	250 µL
10% APS	125 µL
TEMED	25 µL

2A.20. 10X Tris-Glycine-SDS Buffer

1. 30 g Tris base.
2. 144 g glycine.
3. 10 g SDS.
4. Made up to 1 litre with 18.2Ω water.

2A.21. 1X Tris-Glycine-SDS Buffer

1. 900 mL 18.2Ω water.
2. 100 mL 10X Tris-Glycine-SDS buffer.

2A.22. Western Blot Transfer Buffer

1. 200 mL analysis reagent grade methanol.
2. 100 mL 10X TGS.
3. 700 mL 18.2Ω water.

2A.23. 10X Tris-Buffered Saline

1. 6 g Tris base.
2. 9 g sodium chloride.
3. Made up to 1 litre with 18.2Ω water.

2A.24. 1X Tris-Buffered Saline

900 mL 18.2Ω water and 100 mL 10X Tris-buffered saline (TBS).

For 1X TBST, Tween 20 (0.1%) was added to 1X TBS prior to immediate use.

2A.25. Mild Stripping Buffer

1. 15 g glycine.
2. 1 g SDS.
3. 10 mL Tween 20.
4. Dissolved in 800 mL of 18.2Ω water.
5. pH adjusted to 2.2 with HCl.
6. Made up to 1 litre with 18.2Ω water.

2A.26. Cycling Parameters for cDNA Synthesis

Stage	Temperature (Celsius)	Time
Extension	25	10 min
cDNA synthesis	42	60 min
Reaction Termination	85	5 min

2A.27. qRT-PCR Cycling Parameters*

Stage		Temperature (Celsius)	Time
Initial Denaturing		95°C	3 min
X40 cycles	Denaturing	95°C	10 secs
	Annealing	Primer Dependent	30 secs
	Extension	70°C	30 secs
Melt Curve		65-95°C in 5°C increments	5 secs

**Annealing temperature was optimised for each set of primers.*

2A.28. Dey-Engley Neutralising Broth Test

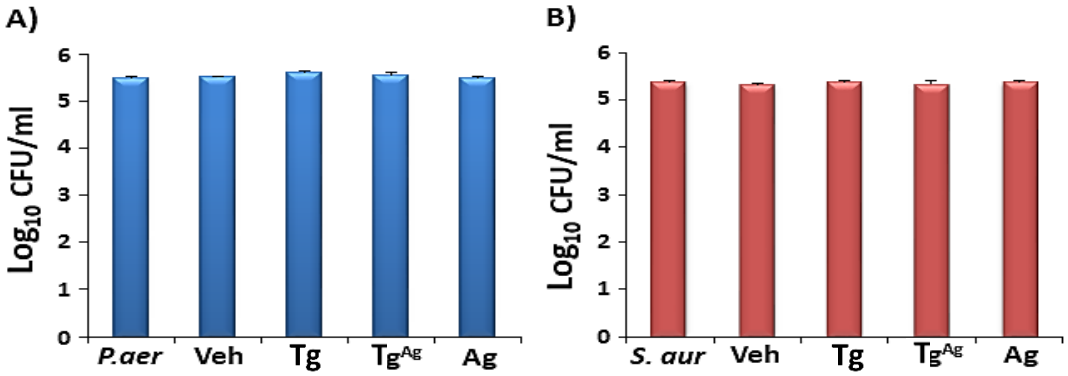

Figure 2A.1. Testing Dey-Engley Neutralising Broth (DENB) against Theraglass™. Here, the neutralisation capacity of DENB was tested against treatments (NIVEA vehicle, "veh"; Theraglass™, "Tg"; Theraglass with silver, "Tg^{Ag}" and; silver oxide control, "Ag"). Untreated bacteria were included as a positive control. DENB (5 mL) was added to each treatment (1 g) and incubated at RT for 15 minutes. Adjusted cultures (see main text) of *Pseudomonas aeruginosa* (*P. aer*; **A**) and *Staphylococcus aureus* (*S. aur*, **B**) were added to the tubes and plated on Mueller Hinton agar to assess viability (colony forming units per millilitre, CFU/mL). As no differences in viability were found, it was assumed that DENB effectively neutralised the treatments under study.

2A.29. Ratiometric Co-Culture Analysis

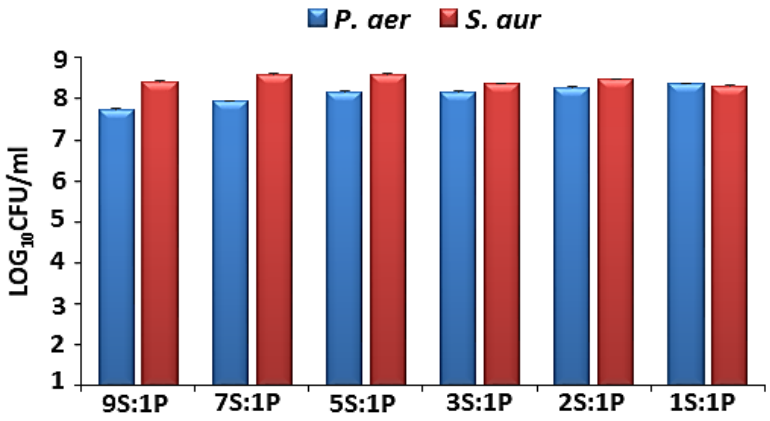

Figure 2A. 2. Ratiometric determination of the relative proportions of *Pseudomonas aeruginosa* (*P. aer*) and *Staphylococcus aureus* (*S. aur*) in membrane biofilms. Adjusted cultures were added in ratios of 9:1, 7:1, 5:1, 3:1, 2:1 and 1:1 *S. aur* (S): *P. aer* (P) to form biofilms over 72 hours. Colony forming units per ml (CFU/mL) were enumerated on agar selective for *P. aer* and *S. aur.* Addition of each species in a 1:1 ratio gave the most equal recovery of each species from biofilms.

2A.30. Zymography Gels

Reagent	Separating Gel (16 mL)	Stacking Gel (5 mL)
Tris-HCl	4 mL (1.5 M pH 8.8)	1.25 mL (0.5 M pH 6.8)
40% Acrylamide: Bis-Acrylamide 37.5:1	3 mL	502.5 µL
dH_2O	5 mL	3.25 mL
Porcine skin gelatin	4 mL (8 mg/mL stock in dH_2O)	Not required
10% SDS	160 µL	50 µL
10% APS (made in dH_2O)	160 µL	50 µL
TEMED	20 µL	10 µL

SDS = sodium dodecyl sulphate; APS = ammonium persulphate. All reagents prepared in 18.2Ω water. APS working solution was aliquoted and stored at -20°C for long term use.

2A.31. Gelatinase Resolving Buffer

1. 1.7 mL 1.5 M Tris-HCl pH 8.8 plus 47.5 mL dH_20.
2. 500 µL Triton X-100 (Sigma-Aldrich).
3. 250 µL 1M stock calcium chloride (Sigma-Aldrich).
4. 80 µL of 10% sodium azide (Thermo Fisher Scientific).
5. 0.5 µL of 0.1 M zinc chloride (Sigma-Aldrich).

2A.32. Murine Primer Sequences for qRT-PCR*

Primer	Forward Sequence	Reverse Sequence
*18s**	AGTCCCTGCCTTTGTACACA	CATCCGAGGGCCTAACTAAC
Arg1	TGACATCAACACTCCCCTGACAAC	GCCTTTTCTTCCTTCCCAGCAG
Calm1	GTTACATCAGTGCGGCAGAA	GTCCGTCGCCATCAATATCT
Casr	TCATTGATGAACAGTCTTTCTCCCT	TCTGTTCTCTTTAGGTCCTGAAACA
Ccl17	TGCTTCTGGGGACTTTTCTG	TGGCCTTCTTCACATGTTTG
Ccl22	CAGGCAGGTCTGGGTGAA	TAAAGGTGGCGTCGTTGG
Cd86	TCAGTGATCGCCAACTTCAG	TTAGGTTTCGGGTGACCTTG
Cdkn1a	CAGTACTTCCTCTGCCCTGC	GCTCAGACACCAGAGTGCAA
Cdkn1b	TTGGGTCTCAGGCAAACTCT	TTCTGTTCTGTTGGCCCTTT
Cdkn2a	GTACCCCGATTCAGGTGATG	CAGTTCGAATCTGCACCGTA
Col1a1	GAGCGGAGAGTACTGGATCG	GCTTCTTTTCCTTGGGGTTC
Col3a1	GCACAGCAGTCCAACGTAGA	CCAGAGATCCCATTTGGAGA
Cxcl1	GCTGGGATTCACCTCAAGAA	TGGGGACACCTTTTAGCATC
Cxcl2	AGTGAACTGCGCTGTCAATG	TTCAGGGTCAAGGCAAACTT
Cxcr2	ATCTTCGCTGTCGTCCTTGT	AGCCAAGAATCTCCGTAGCA
Fn1	AATGGAAAAGGGGAATGGAC	GAGCAAGAAGGACAACCGAG
Fth	CGAGATGATGTGGCTCTGAA	GTGCACACTCCATTGCATTC
Ftl	AATCAGGCCCTCTTGGATCT	GGCGCTCAAAGAGATACTCG
*Gapdh**	TGCACCACCAACTGCTTAGC	GGCATGGACTGTGGTCATGAG
Il1b	GCCCATCCTCTGTGACTCAT	AGGCCACAGGTATTTTGTCG
Irp1	GACTTTGAAAGCTGCCTTGG	AGCTAGTGATGGCAGCGATT
Ivl	AGGAGTCACCTGAGCCAGAA	CTTTCTGATCCCCTGCCATA
Krt1	AACTTCAGCTCAGGCTCTGC	CCTCCTCCTGAAAATCTCCC
Krt14	ATCGAGGACCTGAAGAGCAA	TCGATCTGCAGGAGGACATT
Nos2	GTGGTGACAAGCACATTTGG	AAGGCCAAACACAGCATACC
Pi3k	CCCAAGCTGGATGTGAAGTT	TGCTTCGATAGCCGTTCTTT
S100a8	CCATGCCCTCTACAAGAATGA	ATCACCATCGCAAGGAACTC
S100a9	AGGACCTGGACACAAACCAG	TTACTTCCCACAGCCTTTGC
S1pr2	TCTCAGGGCATGTCACTCTG	CAGCTTTTGTCACTGCCGTA
Slc11a2	TCAGAGCTCCACCATGACTG	GATAGACCGGGTCAGGATCA
Slc40a1	CCCTGCTCTGGCTGTAAAAG	GGTGGGCTCTTGTTCACATT
Sprr2f	GCACTTTGGAGGAGGACAAG	AAGAACAGCAGTGCAAGCAA
Steap3	GCTGGCCTTGAACTCAAAAG	CGTGGTGACACACATCTTCC
Tf	TTCTCATGCTGTTGTGGCTC	CAGCAGGTCTTTCCCAAGAG
Tfr1	TGCAGAAAAGGTTGCAAATG	TGAGCATGTCCAAAGAGTGC
Tnf	GAACTGGCAGAAGAGGCACT	AGGGTCTGGGCCATAGAACT
Tram2	TCCTCATCGGGCTTATGTTC	CAGCATGGAAGATGATGGTG
Trp53	AGAGACCGCCGTACAGAAGA	CTGTAGCATGGGCATCCTTT
Tsg1	GTGCTCACGATCAGACCAGA	CAATGCGATCAGAGGACTCA
Ym1	GGCTACACTGGAGAAAATAGTCCCC	CCAACCCACTCATTACCCTGATAG

**Housekeeping genes.*

2A.33. Human Primer Sequences for qRT-PCR*

Primer	Forward Sequence	Reverse Sequence
ACTA2	ACCCACAATGTCCCCATCTA	GAAGGAATAGCCACGCTCAG
CALM1	TGCTGAATTCAAGGAAGCCT	CTGTTGGGTTCTGACCCAGT
CASR	AGCTAAAGATCAAGATCTCA	TGGGAAGAAGGGCTGGGCTG
CCL17	CTTCTCTGCAGCACATCCAC	AGTACTCCAGGCAG-CACTCC
CCL22	TGCCGTGATTACGTCCGTTA	AAGGTTAGCAACACCACGCC
CD11b	AGAACAACATGCCCAGAACC	GCGGTCCCATATGACAGTCT
CD14	CGAGGACCTAAAGATAACCGGC	GTTGCAGCTGAGATCGAGCAC
CD36	GCCAGTTGGAGACCTGCTTA	CAGCGTCCTGGGTTACATTT
CD54	GGCTGGAGCTGTTTGAGAAC	TCACACTGACTGAGGCCTTG
CDH11	CTTTGCAGCAGAAATCCACA	TGGGAGCATTATCGTTGACA
CDKN1A	GACTCTCAGGGTCGAAAACG	CTCTTGGAGAAGATCAGCCG
CDKN2A	GAGCAGCATGGAGCCTTC	CCGTAACTATTCGGTGCGTT
COL1A1	CACACGTCTCGGTCATGGTA	CGGCTCCTGCTCCTCTTAG
COL1A2	AGCAGGTCCTTGGAAACCTT	GAAAAGGAGTTGGACTTGGC
COL3A1	ATATTTGGCATGGTTCTGGC	TGGCTACTTCTCGCTCTGCT
COL6A1	CTACACCGACTGCGCTATCA	GCCACCGAGAAGACTTTGAC
CXCL1	ATTCACCCCAAGAACATCCA	TGGATTTGTCACTGTTCAGCA
CXCL2	GCAGGGAATTCACCTCAAGA	GGATTTGCCATTTTTCAGCA
FHC	TGGAGTTTTGCTTTCCCATC	GGTTTGCTATTCGACACCGT
FIH	GTGGGCAGGAAGATTGTCAT	GGGTGATGAACAGGGTATGG
FLG	GTGTCCCTCACTGTCCCTGT	CCAGGTACCATTGCAGGAGT
FN1	TGACCCCTACACAGTTTCCCA	TGATTCAGACATTCGTTCCCAC
*GAPDH**	TGCACCACCAACTGCTTAGC	GGCATGGACTGTGGTCATGAG
HIF1A	TGCGTGTGAGGAAACTTCTG	CCTCATGGTCACATGGATGA
HIF2A	CAACAGAGGCCGTACTGTCA	TGCTGGATTGGTTCACACAT
IL1B	CTCGCCAGTGAAATGATGGCT	GTCGGAGATTCGTAGCTGGAT
IRP1	AGGCCTAGCTAAGGACCAGC	CGAAGACGGGTGGACTGTAT
ITPR1	CCATTGCTGGGAAGCTAGAG	CTCTGTTGGGCTTGGAGAAG
IVL	CTGCCTCAGCCTTACTGTGA	GGAGGAGGAACAGTCTTGAGG
KRT1	ATTTCTGAGCTGAATCGTGTGATC	CTTGGCATCCTTGAGGGCATT
KRT14	GGCCTGCTGAGATCAAAGAC	GTCCACTGTGGCTGTGAGAA
LOX	CAGAGGAGAGTGGCTGAAGG	CCAGGTAGCTGGGGTTTACA
LOXL1	CATTACCACAGCATGGACGA	ATGTAGTTCCCAGGCTGCAC
LOXL2	GAGTTGCCTGCTCAGAAACC	GTTGTGGATCTGGGAGGAGA
MMP2	ATGACAGCTGCACCACTGAG	ATTTGTTGCCCAGGAAAGTG
NFE2L2	AAACCAGTGGATCTGCCAAC	ACGTAGCCGAAGAAACCTCA
PDGFA	ACACGAGCAGTGTCAAGTGC	CCTGACGTATTCCACCTTGG
PH4A1	GGCAGCCAAAGCTCTGTTAC	GGCTTGTTCCATCCACAGTT
PH4A2	ACGAGATAGGAGCTGCCAAA	CCTGTGACTTGGTTGTGGTG
PH4B	CTCGACAAAGATGGGGTTGT	GCAAGAACAGCAGGATGTGA
SERPINE1	ATACTGAGTTCACCACGCCC	GTTGGTGAGGGCAGAGAGAG
SLC11A2	GTTCAAGTGCTTCTCCTGCC	GAGTTCGAGACCAGCCTGAC
SLC40A1	CCAAAGGGATTGGATTGTTG	AAATAAAGCCACAGCCGATG
STEAP3	GCAGAGCCACCAAAATGCC	GGCTACTATCGCTGTCCACC
TF	ACTCACACAGGAGGGGTCAC	CTGTGGTAACAGAGGCCCAT

TFR1	CAGGTGGATCACTTGTGGTG	AGTGGCTGGGATTACAGGTG
TNFA	CCAGCTGGAGAAGGGTGAC	AGGCGTTTGGGAAGGTTG
TRAM2	TCCTCATCGGGCTTATGTTC	ATCAGCAAACGGCTTCATCT
TSG1	CCCAAGAGACTAGCAGTGGC	GCTGCCAGTACACCTTGTCA
VIM	TCCCGCATCTCCTCCTCGTA	CTGAATGACCGCTTCGCCAA
*YWHAZ**	ACTTTTGGTACATTGTGGCTTCAA	CCGCCAGGACAAACCAGTAT

**Housekeeping genes.*

2A.34. Bacterial Primer Sequences for qRT-PCR*#

Gene	Forward Sequence	Reverse Sequence
*16S**	GTGGAAAAGAGCTTCTGGCA	CTTCTCGACGATGATTTCCG
16S#	TGATGCAGAGAACTGAACCG	TTCTTTGTGCAAATGCTGCT
*aprA**	CTTCAATACGCCGTGGAAGT	GCGTCGACGAAGTGGATATT
*algD**	ATCAGCATCTTTGGTTTGGG	CACCAATGACTTCATGACCG
*lasB**	GTCGCAGTACTACAACGGCA	ATTGGCCAACAGGTAGAACG
fnbpB#	CGTTATTTGTAGTTGTTTGTGTT	TGGAATGGGACAAGAAAAAGAA
eno#	CGTACAGCTGCAGAACAAGTTGA	CACCGATACGTTCTGTAAGTTGTTC
fnpbA#	ACTTGATTTTGTGTAGCCTTTTT	GAAGAAGCACCAAAAGCAGTA

**Pseudomonas aeruginosa genes. #Staphylococcus aureus genes.*

Chapter 4: Appendix

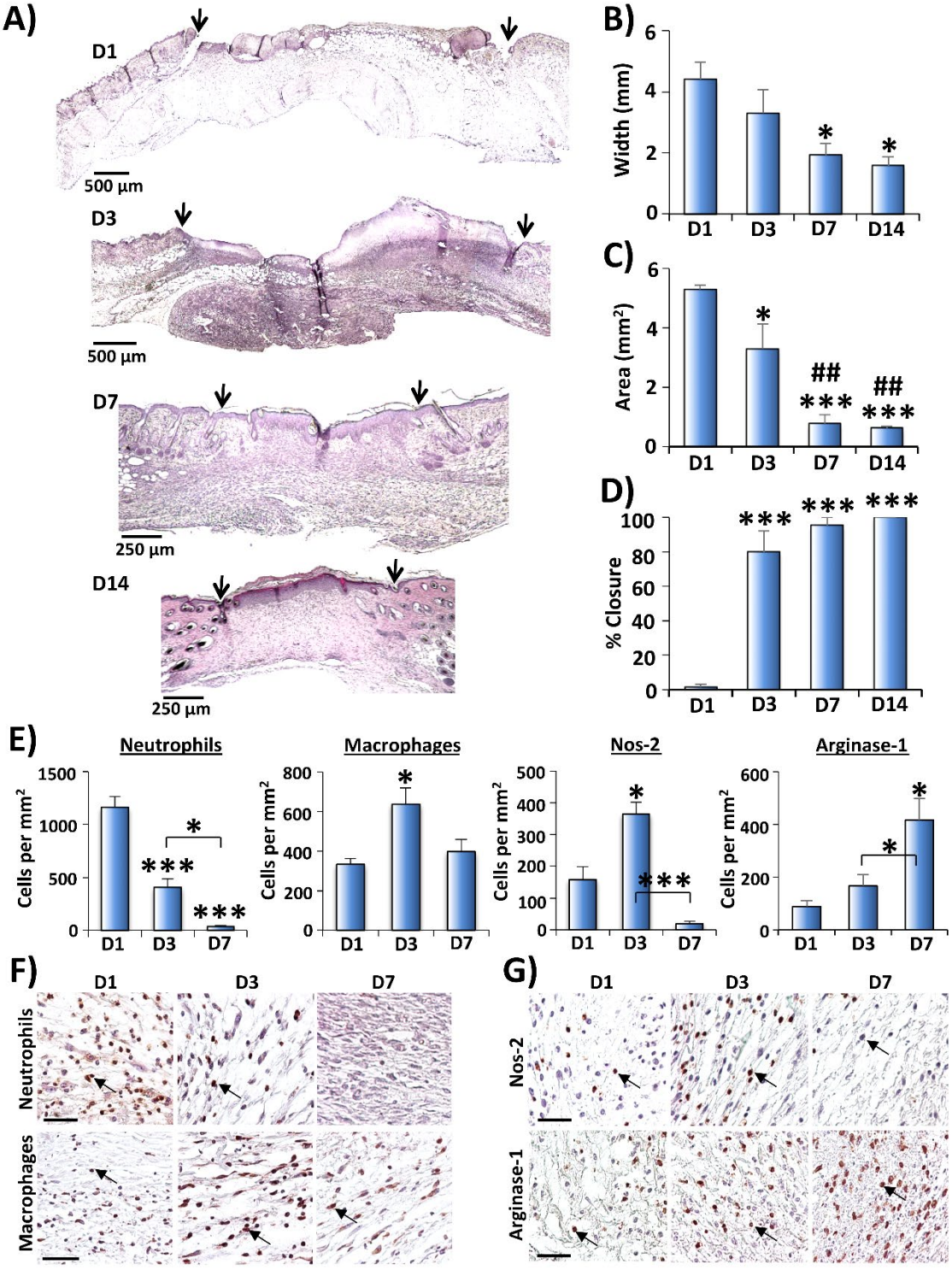

Figure 4A.1. Histological profiling of temporal healing rates across normal murine wound repair. Haematoxylin and Eosin stained wounds at day 1 (D1), D3, D7 and D14 post-injury (**A**). Arrows = wound edges. Wound width (**B**), area (**C**) and % closure (**D**) quantified from **A**. Immunohistochemistry was used to assess neutrophils, macrophages, and Nos-2^{+ve} and Arginase-1^{+ve} macrophages (**E**), representative staining in **F** and **G**. Arrows = positive (brown/red) cells. Bar = 50 µm. Mean +/- SEM. n = 5 mice per group. * = $P < 0.05$, ## = $P < 0.01$, *** = $P < 0.001$. One-way ANOVA with Tukey's *post-hoc* analysis. * versus D0. # versus D3.

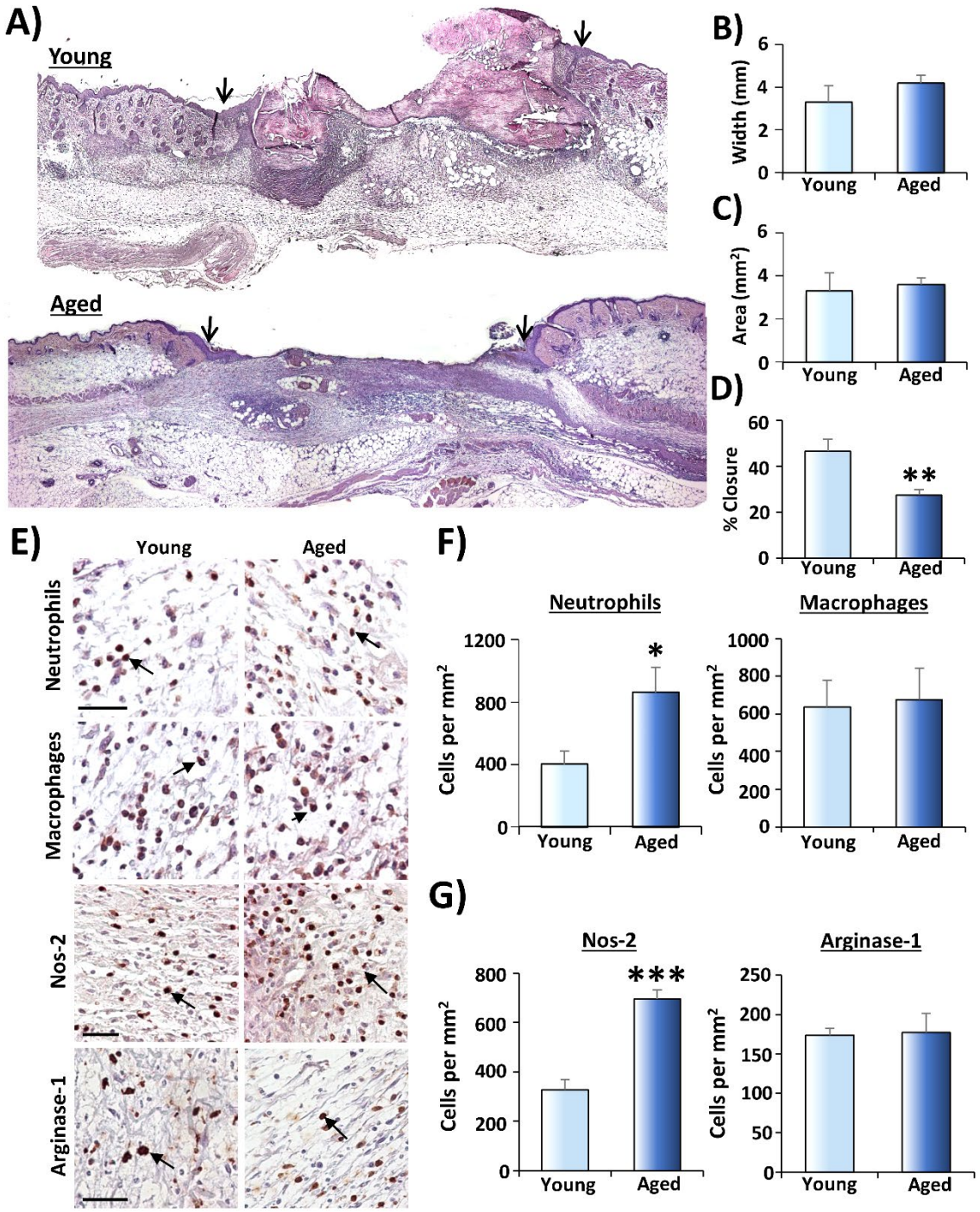

Figure 4A.2. Confirmation of delayed healing in aged versus young murine wounds at day 3 post-injury. Representative Haematoxylin and Eosin staining (**A**). Bar = 500 µm. Arrows = wound edges. Wound width (**B**), area (**C**) and percentage closure (**D**) quantified from **A**. Immunohistochemistry for neutrophils, macrophages, and Nos-2^{+ve} and Arginase-1^{+ve} macrophages (**E**), quantified in **F** and **G**. Arrows = positive (brown/red) cells. Bar = 50 µm. Mean +/- SEM. n = 5 mice per group. * = $P < 0.05$, *** = $P < 0.001$. Independent two-tailed Student's *t* tests.

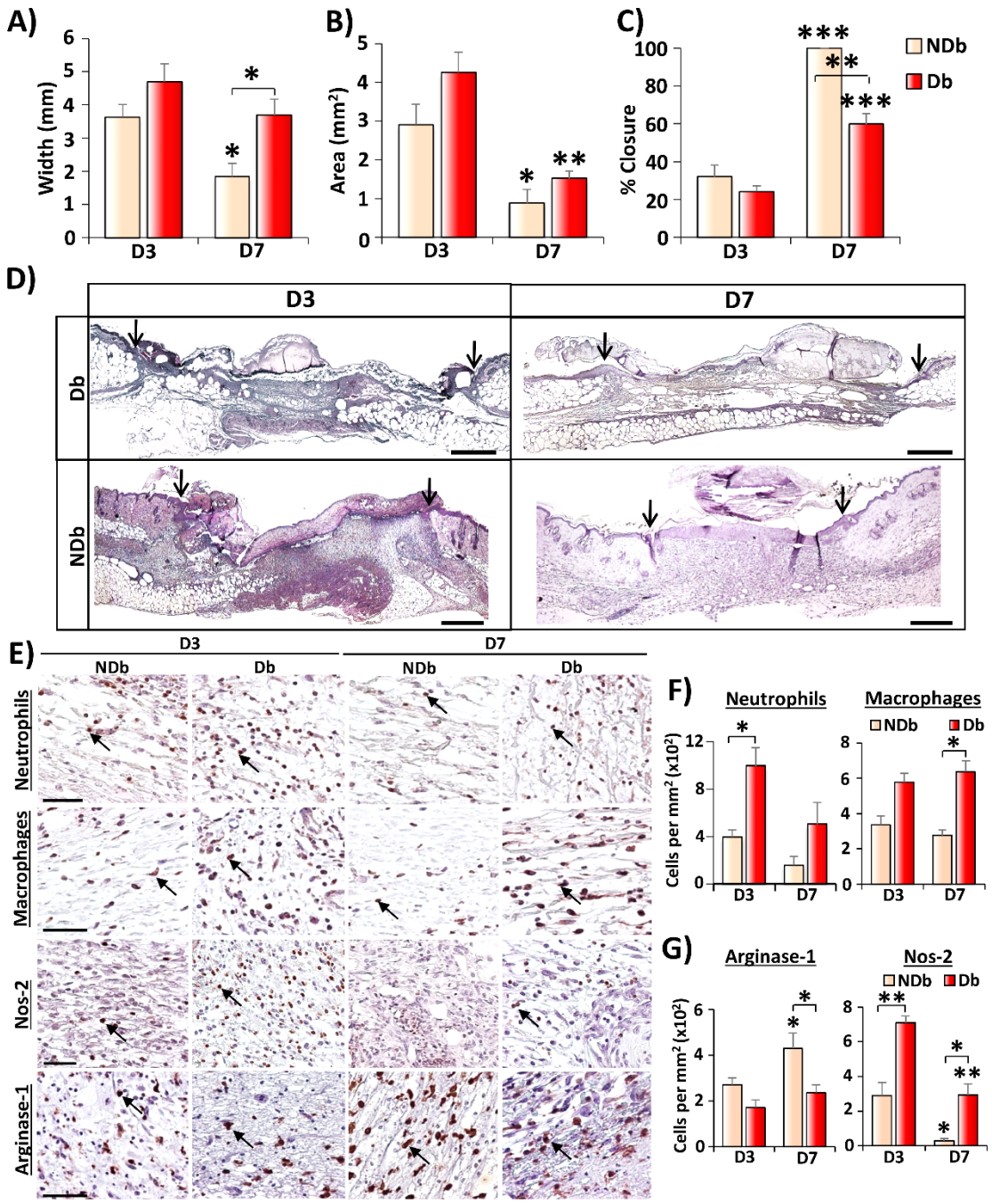

Figure 4A.3. Confirmation of delayed healing in diabetic versus non-diabetic murine wounds at day 3 and day 7 post-injury. Wound width (**A**), area (**B**) and percentage closure (**C**) quantified from representative Haematoxylin and Eosin staining (**D**). Bar = 500 µm. Arrows = wound edges. Immunohistochemistry for neutrophils, macrophages, and Nos-2^{+ve} and Arginase-1^{+ve} macrophages (**E**), quantified in **F** and **G**. Arrows = positive (brown/red) cells. Bar = 50 µm. Mean +/- SEM. n = 5 mice per group. * = $P < 0.05$, ** = $P < 0.01$, *** = $P < 0.001$. Two-way ANOVA with Tukey's *post-hoc* analysis. * alone versus D3.

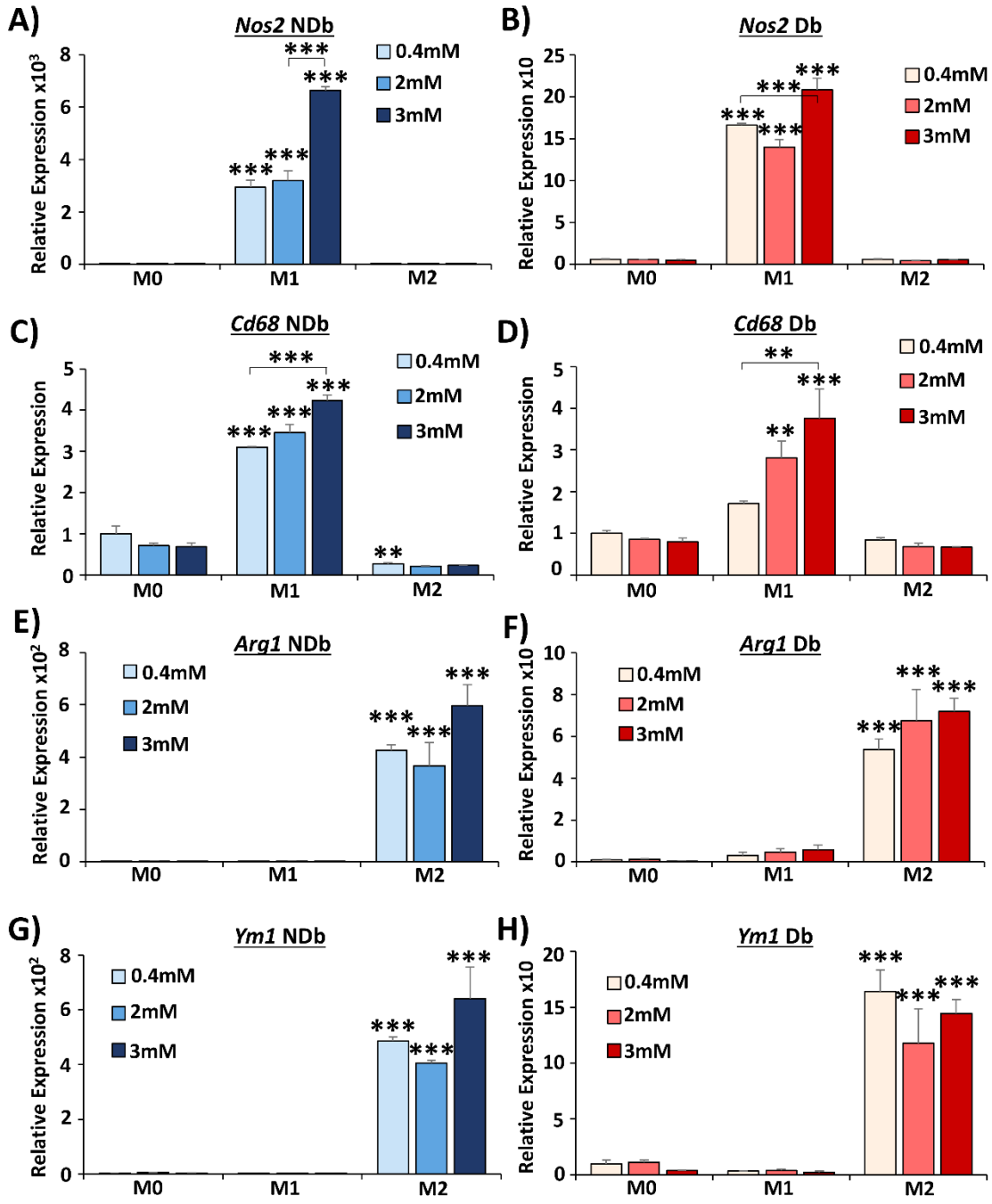

Figure 4A.4. Calcium alters responses to polarisation stimuli in non-diabetic and diabetic macrophages. qRT-PCR was used to assess the expression of M1 (*Nos2* and *Cd86*) and M2 (*Arg1* and *Ym1*) polarisation markers in bone marrow-derived macrophages, stimulated with cytokines at difference calcium concentrations. M0 = unstimulated. NDb = non-diabetic. Db expression relative to NDb. Mean +/- SEM. n = 4 mice per group. ** = $P < 0.01$, *** = $P < 0.001$. Two-way ANOVA with Tukey's *post-hoc* analysis.

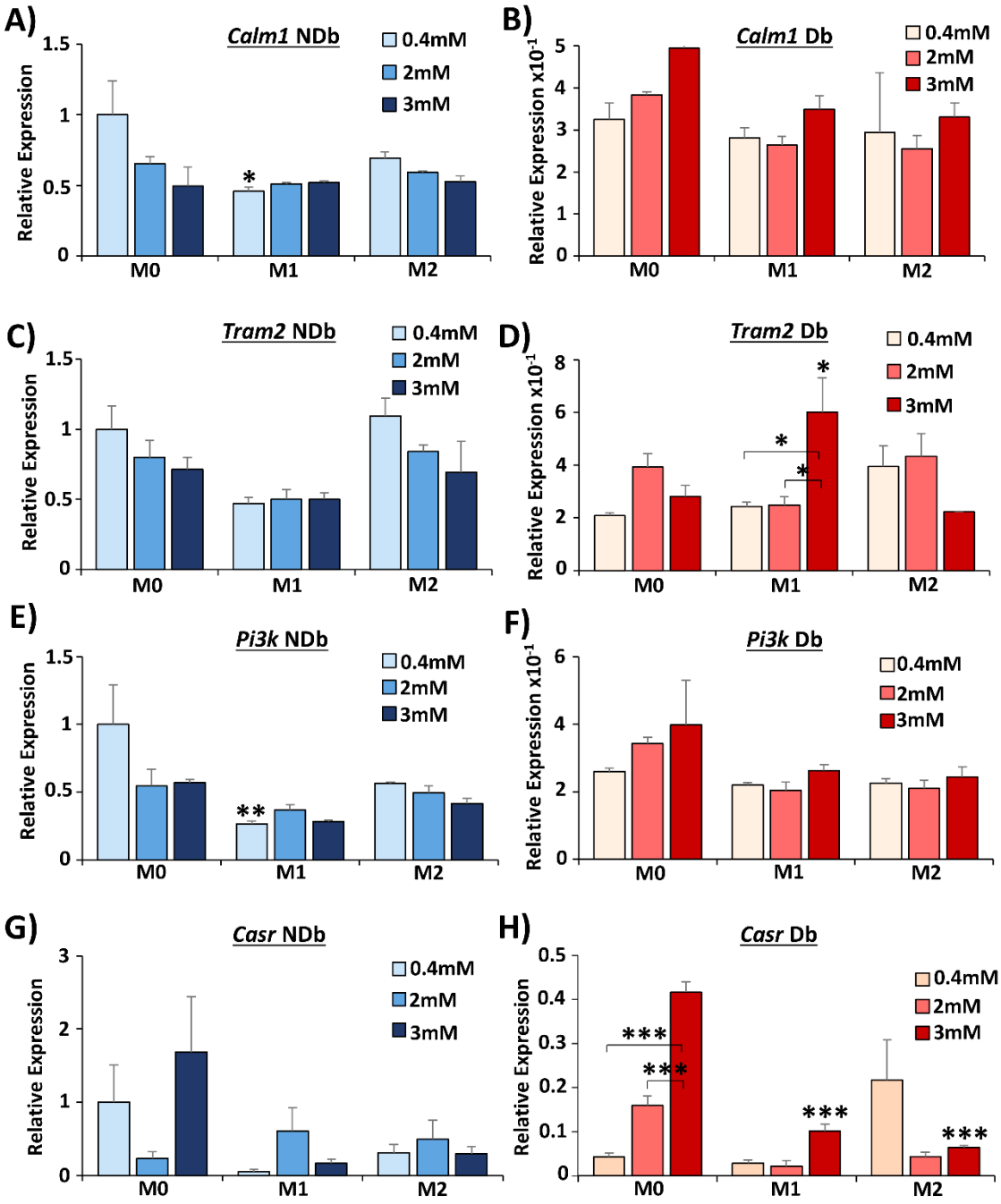

Figure 4A.5. Calcium and polarisation alter the expression of calcium-linked genes in non-diabetic and diabetic macrophages. Bone marrow-derived macrophages were polarised to M1 and M2 states (or left unstimulated, M0). Calcium was added at the same time as cytokines. qRT-PCR was used to assess the expression of calcium-linked genes. NDb = non-diabetic. Db expression relative to NDb. Mean +/- SEM. n = 4 mice per group. ** = $P < 0.01$, *** = $P < 0.001$. Two-way ANOVA with Tukey's *post-hoc* analysis. * alone versus M0 group.

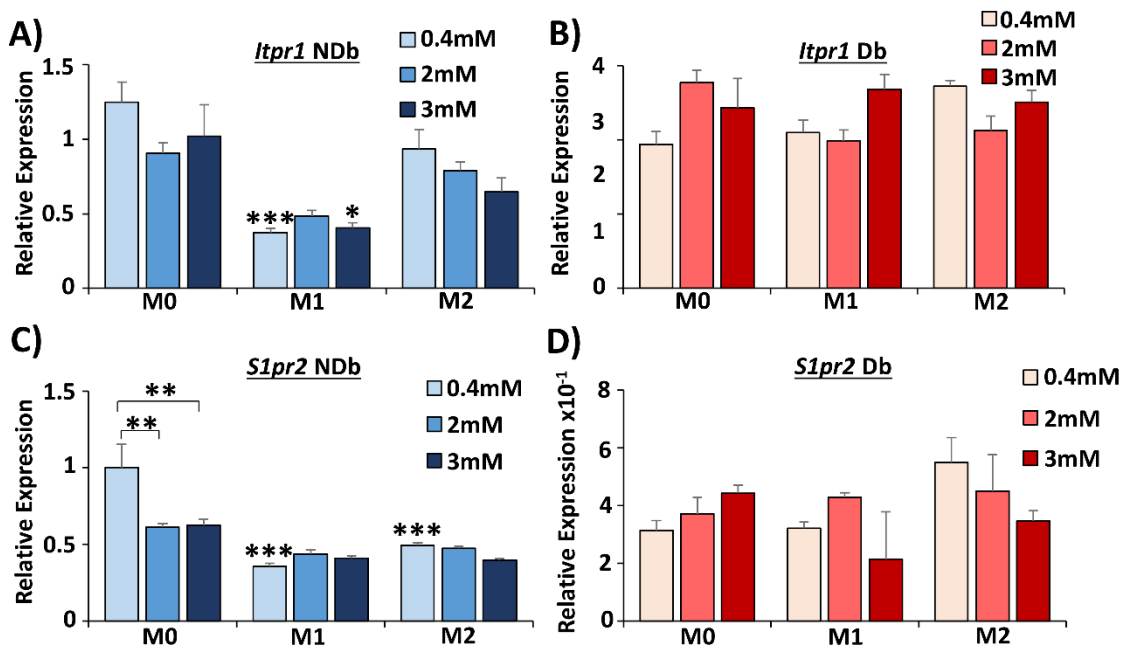

Figure 4A.6. *Itpr1* and *S1pr2* are altered by calcium in non-diabetic, but not diabetic, macrophages. Bone marrow-derived macrophages were polarised to M1 and M2 states (or left unstimulated, M0). Calcium was added with cytokines. qRT-PCR was used to assess the expression of the calcium-linked genes, *Itpr1* and *S1pr2*. NDb = non-diabetic. Db expression relative to NDb. Mean +/- SEM. n = 4 mice per group. * = $P < 0.05$, ** = $P < 0.01$, *** = $P < 0.001$. Two-way ANOVA with Tukey's *post-hoc* analysis. * alone versus M0 group.

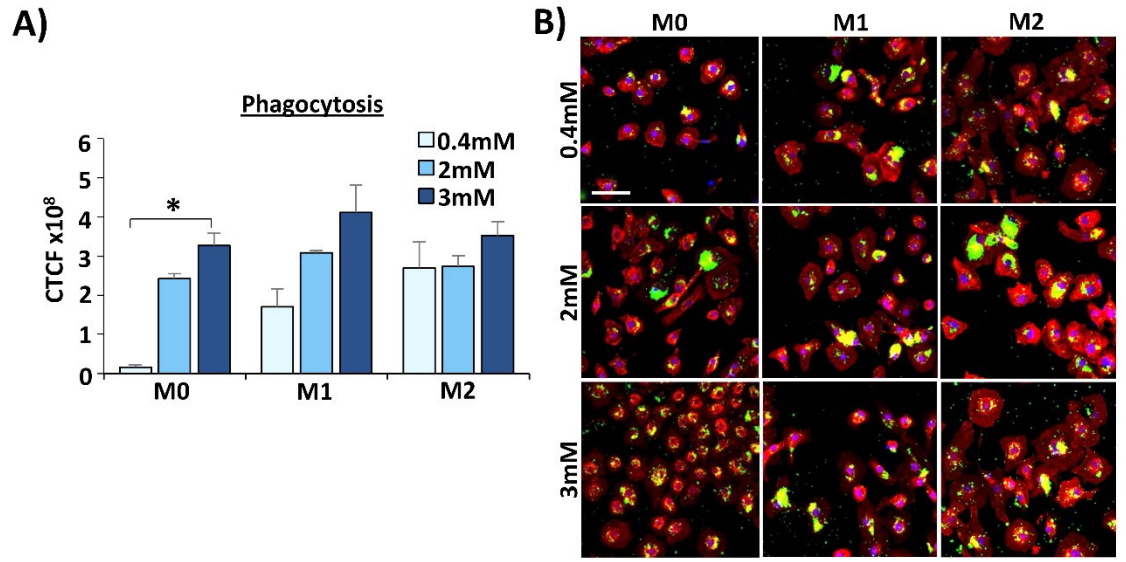

Figure 4A.7. Calcium administration alters the phagocytic ability of non-diabetic macrophages. Bone marrow-derived macrophages (Mφs) were polarised to M1 and M2 states (or left unstimulated, M0). Following stimulation (24 hours), calcium was added to Mφs for six hours. Mφs were then incubated with *E. coli* Bioparticles™ (green) for two hours, counterstained with Phalloidin (red) and DAPI (blue) and imaged. Quantification (**A**) and images (**B**). Bar = 50 µm. CTCF = corrected total cell fluorescence. Mean +/- SEM. n = 4 mice per group. * = $P < 0.05$. Two-way ANOVA with Tukey's *post-hoc*.

Chapter 5: Appendix

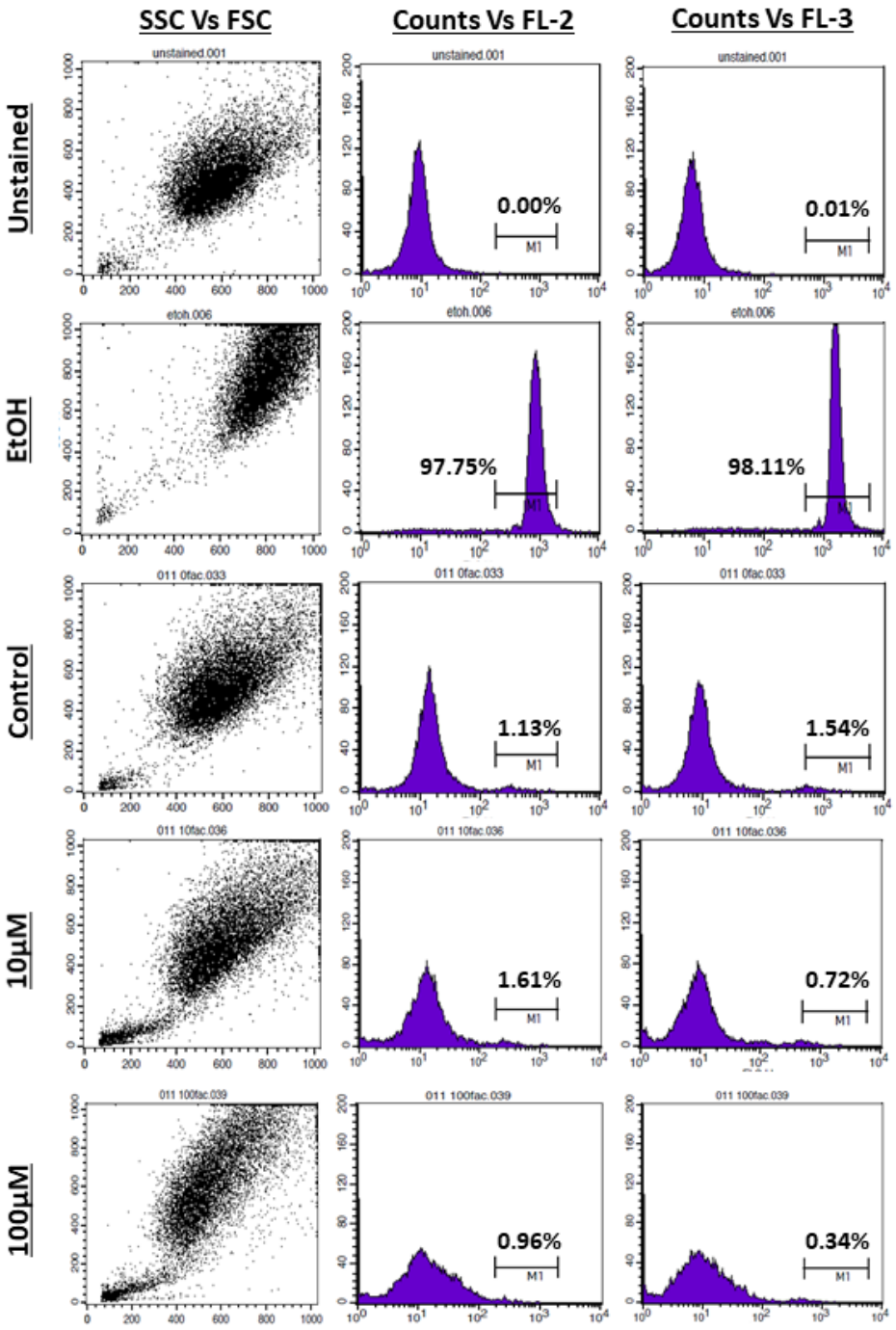

Figure 5A.1. Iron administration does not significantly alter human dermal fibroblast viability after 5 days of treatment. Propidium iodide (PI) staining was performed on human dermal fibroblasts (HDFs) following ferric ammonium citrate treatment. Ethanol (EtOH)-treated HDFs = control. Representative side scatter and forward scatter scatterplots. PI staining read in the FL-2 and FL-3 channels. Representative histograms and markers showing percentage PI^{+ve} staining.

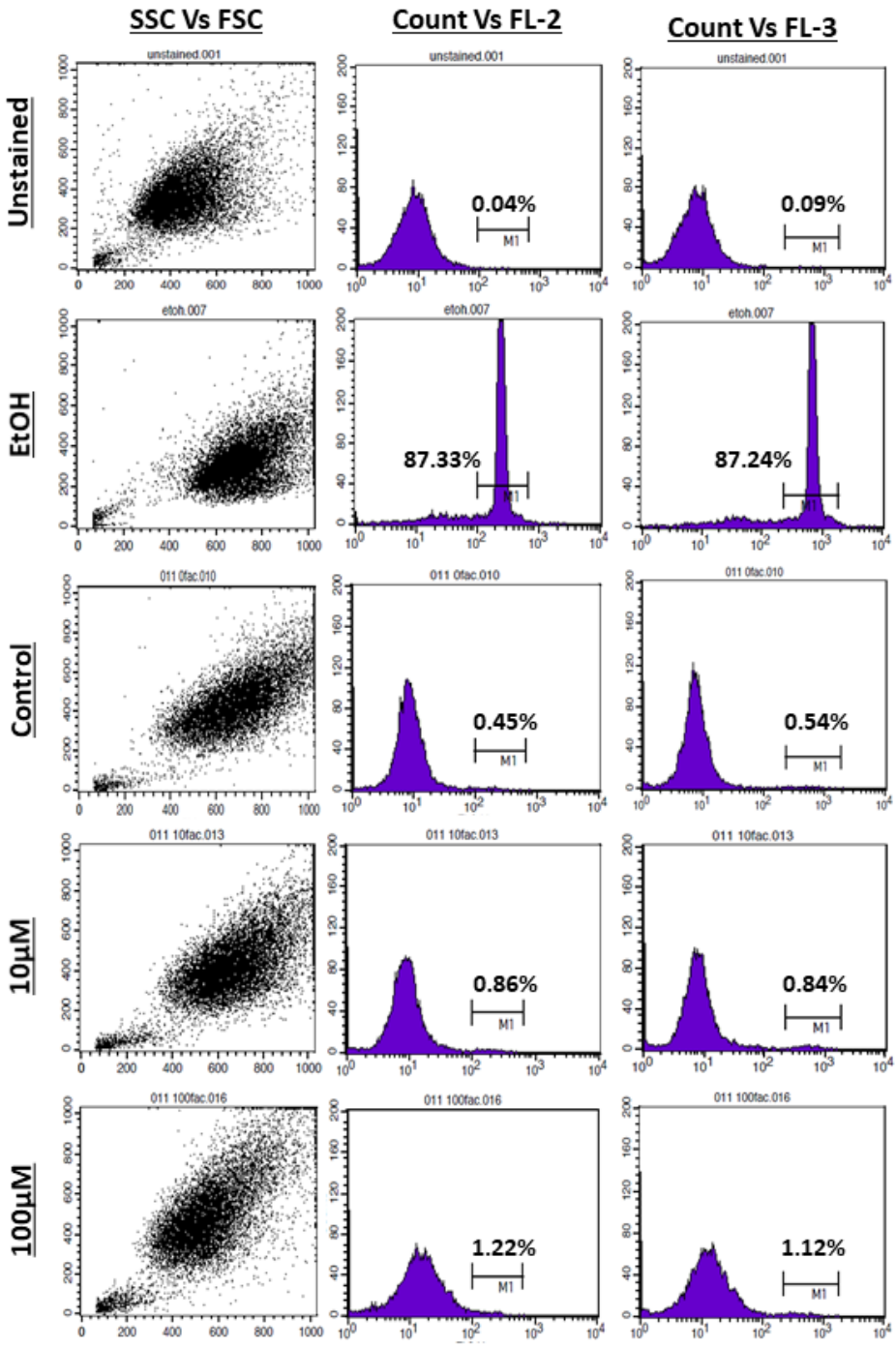

Figure 5A.2. Iron administration does not significantly alter human dermal fibroblast viability after 11 days of treatment. Propidium iodide (PI) staining was performed on human dermal fibroblasts (HDFs) following ferric ammonium citrate treatment. Ethanol (EtOH)-treated HDFs = control. Representative side scatter and forward scatter scatterplots. PI staining read in the FL-2 and FL-3 channels on a BD FACSCalibur™. Representative histograms and markers show PI^{+ve} staining.

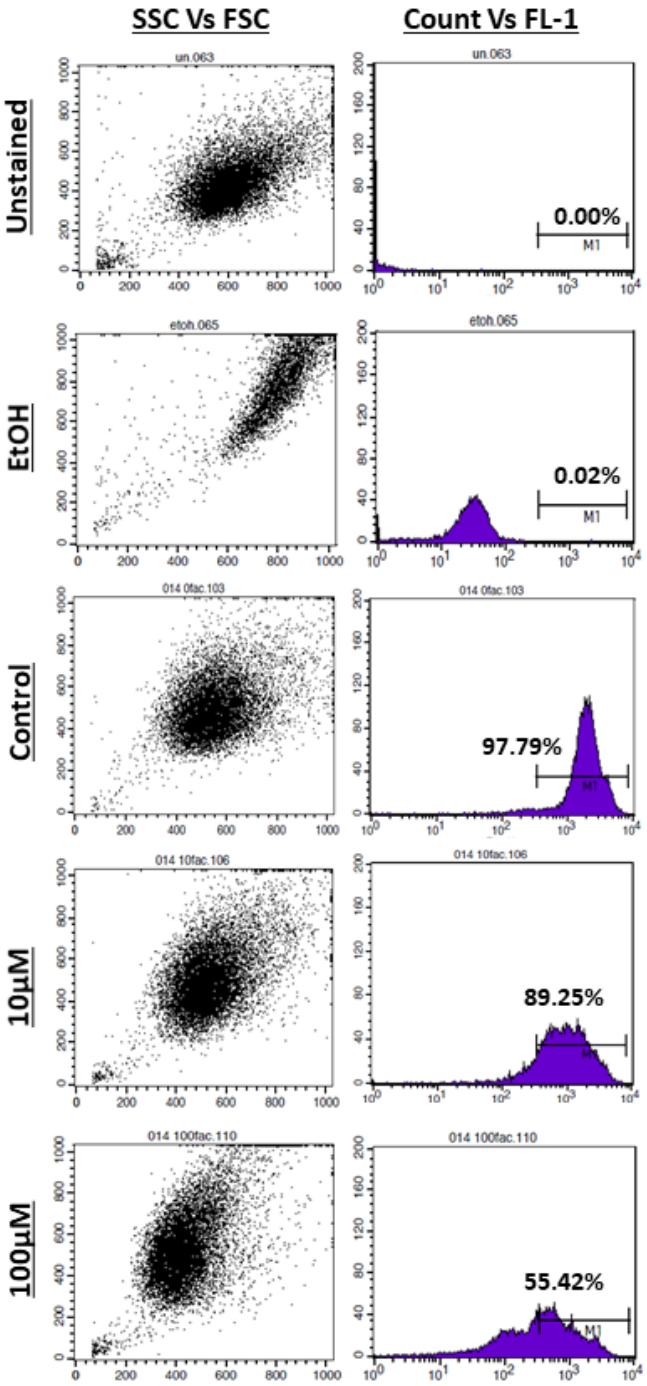

Figure 5A.3. Calcein AM staining of iron treated human dermal fibroblasts 5 days post-initial treatment. Calcein AM staining was performed on human dermal fibroblasts (HDFs) following ferric ammonium citrate treatment to determine HDF viability. Ethanol (EtOH)-treated HDFs = control. Representative side scatter and forward scatter scatterplots. Calcein AM staining read in the FL-1 channel on a BD FACSCalibur™. Representative histograms and markers showing percentage Calcein AM staining.

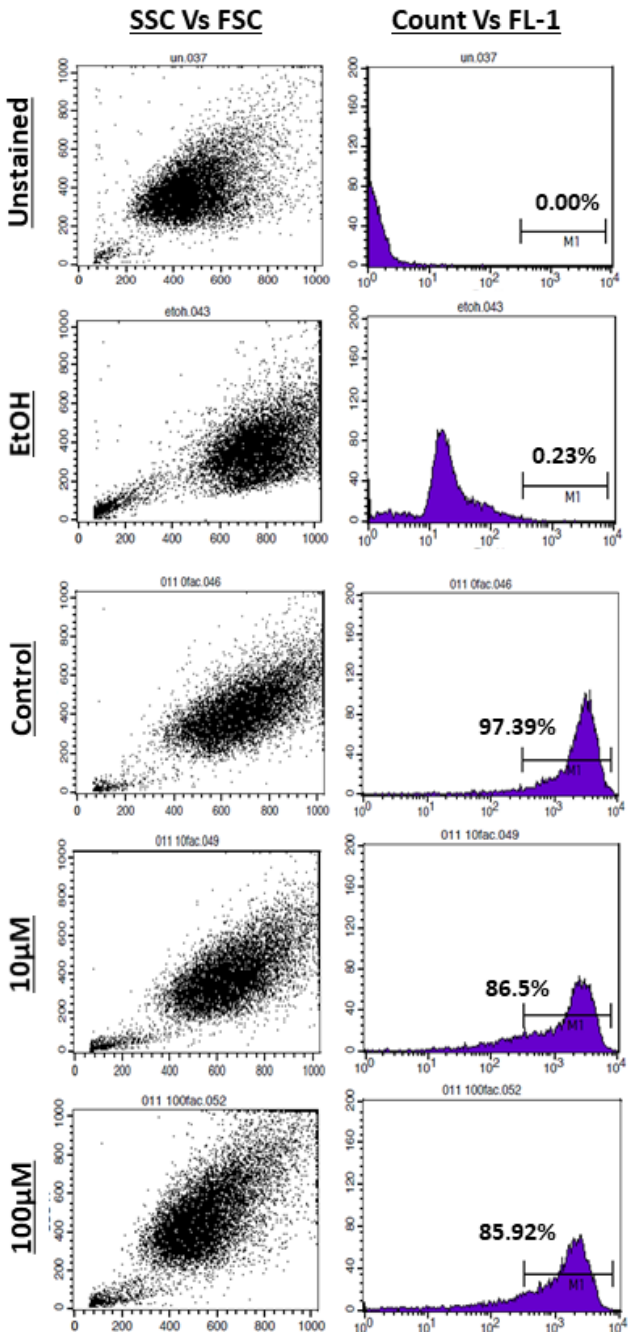

Figure 5A.4. Calcein AM staining of iron treated human dermal fibroblasts 11 days post-initial treatment. Calcein AM staining was performed on human dermal fibroblasts (HDFs) following ferric ammonium citrate treatment to determine HDF viability. Ethanol (EtOH)-treated HDFs = control. Representative side scatter and forward scatter scatterplots. Calcein AM staining read in the FL-1 channel on a BD FACSCalibur™. Representative histograms and markers showing percentage Calcein AM staining.

Table 5A.1. Liquid chromatography mass spectrometry identifies an altered fibroblast extracellular matrix proteome following iron treatment. *

Protein	Score		Peptides		% SC	
	0FAC	100FAC	0FAC	100FAC	0FAC	100FAC
CO1A1	501.9	1069.2	4	15	1.8	7.3
CO1A2	191.9	120.9	2	1.9	2.4	2.16
CO6A1	2691.6	1511.1	11	11	15	17
FINC	2821.3	2376.7	21.5	16	31	10.2
TSP1	1035.7	2549.9	4	20	4.5	26.2
FBN1	684.4	NA	9	NA	3.8	NA
VIME	431.7	607.3	6	6	13.3	16.1
VTNC	536.7	51	1	1	3.1	3.1
TENA	3177.5	2703.1	19	18.4	12.1	0.87
CO6A2	1124.6	529.9	9	8	10.4	10.6
MXRA5	150.6	NA	3	NA	1.2	NA
CALL5	101.3	NA	1	NA	7.5	NA
NET1	NA	99	NA	9	NA	2.6
LEG1	NA	66.4	NA	1	NA	8.9
LEG7	NA	63	NA	1	NA	8.1
ACTA	NA	50.8	NA	1	NA	7.1
TSP2	NA	277.8	NA	4	NA	5.5

**NA = not identified. %SC = percentage sequence coverage. Enrichments, number of peptides and SC were higher in iron-loaded cells for collagens (CO1A1, CO6A1 and CO6A2), thrombosposondins (TSP1 and TSP2), vimentin (VIME) and α-SMA (ACTA).*

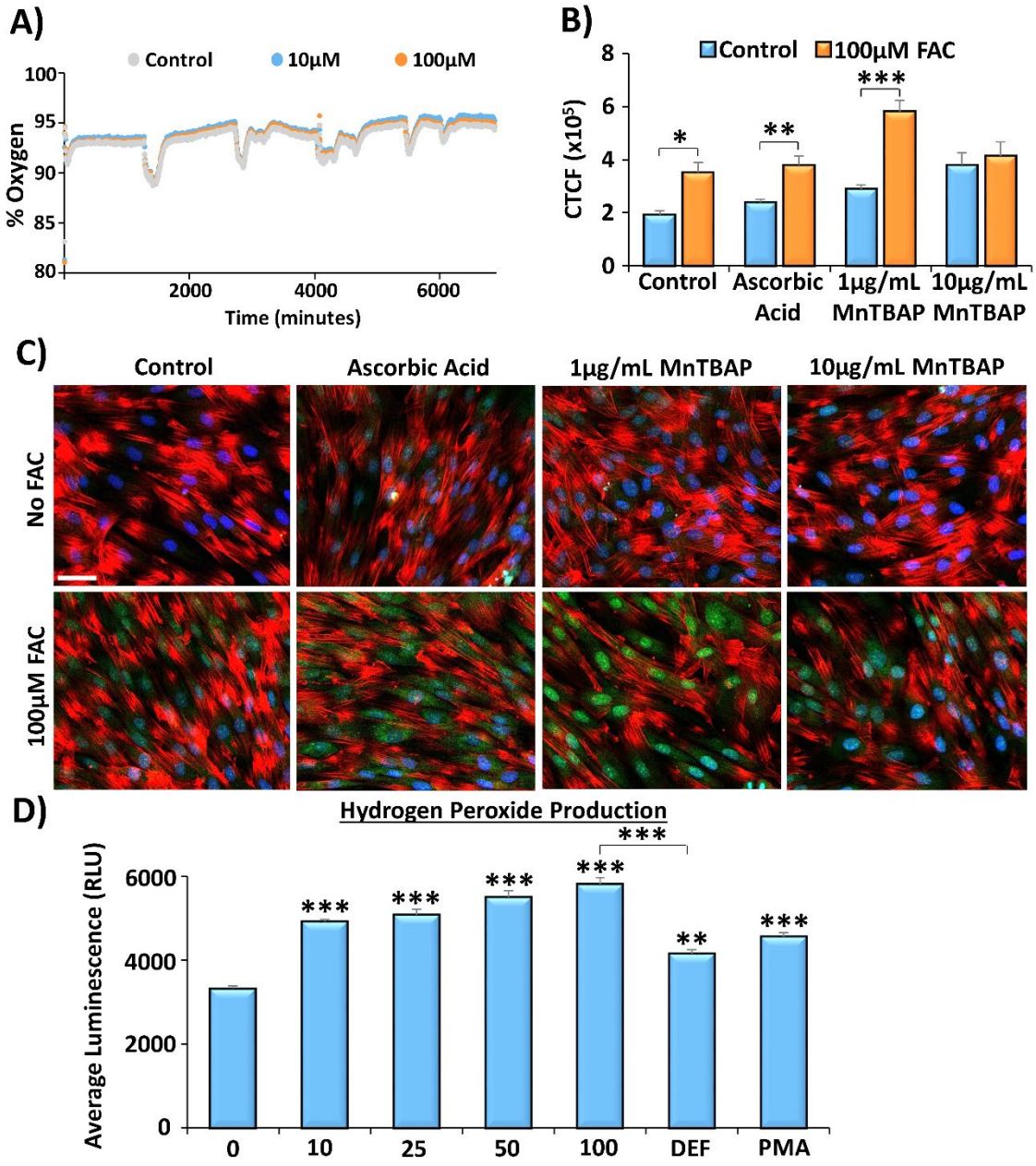

Figure 5A.5. Iron treatment does not substantially alter cell culture oxygen, but induces oxidative stress via CellROX® assessment. A presens oxygen plate monitor was used to measure saturated oxygen in cell culture following ferric ammonium citrate (FAC) treatment over 5 days (**A**). A CellROX® assay measured intracellular reactive oxygen species (ROS; **B-C**). The antioxidants, ascorbic acid and MnTBAP chloride, did not significantly rescue iron-induced oxidative stress. CellROX = green ROS. Phalloidin = red cytoskeleton. DAPI= blue nuclei. H_2O_2 production (ROS-Glo assay, Promega) was increased following FAC treatment (**D**). Bar = 50 µm. n = 3 donors. Representative of three independent experiments. Mean + SEM. Two-way ANOVA and Tukey *post-hoc* analysis on **B**, one-way ANOVA and Tukey's *post-hoc* analysis on **D** (versus no FAC, 0).

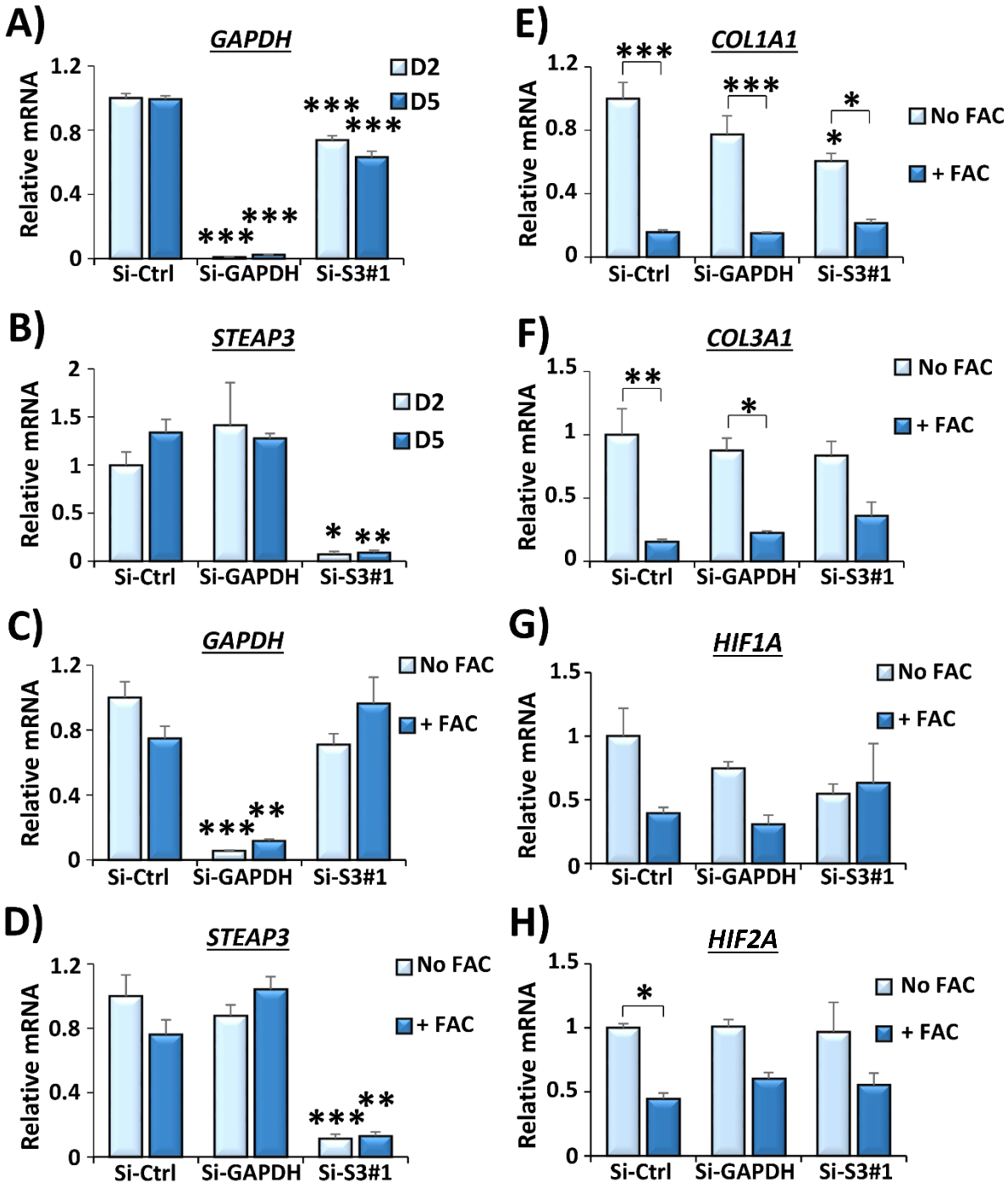

Figure 5A.6. SiRNA knockdown of *STEAP3* is stable at 5 days following iron treatment. Human dermal fibroblasts (HDFs) were transfected with control (Si-Ctrl), GAPDH (Si-GAPDH) or STEAP3 siRNA (Si-S3#1) and collected at 2 and 5 days post-transfection. Silencing of *GAPDH* (**A**) and *STEAP3* (**B**) remained stable over 5 days, and with 100 μM ferric ammonium citrate (+ FAC) administration (**C** and **D**, respectively). *COL1A1* (**E**), *COL3A1* (**F**), *HIF1A* (**G**) and *HIF2A* (**H**) were also assessed. n = 3 donors. Data represent mean + SEM. * = $P < 0.05$, ** = $P < 0.01$, *** = $P < 0.001$. Two-way ANOVA was performed on all data sets with Tukey's *post-hoc* analysis. * alone versus Si-Ctrl.

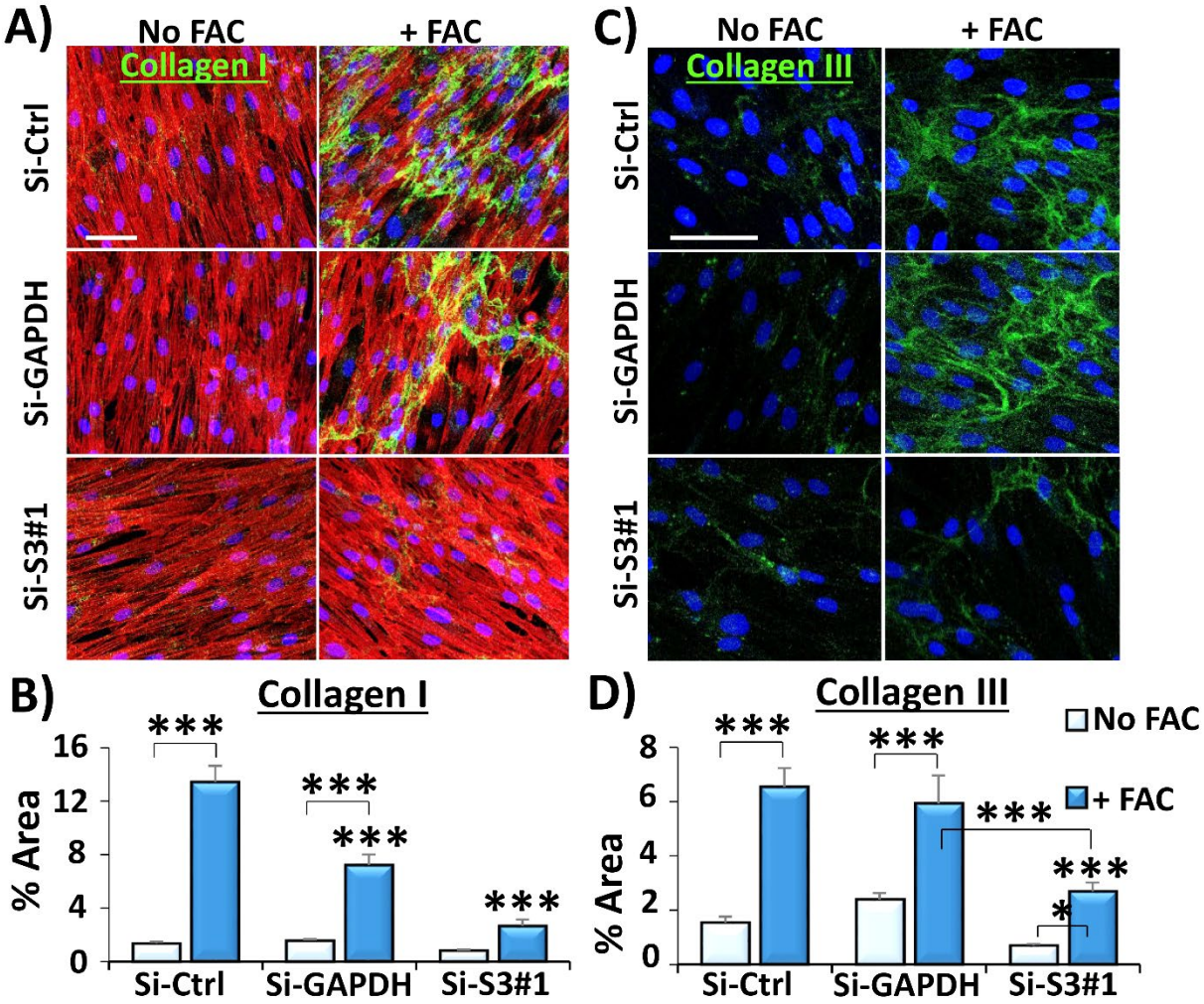

Figure 5A.7. *STEAP3* knockdown reduces extracellular collagen I and collagen III deposition *in vitro*. Human dermal fibroblasts (HDFs) were transfected with control (Si-Ctrl), GAPDH (Si-GAPDH) or STEAP3 (Si-S3#1) siRNA, with or without 100 µM ferric ammonium citrate (FAC) for 5 days. Si-S3#1 treated HDFs produce less collagen I (**A-B**) and collagen III (C-D) following FAC treatment. Collagen I/III (green), nuclei (blue) and phalloidin (red cytoskeleton in **A**). Bar = 50 µm. n = 3 donors. Data represent mean + SEM. * = $P < 0.05$, ** = $P < 0.001$. Two-way ANOVA with Tukey's *post-hoc*. * alone versus Si-Ctrl.

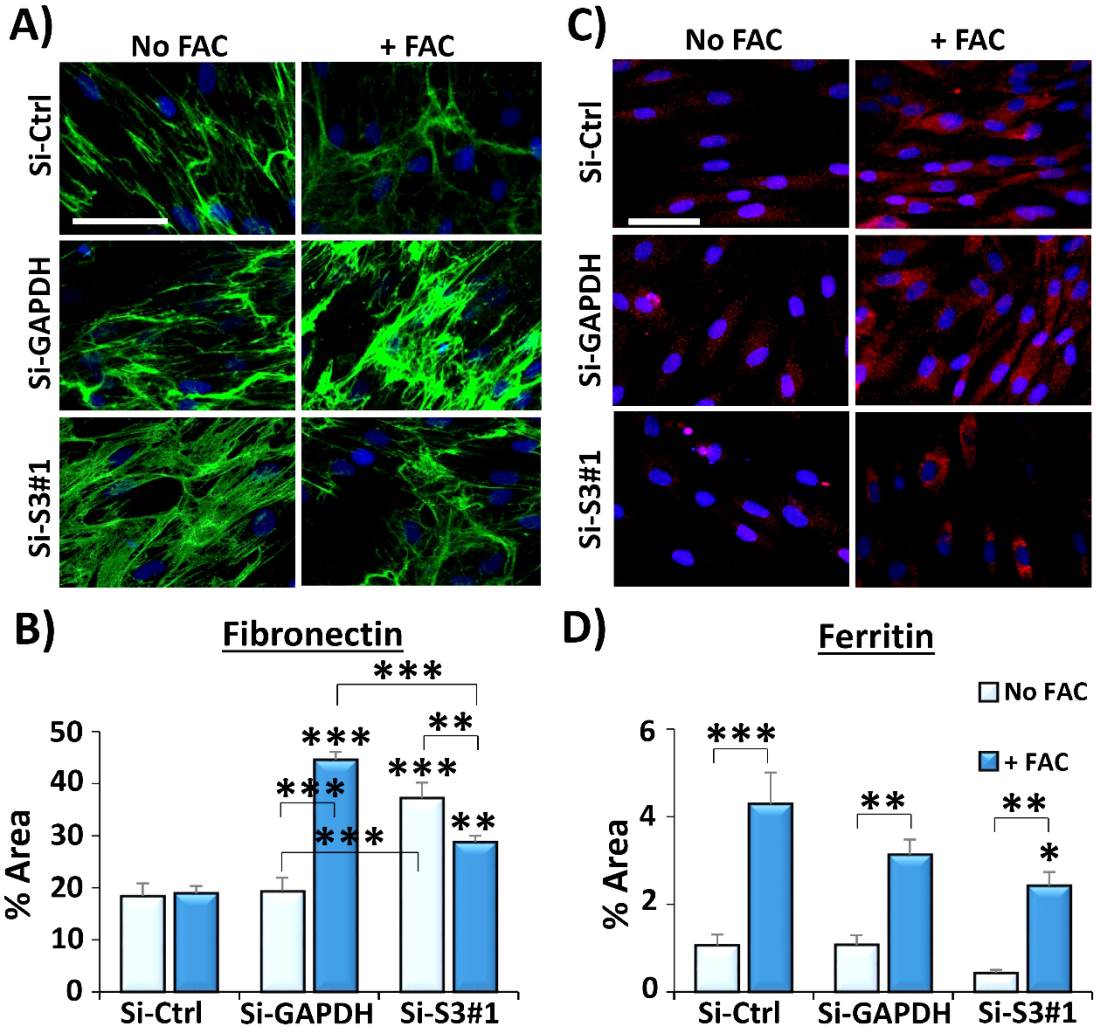

Figure 5A.8. ***STEAP3*** **knockdown alters fibronectin and ferritin expression**. Human dermal fibroblasts (HDFs) were transfected with control (Si-Ctrl), GAPDH (Si-GAPDH) or STEAP3 (Si-S3#1) siRNA, with or without 100 µM ferric ammonium citrate (FAC) for 5 days. HDFs were stained for fibronectin (**A**, green), quantified in **B,** and ferritin (**C**, red), quantified in **D**. DAPI = blue nuclei. Bar = 50 µm. n = 3 donors. Data represent mean + SEM. * = $P < 0.05$, ** = $P < 0.01$, *** = $P < 0.001$. Two-way ANOVA was performed on all data sets with Tukey's *post-hoc* analysis. * alone versus Si-Ctrl.

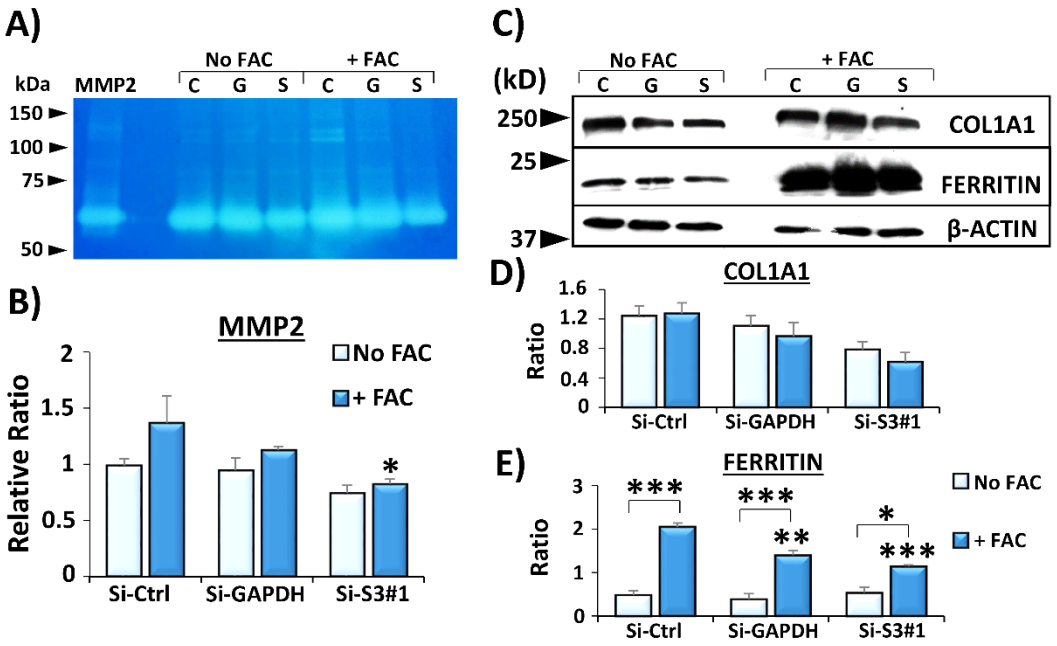

Figure 5A.9. *STEAP3* knockdown reduces protease activity and collagen expression. Human dermal fibroblasts (HDFs) were transfected with control (C, Si-Ctrl), GAPDH (G, Si-GAPDH) or STEAP3 (S, Si-S3#1) siRNA, with or without 100 μM ferric ammonium citrate (FAC) for 5 days. Conditioned media was assessed for MMP2 activity via zymogram (**A**), quantified in **B**. HDFs were also collected for western blot analysis (**C**), quantified in **D** and **E**. β-actin = loading control. n = 3 donors. Data represent mean + SEM. * = $P < 0.05$, ** = $P < 0.01$, *** = $P < 0.001$. Two-way ANOVA was performed on all data sets with Tukey's *post-hoc* analysis. * alone versus Si-Ctrl.

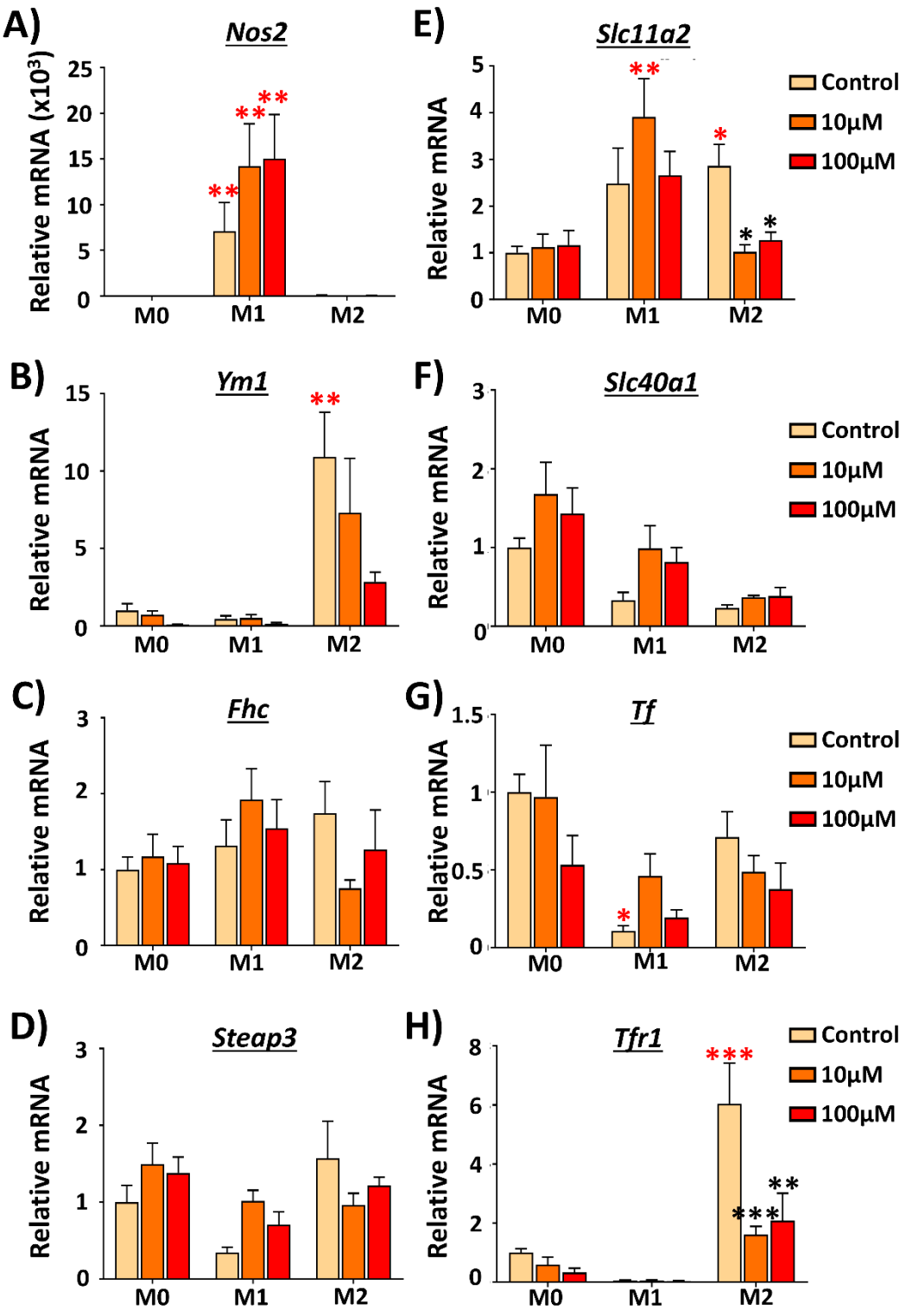

Figure 5A.10. Iron treatment alters iron gene transcription in murine bone marrow-derived macrophages. qRT-PCR shows the expression of the M1 and M2 markers, *Nos2* (**A**) and *Ym1* (**B**), respectively. The iron-regulating genes, *Fhc* (**C**), *Steap3* (**D**), *Slc11a2* (**E**), *Slc40a1* (**F**), *Tf* (**G**) and *Tfr1* (**H**) are also shown. M0 = unstimulated. M1 = M1-stimulated. M2 = M2-stimulated. n = 3 mice per group. Data = mean + SEM. * = $P < 0.05$, ** = $P < 0.01$, *** = $P < 0.001$. Red * = versus M0, black * = versus control within polarisation group. Significance determined via two-way ANOVA and Tukey's multiple comparisons tests.

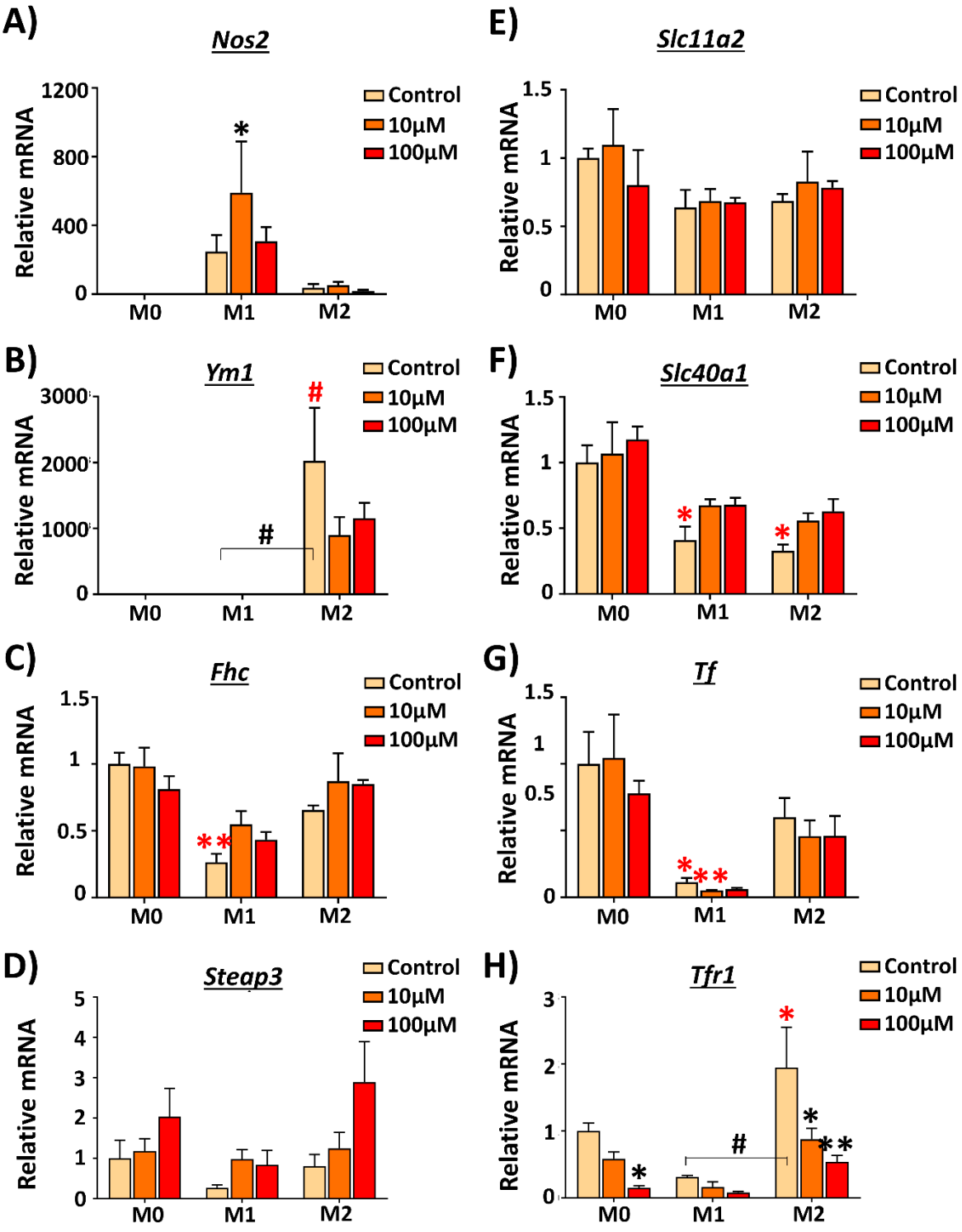

Figure 5A.11. Iron treatment alters iron gene transcription in murine bone marrow-derived macrophages following E. coli phagocytosis. qRT-PCR shows the expression of the M1 and M2 markers, *Nos2* (**A**) and *Ym1* (**B**), respectively. The iron-regulating genes, *Fhc* (**C**), *Steap3* (**D**), *Slc11a2* (**E**), *Slc40a1* (**F**), *Tf* (**G**) and *Tfr1* (**H**) are also shown. M0 = unstimulated. M1 = M1-stimulated. M2 = M2-stimulated. n = 3 mice per group. Data = mean + SEM. * = $P < 0.05$, ** = $P < 0.01$, # = $P < 0.001$. Red */#= versus M0, black */# = versus control within polarisation group. Significance determined via two-way ANOVA and Tukey's *post-hoc* tests.

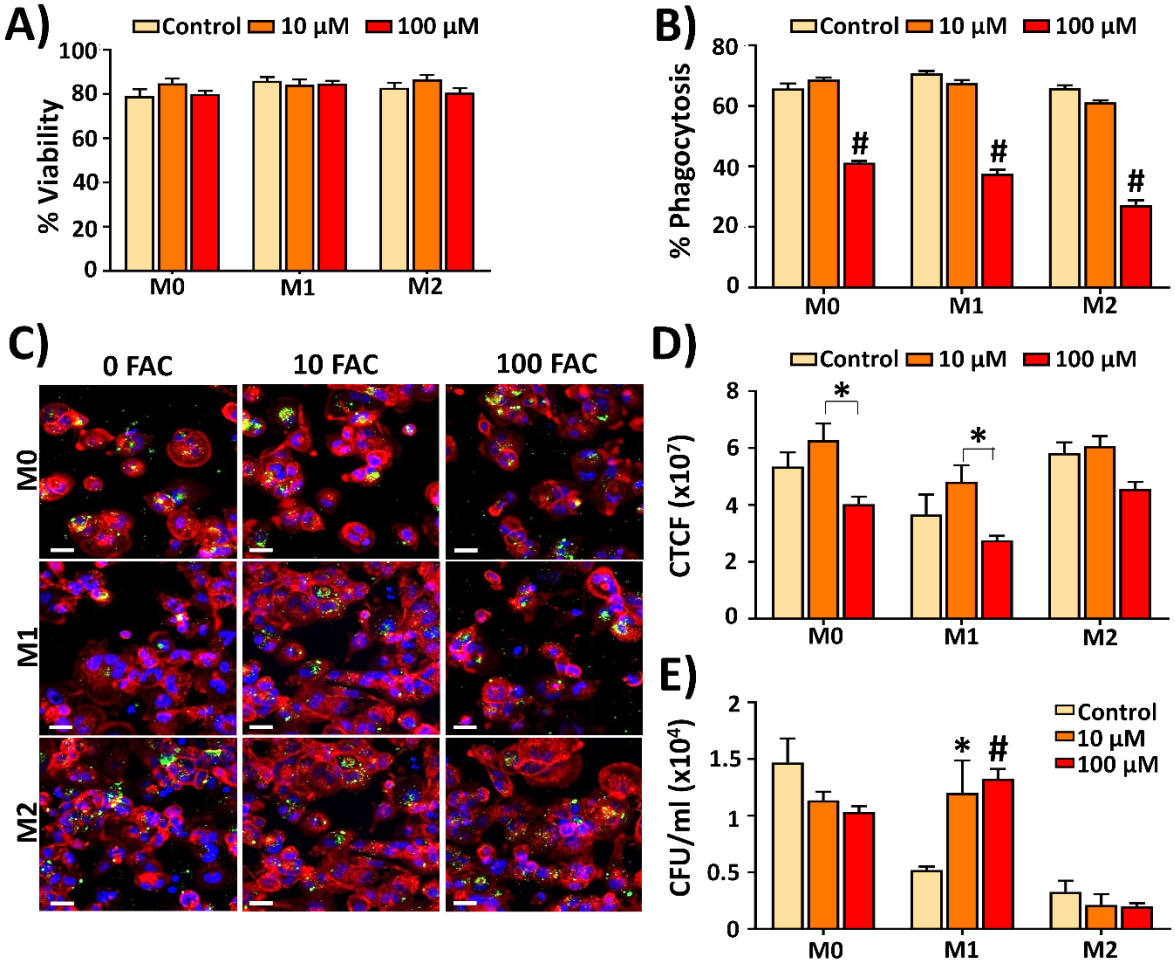

Figure 5A.12. Iron treatment reduces phagocytosis in THP-1 macrophages. Propidium iodide staining of THP-1 macrophage viability following ferric ammonium citrate (FAC) treatment (**A**). *E. coli* Bioparticle™ phagocytosis analysed by flow cytometry (**B**) and confocal microscopy (**C-D**). CTCF = corrected total cell fluorescence. *E. coli* = green. Phalloidin = red cytoskeleton. DAPI = blue nuclei. Bar = 50 µm. Live bacterial phagocytosis (**E**). CFU/mL = colony forming units per millilitre. Three independent experiments. Data = mean + SEM. * = $P < 0.05$, ** = $P < 0.01$, # = $P < 0.001$. Significance determined via two-way ANOVA and Tukey's *post-hoc* tests. */# alone versus M0 group.